EMERGING INFECTIOUS DISEASES®

CDC
Centers for Disease Control and Prevention

Zoonotic Infections

December 2021

Franz Marc (1880–1916), *The Tiger*, 1912. Oil on Canvas. 43.9 in x 40 in111.7 cm x 101.8 cm. Städtische Galerie im Lenbachhaus and Kunstbau Munich, Germany. Image source: Art Resource, New York, New York, USA.

EMERGING INFECTIOUS DISEASES®

Emerging Infectious Diseases is published monthly by the Centers for Disease Control and Prevention, 1600 Clifton Rd NE, Mailstop H16-2, Atlanta, GA 30329-4027, USA. Telephone 404-639-1960; email, eideditor@cdc.gov

EMERGING INFECTIOUS DISEASES®

Zoonotic Infections **December 2021**

On the Cover

Franz Marc (1880–1916), *The Tiger,* 1912. Oil on Canvas. 43.9 in x 40 in111.7 cm x 101.8 cm. Städtische Galerie im Lenbachhaus and Kunstbau Munich, Germany. Image source: Art Resource, New York, New York, USA.

Synopses

Research

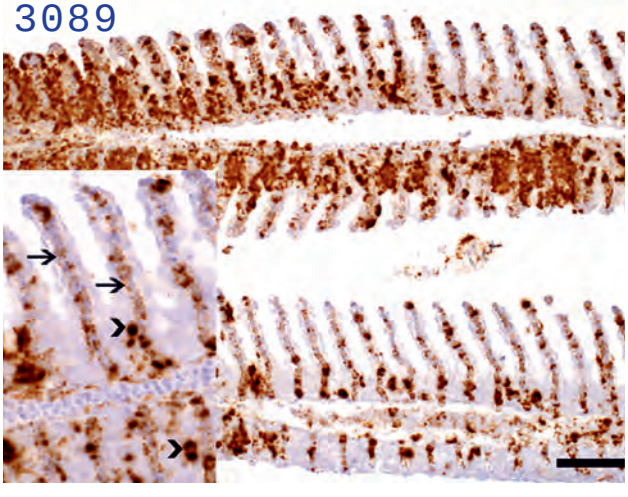

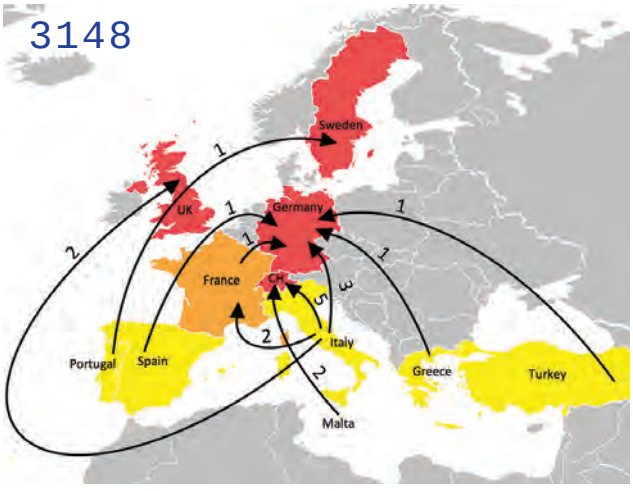

3148

Dispatches

EMERGING INFECTIOUS DISEASES®
December 2021

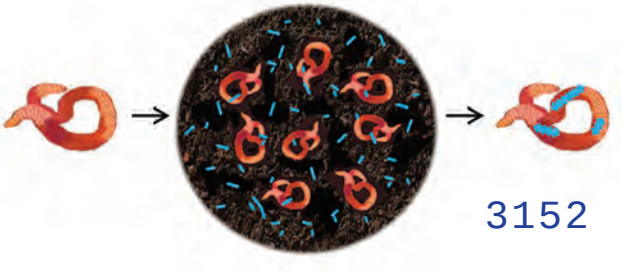
3152

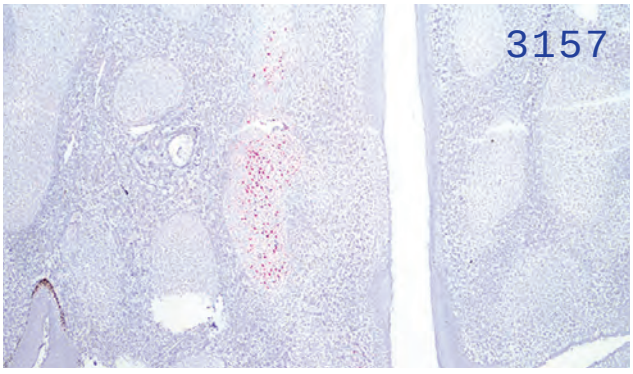

EMERGING INFECTIOUS DISEASES®
December 2021

Research Letters

Books and Media

About the Cover

Reviewer Appreciation

Etymologia

Correction

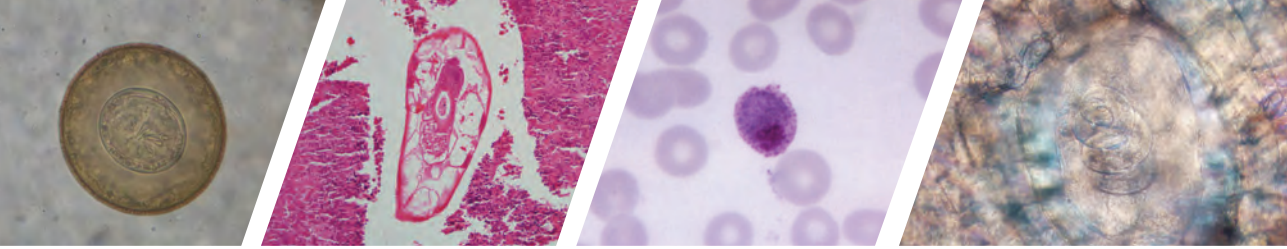

DPDx

Diagnostic Assistance and Training in Laboratory Identification of Parasites

A free service of CDC available to laboratorians, pathologists, and other health professionals in the United States and abroad

- Diagnosis from photographs of worms, histological sections, fecal, blood, and other specimen types
- Expert diagnostic review
- Formal diagnostic laboratory report
- Submission of samples via secure file share

Visit the DPDx website for information on laboratory diagnosis, geographic distribution, clinical features, parasite life cycles, and training via Monthly Case Studies of parasitic diseases.

www.cdc.gov/dpdx
dpdx@cdc.gov

U.S. Department of Health and Human Services
Centers for Disease Control and Prevention

CS272346-DE

Clinical Characteristics of *Corynebacterium* Bacteremia Caused by Different Species, Japan, 2014–2020

Ryosuke Yamamuro, Naoto Hosokawa, Yoshihito Otsuka, Ryosuke Osawa

Medscape EDUCATION ACTIVITY

In support of improving patient care, this activity has been planned and implemented by Medscape, LLC and Emerging Infectious Diseases. Medscape, LLC is jointly accredited by the Accreditation Council for Continuing Medical Education (ACCME), the Accreditation Council for Pharmacy Education (ACPE), and the American Nurses Credentialing Center (ANCC), to provide continuing education for the healthcare team.

Medscape, LLC designates this Journal-based CME activity for a maximum of 1.00 ***AMA PRA Category 1 Credit(s)™***. Physicians should claim only the credit commensurate with the extent of their participation in the activity.

Successful completion of this CME activity, which includes participation in the evaluation component, enables the participant to earn up to 1.0 MOC points in the American Board of Internal Medicine's (ABIM) Maintenance of Certification (MOC) program. Participants will earn MOC points equivalent to the amount of CME credits claimed for the activity. It is the CME activity provider's responsibility to submit participant completion information to ACCME for the purpose of granting ABIM MOC credit.

All other clinicians completing this activity will be issued a certificate of participation. To participate in this journal CME activity: (1) review the learning objectives and author disclosures; (2) study the education content; (3) take the post-test with a 75% minimum passing score and complete the evaluation at http://www.medscape.org/journal/eid; and (4) view/print certificate. For CME questions, see page 3218.

Release date: November 17, 2021; Expiration date: November 17, 2022

Learning Objectives

Upon completion of this activity, participants will be able to:

- Describe the proportion of true bacteremia and differences in clinical characteristics of patients with bacteremia from *C. striatum*, *C. jeikeium*, and other *Corynebacterium* species, based on a retrospective medical record review
- Describe differences in mortality and antimicrobial susceptibility in patients with bacteremia from *C. striatum*, *C. jeikeium*, and other *Corynebacterium* species, based on a retrospective medical record review
- Describe clinical implications of differences in clinical characteristics of patients with bacteremia from *C. striatum*, *C. jeikeium*, and other *Corynebacterium* species, based on a retrospective medical record review

CME Editor

P. Lynne Stockton Taylor, VMD, MS, ELS(D), Technical Writer/Editor, Emerging Infectious Diseases. *Disclosure: P. Lynne Stockton Taylor, VMD, MS, ELS(D), has disclosed no relevant financial relationships.*

CME Author

Laurie Barclay, MD, freelance writer and reviewer, Medscape, LLC. *Disclosure: Laurie Barclay, MD, has disclosed no relevant financial relationships.*

Authors

Disclosures: ***Ryosuke Yamamuro, MD; Naoto Hosokawa, MD, PhD; Yoshihito Otsuka, PhD;*** *and* ***Ryosuke Osawa, MD,*** *have disclosed no relevant financial relationships.*

Author affiliation: Kameda Medical Center, Chiba, Japan

DOI: https://doi.org/10.3201/eid2712.210473

To determine differences in clinical characteristics of patients with bacteremia caused by *Corynebacterium striatum*, *C. jeikeium*, and other species of *Corynebacterium*, we retrospectively reviewed medical records of patients in Japan who had *Corynebacterium* bacteremia during January 2014–May 2020. Of the 115 records evaluated, 60 (52%) were cases of true bacteremia and 55 (48%) were cases of contamination. Proportions of true bacteremia cases caused by *C. striatum* (70%) and by *C. jeikeium* (71%) were significantly higher than those caused by other species of *Corynebacterium* (9%). These 2 organisms were commonly detected in blood cultures of patients with hematologic malignancies and neutropenia. The mortality rates at 90 days were 34% (*C. striatum*), 30% (*C. jeikeium*), and 0% (other species). Given the high mortality rates, assessing true bacteremia when *C. striatum* or *C. jeikeium* is detected in blood cultures, especially in patients with hematologic malignancy, is warranted.

Corynebacterium bacteria are club-shaped gram-positive rods that are ubiquitous in the environment. Because *Corynebacterium* species other than *C. diphtheriae* colonize skin and mucous membranes in humans, *Corynebacterium* is typically considered a clinically nonsignificant contaminant in cultures (*1*). Recently, the frequency of detecting *C. striatum* and *C. jeikeium* as causative agents of severe bloodstream infections (*2*,*3*), infective endocarditis, pneumonia, meningitis, and skin and soft tissue infections (SSTIs) has increased (*4*). Furthermore, these 2 species have been identified most frequently in cultures of clinical specimens, mainly blood, pus, urine, and pleural effusion (*5*).

Studies that have identified *Corynebacterium* infections or bacteremia to the species level are limited, and most are case reports (*6*). The largest study to date of *Corynebacterium* bacteremia investigated 98 cases; however, the species were not identified (*7*). The largest study that identified *Corynebacterium* species included 30 cases of true bacteremia in 339 patients with positive blood cultures (*8*). In our study, we aimed to determine the differences in characteristics and clinical presentations for patients with bacteremia caused by *C. striatum*, *C. jeikeium*, or other species of *Corynebacterium*.

Materials and Methods

Study Design

We retrospectively reviewed electronic medical records and clinical microbiology records of patients with positive blood cultures for *Corynebacterium* spp. in Kameda Medical Center (Chiba, Japan) during January 2014–May 2020. This facility is an 865-bed, tertiary-care general medical center that provides a wide variety of services including general medicine, surgery, oncology, cardiothoracic surgery, hematopoietic stem cell transplantation, and renal transplantation to ≈310,000 persons each year. All patients with blood cultures positive for any organism are automatically referred to the infectious diseases department for consultation. Board-certified infectious disease physicians evaluate the patients and document the consultation report in medical records. The study protocol was reviewed and approved by the Kameda Medical Center Institutional Review Board (reference no. 20-046). The need for written informed consent was waived. The study complied with the principles of the Declaration of Helsinki.

Study Population

We included all patients at the hospital who had blood cultures positive for *Corynebacterium* spp. during the study period. We collected data about age, sex, underlying conditions, clinical diagnosis, 90-day mortality rates, species of *Corynebacterium*, and antimicrobial susceptibility. If the same patient had multiple episodes of *Corynebacterium* bacteremia during the study period, we included only the first episode.

Definitions

We defined a case as true bacteremia when 2 sets of blood cultures from a patient with signs of infection were positive for *Corynebacterium* spp. or when 1 set of blood cultures and a clinically relevant specimen from another site (e.g., urine or sputum) where the infection was thought to exist (on the basis of signs/symptoms and examination findings) were both positive for the same species of *Corynebacterium*. For patients with only 1 set of blood cultures in which *Corynebacterium* spp. were detected and for whom bacteremia was clinically suspected, new blood cultures were performed, and reevaluated as necessary, before antimicrobial agents were initiated. These patients were carefully followed by our infectious disease physicians to ensure the absence of infection. This definition was based on a previous study (*9*).

Catheter-related bloodstream infection (CRBSI) was considered definite for patients who met 1 of the following 3 criteria: 1) ≥1 set of blood cultures and semiquantitative cultures of a catheter segment (>15 CFUs/plate) were both positive for the same *Corynebacterium* species; 2) peripheral blood cultures and blood cultures from a catheter lumen were both positive for the same species of *Corynebacterium*, and its differential time to positivity was >2 hours (*10*); or 3)

2 sets of blood cultures were positive for *Corynebacterium* species, and signs of inflammation or purulence were present at the catheter insertion site (*11*). Diagnosis of other focal infections were based on the US Centers for Disease Control and Prevention National Healthcare Safety Network criteria (*12*).

We classified a case as no focus when physical examination by infectious disease physicians revealed no localized signs of infection, urinalysis was negative for pyuria or bacteriuria, chest images (radiographs or computed tomography scans) showed no infiltrates or masses, and the case still satisfied the criteria for true bacteremia. Chronic kidney disease was defined as being present when serum creatinine level was >2.0 mg/dL. Liver disease was defined as presence of liver cirrhosis or chronic hepatitis B or C.

Laboratory Methods

We used RapID CB Plus (Kyokuto Pharmaceutical Industrial Co. Ltd., https://www.kyokutoseiyaku.co.jp) for bacterial identification during January 2014–May 2015. This kit correctly identifies 95% of *Corynebacterium* isolates to the species level (*13*). Starting in June 2015, we identified strains by using matrix-assisted laser desorption/ionization time-of-flight mass spectrometry and a Bruker MALDI Biotyper (Bruker Daltonics GmbH, https://www.bruker.com). We used score cutoff values according to recommendations proposed by the manufacturer (≥2.0). For some cases in which no identification or ambiguous identification was achieved by these methods, we confirmed identification by using 16S rRNA gene sequence analysis. We performed antimicrobial susceptibility tests by broth microdilution, using Clinical and Laboratory Standards Institute (CLSI, https://clsi.org) M45 A2:2ED 2010 during January 2014–December 2016 and CLSI M45 3rd edition from January 2017 on.

Statistical Analyses

We used Fisher exact or Pearson χ^2 tests to compare categorical variables. For continuous variables, we used Mann–Whitney U or paired *t*-tests, and for estimating survival probabilities we used Kaplan-Meier curves. We estimated and compared the cumulative incidence of mortality by using the log-rank test and compared differences in antimicrobial susceptibility between *Corynebacteria* species by using Fisher exact or Pearson χ^2 tests. We considered $p<0.05$ to indicate statistical significance. We performed all statistical analyses by using EZR (Saitama Medical Center, Jichi Medical University, Saitama, Japan), a graphical user interface for R (The R Foundation, https://www.r-project.org) (*14*).

Results

Proportion of True Bacteremia Cases

Of 115 patients in this study, *C. striatum* was detected in 67 (58%), *C. jeikeium* in 14 (12%), and other *Corynebacteria* species in 34 (30%) patients. The category of other consisted of 15 species (Table 1). In total, there were 60 cases of true bacteremia and 55 cases of contamination, resulting in 52% of patients having true bacteremia. Of the 60 patients with true bacteremia, 55 had ≥2 sets of positive blood cultures with *Corynebacterium* spp.; 5 had 1 set of positive blood cultures but met the definition of true bacteremia in our study. Of 115 patients, ≥2 genera of bacteria were detected in blood culture from only 1 patient; this patient had diverticulitis and bacteremia caused by *Corynebacterium* spp. and *Escherichia coli*. The patient recovered after receiving treatment

Table 1. Patients with *Corynebacterium* species detected in blood cultures, Japan, 2014–2020

Corynebacterium species	Total, n = 115	True bacteremia, n = 60	Contamination, n = 55
C. striatum	67	47	20
C. jeikeium	14	10	4
Other, total	34	3	31
C. accolens	1	0	1
C. afermentans	6	0	6
C. amycolatum	4	1	3
C. aurimucosum	4	0	4
C. coyleae	1	0	1
C. glucuronolyticum	1	0	1
C. minutissimum	4	0	4
C. mucifaciens	1	0	1
C. pseudodiphtheriticum	1	0	1
C. resistens	2	0	2
C. riegelii	1	1	0
C. simulans	3	0	3
C. singulare	2	0	2
C. tuberculostearicum	2	0	2
C. urealyticum	1	1	0

for *E. coli* bacteremia alone; *Corynebacterium* spp. were considered to be contaminants. The percentages of true bacteremia cases caused by *C. striatum* (70%) and *C. jeikeium* (71%) were significantly higher than those for other species (9%; p<0.001 for each) (Table 2).

Clinical Diagnosis and Underlying Diseases

Hematologic malignancy was the most common underlying disease (33%), especially in 64% of patients with *C. jeikeium* bacteremia, followed by solid tumors (24%) and diabetes mellitus (23%) (Table 2). *C. striatum* and *C. jeikeium* were more frequently detected than other species in patients with hematologic malignancy (p = 0.036 and p<0.001, respectively) and neutropenia (p<0.01 and p<0.001, respectively). Of the 60 patients with true bacteremia, 25 (42%) had infection at an unknown site; 17 (28%) had CRBSI; and 18 (30%) had infection at other foci, including SSTI, pyelonephritis, pneumonia, empyema, infective endocarditis, vertebral osteomyelitis, central venous port infection, and spontaneous bacterial peritonitis.

Mortality Rates

Mortality rates among patients with true bacteremia were 34% among those with bacteremia caused by *C. striatum*, 30% by *C. jeikeium*, and 0 by other species of *Corynebacterium*. (Figure). We observed no significant differences in survival rates between these groups (*C. striatum* p = 0.25 and *C. jeikeium* p = 0.32). Six patients experienced a fulminant course of illness that resulted in death within 7 days; for all 6 patients, the causative organism was *C. striatum*.

Antimicrobial Susceptibility

All tested strains of *Corynebacterium*, regardless of species, were susceptible to vancomycin, linezolid, and minocycline (Table 3). *C. striatum* and *C. jeikeium* were less susceptible than other species to penicillin (p<0.001 for each), ceftriaxone (p<0.001 for each), meropenem (p<0.001 for each), erythromycin (p<0.01 for each), and ciprofloxacin (p<0.001 for *C. striatum* and p = 0.02 for *C. jeikeium*).

Discussion

With regard to the characteristics of *Corynebacterium* bacteremia at the species level, we report 3 major findings. First, *C. striatum* and *C. jeikeium* each caused true bacteremia more frequently than did other *Corynebacterium* species. Second, hematologic malignancies were the most common underlying disease in patients with *Corynebacterium* bacteremia (33%).

Table 2. Clinical diagnosis and characteristics of patients with *Corynebacterium* species detected in blood culture, Japan, 2014–2020*

Variable	All, n = 115	*C. striatum*, %, n = 67	*C. jeikeium*, %, n = 14	Other species, %, n = 34	p values: *C. striatum* vs. other species	p values: *C. jeikeium* vs. other species
Age, y	71	71	66	77	0.055	<0.001
Sex						
M	80 (70)	51 (76)	13 (93)	16 (47)	<0.01	<0.001
F	35 (30)	16 (24)	1 (7)	18 (53)	<0.01	<0.001
Underlying disease, no. (%)						
Diabetes mellitus	27 (23)	14 (20)	2 (14)	11 (32)	0.309	0.292
Chronic kidney disease	16 (14)	9 (13)	2 (14)	5 (15)	1	1
Liver disease	4 (4)	4 (6)	0 (0)	0 (0)	0.299	NA
Solid tumor	27 (24)	13 (19)	4 (29)	10 (29)	0.378	1
Leukemia†	20 (17)	11 (16)	8 (57)	1 (3)	0.056	<0.001
Malignant lymphoma‡	14 (12)	8 (12)	3 (21)	3 (9)	0.537	0.171
Hematologic malignancy§	38 (33)	24 (36)	9 (64)	5 (15)	0.036	<0.01
Underlying condition, no. (%)						
Neutropenia, <500 cells/mm^3	29 (25)	19 (28)	8 (57)	2 (6)	<0.01	<0.001
Corticosteroid	8 (7)	5 (8)	2 (14)	1 (3)	0.661	0.2
Chemotherapy, within 3 mo	41 (36)	23(34)	10 (71)	8 (24)	0.377	<0.01
Clinical diagnosis, no. (%)						
True bacteremia	60 (52)	47 (70)	10 (71)	3 (9)	<0.001	<0.001
No focus	25 (22)	19 (29)	6 (43)	0	ND	ND
CRBSI	17 (15)	13 (19)	3 (21)	1 (3)	ND	ND
Other focus¶	18 (16)	15 (22)	1 (7)	2 (6)	ND	ND
Contamination	55 (48)	20 (30)	4 (29)	31 (91)	<0.001	<0.001

*ALL, acute lymphoid leukemia; AML, acute myeloid leukemia; CRBSI: catheter-related blood stream infection; DLBCL, diffuse large B cell lymphoma; MDS, myelodysplastic syndrome; MM, multiple myeloma; NA, not applicable; ND, not done; IVLBCL, intravascular large B cell lymphoma.; PTCL, peripheral T-cell lymphoma.
†No. cases: AML, 17; ALL, 3,
‡No.cases: DLBCL, n = 8: PCTL, n =3; IVLBCL, n = 1; lymphoplasmacytic lymphoma, n= 1,: Burkitt lymphoma, n = 1.
§No. cases: leukemia, n = 20; lymphoma, n = 14; MM, n = 3; MDS, n = 1; myelofibrosis, n = 2.
¶No. cases: pyelonephritis, n = 5; skin and soft tissue infection, n = 4; empyema, n = 2; pneumonia, n = 1; prostatitis, n = 1; infective endocarditis, n = 1; osteomyelitis, n = 1; vascular graft infection, n = 1; central venous port infection, n = 1; spontaneous bacterial peritonitis, n = 1.

Third, although the most common sources of infection were of unknown origin and CRBSI, other sources (e.g., pyelonephritis, SSTI, and empyema) accounted for 30% of true bacteremia cases.

The strengths of our study include having had infectious disease specialists assess infection sites and classify cases as true bacteremia to ensure study quality. Furthermore, detailed clinical and microbiological data were available because we included all cases of *Corynebacterium* bacteremia in our center over 6 years.

A previous study reported that contamination rates varied among species of *Corynebacterium* and that *C. jeikeium* caused true bacteremia more frequently than other species (*8*). The overall contamination rates of 48% in all patients treated in our study approximated those for 2 previous studies in Japan (46% and 42%) (*9*,*15*). However, higher contamination rates were reported in a study performed in Sweden (*8*), where 93% of these cases were considered to be contaminations and *C. afermentans* accounted for 14%, *C. aurimucosum* for 7%, and *C. amycolatum* for 6% of the total *Corynebacterium* species detected in blood culture. Our study also demonstrated a high contamination rate of 93% for those species, but our frequency of detection was less than that in the previous study; detection rates in our study were 5% for *C. afermentans*, 3% for *C. aurimucosum*, and 3% for *C. amycolatum*. The difference in contamination rates in both studies may be underpinned by regional differences in the epidemiology of *Corynebacterium* species. It is plausible that the study populations may differ because the study in Sweden was population based, whereas our study was performed in a tertiary-care hospital. Furthermore, indications for blood culture may differ between these studies.

Bacteremia with *C. striatum* or *C. jeikeium*, the most frequently identified species in our study, seemed to be more associated with a higher 90-day mortality rate when compared with other species, although we observed no significant difference. Factors associated with a poor prognosis for *Corynebacterium* spp. bacteremia are mixed infection, chronic kidney disease, and lack of a central venous catheter (*16*). However, we are unaware of any study that has reported on differences in mortality rate among patients with infections by different species of *Corynebacterium*. One study reported that *C. striatum* formed biofilms on polyurethane catheters in vitro and hypothesized that biofilm may contribute to the establishment of hospital-acquired infections (*17*). Indeed, biofilm formation has been associated with true bacteremia in another study (*18*). *C. jeikeium* has also been reported to form biofilm, which can promote opportunistic infections (*19*). Although further study is needed, the tendency for *C. striatum* and *C. jeikeium* to form biofilm and their association with true bacteremia may be a reason for worse outcomes compared with outcomes for infection with other *Corynebacterium* species.

All strains of *Corynebacterium* spp. detected in this study were sensitive to vancomycin, minocycline, and linezolid. A previous study reported that most isolates were resistant to penicillin, ciprofloxacin, and tetracycline, and in contrast, all isolates were sensitive to

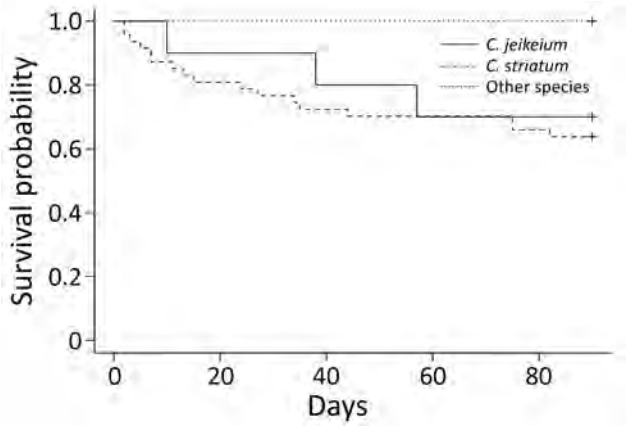

Figure. Kaplan-Meier curve showing survival probability after episodes of true bacteremia caused by *Corynebacterium* species, Japan, 2014–2020.

Table 3. Antimicrobial susceptibility testing of *Corynebacterium* species isolated from blood culture, Japan, 2014–2020*

Species	Susceptible/tested (%)									
	PEN	CRO	MEM	GEN	CIP	MIN	CLI	ERY	VAN	LZD†
C. striatum, n = 67	14/67 (21)	5/67 (7)	17/67 (25)	59/67 (88)	3/67 (4)	67/67 (100)	8/67 (12)	13/67 (19)	67/67 (100)	4/4 (100)
C. jeikeium, n = 14	0/14 (0)	0/14 (0)	5/14 (36)	5/14 (36)	0/14 (0)	14/14 (100)	0/14 (0)	0/14 (0)	14/14 (100)	3/3 (100)
Other species, n = 34	27/34 (79)	22/34 (65)	31/34 (91)	30/34 (88)	10/34 (29)	34/34 (100)	6/34 (18)	16/34 (47)	34/34 (100)	2/2 (100)
All, n = 115	41/115 (36)	27/115 (23)	53/115 (46)	94/115 (82)	13/115 (11)	115/115 (100)	14/115 (12)	29/115 (25)	115/115 (100)	9/9 (100)

*CIP, ciprofloxacin; CLI, clindamycin; CRO, ceftriaxone; ERY, erythromycin; GEN, gentamicin; LZD, linezolid; MEM, meropenem; MIN, minocycline; PEN, penicillin; VAN, vancomycin.
†Antimicrobial susceptibility testing for linezolid was only performed if requested by physicians.

vancomycin (*20*). In another study, only a few strains of *C. jeikeium* were resistant to doxycycline (*21*). The results of our study are consistent with those reports.

The most common underlying disease in patients with *Corynebacterium* bacteremia in our study was hematologic malignancy (33%). Among bacteremic patients with hematologic malignancies, the second most common gram-positive bacteria were *Corynebacterium* spp. (*22*). *C. striatum* was more likely to cause bacteremia in patients with malignancies or neutropenia (*15*), and *C. jeikeium* also caused bacteremia, frequently in patients with neutropenia or a history of previous antimicrobial treatment (*23*). The reason for the higher frequency of *Corynebacterium* bacteremia in patients with hematologic malignancies remains unknown. Among patients with hematologic malignancies, the reported rate of skin or rectal colonization with *Corynebacterium* spp. was 41% (*24*). We hypothesize that skin and mucosal barrier failures resulting from intense chemotherapy, chronic indwelling infusion catheters, and increased colonization may put patients with hematologic malignancies at a higher risk for *Corynebacterium* bacteremia.

Although the most common sources for *Corynebacterium* bacteremia were unknown or CRBSI, other sources accounted for 30% (18/60 cases), including lower respiratory tract infections, urinary tract infections, and SSTIs. Previous studies have reported that *C. striatum* can cause pneumonia (*25*), urinary tract infections, and intra-abdominal infections (*4*). Case studies have also reported *C. jeikeium* as being responsible for infective endocarditis (*6*), pacemaker infections (*26*), and prosthetic joint infections (*27*). *Corynebacterium* spp. are often reported as coryneform and not fully identified unless they are from sterile specimens because they colonize the skin and are ubiquitous in the environment. We emphasize the value of actively identifying coryneforms in specimens, even if they are not sterile (e.g., sputum or urine), especially in suspected cases of *Corynebacterium* bacteremia.

The first limitation of our study is that it was a retrospective single-center study. However, we believe that our results can be generalized to other tertiary institutions because the common species of *Corynebacterium* and susceptibility results obtained in our study do not differ considerably from others (*9*,*20*); moreover, our hospital is a referral center providing tertiary care in the region. Second, because of the difficulty of separating true bacteremia from contamination when *Corynebacterium* spp. are detected in blood culture, it is possible that we may have missed patients with true bacteremia. For example, we may have missed a patient with prosthetic valve endocarditis when *Corynebacterium* spp. were detected in only 1 set of blood cultures as a result of previous antimicrobial drug use because it did not meet the criteria for true bacteremia in our study. It is also possible that detection of *Corynebacterium* in 2 sets of blood cultures may actually represent contamination. To minimize the risk of incorrectly categorizing *Corynebacterium* bacteremia into true bacteremia or contamination, each case was carefully discussed during daily rounds and cases were routinely closely followed up with repeated blood culture if deemed necessary. Third, the number of cases of infection with the other 15 species of *Corynebacterium* was small, and the sample size was insufficient to describe the clinical characteristics of bacteremia caused by each of these species. Last, we used RapID CB Plus and matrix-assisted laser desorption/ionization time-of-flight mass spectrometry mainly for identification and performed 16s rRNA sequencing analysis for only a subset of cases.

In conclusion, the proportion of cases of true bacteremia caused by *C. striatum* or *C. jeikeium* was higher than that caused by other *Corynebacterium* species, and the mortality rate for true bacteremia was ≈30%. *C. striatum* and *C. jeikeium* were frequently detected in patients with hematologic malignancies and neutropenia. Healthcare providers should give special consideration to these 2 species of *Corynebacterium* and consider the possibility of true bacteremia rather than contamination when they are detected in blood cultures, especially in patients with hematologic malignancies.

Acknowledgments

We thank Muneyoshi Kimura and Atsushi Shiraishi for their support with statistical analyses. We also thank the medical technologists in the Kameda Medical Center for their invaluable technical assistance.

About the Author

Dr. Yamamuro is a medical doctor at Kameda Medical Center. His primary research interests include opportunistic infections and immune mechanism in hematologic transplant patients.

References

1. von Graevenitz A, Pünter-Streit V, Riegel P, Funke G. Coryneform bacteria in throat cultures of healthy individuals. J Clin Microbiol. 1998;36:2087–8. https://doi.org/10.1128/JCM.36.7.2087-2088.1998
2. Elkayam N, Urazov A, Tuneev K, Chapnick E. *Corynebacterium striatum* bacteremia associated with cellulitis in a patient with cirrhosis. IDCases. 2019;17:e00575. https://doi.org/10.1016/j.idcr.2019.e00575

3. van der Lelie H, Leverstein-Van Hall M, Mertens M, van Zaanen HC, van Oers RH, Thomas BL, et al. *Corynebacterium* CDC group JK (*Corynebacterium jeikeium*) sepsis in haematological patients: a report of three cases and a systematic literature review. Scand J Infect Dis. 1995;27: 581–4. https://doi.org/10.3109/00365549509047071
4. Lee PP, Ferguson DA Jr, Sarubbi FA. *Corynebacterium striatum*: an underappreciated community and nosocomial pathogen. J Infect. 2005;50:338–43. https://doi.org/10.1016/j.jinf.2004.05.005
5. Bao R, Gao X, Hu B, Zhou Z. Matrix-assisted laser desorption ionization time-of-flight mass spectrometry: a powerful tool for identification of *Corynebacterium* species. J Thorac Dis. 2017;9:3239–45. https://doi.org/10.21037/jtd.2017.09.69
6. Rezaei Bookani K, Marcus R, Cheikh E, Parish M, Salahuddin U. *Corynebacterium jeikeium* endocarditis: a case report and comprehensive review of an underestimated infection. IDCases. 2017;11:26–30. https://doi.org/10.1016/j.idcr.2017.11.004
7. Ghide S, Jiang Y, Hachem R, Chaftari AM, Raad I. Catheter-related *Corynebacterium* bacteremia: should the catheter be removed and vancomycin administered? Eur J Clin Microbiol Infect Dis. 2010;29:153–6. https://doi.org/10.1007/s10096-009-0827-0
8. Rasmussen M, Mohlin AW, Nilson B. From contamination to infective endocarditis–a population-based retrospective study of *Corynebacterium* isolated from blood cultures. Eur J Clin Microbiol Infect Dis. 2020;39:113–9. https://doi.org/10.1007/s10096-019-03698-6
9. Yanai M, Ogasawasa M, Hayashi Y, Suzuki K, Takahashi H, Satomura A. Retrospective evaluation of the clinical characteristics associated with *Corynebacterium* species bacteremia. Braz J Infect Dis. 2018;22:24–9. https://doi.org/10.1016/j.bjid.2017.12.002
10. Raad I, Hanna HA, Alakech B, Chatzinikolaou I, Johnson MM, Tarrand J. Differential time to positivity: a useful method for diagnosing catheter-related bloodstream infections. Ann Intern Med. 2004;140:18–25. https://doi.org/10.7326/0003-4819-140-1-200401060-00007
11. Mermel LA, Allon M, Bouza E, Craven DE, Flynn P, O'Grady NP, et al. Clinical practice guidelines for the diagnosis and management of intravascular catheter-related infection: 2009 update by the Infectious Diseases Society of America. Clin Infect Dis. 2009;49:1–45. https://doi.org/10.1086/599376
12. Horan TC, Andrus M, Dudeck MA. CDC/NHSN surveillance definition of health care-associated infection and criteria for specific types of infections in the acute care setting. Am J Infect Control. 2008;36:309–32. https://doi.org/10.1016/j.ajic.2008.03.002
13. Hudspeth MK, Hunt Gerardo S, Citron DM, Goldstein EJ. Evaluation of the RapID CB Plus system for identification of *Corynebacterium* species and other gram-positive rods. J Clin Microbiol. 1998;36:543–7. https://doi.org/10.1128/JCM.36.2.543-547.1998
14. Kanda Y. Investigation of the freely available easy-to-use software 'EZR' for medical statistics. Bone Marrow Transplant. 2013;48:452–8. https://doi.org/10.1038/bmt.2012.244
15. Ishiwada N, Watanabe M, Murata S, Takeuchi N, Taniguchi T, Igari H. Clinical and bacteriological analyses of bacteremia due to *Corynebacterium striatum*. J Infect Chemother. 2016;22:790–3. https://doi.org/10.1016/j.jiac.2016.08.009
16. Kimura SI, Gomyo A, Hayakawa J, Akahoshi Y, Harada N, Ugai T, et al. Clinical characteristics and predictive factors for mortality in coryneform bacteria bloodstream infection in hematological patients. J Infect Chemother. 2017;23:148–53. https://doi.org/10.1016/j.jiac.2016.11.007
17. Souza C, Faria YV, Sant'Anna LO, Viana VG, Seabra SH, Souza MC, et al. Biofilm production by multiresistant *Corynebacterium striatum* associated with nosocomial outbreak. Mem Inst Oswaldo Cruz. 2015;110:242–8. https://doi.org/10.1590/0074-02760140373
18. Kang SJ, Choi SM, Choi JA, Choi JU, Oh TH, Kim SE, et al. Factors affecting the clinical relevance of *Corynebacterium striatum* isolated from blood cultures. PLoS One. 2018;13:e0199454. https://doi.org/10.1371/journal.pone.0199454
19. Kwaszewska AK, Brewczyńska A, Szewczyk EM. Hydrophobicity and biofilm formation of lipophilic skin corynebacteria. Pol J Microbiol. 2006;55:189–93.
20. Dragomirescu CC, Lixandru BE, Coldea IL, Corneli ON, Pana M, Palade AM, et al. Antimicrobial susceptibility testing for *Corynebacterium* species isolated from clinical samples in Romania. Antibiotics (Basel). 2020;9:31. https://doi.org/10.3390/antibiotics9010031
21. Soriano F, Zapardiel J, Nieto E. Antimicrobial susceptibilities of *Corynebacterium* species and other non-spore-forming gram-positive bacilli to 18 antimicrobial agents. Antimicrob Agents Chemother. 1995;39:208–14. https://doi.org/10.1128/AAC.39.1.208
22. Kara Ö, Zarakolu P, Aşçioğlu S, Etgül S, Uz B, Büyükaşik Y, et al. Epidemiology and emerging resistance in bacterial bloodstream infections in patients with hematologic malignancies. Infect Dis (Lond). 2015;47:686–93. https://doi.org/10.3109/23744235.2015.1051105
23. Rozdzinski E, Kern W, Schmeiser T, Kurrle E. *Corynebacterium jeikeium* bacteremia at a tertiary care center. Infection. 1991;19:201–4. https://doi.org/10.1007/BF01644945
24. Stamm WE, Tompkins LS, Wagner KF, Counts GW, Thomas ED, Meyers JD. Infection due to *Corynebacterium* species in marrow transplant patients. Ann Intern Med. 1979;91:167–73. https://doi.org/10.7326/0003-4819-91-2-167
25. Shariff M, Aditi A, Beri K. *Corynebacterium striatum*: an emerging respiratory pathogen. J Infect Dev Ctries. 2018;12:581–6. https://doi.org/10.3855/jidc.10406
26. Bechara C, Gousseff M, Passeron A, Podglajen I, Day N, Pouchot J, et al. *Corynebacterium jeikeium* pacemaker infection associated with antineutrophil cytoplasmic antibodies: a single positive blood culture could be sufficient for diagnosis. J Med Microbiol. 2011;60:249–51. https://doi.org/10.1099/jmm.0.023283-0
27. Cazanave C, Greenwood-Quaintance KE, Hanssen AD, Patel R. *Corynebacterium* prosthetic joint infection. J Clin Microbiol. 2012;50:1518–23. https://doi.org/10.1128/JCM.06439-11

Address for correspondence: Ryosuke Yamamuro, Department of Infectious Disease, Kameda Medical Center, 929 Higashi-cho, Kamogawa Chiba, 296-8602, Japan; email: xurmra38@gmail.com

Evaluation of Early Warning, Alert and Response System for Ebola Virus Disease, Democratic Republic of the Congo, 2018–2020

Mory Keita, Héloïse Lucaccioni, Michel Kalongo Ilumbulumbu, Jonathan Polonsky, Justus Nsio-Mbeta, Gaston Tshapenda Panda, Pierre Celeste Adikey, John Kombe Ngwama, Michel Kasereka Tosalisana, Boubacar Diallo, Lorenzo Subissi, Adama Dakissaga, Iris Finci, Maria Moitinho de Almeida, Debarati Guha-Sapir, Ambrose Talisuna, Alexandre Delamou, Stephanie Dagron, Olivia Keiser, Steve Ahuka-Mundeke

The 10th and largest Ebola virus disease epidemic in the Democratic Republic of the Congo (DRC) was declared in North Kivu Province in August 2018 and ended in June 2020. We describe and evaluate an Early Warning, Alert and Response System (EWARS) implemented in the Beni health zone of DRC during August 5, 2018–June 30, 2020. During this period, 194,768 alerts were received, of which 30,728 (15.8%) were validated as suspected cases. From these, 801 confirmed and 3 probable cases were detected. EWARS showed an overall good performance: sensitivity and specificity >80%, nearly all (97%) of alerts investigated within 2 hours of notification, and good demographic representativeness. The average cost of the system was US $438/case detected and US $1.8/alert received. The system was stable, despite occasional disruptions caused by political insecurity. Our results demonstrate that EWARS was a cost-effective component of the Ebola surveillance strategy in this setting.

Early case detection is important to control and prevent infectious disease outbreaks (*1*). The 5 identified purposes for early detection surveillance are detecting the first case of the disease in a population previously free, detecting new cases in an area already infected, early detection of an abnormal increase in the level of a disease normally present at a base level, screening for individual cases of noncommunicable diseases, and the first detection of an invasive species in an area previously free of that species (*2*). The International Health Regulations (2005) (*3*) impose obligation on countries to develop, strengthen, and maintain their capacities to detect, verify, assess, report, and respond to any events that may constitute a public health risk and thereby prevent international spread. Public health surveillance systems are poorly developed in many low-income and middle-income countries, as demonstrated by recent Ebola outbreaks, which had devastating consequences in the health and economy of several countries (*4*–*7*).

Ebola virus disease (EVD), if not detected and reported early, can rapidly spread and result in high rates of illness and death (*8*,*9*). In recent years, the world has faced the 2 largest EVD epidemics in recorded history, both of which were declared public health emergencies of international

Author affiliations: Institute of Global Health, University of Geneva, Geneva, Switzerland (M. Keita, J. Polonsky, S. Dagron, O. Keiser); World Health Organization Regional Office for Africa, Brazzaville, Congo (M. Keita, A. Talisuna); European Centre for Disease Prevention and Control, Stockholm, Sweden (H. Lucaccioni, I. Finci); Ministère Provincial de la Santé, Goma, Democratic Republic of the Congo (M.K. Ilumbulumbu, M.K. Tosalisana); World Health Organization, Geneva (J. Polonsky, L. Subissi); Ministère de la Santé, Direction Générale de la Lutte contre la Maladie, Kinshasa, Democratic Republic of the Congo (J. Nsio-Mbeta, G.T. Panda, P.C. Adikey, J.K. Ngwama); Ministère de la Santé, Direction Régionale de la Sante du Plateau central, Ziniaré, Burkina Faso (A. Dakissaga); Centre for Research on Epidemiology of Disasters, Research Institute on Health and Society, Université Catholique de Louvain, Brussels, Belgium (M.M. de Almeida, D. Guha-Sapir); Africa Center of Excellence (CEA-PCMT), University Gamal Abdel Nasser, Conakry, Guinea (A. Delamou); Institut National de Recherche Biomédicale, Kinshasa (S. Ahuka-Mundeke)

DOI: https://doi.org/10.3201/eid2712.210290

concern by the director-general of the World Health Organization (WHO).

EVD case definitions are crucial surveillance tools, both for referring suspected cases and as screening tools to aid admission and laboratory testing decisions at health facilities (*10*). WHO has developed standard case definitions for alert, suspected, probable, and confirmed cases in the context of routine and community-based surveillance (*11*,*12*) (Appendix Table, https://wwwnc.cdc.gov/EID/article/27/12/21-0290-App1.pdf).

Insufficient command of these case definitions at the community and health-facility level has resulted in late detection of EVD outbreaks. For instance, recent epidemics in both West Africa and the Democratic Republic of the Congo (DRC) were officially declared 3 months after the effective start of the epidemics (*13*,*14*). The epidemic in DRC was the second largest EVD outbreak ever documented after the West Africa EVD epidemic (2013–2016); a total of 3,481 cases (3,323 confirmed and 158 probable) and 2,299 deaths were recorded in August 2018–June 2020 in North Kivu, Ituri, and South Kivu Provinces. This outbreak was particularly complex because it occurred in an active conflict zone (*15*). Public health performance indicators at the beginning of this EVD response were poor, including many community deaths, poor contact tracing, and delays between symptom onset and case isolation. A decline in incidence toward the end of 2019 was thought to be the result of improvement in the quality of surveillance activities, including prompt investigation, early detection and isolation of cases, enhanced community-based surveillance, rapid follow-up of high-risk contacts, and an adaptive vaccination strategy (*16*).

Soon after the declaration of the 10th EVD outbreak in the DRC, an Early Warning, Alert and Response System (EWARS) was implemented throughout North Kivu and Ituri Provinces, to report, collect, investigate, validate, and take early action (isolation, safe burial, or referral) on alerts that met the suspected case definition for EVD. We describe and evaluate this system as implemented in the subcoordination of Beni, established to manage the response across several health zones.

Methods

Description of the EWARS

The Alert Unit was the core functional unit around which the EWARS was organized (Figure 1); it was composed of an overall operational leader who coordinated activities, a database and information administrator, a case management leader, a Safe and Dignified Burial (SDB) leader, 3 telephone operators, 1 alert monitoring officer, 1 database manager, 1 data clerk, and 1 archivist. The main role of the Alert Unit was to gather and scan alerts from various sources, coordinate the field investigations with the rapid intervention teams, and, if relevant, organize the referral and ambulance transfer or safe burial in collaboration with the case management or SDB team. All alerts and their outcomes were entered and archived into paper-based alert and investigation forms and a Microsoft Excel database (https://www.microsoft.com). There were 4 main sources of alerts: community, in which community health workers, community members, and political and administrative authorities raised alerts; active case finding conducted in health facilities and other structures (pharmacies, churches, traditional practitioners); surveillance sites, including contact tracing teams, vaccination sites, and points of entry/points of control (PoE/PoC); and finally, public and private health facilities that ensured passive reporting.

Two toll-free numbers were activated on August 26, 2018, to enable rapid and easy alert reporting from all the sources. Calls were directed to telephone operators in the Alert Unit, which was operational 24 hours per day, 7 days per week; a smaller team for night shifts comprised the operations leader and phone managers only. In active case finding, passive reporting, or PoE/PoC, the alert notifier completed an alert form, or for community and contact tracing alerts, the telephone operator or alert monitoring officer completed the form. When telephone operators received the alerts, they checked for duplication and conducted preliminary triage to prioritize them by epidemiologic and clinical factors. Rapid intervention teams were then notified to investigate the alert onsite.

Rapid intervention teams were made up of a field epidemiologist, an infection prevention and control (IPC) officer, a communication officer, and a psychosocial worker. All these response pillars were positioned in each health area covered by the alert system, from which a senior epidemiologist would organize rapid intervention teams. The investigation consisted of a detailed history, assessment of the epidemiologic link, clinical symptoms for validation against the suspected case definition (*17*), and initial listing of contacts. Investigation forms were stored in the Alert Unit, and copies were sent to Ebola treatment centers (ETC) for patients requiring admission. The rapid intervention team validated or invalidated the alert on

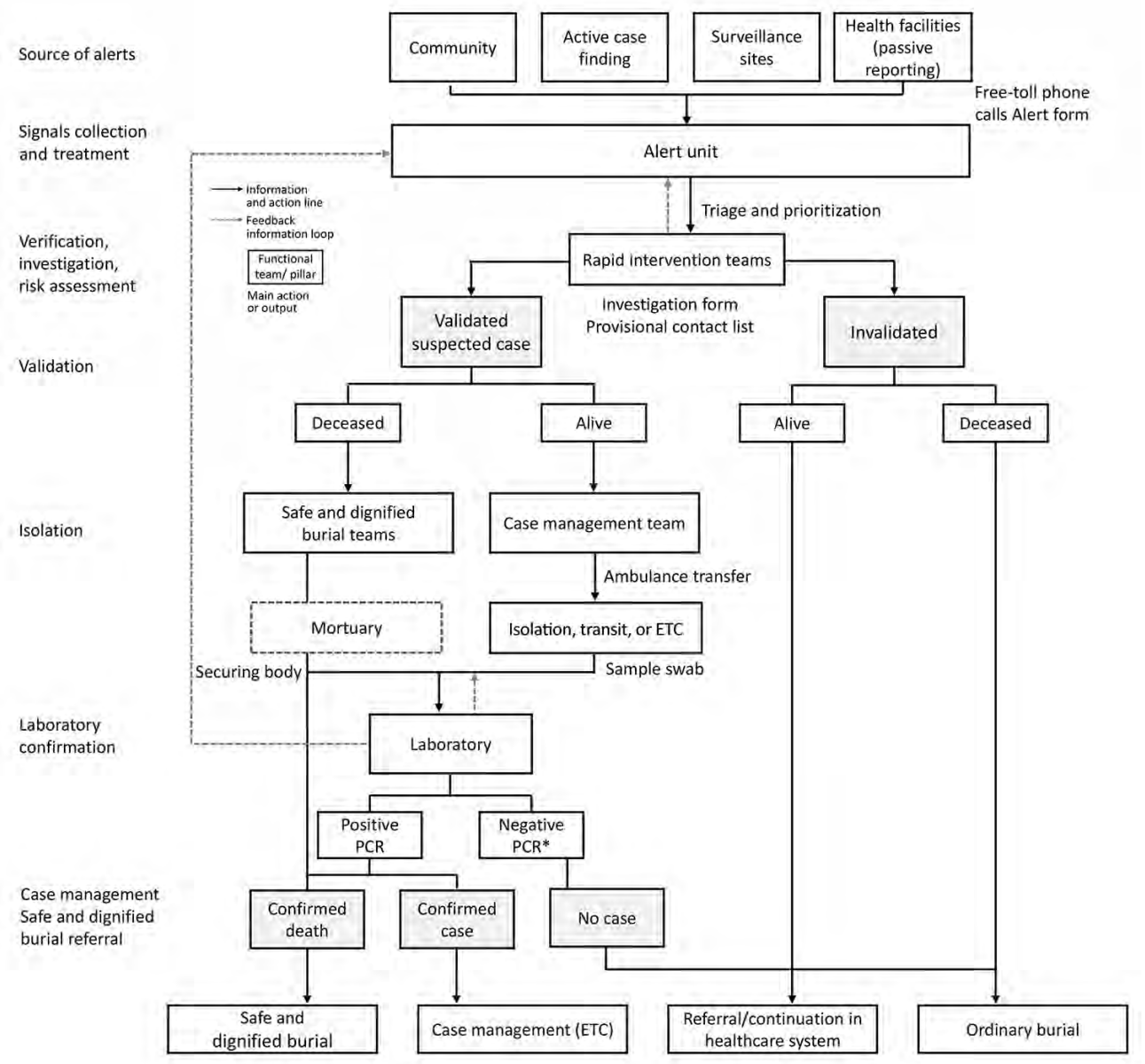

Figure 1. Organization of the Early Warning, Alert and Response System as used in the Democratic Republic of the Congo, August 2018–June 2020. Asterisk (*) indicates 1 negative result for a deceased suspected case-patient or 2 negative results within 72 hours for an alive suspected case-patient. ETC, Ebola treatment center.

the basis of the investigation findings and provided immediate feedback to the Alert Unit contact persons, who coordinated the next steps.

For invalidated alerts, the family can proceed with ordinary burial of deceased patients, whereas living patients were referred to public healthcare facilities for free healthcare. Living patients with validated alerts were immediately transferred to a transit center, isolation center, or ETC, depending on the patient's condition and location. There was no additional validation at triage in ETC. To reduce the risk that a transfer would refuse a patient, the intervention team would propose 2 options according to patient condition and preference: transfer the patient by ambulance or by motorcycles driven by Ebola survivors. After admission to the isolation center, patients followed the suspected case management algorithm: blood samples were taken and tested by using GeneXpert (Cepheid, https://www.cepheid.com) within 3 hours after admission. Cases confirmed by PCR were immediately admitted to an ETC for treatment. Those patients with an

initial negative test were discharged pending a second negative result 72 hours later.

The SDB team were notified of validated alerts of deceased patients, then joined the rapid intervention team onsite to engage with the family. The body was secured and a swab sample taken and sent to the laboratory for testing. With family consent, SDB proceeded immediately. However, if the family refused, the body was kept at the mortuary until the laboratory result was available. If the result was negative, the body was returned to the family to proceed with ordinary burial; if the results was positive, SDB was mandatory and enforced by authorities.

Evaluation Approach and Data Sources and Indicators

We conducted a quantitative evaluation according to guidelines published by WHO (*18*) and the US Centers for Disease Control and Prevention (CDC) (*19*). We used the anonymized Alert Unit database, covering the health zones of Beni, Mutwanga, and Oicha, during August 5, 2018–June 30, 2020, to assess EWARS using the EVD suspected case definition as the standard. An alert was considered validated if it met the definition of an alert case by community-based surveillance or the definition of a suspected case by mobile teams or health stations or centers (*12*). An investigator would validate a suspected case on the evidence of clinical signs in the patient (Appendix Figure).

To assess the true sensitivity, specificity, positive predictive value (PPV), and negative predictive value (NPV) would require laboratory testing for all patients, which would not have been feasible. We calculated sensitivity as the proportion of alerts validated among all alerts meeting the suspected case definition, specificity as the proportion of invalidated alerts among all alerts not meeting the suspected case definition, PPV as the proportion of alerts that met the suspected case definition among all validated alerts, and NPV as the proportion of alerts that did not meet the suspected case definition among all invalidated alerts. We assessed timeliness as the median, range, and interquartile range (IQR) of the delay between the transmission of alert to the Alert Unit and the start of the onsite investigation. We evaluated representativeness through the geographic and demographic coverage of the alerts by comparing alert incidence by sex, age group, and health zone. We appraised usefulness by considering the number of confirmed and probable cases that were detected through the alert system. Finally, we assessed stability by considering how the system was operating over time, disruptions, and sustainability of functioning beyond the emergency response phase, notably in relation with costs and human resources. We conducted all analyses using R statistical software version 4.0.3 (*20*).

Results

Outcomes of EWARS

During the study period, 195,601 alerts were received; 194,768 (99.6%) from the health zones of Beni, Mutwanga, and Oicha, and 833 (0.4%) from other health zones (Figure 2). A small number (52,240, 2.7%) were reports of community deaths.

On average, there were 280 alerts/day (range 2–955, median 127 alerts/day), although this value greatly varied over time. The number of daily alerts increased progressively, from 6 at the outset in August 2018 to a peak of 922 at the beginning of March 2020. We observed multiple sudden, short-lived decreases in the daily number of alerts, particularly in mid-November 2019 and early April 2020, coinciding with security incidents (see Stability) (Figure 3).

A total of 30,728 (15.8%) alerts were validated as suspected cases. Among those, 801 (2.6%) were finally classified as confirmed cases and 3 (<0.1%) as probable cases. No invalidated alerts became confirmed cases; the information recorded the first time remains in the database, and a new alert with the same information could be quickly detected.

Most (62.6%) alerts were raised by active case finding teams, followed by passive reporting from health facilities (19.0%), and community alerts (15.0%). The remainder (3.6%) originated from other sources (Table 1).

Sensitivity, Specificity, Positive Predictive Value, Negative Predictive Value

We excluded 434 alerts (0.2%) that were not investigated and 201 alerts (0.1%; 197 invalidated and 4 validated) that could not be classified according to the case definition because of missing data. A total of 17,927 (9.2%) alerts met the EVD suspected case definition. Sensitivity was 84.6% (95% CI 84.1%–85.1%) and specificity 91.2% (95% CI 91.0%–91.3%). PPV was 49.4% (95% CI 48.8%–49.9%) and NPV 98.3% (95% CI 98.2%–98.4%) (Table 2).

Indicators varied with time, health zone, and source of notification (Table 3). Overall, sensitivity increased over time, and specificity remained high throughout the study period. PPV decreased while NPV increased, which is consistent with the outbreak

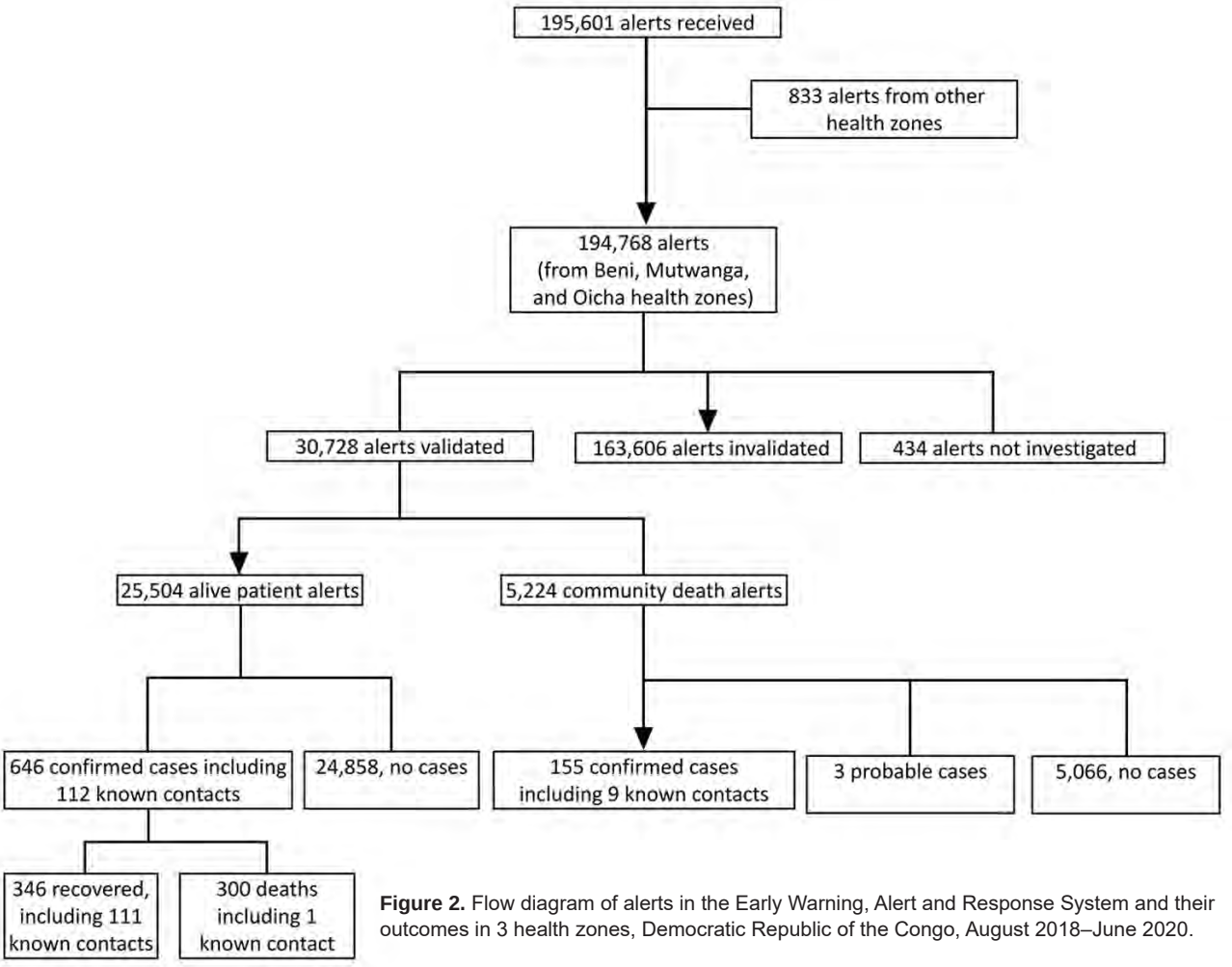

Figure 2. Flow diagram of alerts in the Early Warning, Alert and Response System and their outcomes in 3 health zones, Democratic Republic of the Congo, August 2018–June 2020.

dynamics and the decrease in incidence toward the end of the epidemic (Appendix Figure).

Sensitivity was higher for alerts arising from surveillance sites (98.0%, 95% CI 97.4%–98.7%), community alerts (91.4%, 95% CI 90.1%–92.7%), and active case finding (87.5%, 95% CI 86.9%–88.1%) and lower for those arising from passive reporting from health facilities (65.4%, 95% CI 63.8%–67.0%). Conversely, specificity was highest in health facilities (96.2%, 95% CI 96.0%–96.4%), and was high (>90%) for all other sources except surveillance sites. Sensitivity was higher in Beni (94.8%, 95% CI 94.4%–95.2%) than in Mutwanga (54.9%, 95% CI 52.4%–57.3%) and Oicha (64.3%, 95% CI 62.8%–65.8%), but specificity was higher in Mutwanga (96.4%, 95% CI 96%–96.7%) and Oicha (93.3%, 95% CI 92.8–93.8).

Timeliness

An investigation was initiated within 2 hours from the time of alert for 188,184 (96.6%) alerts. The median time from alert transmission to the arrival of the investigation team on site was 11 minutes (IQR 10–15 minutes). Information about the time of investigation was not available for 3,475 (1.8%) alerts.

Timeliness of responses varied over time; substantial delays were observed at the outset of the system implementation, with greatest delays in Mutwanga (Figure 4). We saw no marked difference in timeliness by source of notification.

Representativeness

We observed substantial variations in the alert incidence between the health zones. On average, there were 241 (range 2–789) alerts/day in Beni, 42.3 (range 1–181) alerts/day in Mutwanga, and 25.4 (range 1–138) alerts/day in Oicha. The alert incidence in the population followed a similar pattern: an average of 36 alerts/1,000 inhabitants/week in Beni, 2.5 alerts/1,000 inhabitants/week in Oicha, and 2.4 alerts/1,000 inhabitants/week in Mutwanga. In Beni,

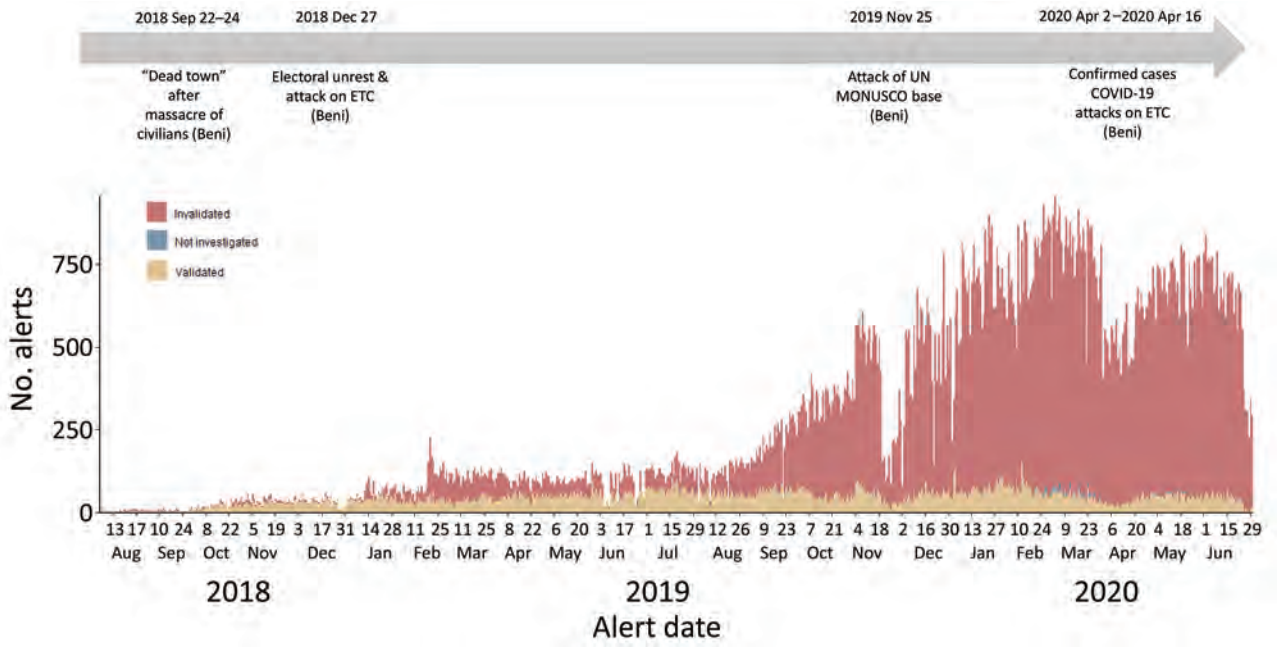

Figure 3. Trend in daily number of alerts from the Early Warning, Alert and Response System by final validation status in 3 health zones, Democratic Republic of the Congo, August 2018–June 2020. Key security incidents during the epidemic period are depicted along the timeline above the graphic. MONUSCO is the name of the UN peacekeeping force in the country. ETC, Ebola treatment center.

the incidence of alerts increased progressively from the outset (Figure 5). However, in Mutwanga and Oicha, incidence remained low until the beginning of November 2019, when it rapidly increased following community transmission.

We observed more alerts among female (56.3%) than male (43.4%) patients. Children <5 years of age were the most represented (23.6%), followed by patients 20–29 years of age (18.9%) and 10–19 years of age (18.9%); these percentages approximate the age and sex breakdown of the local population, with the exception of children 5–9 years of age, who were underrepresented (11%).

Usefulness and Cost

The EWARS system led to the detection of 801 confirmed and 3 probable cases, which equates to 242 alerts notified and 38 alerts validated for each case detected by the system. The total direct and indirect costs associated with EWARS implementation and maintenance was US $353,525 over the 2-year period of operation (Table 4), yielding a minimum value of US $1.8/alert and US $438/case detected.

Stability

The alert system operated 24 hours per day, 7 days per week, including a minimal night team to ensure continuity. Continuous communication and reporting of alerts was possible by a comprehensive and stable mobile phone coverage covering all health areas. As such, alerts were collected and analyzed on a continuous basis, and reports were produced and distributed daily. However, despite the continuous availability of human resources and communication networks, the system was severely disrupted by security incidents. Security incidents coincided with decreases in the number of alerts, affecting both the reporting and investigation of alerts (Figure 3). The Alert Unit ceased operations following the standard 90-day period of heightened surveillance after the declaration of the end of the outbreak, as determined by WHO (*21*).

Discussion

During August 2018–June 2020, EWARS led to the notification and investigation of 194,768 alerts and the detection of 801 confirmed and 3 probable EVD cases. The evaluation showed an overall good performance of the system regarding the main attributes we assessed, highlighting the many strengths of such a system. However, it also revealed disparities in performance between the health zones covered by the system, reflecting differences in the timing of implementation and, most notably, unequal operating conditions (e.g., security incidents).

This system encompassed both event-based and indicator-based surveillance (*22*,*23*), resulting

Table 1. Characteristics of Ebola virus disease alerts received in Beni subcoordination, Democratic Republic of the Congo, August 5, 2018–June 30, 2020

Characteristic	No. (%) alerts, n = 194,768
Year	
2018	3,211 (1.6)
2019	67,579 (34.7)
2020	123,978 (63.7)
Final alert status	
Invalidated	163,606 (84.0)
Validated	30,728 (15.8)
Not investigated	434 (0.2)
Alert initial status	
Deceased	5,230 (2.7)
Alive	189,538 (97)
Final case classification	
Not a case	193,964 (99.6)
Confirmed case	801 (0.4)
Probable	3 (<0.1)
Source of alert	
Active case finding	121,970 (62.6)
Health structure	36,911 (19.0)
Community	28,928 (15.0)
Other surveillance sites	6,959 (3.6)
Health zone	
Beni	167,503 (86.0)
Mutwanga	12,891 (6.6)
Oicha	14,374 (7.4)
Sex	
F	109,605 (56.3)
M	84,442 (43.4)
Unknown	721 (0.4)
Age group	
0–4	45,934 (23.6)
5–9	22,220 (11.4)
10–19	36,825 (18.9)
20–29	37,945 (19.5)
30–39	21,975 (11.3)
40–49	11,186 (5.7)
50–59	6,668 (3.4)
≥60	8,679 (4.5)
Unknown	3,336 (1.7)
Known contact of confirmed or probable case	
No	194,052 (99.6)
Yes	672 (0.3)
Unknown	44 (0.1)

in 7.8% of alerts meeting the definition of EVD suspected case, 4-fold higher than the event-based surveillance system at the community level during the Ebola outbreak in Sierra Leone in 2014–2016, and a 6-fold higher 49.4% PPV (*24*). Approximately 92% of our alerts did not meet the suspected case definition because of a time lag of days between symptom onset, on which the alert launch was based, and the symptoms that were actually present in these patients during investigation.

Although the overall proportion of detected cases among alerts was low (0.4% of all alerts), EWARS aimed to be highly sensitive; actions taken around those confirmed cases successfully interrupted transmission chains and prevented further spread of the disease. Indeed, the system showed a high sensitivity and specificity (>80%) and a low PPV, which reflects the low EVD incidence in the population. All health areas covered by the system reported alerts that did not differ greatly from the population structure, thus suggesting a good demographic representativeness. The system presented prompt timeliness of investigation of alerts throughout its 2 years of operation. Finally, the minimum cost per alert or cases was relatively low compared with that for a nationwide telephone alert system established for rapid notification and response during the 2014–2015 Ebola disease epidemic in Sierra Leone (*25*).

This good performance of EWARS can be explained by the intensive, comprehensive, and continuous reporting flow. First, the system relied on the use of various sources of alerts, involving both passive and active case reporting from the community, health structures, and other surveillance sites. Second, it built upon a stable and extensive telephone network further supported by toll-free numbers, a means of communication that is easily accessible, acceptable, and already commonly used by all stakeholders involved in surveillance. Third, it adopted a decentralized approach for the organization of the investigation teams, which enabled comprehensive coverage of all health areas and prompt reactivity for early action. The existence of a dedicated team at the subcoordination level further supported the coordination of activities at the local level while aiding in the centralization and consolidation of the information circuit. The unceasing availability of all key actors of the reporting system (surveillance, investigation teams, alert unit, and case management/SDB) ensured the continuous reporting and actions around alerts in timely manner. How fast a system detects and responds effectively

Table 2. Evaluation results and overall characteristics of Ebola virus disease alerts from EWARS, Democratic Republic of the Congo, August 5, 2018–June 30, 2020*0

	Suspected case definition			% (95% CI)			
Alert system	No. met	No. unmet	Total	Sensitivity	Specificity	PPV	NPV
Validated	15,163	15,561	30,724				
Invalidated	2,764	160,645	163,409				
Total	15,245	184,104	194,133	84.6 (84.1–85.1)	91.2 (91.0–91.3)	49.4 (48.8–49.9)	98.3 (98.2–98.4)

*Total excludes 434 (0.2%) alerts that were not investigated and 201 (0.1%) alerts that could not be classified according to the case definition due to missing data. EWARS, Early Warning, Alert and Response System; NPV, negative predictive value; PPV, positive predictive value.

Table 3. Evaluation of EWARS alerts by source of Ebola virus disease alert and health zone, Democratic Republic of the Congo, August 5, 2018–June 30, 2020

Category	% (95% CI)			
	Sensitivity	Specificity	PPV	NPV
Source of alert				
Active case finding/IPC	87.5 (86.9–88.1)	91.7 (91.6–91.9)	51.2 (50.4–51.9)	98.7 (98.6–98.7)
Community	91.4 (90.1–92.7)	93.6 (93.3–93.9)	48.3 (46.6–50.0)	99.4 (99.3–99.5)
Health facility	65.4 (63.8–67.0)	96.2 (96.0- 96.4)	64.5 (62.9–66.1)	96.4 (96.2–96.6)
Other surveillance sites	98.0 (97.4–98.7)	34.3 (33.0–35.6)	33.0 (31.7–34.2)	98.1 (97.5–98.8)
Health zone				
Beni	94.8 (94.4–95.2)	90.6 (90.5–90.8)	44.9 (44.3–45.5)	99.5 (99.5–99.6)
Mutwanga	54.9 (52.4–57.3)	96.4 (96–96.7)	68.2 (65.7–70.8)	93.8 (93.3–94.2)
Oicha	64.3 (62.8–65.8)	93.3 (92.8–93.8)	78.6 (77.2–80.1)	87.2 (86.6–87.9)

*EWARS, Early Warning, Alert and Response System; IPC, Infection Prevention and Control; NPV, negative predictive value; PPV, positive predictive value.

to a threat is the optimal measure of performance. Continuously evaluating and improving timeliness can identify performance bottlenecks and help to accelerate progress, improving detection speed and response quality (*26*).

The alert system performed better in Beni for all attributes we studied. In Mutwanga and Oicha, sensitivity was <80%, alert incidence was low (even after an increase in the number of daily alerts in late 2019), geographic coverage appeared less comprehensive as many health areas reported few alerts, and delays in investigation were longer, particularly at the outset. Mutwanga and Oicha are 2 rural health zones located at the epicenter of nonstate armed groups' territories, which greatly affected the operations. Surveillance and investigation activities faced regular security incidents and restrictions, long distances to alert sites, and poor road networks in many health areas. In this context, the alert system was initially implemented in Beni and progressively extended and strengthened in Mutwanga and Oicha. For example, in the early phase, rapid intervention teams were staffed in the Beni subcoordination office only, such that alert investigations in Mutwanga and Oicha suffered longer delays. Surveillance and reporting capacities were also weaker in Mutwanga and Oicha. In November 2019, a training of response personnel (registered nurses, supervisors, and investigators) was organized to address the low incidence of alerts; to strengthen data management capacities, data managers were deployed, leading to a rapid increase in alerts from these health zones.

Despite the effects of security incidents, the EWARS continued to operate throughout the whole period, managing an increasing volume of alerts, leading to the detection of hundreds of cases. In a context of limited surveillance capacities and weak health systems, such an intensive and steadily reporting alert system was vital for the early detection of cases and interruption of the spread of the disease in the population. However, the system was conceived and implemented in an ad hoc manner within the frame-

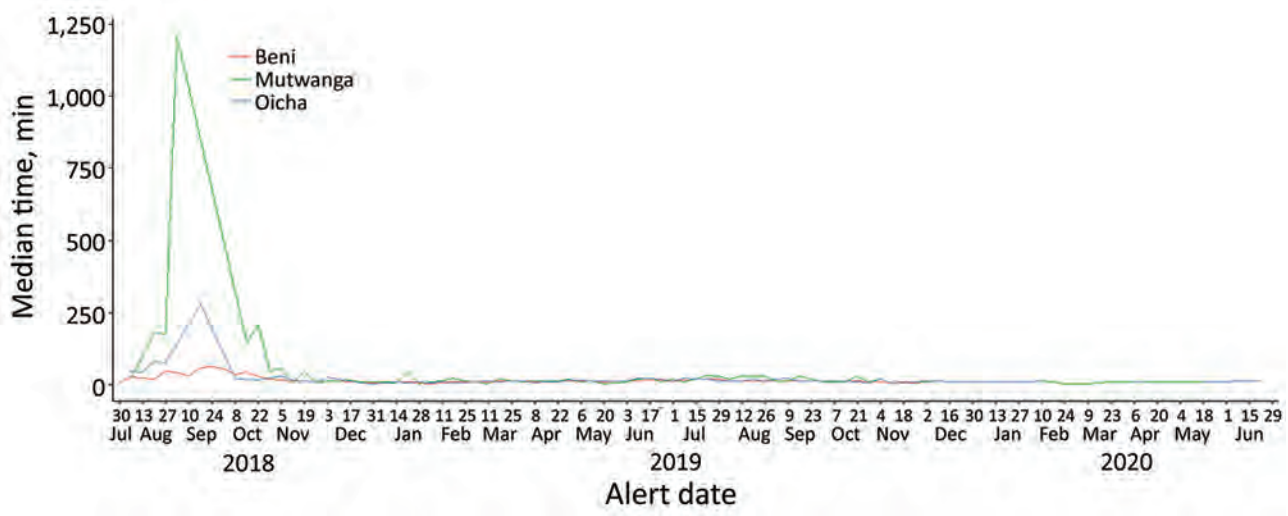

Figure 4. Timeliness over time of alerts from the Early Warning, Alert and Response System, Democratic Republic of the Congo, August 2018–June 2020. Timeliness is defined as weekly median time (in minutes) from alert transmission to the start of the investigation.

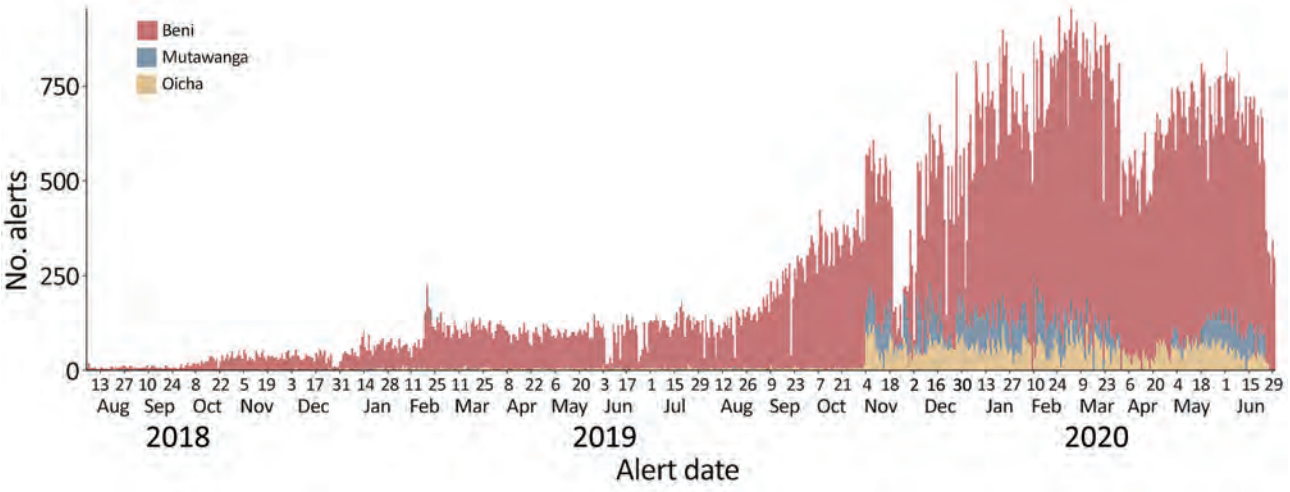

Figure 5. Trend in daily number of alerts in the Early Warning, Alert and Response System in 3 health zones in the Democratic Republic of the Congo, August 2018–June 2020.

work of the Ebola outbreak response, which limited its sustainability beyond the resources and time period of the outbreak response. The financial, logistical, and human resources needed to implement and maintain the system were made possible by dedicated response funds and the time-bound engagement of both national support teams and international financial and technical partners. The EWARS ceased operations within 12 weeks of the declared end of the outbreak. The long-term sustainability of systems such as EWARS remains unknown. An additional limitation was the challenge in assessing overall performance measures of the system, such as completeness, acceptability, and flexibility. We evaluated EWARS with regard to its objectives, but we could not extrapolate the effects of the system on the overall outbreak dynamics.

In conclusion, the magnitude and duration of the 10th and largest Ebola outbreak in DRC, occurring in an active conflict zone, highlighted the need for prompt, functional, and effective infectious disease surveillance systems. We have demonstrated that the EWARS implemented was a cost-effective component of this surveillance system. Our findings underscore the importance of early-warning systems, along with the necessity of ensuring efficiency and sustainability beyond the duration of the emergency response phase. As such, Integrated Disease Surveillance and Response is a relevant framework to further strengthen the International Health Regulations (2005) core

Table 4. Costs for EWARS in Beni, Mutwanga, and Oicha, Democratic Republic of the Congo, August 2018–June 2020*

Health zone	Item	Implementation period costs, USD			Total cost, USD
		2018 Aug 5–Dec 31	2019 Jan 1– Dec 31	2020 Jan 1–Jun 30	
Beni	Prime staff for alerts management teams	6,000	25,200	12,600	43,800
	Prime staff for data managers	900	10,350	5,400	16,650
	Ambulance rental	6,000	72,000	36,000	114,000
	Fuel	9,600	36,000	18,000	63,600
	Purchase of telephones	175	NA	NA	175
	Purchase of materials†	5,500	12,000	6,000	23,500
	Communication credit	750	3,600	2,100	6,450
	Green numbers‡	15,200	15,200	NA	30,400
Oicha	Prime for alerts management teams	NA	12,150	6,300	18,450
	Prime for data managers	NA	5,400	2,700	8,100
	Communication credit	NA	1,200	600	1,800
Mutwanga	Prime for alerts management teams	NA	7,200	5,400	12,600
	Prime for data managers	NA	7,200	5,400	12,600
	Communication credit	NA	800	600	1,400
Total		44,125	208,300	101,100	353,525

*Expenditures included direct and indirect costs. EWARS, Early Warning, Alert and Response System; NA, not applicable.
†Flip charts, markers, printed forms.
‡Telephone numbers 0820800001 and 0999009405, which health workers and community members could use for no charge. WHO covered this expense.

capacities (*27*,*28*). The need to evaluate and learn from field implementation of surveillance systems in infectious disease outbreaks, even in such difficult contexts, is an opportunity to better understand response efforts and improve future responses (*29*).

Acknowledgments

We thank the alert unit team and all the actors who have been involved in the EWARS in Beni, Mutwanga, and Oicha, DRC.

About the Author

Dr. Keita is a medical doctor and public health specialist, currently working as technical officer for risk assessment with the WHO Regional Office for Africa. During the 10th EVD outbreak in DRC, he was deployed as senior field coordinator in Beni. His research interests include infectious diseases epidemiology, risk assessment, public health response in humanitarian and emergency settings, health systems strengthening, healthcare management, and global health policy.

References

1. Bai Z, Gong Y, Tian X, Cao Y, Liu W, Li J. The rapid assessment and early warning models for COVID-19. Virol Sin. 2020;35:272–9. https://doi.org/10.1007/s12250-020-00219-0
2. Cameron AR, Meyer A, Faverjon C, Mackenzie C. Quantification of the sensitivity of early detection surveillance. Transbound Emerg Dis. 2020;67:2532–43. https://doi.org/10.1111/tbed.13598
3. World Health Organization. International health regulations (2005). 3rd edition. 2016 Jan 1 [cited 2021 Oct 8]. https://www.who.int/publications/i/item/9789241580496
4. Njeru I, Kareko D, Kisangau N, Langat D, Liku N, Owiso G, et al. Use of technology for public health surveillance reporting: opportunities, challenges and lessons learnt from Kenya. BMC Public Health. 2020;20:1101. https://doi.org/10.1186/s12889-020-09222-2
5. Hoffman SJ, Silverberg SL. Delays in global disease outbreak responses: lessons from H1N1, Ebola, and Zika. Am J Public Health. 2018;108:329–33. https://doi.org/10.2105/AJPH.2017.304245
6. Stamm LV. Ebola virus disease: rapid diagnosis and timely case reporting are critical to the early response for outbreak control. Am J Trop Med Hyg. 2015;93:438–40. https://doi.org/10.4269/ajtmh.15-0229
7. Siedner MJ, Gostin LO, Cranmer HH, Kraemer JD. Strengthening the detection of and early response to public health emergencies: lessons from the West African Ebola epidemic. PLoS Med. 2015;12:e1001804. https://doi.org/10.1371/journal.pmed.1001804
8. Gostin LO, Tomori O, Wibulpolprasert S, Jha AK, Frenk J, Moon S, et al. Toward a common secure future: four global commissions in the wake of Ebola. PLoS Med. 2016;13:e1002042. https://doi.org/10.1371/journal.pmed.1002042
9. Camacho A, Kucharski AJ, Funk S, Breman J, Piot P, Edmunds WJ. Potential for large outbreaks of Ebola virus disease. Epidemics. 2014;9:70–8. https://doi.org/10.1016/j.epidem.2014.09.003
10. Caleo G, Theocharaki F, Lokuge K, Weiss HA, Inamdar L, Grandesso F, et al. Clinical and epidemiological performance of WHO Ebola case definitions: a systematic review and meta-analysis. Lancet Infect Dis. 2020;20:1324–38. https://doi.org/10.1016/S1473-3099(20)30193-6
11. Jacob ST, Crozier I, Fischer WA II, Hewlett A, Kraft CS, Vega MA, et al. Ebola virus disease. Nat Rev Dis Primers. 2020;6:13. https://doi.org/10.1038/s41572-020-0147-3
12. World Health Organization. Case definition recommendations for Ebola or Marburg virus diseases. Interim guideline. 2014 Aug 9 [cited 2021 Oct 1]. http://apps.who.int/iris/bitstream/10665/146397/1/WHO_EVD_CaseDef_14.1_eng.pdf?ua=1
13. World Health Organization. Ground zero in Guinea: the Ebola outbreak smoulders—undetected—for more than 3 months. A retrospective on the first cases of the outbreak [cited 2020 May 28]. https://www.who.int/news/item/04-09-2015-ground-zero-in-guinea-the-ebola-outbreak-smoulders-undetected-for-more-than-3-months
14. Ilunga Kalenga O, Moeti M, Sparrow A, Nguyen VK, Lucey D, Ghebreyesus TA. The ongoing Ebola epidemic in the Democratic Republic of Congo, 2018–2019. N Engl J Med. 2019;381:373–83. https://doi.org/10.1056/NEJMsr1904253
15. World Health Organization. Ebola virus disease—Democratic Republic of the Congo. Disease outbreak news: update 21 May 2020. Geneva: The Organization; 2020.
16. Mobula LM, Samaha H, Yao M, Gueye AS, Diallo B, Umutoni C, et al. Recommendations for the COVID-19 response at the national level based on lessons learned from the Ebola virus disease outbreak in the Democratic Republic of the Congo. Am J Trop Med Hyg. 2020;103:12–7. https://doi.org/10.4269/ajtmh.20-0256
17. World Health Organization. Ebola and Marburg virus disease epidemics: preparedness, alert, control, and evaluation. 2014 [cited 2021 Aug 5]. https://apps.who.int/iris/bitstream/handle/10665/130160/WHO_HSE_PED_CED_2014.05_eng.pdf
18. World Health Organization. Communicable disease surveillance and response systems: guide to monitoring and evaluating. 2006 [cited 2021 Aug 5]. http://www.who.int/csr/resources/publications/surveillance/WHO_CDS_EPR_LYO_2006_2.pdf
19. Buehler JW, Hopkins RS, Overhage JM, Sosin DM, Tong V. Framework for evaluating public health surveillance systems for early detection of outbreaks: recommendations from the CDC Working Group. MMWR Recomm Rep. 2004;53(RR-5):1–11.
20. R Foundation for Statistical Computing. R: a language and environment for statistical computing. 2014 [cited 2021 Aug 5]. http://www.R-project.org
21. Lee H, Nishiura H. Recrudescence of Ebola virus disease outbreak in West Africa, 2014–2016. Int J Infect Dis. 2017 Nov 1;64:90–2. https://doi.org/10.1016/j.ijid.2017.09.013
22. Centers for Disease Control and Prevention. Event-based surveillance. 2019 [cited 2021 Aug 5]. https://www.cdc.gov/globalhealth/healthprotection/gddopscenter/how.html
23. World Health Organization. Integrated disease surveillance and response technical guidelines, booklet 1: introduction section. Brazzaville (Republic of the Congo): WHO Regional Office for Africa; 2019.
24. Ratnayake R, Crowe SJ, Jasperse J, Privette G, Stone E, Miller L, et al. Assessment of community event–based

surveillance for Ebola virus disease, Sierra Leone, 2015. Emerg Infect Dis. 2016;22:1431–7. https://doi.org/10.3201/eid2208.160205
25. Alpren C, Jalloh MF, Kaiser R, Diop M, Kargbo S, Castle E, et al. The 117 call alert system in Sierra Leone: from rapid Ebola notification to routine death reporting. BMJ Glob Health. 2017;2:e000392. https://doi.org/10.1136/bmjgh-2017-000392
26. Frieden TR, Lee CT, Bochner AF, Buissonnière M, McClelland A.7-1-7: an organising principle, target, and accountability metric to make the world safer from pandemics. Lancet. 2021;398:638–40. https://doi.org/10.1016/S0140-6736(21)01250-2
27. World Health Organization. International health regulations (2005): areas of work for implementation. Geneva: The Organization; 2007.
28. Kasolo F, Yoti Z, Bakyaita N, Gaturuku P, Katz R, Fischer JE, et al. IDSR as a platform for implementing IHR in African countries. Biosecur Bioterror. 2013;11:163–9. https://doi.org/10.1089/bsp.2013.0032
29. Cordes KM, Cookson ST, Boyd AT, Hardy C, Malik MR, Mala P, et al. Real-time surveillance in emergencies using the early warning alert and response network. Emerg Infect Dis. 2017;23(Suppl 1):S131. https://doi.org/10.3201/eid2313.170446

Address for correspondence: Mory Keita, Emergency Preparedness and Response Unit (Dakar Hub), WHO Regional Office for Africa, Dakar, Almadies Lotissement Ngor-Extension; Zone 10, Lot No19, PO Box. 4039, Senegal; email: mokeita@who.int

Coronavirus Disease Contact Tracing Outcomes and Cost, Salt Lake County, Utah, USA, March–May 2020

Victoria L. Fields, Ian T. Kracalik, Christina Carthel, Adriana Lopez, Amy Schwartz, Nathaniel M. Lewis, Mackenzie Bray, Carlene Claflin, Kilee Jorgensen, Ha Khong, Walter Richards, Ilene Risk, Maureen Smithee, Madison Clawson, Lee Cherie Booth, Tara Scribellito, Jason Lowry, Jessica Huynh, Linda Davis, Holly Birch, Tiffany Tran, Joseph Walker, Alicia Fry, Aron Hall, Jodee Baker, Eric Pevzner, Angela C. Dunn, Jacqueline E. Tate, Hannah L. Kirking, Tair Kiphibane, Cuc H. Tran

Outcomes and costs of coronavirus disease (COVID-19) contact tracing are limited. During March–May 2020, we constructed transmission chains from 184 index cases and 1,499 contacts in Salt Lake County, Utah, USA, to assess outcomes and estimate staff time and salaries. We estimated 1,102 staff hours and $29,234 spent investigating index cases and contacts. Among contacts, 374 (25%) had COVID-19; secondary case detection rate was ≈31% among first-generation contacts, ≈16% among second- and third-generation contacts, and ≈12% among fourth-, fifth-, and sixth-generation contacts. At initial interview, 51% (187/370) of contacts were COVID-19–positive; 35% (98/277) became positive during 14-day quarantine. Median time from symptom onset to investigation was 7 days for index cases and 4 days for first-generation contacts. Contact tracing reduced the number of cases between contact generations and time between symptom onset and investigation but required substantial resources. Our findings can help jurisdictions allocate resources for contact tracing.

By July 2021, >33 million cases of coronavirus disease (COVID-19), caused by severe acute respiratory syndrome coronavirus 2 (SARS-CoV-2), were documented in the United States, and most cases involved contact tracing by health departments (*1*). Preventing SARS-CoV-2 transmission through contact tracing requires rapid diagnosis, immediate isolation of cases, and rigorous tracking and precautionary isolation of close contacts (*2*–*4*). Because SARS-CoV-2 appears to be most transmissible before and immediately after symptom onset, clinical and transmission studies have shown that timely identification of cases and contacts is essential to preventing transmission (*5*–*7*). In addition, mathematical models have shown contact tracing, when implemented with other mitigation measures, can effectively reduce community spread of SARS-CoV-2 (*8*,*9*).

Evaluations of contact tracing for tuberculosis and HIV have found that contact tracing is an effective and sustainable approach to transmission reduction when disease prevalence is low but that contact tracing becomes less cost-effective as disease prevalence increases compared with other approaches, such as provider-initiated testing and intensified case finding (*10*,*11*). Programmatic data on outcomes and costs of contact tracing for COVID-19 are limited but essential for aiding public health agencies in designing or improving existing contact tracing programs (*12*). We aimed to quantify contact tracing efforts in Salt Lake County, Utah, USA, to examine how contact tracing affected case-finding, evaluate key contact tracing time intervals, and estimate the staff time and salary costs required to conduct investigations.

Methods

We examined persons with laboratory-confirmed or probable COVID-19 cases and their close contacts

Author affiliations: Centers for Disease Control and Prevention, Atlanta, Georgia, USA (V.L. Fields, I.T. Kracalik, A. Lopez, A. Schwartz, N.M, Lewis, T. Tran, J. Walker, A. Fry, A. Hall, E. Pevzner, J.E. Tate, H.L. Kirking, C.H. Tran); Salt Lake County Health Department, Salt Lake City, Utah, USA (C. Carthel, M. Bray, C. Claflin, K. Jorgensen, H. Khong, W. Richards, I. Risk, M. Smithee, M. Clawson, L.C. Booth, T. Scribellito, J. Lowry, J. Huynh, L. Davis, H. Birch, A.C. Dunn, T. Kiphibane); Utah Department of Health, Salt Lake City (J. Baker)

DOI: https://doi.org/10.3201/eid2712.210505

retrospectively by using Salt Lake County Health Department (SLCoHD) surveillance data. We quantified the yield from each index case that generated a contact investigation and created transmission chains. We also examined 25 index cases and close contacts prospectively to estimate staff time and salary cost spent in contact tracing efforts.

SLCoHD Contact Tracing Procedures and Testing Guidelines

During March 12–May 3, 2020, SLCoHD staff traced all reported case-patients with laboratory-confirmed SARS-CoV-2 infection and their close contacts. Close contacts of any confirmed or probable case-patients were traced until no further symptomatic or positive contacts could be identified. Early in the study period, state guidelines called for prioritizing testing symptomatic close contacts of confirmed COVID-19 case-patients. Later in the study period, testing was available to anyone with approval from their healthcare provider.

Definitions

We defined a confirmed COVID-19 case as detection of SARS-CoV-2 RNA by real-time reverse transcription PCR (*13*). According to the Council of State and Territorial Epidemiologists definition, a probable case is one that meets clinical criteria and epidemiologic evidence with no confirmatory laboratory testing performed for COVID-19, meets presumptive laboratory evidence and either clinical criteria or epidemiologic evidence, or meets vital records criteria with no confirmatory laboratory testing performed for COVID-19 (*13*). We defined a probable case as a symptomatic close contact to a confirmed case-patient. We defined close contacts as anyone ≤6 feet of a confirmed case-patient or a symptomatic contact to a confirmed case-patient (i.e., a probable case) for ≥15 minutes, ≥2 days before the case-patient's symptom onset and until the case-patient began strict isolation or until the contact's last exposure to the case.

Index Case Identification and Transmission Chains

SLCoHD staff conducted contact tracing investigations via telephone interview. Interviews included 5 components: providing isolation or quarantine guidance; monitoring contacts for 14 days after their last exposure to a case, with the option for daily phone calls or text messages; entering demographic data for contacts into the Utah National Electronic Disease Surveillance System (EpiTrax, https://epi.health.utah.gov/utah-national-electronic-disease-surveillance-system-ut-nedss) for linkage and tracking; community notifications, including notifying businesses, workplaces, event venues, churches, or persons who might have been exposed to confirmed cases; and providing resources, such as information on housing or financial support, SARS-CoV-2 testing locations, and where and when to seek medical care.

We grouped contacts into 3 main categories: confirmed cases, probable cases, and contacts under observation. We further divided the 3 categories into 8 subclassifications: confirmed cases comprised index, symptomatic positive, and asymptomatic positive cases; probable cases comprised untested but symptomatic persons; and contacts under observation comprised persons who were asymptomatic not tested, symptomatic negative, or asymptomatic negative, as well as unknown status cases (Appendix, https://wwwnc.cdc.gov/EID/article/27/12/21-1505-App1.pdf). Status of probable cases and contacts under observation could change during the quarantine period; for instance, a probable case could become a symptomatic positive case if the contact had a SARS-CoV-2–positive test result during the quarantine period.

Data Source

We used EpiTrax surveillance data to retrospectively construct COVID-19 transmission chains for all confirmed index case-patients and contacts. We abstracted demographics, exposure history, SARS-CoV-2 test results, symptoms, and underlying conditions for confirmed or probable cases. We also abstracted investigation notes and applicable dates for last exposure to the confirmed or probable case, symptom onset, symptom resolution, initial health department contact, COVID-19 tests, monitoring period, hospital admission and discharge, and death. We also identified each contact's relationship to their respective index case-patient, such as household or nonhousehold contact and generation of contact (first through sixth generation).

We chose a priori to systematically select 10% of laboratory-confirmed cases diagnosed during March 12–May 3, 2020, in Salt Lake County. However, during that period, the number of cases identified in Salt Lake County grew. Our final sample represented 8% of the total 2,757 cases.

Effort Time and Cost

We selected 25 index case-patients and prospectively documented the time spent interviewing them and their 144 contacts, from time of initial health department interaction with the index case-patient to the end of each contact's 14-day monitoring period. Interviewers prospectively recorded time needed to complete all 5 investigation components for the selected index cas-patients. We grouped contacts into 1 of the 8 subclassifications and applied a β-PERT

distribution to Monte Carlo simulation to estimate time and staff salary required to conduct contact tracing investigations for each of the 8 disease statuses (Appendix). We used the minimum, mean, and maximum time documented investigating each of the 8 disease subclassifications as parameters for the simulation (Appendix). We estimated salary cost by multiplying the median wage of all staff involved in contact tracing by the total number of hours spent on the contact tracing investigation (Appendix). Costs comprised time spent conducting all interviews (i.e., cost per index case and cost per contact, including those that were ultimately unreachable or out of jurisdiction) and for community notifications. We excluded nonstandardized costs, such as overhead, overtime, and time and costs for trainings.

Data Management and Analysis

To quantify contact tracing efforts, we evaluated the number of contacts yielded and investigated from each index case. We did not reclassify symptomatic contacts to an index case-patient if their symptom onset date was earlier than their respective index case-patient, but we did include them in the analysis. We used R (R Foundation for Statistical Computing, https://www.r-project.org) and Stata (StataCorp LLC, https://www.stata.com) software for data management and descriptive analysis. We calculated 95% CIs for estimated time intervals between events, such as symptom onset, testing, and initial contact, and for estimated cost per type of case or contact investigation. This activity was reviewed by the Centers for Disease Control and Prevention and was conducted consistent with its policy and applicable federal laws (*14*–*19*).

Results

Index Case Identification and Contact Tracing

Of the 229 cases identified from the line list, 45 were excluded; 12 were excluded because the case-patient was a contact of a previously included index case and 33 because of incomplete data (Figure 1). Our final analysis included 184 index cases and 1,499 linked contacts. Among linked contacts, 922 were first-generation, 387 second-generation, 99 third-generation, 39 fourth-generation, 49 fifth-generation, and 3 sixth-generation contacts. Third-, fourth-, fifth-, and sixth-generation contacts were directly or indirectly linked to first-generation contacts of patients who tested positive, who had confirmed cases, or who had symptomatic but untested probable cases (Figure 1). Among 184 index case-patients, 153 (83%) did not have known contact with a laboratory-confirmed COVID-19 case-patient. Across all generations, we identified a median of 5 (range 0–97) contacts and a mean of 2.03 confirmed and probable secondary cases for each index case (Table 1). Of 1,499 contacts, 96 were unreachable; 89 were unreachable or did not have adequate information to trace, and 7 were out of jurisdiction and did not have final disease status. Of 1,499 contacts, 374 (25%) became confirmed or probable cases, of which 285 (19%) were confirmed and 89 (6%) were probable. The rate of secondary case detection was ≈31% among first-generation contacts; ≈16% among both second- and third-generation contacts; and ≈12% among fourth-, fifth-, and sixth-generation contacts.

Disease Status at Initiation and End of the Contact's Monitoring Period

Among 1,499 contacts, 277/1,027 (27%) were tested during their monitoring period (Figure 2). Of the 277 tested contacts, 98 (35%) were SARS-CoV-2–positive after initial health department interaction. Among the 362 (24%) SARS-CoV-2–negative contacts, 183 (51%) had tested negative before their initial health department interview and 179 (49%) tested negative after the initial interview.

The proportion of household contacts who were symptomatic and positive increased from 11% at initial health department interaction to 18% after the monitoring period (Figure 2). When comparing the final disease status of contacts exposed within their household versus outside of their household, more contacts exposed within their households received testing (23% vs. 13%) (data not shown).

Key COVID-19–Associated Dates

The median time from symptom onset to initial health department interaction was 7 days (interquartile range [IQR] 4–10 days) for index cases compared with 4 days (IQR 1–7.25 days) for first-generation contacts (Figure 3; Appendix). The median time from laboratory PCR test collection to initial interview was 2 days (IQR 2–4 days) for index case-patients compared with 0 days (IQR 2–4 days) for first-generation contacts. Index case-patients generally started isolation on the day of the initial SLCo-HD interview (median 0 days, IQR 0–3 days). First-generation contacts reported having quarantined themselves for a median of 0 days (IQR 0–5 days) before initial interview. First-generation contacts reported a date of last exposure as a median of 4 days (IQR 0–7 days) before the initial interview; household contacts reported a median of 1 day (IQR 0–5 days), and nonhousehold contacts reported a median of 6 days (IQR 4–9 days). The

time between last exposure to isolation decreased for each subsequent generation (Appendix). Among 270 contacts who reported ongoing exposure, such as persons who could not or did not isolate, 96% were household contacts.

Effort and Staffing Cost

We calculated time and salary cost (in USD) required to conduct contact tracing (Figure 4). Total time required to investigate 184 index cases and their 1,499 contacts was 1,102 staff hours at a total cost of $29,234 (Appendix). Median time and cost spent investigating an index case and all successive generations of contacts was 4.16 hours (95% CI 4.06–4.72 hours) at $107.22 (95% CI $92.60–$120.70).

Time and costs varied depending on the status of the contact. For each index case, the median investigation time was 79.23 (95% CI 76.56–81.40) minutes and

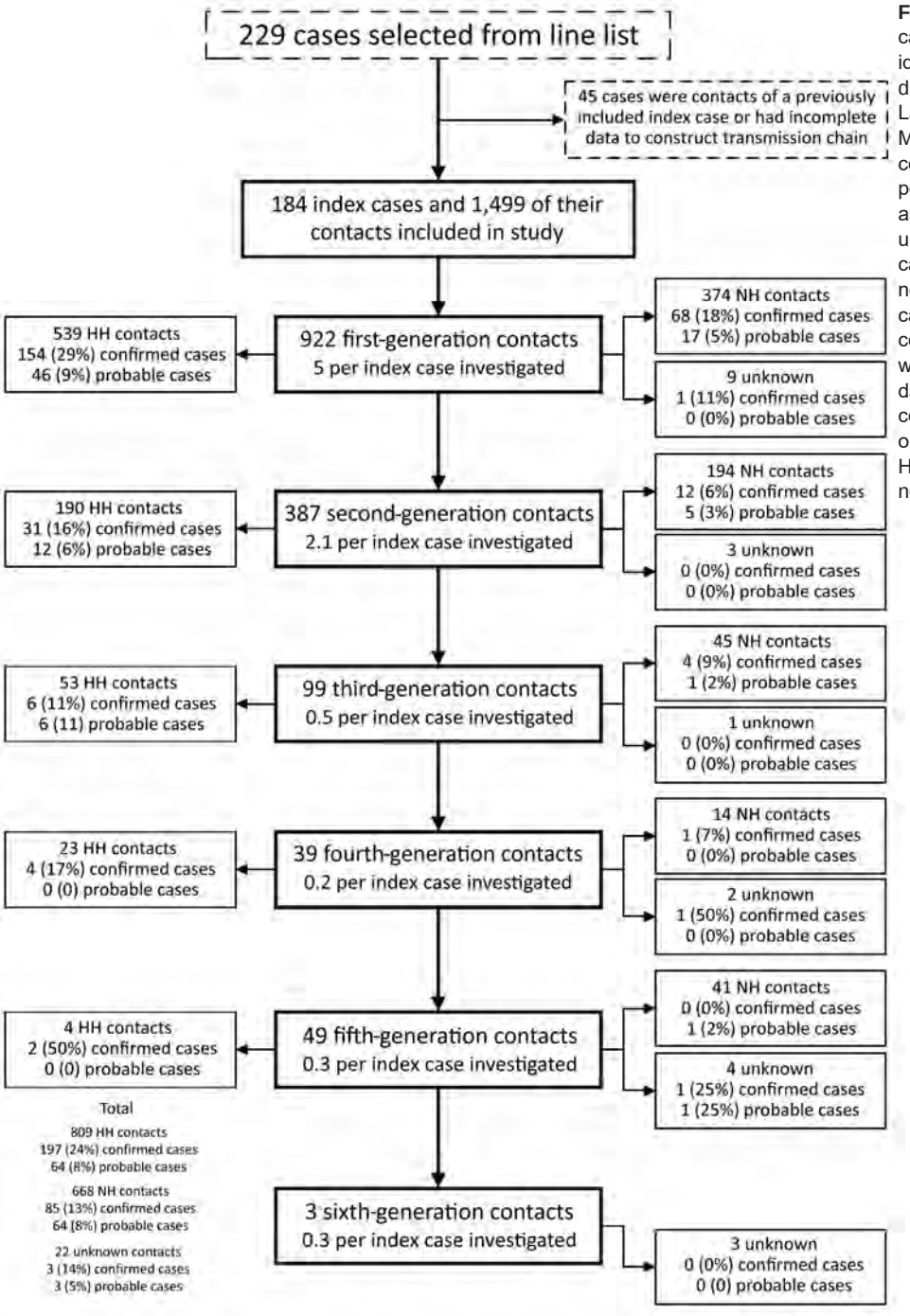

Figure 1. Flowchart of index case-patients and their contacts identified during coronavirus disease contact tracing, Salt Lake County, Utah, USA, March–May 2020. Confirmed cases comprised disease categories positive symptomatic, positive asymptomatic, and positive unknown symptoms. Probable cases comprised contacts in the not tested symptomatic disease category. Twenty-three HH contacts and 13 NH contacts were symptomatic on the same day or before the index case; contacts with an earlier symptom onset date were not reclassified. HH, household contacts; NH, nonhousehold contacts.

Table. Number of contacts identified and COVID-19 status by generation among persons during COVID-19 contact tracing, Salt Lake County, Utah, USA, March–May 2020*

Generation	Final status†	No. (%)	No. contacts/no. index cases investigated‡	No. contacts traced to identify 1 case (mean)§
All, n = 1,499	Confirmed case	285 (19)	1.55	5.26 (4.01)
	Probable case	89 (6)	0.48	16.84 (4.01)
	Not a case	1,029 (69)	5.59	1.46 (NA)
	Unreachable or out of jurisdiction	96 (6)	0.52	15.61 (NA)
First, n = 922	Confirmed case	223 (24)	1.21	4.13 (3.22)
	Probable case	63 (7)	0.34	14.63 (3.22)
	Not a case	588 (64)	3.20	1.57 (NA)
	Unreachable or out of jurisdiction	48 (5)	0.26	19.21 (NA)
Second, n = 387	Confirmed case	43 (11)	0.23	9.00 (6.45)
	Probable case	17 (4)	0.09	22.76 (6.45)
	Not a case	304 (79)	1.65	1.27 (NA)
	Unreachable or out of jurisdiction	23 (6)	0.13	16.83 (NA)
Third, n = 99	Confirmed case	10 (10)	0.05	9.90 (5.82)
	Probable case	7 (7)	0.04	14.14 (5.82)
	Not a case	73 (74)	0.40	1.36 (NA)
	Unreachable or out of jurisdiction	9 (9)	0.05	11.00 (NA)
Fourth–sixth, n = 91	Confirmed case	9 (10)	0.05	10.11 (8.27)
	Probable case	2 (2)	0.01	45.50 (8.27)
	Not a case	64 (70)	0.35	1.42 (NA)
	Unreachable or out of jurisdiction	16 (18)	0.09	5.69 (NA)

*COVID-19, coronavirus disease; NA, not applicable.
†Contacts were categorized as follows: confirmed cases comprised symptomatic-positive persons, asymptomatic-positive persons, and persons with unknown symptoms who tested positive; probable cases comprised symptomatic persons who were not tested; not a case comprised asymptomatic persons who were not tested, asymptomatic-negative persons, and symptomatic-negative persons. See Appendix (https://wwnc.cdc.gov/EID/article/27/12/21-0505-App1.pdf) for each generation breakdown by final status.
‡The number of contacts per index case investigated was calculated by dividing the number of contacts in each category by the 184 index cases.
§The number of contacts traced to find a confirmed or probable case in each generation was calculated by dividing the total number of contacts (n = 1,499) by the number of cases in each category.

median cost was $33.67 (95% CI $32.34–$35.22). Negative asymptomatic cases required the least amount of staff time, 21.50 (95% CI 21.05–22.08) minutes costing a median of $9.29 (95% CI $9.07–$9.50). The total time spent on community notification for exposure to a confirmed case was 84.13 hours (Figure 4). Each notification took a median of 34.67 (95% CI 32.45–37.78) minutes, including 121 (66%) index case-patients who requested work excuse letters and 14 (7.6%) index case-patients who requested notifications to community locations, such as medical facilities, event venues, churches, and grocery stores. The average gross hourly wage for salaried epidemiologists, nurses, and office support staff involved in contact tracing efforts was $29.52 (range $23.61–$35.42) (Appendix Table 4).

Discussion

Our analysis of contact tracing of 184 index cases and 1,499 close contacts in Salt Lake County, Utah, highlights the substantial cost and time needed for these investigations. In addition, we found that, for successive generations of contacts traced, fewer cases were identified, and the time between symptom onset and SARS-CoV-2 testing decreased. However, changing quarantine or social distancing guidance during the investigation period also might have resulted in fewer cases in later generations. These findings highlight the effectiveness of contact tracing to guide control measures and reduce onward transmission of SARS-COV-2. Other jurisdictions can use these findings to examine their contact tracing yields, effort, and key COVID-19–associated time intervals to help guide programmatic changes.

Contact tracing is resource intensive (*8*). Every index case investigated produced a transmission chain containing a median of 5 linked contacts. The median time to investigate these transmission chains was 4.16 (95% CI 4.06–4.72) hours at a cost of $107.22 (95% CI $92.60–$120.70). During the study period, 2,757 COVID-19 cases in Salt Lake County required investigation, which we estimate to have resulted in ≈$300,000 and ≈11,500 staff hours spent conducting these investigations. The time spent by contact tracers reflects resources needed to interview, educate, and enter data for cases and contacts and to write work excuse letters and conduct community notifications. The finding of lower yields in later generations highlights the need for further studies to examine the cost-benefit of tracing multiple generations of contacts (*20*).

We found that 6% of contacts were unreachable or out of jurisdiction, which is lower than the 17% unreachable contacts identified through a text messaging–based system in a previous study (*21*). However, consistent with another study (*22*), we found a high proportion (83%) of index case-patients that did not have known contact with a laboratory-

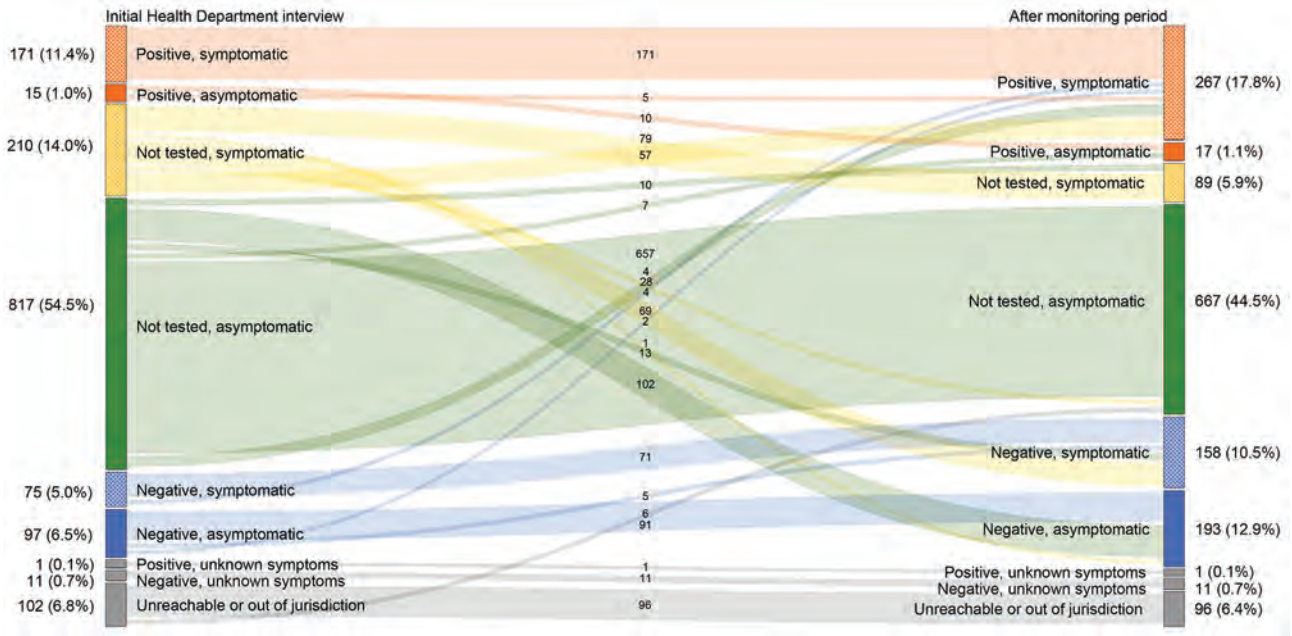

Figure 2. Coronavirus disease status at initial health department interaction and after 14-day monitoring period, Salt Lake County, Utah, USA, March–May 2020. Numbers in the center signify the change in status from initial interaction by health department after the monitoring period. Numbers on left and right represent total (%) of cases in each group. The median monitoring period was the time from initial health department interview to 14 days after the last exposure to the index case. Colors represent disease status classification category.

confirmed COVID-19 case-patient. The prevalence of cases without an identified epidemiologic link raises concerns over unrecognized transmission (*23*), which suggests contact tracing efforts alone might not be sufficient to stop disease transmission.

Our contact tracing yields, laboratory confirmation of infection among 19% of contacts, were higher than those in South Korea (4%), and Shenzhen (15%) and Guangzhou (17%) in China (*2*,*7*,*24*). Consistent with findings from recent studies (*1*,*2*,*24*,*25*), we found household contacts were infected at a higher rate (32%) than nonhousehold contacts (16%). The finding of higher infection rates among household contacts reinforces the importance of evaluating prevention measures, such as using hotels for contacts unable to separate themselves from other household members (*26*). Compared with index cases (n = 184), confirmed secondary cases (n = 285) identified through contact tracing generated about one fourth of the contacts and less than one fifth of the secondary cases. During the study period, testing capacity was limited, delaying health department notifications and initiation of contact tracing investigations, which might have increased yields because case-patients spent more time not knowing their infection status (*8*). In addition, because primarily symptomatic persons received testing, positive results might have resulted in higher rates and thus higher yields.

Modeling shows the probability of COVID-19 control decreases with long delays from symptom onset to case isolation, fewer cases ascertained by contact tracing, and increasing transmission before symptom onset (*8*). Thus, time intervals between symptom onset, laboratory testing, and initial health department interview provide insight into the efficiency of contact tracing investigations (*27*). One study found that contact tracing for COVID-19 reduced the time to test confirmation by 2.3 days and time to contact isolation by 1.9 days (*24*). Similarly, we observed a 3-day decrease in the time from symptom onset to initial health department interview starting with first-generation contacts and noted to be the same or further decreasing in most subsequent generations. The time interval from symptom onset to initial health department interview was longer than that from symptom onset to first positive test or from symptom onset to isolation initiation. This time interval decreased between the first-generation and sixth-generation contacts; later generation contacts might have had more opportunity to follow health department recommendations and for the health department to promptly recommend testing when indicated. Although the usefulness of contact tracing in the setting of sustained SARS-CoV-2 transmission has been questioned (*28*,*29*), consistent with other studies, our findings show that contact tracing reduced transmission; only one fourth of contacts traced and

quarantined experienced COVID-19–like symptoms or tested SARS-CoV-2–positive.

New technologies, such as mobile telephone application–based symptom monitoring and electronic contact tracing platforms, might alleviate some of the burden needed to carry out investigations. In Utah, contacts could opt to receive daily phone calls or text message notifications. Text messaging might improve efficiency by decreasing time for contact follow-up, but it requires additional resources, a robust information technology infrastructure, and strong data protection safeguards (*21*). Smartphone technology is another powerful tool for contact tracing; a widely accepted smartphone application that does not have major privacy concerns, including the collection of personal data such as location, might prove useful (*30*). In addition, technology such as point-of-care SARS-CoV-2 testing, where results can be obtained within 48 hours, could reduce laboratory turnaround time. Rapid tests aid in quickly identifying index cases and contacts to implement isolation protocols (J. Joung et al., unpub. data, https://doi.org/10.1101/2020.05.04.20091231) and could improve contact tracing metrics. Online platforms that can identify how cases and contacts are linked, such as MicrobeTrace (https://microbetrace.cdc.gov/MicrobeTrace), also could aid in the management of investigations by reducing duplicative efforts, thereby improving efficiency.

The ongoing COVID-19 pandemic and emergence of the SARS-CoV-2 B.1.617.2 (Delta) variant have demonstrated the need for continuing layered prevention strategies, including contact tracing (*31*). Our findings can help local and state jurisdictions

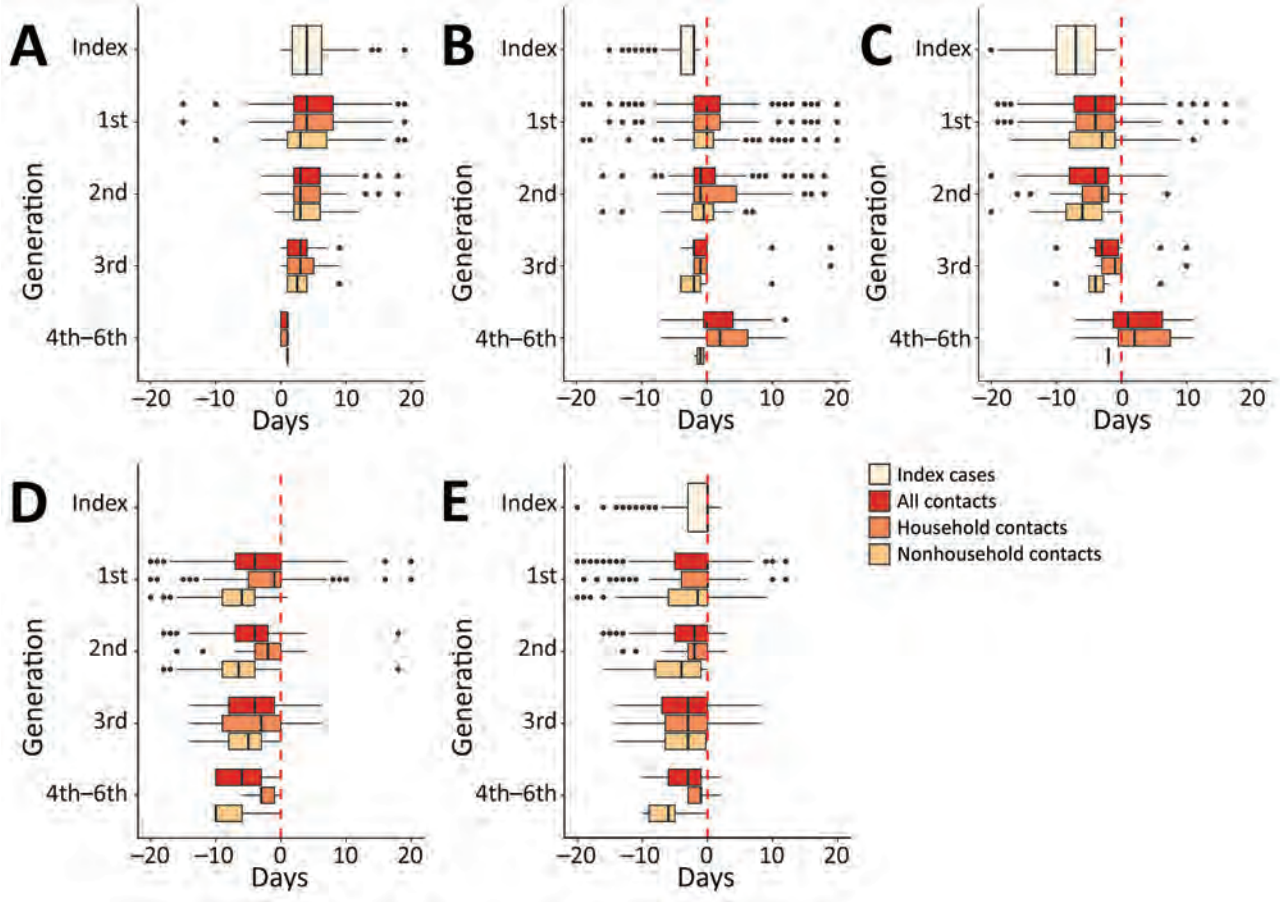

Figure 3. Box-and-whisker plots showing time from key coronavirus disease contact tracing–associated dates to other key dates, Salt Lake County, Utah, USA, March–May 2020. A) Days from symptom onset to PCR testing; B) days from PCR testing to initial interaction with Salt Lake County Health Department (SLCoHD); C) days from symptom onset to initial interaction with SLCoHD; D) days from last day of exposure to a confirmed or probable case to initial interaction with SLCoHD; E) days from monitoring start date to initial interaction with SLCoHD. The all contacts category includes contacts with an unknown relationship to a confirmed or probable case. Dotted red lines represent when the Salt Lake County Health Department had initial interactions with cases or contacts. Vertical lines within boxes indicate the median, left and right box edges indicate the interquartile range (IQR), and whiskers indicate the lower extreme and upper extreme quartiles; black dots indicate outliers. Negative values along the x-axis indicate that the second event happened before the first event.

determine the cost, effort, and yields associated with implementing a comprehensive contact tracing program, factors that are crucial for guiding policy decisions. Our data, coupled with further cost studies, can help inform resource allocation, including staffing needs and roles, technology requirements, and strategies to evaluate cost-effectiveness. In addition, our findings can be used to develop mathematical models to determine the need to scale up contact tracing to focus on all cases and contacts or to scale down and focus only on first-, second-, and third-generation contacts, as well as to decide who to interview, such as high-risk contacts or household contacts.

Our study's first limitation is that our approach might not be generalizable because Utah's surveillance system enables linkage between cases and contacts, which might not be available in other jurisdictions; differences could also exist in contact

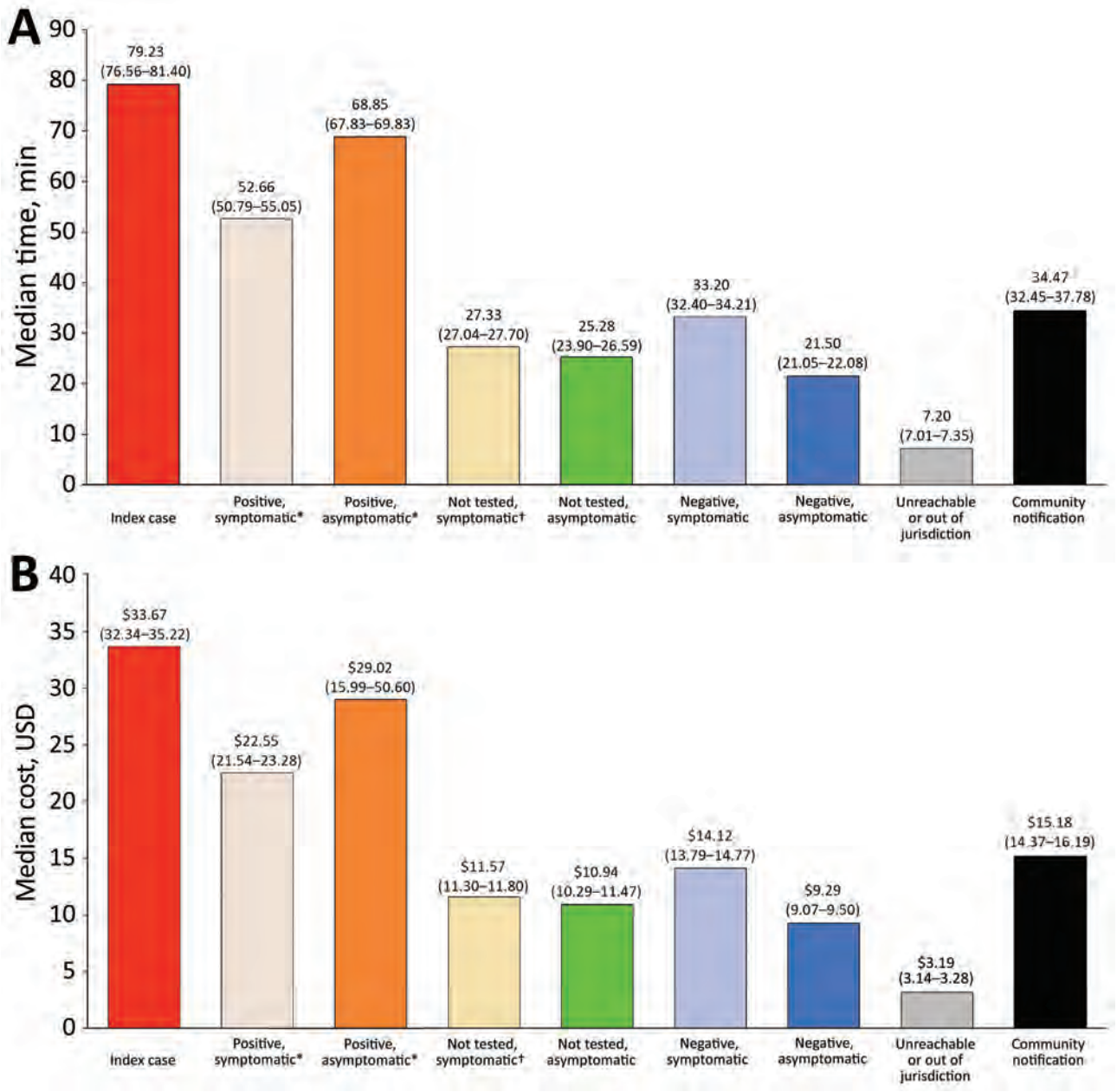

Figure 4. Estimated median time and cost spent educating, interviewing, and charting index cases and their contacts by final coronavirus disease status, Salt Lake County, Utah, USA, March–May 2020. Community notifications consisted of notifying businesses or persons that might have been exposed to the confirmed case such as in a workplace, at a wedding, or in a church. Asterisk (*) indicates case; dagger (†) indicates probable case. A) Median time in minutes and 95% CIs are reported above each bar. B) Median cost in USD and 95% CIs are reported above each bar.

participation across jurisdictions. Second, during March 2020, testing was available only for persons meeting initial COVID-19 symptom criteria (Appendix), which might have reduced case identification and the ability to test contacts. Third, interventions such as social distancing guidance and stay-at-home-orders introduced during March–May 2020 might have decreased transmission. Fourth, information was derived from interviews, which have a potential for recall bias, including naming all contacts (*32*). Fifth, costs of contact tracing are underestimated because we could not account for overtime benefits, such as time-and-a-half pay; overhead, such as staff health insurance and facility utility costs; staff training time; time spent providing services to the community, such as time to drop off masks; and other expenditures. Sixth, we could not track how many persons complied with recommendations to self-isolate or quarantine; the ability to determine whether cases and contacts complied with recommendations would aid in further quantifying contact tracing yield and effort. Finally, patients who do not seek care, potentially because of presymptomatic or asymptomatic infection, are a further challenge to preventing additional cases because SARS-CoV-2 shedding is highest early in illness (*8*). We found that 2% of asymptomatic contacts tested SARS-CoV-2–positive and 76% of asymptomatic contacts were not tested. Therefore, the attack rate might have been underestimated given the large proportion of asymptomatic contacts who did not get tested.

In conclusion, our analysis highlights the importance of contact tracing to reduce transmission of SARS-CoV-2. However, the effectiveness of contact tracing is contingent upon availability of substantial resources and rapid testing capacity. Persons should seek testing as soon as they experience COVID-19–like symptoms and begin isolation while results are pending. Because of early viral shedding, health department messaging should strongly direct contacts to obtain testing when possible, especially contacts with a higher risk for exposure, such as caregivers within households, populations in congregate settings, and contacts with underlying conditions; or for contacts who have an occupation requiring them to be in contact with other vulnerable persons, such as long-term care facility workers, daycare workers, and those who work with unvaccinated persons (*33*,*34*). Contact tracing metrics evaluated in this study can help other jurisdictions design, improve, and scale up contact tracing programs as needed for their specific epidemiologic contexts. Health departments should consider adjusting their approach to contact tracing as the situation evolves and adopting new technologies as these become available.

Acknowledgments

We thank Andrew Hill and Prabasaj Paul for their critical review of this analysis and Dagmar Vitek for supporting and approving this evaluation. We thank the Salt Lake County residents for their cooperation working with the health department in their contact tracing efforts. We thank the Salt Lake County Health Department and Utah Department of Health for their participation and involvement in this project, which contributed to its success; we would not have been able to carry out this evaluation without their support.

About the Author

Dr. Fields is an Epidemic Intelligence Service Officer assigned to the Child Development and Disability Branch, Division of Human Development and Disability, National Center on Birth Defects and Developmental Disabilities, Centers for Disease Control and Prevention. Her research interests include autism and other developmental disabilities, antimicrobial resistance, zoonotic disease, and a One Health approach.

References

1. Bing.com. COVID-19 tracker [cited 2021 Feb 19]. https://bing.com/covid/local/unitedstates
2. Park YJ, Choe YJ, Park O, Park SY, Kim YM, Kim J, et al.; COVID-19 National Emergency Response Center, Epidemiology and Case Management Team. Contact tracing during coronavirus disease outbreak, South Korea, 2020. Emerg Infect Dis. 2020;26:2465–8. https://doi.org/10.3201/eid2610.201315
3. World Health Organization. Contact tracing in the context of Covid-19. Interim guidance [cited 2020 Sep 24]. https://apps.who.int/iris/bitstream/handle/10665/332049/WHO-2019-nCoV-Contact_Tracing-2020.1-eng.pdf
4. Salathé M, Althaus CL, Neher R, Stringhini S, Hodcroft E, Fellay J, et al. COVID-19 epidemic in Switzerland: on the importance of testing, contact tracing and isolation. Swiss Med Wkly. 2020;150:w20225. https://doi.org/10.4414/smw.2020.20225
5. Zou L, Ruan F, Huang M, Liang L, Huang H, Hong Z, et al. SARS-CoV-2 viral load in upper respiratory specimens of infected patients. N Engl J Med. 2020;382:1177–9. https://doi.org/10.1056/NEJMc2001737
6. Cheng HY, Jian SW, Liu DP, Ng TC, Huang WT, Lin HH; Taiwan COVID-19 Outbreak Investigation Team. Contact tracing assessment of COVID-19 transmission dynamics in Taiwan and risk at different exposure periods before and after symptom onset. JAMA Intern Med. 2020;180:1156–63. https://doi.org/10.1001/jamainternmed.2020.2020
7. Jing QL, Liu MJ, Zhang ZB, Fang LQ, Yuan J, Zhang AR, et al. Household secondary attack rate of COVID-19 and associated determinants in Guangzhou, China: a retrospective cohort study. Lancet Infect Dis. 2020;20:1141–50. https://doi.org/10.1016/S1473-3099(20)30471-0
8. Kretzschmar ME, Rozhnova G, Bootsma MCJ, van Boven M, van de Wijgert JHHM, Bonten MJM. Impact of delays on effectiveness of contact tracing strategies for COVID-19:

a modelling study. Lancet Public Health. 2020;5:e452–9. https://doi.org/10.1016/S2468-2667(20)30157-2
9. Hellewell J, Abbott S, Gimma A, Bosse NI, Jarvis CI, Russell TW, et al.; Centre for the Mathematical Modelling of Infectious Diseases COVID-19 Working Group. Feasibility of controlling COVID-19 outbreaks by isolation of cases and contacts. Lancet Glob Health. 2020;8:e488–96. https://doi.org/10.1016/S2214-109X(20)30074-7
10. Kakinda M, Matovu JKB. A yield and cost comparison of tuberculosis contact investigation and intensified case finding in Uganda. PLoS One. 2020;15:e0234418. https://doi.org/10.1371/journal.pone.0234418
11. Armbruster B, Helleringer S, Kalilani-Phiri L, Mkandawire J, Kohler HP. Exploring the relative costs of contact tracing for increasing HIV case finding in sub-Saharan countries. J Acquir Immune Defic Syndr. 2011;58:e29–36. https://doi.org/10.1097/QAI.0b013e31822a9fa8
12. Burke RM, Midgley CM, Dratch A, Fenstersheib M, Haupt T, Holshue M, et al. Active monitoring of persons exposed to patients with confirmed COVID-19—United States, January–February 2020. MMWR Morb Mortal Wkly Rep. 2020;69:245–6. https://doi.org/10.15585/mmwr.mm6909e1
13. Centers for Disease Control and Prevention. Coronavirus disease 2019 (COVID-19), 2020 interim case definition, approved April 5, 2020 [cited 2020 Sep 30]. https://ndc.services.cdc.gov/case-definitions/coronavirus-disease-2019-2020
14. Centers for Disease Control and Prevention. Human participant protection in CDC research [cited 2021 Sep 10]. https://www.cdc.gov/os/integrity/hrpo/index.htm
15. Code of Federal Regulations. 45 CFR part 46: protection of human subjects [cited 2021 Sep 10]. https://ecfr.federalregister.gov/current/title-45
16. Code of Federal Regulations. 21 CFR part 56: institutional review boards [cited 2021 Sep 10]. https://ecfr.federalregister.gov/current/title-21/chapter-I/subchapter-A/part-56
17. United States Code. 42 USC section 241(d): research and investigations [cited 2021 Sep 10]. https://www.govinfo.gov/app/details/USCODE-2011-title42/USCODE-2011-title42-chap6A-subchapII-partA-sec241/summary
18. United States Code. 5 USC section 552a: records maintained on individuals [cited 2021 Sep 10]. https://www.govinfo.gov/app/collection/uscode/2019/title5/partI/chapter5/subchapterII/Sec.%20552a
19. United States Code. 44 USC section 3501: federal information policy [cited 2021 Sep 10]. https://www.govinfo.gov/app/collection/uscode/2019/title44/chapter35/subchapterI
20. Armbruster B, Brandeau ML. Contact tracing to control infectious disease: when enough is enough. Health Care Manage Sci. 2007;10:341–55. https://doi.org/10.1007/s10729-007-9027-6
21. Barrett PM, Bambury N, Kelly L, Condon R, Crompton J, Sheahan A; regional Department of Public Health. Measuring the effectiveness of an automated text messaging active surveillance system for COVID-19 in the south of Ireland, March to April 2020. Euro Surveill. 2020;25:2000972. https://doi.org/10.2807/1560-7917.ES.2020.25.23.2000972
22. Marshall K, Vahey GM, McDonald E, Tate JE, Herlihy R, Midgley CM, et al.; Colorado Investigation Team. Exposures before issuance of stay-at-home orders among persons with laboratory-confirmed COVID-19—Colorado, March 2020. MMWR Morb Mortal Wkly Rep. 2020;69:847–9. https://doi.org/10.15585/mmwr.mm6926e4
23. Oshitani H; Expert Members of The National COVID-19 Cluster Taskforce at The Ministry of Health, Labour and Welfare, Japan. Cluster-based approach to coronavirus disease 2019 (COVID-19) response in Japan, from February to April 2020. Jpn J Infect Dis. 2020;73:491–3. https://doi.org/10.7883/yoken.JJID.2020.363
24. Bi Q, Wu Y, Mei S, Ye C, Zou X, Zhang Z, et al. Epidemiology and transmission of COVID-19 in 391 cases and 1286 of their close contacts in Shenzhen, China: a retrospective cohort study. Lancet Infect Dis. 2020;20:911–9. https://doi.org/10.1016/S1473-3099(20)30287-5
25. Lewis NM, Duca LM, Marcenac P, Dietrich EA, Gregory CJ, Fields VL, et al. Characteristics and timing of initial virus shedding in severe acute respiratory syndrome coronavirus 2, Utah, USA. Emerg Infect Dis. 2021;27:352–9. https://doi.org/10.3201/eid2702.203517
26. Centers for Disease Control and Prevention. Case investigation and contact tracing: part of a multipronged approach to fight the COVID-19 pandemic [cited 2020 Sep 14]. https://www.cdc.gov/coronavirus/2019-ncov/php/principles-contact-tracing.html
27. Prevent Epidemics. Eleven epidemiological fallacies in COVID-19 [cited 2020 Sep 14]. https://preventepidemics.org/covid19/science/insights/eleven-epidemiological-fallacies-in-covid-19
28. Ferretti L, Wymant C, Kendall M, Zhao L, Nurtay A, Abeler-Dörner L, et al. Quantifying SARS-CoV-2 transmission suggests epidemic control with digital contact tracing. Science. 2020;368:eabb6936. https://doi.org/10.1126/science.abb6936
29. MacIntyre CR. Case isolation, contact tracing, and physical distancing are pillars of COVID-19 pandemic control, not optional choices. Lancet Infect Dis. 2020;20:1105–6. https://doi.org/10.1016/S1473-3099(20)30512-0
30. Yasaka TM, Lehrich BM, Sahyouni R. Peer-to-peer contact tracing: development of a privacy-preserving smartphone app. JMIR Mhealth Uhealth. 2020;8:e18936. https://doi.org/10.2196/18936
31. Christie A, Brooks JT, Hicks LA, Sauber-Schatz EK, Yoder JS, Honein MA; CDC COVID-19 Response Team. Guidance for implementing COVID-19 prevention strategies in the context of varying community transmission levels and vaccination coverage. MMWR Morb Mortal Wkly Rep. 2021;70:1044–47. PubMed https://doi.org/10.15585/mmwr.mm7030e2
32. Furuse Y, Sando E, Tsuchiya N, Miyahara R, Yasuda I, Ko YK, et al.; CDC COVID-19 Response Team. Clusters of coronavirus disease in communities, Japan, January–April 2020. Emerg Infect Dis. 2020;26:2176–9. https://doi.org/10.3201/eid2609.202272
33. Fields VL, Kiphibane T, Eason JT, Hafoka SF, Lopez AS, Schwartz A, et al. Assessment of contact tracing for COVID-19 among people experiencing homelessness, Salt Lake County Health Department, March–May 2020. Ann Epidemiol. 2021;59:50–5. https://doi.org/10.1016/j.annepidem.2021.04.002
34. Lopez AS, Hill M, Antezano J, Vilven D, Rutner T, Bogdanow L, et al. Transmission dynamics of COVID-19 outbreaks associated with child care facilities—Salt Lake City, Utah, April–July 2020. MMWR Morb Mortal Wkly Rep. 2020;69:1319–23. https://doi.org/10.15585/mmwr.mm6937e3

Address for correspondence: Cuc H. Tran, Centers for Disease Control and Prevention, 1600 Clifton Road NE, Mailstop US1-1, Atlanta, GA 303029-4027; email: CHTran@cdc.gov

Transmission of Severe Acute Respiratory Syndrome Coronavirus 2 in Households with Children, Southwest Germany, May–August 2020

Maximilian Stich,[1] Roland Elling,[1] Hanna Renk,[1] Aleš Janda,[1] Sven F. Garbade, Barbara Müller, Hans-Georg Kräusslich, Dorit Fabricius, Maria Zernickel, Peter Meissner, Daniela Huzly, Jürgen Grulich-Henn, Anneke Haddad, Tessa Görne, Benedikt Spielberger, Linus Fritsch, Alexandra Nieters, Hartmut Hengel, Andrea N. Dietz, Thomas Stamminger, Tina Ganzenmueller, Natalia Ruetalo, Andreas Peter, Jonathan Remppis, Thomas Iftner, Kathrin Jeltsch, Tim Waterboer, Axel R. Franz, Georg Friedrich Hoffmann, Corinna Engel,[2] Klaus-Michael Debatin,[2] Burkhard Tönshoff,[2] Philipp Henneke[2]

Resolving the role of severe acute respiratory syndrome coronavirus 2 (SARS-CoV-2) transmission in households with members from different generations is crucial for containing the current pandemic. We conducted a large-scale, multicenter, cross-sectional seroepidemiologic household transmission study in southwest Germany during May 11–August 1, 2020. We included 1,625 study participants from 405 households that each had ≥1 child and 1 reverse transcription PCR–confirmed SARS-CoV-2–infected index case-patient. The overall secondary attack rate was 31.6% and was significantly higher in exposed adults (37.5%) than in children (24.6%–29.2%; p = ≤0.015); the rate was also significantly higher when the index case-patient was ≥60 years of age (72.9%; p = 0.039). Other risk factors for infectiousness of the index case-patient were SARS-CoV-2–seropositivity (odds ratio [OR] 27.8, 95% CI 8.26–93.5), fever (OR 1.93, 95% CI 1.14–3.31), and cough (OR 2.07, 95% CI 1.21–3.53). Secondary infections in household contacts generate a substantial disease burden.

Severe acute respiratory syndrome coronavirus 2 (SARS-CoV-2) has rapidly spread globally since its emergence in December 2019. As of March 2021, >120 million infections have been reported, and >2.7 million deaths have been attributed to the novel coronavirus disease (COVID-19) (*1*). The severity of COVID-19 and the risk for a complicated course of illness or death increase with age (*2*,*3*). In terms of SARS-CoV-2 transmission, conjectures early in the pandemic were that asymptomatic (i.e., healthy) but infectious children played a particularly substantial role. The underlying assumption that children were drivers of the pandemic was based on experience with seasonal influenza virus. Consequently, closures of schools and preschools were among the earliest nonpharmaceutical interventions for transmission (*4*). However, the role of children in the transmission of SARS-CoV-2 remains controversial (*5*–*7*).

Next to superspreading events (*8*), intrahousehold transmission of SARS-CoV-2 is a major driver of the pandemic (*9*). A recent systematic review and meta-analysis based on reverse transcription PCR

Author affiliations: Heidelberg University Hospital, Heidelberg, Germany (M. Stich, S.F. Garbade, B. Müller, H.-G. Kräusslich, J. Grulich-Henn, K. Jeltsch, G.F. Hoffmann, B. Tönshoff); University Medical Centre and Faculty of Medicine Freiburg, Freiburg, Germany (R. Elling, D. Huzly, A. Haddad, T. Görne, B. Spielberger, L. Fritsch, A. Nieters, H. Hengel, P. Henneke); University Hospital and Faculty of Medicine Tübingen, Tübingen, Germany (H. Renk, T. Ganzenmueller, N. Ruetalo, A. Peter, J. Remppis, T. Iftner, A.R. Franz, C. Engel); Ulm University Medical Center, Ulm, Germany (A. Janda, D. Fabricius, M. Zernickel, P. Meissner, A.N. Dietz, T. Stamminger, K.-M. Debatin); German Cancer Research Center (DKFZ), Heidelberg (T. Waterboer)

DOI: https://doi.org/10.3201/eid2712.210978

[1]These first authors contributed equally to this article.

[2]These senior authors contributed equally to this article.

(RT-PCR) testing of SARS-CoV-2 RNA from nasopharyngeal or oropharyngeal swab specimens calculated a secondary attack rate (SAR) of 16.6% in households (*10*). In individual studies, the SAR in children varied from 4% (*11*) to 36% (*12*); hence, the data vary widely. Only a minority of studies reported separate SARs from pediatric index cases, and children accounted for <10% of index cases when reported (*8*,*9*,*13*,*14*).

Low detection rates of SARS-CoV-2 RNA by RT-PCR in children might not precisely reflect the frequency of infections. Mild or even asymptomatic disease in children combined with higher rates of aversion and incorrect swab collection might lead to underestimation of the infection risk, especially in symptom-based transmission studies. Determining the presence of SARS-CoV-2 antibodies could overcome some of these limitations (*15*). In a cross-sectional investigation of 2,482 child–parent pairs without known prior SARS-CoV-2 infection, we found a 3-fold lower SARS-CoV-2 seroprevalence in children than in their parents (*16*). Previous household transmission studies found SARS-CoV-2–specific IgG in 28% (*17*), 34% (*18*), 42% (*19*), 45% (*20*) and 52% (*21*) of exposed children; SARs were lower (*18*), similar to (*17*,*21*), or higher (*19*) than in exposed adult household members. However, the low number of studied households with children (21–130 households) (*17*–*21*) was a limitation.

We performed a large-scale multicenter seroepidemiologic study on transmission of SARS-CoV-2 in households with ≥1 child. Our objectives were to determine the SARS-CoV-2 seroprevalence and SAR in children compared with adults from the same households and, second, to identify risk factors associated with infectiousness of index case-patients and susceptibility of contacts.

Methods

Study Design and Conduct

We conducted a multicenter, cross-sectional SARS-CoV-2 transmission study on the prevalence of SARS-CoV-2 antibodies in members of households with 1 index case-patient with a previous SARS-CoV-2 infection confirmed by RT-PCR from a nasopharyngeal or oropharyngeal swab specimen. Households that met the eligibility criteria were invited to participate through the local health authorities Alb-Donau, Breisgau-Hochschwarzwald, Heidelberg/Rhein-Neckar, Karlsruhe, Mannheim, Neckar-Odenwald, Reutlingen, and Tübingen in the Federal State of Baden-Württemberg, Germany. We enrolled participants at the University Children's Hospitals in Freiburg, Heidelberg, Tübingen, and Ulm during May 11–August 1, 2020. At time of study enrollment, we collected blood samples from participants for antibody measurement and retrospectively determined symptom and infection history through a questionnaire and serologic tests. The study was designed, analyzed, and reported according to the Strengthening the Reporting of Observational Studies in Epidemiology (STROBE) reporting guidelines (https://www.strobe-statement.org).

Ethics

The study protocol was approved by the independent ethics committees of the Medical Faculty Heidelberg (approval no. S-294/2020), Medical Faculty Tübingen (approval no. 293/2020BO2), University of Ulm (approval no. 152/20), and University of Freiburg (approval no. 256/20_201553). The study was conducted according to the Declaration of Helsinki. Written informed consent was obtained from all household members and parents or guardians; children gave consent when appropriate for their age.

Eligibility Criteria and Study Procedure

Households were eligible for enrollment if they met all of these inclusion criteria: SARS-CoV-2 detection by RT-PCR from a nasopharyngeal or oropharyngeal swab specimen in ≥1 household member, ≥1 household member <18 years of age, residency in the state of Baden-Württemberg, and all household members having been officially released from quarantine. Key exclusion criteria were lack of written consent and insufficient knowledge of the German language.

Questionnaire items were number of household members and, for each member, age, sex, and whether they had ever tested positive for SARS-CoV-2. We asked participants reporting an RT-PCR-confirmed SARS-CoV-2 infection for the date when the positive specimen was collected, COVID-19–related symptoms (fever, cough, diarrhea, or dysgeusia), and whether they were hospitalized for COVID-19. We defined the index case-patient as the household member with the first SARS-CoV-2 RNA–positive specimen collected. We validated this definition in a subset of 54 households from 1 study center for which additional questionnaire information on transmission routes from nonhousehold contacts with COVID-19 were available. In 52 (96.3%) of 54 households, the definition of the index case based on timing of the RT-PCR test was consistent with the definition based on this anamnestic information. The RT-PCR test was performed within 24 hours, and a positive test result immediately triggered a strict home isolation and

quarantine for all household members for ≥14 days unless hospitalization was required.

Laboratory Analysis

We sent blood samples to the respective diagnostic laboratories in the 4 study centers, and serum was prepared on the same day. Samples were either immediately analyzed or stored at 4°C until further processing. Samples were analyzed for IgG reactive to the S1 domain of the viral spike glycoprotein and the SARS-CoV-2 nucleocapsid (N) protein. Antibodies reactive to the N protein were measured either with the Elecsys Anti-SARS-CoV-2 IgG/IgM ECLIA test kit (Roche, https://www.roche.com) processed on a Roche Cobas e601 or e411 module (in Heidelberg, Tübingen, and Ulm), or by recomWell SARS-CoV-2 IgG ELISA (Mikrogen Diagnostik, https://www.mikrogen.de/start.html) run on a BEP III analyzer in (Freiburg). SARS-CoV-2 IgG for the S1 domain of the spike protein were measured with the Euroimmun Anti-SARS-CoV-2-ELISA (IgG) test kit (Euroimmun, https://www.euroimmun.com) in Freiburg and Ulm. In Heidelberg and Tübingen, IgG/IgM directed against the receptor-binding domain of S1 were analyzed with the SARS-CoV-2 Total (COV2T) CLIA Assay (Siemens Healthineers, https://www.siemens-healthineers.com) on a Siemens ADVIA Centaur XP analyzer.

We categorized serum samples with concordant results in both assays as seropositive or seronegative. In case of discordant results, we performed additional, study site–specific measurements. These measurements were a neutralization assay (Tübingen) (*22*); the Euroimmun Anti-SARS-CoV-2-ELISA (IgG) (Euroimmun) (Heidelberg); the Elecsys Anti-SARS-CoV-2 IgG/IgM ECLIA (Roche) (Freiburg); or the ARCHITECT SARS-CoV-2 IgG, a test for IgG against the viral N protein (Abbott Laboratories, https://www.abbott.com) on an Abbott ARCHITECT 1000 instrument (Ulm). We classified serum samples with a positive reaction in the additional assay as seropositive.

Statistical Analysis

We performed analyses with R version 4.0.0 (R Foundation for Statistical Computing, https://www.r-project.org). We present results for continuous variables as mean with SD (for data with normal distribution) or median with interquartile ranges (IQR) and minimum and maximum values, unless stated otherwise. SARS-CoV-2 seropositivity served as a proxy for previous infection. We calculated the observed SAR by dividing the number of exposed SARS-CoV-2 IgG-positive household members by all exposed household members. To model and predict SAR, we used generalized linear mixed-effects logistic regression models (GLMM) with a logit function and the dependent variable "SARS-CoV-2 infection (yes/no)" of exposed household members and the predictors age of index case-patient, age of exposed household member, sex of index case-patient, sex of exposed household member, household size, and SARS-CoV-2–seropositivity in the index case.

We used a generalized linear mixed-effects model tree (*23*) to detect subgroup interactions in SAR of exposed household members (R package glmertree). This method uses model-based recursive partitioning to detect subgroup interactions and a GLMM to estimate the random-effects parameters (*23*). No a priori formulated hypotheses were tested, and therefore all p values and CIs are reported as descriptive measures. We compiled a more detailed description of GLMM models, simulations, violin plots, and R code (Appendix, https://wwwnc.cdc.gov/EID/article/27/12/21-0978-App1.pdf).

Results

Study Population

We enrolled 473 households during May 11–August 1, 2020 (Appendix Figure). We excluded households in which the index case could not be determined (n = 61). SARS-CoV-2–seropositivity plateaued at ≈30 days after a positive RT-PCR test for SARS-CoV-2 RNA (Appendix Table 1). To reduce the probability of negative serologic results because of imminent seroconversion, we excluded households that participated <30 days after a positive RT-PCR test of the index case (n = 7). A total of 405 households with 1,625 members (922 adults and 703 children) were available for final analysis (Table 1; Figure 1). The median age of index case-patients (n = 405) was 43.6 (range 1.36–71.5) years; 25 index case-patients (6.2%) were children. Among exposed household members (n = 1,220), 678 participants (55.6%) were children and 542 (44.4%) were adults. The sex distribution of index case-patients and exposed household members was balanced (Table 1).

SARS-CoV-2 Seropositivity and Observed Secondary Attack Rates

A total of 400 of 1,220 exposed household members tested positive for SARS-CoV-2 IgG and were categorized as previously infected (Figure 1), resulting in an overall observed SAR of 32.8%. Among the 405

Table 1. Demographic characteristics of study participants from 405 households, southwest Germany, May–August 2020

Characteristic	Total cohort	Adults	Children
No. participants	1,625	922	703
Median age, y	30.0	42.6	10.0
Interquartile range	11.0–45.0	37.0–50.0	5.79–13.9
Range	0.50–81.1	18.0–81.1	0.50–17.9
No. index case-patients	405	380	25
Median age, y	43.6	44.8	13.3
Interquartile range	37.2–49.5	38.0–49.9	9.03–16.2
Range	1.36–71.5	18.3–71.5	1.36–17.6
No. exposed household members	1220	542	678
Median age, y	16.2	42.8	9.83
Interquartile range	8.99–41.0	35.4–50.0	5.58–13.8
Range	0.50–81.1	18.0–81.1	0.50–17.9
Sex			
M	807	457	350
F	818	465	353
Household size*			
2–3	267	174	93
4	804	449	355
5	360	192	168
≥6	194	107	87
Region			
Freiburg	577	329	248
Heidelberg	532	306	226
Tübingen	319	175	144
Ulm	197	112	85

*Includes household members who did not participate.

index case-patients with RT-PCR–confirmed SARS-CoV-2 infection, 363 (89.6%) were seropositive and 42 (10.4%) were seronegative at the time of study participation. The rate of seropositivity in households with a seropositive index case-patient (393 of 1,090 [36.1%]) was 6-fold higher than the rate in households with a seronegative index case-patient (7 of 130 [5.4%]) (Table 2). The observed SAR in adults was 38.0% (206 of 542) compared with 28.6% (194 of 678) in children; it did not differ substantially among the 3 pediatric age groups (<6 years, 26.6%; 6–11.9 years, 30.7%; 12.0–17.9 years, 27.9%).

The observed SAR in exposed household members increased with the age of the index case-patient, from 13.3% for those <12 years of age to 71.4% for those ≥60 years of age (Table 2). The observed SAR in exposed male (32.5%) and female (33.1%) household members and in those with a male (33.9%) or female (31.6%) index case-patient were similar. Among the 405 index case-patients, 394 (97.3%) reported COVID-19–related symptoms and 9 (2.2%) were asymptomatic; no data were reported for 2 index case-patients. The most prevalent symptom was dysgeusia; cough, fever, and diarrhea were next most prevalent (Appendix Table 2). Overall symptoms (98.3% vs. 88.1%), and especially fever (58.4% vs. 33.3%) and dysgeusia (66.1% vs. 31.0%), were more prevalent in seropositive index case-patients than in seronegative index case-patients. A total of 22 (5.4%) index case-patients were hospitalized.

Risk Factors for SARS-CoV-2 Transmission

We used a linear mixed-effects logistic regression model to analyze these risk factors for virus transmission: age and sex of index case-patients and of exposed household members, household size, and SARS-CoV-2 seropositivity of the index case-patient (Table 2). SARS-CoV-2 seropositivity of the index case-patient was the risk factor most strongly associated with the SAR (odds ratio [OR] 27.8, 95% CI 8.26–93.5; p<0.001).

The predicted SAR in adults was higher than the predicted SARs in the 3 pediatric age groups, which were broadly similar (Table 2). Age of the index case-patient was also a risk factor for virus transmission. The predicted SAR in exposed household members was lowest when the index case-patient was <12 years of age (12.0%) and highest with an index case-patient ≥60 years of age (72.9%) and plateaued around 31% for index case-patients 12.0–59.9 years of age. It differed significantly between adults 18.0–59.9 years of age and those ≥60 years of age (OR 9.02, 95% CI 1.19–72.8; p = 0.039). Sex of the index case-patient and sex of the exposed household member were not associated with the SAR (Table 2). Larger households tended toward lower predicted SARs (Table 2); when we applied a Fisher exact test to the observed data, households with ≥4 household members were associated with a lower SAR (Appendix Table 3).

We compared the observed and predicted SAR associated with age of the index case-patient, age of

exposed household members, household size, and SARS-CoV-2 seropositivity of the index case-patient (Figure 2). We calculated the predicted SAR by using the generalized mixed-effects logistic regression model with simulations. In all 4 analyses, the observed and predicted SARs were almost identical, indicating that this logistic regression model was valid.

We used the same risk factors for a generalized linear mixed model binary decision tree to study subgroup interactions of risk factors for SAR. The most dominant risk factor for transmission was SARS-CoV-2-seropositivity of the index case-patient; the next most dominant risk factor was increased age of exposed household members (Figure 3, panel A). In an alternative generalized linear mixed model binary decision tree, only age of the index case-patient was considered a risk factor, and the age of exposed household members was fixed in each terminal node (Figure 3, panel B). In this model, the SAR increased with age of the index case-patient. Within each age group of index case-patient, the SAR also increased with age of the exposed household member (Figure 3, panel B). The observed SAR was 23.1% (80/346) if the index case-patient was <37.8 years of age, 34.7% (287/827) if the index case-patient was 37.8–57.9 years of age, and 70.2% (33/47) if the index case-patient was >57.9 years of age. However, cutoff values determined by generalized linear mixed-effects model trees are data-driven and should not be interpreted as fixed parameters. When we excluded the 42 households with a seronegative index case-patient and analyzed the remaining 363 households (Appendix Table 4) or included the time interval from positive SARS-CoV-2 RNA specimen collection in the index case-patient to the serologic assessment of the household (Appendix Table 5), we obtained comparable results.

We analyzed the COVID-19–related symptoms cough, fever, dysgeusia, and diarrhea, as well as hospitalization in the index case-patient, in an additional linear mixed-effect logistic regression model, consisting only of households with a symptomatic index case-patient with known hospitalization status

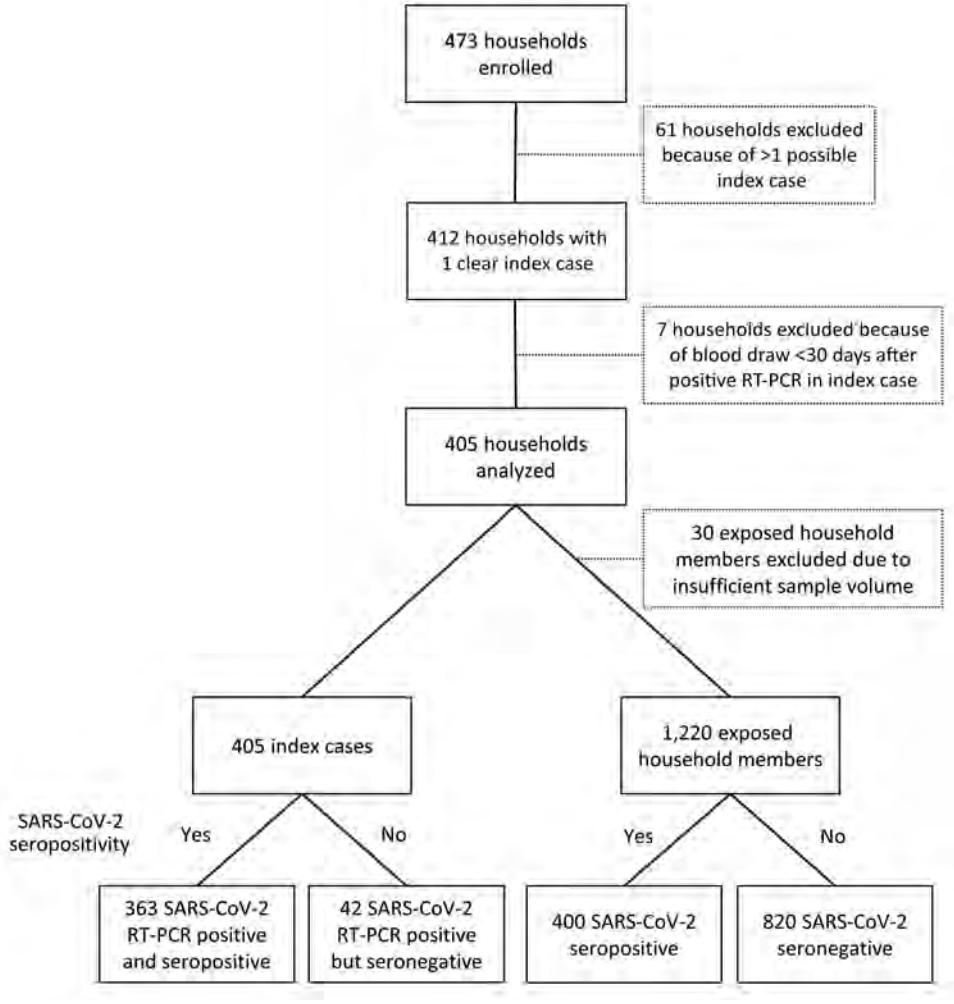

Figure 1. Flowchart of participant enrollment in study of transmission of severe acute respiratory syndrome coronavirus 2 in households with children, southwest Germany, May–August 2020. RT-PCR, reverse transcription PCR; SARS-CoV-2, severe acute respiratory syndrome coronavirus 2.

Table 2. Secondary attack rates in household members exposed to severe acute respiratory syndrome coronavirus 2 from 405 households, southwest Germany, May–August 2020*

Characteristic	No. index cases	No. exposed	No. seropositive exposed	Observed SAR, %	Predicted SAR, % (IQR)†	Odds ratio (95% CI)	p value
No. participants	405	1,220	400	32.8	31.6 (8.31–52.2)	NA	NA
Age of index case-patients, y							
≥60	6	21	15	71.4	72.9 (54.9–88.9)	9.02 (1.19–72.8)	0.039
18.0–59.9	374	1122	366	32.6	31.3 (8.41–51.1)	Referent	
12.0–17.9	16	47	15	31.9	30.8 (3.11–55.9)	1.32 (0.31–5.57)	0.704
0.0–11.9	9	30	4	13.3	12.0 (0.59–11.4)	0.34 (0.04–3.19)	0.343
Age of exposed household members, y							
≥18	NA	542	206	38.0	37.5 (13.2–59.4)	Referent	
12.0–17.9	NA	244	68	27.9	25.8 (6.24–40.2)	0.39 (0.25–0.63)	<0.001
6.0–11.9	NA	257	79	30.7	29.2 (8.02–47.9)	0.55 (0.35–0.89)	0.015
0.0–5.9	NA	177	47	26.6	24.6 (5.09–43.8)	0.33 (0.18–0.58)	<0.001
Sex of index case-patients							
M	207	629	213	33.9	32.6 (8.52–53.6)	Referent	
F	198	591	187	31.6	30.4 (8.12–50.8)	1.07 (0.62–1.87)	0.803
Sex of exposed household members							
M	NA	600	195	32.5	31.1 (7.62–51.9)	Referent	
F	NA	620	205	33.1	31.9 (8.54–53.5)	1.08 (0.75–1.56)	0.676
Household size							
2–3	92	175	69	39.4	38.1 (12.5–67.1)	Referent	
4	206	598	185	30.9	29.4 (8.26–44.0)	0.50 (0.24–1.01)	0.055
5	75	285	98	34.4	33.5 (8.57–53.7)	0.77 (0.33–1.78)	0.543
≥6	32	162	48	29.6	28.8 (4.64–55.6)	0.40 (0.14–1.18)	0.095
SARS-CoV-2–seropositive index case-patient							
No	42	130	7	5.38	3.59 (0.71–2.17)	Referent	
Yes	363	1090	393	36.1	34.9 (12.0–56.4)	27.8 (8.26–93.5)	<0.001

*IQR, interquartile range; NA, not applicable; SAR, secondary attack rate.
†The predicted SARs, odds ratios, and p values were calculated from a multivariable generalized linear mixed-effects logistic regression model. The respective references were "adult index 18.0-59.9 years," "adult exposed," "male index," "male exposed," "household size 2–3," and "seronegative index."

(n = 393) and adjusted for age of the index case-patient. The occurrences of fever and cough, but not of diarrhea, dysgeusia, or hospitalization, were significantly associated with a higher predicted SAR (Table 3).

Discussion

This large multicenter serologic SARS-CoV-2 household transmission study focusing on children revealed that the predicted SAR in household members <18 years of age is ≈8–13 percentage points lower than in adults. The predicted SAR also increased with increasing age of the index case-patient, which resulted in SARs of exposed household members ranging from 12.0% when the index case-patient was <12 years of age to 72.9% when the index case-patient was ≥60 years of age. The infectiousness of teenagers was similar to adults <60 years of age, and the predicted SAR was 31% in both groups.

Next to age, a systemic immune response after SARS-CoV-2 infection in the index case-patient, as indicated by circulating virus-specific antibodies, was strongly associated with the occurrence of secondary household cases. The biologic basis for the strikingly low SAR of 5.4% in households with a seronegative index case-patient (42/405) is unclear. Given the high specificity of SARS-CoV-2 RT-PCR testing, a proportion of 10% false-positive results is unlikely. Presumably the individual viral load is associated with both a stronger adaptive immune response and the extent of symptoms, which in turn increase virus transmission. Our observations that fever and dysgeusia were less prevalent in seronegative index case-patients and that presence of fever and cough in the index case-patient increases SAR in exposed household members are in line with this hypothesis. Furthermore, our findings are in accordance with other studies, in which specific SARS-CoV-2 antibodies were frequently absent in patients with mild symptoms (*15*). However, the hypothesis that SARS-CoV-2 transmission is more likely in cases with higher or persisting viral load in the nasopharynx has not been formally tested.

Our observation of a SAR ≈10 percentage points higher in adults than in children is consistent with household studies based on RT-PCR–confirmed SARS-CoV-2 infection (*10*). In contrast, previous household transmission studies based on SARS-CoV-2 serologic testing reported lower (*18*), similar (28%) (*17*), or higher (43%–52%) (*19*–*21*) SARs in children. However, these studies were relatively small.

A low proportion of pediatric index case-patients (6.2%) and an increasing SAR with increasing age of the index case-patient is in line with most previous serologic testing–based (*24*) or RT-PCR–based (*10*,*13*,*25*) household transmission studies

comparing infectiousness of pediatric and adult index case-patients. In addition, Soriano-Arandes et al. (*13*) found fewer intrahousehold transmissions after reopening schools, whereas intraschool transmissions were rare events in several countries after schools reopened in 2020 (*26*–*32*). Keeping schools open with strict hygiene measures in place could reduce overall SARS-CoV-2 transmission because close intrahousehold contact is reduced and children might act as sentinels for household transmissions when regularly tested at school.

Lower SARs in children have been previously attributed to differences in contact patterns; for example, physical interactions between spouses might be more intimate than between children and adults (*33*). Accordingly, we hypothesized that among children, toddlers might have more frequent and close physical contact with their parents than older children and adolescents, which might result in a SAR inversely correlated with age. However, we found the SAR to be similar among toddlers, older children, and adolescents, which indicates that behavior might not have a major effect on virus transmission within families. In contrast, the lower susceptibility to SARS-CoV-2 in children points toward the possible role of developmental factors related to host resistance and immunity. Low expression levels of angiotensin-converting enzyme 2, the cellular entry receptor of SARS-CoV-2 in the nasal epithelium of children has been previously suggested as a mechanistic factor (*34*). Moreover, previous endemic coronavirus infections in children might provide some protection, as indicated by frequently

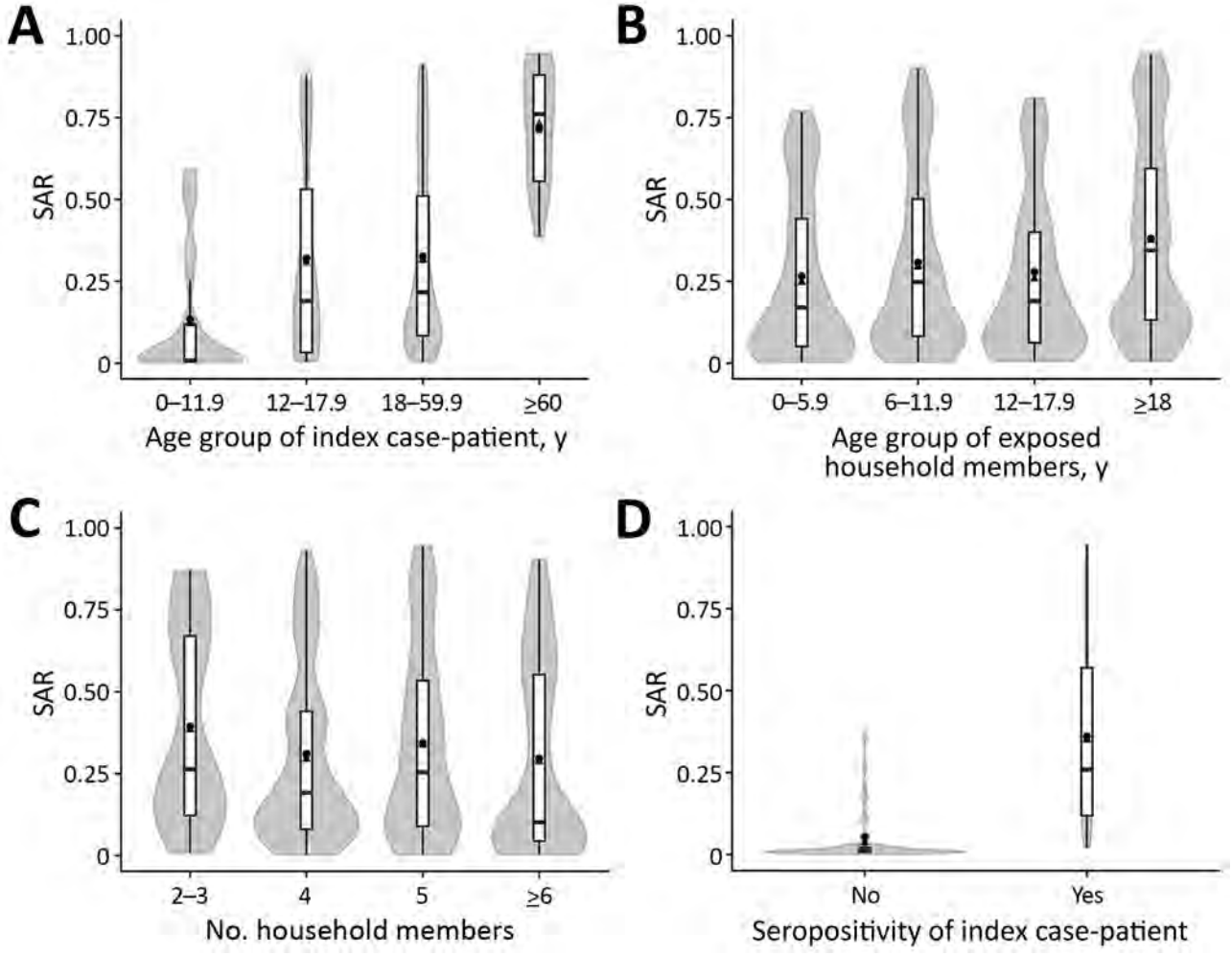

Figure 2. Observed and predicted SARs in household members exposed to severe acute respiratory syndrome coronavirus 2, southwest Germany, May–August 2020. SARs shown are associated with age of index case-patient (A), age of exposed household member (B), household size (C), and SARS-CoV-2 seropositivity of the index case-patient (D). The mean observed SAR is shown as a black dot. The mean (black triangles), interquartile range (white bars), maximum and minimum (ends of vertical black line), and distribution (gray shading) of the predicted SAR are shown in the violin plots. The predicted SARs were calculated from the generalized linear mixed-effects logistic regression model. SAR, secondary attack rate.

circulating cross-reacting antibodies (*35*) and SARS-CoV-2–reactive CD4+ T cells in ≤60% of unexposed children and adolescents (*36*). Furthermore, the innate immune response in children with SARS-CoV-2 exposure and infection might differ from that in adults, such as with respect to circulating neutrophil subsets, the induction of interferons (*37*), and cytokines (*38*).

The strengths of this study are its multicenter design, the high number of study participants, the application of robust statistical models, and a relatively low risk for recruitment bias, because potentially eligible households were invited through health authorities. Limitations are the high proportion of symptomatic index case-patients (97%) and adult (94%) index case-

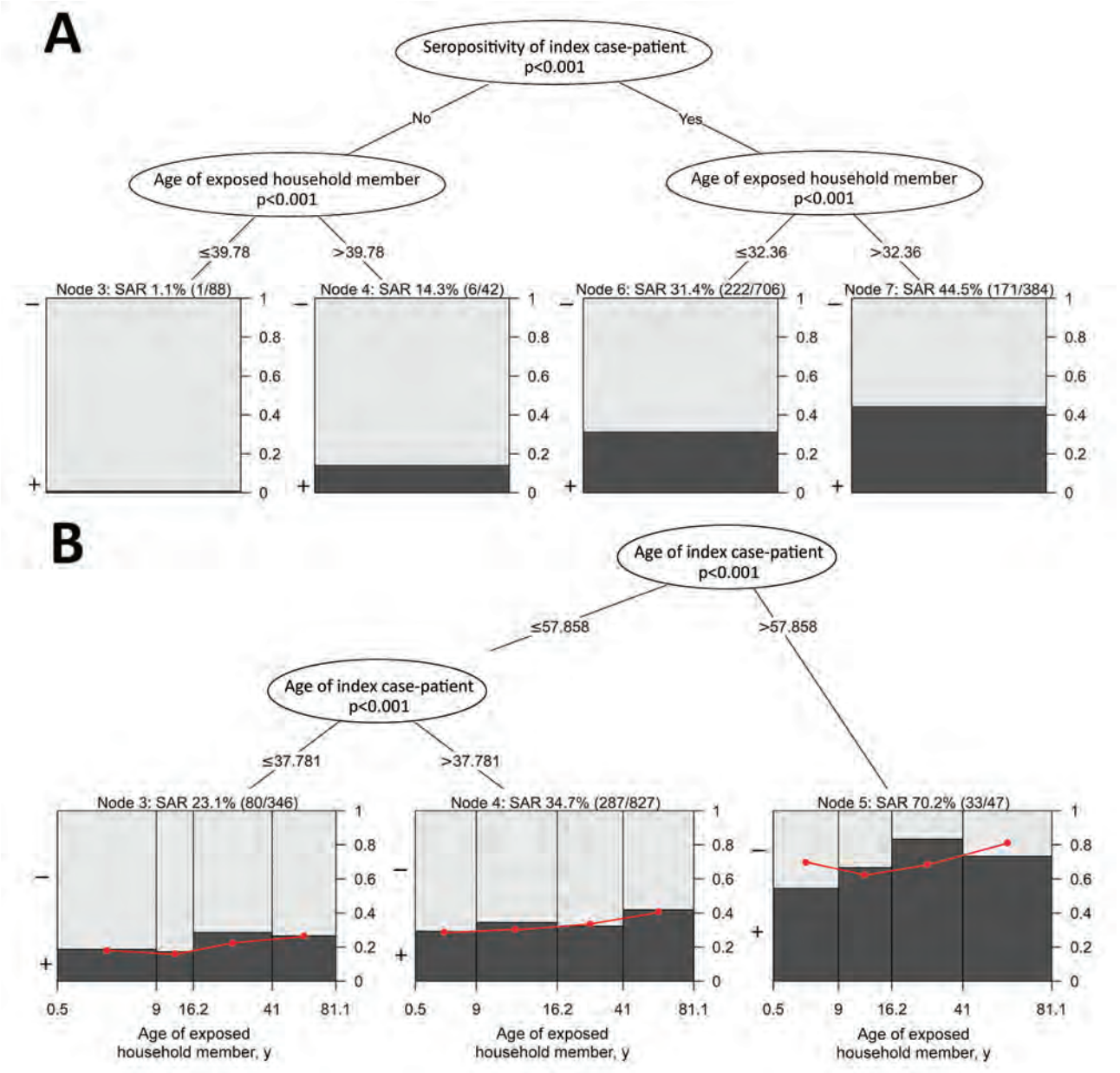

Figure 3. Generalized linear mixed model binary decision trees in study of transmission of severe acute respiratory syndrome coronavirus 2 in households with children, southwest Germany, May–August 2020. A) Model incorporating the 2 most dominant effects (p<0.001) on the SAR of exposed household members, SARS-CoV-2 seropositivity of the index case-patient and age of exposed household members with a seronegative or a seropositive index case-patient. B) Model incorporating only age of the index case-patient as a risk factor; SAR was modeled by age of exposed household member within each node. In both panels, the observed SAR as a proportion of seropositive (black) and seronegative (gray) exposed household members with these characteristics are shown within final nodes and as a percentage with the total number of seropositive/total exposed household members in parentheses above each node. In panel B, the predicted SARs are indicated within each final node as a red dot and red straight line. SAR, secondary attack rate.

Table 3. Association between coronavirus disease–related symptoms or hospitalization in index case-patients and secondary attack rates in exposed household members from 393 households with a symptomatic index case-patient whose hospitalization status is known, southwest Germany, May–August 2020*

Index case symptom or hospitalization	No. index cases, n = 393	No. exposed, n = 1,182	No. seropositive exposed, n = 390	Observed SAR, %	Predicted SAR, % (IQR)†	Odds ratio (95% CI)†	p value†
Fever	225	666	253	38.0	36.8 (11.8–58.4)	1.93 (1.14–3.31)	0.015
Cough	236	717	272	37.9	36.8 (11.7–58.2)	2.07 (1.21–3.53)	0.008
Diarrhea	91	271	94	34.7	33.2 (9.34–54.5)	0.80 (0.43–1.49)	0.481
Dysgeusia	253	748	252	33.7	32.2 (10.4–48.7)	1.41 (0.82–2.43)	0.213
Hospitalization	22	67	30	44.8	43.9 (15.2–68.9)	1.22 (0.40–3.75)	0.726

*IQR, interquartile range; NA, not applicable; SAR, secondary attack rate.
†The predicted SARs, odds ratios, and p values were calculated from a multivariable generalized linear mixed-effects logistic regression model. The respective references were absence of the symptom or "hospitalization" and adjusted for age of index case-patient as a numeric variable (OR 1.04, 95% CI 1.01–1.06; p = 0.0055).

patients. Potential explanations are the limited diagnostic test capacities at the time of the study, which favored testing of symptomatic adults and those with work-related exposure (e.g., in the healthcare sector) or a history of travel to high-risk regions. In households with an asymptomatic index case-patient, symptomatic secondary case-patients were possibly mislabeled as index case-patients as a result of this testing policy. An overestimation of the SAR in adults and an underestimation in children is likely, because COVID-19-associated symptoms were a good predictor for SARS-CoV-2 infection in adults but not in children (*16*). COVID-19–related symptoms were not reported more frequently in seropositive children than seronegative children, and other respiratory viruses were >100 times more prevalent than SARS-CoV-2 in children with acute respiratory symptoms across Germany during February–May 2020 (*39*). Another factor that leads to an underestimation of the SAR is a negative SARS-CoV-2 IgG test result in ≤10% of previously infected participants, which might partly be because of false-negative test results and a physiologic reduction of SARS-CoV-2 IgG levels over time.

Other potential weaknesses of serologic testing–based household transmission studies are the difficulty of differentiating between secondary and tertiary transmission within the same household and the inability to rule out nonhousehold infections of exposed household members. This could result in an overestimation of the SAR per index case. The possibility that 1 nonhousehold (community) index case-patient infected several household members is a potential bias of this study. However, the probability of SARS-CoV-2 infections from 2 different nonhousehold (community) index case-patients can be assumed to be low, because this study was performed shortly after the first pandemic wave and the strict government-imposed lockdown (Appendix Figure), when the SARS-CoV-2 seroprevalence in southwest Germany was as low as 1.8% in adults and 0.6% in children (*16*). Finally, the findings regarding SAR and its age dependency only apply to the SARS-CoV-2 variants circulating in Germany at that time and might not be translated to the more transmissible Delta variant.

In conclusion, this multicenter SARS-CoV-2 household transmission study focusing on children demonstrates that secondary infections in household contacts generate a substantial disease burden. Age is a risk factor both for infectiousness of index cases and susceptibility of exposed household members. Furthermore, fever and cough in index case-patients were associated with higher levels of infectiousness. Households can be expected to remain sites for SARS-CoV-2 transmission because home quarantine and home isolation are key measures in cases of suspected or confirmed infections in most countries.

Acknowledgments

We are especially indebted to all households who participated in this study. The engagement and great motivation of the participating recruiting physicians and nurses of the participating University Children's Hospitals working 7 days per week to execute the study timely and quickly. Similarly, the staff in the 4 testing laboratories in Freiburg, Heidelberg, Tübingen, and Ulm require special recognition. We thank the staff of the following public health departments for their organizational support: Robin Schöttke (Alb-Donau); Sigrid Maassen (Breisgau-Hochschwarzwald); Andreas Welker, Rainer Schwertz (Heidelberg/Rhein-Neckar); Peter Friebel, Barbara Koch (Karlsruhe); Daniele Schutz, Nadja Oster, Katrin Schwöbel, Peter Schäfer (Mannheim); Martina Teinert, Lena Fuchs (Neckar-Odenwald); Gottfried Roller (Reutlingen); Martina Benzing, and Oliver Piehl (Tübingen). We thank the following persons for excellent organizational support: Julia Euler, Anette Ulbrich, Iris Schelletter, Heike Matzkuhn, Kristine Chobanyan-Jürgens (Heidelberg); Aileen Heselich, Alicia Zink, Tara Marianna Ziegelbauer, Bianca Rippberger, Simone Hock (Freiburg); Andrea Bevot, Sarah Johler (Tübingen); Sandra Steinmann, Boram Song, Eva-Maria Jacobsen (Ulm). We thank Dorothea Kronsteiner (Heidelberg), Martin

Wolkewitz (Freiburg), and Rainer Muche (Ulm) for statistical consulting. We thank Florian Gleich (Heidelberg) for database assistance. We gratefully acknowledge Stefanie Wolf, Maria Anders-Össwein, Ira Pistorius-Knopf, and Markus Zorn (Heidelberg) for support in serological analyses. We thank Michael Schindler (Tübingen) for skillful assistance in conduction and interpretation of neutralization assays, Marlies Just (Ulm) for technical assistance, Ann-Kathrin Horlacher and Angelika Iftner (Tübingen) for support in serologic and RT-PCR analyses and Sigrid Enkel (Clinical Transfusion Medicine, Tübingen). We are grateful to the HILDA-Biobank, in particular Ali-Riza Kaya, and Marco Teller and Dirk Lebrecht at the FREEZE-Biobank (Freiburg). The work of Tim Waterboer was supported by a generous donation of the Dieter Morszeck Foundation.

The COVID-19 BaWü study was funded by the Ministry of Science, Research and the Arts Baden-Württemberg, Germany, within the framework of the special funding line for COVID-19 research, part of the measures to combat Coronavirus SARS-CoV-2 pandemic in the field of medical research. The funder of the study had no role in design or conduct of the study; collection, management, analysis, and interpretation of the data; and preparation, review, or approval of the manuscript; or the decision to submit the manuscript for publication.

About the Author

Dr. Stich is a resident at the Department of Pediatrics I, University Children's Hospital Heidelberg, Germany. His research interests are viral diseases with a focus on human papillomavirus and SARS-CoV-2.

References

1. Dong E, Du H, Gardner L. An interactive web-based dashboard to track COVID-19 in real time. Lancet Infect Dis. 2020;20:533–4. https://doi.org/10.1016/S1473-3099(20)30120-1
2. Zhou F, Yu T, Du R, Fan G, Liu Y, Liu Z, et al. Clinical course and risk factors for mortality of adult inpatients with COVID-19 in Wuhan, China: a retrospective cohort study. Lancet. 2020;395:1054–62. https://doi.org/10.1016/S0140-6736(20)30566-3
3. Dong Y, Mo X, Hu Y, Qi X, Jiang F, Jiang Z, et al. Epidemiology of COVID-19 among children in China. Pediatrics. 2020;145:e20200702. https://doi.org/10.1542/peds.2020-0702
4. Buonsenso D, Roland D, De Rose C, Vásquez-Hoyos P, Ramly B, Chakakala-Chaziya JN, et al. Schools closures during the COVID-19 pandemic: a catastrophic global situation. Pediatr Infect Dis J. 2021;40:e146–50. https://doi.org/10.1097/INF.0000000000003052
5. Lee EC, Wada NI, Grabowski MK, Gurley ES, Lessler J. The engines of SARS-CoV-2 spread. Science. 2020;370:406–7. https://doi.org/10.1126/science.abd8755
6. Viner RM, Mytton OT, Bonell C, Melendez-Torres GJ, Ward J, Hudson L, et al. Susceptibility to SARS-CoV-2 infection among children and adolescents compared with adults: a systematic review and meta-analysis. JAMA Pediatr. 2021;175:143–56. https://doi.org/10.1001/jamapediatrics.2020.4573
7. Spielberger BD, Goerne T, Geweniger A, Henneke P, Elling R. Intra-household and close-contact SARS-CoV-2 transmission among children—a systematic review. Front Pediatr. 2021;9:613292. https://doi.org/10.3389/fped.2021.613292
8. Laxminarayan R, Wahl B, Dudala SR, Gopal K, Mohan B C, Neelima S, et al. Epidemiology and transmission dynamics of COVID-19 in two Indian states. Science. 2020;370:691–7. https://doi.org/10.1126/science.abd7672
9. Park YJ, Choe YJ, Park O, Park SY, Kim YM, Kim J, et al.; COVID-19 National Emergency Response Center, Epidemiology and Case Management Team. Contact tracing during coronavirus disease outbreak, South Korea, 2020. Emerg Infect Dis. 2020;26:2465–8. https://doi.org/10.3201/eid2610.201315
10. Madewell ZJ, Yang Y, Longini IM Jr, Halloran ME, Dean NE. Household transmission of SARS-CoV-2: a systematic review and meta-analysis. JAMA Netw Open. 2020;3:e2031756. https://doi.org/10.1001/jamanetworkopen.2020.31756
11. Li W, Zhang B, Lu J, Liu S, Chang Z, Peng C, et al. Characteristics of household transmission of COVID-19. Clin Infect Dis. 2020;71:1943–6. https://doi.org/10.1093/cid/ciaa450
12. Wang Y, Tian H, Zhang L, Zhang M, Guo D, Wu W, et al. Reduction of secondary transmission of SARS-CoV-2 in households by face mask use, disinfection and social distancing: a cohort study in Beijing, China. BMJ Glob Health. 2020;5:e002794. https://doi.org/10.1136/bmjgh-2020-002794
13. Soriano-Arandes A, Gatell A, Serrano P, Biosca M, Campillo F, Capdevila R, et al.; COPEDI-CAT research group. Household SARS-CoV-2 transmission and children: a network prospective study. Clin Infect Dis. 2021 Mar 12 [Epub ahead of print]. https://doi.org/10.1093/cid/ciab228
14. Bi Q, Wu Y, Mei S, Ye C, Zou X, Zhang Z, et al. Epidemiology and transmission of COVID-19 in 391 cases and 1286 of their close contacts in Shenzhen, China: a retrospective cohort study. Lancet Infect Dis. 2020;20:911–9. https://doi.org/10.1016/S1473-3099(20)30287-5
15. Gudbjartsson DF, Norddahl GL, Melsted P, Gunnarsdottir K, Holm H, Eythorsson E, et al. Humoral immune response to SARS-CoV-2 in Iceland. N Engl J Med. 2020;383:1724–34. https://doi.org/10.1056/NEJMoa2026116
16. Tönshoff B, Müller B, Elling R, Renk H, Meissner P, Hengel H, et al. Prevalence of SARS-CoV-2 infection in children and their parents in southwest Germany. JAMA Pediatr. 2021;175:586–93. https://doi.org/10.1001/jamapediatrics.2021.0001
17. Laws RL, Chancey RJ, Rabold EM, Chu VT, Lewis NM, Fajans M, et al. Symptoms and transmission of SARS-CoV-2 among children—Utah and Wisconsin, March–May 2020. Pediatrics. 2021;147:e2020027268. https://doi.org/10.1542/peds.2020-027268
18. Dattner I, Goldberg Y, Katriel G, Yaari R, Gal N, Miron Y, et al. The role of children in the spread of COVID-19: Using household data from Bnei Brak, Israel, to estimate the relative susceptibility and infectivity of children. PLOS Comput Biol. 2021;17:e1008559. https://doi.org/10.1371/journal.pcbi.1008559

19. Lewis NM, Chu VT, Ye D, Conners EE, Gharpure R, Laws RL, et al. Household transmission of SARS-CoV-2 in the United States. Clin Infect Dis. 2020 Aug 16 [Epub ahead of print]. https://doi.org/10.1093/cid/ciaa1166
20. Ladhani SN, Andrews N, Aiano F, Baawuah F, Amin-Chowdhury Z, Brown KE, et al. Secondary attack rate and family clustering of SARS-CoV-2 infection in children of healthcare workers with confirmed COVID-19. Clin Infect Dis. 2021;73:e260–3. https://doi.org/10.1093/cid/ciaa1737
21. Buonsenso D, Valentini P, De Rose C, Pata D, Sinatti D, Speziale D, et al.; Gemelli Against COVID-19 Post-Acute Care Study Group. Seroprevalence of anti-SARS-CoV-2 IgG antibodies in children with household exposure to adults with COVID-19: preliminary findings. Pediatr Pulmonol. 2021;56:1374–7. https://doi.org/10.1002/ppul.25280
22. Ruetalo N, Businger R, Althaus K, Fink S, Ruoff F, Pogoda M, et al. Antibody response against SARS-CoV-2 and seasonal coronaviruses in nonhospitalized COVID-19 patients. MSphere. 2021;6:e01145–20. https://doi.org/10.1128/mSphere.01145-20
23. Fokkema M, Smits N, Zeileis A, Hothorn T, Kelderman H. Detecting treatment-subgroup interactions in clustered data with generalized linear mixed-effects model trees. Behav Res Methods. 2018;50:2016–34. https://doi.org/10.3758/s13428-017-0971-x
24. Galow L, Haag L, Kahre E, Blankenburg J, Dalpke AH, Lück C, et al. Lower household transmission rates of SARS-CoV-2 from children compared to adults. J Infect. 2021;83:e34–6. https://doi.org/10.1016/j.jinf.2021.04.022
25. Thompson HA, Mousa A, Dighe A, Fu H, Arnedo-Pena A, Barrett P, et al. Severe acute respiratory syndrome coronavirus 2 (SARS-CoV-2) setting-specific transmission rates: a systematic review and meta-analysis. Clin Infect Dis. 2021;73:e754–64. https://doi.org/10.1093/cid/ciab100
26. Buonsenso D, De Rose C, Moroni R, Valentini P. SARS-CoV-2 infections in Italian schools: preliminary findings after 1 month of school opening during the second wave of the pandemic. Front Pediatr. 2021;8:615894. https://doi.org/10.3389/fped.2020.615894
27. Ismail SA, Saliba V, Lopez Bernal J, Ramsay ME, Ladhani SN. SARS-CoV-2 infection and transmission in educational settings: a prospective, cross-sectional analysis of infection clusters and outbreaks in England. Lancet Infect Dis. 2021;21:344–53. https://doi.org/10.1016/S1473-3099(20)30882-3
28. Zimmerman KO, Akinboyo IC, Brookhart MA, Boutzoukas AE, McGann KA, Smith MJ, et al.; ABC SCIENCE COLLABORATIVE. Incidence and secondary transmission of SARS-CoV-2 infections in schools. Pediatrics. 2021;147:e2020048090. https://doi.org/10.1542/peds.2020-048090
29. Yung CF, Kam KQ, Nadua KD, Chong CY, Tan NWH, Li J, et al. Novel coronavirus 2019 transmission risk in educational settings. Clin Infect Dis. 2021;72:1055–8. https://doi.org/10.1093/cid/ciaa794
30. Macartney K, Quinn HE, Pillsbury AJ, Koirala A, Deng L, Winkler N, et al.; NSW COVID-19 Schools Study Team. Transmission of SARS-CoV-2 in Australian educational settings: a prospective cohort study. Lancet Child Adolesc Health. 2020;4:807–16. https://doi.org/10.1016/S2352-4642(20)30251-0
31. Otte Im Kampe E, Lehfeld AS, Buda S, Buchholz U, Haas W. Surveillance of COVID-19 school outbreaks, Germany, March to August 2020. Euro Surveill. 2020;25:2001645. https://doi.org/10.2807/1560-7917.ES.2020.25.38.2001645
32. Ehrhardt J, Ekinci A, Krehl H, Meincke M, Finci I, Klein J, et al. Transmission of SARS-CoV-2 in children aged 0 to 19 years in childcare facilities and schools after their reopening in May 2020, Baden-Württemberg, Germany. Euro Surveill. 2020;25:25. https://doi.org/10.2807/1560-7917.ES.2020.25.36.2001587
33. Goldstein E, Lipsitch M, Cevik M. On the effect of age on the transmission of SARS-CoV-2 in households, schools, and the community. J Infect Dis. 2021;223:362–9. https://doi.org/10.1093/infdis/jiaa691
34. Bunyavanich S, Do A, Vicencio A. Nasal gene expression of angiotensin-converting enzyme 2 in children and adults. JAMA. 2020;323:2427–9. https://doi.org/10.1001/jama.2020.8707
35. Ng KW, Faulkner N, Cornish GH, Rosa A, Harvey R, Hussain S, et al. Preexisting and de novo humoral immunity to SARS-CoV-2 in humans. Science. 2020;370:1339–43. https://doi.org/10.1126/science.abe1107
36. Grifoni A, Weiskopf D, Ramirez SI, Mateus J, Dan JM, Moderbacher CR, et al. Targets of T cell responses to SARS-CoV-2 coronavirus in humans with COVID-19 disease and unexposed individuals. Cell. 2020;181:1489–1501.e15. https://doi.org/10.1016/j.cell.2020.05.015
37. Neeland MR, Bannister S, Clifford V, Dohle K, Mulholland K, Sutton P, et al. Innate cell profiles during the acute and convalescent phase of SARS-CoV-2 infection in children. Nat Commun. 2021;12:1084. https://doi.org/10.1038/s41467-021-21414-x
38. Buonsenso D, Sali M, Pata D, De Rose C, Sanguinetti M, Valentini P, et al. Children and COVID-19: microbiological and immunological insights. Pediatr Pulmonol. 2020;55:2547–55. https://doi.org/10.1002/ppul.24978
39. Oh DY, Buda S, Biere B, Reiche J, Schlosser F, Duwe S, et al. Trends in respiratory virus circulation following COVID-19-targeted nonpharmaceutical interventions in Germany, January–September 2020: analysis of national surveillance data. Lancet Reg Health Eur. 2021;6:100112. https://doi.org/10.1016/j.lanepe.2021.100112

Address for correspondence: Burkhard Tönshoff, Department of Pediatrics I, University Children's Hospital, Im Neuenheimer Feld 430, D-69120 Heidelberg, Germany; email: Burkhard.Toenshoff@med.uni-heidelberg.de

SARS-CoV-2 Seroprevalence in a Rural and Urban Household Cohort during First and Second Waves of Infections, South Africa, July 2020–March 2021

Jackie Kleynhans, Stefano Tempia, Nicole Wolter, Anne von Gottberg, Jinal N. Bhiman, Amelia Buys, Jocelyn Moyes, Meredith L. McMorrow, Kathleen Kahn, F. Xavier Gómez-Olivé, Stephen Tollman, Neil A. Martinson, Floidy Wafawanaka, Limakatso Lebina, Jacques du Toit, Waasila Jassat, Mzimasi Neti, Marieke Brauer, Cheryl Cohen, for the PHIRST-C Group[1]

Severe acute respiratory syndrome coronavirus 2 (SARS-CoV-2) infections may be underestimated because of limited access to testing. We measured SARS-CoV-2 seroprevalence in South Africa every 2 months during July 2020–March 2021 in randomly selected household cohorts in 2 communities. We compared seroprevalence to reported laboratory-confirmed infections, hospitalizations, and deaths to calculate infection–case, infection–hospitalization, and infection–fatality ratios in 2 waves of infection. Post–second wave seroprevalence ranged from 18% in the rural community children <5 years of age, to 59% in urban community adults 35–59 years of age. The second wave saw a shift in age distribution of case-patients in the urban community (from persons 35–59 years of age to persons at the extremes of age), higher attack rates in the rural community, and a higher infection–fatality ratio in the urban community. Approximately 95% of SARS-CoV-2 infections were not reported to national surveillance.

The first laboratory-confirmed case of coronavirus disease (COVID-19) in South Africa was reported on March 5, 2020, and the country has since experienced 2 waves of COVID-19, the first peaking in July 2020 and the second in January 2021 (*1*). Across Africa, the second wave was more severe than the first (*2*), and specifically in South Africa, higher weekly incidence, hospitalizations, and deaths were reported for the second wave, compared with the first (*3*–*5*). The second wave in South Africa was coupled with the emergence of a new variant of severe acute respiratory syndrome coronavirus 2 (SARS-CoV-2), B.1.351, also known as 501Y.V2 or Beta (*6*).

South Africa reported >1.6 million laboratory-confirmed cases by mid-May 2021 (*3*), but many cases go undiagnosed because of mild or absent symptoms or the lack of (or reluctance to access) care or testing. Data on the proportion of persons with serologic evidence of prior SARS-CoV-2 infection are critical to assess infection rates, calculate infection–hospitalization ratios (IHRs) and infection–fatality ratios (IFRs), compare infection prevalence between waves of infection and to guide public health responses (*7*). SARS-CoV-2 seroprevalence is higher in close contacts of case-patients and at-risk healthcare workers and lower in persons <20 years of age or ≥65 years

Author affiliations: National Institute for Communicable Diseases of the National Health Laboratory Service, Johannesburg, South Africa (J. Kleynhans, S. Tempia, N. Wolter, A. von Gottberg, J.N. Bhiman, A. Buys, J. Moyes, W. Jassat, M. Neti, C. Cohen); University of the Witwatersrand, Johannesburg (J. Kleynhans, S. Tempia, N. Wolter, A. von Gottberg, J.N. Bhiman, J. Moyes, C. Cohen); Centers for Disease Control and Prevention, Atlanta, Georgia, USA (S. Tempia, M.L. McMorrow); Influenza Program, Centers for Disease Control and Prevention, Pretoria, South Africa (M.L. McMorrow); MRC/Wits Rural Public Health and Health Transitions Research Unit (Agincourt), University of the Witwatersrand, Johannesburg (K. Kahn, F.X. Gómez-Olivé, S. Tollman, F. Wafawanaka, J. du Toit); Perinatal HIV Research Unit, University of the Witwatersrand, Johannesburg (N.A. Martinson, L. Lebina); Johns Hopkins University Center for TB Research, Baltimore, Maryland, USA (N.A. Martinson); Ampath Pathology, Pretoria (M. Brauer)

DOI: https://doi.org/10.3201/eid2712.211465

[1]Additional members of the PHIRST-C group who contributed to this manuscript are listed at the end of this article.

of age, with no differences based on sex (*8*). Whether HIV infection increases the risk for SARS-CoV-2 infection is still unclear, and results from studies thus far have varied (*9*,*10*).

We describe the seroprevalence of SARS-CoV-2 in 2 household cohorts in a rural and an urban community at 5 timepoints from July 2020 to March 2021, during 2 epidemic waves. We compare disease prevalence between the first and second wave by comparing the seroprevalence by wave to reported laboratory-confirmed infections, hospitalizations, and deaths within the respective districts.

Methods

Study Population

We conducted a prospective study on a randomly selected household cohort in a rural community (Agincourt, Ehlanzeni District, Mpumalanga Province) and an urban community (Jouberton, Dr. Kenneth Kaunda District, North West Province) as part of the Prospective Household Study of SARS-CoV-2, Influenza, and Respiratory Syncytial Virus Community Burden, Transmission Dynamics, and Viral Interaction (PHIRST-C) study in South Africa. Methods for the cohort study are detailed in the Appendix (https://wwwnc.cdc.gov/EID/article/27/12/21-1465-App1.pdf). Recruitment to this study began in July 2020, and follow-up will continue through August 2021. Households that previously participated in the PHIRST study during 2016–2018 (*11*,*12*) and additional randomly selected households were eligible. Households with ≥3 household members of any age were enrolled if ≥80% of members consented.

The study was approved by the University of the Witwatersrand Human Research Ethics Committee (reference no. 150808). The US Centers for Disease Control and Prevention relied on local clearance (Institutional Review Board approval no. 6840).

Seroprevalence

We collected baseline data and blood (blood draw [BD] 1) at enrollment (July 20–September 17, 2020) and every 2 months thereafter: BD2, September 21–October 10; BD3, November 23–December 12, 2020; BD4, January 25–February 20, 2021; and BD5, March 22–April 11, 2021). We confirmed HIV status from medical records (if a person was HIV-infected) and by using a rapid test for participants with unknown or self-reported negative status. We determined previous SARS-CoV-2 infection by using the Roche Elecsys anti-SARS-CoV-2 assay (Roche Diagnostics, https://www.roche.ch/en/standorte/rotkreuz.htm) to detect antibodies against the SARS-CoV-2 nucleocapsid protein. We performed the assay on the Cobas e601 instrument (Roche Diagnostics), and we considered a cutoff index (COI) ≥1.0 as an indication of prior infection (i.e., seropositivity). We performed data analysis in Stata 14 (StataCorp, https://www.stata.com) (*13*). We adjusted seroprevalence estimates for sensitivity and specificity, as previously described (*14*), on the basis of the manufacturers' reported 99.5% sensitivity and 99.8% specificity (*15*). We obtained seroprevalence 95% credible intervals (CrIs) by using Bayesian inference with 10,000 posterior draws (*14*). We used Pearson's χ^2 test to assess the statistical significance of differences in SARS-CoV-2 seropositivity between the 2 communities and across BDs, waves of infection, and HIV status.

Calculation of Infection–Case Ratio, Infection–Hospitalization Ratio, and Infection–Fatality Ratio by Wave of Infection

To assess the prevalence of SARS-CoV-2 and compare the severity of illness between the 2 waves, we performed an ecologic study comparing estimated number of infections on the basis of seroprevalence in our cohort study to reported number of cases, hospitalizations, and in-hospital and excess deaths in the same district for each wave. We calculated the age- and sex-adjusted total number of infections, laboratory-confirmed cases, hospitalizations, deaths, infection–case ratio (ICR) (i.e., number of infections compared with laboratory-confirmed cases), IHR, and in-hospital and excess deaths IFR (Appendix) for the first (March 1–November 21, 2020) and second (November 22, 2020–March 27, 2021) wave of infection (Figure 1).

Comparison of Cases between First and Second Wave of Infection

We compared characteristics of participants who showed seroconversion during the first and second wave of infections by using unconditional logistic regression. We compared participants who showed seroconversion in wave 1 (BD3) with those who showed seroconversion in wave 2 (BD5, excluding BD3 seroconversions). For this analysis, we only included participants with a BD3 and BD5 paired serum sample. For the multivariable model, we assessed all variables that were significant at $p<0.2$ on univariate analysis and dropped nonsignificant factors ($p\geq0.05$) with manual backward elimination. We also compared the site, age, sex, and HIV status of persons with a BD

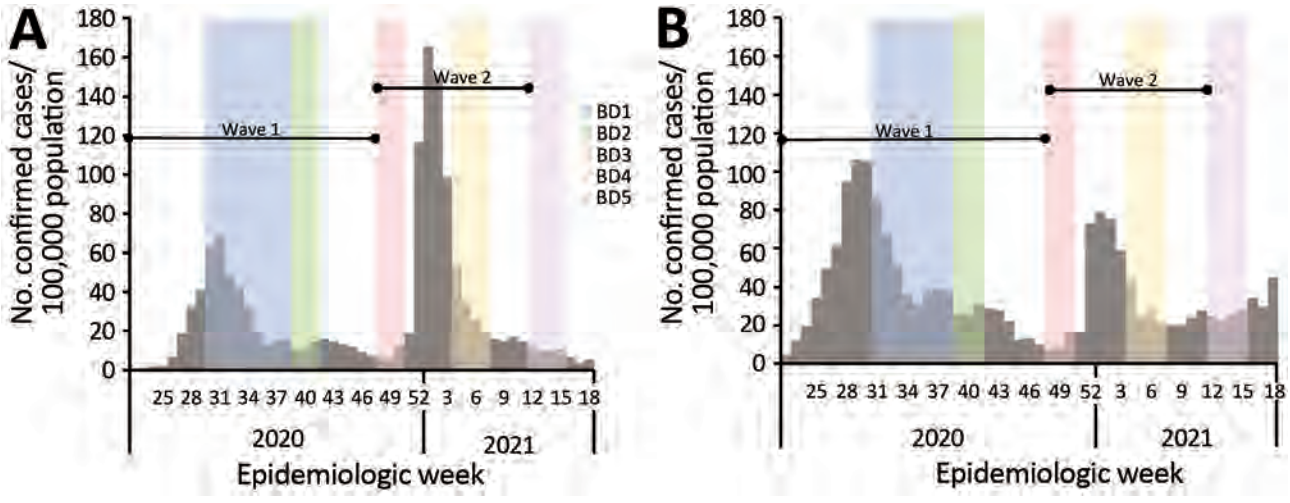

Figure 1. Timing of blood collection and weekly incidence of severe acute respiratory syndrome coronavirus 2 infection in the rural community district (A) and the urban community district (B), South Africa, March 2020–March 2021. BD, blood draw.

3+5 pair with those without a BD 3+5 pair by using logistic regression.

Persistence of SARS-CoV-2 Antibodies

For participants with 5 serum samples collected and who showed seroconversion during BD2 to BD5, we plotted COI values with the BD at which seroconversion took place as point 0. For participants who were seropositive at baseline, we plotted COI results from each BD. We calculated mean COI and the exact 95% CI at each point by using the Clopper–Pearson method. We assessed percentage of participants with COI $\geq$1 at each subsequent BD as number of participants with COI $\geq$1 divided by total number of participants who showed seroconversion during BD2 to BD5 with a serum sample at the timepoint.

Results

Study Population

In the rural community, we approached 185 households, 118 (64%) were enrolled, and 641/692 (92%) of household members consented, agreed to participate, or both. In the urban community, 352 households were approached, 114 (32%) enrolled, and 570/607 (93%) of household members consented, agreed to participate, or both. In both communities, the percentage of children, women or girls, and unemployed persons included in the cohort were higher than in district census data (Appendix Table 1). Median age was 13 (interquartile range 7–29) and 21 (interquartile range 10–43) years, and HIV prevalence was 14% (95% CI 11%–17%) in the rural community and 18% (95% CI 14%–21%) in the urban community.

Seroprevalence

Most (83% [n = 553]) participants who lived in the rural community and most (83% [n = 499]) who lived in the urban community had both BD3 and BD5 blood collected (Appendix). Seroprevalence, adjusted for assay sensitivity and specificity, in the rural community was lower at BD1 than in the urban community (1% [95% CrI 0%–2%] vs. 15% [95% CrI 12%–18%]; p<0.001), increasing after the first wave of infections (at BD3) to 7% (95% CrI 5%–9%) in the rural community and 27% (95% CrI 23%–31%) in the urban community (p<0.001) (Figure 2; Appendix). After the second wave (BD5), seroprevalence increased to 26% (95% CrI 22%–29%; p<0.001) in the rural community and to 41% (95% CrI 37%–45%; p<0.001) in the urban community (Appendix)..

At BD5, seroprevalence was highest in the 19–34 years age group (37% [95% CrI 28%–47%]) in the rural community and the 35–59 years age group (59% [95% CrI 49%–68%]) in the urban community (Figure 2; Appendix Table 3). The seroprevalence was lowest in children <5 years of age, 18% (95% CrI 10%–26%) in the rural community and 28% (95% CrI 17%–41%) in the urban community.

At BD5, SARS-CoV-2 seroprevalence was similar between HIV-infected and HIV-uninfected participants (Appendix Table 4). Persons who were HIV-positive were not more likely to be seropositive (adjusted odds ratio 1.0 [95% CI 0.7–1.5]).

Infection–Case Ratio, Infection–Hospitalization Ratio, and Infection–Fatality Ratio by District and Wave of Infection

During the first wave of infections (BD3) the age- and sex-adjusted seroprevalence at the rural site was

11.75% (95% CrI 3.42%–24.60%), resulting in an ICR of only 4.74% (95% CI 2.36%–15.62%). We observed a 0.64% (95% CI 0.34%–1.96%) IHR and an in-hospital IFR of 0.12% (95% CI 0.07%–0.31%) and an excess deaths IFR of 0.43% (95% CI 0.21%–1.47%) (Figure 3, 4).

The seroprevalence in the rural community was 22.43% (95% CrI 10.46%–37.67%) for the second wave. The ICR was 3.71% (95% CI 2.28%–7.68%), IHR was 0.61% (95% CI 0.40%–1.22%), in-hospital IFR was 0.18% (95% CI 0.12%–0.34%), and excess deaths IFR was 0.65% (95% CI 0.39%–1.39%) (Figure 3, 4).

In the urban community, the seroprevalence at BD3 was 29.58% (95% CrI 18.04%–43.20%). We found a 3.54% (95% CI 2.53%–5.55%) ICR and 1.93% (95% CI 1.41%–2.98%) IHR. The in-hospital IFR was 0.16% (95% CI 0.13%–0.23%) and excess deaths IFR was 0.12% (95% CI 0.09%–0.20%) (Figure 3, 4). During the second wave, the seroprevalence in the urban community was 15.19% (95% CrI 6.49%–26.96%), resulting in an ICR estimate of 3.67% (95% CI 2.21%–8.07%), an IHR of 2.29% (95% CI 1.39%–4.96%), an in-hospital IFR of 0.36% (95% CI 0.24%–0.72%), and an excess deaths IHR of 0.50% (95% CI 0.29%–1.17%) (Figure 3, 4). These estimates standardized to World Health Organization world population estimates are shown in Appendix Figure 2.

Comparison of Case-Patients between First and Second Wave of Infection

Compared with the urban community, persons in the rural community who showed seroconversion were 4.7 (95% CI 2.9–7.6) times more likely to show seroconversion during the second wave. Compared with persons 35–59 years of age, persons 5–12 years of age were 2.1 (95% CI 1.1–4.2) times more likely to show seroconversion in the second wave and persons ≥60 years of age were 2.8 (95% CI 1.1–7.0) times more likely to show seroconversion in the second wave (Table). When we stratified the analysis by site, this association was only detected in the urban community (Appendix Table 6). Persons who did not have a BD 3+5 pair were more likely to be <5 or 19–34 years of age (Appendix Table 7).

Persistence of SARS-CoV-2 Antibodies

Of the 72 participants who were seropositive at BD1 and with BDs 1–5 samples collected, 99% (71/72) still had a COI ≥1 by BD5. The mean COI at baseline for seropositive participants was 64, which increased to 125 at BD2 and dropped to 59 at BD5 (Figure 5, panel A). The participant who no longer had detectable SARS-CoV-2 antibodies at BD5 had a starting COI of 9. Of the 210 participants with BD 1–5 samples, 99% (167/169), 99% (70/71%), and 93% (41/44) still had a COI ≥1 in the first, second, and third BD after initial seroconversion, respectively (Figure 5, panel B). The participants who seroreverted had starting COIs ranging from 2 to 6, and none showed seroconversion again after reversion during the study period. The mean COI at the point of seroconversion was 48, which increased to 86 at the first BD after seroconversion and reduced to 61 at the third BD after seroconversion.

Discussion

We assessed SARS-CoV-2 seroprevalence in 1,211 persons living in 2 diverse communities in South Africa and show that laboratory-confirmed cases reported from study districts greatly underestimate the actual prevalence of SARS-CoV-2 infections. At baseline, seroprevalence was 1% and 15%, increasing to 7% and 27%, respectively, after the first wave, by March 2021. After the second epidemic wave, seroprevalence was

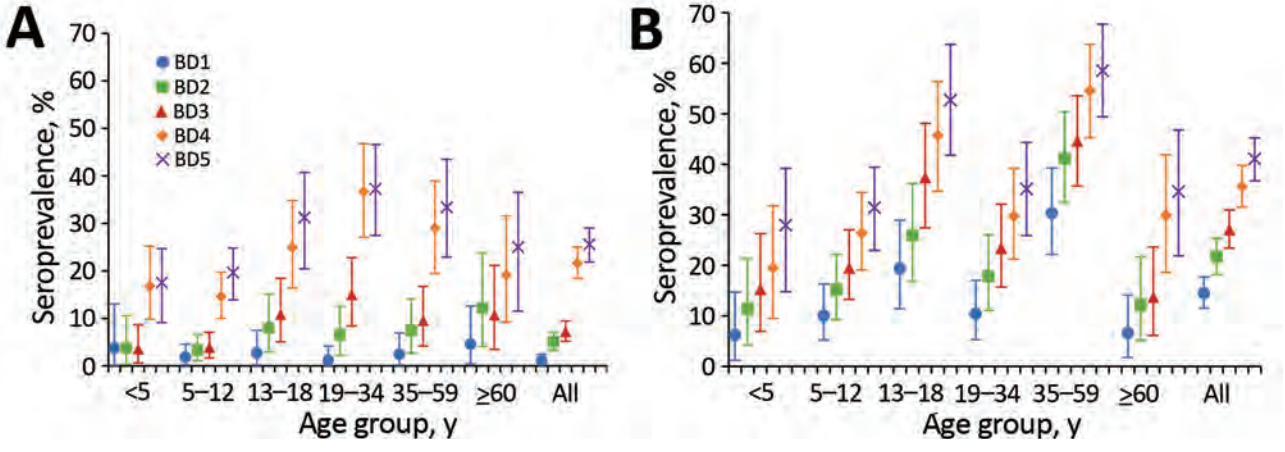

Figure 2. Seroprevalence of severe acute respiratory syndrome coronavirus 2 at each blood collection, by age group, in a rural community (A) and an urban community (B), South Africa, March 2020–March 2021.

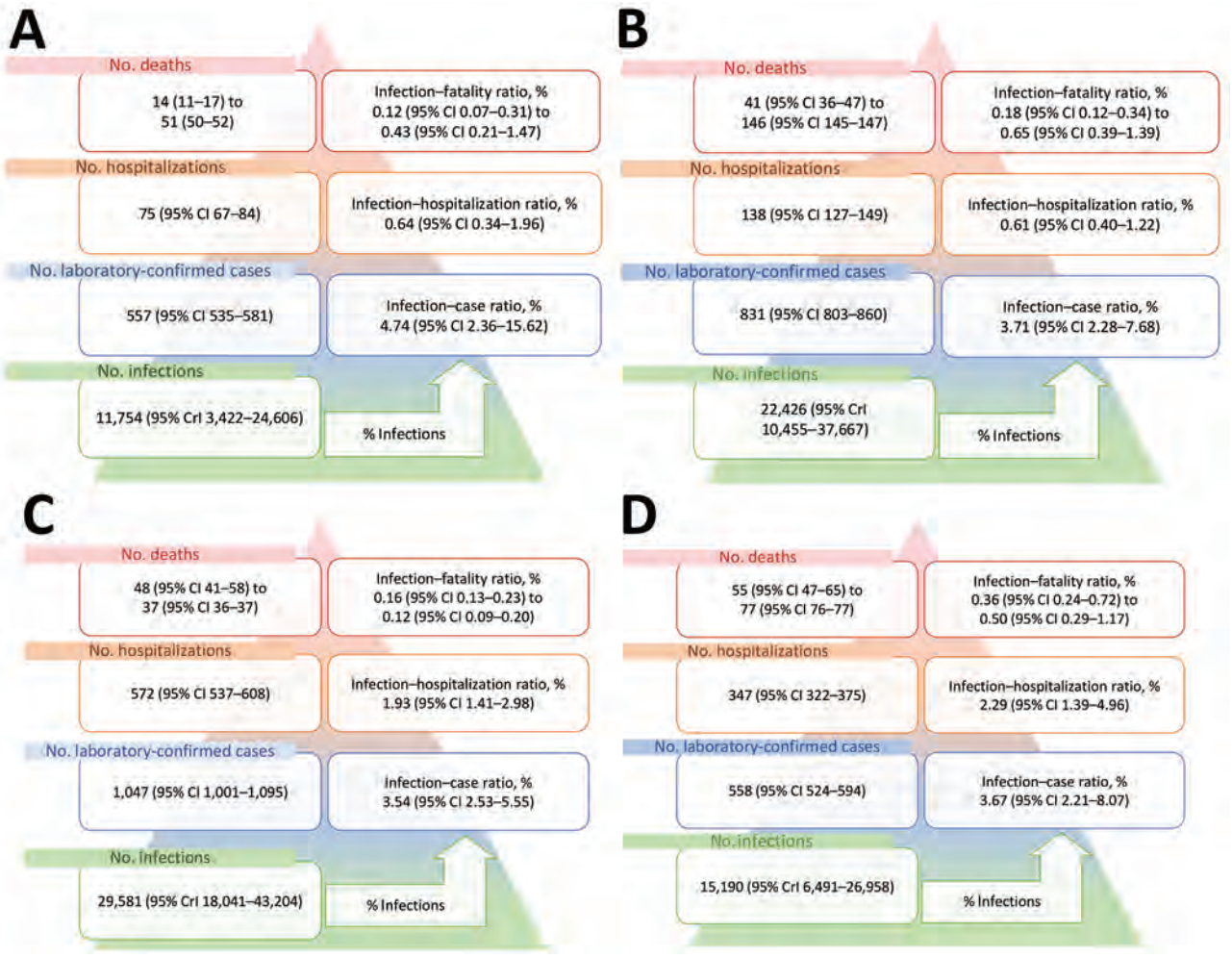

Figure 3. Age- and sex-standardized number of severe acute respiratory syndrome coronavirus 2 infections, laboratory-confirmed diagnoses, hospitalizations, and deaths per 100,000 population in a rural community during infection wave 1 (A) and wave 2 (B) and an urban community during infection wave 1 (C) and wave 2 (D), South Africa, March 2020–March 2021. CrI, credible interval.

26% in the rural community and 41% in the urban community. The highest seroprevalence was 59% in adults 35–59 years of age in the urban community, and the lowest was 18% in rural community children <5 years of age. During the second wave, compared with the first wave, the rural site was more affected, and infections in the second wave more likely affected children 5–12 and adults ≥60 years of age in the urban community. In the urban community, IFR was higher in the second wave (0.36%–0.50%) compared with the first (0.12%–0.16%), and numbers of infections were lower, suggesting possible increased severity associated with the emergence of novel variant B.1.351. Most persons who showed seroconversion maintained detectable SARS-CoV-2 antibodies in subsequent serum samples.

Low seropositivity was observed at the rural site at baseline, and seroprevalence remained low after the first wave of infections, reaching 7%, which was considerably lower than the 27% at the urban site at the same time. This observation could be related to the relatively isolated location and lower population density in the rural community compared with more densely populated urban community. Seroprevalence in the rural site increased to 26% after the second wave of infections within the district. This increase could have been attributable to possible increased transmissibility of the B.1.135 lineage that was circulating in the second wave (*16*), as well as additional transmission networks in the community during the December holiday period, when largescale urban-to-rural migration takes place as persons return home for year-end holidays. The urban site had fewer seroconversions in the second wave compared with the first, which may be attributable to existing immunity among persons in the community after the first wave.

As seen in previous studies (*8*), adults had the highest seroprevalence levels, although a relatively high seroprevalence of 18% and 28% persisted in children <5 years of age at the rural and urban community, respectively.

When comparing the characteristics of persons infected in the second wave to those infected in the first, persons infected in the second wave were more likely to be from the rural site and to be <13 or >60 years of age, compared with persons 35–59 years of age. The shift in age groups affected was only detected in the urban community, possibly because of the large number of adults infected during wave 1, whereas the number of infections in wave 1 in the rural community was lower.

A study conducted among blood donors in South Africa during the second wave found a seroprevalence of 32%–63% in 5 provinces of South Africa that have both rural and urban communities (W. Sykes et al., unpub. data, https://doi.org/10.21203/rs.3.rs-233375/v1). In our study, we observed a seroprevalence in adults ranging from 25% to 37% in rural households, and from 35% to 59% in urban households, suggesting that seroprevalence is heterogeneous between communities. In Kenya, the seroprevalence in blood donors during the country's first wave of infections was 4% and was also higher in urban communities (*17*). In a population-level household serosurvey conducted in Zambia during their first wave of infections, 11% of persons had evidence of SARS-CoV-2 infection (*18*).

Based on our estimates, only 4%–6% of cases were laboratory-confirmed, suggesting that substantially higher prevalence of infection was ascertained through serologic testing and that the differences may have been greater in the urban community than the rural community; however, more extensive studies are needed to assess whether this observation is consistent in other areas. Compared with the urban community, the rural community had less than half the rate of hospitalization (0.6% vs. 2.0%). These observations may be attributable to differences in referral and testing policies, health-seeking behavior, and access to care, as well as differences in circulating lineages within these districts.

A study comparing the severity of the first and second waves of infections in South Africa in hospitalized patients found a higher mortality rate in the second wave, compared with the first (*19*). At the urban site, the IFR was higher in the second wave (0.36%–0.50%) compared with the first (0.12%–0.16%), although no differences were observed in IHR between the 2 waves. The lower overall number of infections in the second wave in this site means that our finding of increased mortality is unlikely to be related to pressure on health services. The increased severity of the second wave may be related to increased severity of the B.1.135 variant, but further studies are needed to confirm this relation. The excess death IFR during the first wave in the urban site was smaller than the in-hospital IFR. This difference may be attributable to uncertainty on the process for excess death estimation, or that the 85% contribution of COVID-19 to excess deaths was an underestimation within the province. However, the in-hospital IFR followed the same trend of increase between wave 1 and 2 (0.16% to 0.36%). Although no significant increase was observed between the IFR in the rural community between wave

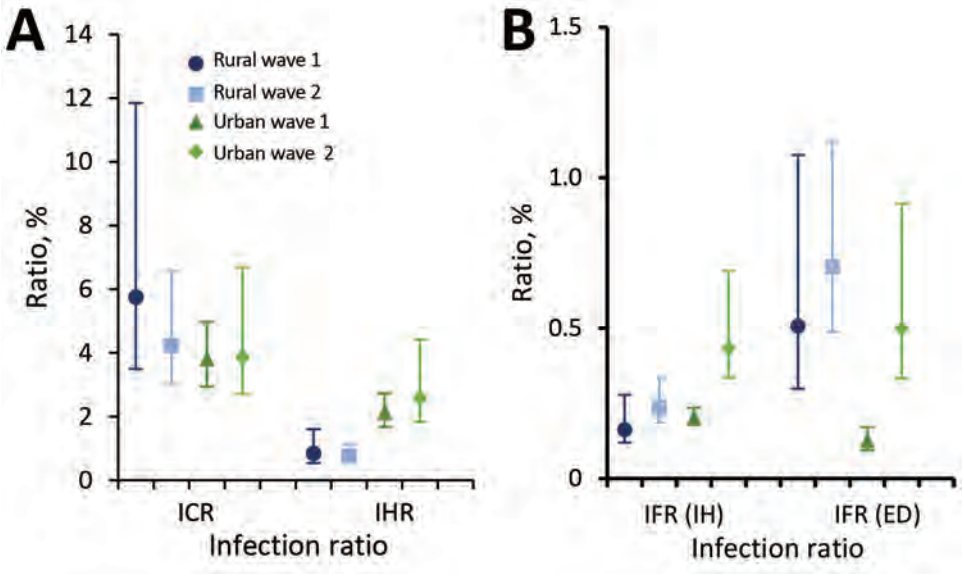

Figure 4. Severe acute respiratory syndrome coronavirus 2 infection–case and infection–hospitalization ratios (A) and in-hospital and excess deaths infection-fatality ratios (B) in a rural and urban community during the first and second wave of infections, South Africa, March 2020–March 2021. Vertical lines represent 95% CIs. Wave 1: March 1–November 21, 2020. Wave 2: November 2020 22–March 27, 2021. ED, excess deaths; ICR, infection–case ratio; IFR, infection–fatality ratio; IH, in-hospital; IHR, infection–hospitalization ratio.

Table. Comparison of participants with detectable SARS-CoV-2 antibodies after the first wave (blood draw 3) and second wave (blood draw 5), South Africa, July 2020–April 2021*

Characteristic	Infected in wave 1, no. (%)	Infected in wave 2, no. (%)	Univariate OR (95% CI)	Multivariable aOR (95% CI)
Site				
Rural	40/140 (29)	100/140 (71)	**4.9 (3.1–7.8)**	**4.7 (2.9–7.6)**
Urban	139/210 (66)	71/210 (34)	Referent	Referent
Sex				
M	65/123 (53)	58/123 (47)	Referent	
F	114/227 (50)	113/227 (50)	1.1 (0.7–1.7)	
Age group, y				
<5	9/25 (36)	16/25 (64)	**3.2 (1.3–8.0)**	2.7 (1.0–7.2)
5–12	30/74 (41)	44/74 (59)	**2.6 (1.4–4.9)**	**2.1 (1.1–4.2)**
13–18	36/64 (56)	28/64 (44)	1.4 (0.7–2.7)	1.3 (0.6–2.6)
19–34	34/67 (51)	33/67 (49)	1.7 (0.9–3.3)	1.3 (0.7–2.6)
35–59	59/92 (64)	33/92 (36)	Referent	Referent
≥60	11/28 (39)	17/28 (61)	**2.8 (1.2–6.6)**	**2.8 (1.1–7.0)**
HIV status				
Negative	139/271 (51)	132/271 (49)	1.0 (0.6–1.7)	
Positive	35/68 (51)	33/68 (49)	Referent	
CD4 count, cells/μL				
≥200	28/54 (52)	26/54 (48)	1.9 (0.2–21.7)	
<200	2/3 (67)	1/3 (33)	Referent	
Viral load, copies/mL				
<1,000	28/51 (55)	23/51 (45)	Referent	
≥1,000	2/7 (29)	5/7 (71)	3.0 (0.5–17.2)	
Other underlying illness‡				
No	161/316 (51)	155/316 (49)	1.1 (0.5–2.2)	
Yes	18/34 (53)	16/34 (47)	Referent	
Body mass index category				
Underweight	10/22 (45)	12/22 (55)	1.5 (0.6–3.9)	
Normal weight	65/141 (46)	76/141 (54)	1.5 (0.9–2.5)	
Overweight	46/84 (55)	38/84 (45)	1.1 (0.6–1.9)	
Obese	58/103 (56)	45/103 (44)	Referent	
Currently smoking‡				
No	109/190 (57)	81/190 (43)	Referent	
Yes	20/36 (56)	16/36 (44)	1.1 (0.5–2.2)	
Alcohol use‡				
No	88/167 (53)	79/167 (47)	2.0 (1.1–3.8)	
Yes	41/59 (69)	18/59 (31)	Referent	
Employment status§				
Unemployed	70/128 (55)	58/128 (45)	1.9 (0.5–6.4)	
Student	9/13 (69)	4/13 (31)	Referent	
Employed	25/41 (61)	16/41 (39)	1.4 (0.4–5.5)	

*Includes all participants with blood draw 3 and 5 serum pairs and who showed seroconversion at either draw. Bold indicates a statistically significant difference. aOR, adjusted odds ratio; OR, odds ratio; SARS-CoV-2, severe acute respiratory syndrome coronavirus 2.
†Self-reported history of asthma, lung disease, heart disease, stroke, spinal cord injury, epilepsy, organ transplant, immunosuppressive therapy, organ transplantation, cancer, liver disease, renal disease, or diabetes.
‡Among persons ≥15 years of age.
§Among persons ≥18 years of age.

1 and 2, the excess (maximum) IFR estimate (0.43%) was already high in wave 1, similar to the IFR for wave 2 in the urban community (0.50%). Considering the lower IHR in the rural community for both waves compared with the urban community, this observation may point toward lack of access to care or delays in seeking care. In-hospital SARS-CoV-2 mortality rates have previously also been shown to be higher in Mpumalanga Province where the rural community is located (*19*).

Our first wave in-hospital IFR estimates (0.12% rural, 0.16% urban) were similar to the age-adjusted 0.15% reported from India for the first wave of laboratory-confirmed deaths from SARS-CoV-2 infection (*20*). In addition, our first wave excess death IFR was higher in the rural (0.431%) and lower in the urban (0.12%) community compared with the age-adjusted 0.28% IFR excess deaths reported from Brazil during their first wave of infections (*21*).

Although previous studies have shown that antibodies against the SARS-CoV-2 nucleocapsid wanes more quickly than those against the spike protein (*22*,*23*), 93% of persons who showed seroconversion at BD2 still had detectable nucleocapsid antibodies 6 months later. Direct antigen-sandwich format assays, such as the Roche anti-N assay used in our study,

have been found to reliably detect antibodies in longitudinal samples (*24*). Of the few that seroreverted in this timeframe, the starting COI was low.

We did not observe a difference in SARS-CoV-2 seroprevalence in HIV-infected and HIV-uninfected persons at either site. Although our sample size was too small to detect small differences in a stratified analysis, we also did not observe a signal when using logistic regression. Because HIV causes immune suppression, a concern exists that HIV-infected persons may be more susceptible to SARS-CoV-2 infection (*9*,*10*). Although HIV infection may not increase susceptibility to infection, it has been demonstrated to be a risk factor for having onset of severe COVID-19 and death after infection (*9*,*25*).

Our study is limited by a small sample size, reducing the power for accurate seroprevalence estimates in small age strata, and inclusion of only 2 geographic sites, and therefore may not be representative of other districts and provinces in South Africa. Because we used seroprevalence to estimate infections by wave, we could have missed reinfections in the second wave. Based on data from the same cohort, these reinfections occurred in only a small portion (3%) of the cohort (C. Cohen et al., unpub. data, https://doi.org/10.1101/2021.07.20.21260855) and would have had a negligible influence on the infection ratios. ICR, IHR, and IFR formed part of an ecologic analysis, which is inherently prone to biases. Excess deaths in the first wave may be underestimated because the reporting period only started in June. Transmission dynamics within our cohort may not be similar to the transmission dynamics within the district. Seventeen percent of persons did not have a BD 3+5 pair, and bias could have been introduced if the seroprevalence were different for those without a BD 3+5 blood pair. Ongoing follow-up of this cohort will track future infections and monitor antibody waning, and compare these data to laboratory-confirmed infections and symptoms from twice-weekly follow-up.

A strength of our study is the collection of samples from prospectively followed-up persons from randomly selected households within the study communities and inclusion of persons of all ages. As a longitudinal study, our study provides the advantage

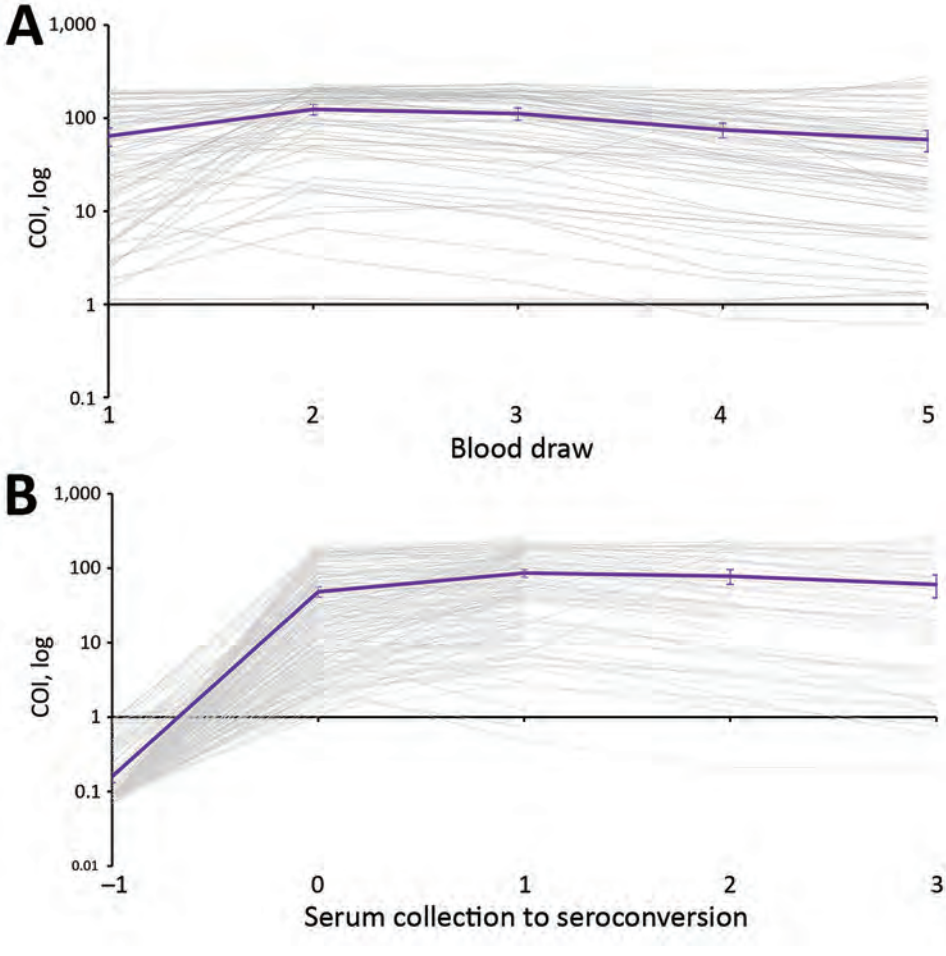

Figure 5. Cutoff index (COI) on Roche Elecsys (Roche Diagnostics, https://www.roche.ch/en/standorte/rotkreuz.htm) anti–severe acute respiratory syndrome coronavirus 2 assay for persons with blood draws 1–5 samples who were seropositive at baseline (A) or showed seroconversion during blood draws 2–5, South Africa, July 2020–April 2021. Purple line indicates mean COI with 95% CIs. COI values in panel B are aligned to first draw before seroconversion, COI, cutoff index.

of serial comparisons of antibody responses in relation to reported laboratory-confirmed SARS-CoV-2 infections within the community through 2 successive SARS-CoV-2 waves.

We estimate that ≈95% of SARS-CoV-2 infections in these 2 communities were not laboratory-confirmed and reported to the national surveillance system, which has major implications for contact tracing and isolation and other measures to contain infection. We observed heterogeneity between seroprevalence estimates based on pandemic wave, community, and age group, indicating the need for ongoing studies that include diverse settings.

Additional members of the PHIRST-C group who contributed to this manuscript were Kgaugelo Patricia Kgasago, Linda de Gouveia, Maimuna Carrim, Mignon du Plessis, Retshidisitswe Kotane, and Tumelo Moloantoa.

Acknowledgments

We thank all persons participating in the study and the field teams for their hard work and dedication to the study, especially Tumelo Moloantoa, Kgaugelo Kgasago, Nompumelelo Yende, and Sizzy Ngobeni for coordination of site activities; Charlotte Yaldwyn and Shingirai Chipungu for processing of collected bloods; the Centre for Respiratory Diseases and Meningitis Laboratory Team; Doreen Janse van Rensburg for managing logistics surrounding testing of collected bloods and result extraction; Nevashan Govender, Genevie Ntshoe, Andronica Moipone Shonhiwa, Darren Muganhiri, Itumeleng Matiea, Eva Mathatha, Fhatuwani Gavhi, Teresa Mashudu Lamola, Matimba Makhubele, Mmaborwa Matjokotja, Simbulele Mdleleni, and Masingita Makhubela from the national SARS-CoV-2 National Institute for Communicable Diseases Surveillance Team; Lincoln Darwin, Fazil Mckenna, Trevor Graham Bell, Ndivhuwo Munava, Muzammil Raza Bano, and Jimmy Khosa from National Institute for Communicable Diseases Information Technology Department; Rob Dorrington from the Centre for Actuarial Research for providing wave-specific excess death estimates; Ben Cowling, Kanta Subbarao, Juliet Pulliam, Melissa Rolfes, and Mosa Moshabela from the PHIRST-C Scientific Committee; and Andrew Whitelaw, June Fabian, Jennifer Verani, Lindiwe Qwabe, Banele Faku, and Saheen Methar from the PHIRST-C Safety Committee.

This work was supported by the National Institute for Communicable Diseases of the National Health Laboratory Service and the US Centers for Disease Control and Prevention (cooperative agreement no. 6U01IP001048-04-02 awarded to C.C.). C.C. reports receiving grant funds from US Centers for Disease Control and Prevention, Wellcome Trust, and South African Medical Research Council.

The investigators welcome enquiries about possible collaborations and requests for access to the dataset. Data will be shared after approval of a proposal and with a signed data access agreement. Investigators interested in more details about this study, or in accessing these resources, should contact the corresponding author.

About the Author

Ms. Kleynhans is an epidemiologist in the Centre for Respiratory Diseases and Meningitis, National Institute for Communicable Diseases. Her primary research interests include the epidemiology of respiratory diseases like influenza and COVID-19, vaccine impact studies, and modelling of infectious disease transmission dynamics.

References

1. National Institute for Communicable Diseases. COVID-19 testing summary. 2021 12 Feb 2021 [cited 2021 Feb 16]. https://www.nicd.ac.za/wp-content/uploads/2021/03/COVID-19-Testing-Summary-Week-8-2021.pdf
2. Salyer SJ, Maeda J, Sembuche S, Kebede Y, Tshangela A, Moussif M, et al. The first and second waves of the COVID-19 pandemic in Africa: a cross-sectional study. Lancet. 2021;397:1265–75. https://doi.org/10.1016/S0140-6736(21)00632-2
3. National Institute for Communicable Diseases. COVID-19 weekly epidemiology brief, week 19. 2021 May 22 [cited 2021 May 22]. https://www.nicd.ac.za/wp-content/uploads/2021/05/COVID-19-Weekly-Epidemiology-Brief-week-19-2021.pdf
4. National Institute for Communicable Diseases. COVID-19 sentinel hospital surveillance update, week 18. 2021 May 14 [cited 2021 May 22]. https://www.nicd.ac.za/wp-content/uploads/2021/05/NICD-COVID-19-Weekly-Sentinel-Hospital-Surveillnace-update-Week-18-2021.pdf
5. South African Medical Research Council. Report on weekly deaths in South Africa, week 18. 2021 May 10 [cited 2021 May 22]. https://www.samrc.ac.za/reports/report-weekly-deaths-south-africa
6. Wibmer CK, Ayres F, Hermanus T, Madzivhandila M, Kgagudi P, Oosthuysen B, et al. SARS-CoV-2 501Y.V2 escapes neutralization by South African COVID-19 donor plasma. Nat Med. 2021;27:622–5. https://doi.org/10.1038/s41591-021-01285-x
7. Murhekar MV, Clapham H. COVID-19 serosurveys for public health decision making. Lancet Glob Health. 2021;9:e559–60. https://doi.org/10.1016/S2214-109X(21)00057-7
8. Chen X, Chen Z, Azman AS, Deng X, Sun R, Zhao Z, et al. Serological evidence of human infection with SARS-CoV-2: a systematic review and meta-analysis. Lancet Glob Health. 2021;9:e598–609. https://doi.org/10.1016/S2214-109X(21)00026-7
9. Spinelli MA, Lynch KL, Yun C, Glidden DV, Peluso MJ, Henrich TJ, et al. SARS-CoV-2 seroprevalence, and IgG concentration and pseudovirus neutralising antibody titres after infection, compared by HIV status: a matched case-control observational study. Lancet HIV. 2021;8:e334–41. https://doi.org/10.1016/S2352-3018(21)00072-2

10. Ssentongo P, Heilbrunn ES, Ssentongo AE, Advani S, Chinchilli VM, Nunez JJ, et al. Epidemiology and outcomes of COVID-19 in HIV-infected individuals: a systematic review and meta-analysis. Sci Rep. 2021;11:6283. https://doi.org/10.1038/s41598-021-85359-3
11. Cohen C, McMorrow ML, Martinson NA, Kahn K, Treurnicht FK, Moyes J, et al. Cohort profile: a prospective household cohort study of influenza, respiratory syncytial virus and other respiratory pathogens community burden and transmission dynamics in South Africa, 2016–2018. Influenza Other Respir Viruses. 2021 Jul 23 [Epub ahead of print].
12. Cohen C, Kleynhans J, Moyes J, McMorrow ML, Treurnicht FK, Hellferscee O, et al.; PHIRST group. Asymptomatic transmission and high community burden of seasonal influenza in an urban and a rural community in South Africa, 2017-18 (PHIRST): a population cohort study. Lancet Glob Health. 2021;9:e863–74. https://doi.org/10.1016/S2214-109X(21)00141-8
13. South African Government. COVID-19: vaccine strategy. 2021[cited 2021 Feb 16]. https://sacoronavirus.co.za/2021/01/03/covid-19-vaccine-strategy
14. Larremore DB, Fosdick BK, Bubar KM, Zhang S, Kissler SM, Metcalf CJE, et al. Estimating SARS-CoV-2 seroprevalence and epidemiological parameters with uncertainty from serological surveys. eLife. 2021;10:e64206. https://doi.org/10.7554/eLife.64206
15. Roche. Elecsys anti-SARS-CoV-2. 2020 [cited 2021 Mar 21]. https://diagnostics.roche.com/global/en/products/params/elecsys-anti-sars-cov-2.html
16. Tegally H, Wilkinson E, Giovanetti M, Iranzadeh A, Fonseca V, Giandhari J, et al. Detection of a SARS-CoV-2 variant of concern in South Africa. Nature. 2021;592:438–43. https://doi.org/10.1038/s41586-021-03402-9
17. Uyoga S, Adetifa IMO, Karanja HK, Nyagwange J, Tuju J, Wanjiku P, et al. Seroprevalence of anti-SARS-CoV-2 IgG antibodies in Kenyan blood donors. Science. 2021;371:79–82. https://doi.org/10.1126/science.abe1916
18. Mulenga LB, Hines JZ, Fwoloshi S, Chirwa L, Siwingwa M, Yingst S, et al. Prevalence of SARS-CoV-2 in six districts in Zambia in July, 2020: a cross-sectional cluster sample survey. Lancet Glob Health. 2021;9:e773–81. https://doi.org/10.1016/S2214-109X(21)00053-X
19. Jassat W, Mudara C, Ozougwu L, Tempia S, Blumberg L, Davies M-A, et al.; DATCOV author group. Difference in mortality among individuals admitted to hospital with COVID-19 during the first and second waves in South Africa: a cohort study. Lancet Glob Health. 2021;9:e1216–25. https://doi.org/10.1016/S2214-109X(21)00289-8
20. Murhekar MV, Bhatnagar T, Selvaraju S, Rade K, Saravanakumar V, Vivian Thangaraj JW, et al. Prevalence of SARS-CoV-2 infection in India: findings from the national serosurvey, May–June 2020. Indian J Med Res. 2020;152:48–60. https://doi.org/10.4103/ijmr.IJMR_3290_20
21. Silva AAMD, Lima-Neto LG, Azevedo CMPES, Costa LMMD, Bragança MLBM, Barros Filho AKD, et al. Population-based seroprevalence of SARS-CoV-2 and the herd immunity threshold in Maranhão. Rev Saude Publica. 2020;54:131. https://doi.org/10.11606/s1518-8787.2020054003278
22. Lumley SF, Wei J, O'Donnell D, Stoesser NE, Matthews PC, Howarth A, et al.; Oxford University Hospitals Staff Testing Group. The duration, dynamics, and determinants of severe acute respiratory syndrome coronavirus 2 (SARS-CoV-2) antibody responses in individual healthcare workers. Clin Infect Dis. 2021;73:e699–709. https://doi.org/10.1093/cid/ciab004
23. Fenwick C, Croxatto A, Coste AT, Pojer F, André C, Pellaton C, et al. Changes in SARS-CoV-2 spike versus nucleoprotein antibody responses impact the estimates of infections in population-based seroprevalence studies. J Virol. 2021;95:e01828–20. https://doi.org/10.1128/JVI.01828-20
24. Di Germanio C, Simmons G, Kelly K, Martinelli R, Darst O, Azimpouran M, et al. SARS-CoV-2 antibody persistence in COVID-19 convalescent plasma donors: dependency on assay format and applicability to serosurveillance. Transfusion. 2021 Jun 15 [Epub ahead or print]. https://doi.org/10.1111/trf.16555
25. Western Cape Department of Health and National Institute for Communicable Diseases SA. Risk factors for coronavirus disease 2019 (COVID-19) death in a population cohort study from the Western Cape Province, South Africa. Clin Infect Dis. 2020 Aug 29 [Epub ahead of print].

Address for correspondence: Jackie Kleynhans, Centre for Respiratory Diseases and Meningitis, National Institute for Communicable Diseases of the National Health Laboratory Service, 1 Modderfontein Rd, Sandringham, 2192, Johannesburg, South Africa; email: jackiel@nicd.ac.za

Human Melioidosis Caused by Novel Transmission of *Burkholderia pseudomallei* from Freshwater Home Aquarium, United States[1]

Patrick Dawson,[2] Monique M. Duwell,[2] Mindy G. Elrod, Ruth J. Thompson, David A. Crum, Ruth M. Jacobs, Jay E. Gee, Cari B. Kolton, Lindy Liu, David D. Blaney, LaToya Griffin Thomas, Denise Sockwell, Zachary Weiner, William A. Bower, Alex R. Hoffmaster, Johanna S. Salzer

Nearly all cases of melioidosis in the continental United States are related to international travel to areas to which *Burkholderia pseudomallei*, the bacterium that causes melioidosis, is endemic. We report the diagnosis and clinical course of melioidosis in a patient from the United States who had no international travel history and the public health investigation to determine the source of exposure. We tested environmental samples collected from the patient's home for *B. pseudomallei* by PCR and culture. Whole-genome sequencing was conducted on PCR-positive environmental samples, and results were compared with sequences from the patient's clinical specimen. Three PCR-positive environmental samples, all collected from a freshwater home aquarium that had contained imported tropical fish, were a genetic match to the clinical isolate from the patient. This finding suggests a novel route of exposure and a potential for importation of *B. pseudomallei*, a select agent, into the United States from disease-endemic areas.

Melioidosis is a severe, potentially life-threatening bacterial disease caused by *Burkholderia pseudomallei*, a gram-negative bacterium found in water and soil in tropical and subtropical environments worldwide (*1*). Melioidosis might manifest as localized, pulmonary, systemic, or disseminated infections. However, melioidosis symptoms are nonspecific, and it is often misdiagnosed (*1*,*2*). Exposure to *B. pseudomallei* occurs through inhalation of contaminated dust or water droplets, ingestion of contaminated water, and direct contact with contaminated water or soil, particularly through cuts or abrasions (*3*). The incubation period in acute cases ranges from 1 to 21 days, although activation of latent infections might develop many years later (*4*,*5*). Persons at greater risk for developing melioidosis include those with diabetes, liver disease, renal disease, chronic lung disease, thalassemia, cancer, and other immunocompromising conditions (*6*,*7*).

Melioidosis (formerly Whitmore's disease) was described in 1912 (*8*), and cases were historically identified primarily in northern Australia and areas of Southeast Asia, such as Thailand, where melioidosis is hyperendemic (*9*). However, the known geographic range has expanded considerably in recent decades; the estimated global burden is 165,000 human cases/year (*10*). On the basis of clinical cases or environmental isolation, *B. pseudomallei* is now suspected to be endemic to the environment in parts of Central and South America, the Caribbean, Mexico, and potentially in areas of the continental United States, such as Texas (*11*–*14*). Despite increased recognition of the expansive range of *B. pseudomallei*,

Author affiliations: Centers for Disease Control and Prevention, Atlanta, Georgia, USA (P. Dawson, M.G. Elrod, J.E. Gee, C.B. Kolton, L. Liu, D.D. Blaney, Z. Weiner, W.A. Bower, A.R. Hoffmaster, J.S. Salzer); Maryland Department of Health, Baltimore, Maryland, USA (M.M. Duwell, R.J. Thompson, D.A. Crum); Holy Cross Germantown Hospital, Germantown, Maryland, USA (R.M. Jacobs); Virginia Department of General Services, Richmond, Virginia, USA (L. Griffin Thomas); Virginia Department of Health, Richmond (D. Sockwell)

DOI: https://doi.org/10.3201/eid2712.211756

[1]Preliminary results of this study were presented at the Virtual IDWeek 2020 Conference; October 21–25, 2020.

[2]These authors contributed equally to this article.

nearly all US cases are related to previous residence in or travel to disease-endemic areas outside the continental United States (*15*).

Case Report

In October 2019, the US Centers for Disease Control and Prevention (CDC) was notified by the Maryland Department of Health and through the CDC Laboratory Response Network (LRN) of a preliminary positive bacterial isolate of *B. pseudomallei* from a blood culture specimen from a Maryland resident. The clinical specimen had been forwarded to the Virginia Division of Consolidated Laboratory Services, where it was confirmed, and shipped to CDC for simultaneous confirmation and genomic analysis.

The patient, a 56-year-old woman, was hospitalized on September 20, 2019 (day 0; Figure), because of fever, cough, and chest pain with onset 2 days earlier. The patient had a history of polymyositis, rheumatoid arthritis, and diabetes mellitus, and reported to have stopped long-term immunosuppressive medications (methotrexate, azathioprine, and prednisone) 1 month before symptom onset.

A thoracic radiograph on day 0 showed a right perihilar and lower lobe infiltrate, consistent with pneumonia. A noncontrast computed tomography (CT) scan on day 3 showed air space consolidation in the right lower lobe consistent with pneumonia, additional bibasilar air space densities, and a small right pleural effusion. Other notable clinical laboratory results at presentation included an increased leukocyte count of 22,800 cells/μL (reference range 4,500–11,000 cells/μL) and a decreased sodium level of 125 mmol/L (reference range 135–145 mmol/L).

We obtained blood cultures on day 0 before administration of antimicrobial drugs. Gram-negative rods were identified in 4 initial blood cultures; the rods were subsequently identified as *B. pseudomallei*. Three additional blood cultures obtained on days 2–4 grew the same organism. The patient was given ceftriaxone and azithromycin on days 0–3, then on day 4, treatment was changed to meropenem after *B. pseudomallei* was identified. The patient showed gradual symptom improvement; fever resolved, and leukocyte count normalized. The intensive phase duration was extended because of persistent bacteremia. She was discharged on day 11 and continued taking intravenous meropenem as an outpatient. Antimicrobial drug susceptibility testing was not performed because the patient had been

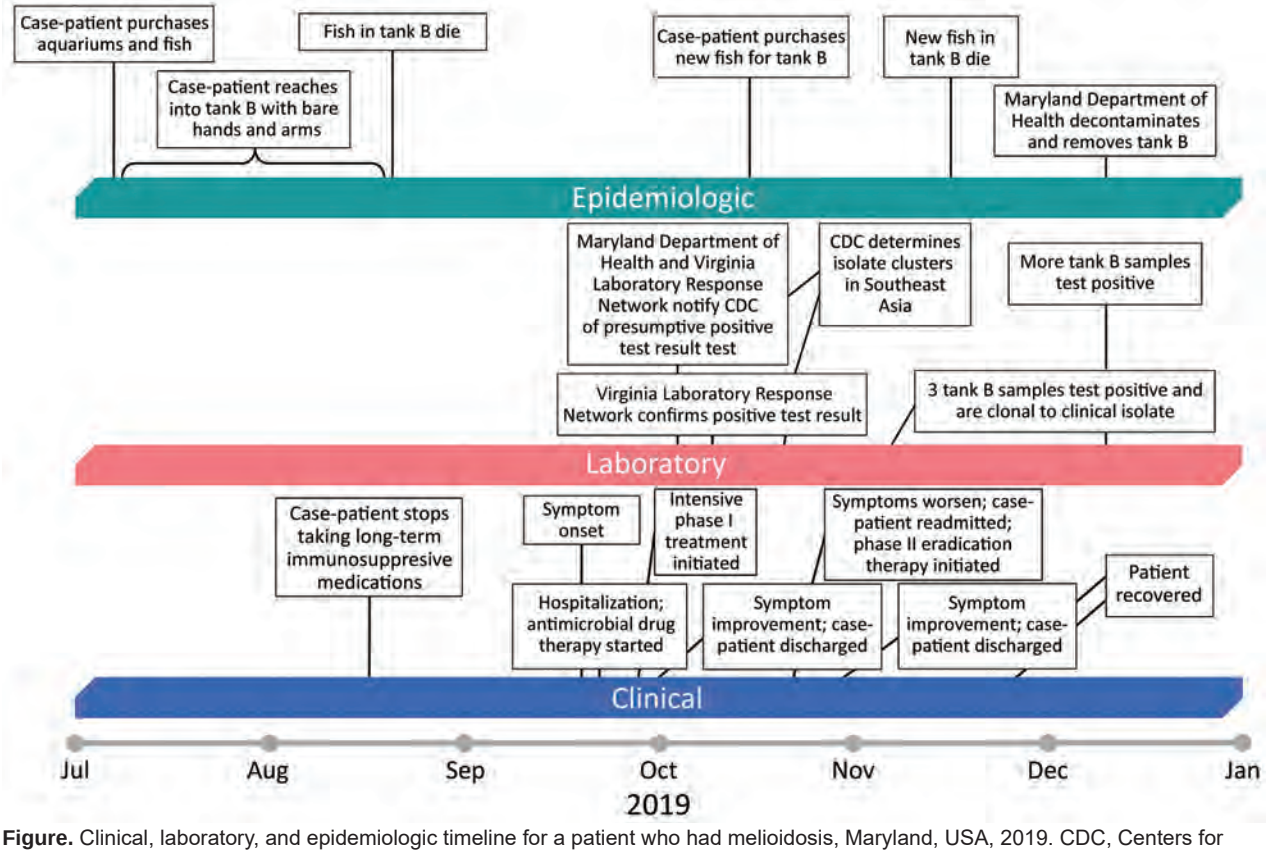

Figure. Clinical, laboratory, and epidemiologic timeline for a patient who had melioidosis, Maryland, USA, 2019. CDC, Centers for Disease Control and Prevention.

responding to treatment with meropenem before LRN confirmation of *B. pseudomallei*.

After 3 weeks of taking meropenem, the patient's leukocyte count increased to 14,700 cells/μL, and fever developed (temperature 100.1°F [37.8°C]). A repeat CT scan showed a patchy opacity at the right lung base and bilateral interstitial process consistent with pneumonia, but a 45 × 24 mm mass in the right lung posteriorly could not be excluded and increased concern for pulmonary abscess. The patient was readmitted, sulfamethoxazole/trimethoprim was given, and treatment with meropenem continued. She clinically improved and was discharged after 1 week. Repeat, noncontrast, thoracic CT scans showed improvement of right basilar consolidation after 6 weeks of meropenem and sulfamethoxazole/trimethoprim and resolution after 10 weeks. The patient completed eradication therapy with a 10-week course of meropenem and 12-week course of sulfamethoxazole/trimethoprim.

Methods

Case Investigation

We conducted an initial epidemiologic investigation to assess the travel history of the patient and other possible exposures to *B. pseudomallei*. Interviews were conducted October–December 2019, with the patient and other household members. After establishing no international travel history and identification of positive environmental samples, the interviews focused on the freshwater home aquariums, tropical fish, and contact with the fish and aquariums of the patient.

Environmental Sampling

During November 2019, the investigation team visited the home of the patient to collect environmental samples and assess potential sources of *B. pseudomallei*. The patient had 2 freshwater aquariums (tanks A and B, both ≈5 liters). We collected bulk water samples (≈50 mL) from each aquarium and swab specimens of biofilms (3 from tank A and 2 from tank B). We collected an additional 16 samples, including swab specimens of all household faucets, soil from potted plants and around the property, 2 beauty products, and 4 liquid vaping products. During December 2019, the team collected 6 additional specimens: bulk water from tanks A and B, gravel from tank B, filters from tank B, dead fish carcasses from tank B, and a dry artificial plant that had been in tank B but was removed during August 2019. During the second visit, the Maryland Department of Health also performed decontamination, removal, and safe disposal of fish tank B from the home of the patient.

Laboratory Confirmation

The clinical isolate was confirmed as *B. pseudomallei* at the Virginia Division of Consolidated Laboratory Services and CDC by using the LRN algorithm, including biochemicals and PCR. All 29 environmental samples were sent to CDC for culture and identification. We directly inoculated all environmental samples into TBSS-C50 (Galimand) broth and incubated broths in a shaking incubator at 37°C for 6 days. We then cultured enriched broths onto Ashdown agar, and extracted DNA by using a QIAamp Fast Stool Mini Kit (QIAGEN, https://www.qiagen.com) or testing by real-time PCR. Suspected colonies from Ashdown agar were selected for further workup, and confirmation of isolates followed the LRN algorithm.

Multilocus Sequence Typing and Whole-Genome Sequencing

CDC performed multilocus sequence typing on isolate MD2019a (clinical). CDC also performed whole-genome sequencing (WGS) for isolates MD2019a (clinical), MD2019b (water from tank B collected during November 2019), and MD2019c (swab specimen of biofilms from tank B collected during November 2019) by using the Nextera FLEX Kit (https://www.illumina.com) for library preparation and the iSeq 100 instrument (Illumina) with a 2 × 151-bp kit. We analyzed draft genomes along with a reference panel of *B. pseudomallei* genomes from publicly available sources representing geographic diversity by using Parsnp in the HARVEST 1.3 suite (https://harvest.readthedocs.io/en/latest/content/parsnp.html) to detect single-nucleotide polymorphisms (SNPs).

Results

Initial Investigation

The initial epidemiologic investigation showed that the patient was a long-time resident of Maryland who had never traveled outside the continental United States. She reported previous pet ownership of reptiles and cats >5 years ago. She denied any other direct soil or environmental water exposure. She also denied use of herbal products or products known to be imported from Asia or Australia. She reported use of vaping products. No family members or close contacts had an illness similar to that of the patient.

Multilocus sequence typing yielded sequence type 369, which had been seen in examples from Malaysia, Thailand, and Vietnam (*16*). WGS of the

clinical isolate, MD2019a, showed that when compared to a panel of publicly available genomes composed to represent geographic diversity, it clustered with genomes from Southeast Asia predominantly associated with Singapore and Malaysia (Appendix Figure, https://wwwnc.cdc.gov/EID/article/27/12/21-1756-App1.pdf). The genetic link of the isolate to Southeast Asia, coupled with lack of international travel history for the patient, led the investigation team to conduct follow-up interviews and environmental sampling in the home of the patient.

Isolation of *B. pseudomallei* from Environmental Samples

Of the 23 environmental samples collected during November 2019, a total of 3 samples, all from tank B, were positive for *B. pseudomallei* by culture and real-time PCR. All other November 2019 samples were negative. The water and gravel samples from tank B collected during December 2019 were also positive for *B. pseudomallei* by PCR and culture. The artificial plant that was removed from the tank during August 2019 was positive by PCR, but no growth was observed in culture. The December 2019 water sample from tank A was negative.

Genetic Match of Aquarium Isolates with the Clinical Isolate

Comparison of the draft genome sequences between the clinical isolate (MD2019a) and the 2 aquarium samples from tank B (MD2019b and MD2019c) showed no SNPs between MD2019a and MD2019c, and only 1 SNP was detected between MD2019a and MD2019b. This finding indicates that all 3 isolates were clonal.

Follow-Up Patient Interviews

The patient reported she had purchased fish, aquariums, and associated supplies during July 2019 (Figure). She purchased the tanks and gravel substrate at a large retail store. She purchased 3 cherry barbs (*Puntius titteya*) for tank A from a retail pet store, and all were alive at the time of her interview. She purchased 3 fancy-tailed guppies (*Poecilia reticulata*) for tank B from the same store, and they died during August 2019. During October 2019, after her illness onset, she purchased 3 tiger barbs (*Puntigrus tetrazona*) for tank B from the same store, and they died during November 2019.

The patient reported that the water in tank B was persistently cloudier than the water in tank A and more difficult to keep clean. She reported that she was the primary caretaker of the fish and recalled reaching bare hands and arms into the water and gravel of tank B to disrupt sediment while cleaning it, as recently as August 2019.

Discussion

This investigation of a patient who had melioidosis and no history of travel to disease-endemic areas provides strong evidence for documented transmission of *B. pseudomallei* from a freshwater home aquarium to a human. Although this type of transmission has not been described in the literature, contamination of aquarium transport water with *B. pseudomallei* used for freshwater tropical fish originating from Singapore has been reported in France (*17*). Furthermore, freshwater fishing practices have been identified as risk factors in countries to which melioidosis is endemic (*7*,*18*,*19*).

With freshwater aquariums as a newly recognized source of possible transmission of *B. pseudomallei* to humans, further investigations are underway to determine the extent of *B. pseudomallei* contamination at the pet store retailer where the patient purchased the pet fish with accompanying aquarium water and at the vendors that imported and supplied freshwater ornamental fish, aquatic plants, and associated aquarium water to this retail location. Because these vendors might distribute freshwater animals and aquatic plants to pet store retailers throughout the United States, identifying possible source(s) of introduction with *B. pseudomallei* in the supply chain is essential to public health.

Federal regulators classify *B. pseudomallei* as a Tier 1 Select Agent because of its heightened risk for deliberate misuse and major potential for mass casualties, economic disruption, critical infrastructure effects, or damaging public confidence (*20*). The United States is the largest importer of ornamental fish, most of which are freshwater and originate in Southeast Asia (*21*,*22*), where *B. pseudomallei* is widespread in the environment. An estimated 11.5 million US households have pet fish; ≈139 million freshwater fish are owned (*23*,*24*). Determining where in the supply chain introduction of the bacteria might occur can lead to development of enhanced surveillance and mitigation procedures at the critical control points, which might prevent further introductions and spread of the bacteria to retailers and homes of consumers.

To prevent or reduce risk of exposure, particularly among persons who have major risk factors, simple precautions can be taken when handling freshwater fish, snails, aquatic plants, aquariums, or other materials in contact with aquarium

water, such as gravel, substrate, decorations, filters, and other equipment. CDC recommends thorough handwashing with soap and water before and after handling or cleaning aquariums and feeding fish, wearing gloves to cover any cuts or wounds in the hand while handling fish or aquariums or allowing wounds to fully heal first, avoiding cleaning fish aquariums if immunocompromised or in areas where immunocompromised persons might be present, and not allowing children <5 years of age to clean fish aquariums (*25*).

This report highlights the essential role of molecular epidemiology in public health investigations of melioidosis cases, which identified the likely geographic origin of the bacteria and prompted a public health response that characterized a novel route of exposure. There is growing evidence that US melioidosis cases are not limited to international travelers, including a 2021 multistate cluster involving an organism that is not clonal to the isolates described here, as determined by WGS (*14*,*26*–*29*).

We urge clinicians in the United States to consider melioidosis in patients who have clinically compatible symptoms and exposure to tropical ornamental fish and freshwater aquariums, particularly if patients are immunocompromised, even though such exposure events might be exceedingly rare and few persons show development of melioidosis after exposure to *B. pseudomallei* (*5*). This organism might be difficult for hospital laboratories to diagnose, and automated identification systems in clinical laboratories can misidentify *B. pseudomallei*, highlighting the need for LRN confirmation (*28*).

Clinicians treating melioidosis should consult established treatment guidelines, which were updated in 2020 (*30*,*31*). Likewise, public health investigators should consider inquiring about pet freshwater fish exposure in patients given a diagnosis of melioidosis who have not traveled to a disease-endemic area or have only traveled to locations inconsistent with the geographic profile of the genome of their isolate.

Acknowledgment

We thank David Blythe for providing contributions to this study.

About the Author

Dr. Dawson is an epidemiologist in the Office of Science, Centers for Disease Control and Prevention, Atlanta, GA. His primary research interests are emerging infectious diseases, zoonotic diseases, and health equity.

References

1. Wiersinga WJ, Currie BJ, Peacock SJ. Melioidosis. N Engl J Med. 2012;367:1035–44. https://doi.org/10.1056/NEJMra1204699
2. Hoffmaster AR, AuCoin D, Baccam P, Baggett HC, Baird R, Bhengsri S, et al. Melioidosis diagnostic workshop, 2013. Emerg Infect Dis. 2015;21:e141045.
3. Centers for Disease Control and Prevention. Melioidosis transmission [cited 2021 Sep 17]. https://www.cdc.gov/melioidosis/transmission/index.html.
4. Currie BJ, Fisher DA, Howard DM, Burrow JN, Selvanayagam S, Snelling PL, et al. The epidemiology of melioidosis in Australia and Papua New Guinea. Acta Trop. 2000;74:121–7. https://doi.org/10.1016/S0001-706X(99)00060-1
5. Currie BJ. Melioidosis: evolving concepts in epidemiology, pathogenesis, and treatment. Semin Respir Crit Care Med. 2015;36:111–25. https://doi.org/10.1055/s-0034-1398389
6. Centers for Disease Control and Prevention. Melioidosis signs and symptoms [cited 2021 Sep 17]. https://www.cdc.gov/melioidosis/symptoms/index.html
7. Currie BJ, Ward L, Cheng AC. The epidemiology and clinical spectrum of melioidosis: 540 cases from the 20 year Darwin prospective study. PLoS Negl Trop Dis. 2010;4:e900. https://doi.org/10.1371/journal.pntd.0000900
8. Whitmore A, Krishnaswami CS. A hitherto undescribed infective disease in Rangoon. Ind Med Gaz. 1912;47:262–7.
9. Currie BJ, Dance DA, Cheng AC. The global distribution of *Burkholderia pseudomallei* and melioidosis: an update. Trans R Soc Trop Med Hyg. 2008;102(Suppl 1):S1–4. https://doi.org/10.1016/S0035-9203(08)70002-6
10. Limmathurotsakul D, Golding N, Dance D, Messina J, Pigott D, Moyes C, et al. Predicted global distribution of *Burkholderia pseudomallei* and burden of melioidosis. Nat Microbiol. 2016;1:15008. https://doi.org/10.1038/nmicrobiol.2015.8
11. Benoit TJ, Blaney DD, Doker TJ, Gee JE, Elrod MG, Rolim DB, et al. A review of melioidosis cases in the Americas. Am J Trop Med Hyg. 2015;93:1134–9. https://doi.org/10.4269/ajtmh.15-0405
12. Sanchez-Villamil JI, Torres AG. Melioidosis in Mexico, Central America, and the Caribbean. Trop Med Infect Dis. 2018;3:24. https://doi.org/10.3390/tropicalmed3010024
13. Doker TJ, Sharp TM, Rivera-Garcia B, Perez-Padilla J, Benoit TJ, Ellis EM, et al. Contact investigation of melioidosis cases reveals regional endemicity in Puerto Rico. Clin Infect Dis. 2015;60:243–50. https://doi.org/10.1093/cid/ciu764
14. Cossaboom CM, Marinova-Petkova A, Strysko J, Rodriguez G, Maness T, Ocampo J, et al. Melioidosis in a resident of Texas with no recent travel history, United States. Emerg Infect Dis. 2020;26:1295–9. https://doi.org/10.3201/eid2606.190975
15. Elrod MG, Gee JE, Gulvik CA, Liu L, Salzer JS, Deka MA, et al. Update on melioidosis in the Americas. Presented at: 9th World Melioidosis Congress; Hanoi, Vietnam; October 15–18, 2019.
16. Godoy D, Randle G, Simpson AJ, Aanensen DM, Pitt TL, Kinoshita R, et al. Multilocus sequence typing and evolutionary relationships among the causative agents of melioidosis and glanders, *Burkholderia pseudomallei* and *Burkholderia mallei*. J Clin Microbiol. 2003;41:2068–79. https://doi.org/10.1128/JCM.41.5.2068-2079.2003
17. Galimand M, Escallier G, Dodin A. The health risks of importing tropical fish [in French]. Revue Française d'Aquariologie Herpétologie. 1981;8:19–22.

18. Hassan MR, Pani SP, Peng NP, Voralu K, Vijayalakshmi N, Mehanderkar R, et al. Incidence, risk factors and clinical epidemiology of melioidosis: a complex socio-ecological emerging infectious disease in the Alor Setar region of Kedah, Malaysia. BMC Infect Dis. 2010;10:302. https://doi.org/10.1186/1471-2334-10-302
19. Fang Y, Chen H, Li Y-L, Li Q, Ye Z-J, Mao X-H. Melioidosis in Hainan, China: a restrospective study. Trans R Soc Trop Med Hyg. 2015;109:636–42. https://doi.org/10.1093/trstmh/trv065
20. Federal Select Agent Program. Biosafety/biocontainment plan guidance [cited 2021 Sep 17]. https://www.selectagents.gov/bbp-definitions.html
21. Dey V. The global trade in ornamental fish. Infofish International. 2016;4:52–5.
22. Livengood EJ, Chapman FA. The ornamental fish trade: an introduction with perspectives for responsible aquarium fish ownership. Gainesville (FL): US Department of Agriculture, University of Florida, UF/IFAS Extension Service; 2007.
23. American Pet Products Association. 2019–2020 APPA national pet owners survey, 2020 [cited 2021 Sep 17]. https://www.americanpetproducts.org/press_industry-trends.asp
24. American Pet Products Association. 2017–2018 APPA national pet owners survey, 2018 [cited 2021 Sep 17]. https://www.americanpetproducts.org/press_industry-trends.asp.
25. Centers for Disease Control and Prevention. Healthy pets, healthy people: fish [cited 2021 Sep 17]. https://www.cdc.gov/healthypets/pets/fish.html
26. Hall CM, Jaramillo S, Jimenez R, Stone NE, Centner H, Busch JD, et al. *Burkholderia pseudomallei*, the causative agent of melioidosis, is rare but ecologically established and widely dispersed in the environment in Puerto Rico. PLoS Negl Trop Dis. 2019;13:e0007727. https://doi.org/10.1371/journal.pntd.0007727
27. Stewart T, Engelthaler DM, Blaney DD, Tuanyok A, Wangsness E, Smith TL, et al. Epidemiology and investigation of melioidosis, Southern Arizona. Emerg Infect Dis. 2011;17:1286–8. https://doi.org/10.3201/eid1707.100661
28. Doker TJ, Quinn CL, Salehi ED, Sherwood JJ, Benoit TJ, Glass Elrod M, et al.; Melioidosis Investigation Team. Fatal *Burkholderia pseudomallei* infection initially reported as a *Bacillus* species, Ohio, 2013. Am J Trop Med Hyg. 2014;91:743–6. https://doi.org/10.4269/ajtmh.14-0172
29. Centers for Disease Control and Prevention. CDCHAN-00448. New case identified: multistate investigation of non-travel associated *Burkholderia pseudomallei* infections (melioidosis) in four patients: Georgia, Kansas, Minnesota, and Texas—2021, August 9, 2021 [cited 2021 Sep 9]. https://emergency.cdc.gov/han/2021/han00448.asp
30. Pitman MC, Luck T, Marshall CS, Anstey NM, Ward L, Currie BJ. Intravenous therapy duration and outcomes in melioidosis: a new treatment paradigm. PLoS Negl Trop Dis. 2015;9:e0003586. https://doi.org/10.1371/journal.pntd.0003586
31. Sullivan RP, Marshall CS, Anstey NM, Ward L, Currie BJ. 2020 Review and revision of the 2015 Darwin melioidosis treatment guideline; paradigm drift not shift. PLoS Negl Trop Dis. 2020;14:e0008659. https://doi.org/10.1371/journal.pntd.0008659

Address for correspondence: Patrick Dawson, Centers for Disease Control and Prevention, 1600 Clifton Rd NE, Mailstop H21-8, Atlanta, GA 30329-4027, USA; email: wpb7@cdc.gov

Trends in Incidence and Clinical Outcomes of *Clostridioides difficile* Infection, Hong Kong

Cosmos L.T. Guo[1], Thomas N.Y. Kwong[1], Joyce W.Y. Mak, Lin Zhang, Grace C.Y. Lui, Grace L.H. Wong, Margaret Ip, Jun Yu, Joseph J.Y. Sung, William K.K. Wu,[2] Sunny H. Wong[2]

Medscape ACTIVITY EDUCATION

In support of improving patient care, this activity has been planned and implemented by Medscape, LLC and Emerging Infectious Diseases. Medscape, LLC is jointly accredited by the Accreditation Council for Continuing Medical Education (ACCME), the Accreditation Council for Pharmacy Education (ACPE), and the American Nurses Credentialing Center (ANCC), to provide continuing education for the healthcare team.

Medscape, LLC designates this Journal-based CME activity for a maximum of 1.00 ***AMA PRA Category 1 Credit(s)™***. Physicians should claim only the credit commensurate with the extent of their participation in the activity.

Successful completion of this CME activity, which includes participation in the evaluation component, enables the participant to earn up to 1.0 MOC points in the American Board of Internal Medicine's (ABIM) Maintenance of Certification (MOC) program. Participants will earn MOC points equivalent to the amount of CME credits claimed for the activity. It is the CME activity provider's responsibility to submit participant completion information to ACCME for the purpose of granting ABIM MOC credit.

All other clinicians completing this activity will be issued a certificate of participation. To participate in this journal CME activity: (1) review the learning objectives and author disclosures; (2) study the education content; (3) take the post-test with a 75% minimum passing score and complete the evaluation at http://www.medscape.org/journal/eid; and (4) view/print certificate. For CME questions, see page 3219.

Release date: November 18, 2021; Expiration date: November 18, 2022

Learning Objectives

Upon completion of this activity, participants will be able to:

- Describe disease burden, incidence, and clinical outcomes of CDI among hospitalized patients in Hong Kong, according to an updated territory-wide survey study
- Determine antibiotic usage and other CDI-associated risk factors and clinical outcomes among hospitalized patients in Hong Kong, according to an updated territory-wide survey study
- Identify clinical and public health implications of the epidemiologic pattern of CDI, CDI-associated risk factors, and clinical outcomes among hospitalized patients in Hong Kong, according to an updated territory-wide survey study.

CME Editor

Dana C. Dolan, BS, Copyeditor, Emerging Infectious Diseases. *Disclosure: Dana C. Dolan, BS, has disclosed no relevant financial relationships.*

CME Author

Laurie Barclay, MD, freelance writer and reviewer, Medscape, LLC. *Disclosure: Laurie Barclay, MD, has disclosed no relevant financial relationships.*

Authors

Disclosures: ***Cosmos L.T. Guo; Thomas N.Y. Kwong, PhD; Lin Zhang, PhD; Grace C.Y. Lui, MBChB; Jun Yu, MD, PhD; Joseph J.Y. Sung, MD, PhD; William K.K. Wu, PhD;*** *and* ***Sunny H. Wong, MBChB, DPhil,*** *have disclosed no relevant financial relationships.* ***Joyce W.Y. Mak, MBBS, MRCP(UK),*** *has disclosed the following relevant financial relationships: received grants for clinical research from Gilead Sciences, Inc.; Janssen Pharmaceuticals, Inc.* ***Grace L.H. Wong, MBChB (Hons), MD,*** *has disclosed the following relevant financial relationships: served as an advisor or consultant for Gilead Sciences, Inc.; Janssen Pharmaceuticals, Inc.; served as a speaker or a member of a speakers bureau for Abbott Laboratories; AbbVie Inc.; Bristol-Myers Squibb Company; Echosens; Gilead Sciences, Inc.; received grants for clinical research from: AbbVie Inc.; Gilead Sciences, Inc.* ***Margaret Ip, MD,*** *has disclosed the following relevant financial relationships: served as an advisor or consultant for Cepheid; Merck Sharp & Dohme GmbH; served as a speaker or a member of a speakers bureau for Cepheid; Merck Sharp & Dohme GmbH; received grants for clinical research from Merck Sharp & Dohme GmbH.*

Author affiliations: The Chinese University of Hong Kong, Hong Kong, China (C.L.T. Guo, T.N.Y. Kwong, J.W.Y. Mak, L. Zhang, G.C.Y. Lui, G.L.H. Wong, M. Ip, J. Yu, J.J.Y. Sung, W.K.K. Wu, S.H. Wong); Lee Kong Chian School of Medicine, Nanyang Technological University, Singapore (J.J.Y. Sung, S.H. Wong)

DOI: https://doi.org/10.3201/eid2712.213769

[1]These authors contributed equally to this work.

[2]These authors were co–principal investigators.

We conducted a territorywide survey to investigate the epidemiology, risk factors, and clinical outcomes of *Clostridioides difficile* infection (CDI) among hospitalized patients in Hong Kong. A total of 17,105 cases of CDI were identified, of which 15,717 (91.9%) were healthcare-associated and 1,025 (6.0%) were community-associated. Although CDI incidence increased substantially from 2006 to 2017, it plateaued in 2018 and 2019. The 30-day mortality rates decreased from 20.1% in 2015 to 16.8% in 2019, whereas the 60-day recurrence rates remained constant at ≈11% during the study period. Cross-correlation statistic showed significant correlations between incidence trend and overall antimicrobial drug use ($r = 0.865$, $p<0.001$), which has decreased as a result of an antibiotic stewardship program initiated in 2017. Our data suggest a turning point in *C. difficile* epidemiology that could be related to the changing pattern of antimicrobial drug use.

Clostridioides difficile infection (CDI) is a common nosocomial disease; symptoms range from mild diarrhea to life-threatening colitis and toxic megacolon. CDI is associated with a high mortality rate, particularly for patients >75 years of age (*1*). Epidemiologic studies have identified its substantial incidence especially in the United States and in many countries in Europe (*2*,*3*). Recent data suggested that its overall incidence in some of these countries have reached a plateau. For instance, the US Centers for Disease Control and Prevention (CDC) reported a decrease in CDI incidence from 2014 to 2017 (*2*), whereas the overall CDI incidence in Sweden has decreased by 22% from 2012 to 2016 (*4*). These declines are often attributed to the implementation of antibiotic stewardship programs. Nonetheless, community-acquired CDI (CA-CDI) represents a growing threat; incidence of CA-CDI doubled from 2011–2015 (*5*).

The epidemiologic patterns in different geographic regions are highly dynamic. Outbreaks of CDI in North America and Europe were once predominantly caused by the *C. difficile* ribotype 027 (*6*), which was rarely reported about in Asia (*7*). Instead, *C. difficile* ribotype 017 has been the predominant strain in Asia (*8*). Other toxigenic strains, such as *C. difficile* ribotype 369, which was associated with multiple epidemics in Japan, have been reported in various Southeast Asia countries (*9*), whereas *C. difficile* ribotype 002 was reported to be common in Hong Kong, China, and was associated with increased virulence (*10*,*11*). Continuous surveillance, therefore, is important to prevent outbreaks of CDI. However, epidemiologic data of CDI in Asia remain sparse. We have previously characterized the molecular and antimicrobial susceptibility patterns of prevalent *C. difficile* ribotypes in Hong Kong (*12*). We also conducted an observational study to investigate CDI disease burden and clinical outcomes among hospitalized patients in Hong Kong, which showed a rapidly increasing incidence until 2014 (*13*). In this study, we continued to update the epidemiologic pattern of CDI among hospitalized patients in Hong Kong and characterize CDI-associated risk factors and clinical outcomes.

We conducted this study in accordance with the Declaration of Helsinki (2013 version). The Joint Clinical Research Ethics Committee of the Chinese University of Hong Kong and Hospital Authority New Territory East Cluster approved the study. All clinical data were anonymized by the Clinical Data Analysis and Reporting System (CDARS), and all potential identifiers were removed upon return of database searches.

Methods

Study Population and Data Extraction

We identified digital records of all patients hospitalized in public hospitals with a laboratory-confirmed diagnosis of CDI in Hong Kong during January 1, 2015–December 31, 2019, from CDARS, a database of public hospital patient records managed by the Hong Kong Hospital Authority. We obtained clinical data including the patient demographics, laboratory results, drug prescription records, clinical outcomes, and diagnoses of underlying conditions. Patient demographic data include age and gender. We identified relevant diagnoses using codes from the International Classification of Diseases, 9th Revision, in accordance with the Charlson Comorbidity Index (*14*). We also obtained data on antimicrobial drug use and other drug use within 8 weeks before CDI diagnosis.

Case Identification and Definitions

We defined a CDI case as positive result obtained from culture, toxin, or molecular assay for a diarrheal fecal specimen collected from inpatient residents ≥18 years of age. As described previously (*13*), patients with samples obtained >48 hours after admission or those who were hospitalized in a healthcare facility within the previous 4 weeks were classified as cases of healthcare-associated CDI (HA-CDI). We defined community-associated CDI (CA-CDI) as patients who had not been hospitalized in a healthcare facility within the previous 12 weeks. We defined patients who had been hospitalized in a healthcare facility within the previous 4–12 weeks as indeterminate. We classified patients with a maximum leukocyte count

>15,000 cells/μL or >50% increase in serum creatinine level as having cases of severe CDI, as defined by the Infectious Diseases Society of America (*15*). We defined refractory disease as a nonresponding disease requiring >14 days of continued treatment and a treatment period as a period during which records of drug prescription records indicate continuous antimicrobial treatment with ≤3 days of interruption.

Antimicrobial Drug Use Data

Because the use of antimicrobial drugs is a major risk factor for CDI, we extracted from the data the overall corporate use of antimicrobial drugs in public hospitals in Hong Kong and analyzed. The data were recorded as daily defined doses (DDDs), which is the assumed average maintenance dose per day for each drug. These can demonstrate the absolute changes in use, as well as DDDs per 1,000 bed-days occupied (DDD/1,000 BDO), which can demonstrate changes in use relative to hospital occupancy. Broad-spectrum antimicrobial drugs include cefepime, ceftazidime, cefotaxime, cefoperazone/sulbactam, piperacillin, piperacillin/tazobactam, carbapenems, and quinolones. We determined the risk for CDI for each drug class on the basis of its association with CDI (*1*). High-risk drugs were lincosamides, cephalosporins, fluoroquinolones, amoxicillin, and ampicillin. Medium-risk drugs included sulphonamides and macrolides. Low-risk drugs included tetracyclines (*1*).

Statistical Analysis

We analyzed data with R version 3.6.0. (R Foundation for Statistical Computing, https://www.r-project.org) We defined annual crude incidence of CDI as the number of patients given a diagnosis of CDI per 100,000 adult population, using data obtained from the Hong Kong Census and Statistics Department. We analyzed potential predictors for 30-day mortality rate and 60-day recurrence rate using univariate and multivariate forward Wald logistic regression. We used Cox proportional hazard regression to identify factors that decreased the time to recurrence after an episode. We used χ^2 test of proportion to compare differences in incidences, mortality rates, and recurrence rates. We used cross-correlation to identify correlation between CDI incidence and antimicrobial drug use and $p = 0.05$ as a measure of statistical significance.

Results

Disease Burden and Incidence

During 2015–2019, we identified 17,105 cases of CDI among hospitalized patients in Hong Kong (average 3,421 cases/year). Of these cases, 15,717 (91.9%) were HA-CDI and 1,025 (6.0%) were CA-CDI. The remaining 363 cases (2.1%) were indeterminate (Table 1; Appendix Figure 1).

Although a rapid increase of CDI incidence was observed during 2006–2014, the crude incidence of CDI in Hong Kong remained relatively stable and the average annual percentage change (APC) from 2015 to 2019 showed a modest increase of 1.53% (Table 1; Figure, panel A). Among the different age groups, the CDI incidence showed a significant decrease for patients ≥75 years of age (Figure, panel B). We observed a similar downward trend in the overall incidences of HA-CDI (Figure, panel A), the first time since the start of our previous study in 2006 (*13*). However, this decrease was not evident in the younger patient groups between 2015 and 2019, despite these groups only representing a minor proportion of CDI incidence (Table 1; Figure).

The median age of patients was 77 years (interquartile range [IQR] 63–86 years); 51.8% were female and 48.2% male (Table 2). The number of patients from old-age homes has significantly decreased, from 29.2% in 2015 to 22.8% in 2019 ($p<0.001$) (Table 3), compared with an average of 30.2% in the period 2006–2014. Most patients have taken high-risk antimicrobial drugs (81.4%), broad-spectrum antimicrobial drugs (59.3%), or proton-pump inhibitors (PPI) (62.1%) within 8 weeks before diagnosis of CDI (Table 2). Of note, during the period of 2015–2019, the proportion of severe CDI has decreased from 38.2% to 31.2% of patients ($p<0.001$) (Table 3).

Table 1. Crude incidence of *Clostridioides difficile* infections, by epidemiologic category, Hong Kong, China, 2015–2019*

Year	Adult population	No. cases			Incidence†		
		Overall	HA-CDI	CA-CDI	Overall	HA-CDI	CA-CDI
2015	6,247,460	3,160	2,921	181	50.6	46.8	2.9
2016	6,301,560	3,303	3,058	185	52.4	48.5	2.9
2017	6,357,420	3,618	3,303	231	56.9	52.0	3.6
2018	6,410,080	3,557	3,248	223	55.5	50.7	3.5
2019	6,481,000	3,467	3,187	205	53.5	49.2	3.2

*Adult is defined as a person >18 years of age. CA-CDI, community-associated *Clostridioides difficile* infection; HA-CDI, healthcare-associated *Clostridioides difficile* infection.
†No. cases/100,000 adults.

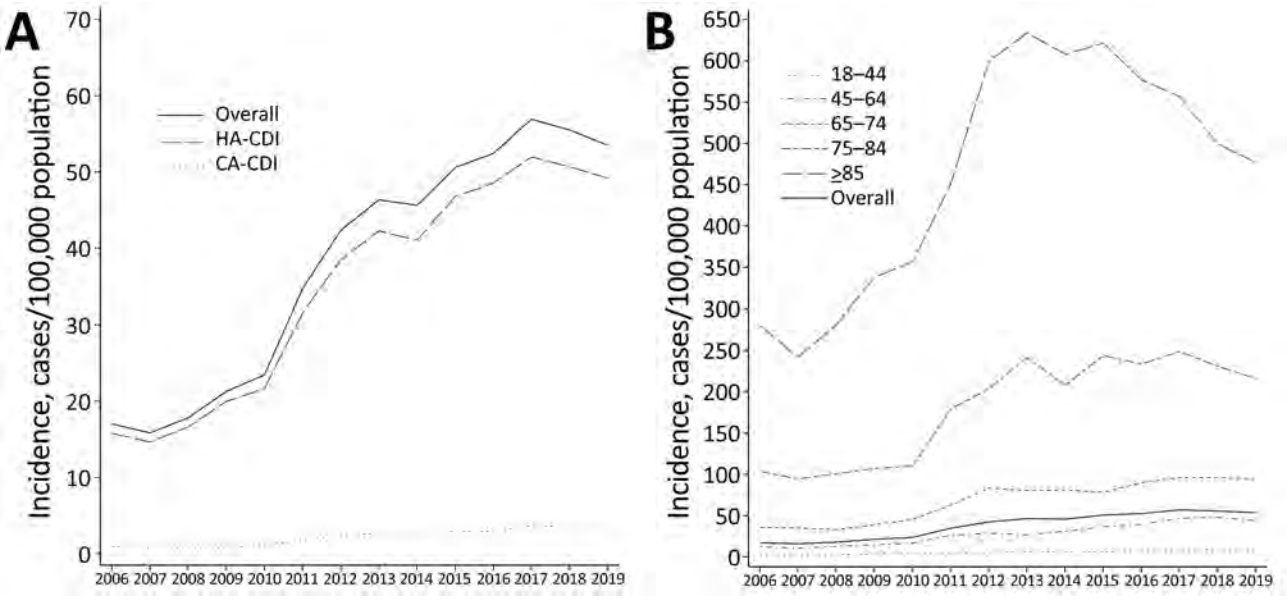

Figure. *Clostridioides difficile* infections in adults, Hong Kong, 2006–2019. Data for 2006–2014 were acquired from a previous study (*13*). A) Crude incidence of healthcare-associated and community-associated *C. difficile* infections. B) Incidence of infections by age group.

Clinical Outcomes and Risk Factors

The 30-day all-cause mortality rates have decreased from 20.1% in 2015 to 16.8% in 2019 (p = 0.002), substantially lower than the previous decrease of 22.5% during the period 2006–2014 (Appendix Table 1) (*13*). Multivariate logistic regression analysis indicated that the main predictors for death in 30 days were advanced age (>85 years, adjusted OR [aOR] 7.23, 95% CI 5.29–10.12; 75–84 years, aOR 4.30, 95% CI 3.16–5.98) and metastatic tumor (aOR 2.63, 95% CI 2.21–3.12) (Table 3).

The 60-day recurrence rate remained at ≈11% (Appendix Table 1). Cox regression analysis showed that the main predictors of 60-day recurrence were healthcare-associated CDI (adjusted hazard ratio [aHR] 8.15, 95% CI 5.25–12.63) and use of quinolones (aHR 1.59, 95% CI 1.41–1.78) or broad-spectrum antibiotics (aHR 1.37, 95% CI 1.18–1.59) within 8 weeks before diagnosis of CDI (Appendix Table 2). Refractory disease rates decreased from 13.6% in 2015 to 11.3% in 2019, but the change was not statistically significant (p<0.076).

The number of patients who used tetracyclines within 8 weeks before CDI increased from 2.7% in 2015 to 6.2% in 2019 (p<0.001). In contrast, patient exposure to certain known risk factors has decreased during the period, including the use of H2 antagonists (from 35.2% to 25.0%; p<0.001), high-risk antibiotics (from 85.5% to 77.7%; p<0.001), penicillin group of drugs (from 74.2% to 68.5%; p<0.001) and fluoroquinolones (from 27.4% to 20.7%; p<0.001). The risk factor of having cerebrovascular accident as an underlying condition also decreased in these patients (from 21.9% to 15.9%; p<0.001) (Appendix Table 3).

Comparison of HA-CDI and CA-CDI

The proportion of HA-CDI among all patients has remained at ≈90% and of CA-CDI at ≈5% (Appendix Figure). The year-to-year changes for the CA-CDI and HA-CDI incidence rates were not statistically significant, suggesting a static trend during the period (Table 1). Comparisons between the patients showed that HA-CDI patients had a median age of 77 (IQR 63–86) years, versus a median age of 74 (IQR 58–85) years for CA-CDI patients. Significantly more HA-CDI patients had severe CDI (36.5% vs 29.0%; p<0.001) and underlying conditions compared with CA-CDI patients (Table 2). HA-CDI patients were more likely to have exposure to high-risk antimicrobial drugs (86.0% vs. 26.5%; p<0.001) and broad-spectrum antimicrobials (63.5% vs 9.2%; p<0.001) within 8 weeks before CDI. The 30-day mortality rate was 19.7% for HA-CDI but 8.5% for CA-CDI patients (p<0.001), although both rates have decreased compared with the earlier period of 2006–2014 (*13*). Although the 30-day mortality rate for HA-CDI decreased from 2015 to 2019, we did not observe an obvious trend in mortality rate for CA-CDI patients (p = 0.354) (Appendix Table 1). The 60-day recurrence rate was 12.4% for HA-CDI, whereas none of the CA-CDI patients had a recurrence (Table 2).

Data on Antimicrobial Drug Use

The overall use of antimicrobial drugs per year, measured as DDD/1,000 BDO, increased from 1,206 in 2006 to 4,747 in 2018 but then decreased to 3,968 in 2019 (Appendix Table 4). Annual use shared a significant correlation (r = 0.865; p<0.001) with the CDI incidence. In terms of DDD/1,000 BDO, we observed the highest levels of correlation for lincosamides (r = 0.907; p<0.001), carbapenems (r = 0.893; p<0.001) and sulphonamides (r = 0.872;

Table 2. Characteristics, outcomes, and procedures of patients with *Clostridioides difficile* infections, Hong Kong, China, 2015–2019*

Characteristic	Overall	CA-CDI	HA-CDI	Indeterminate
All patients	17,105	1,025 (6.0)	15,717 (91.9)	363 (2.1)
Age, y				
Median (IQR)	77 (63–86)	74 (58–85)	77 (63–86)	78 (62–86)
<44	1,056 (6.2)	138 (13.5)	901 (5.7)	17 (4.7)
45–64	3,679 (21.5)	221 (21.6)	3,375 (21.5)	83 (22.9)
65–74	3,027 (17.7)	173 (16.9)	2,793 (17.8)	61 (16.8)
75–84	4,340 (25.4)	207 (20.2)	4,044 (25.7)	89 (24.5)
≥85	5,003 (29.2)	286 (27.9)	4,604 (29.3)	113 (31.1)
Sex				
M	8,252 (48.2)	442 (43.1)	7,642 (48.6)	168 (46.3)
F	8,853 (51.8)	583 (56.9)	8,075 (51.4)	195 (53.7)
Admission from OAH	4,321 (25.3)	209 (20.4)	4,003 (25.5)	109 (30.0)
IDSA-defined severe disease	5,871 (35.8)	295 (29.0)	5,482 (36.5)	94 (26.2)
Diagnostic test				
Bacterial culture	8,191 (40.9)	468 (39.4)	7,560 (41.0)	163 (38.6)
Nucleic acid amplification test	8,994 (44.9)	547 (46.0)	8,261 (44.8)	186 (44.1)
Toxin detection	2,855 (14.2)	173 (14.6)	2,609 (14.2)	73 (17.3)
Antimicrobial drug use				
High-risk drugs	13,932 (81.4)	272 (26.5)	13,519 (86.0)	141 (38.8)
Medium-risk drugs	1,562 (9.1)	23 (2.2)	1,526 (9.7)	13 (3.6)
Low-risk drugs	4,286 (25.1)	17 (1.7)	4,257 (27.1)	12 (3.3)
Broad-spectrum drugs	10,147 (59.3)	94 (9.2)	9,986 (63.5)	67 (18.5)
Use of other drugs				
Proton pump inhibitor	10,614 (62.1)	201 (19.6)	10,255 (65.2)	158 (43.5)
H2 antagonist	4,950 (28.9)	158 (15.4)	4,722 (30.0)	70 (19.3)
Corticosteroid	4,477 (26.2)	81 (7.9)	4,350 (27.7)	46 (12.7)
Underlying conditions				
Myocardial infarction	1,212 (7.1)	37 (3.6)	1,144 (7.3)	31 (8.5)
Congestive heart failure	2,407 (14.1)	64 (6.2)	2,292 (14.6)	51 (14.0)
Peripheral vascular disease	556 (3.3)	10 (1.0)	536 (3.4)	10 (2.8)
Cerebrovascular disease	3,051 (17.8)	91 (8.9)	2,887 (18.4)	73 (20.1)
Chronic pulmonary disease	1,937 (11.3)	84 (8.2)	1,806 (11.5)	47 (12.9)
Mild liver disease	338 (2.0)	18 (1.8)	301 (1.9)	19 (5.2)
Severe liver disease	243 (1.4)	11 (1.1)	221 (1.4)	11 (3.0)
Diabetes mellitus	3,624 (21.2)	131 (12.8)	3,414 (21.7)	79 (21.8)
Diabetes mellitus with complications	1,492 (8.7)	44 (4.3)	1,406 (8.9)	42 (11.6)
Moderate/severe kidney disease	3,363 (19.7)	94 (9.2)	3,178 (20.2)	91 (25.1)
Nonmetastatic cancer	3,403 (19.9)	75 (7.3)	3,268 (20.8)	60 (16.5)
Metastatic cancer	970 (5.7)	21 (2.0)	932 (5.9)	17 (4.7)
HIV	16 (0.1)	1 (0.1)	15 (0.1)	0
Paraplegia	356 (2.1)	12 (1.2)	336 (2.1)	8 (2.2)
Connective tissue disease	174 (1.0)	15 (1.5)	152 (1.0)	7 (1.9)
Dementia	863 (5.0)	47 (4.6)	793 (5.0)	23 (6.3)
Peptic ulcer	867 (5.1)	24 (2.3)	826 (5.3)	17 (4.7)
Outcomes				
Episode death	3,220 (18.8)	73 (7.1)	3,117 (19.8)	30 (8.3)
30-day mortality	3,225 (18.9)	87 (8.5)	3,100 (19.7)	38 (10.5)
60-day mortality	4,738 (27.7)	117 (11.4)	4,562 (29.0)	59 (16.3)
30-day recurrence	1,968 (11.5)	0	1,947 (12.4)	21 (5.8)
Refractory disease	2,155 (12.6)	59 (5.8)	2,064 (13.1)	32 (8.8)
Procedures				
Partial colectomy	3 (0.0)	1 (0.1)	2 (0.0)	0
Left colectomy	3 (0.0)	0	3 (0.0)	0
Right colectomy	6 (0.0)	0	6 (0.0)	0
Sigmoid colectomy	1 (0.0)	0	1 (0.0)	0
Total colectomy	4 (0.0)	1 (0.1)	3 (0.0)	0
Fecal microbiota transplant	3 (0.0)	0	3 (0.0)	0

*Values are no. (%) patients except as indicated. CA-CDI, community-associated *Clostridioides difficile* infection; HA-CDI, healthcare-associated *Clostridioides difficile* infection; IDSA, Infectious Diseases Society of America; IQR, interquartile range; OAH, old age home.

Table 3. Logistic regression analysis of potential independent variables associated with 30-day mortality for *Clostridioides difficile* infection, Hong Kong, China, 2015–2019*

Variable	Univariate		Multivariate	
	OR (95% CI)	p value	OR (95% CI)	p value
Age, y				
<44	Referent	NA	Referent	NA
45–64	3.115 (2.301–4.322)	<0.001	2.458 (1.794–3.449)	<0.001
65–74	4.203 (3.105–5.829)	<0.001	3.203 (2.334–4.502)	<0.001
75–84	6.237 (4.643–8.595)	<0.001	5.384 (3.944–7.531)	<0.001
≥85	7.986 (5.959–10.986)	<0.001	7.633 (5.583–10.70)	<0.001
Male sex	1.124 (1.041–1.213)	0.0029	1.221 (1.121–1.330)	<0.001
IDSA-defined severe disease	2.296 (2.121–2.486)	<0.001	2.159 (1.986–2.347)	<0.001
Healthcare-associated disease	2.483 (2.066–3.010)	<0.001	1.378 (1.119–1.708)	0.003
Admission from OAH	1.716 (1.579–1.864)	<0.001	1.327 (1.203–1.463)	<0.001
Diagnostic test				
Bacterial culture	Referent	NA	Referent	NA
Nucleic acid amplification test	1.070 (0.991–1.157)	0.0845	1.046 (0.962–1.138)	0.294
Toxin detection	0.995 (0.669–1.438)	0.9799	0.904 (0.592–1.343)	0.629
Antimicrobial drug use				
High-risk drugs	2.243 (1.990–2.534)	<0.001	0.753 (0.603–0.939)	0.012
Medium-risk drugs	1.021 (0.893–1.164)	0.7602	1.988 (0.653–8.670)	0.281
Low-risk drugs	1.193 (1.094–1.300)	0.0001	0.841 (0.647–1.092)	0.193
Broad-spectrum drugs	1.673 (1.542–1.817)	<0.001	1.402 (1.244–1.581)	<0.001
Aminoglycosides	0.907 (0.773–1.059)	0.2223	1.026 (0.825–1.272)	0.815
Beta-lactamase inhibitor	2.276 (2.063–2.516)	<0.001	1.465 (1.047–2.052)	0.026
Carbapenem	1.229 (1.118–1.349)	<0.001	1.233 (0.967–1.571)	0.091
Cephalosporin	1.180 (1.087–1.279)	0.0001	0.936 (0.848–1.033)	0.187
Lincosamides	0.901 (0.554–1.400)	0.6580	1.126 (0.674–1.800)	0.634
Macrolides	1.411 (1.201–1.650)	<0.001	0.604 (0.140–1.812)	0.425
Penicillin	2.208 (2.003–2.438)	<0.001	1.165 (0.840–1.624)	0.362
Quinolones	1.115 (1.020–1.218)	0.0161	0.939 (0.843–1.045)	0.251
Sulphonamides	0.588 (0.465–0.734)	<0.001	0.395 (0.092–1.167)	0.138
Tetracyclines	1.291 (1.081–1.534)	0.0043	1.219 (0.955–1.548)	0.108
Use of other drugs				
Proton pump inhibitor	1.614 (1.486–1.755)	<0.001	1.182 (1.073–1.304)	<0.001
H2 antagonist	1.237 (1.136–1.346)	<0.001	1.225 (1.109–1.353)	<0.001
Corticosteroid	0.954 (0.876–1.038)	0.2759	0.919 (0.835–1.010)	0.080
Underlying conditions				
Myocardial infarction	1.268 (1.100–1.457)	0.0009	1.022 (0.871–1.195)	0.791
Congestive heart failure	1.632 (1.475–1.804)	<0.001	1.358 (1.208–1.525)	<0.001
Peripheral vascular disease	1.218 (0.989–1.489)	0.0588	0.980 (0.781–1.221)	0.859
Cerebrovascular disease	1.204 (1.092–1.325)	0.0002	1.021 (0.911–1.143)	0.722
Nonmetastatic cancer	1.498 (1.368–1.638)	<0.001	1.657 (1.468–1.869)	<0.001
Metastatic cancer	2.827 (2.466–3.237)	<0.001	2.627 (2.209–3.124)	<0.001
Diabetes mellitus	1.267 (1.157–1.386)	<0.001	1.052 (0.948–1.168)	0.339
Diabetes mellitus with complications	1.226 (1.076–1.394)	0.0020	1.205 (1.029–1.409)	0.020
Mild liver disease	1.005 (0.758–1.314)	0.9694	1.192 (0.829–1.690)	0.333
Severe liver disease	1.204 (0.878–1.623)	0.2360	1.643 (1.090–2.451)	0.016
Peptic ulcer	1.283 (1.087–1.508)	0.0029	1.060 (0.885–1.264)	0.523
Chronic pulmonary disease	1.302 (1.161–1.459)	<0.001	1.006 (0.883–1.144)	0.926
Moderate/severe kidney disease	1.203 (1.095–1.320)	0.0001	1.383 (1.231–1.553)	<0.001
Connective tissue disease	0.556 (0.338–0.865)	0.0139	0.970 (0.573–1.563)	0.904
Paraplegia	1.152 (0.885–1.482)	0.2810	1.054 (0.779–1.410)	0.726
Dementia	1.364 (1.158–1.600)	0.0002	1.033 (0.864–1.231)	0.718
HIV	0.287 (0.016–1.415)	0.2253	0.562 (0.030–3.080)	0.590

*IDSA, Infectious Diseases Society of America; NA, not applicable; OAH, old age home.

p<0.001), followed by penicillin (r = 0.847; p<0.001) and quinolones (r = 0.825; p<0.001). Similar to the trend in overall antimicrobial drug use, all of these drugs had a decrease in use in 2019, after consistent increases from 2006–2018. We grouped ampicillin and amoxicillin together with other penicillin group drugs because their combined use attributed to 80% of all penicillin use from 2006–2019. In the same period, we observed increased use of tetracyclines, from 9.22 DDD/1,000 BDO in 2006 to 193.44 DDD/1,000 BDO in 2019.

Discussion

In this study, we investigated the latest disease burden of CDI in Hong Kong to provide a complete picture of continual disease surveillance since 2006. Because the public hospitals provide >90% of inpatient medical service in Hong Kong, this study provides a

comprehensive and near-complete data on the disease epidemiology among hospitalized patients in the territory. Our main finding was a decrease in the incidence of CDI in 2018 and 2019, in contrast with the distinctive increasing trend in 2006–2017 (*13*). The average APC during 2015–2019 showed a 1.53% increase, in contrast with the 13.76% increase for the average APC from 2006–2014. Year-to-year changes of crude CDI incidence in 2015–2019, except for 2016–2017, were statistically insignificant, suggesting that the incidence might have reached a plateau. Our reported incidence in Hong Kong (56.9 cases/100,000 population in 2017) was higher than incidence in the United Kingdom (24 cases/100,000 population in 2017), where CDI incidence has seen a decrease that was mostly attributed to a successful antimicrobial drug stewardship program (*16*,*17*). In comparison, Guh et al. reported an estimated crude incidence of 143.6 cases/100,000 population in the United States for 2017 (*2*). Despite the decrease in CDI incidence since 2011, it is still more than double the incidence in Hong Kong (*18*). In contrast, Liao et al. reported an overall crude CDI incidence in China during 2009–2016 was 34 cases/100,000 population, a relatively low value compared with our observations (*19*).

The trends in CDI incidence from 2006–2019 may partially be explained by changes in antimicrobial drug use. Usage rates of many drugs, such as penicillin, lincosamides (including clindamycin), quinolones, sulphonamides, and carbapenems have demonstrated significant correlations with CDI incidence. Penicillin, lincosamides, and quinolones are known to be high-risk for CDI, whereas sulphonamides and carbapenems carry a medium to low risk (*1*). The changes in penicillin use are likely the most relevant, because they were the most prescribed class of drugs during this period. We saw in the same period increased use of tetracyclines, which have been repeatedly demonstrated to have a relatively low risk for CDI (*20*). The changes in antimicrobial drug use may be attributable to Hong Kong's antibiotic stewardship program, which was updated in 2017 (*21*). These changes are consistent with our observation on the decreased use of antimicrobial drugs, including the penicillin group, fluoroquinolones, and other high-risk drugs, in CDI patients from 2015–2019. By extrapolating the CDI incidence from 2006–2017 to predict incidence in 2018–2019, we observed that the predicted incidence in 2019 would be 20% higher than the actual incidence, showing that the potential effect antibiotic stewardship had on the status quo.

In addition to a decrease in incidence, we observed a decrease in 30-day mortality rates, for which there are myriad plausible explanations. The decrease may be attributed to improved effectiveness of treatment and management efforts for CDI, successful antibiotic stewardship programs, or increased use of fecal microbiota transplant as a treatment (*22*). Alternatively, a decrease in deaths may be attributable to a change in prevalence of ribotypes or their virulence, such as ribotype 002, which is common in Hong Kong. This difference may also explain the decrease in the relative proportion of severe CDI. Furthermore, ribotypes 002 and 017 are both virulent strains with high antimicrobial resistance (*8*,*10*,*12*), which may have been positively selected in the past because of excessive antimicrobial drug use. Now that the use of antimicrobial drugs has been declining, these strains may have seen a decline in prevalence, which lowered mortality rates. However, more data, such as those gathered through molecular typing and antibiotic resistance analysis, are required to validate this hypothesis.

Despite changes in CDI incidence, the proportion of CA-CDI cases of all CDI cases annually has remained steady from 2006–2019, at ≈4–5%. Risk factors for CA-CDI are unclear, although our data suggest that gastric acid suppression, antimicrobial drug use, and old age may be potential factors. Nonetheless, CA-CDI patients tend to be relatively younger. Previous studies have indicated that there is an increase in CA-CDI incidence and severe outcomes (*5*,*23*). Our study, however, indicates the proportion of CA-CDI has remained relatively constant and that their clinical outcomes are generally more favorable, including lower rates of mortality and recurrence, than outcomes for HA-CDI patients. Furthermore, we did not observe any significant trend of increase in CA-CDI cases. One potential explanation is that Hong Kong still has lower rates of inflammatory bowel disease compared with Western countries, despite an increasing trend in these illnesses over the past few decades (*22*,*24*).

The main strength of this study is that it is territorywide, driven by data extracted from all public hospitals in Hong Kong. All data, including demographics, laboratory results, drug prescription data, and procedures, were extracted from the public hospital database, thus reducing the possibility of recall bias. Furthermore, this study followed on our previous study (*13*) that investigated the epidemiology of CDI in Hong Kong during 2006–2014, providing a comprehensive epidemiologic pattern and comparisons for CDI in Hong Kong. Nonetheless, we acknowledge several limitations in our study. First, the data in this study were based only on

inpatient data; we may have missed diagnoses made in outpatient clinics. Patients with mild symptoms could be sufficiently treated in outpatient clinics, which may result in an underestimation of the actual CDI incidence. Second, patient exposure to antimicrobial drugs and other drugs within 8 weeks of CDI was indicated as a logical indicator (i.e., true or false), regardless of dose, frequency, and prescription time, which may overestimate or underestimate the extent of the exposure. Third, there was a lack of data regarding changes in CDI diagnostic tests used from before 2015, making comparisons of CDI incidence unable to account for any shifts toward the use of the nucleic acid amplification test (NAAT), which is known to be a more sensitive test for CDI (2). Fortunately, the use of NAAT from 2015–2019 has remained within 40%–50%, which may mean a smaller impact on the trend of CDI incidence. Last, this is a retrospective study and there are unforeseeable covariates that were not adjustable or measurable, which may affect the analyses and results. Nevertheless, the epidemiology of CDI is dynamic, and changes can occur rapidly. We recommend continued surveillance of this infection in healthcare settings.

This project is supported by the Hong Kong University Grants Committee Research Grant Council (Early Career Scheme no. 21153816/24103516) and the Hong Kong Food and Health Bureau Commissioned Health and Medical Research Fund (CID-CUHK-C).

Author contributions: S.H.W. and W.K.K.W. conceived the study. C.L.T.G. and T.N.Y.K. extracted the data, performed the analysis, and drafted the manuscript. J.W.Y.M., L.Z., G.C.Y.L., G.L.H.W., M.I., S.S.L., J.Y., and J.J.Y.S. provided important intellectual input and revised the manuscript. J.J.Y.S., W.K.K.W., and S.H.W. managed and oversaw the study. All authors critically reviewed and agreed to be accountable for the works.

About the Authors

Mr. Guo is a medical student at the Chinese University of Hong Kong. Dr. Kwong is a postdoctoral researcher at the Chinese University of Hong Kong; his research interests include infectious diseases epidemiology and specifically *Clostridioides difficile*.

References

1. Leffler DA, Lamont JT. *Clostridium difficile* infection. N Engl J Med. 2015;372:1539–48. https://doi.org/10.1056/NEJMra1403772
2. Guh AY, Mu Y, Winston LG, Johnston H, Olson D, Farley MM, et al.; Emerging Infections Program Clostridioides difficile Infection Working Group. Trends in U.S. burden of *Clostridioides difficile* infection and outcomes. N Engl J Med. 2020;382:1320–30. https://doi.org/10.1056/NEJMoa1910215
3. Heimann SM, Cruz Aguilar MR, Mellinghof S, Vehreschild MJGT. Economic burden and cost-effective management of *Clostridium difficile* infections. Med Mal Infect. 2018;48:23–9. https://doi.org/10.1016/j.medmal.2017.10.010
4. Rizzardi K, Norén T, Aspevall O, Mäkitalo B, Toepfer M, Johansson Å, et al. National surveillance for *Clostridioides difficile* infection, Sweden, 2009–2016. Emerg Infect Dis. 2018;24:1617–25. https://doi.org/10.3201/eid2409.171658
5. Ofori E, Ramai D, Dhawan M, Mustafa F, Gasperino J, Reddy M. Community-acquired *Clostridium difficile*: epidemiology, ribotype, risk factors, hospital and intensive care unit outcomes, and current and emerging therapies. J Hosp Infect. 2018;99:436–42. https://doi.org/10.1016/j.jhin.2018.01.015
6. Valiente E, Cairns MD, Wren BW. The *Clostridium difficile* PCR ribotype 027 lineage: a pathogen on the move. Clin Microbiol Infect. 2014;20:396–404. https://doi.org/10.1111/1469-0691.12619
7. Collins DA, Sohn KM, Wu Y, Ouchi K, Ishii Y, Elliott B, et al.; Clostridioides difficile Asia-Pacific Study Group. *Clostridioides difficile* infection in the Asia-Pacific region. Emerg Microbes Infect. 2019;9:42–52. https://doi.org/10.1080/22221751.2019.1702480
8. Imwattana K, Knight DR, Kullin B, Collins DA, Putsathit P, Kiratisin P, et al. *Clostridium difficile* ribotype 017—characterization, evolution and epidemiology of the dominant strain in Asia. Emerg Microbes Infect. 2019;8:796–807. https://doi.org/10.1080/22221751.2019.1621670
9. Collins DA, Riley TV. *Clostridium difficile* in Asia: opportunities for One Health management. Trop Med Infect Dis. 2018;4:E7. https://doi.org/10.3390/tropicalmed4010007
10. Kong KY, Kwong TNY, Chan H, Wong K, Wong SSY, Chaparala AP, et al. Biological characteristics associated with virulence in *Clostridioides difficile* ribotype 002 in Hong Kong. Emerg Microbes Infect. 2020;9:631–8. https://doi.org/10.1080/22221751.2020.1739564
11. Wong SH, Ip M, Hawkey PM, Lo N, Hardy K, Manzoor S, et al. High morbidity and mortality of *Clostridium difficile* infection and its associations with ribotype 002 in Hong Kong. J Infect. 2016;73:115–22. https://doi.org/10.1016/j.jinf.2016.05.010
12. Chow VCY, Kwong TNY, So EWM, Ho YII, Wong SH, Lai RWM, et al. Surveillance of antibiotic resistance among common *Clostridium difficile* ribotypes in Hong Kong. Sci Rep. 2017;7:17218. https://doi.org/10.1038/s41598-017-17523-7
13. Ho J, Dai RZW, Kwong TNY, Wang X, Zhang L, Ip M, et al. Disease burden of *Clostridium difficile* infections in adults, Hong Kong, China, 2006–2014. Emerg Infect Dis. 2017;23:1671–9. https://doi.org/10.3201/eid2310.170797
14. Sundararajan V, Henderson T, Perry C, Muggivan A, Quan H, Ghali WA. New ICD-10 version of the Charlson comorbidity index predicted in-hospital mortality. J Clin Epidemiol. 2004;57:1288–94. https://doi.org/10.1016/j.jclinepi.2004.03.012
15. Cohen SH, Gerding DN, Johnson S, Kelly CP, Loo VG, McDonald LC, et al.; Society for Healthcare Epidemiology of America; Infectious Diseases Society of America. Clinical practice guidelines for *Clostridium difficile* infection in adults: 2010 update by the Society for Healthcare Epidemiology of America (SHEA) and the Infectious Diseases Society of America (IDSA). Infect Control Hosp

Epidemiol. 2010;31:431–55. https://doi.org/10.1086/651706
16. Thelwall S, Nsonwu O, Rooney G, Wasti S, Anselmo J, Hope R; Public Health England. *Clostridium difficile* infection: mandatory surveillance 2017/18. London: Public Health England; 2018.
17. Wilcox MH. *Clostridium difficile* surveillance in England. Infectious Agents Surveillance Report. 2020;41:39–41.
18. US Centers for Disease Control and Prevention. 2017 annual report for the Emerging Infections Program for *Clostridioides difficile* infection. 2017 [cited 2021 Oct 15]. https://www.cdc.gov/hai/eip/pdf/cdiff/2017-CDI-Report-H.pdf
19. Liao F, Li W, Gu W, Zhang W, Liu X, Fu X, et al. A retrospective study of community-acquired *Clostridium difficile* infection in southwest China. Sci Rep. 2018;8:3992. https://doi.org/10.1038/s41598-018-21762-7
20. Tariq R, Cho J, Kapoor S, Orenstein R, Singh S, Pardi DS, et al. Low risk of primary *Clostridium difficile* infection with tetracyclines: a systematic review and metaanalysis. Clin Infect Dis. 2018;66:514–22. https://doi.org/10.1093/cid/cix833
21. Ho P, Wu T, Chao DV, Hung IF, Lui L, Lung DC, et al. Reducing bacterial resistance with IMPACT, 5th edition, Hong Kong. Hong Kong: Centre for Health Protection—Department of Health; 2017.
22. Lui RN, Wong SH, Lau LHS, Chan TT, Cheung KCY, Li A, et al. Faecal microbiota transplantation for treatment of recurrent or refractory *Clostridioides difficile* infection in Hong Kong. Hong Kong Med J. 2019;25:178–82.
23. Gupta A, Khanna S. Community-acquired *Clostridium difficile* infection: an increasing public health threat. Infect Drug Resist. 2014;7:63–72.
24. Ng SC, Leung WK, Shi HY, Li MK, Leung CM, Ng CK, et al. Epidemiology of inflammatory bowel disease from 1981 to 2014: results from a territory-wide population-based registry in Hong Kong. Inflamm Bowel Dis. 2016;22:1954–60. https://doi.org/10.1097/MIB.0000000000000846

Address for correspondence: Sunny H. Wong, Lee Kong Chian School of Medicine, 11 Mandalay Rd, Nanyang Technological University, Singapore 308232, Singapore; email: sunny.wong@ntu.edu.sg

Characterization of Swine Influenza A(H1N2) Variant, Alberta, Canada, 2020

Jamil N. Kanji,[1] Kanti Pabbaraju, Matthew Croxen, Susan Detmer, Nathalie Bastien, Yan Li, Anna Majer, Hussein Keshwani, Nathan Zelyas, Ifeoma Achebe, Corinne Jones, Maureen Rutz, Angela Jacobs, Keith Lehman, Deena Hinshaw, Graham Tipples

Influenza strains circulating among swine populations can cause outbreaks in humans. In October 2020, we detected a variant influenza A subtype H1N2 of swine origin in a person in Alberta, Canada. We initiated a public health, veterinary, and laboratory investigation to identify the source of the infection and determine whether it had spread. We identified the probable source as a local pig farm where a household contact of the index patient worked. Phylogenetic analysis revealed that the isolate closely resembled strains found at that farm in 2017. Retrospective and prospective surveillance using molecular testing did not identify any secondary cases among 1,532 persons tested in the surrounding area. Quick collaboration between human and veterinary public health practitioners in this case enabled a rapid response to a potential outbreak.

Rapid detection and reporting of novel influenza A virus (IAV) strains are critical to prompt evaluation of a pandemic threat (*1*). For example, in 2009, health officials in Mexico reported a variant influenza A(H1N1) virus of swine origin; that variant quickly caused a pandemic (*2*). Although uncommon, transmission of swine variant IAV strains from pigs to humans has been documented on several occasions (*3*). Pig farming is structured such that the animals move to different types farms as they grow. Usually, piglets are born in farrowing farms, transferred to nurseries upon weaning, and then sent to finisher barns at 10–12 weeks of age. These farms usually span >2 geographically separate sites. Collectively, the combination of farrowing, nursery, and finisher farms form a chain where later farms are referred to as downstream from prior ones in the chain.

In 2005, updates to the International Health Regulations instituted mandatory reporting of pathogens such as novel influenza variants in all member states of the World Health Organization (*2*). Since then, 29 cases of swine influenza A(H1N2) variant H1N2v) strains have been reported to the World Health Organization, including 25 cases in the United States during 2011–2018, 1 case in Brazil in 2015, and 2 cases in Brazil in 2020 (*4*–*7*). In addition, 2 cases of H1N2v infection were detected in Canada: 1 in Alberta in October 2020 and 1 in Manitoba in April 2021 (*8*). Since the 2010–11 influenza season, the US Centers for Disease Control and Prevention has reported >465 cases of swine IAV variants, including H1N1v, H1N2v, and H3N2v, in humans (*9*). We report the detection and genetic characterization of an H1N2v IAV isolated from a patient in Alberta. We also describe the public health response and relevant investigations regarding the case.

Methods

Case Description

During the second week of October 2020, a child <18 years of age was brought to a local emergency department with a 4-day history of cough, fever, pharyngitis, and rhinorrhea. At admission, the patient was afebrile, had mild tachycardia and tachypnea, and had

Author affiliations: Alberta Precision Laboratories, Edmonton, Alberta, Canada (J.N. Kanji, K. Pabbaraju, M. Croxen, N. Zelyas, G. Tipples); University of Alberta, Edmonton (J.N. Kanji, M. Croxen, N. Zelyas, I. Achebe, D. Hinshaw, G. Tipples); University of Saskatchewan, Regina, Saskatchewan, Canada (S. Detmer); Public Health Agency of Canada, Winnipeg, Manitoba, Canada (N. Bastien, Y. Li, A. Majer); Alberta Agriculture and Forestry, Edmonton (H. Keshwani, K. Lehman); Alberta Health Services, Red Deer, Alberta, Canada (I. Achebe, C. Jones, M. Rutz); Alberta Health Services, Edmonton (A. Jacobs); University of Calgary, Calgary, Alberta, Canada (D. Hinshaw)

DOI: https://doi.org/10.3201/eid2712.210298

[1]Current affiliation: University of Calgary, Calgary, Alberta, Canada.

an oxygen saturation of 93% on ambient air. We did not find signs of respiratory distress and discharged the patient after collecting specimens for respiratory virus testing. The patient was born in Canada and up-to-date with all routine immunizations and influenza vaccinations until 2016.

Consent was provided for the patient and the patient's household members to be included in this report provided that no identifiable information was published. Presentation of the data contained in this report has been approved by the Human Research Ethics Board at the University of Alberta (Edmonton, Alberta, Canada; study no. Pro00105933).

Diagnostic Evaluation

The patient's nasopharyngeal swab sample tested negative for severe acute respiratory syndrome coronavirus 2 (SARS-CoV-2) by real-time reverse transcription PCR (rRT-PCR) (*10*). Multiplex molecular respiratory virus testing (NxTAG Respiratory Pathogen Panel; Luminex Corporation, https://www.luminexcorp.com) detected the presence of IAV; however, the virus could not be subtyped. A second rRT-PCR confirmed the presence of IAV but not influenza A(H1N1)pdm09 virus (*11*,*12*). Partial Sanger sequencing of the hemagglutinin (HA) and neuraminidase (NA) genes using universal primers (*13*) yielded sequences that closely resembled isolates of swine H1N2 IAVs available in GenBank.

Epidemiologic Inquiry

The patient had no history of travel, contact with persons from outside the county, or contact with persons who had respiratory illness. One of the patient's household contacts worked with animals at a local pig farm. No household contacts reported symptoms of influenza-like illness or coronavirus disease (COVID-19) before the onset of illness in the index patient. However, 1 household contact reported influenza-like illness symptoms ≈2 days after symptom onset in the index patient. All household contacts remained at home for 10 days after symptom onset in the household contact. Both symptomatic persons recovered. Two asymptomatic household members, including one who worked at the farm of interest, consented to serologic testing by hemagglutination inhibition (HI) assay; samples were collected 35 days after identification of the index patient. The index patient and symptomatic household member declined serologic testing.

Public Health Response

Upon confirmation of swine IAV, which occurred 3 weeks after collection of the original nasopharyngeal swab sample, provincial public health teams, in collaboration with the Alberta Precision Laboratories (Edmonton, Alberta, Canada), undertook heightened influenza surveillance measures in the geographic zone of Alberta where the case was identified. All respiratory specimens collected for community and hospital-based SARS-CoV-2 testing in that region during October 5–November 4, 2020, were retrieved from storage and tested for IAV (*12*). We conducted prospective testing for IAV on all respiratory specimens submitted for SARS-CoV-2 testing from that area during November 4–10, 2020. Patients being tested for SARS-CoV-2 were informed they would also be tested for IAV.

Upon notification of the case, the Office of the Chief Provincial Veterinarian (Edmonton, Alberta, Canada) began a veterinary investigation in collaboration with industry veterinarians and university partners to explore potential links to local pig herds. Staff of the Chief Provincial Veterinarian investigated the health, history and biosecurity practices of the farm where the household contact worked. Past samples collected from local pig herds showed IAVs of multiple subtypes in the farms supplying piglets to the herd of interest. In December 2017, a closely related H1N2 virus had been isolated from the nursery supplying the farm. In October 2019, a virus from the influenza A(H1N1)pdm09 clade was isolated from the nursery; this strain was most recently detected at the nursery in February 2020.

Characterization of H1N2v Strain

We forwarded the patient's sample to the National Microbiology Laboratory (Winnipeg, Manitoba, Canada) for isolation and further characterization. The virus was cultured on Madin-Darby canine kidney cells in 1 passage using standard techniques (*14*).

We conducted HI assays with 0.5% vol/vol turkey red blood cells and 4 HA units of A/Alberta/01/2020 (H1N2)v. We treated each serum with receptor-destroying enzyme (Denka Seiken, https://www.denka.co.jp) at a 1:4 dilution for 18 hrs at 37°C and 45 min at 56°C, then performed adsorption with packed turkey red blood cells (*15*). We defined the HI titer as the highest dilution of the serum capable of inhibiting hemagglutination.

We determined phenotypic susceptibility for oseltamivir and zanamivir by using a chemiluminescent NA inhibition assay (NA-Star Influenza Neuraminidase Inhibitor Resistance Detection Kit; Thermo Fisher Scientific, https://www.thermofisher.com) at the National Microbiology Laboratory. The assay used viruses standardized to equivalent

NA enzyme activity and incubated with 0.0316–1,000 nmol of oseltamivir or zanamivir. We calculated the 50% inhibitory concentration (IC_{50}) by plotting the percentage inhibition of NA activity against the inhibitor concentration, using PRISM version 4 (GraphPad Software, https://www.graphpad.com) for curve fitting.

We conducted whole-genome sequencing of the H1N2v isolate on the MinION (Oxford Nanopore Technologies, https://nanoporetech.com) and MiSeq (Illumina, https://www.illumina.com) platforms. We generated sequence data and prepared and sequenced libraries using the DNA Library Prep Kit and iSeq 100 (Illumina; Appendix, https://wwwnc.cdc.gov/EID/article/27/12/21-0298-App1.pdf). We conducted phylogenetic characterization of the H1N2v isolate by comparing human H1N2v and swine H1N2 HA (segment 4) sequences available on GenBank. We also aligned sequences and visualized the phylogenetic trees (Appendix).

Sampling

We used the rope technique to collect samples from several farms, including the farm of interest (*16*). We also collected 56 deep nasal swab and 11 pen-based oral fluid samples from farms downstream of the farm of interest, as well as 12 nasal swab and 6 oral fluid samples from the farm of interest. We placed individual nasal swab samples in 1.5 mL of Dulbecco's modified Eagle medium (Thermo Fisher Scientific) and vortexed them before extracting 500 μL pooled samples from 3–4 swabs for PCR (*17*). We subtyped the RNA from the strongest positive pooled nasal swab or oral fluid sample from each farm. Samples were analyzed at the University of Saskatchewan (Regina, Saskatchewan, Canada) by using the VetMAX-Gold Swine Influenza Virus Detection rRT-PCR kit and the VetMAX-Gold Swine Influenza Virus Subtyping rRT-PCR kit (Thermo Fisher Scientific) (*18*).

Results

BLAST (https://blast.ncbi.nlm.nih.gov/Blast.cgi) analysis of historical swine H1N2 and H1N2 isolates from western Canada yielded a close match to a virus strain found on only a few farms in central Alberta, including a farm in the pig supply chain of the herd of interest. Phylogenetic analysis showed that the human A/Alberta/01/2020 H1N2v isolate belonged to the evolutionary branch found at the nursery that supplied the farm where the household contact worked (A/swine/Alberta/SD0237/2017 and A/swine/Alberta/SD0267/2017); the most similar sequence was collected from the source farm in 2017 (Figure; Appendix Table). The A/Alberta/01/2020 H1N2v sequence shared high genetic similarity (98%–>99%) with 8 genes from multiple swine H1N2v and H3N2 strains from western Canada and the United States (Table). The H1 gene sequence most resembled sequences found in the H1α-3a subclade.

Two members of patient's household had HI titers of 20. Seasonal vaccine serum for A/Hawaii/70/2019 H1N1 elicited no HI titer against A/Alberta/01/2020 H1N2v. We found that A/Alberta/01/2020/H1N2v was susceptible to oseltamivir (IC_{50} 0.41 nmol) and zanamivir (IC_{50} 2.16 nmol). The control strain, A/Brisbane/10/07 H3N2, was sensitive to oseltamivir (IC_{50} 0.61 nmol) and zanamivir (IC_{50} 3.19 nmol).

Surveillance for Additional H1N2v Cases

This case occurred during the response to the COVID-19 pandemic, when there was no circulating seasonal influenza in the province (*19*). We did not identify additional cases of IAV from retrospective testing of 1,276 archived respiratory specimens nor prospective testing of 256 specimens submitted for respiratory virus testing.

IAV Testing

In total, 3/13 pooled nasal swab and 2/6 oral fluid samples from the farm of interest tested positive for IAV. Cycle threshold (C_t) values were 34.7–36.6; we considered values <38 to be positive. We found that all positive pooled nasal swab and oral fluid samples from the 2 sites of interest with the lowest C_t value (34.7) had the H1 gene; however, we could not identify the NA type. The sample with the second lowest C_t value (35.4) from the same downstream site was subtyped as N2, as was the only positive (C_t 36.0) sample from the other downstream farm tested.

At the nursery, all 3 pooled nasal swab and all 6 oral fluid samples tested positive for IAV (C_t 29.8–34.7). We identified H1, H3, N1, and N2 genes in the pooled nasal swab sample with the lowest C_t value (29.8) from the nursery.

Discussion

We report pig-to-human transmission of H1N2v virus in Alberta, Canada. The source of H1N2v infection in the index patient is unclear, but one of the patient's household contacts worked at a pig farm where a similar H1N2 virus was found in 2017.

IAV is transmitted through close contact and contaminated objects (*5*). Transmission of IAV from swine to humans is usually the result of close contact or self-inoculation from contaminated farm surfaces (*3*,*20*,*21*). In Canada, pig farms must adhere to strict

farm biosecurity measures, such as policies requiring workers to shower before leaving, use of facility-specific uniforms and boots, and designation of clean and dirty zones (*22*–*24*). Thus, the likelihood of the index patient acquiring infection through fomite-related transmission is very low. Because the index patient never visited the farm of interest, the virus was probably transmitted through respiratory droplets from the household contact who worked at the farm. Humans have poor seroconversion to H1N2 viruses (*20*), so it is possible that the household contact had partial protection from previous exposure, despite having an HI titer of 20. Partial protection might also explain the limited forward transmission observed in this study, especially because H1N2v virus is associated with mild illness and limited transmission (*5*).

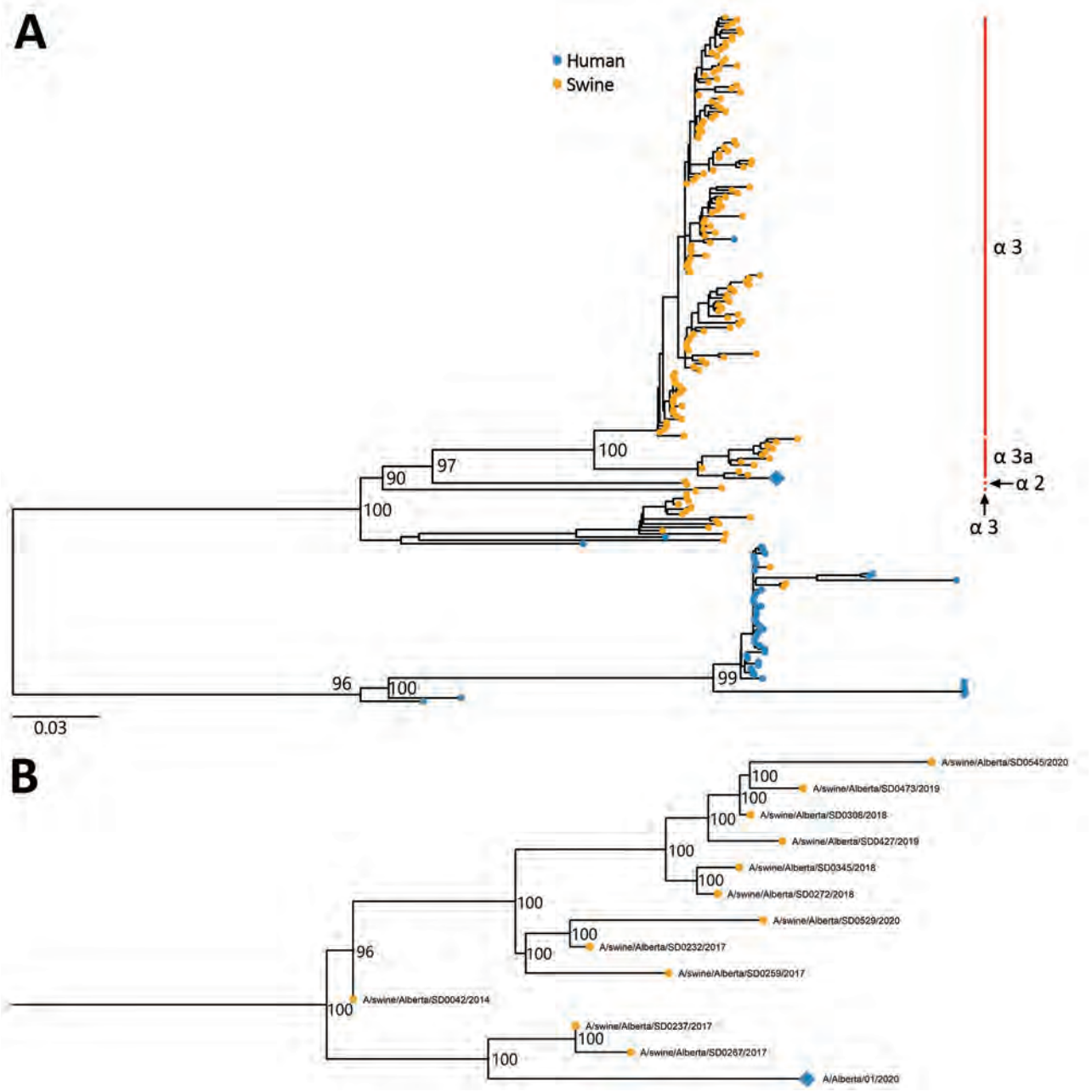

Figure. Phylogenetic trees of A/Alberta/01/2020 H1N2v and related strains, United States and Canada, 2016–2020. A) The H1α-3a subclade. B) The H1α-3a subclade with ≈2 years of changes (2017–2018) of A/swine/Alberta/SD0237/2017 and A/swine/Alberta/SD0267/2017. The trees were built with IQ-TREE version 2.0.3 (http://www.iqtree.org) on the basis of hemagglutinin sequences. Numbers at nodes indicate bootstrap values based on 1,000 replicates. Red bars identifies clades; all clades presented have % age bootstrap values >70. Diamond indicates A/Alberta/01/2020 (H1N2)v. Scale bar indicates number of nucleotide substitutions per site.

Table. Genetic comparison of A/Alberta/01/2020 (H1N2)v and other influenza strains in swine and humans, United States and Canada, 2016–2020*

GISAID ID	Segment	Gene	GenBank accession no.	% Identity	Host	Genotype	Country	Strain	Clade
EPI1815176	1	PB2	MK475180	99.3	Human	H1N1	USA	A/Connecticut/37/2018	npdm
			MK475443	99.3	Human	H1N1	USA	A/Montana/39/2018	npdm
			MK623898	99.3	Human	H1N1	USA	A/Wisconsin/517/2018	npdm
EPI1056722				91.4	Human	H1N2v	USA	A/Ohio/24/2017†	H1α-3 variant
EPI1815177	2	PB1	MK631128	99.3	Human	H1N1	USA	A/Iowa/01/2019	npdm
EPI1056723				91.3	Human	H1N2v	USA	A/Ohio/24/2017†	H1α-3 variant
EPI1815175	3	PA	MK462359	98.7	Swine	H3N2	Canada	A/swine/Saskatchewan/ SD0247/2017	Swine H3
			MK462496	98.7	Swine	H3N2	Canada	A/swine/Saskatchewan/ SD0258/2017	Swine H3
EPI1056721				96.4	Human	H1N2v	USA	A/Ohio/24/2017†	H1α-3 variant
EPI1815179	4	HA	MK462499	97.9	Swine	H1N2	Canada	A/swine/Alberta/SD0237/2017	H1α-3a
EPI1056725				91.7	Human	H1N2v	USA	A/Ohio/24/2017†	H1α-3 variant
EPI1815172	5	NP	MK445889	99.0	Human	H1N1	USA	A/North Dakota/42/2018	npdm
EPI1056718				94.9	Human	H1N2v	USA	A/Ohio/24/2017†	H1α-3 variant
EPI1815178	6	NA	MK462493	98.2	Swine	H3N2	Canada	A/swine/Saskatchewan/ SD0258/2017	Swine H3
EPI1056724				95.4	Human	H1N2v	USA	A/Ohio/24/2017†	H1α-3 variant
EPI1815174	7	M	CY246708	99.5	Swine	H1N2	Canada	A/swine/Saskatchewan/ SD0204/2016H1N2	H1α-3
			CY246716	99.5	Swine	H1N2	Canada	A/swine/Manitoba/SD0203/ 2016H1N2	H1α-3
			MK462355	99.5	Swine	H3N2	Canada	A/swine/Saskatchewan/ SD0247/2017	Swine H3
EPI1056720				96.6	Human	H1N2v	Canada	A/Ohio/24/2017†	H1α-3 variant
EPI1815173	8	NS	MK462463	99.2	Swine	H1N2	Canada	A/swine/Alberta/SD0267/2017	H1α-3a
EPI1056719				94.1	Human	H1N2v	USA	A/Ohio/24/2017†	H1α-3 variant

*GISAID, https://www.gisaid.org. HA, hemagglutinin; ID, identification; M, matrix; NA, neuraminidase; NP, nucleoprotein; npdm, influenza A(H1N1)pdm09-like virus; NS, nonstructural protein; PA, polymerase acidic protein; PB1, polymerase base protein 1; PB2, polymerase basic protein 2.
†A/Ohio/24/2017 data was deposited into GISAID by the Centers for Disease Control (Atlanta, Georgia, USA) and first identified in the Ohio Department of Health Laboratories (Reynoldsburg, Ohio, USA).

Although not an exact predictor of protection, HI titers of 40 are considered the minimum protective level for humans (*25*). Therefore, titers of 20 against the isolated strain would not indicate a recent stimulation of the antibodies or a protective cross-reaction. However, a very mild or asymptomatic infection might not result in a high titer immune response (*26*). Because testing with A/Hawaii/70/2019 (H1N1) antiserum elicited no titer, seasonal vaccination would probably not provide protection against A/Alberta/01/2020/H1N2v.

Extensive surveillance testing in the geographic area of the index patient did not detect additional cases, indicating minimal spread. After detection of a variant influenza, active case-finding is critical because of the potential pandemic threat posed by emerging strains. A comparative evaluation of H1N1v and H1N2v viruses isolated during 2011–2016 found that many swine H1 strains capable of infecting humans possess adaptations for efficient replication and enhanced transmission through respiratory droplets (*27*). Furthermore, the H1 antigens in most isolates were distinct from those of vaccine strains; thus, routine influenza vaccine is unlikely to provide adequate protection against variant strains. Even 1 zoonotic event could enable adaptations for human infection and transmission (*28*).

We found low levels of circulating virus among pigs at the farm where the index patient's household member worked and those downstream from it, possibly because the 2 sites were finisher barns where medium-sized grower pigs are raised until they reach market weight. Sows who have antibodies to IAV from vaccination or natural exposure can pass maternally derived antibodies to their offspring through colostrum. The amount of maternally derived antibodies

detected in newborn piglets varies within litters, not only because antibodies vary among sows, but also because the firstborn piglets consume the most colostrum. In total, 60%–100% of nursing piglets born to a vaccinated sow have HI titers >120 at 5 days old. On average, 75% of the nursing piglets of vaccinated sows have a strong titer (>120) that is homologous between the vaccine and circulating strains (i.e., autogenous vaccines) (S. Detmer, University of Saskatchewan, pers. comm., 2021 Jun 5). As such, there is limited detection of virus in farrowing barns. In contrast, IAVs are often detected in and isolated from nursing piglets 14–24 days of age on farms that do not vaccinate sows, further demonstrating that maternally derived antibodies from vaccinated sows limit infection in nursing piglets until these antibodies wane at 6–8 weeks of age (*29*). By the time pigs reach the finisher barns, they often have experienced infection in the nursery, farrowing barn, or both and have acquired their own immune response to endemic strains of IAV. In finisher barns, acquired immunity among pigs causes many IAV infections to be subclinical and undetected (*30*).

In 2016, analysis of whole influenza genomes isolated from pigs in Canada and the United States demonstrated the splitting of the H1α clade into 3 distinct subclades: H1α-1, H1α-2, and H1α-3 (*31*). We found that A/Alberta/01/2020/H1N2v most closely resembles strains belonging to the H1α-3 virus clade; however, the variant strain does not contain the amino acid deletions at sites 129 and 130 in the HA gene. Therefore, A/Alberta/01/2020/H1N2v probably belongs to the H1α-3a virus clade. Further study is required to assess if the H1α-3a virus cluster is antigenically in addition to genetically distinct from the H1α-3 virus cluster.

A zoonotic H1α-3 H1N2v virus strain (A/Ohio/24/2017/H1N2) was isolated from a human in the United States in 2017 (*32*). The A/Ohio/24/2017/H1N2 and A/Alberta/01/2020 strains share high nucleotide identity (91.3%–96.6%) within 8 major genes; however, this proportion is lower than that of other H1N2 strains (Table). As of July 2021, 9 distinct H1α-3a viruses have been detected in the United States. These 9 viruses were probably associated with animal movements from Alberta to the US states of Iowa and South Dakota. These animal movements stopped in 2018 and there is no evidence of continued transmission or geographic spread of these strains in the United States (*31*).

A major limitation of this study is the 3-week delay in confirming the patient's H1N2v infection. Therefore, active surveillance testing of persons and pigs in the patient's geographic region was delayed, possibly diminishing our ability to detect additional active cases. However, we mitigated this limitation in human sampling by testing banked samples collected for SARS-CoV-2 testing beginning ≈1 week before the collection of the patient's nasopharyngeal swab sample. The delay might have contributed to the higher C_t values for IAV testing of samples from pigs at the farm of interest, because the active phase of infection probably occurred several weeks earlier in most pigs. The higher C_t values of >30 also decreased our ability to amplify certain gene segments for strain identification.

As of September 2021, no further H1N2v virus cases have been identified in humans in that area of Alberta. This case occurred when IAV incidence among humans was uncharacteristically low, probably because of nonpharmaceutical interventions implemented in response to the COVID-19 pandemic (*33*). These interventions simplified IAV screening. Our results highlight the importance of expanding collaborations between the human and veterinary sectors to enable timely identification, reporting, and investigation of emerging zoonotic pathogens of pandemic potential.

About the Author

Dr. Kanji is a medical microbiologist at Alberta Precision Laboratories, Calgary, Alberta, Canada. His research interests include zoonotic pathogens, clinical laboratory diagnostics, and infection control measures.

References

1. Cook PW, Stark T, Jones J, Kondor R, Zanders N, Benfer J, et al. Detection and characterization of swine origin influenza A(H1N1) pandemic 2009 viruses in humans following zoonotic transmission. J Virol. 2020;95:e01066-20. https://doi.org/10.1128/JVI.01066-20
2. Katz R. Use of revised International Health Regulations during influenza A (H1N1) epidemic, 2009. Emerg Infect Dis. 2009;15:1165–70. https://doi.org/10.3201/eid1508.090665
3. Bowman AS, Nelson SW, Page SL, Nolting JM, Killian ML, Sreevatsan S, et al. Swine-to-human transmission of influenza A(H3N2) virus at agricultural fairs, Ohio, USA, 2012. Emerg Infect Dis. 2014;20:1472–80. https://doi.org/10.3201/eid2009.131082
4. Government of Canada (Public Health Agency of Canada). Human emerging respiratory pathogens bulletin 2020 [cited 2021 Jan 18]. https://www.canada.ca/en/public-health/services/surveillance/human-emerging-respiratory-pathogens-bulletin.html
5. Centers for Disease Control and Prevention. Reported infections with variant influenza viruses in the United States 2017 [cited 2020 Nov 18]. https://www.cdc.gov/flu/swineflu/variant-cases-us.htm
6. World Health Organization. Influenza A(H1N2) variant virus—Brazil 2020 Jul 9 [cited 2020 Nov 18]. https://www.who.int/csr/don/09-jul-2020-influenza-a-brazil/en

7. Resende PC, Born PS, Matos AR, Motta FC, Caetano BC, Debur MD, et al. Whole-genome characterization of a novel human influenza A(H1N2) virus variant, Brazil. Emerg Infect Dis. 2017;23:152–4. https://doi.org/10.3201/eid2301.161122
8. Government of Canada. Human influenza A with swine origin. 2021 [cited 2021 May 29]. https://www.canada.ca/en/public-health/services/diseases/human-influenza-a-h1n2-v-swine-origin.html
9. Centers for Disease Control and Prevention. Novel influenza A virus infections. 2021 [cited 2021 May 8]. https://gis.cdc.gov/grasp/fluview/Novel_Influenza.html
10. Pabbaraju KWA, Douesnard M, Ma R, Gill K, Dieu P, Fonseca K, et al. Development and validation of reverse transcriptase-PCR assays for testing of SARS-CoV-2. Official Journal of the Association of Medical Microbiology and Infectious Disease Canada. 2020;6:16–22.
11. Centers for Disease Control and Prevention. CDC protocol of realtime RTPCR for swine influenza A(H1N1). 2007 [cited 2021 Jan 7]. https://www.who.int/csr/resources/publications/swineflu/CDCrealtimeRTPCRprotocol_20090428.pdf
12. Pabbaraju K, Wong S, Wong AA, Appleyard GD, Chui L, Pang X-L, et al. Design and validation of real-time reverse transcription-PCR assays for detection of pandemic (H1N1) 2009 virus. J Clin Microbiol. 2009;47:3454–60. https://doi.org/10.1128/JCM.01103-09
13. Hoffmann E, Stech J, Guan Y, Webster RG, Perez DR. Universal primer set for the full-length amplification of all influenza A viruses. Arch Virol. 2001;146:2275–89. https://doi.org/10.1007/s007050170002
14. Hamamoto I, Takaku H, Tashiro M, Yamamoto N. High yield production of influenza virus in Madin Darby canine kidney (MDCK) cells with stable knockdown of IRF7. PLoS One. 2013;8:e59892. https://doi.org/10.1371/journal.pone.0059892
15. Kendal APPM, Skehel JJ. Concepts and procedures for laboratory-based influenza surveillance. Geneva: World Health Organization; 1982.
16. Detmer SE, Patnayak DP, Jiang Y, Gramer MR, Goyal SM. Detection of influenza A virus in porcine oral fluid samples. J Vet Diagn Invest. 2011;23:241–7. https://doi.org/10.1177/104063871102300207
17. Detmer S, Gramer M, Goyal S, Torremorell M, Torrison J. Diagnostics and surveillance for swine influenza. Curr Top Microbiol Immunol. 2013;370:85–112. https://doi.org/10.1007/82_2012_220
18. Zhang J, Harmon KM. RNA extraction from swine samples and detection of influenza A virus in swine by real-time RT-PCR. Methods Mol Biol. 2020;2123:295–310. https://doi.org/10.1007/978-1-0716-0346-8_21
19. Government of Canada. Influenza weekly reports 2020–21 season. 2021 [cited 2020 Nov 18]. https://www.canada.ca/en/public-health/services/diseases/flu-influenza/influenza-surveillance/weekly-reports-2020-2021-season.html
20. Terebuh P, Olsen CW, Wright J, Klimov A, Karasin A, Todd K, et al. Transmission of influenza A viruses between pigs and people, Iowa, 2002–2004. Influenza Other Respir Viruses. 2010;4:387–96. https://doi.org/10.1111/j.1750-2659.2010.00175.x
21. Lauterbach SE, Wright CM, Zentkovich MM, Nelson SW, Lorbach JN, Bliss NT, et al. Detection of influenza A virus from agricultural fair environment: air and surfaces. Prev Vet Med. 2018;153:24–9. https://doi.org/10.1016/j.prevetmed.2018.02.019
22. Government of Canada. Swine biosecurity. 2012 [cited 2021 May 30]. https://inspection.canada.ca/animal-health/terrestrial-animals/biosecurity/standards-and-principles/swine/eng/1344746044066/1344746179549
23. Canadian Pork Council. Visitors and farm biosecurity. 2021 [cited 2021 May 30]. https://www.cpc-ccp.com/visitor-and-farm-biosecurity
24. Alarcón LV, Allepuz A, Mateu E. Biosecurity in pig farms: a review. Porcine Health Management. 2021;7:5.
25. Hancock K, Veguilla V, Lu X, Zhong W, Butler EN, Sun H, et al. Cross-reactive antibody responses to the 2009 pandemic H1N1 influenza virus. N Engl J Med. 2009;361:1945–52. https://doi.org/10.1056/NEJMoa0906453
26. To KKW, Zhang AJX, Hung IFN, Xu T, Ip WCT, Wong RTY, et al. High titer and avidity of nonneutralizing antibodies against influenza vaccine antigen are associated with severe influenza. Clin Vaccine Immunol. 2012;19:1012–8. https://doi.org/10.1128/CVI.00081-12
27. Pulit-Penaloza JA, Pappas C, Belser JA, Sun X, Brock N, Zeng H, et al. Comparative in vitro and in vivo analysis of H1N1 and H1N2 variant influenza viruses isolated from humans between 2011 and 2016. J Virol. 2018;92:e01444–18. https://doi.org/10.1128/JVI.01444-18
28. Lee JH, Pascua PN, Decano AG, Kim SM, Park SJ, Kwon HI, et al. Evaluation of the zoonotic potential of a novel reassortant H1N2 swine influenza virus with gene constellation derived from multiple viral sources. Infect Genet Evol. 2015;34:378–93. https://doi.org/10.1016/j.meegid.2015.06.005
29. Chamba Pardo FO, Wayne S, Culhane MR, Perez A, Allerson M, Torremorell M. Effect of strain-specific maternally-derived antibodies on influenza A virus infection dynamics in nursery pigs. PLoS One. 2019;14:e0210700. https://doi.org/10.1371/journal.pone.0210700
30. Poljak Z, Dewey CE, Martin SW, Christensen J, Carman S, Friendship RM. Prevalence of and risk factors for influenza in southern Ontario swine herds in 2001 and 2003. Can J Vet Res. 2008;72:7–17.
31. Nelson MI, Culhane MR, Trovão NS, Patnayak DP, Halpin RA, Lin X, et al. The emergence and evolution of influenza A (H1α) viruses in swine in Canada and the United States. J Gen Virol. 2017;98:2663–75. https://doi.org/10.1099/jgv.0.000924
32. Rambo-Martin BL, Keller MW, Wilson MM, Nolting JM, Anderson TK, Vincent AL, et al. Influenza A virus field surveillance at a swine-human interface. MSphere. 2020;5:e00822–19. https://doi.org/10.1128/mSphere.00822-19
33. Partridge E, McCleery E, Cheema R, Nakra N, Lakshminrusimha S, Tancredi DJ, et al. Evaluation of seasonal respiratory virus activity before and after the statewide COVID-19 shelter-in-place order in Northern California. JAMA Netw Open. 2021;4:e2035281.

Address for correspondence: Jamil Kanji, Public Health Laboratory, Alberta Precision Laboratories, Foothills Medical Centre, 3030 Hospital Dr NW, Calgary, AB T2N 4W4, Canada; email: jamil.kanji@ahs.ca

Surface–Aerosol Stability and Pathogenicity of Diverse Middle East Respiratory Syndrome Coronavirus Strains, 2012–2018

Neeltje van Doremalen,[1] Michael Letko,[1] Robert J. Fischer, Trenton Bushmaker, Jonathan Schulz, Claude K. Yinda, Stephanie N. Seifert, Nam Joong Kim, Maged G. Hemida, Ghazi Kayali, Wan Beom Park, Ranawaka A.P.M. Perera, Azaibi Tamin, Natalie J. Thornburg, Suxiang Tong, Krista Queen, Maria D. van Kerkhove, Young Ki Choi, Myoung-don Oh, Abdullah M. Assiri, Malik Peiris, Susan I. Gerber, Vincent J. Munster

Middle East respiratory syndrome coronavirus (MERS-CoV) infects humans and dromedary camels and is responsible for an ongoing outbreak of severe respiratory illness in humans in the Middle East. Although some mutations found in camel-derived MERS-CoV strains have been characterized, most natural variation found across MERS-CoV isolates remains unstudied. We report on the environmental stability, replication kinetics, and pathogenicity of several diverse isolates of MERS-CoV, as well as isolates of severe acute respiratory syndrome coronavirus 2, to serve as a basis of comparison with other stability studies. Although most MERS-CoV isolates had similar stability and pathogenicity in our experiments, the camel-derived isolate C/KSA/13 had reduced surface stability, and another camel isolate, C/BF/15, had reduced pathogenicity in a small animal model. These results suggest that although betacoronaviruses might have similar environmental stability profiles, individual variation can influence this phenotype, underscoring the need for continual global viral surveillance.

Author affiliations: National Institutes of Health, Hamilton, Montana, USA (N. van Doremalen, M. Letko, R.J. Fischer, T. Bushmaker, J. Schulz, C.K. Yinda, S.N. Seifert, V.J. Munster); Washington State University, Pullman, Washington, USA (M. Leitko, S.N. Seifert); Seoul National University College of Medicine, Seoul, South Korea (N.J. Kim, W.B. Park, M.-d. Oh); King Faisal University, Al-Hasa, Saudi Arabia (M.G. Hemida); Kafrelsheikh University, Kafrelsheikh, Egypt (M.G. Hemida); University of Texas Health Sciences Center, Houston, Texas, USA (G. Kayali); University of Hong Kong, Hong Kong, China (R.A.P.M. Perera, M. Peiris); Centers for Disease Control and Prevention, Atlanta, Georgia, USA (A. Tamin, N.J. Thornburg, S. Tong, K. Queen, S.I. Gerber); World Health Organization, Geneva, Switzerland (M.D. van Kerkhove); Chungbuk National University, Cheongju City, South Korea (Y.K. Choi); Ministry of Health, Riyadh, Saudi Arabia (A.M. Assiri)

DOI: https://doi.org/10.3201/eid2712.210344

Middle East respiratory syndrome coronavirus (MERS-CoV) was detected during 2012 and continues to cause outbreaks as a result of frequent spillover from dromedary camels to humans. Human infection with MERS-CoV has a mortality rate of ≈35%, and the virus has spread to 27 countries (*1*). Approximately 41% of human MERS-CoV infections in Saudi Arabia are primary, resulting from direct camel-to-human transmission (*2*). To date, MERS-CoV has been detected in camels in Burkina Faso, Egypt, Ethiopia, Jordan, Kenya, Morocco, Nigeria, Saudi Arabia, Senegal, Sudan, Tunisia, and Uganda (*3*–*11*).

Human-to-human transmission of MERS-CoV primarily occurs in hospital settings and within households (*12*). Epidemiologic studies have mapped indirect patient contact within hospitals, providing evidence for aerosol-mediated and hospital-worker–mediated spread (*13*–*16*). The largest outbreak of infection with MERS-CoV outside the Middle East occurred when 1 traveler from the Middle East brought MERS-CoV to South Korea, resulting in 185 subsequent infections (*17*).

Coronaviruses have large, nonsegmented, positive-sense RNA genomes. The 1% nucleotide sequence variation reported between various MERS-CoV isolates collected in the Middle East and North Africa is equivalent to 300 nt changes in the 30-kB viral genome (*18*). Many of these changes are nonsynonymous and distributed throughout the viral genome. Even single amino acid changes in MERS-CoV can alter viral replication (*19*), and deletions in MERS-CoV have been shown to attenuate

[1]These authors contributed equally to this article.

pathology in an animal model (*18*). These findings underscore the need for characterizing how MERS-CoV genetic variation alters viral replication, pathogenicity, and stability.

We tested a broad panel of viral isolates collected from humans and camels, representing every major geographic region that has had MERS-CoV outbreaks and spanning from early to contemporary outbreaks. Because MERS-CoV spreads within households and hospitals, we characterized viral phenotypes with immediate implications for public health. We focused on environmental stability in aerosols as well as surface stability on common materials found in hospitals, replication kinetics in immortalized human cell lines and primary human airway epithelial cultures, and pathogenicity in a transgenic mouse model our laboratory developed to test vaccine efficacy (*20*). For environmental stability studies, we included severe acute respiratory syndrome coronavirus 2 (SARS-CoV-2) to enable better comparison of these findings with those of previously published stability studies (*21*).

Methods

Ethics

Animal experiment approval was obtained by the Institutional Animal Care and Use Committee at Rocky Mountain Laboratories, National Institutes of Health (Hamilton, MT, USA). All animal experiments were executed in an Association for Assessment and Accreditation of Laboratory Animal Care–approved facility, following the guidelines in National Institutes of Health Guide for the Care and Use of Laboratory Animals, Animal Welfare Act, US Department of Agriculture, and United States Public Health Service Policy on Humane Care and Use of Laboratory Animals. The Institutional Biosafety Committee approved work with MERS-CoV strains under Biosafety Level 3 conditions.

Viral Stock Propagation

We provide strain-specific details for the viruses used in this study (Table). Viruses were isolated by others and provided for this study. SARS-CoV-2/Washington was isolated by the Centers for Disease Control and Prevention (Atlanta, GA, USA).

We obtained MERS-CoV strains from the following sources: EMC12 from Erasmus Medical Center (Rotterdam, the Netherlands); U/14, KSA/15, and KSA/18 from the Centers for Disease Control and Prevention; SK/15 from Chungbuk National University (Cheongju, South Korea); and C/KSA/13, C/E/13, and C/BF/15 from Hong Kong University (Hong Kong, China). We passaged MERS-CoV and SARS-CoV-2 strains once in Vero E6 cells in Dulbecco's modified Eagle medium (DMEM; Sigma Aldrich, https://www.sigmaaldrich.com) supplemented with 2% fetal bovine serum (Thermo Fisher Scientific, https://www.thermofisher.com), 50 U/mL of penicillin (Thermo Fisher), and 50 μg/m of streptomycin (Thermo Fisher).

We maintained Vero E6 cells in DMEM supplemented with 10% fetal bovine serum, 1 mmol/L of L-glutamine, 50 U/mL of penicillin, and 50 μg/mL of streptomycin. We clarified virus stocks by

Table. Characteristics of Middle East respiratory syndrome coronaviruses tested*

Name	Host	Year	Location	Full name	GenBank accession no.	SNPs >50%
EMC/12	Human	2012	Saudi Arabia	HCoV-EMC/2012	JX869059	G27162A (ORF5, W108†)
U/14	Human	2014	United States	Hu/Florida/USA-2/Saudi Arabia/2014	KP223131	None
KSA/15	Human	2015	Saudi Arabia	Hu/Hofuf/KSA-11002/2015	KY688120	None
SK/15	Human	2015	South Korea	Hu/Korea/Seoul/177–3/2015	KX034100	C2149A (NSP2, S431Y); A6884G (synonymous); T9566C (synonymous); G10155T (NSP5, A46S); A11376T (NSP6, S147C); C14162T (synonymous); C26189T (ORF4b R33C)
KSA/18	Human	2018	Saudi Arabia	Hu/Saudi Arabia/3015600912/2018	MN723544	C21149A (NSP16, L183I); G22366A† (S, R304Q); C25009T (S, S1185L)
C/KSA/13	Camel	2013	Saudi Arabia	Camel/Saudi Arabia/KFU-HKU1/2013	KJ650297	C25207T (S, S1251F); C27875T (M, T8I)
C/E/13	Camel	2013	Egypt	Camel/Egypt/NRCE/HKU270/2013	KJ477103	T16318C (synonymous); C24112T (S, A886V); 26892T (ORF5, P18L)
C/BF/15	Camel	2015	Burkina Faso	Camel/Burkina Faso/CIRAD-HKU785/2015	MG923471	None

*NSP, nonstructural protein; ORF, open reading frame; SNP, single-nucleotide polymorphism.
†Present in other sequences.

centrifugation and froze them at −80°C. We performed virus titrations by using endpoint titration in Vero E6 cells inoculated with 10-fold serial dilutions of virus. We scored cytopathic effect at day 5 (for MERS-CoV) or day 6 (for SARS-CoV-2) and calculated median tissue culture infectious dose ($TCID_{50}$) from 4 replicates by using the Spearman–Karber method (*22*).

Sequencing Stocks

We treated MERS-CoV samples with RiboZero H/M/R rRNA Depletion Mix (Illumina, https://www.illumina.com) according to the manufacturer's instructions. After purification with Ampure RNA-CleanXP (Beckman Coulter, ttps://www.beckmancoulter.com), we eluted enriched RNA and assessed it on a BioAnalyzer RNA Pico Chip (Agilent Technologies, https://www.agilent.com). We prepared second-strand cDNA according to the Truseq Stranded mRNA Library Preparation Guide (Illumina). We treated samples with RiboShredder RNase Blend (https://www.cambio.co.uk).

We visualized final libraries on a BioAnalyzer DNA1000 Chip (Agilent Technologies), and quantified them by using a KAPA Library Quant Kit (Illumina) and a universal qPCR Mix (Kapa Biosystems, https://www.roche.com) on a CFX96 Real-Time System (Bio-Rad Laboratories, https://www.bio-rad.com). We pooled libraries together in equimolar concentrations and sequenced them using MiSeq (Illumina) with on-board cluster generation and 2 × 250 paired-end sequencing. The cluster density was at 454 k/mm^2/lane, resulting in 8.7 million reads passing filter/run and an average 85% greater than the Q30 score.

Phylogenetics

We downloaded all available MERS-CoV genome sequences from GenBank and curated them to remove sequences that were not independently sampled. We aligned sequences with the consensus sequences for MERS-CoV isolates used in this study by using MAFFT version 7.388 plugin (*23*) in Geneious Prime (https://www.geneious.com). We inferred a phylogenetic tree by using the maximum-likelihood method under the general time reversible plus gamma model of nucleotide substitution with 1,000 bootstrap replicates implemented with PhyML version 3.3.20190321 (https://www.atgc-montpellier.fr).

Stability of MERS-CoV on Surfaces and in Aerosols

We sterilized 15-mm polypropylene discs (ePlastics, https://www.eplastics), AISI 304 alloy stainless steel discs (Metal Remnants, https://metalremnants.com), copper discs (99.9%; Metal Remnants), and silver discs (99.9%) (Sigma-Aldrich, https://www.sigmaaldrich.com), placed them in 24-well plates, and added 50 μL of MERS-CoV (10^5 $TCID_{50}$/mL). For timepoints taken at 0, 1, 24, 48, and 72 h, we added 1 mL of DMEM to wells, aliquoted, and stored at −80°C. We titrated samples on Vero E6 cells and maintained the temperature (21°C–22°C) and humidity (45%–55%).

We determined virus stability in aerosols as described (*24*). In brief, we loaded a collison nebulizer with $10^{6.5}$ $TCID_{50}$/mL of MERS-CoV in DMEM containing 2% fetal bovine serum. Aerosols were maintained in a Goldberg drum and samples collected at 0, 30, 60, 120, and 180 min after aerosolization by passing air at a volume of 6 L/min for 30 s from the drum through a 47-mm gelatin filter (Sartorius, https://www.sartorius.com). Filters were dissolved in 10 mL of DMEM containing 10% fetal bovine serum and stored at −80°C. All samples were titrated on Vero E6 cells.

Replication of MERS-CoV Strains In Vitro

We inoculated Vero E6 cells with virus (multiplicity of infection = 0.01) and collected supernatants at 8, 24, 48 and 72 hours postinfection (hpi). Human airway epithelium (HAE) inserts (Epithelix, https://www.epithelix.com) were maintained as specified by the manufacturer. We washed HAEs with 200 μL of phosphate-buffered saline for 30 min, followed by inoculation with MERS-CoV at a multiplicity of infection of 0.1. We obtained samples at 8, 24, 48, 72, and 96 hpi.

Animal Experiments

We inoculated intranasally transgenic BALB/c mice expressing human DPP4 with 10^3 $TCID_{50}$ MERS-CoV. Mice were weighed and swabbed daily. At day 3, we euthanized 4 mice and harvested lung tissue. We monitored the remaining 6 mice for survival. We euthanized mice if there were signs of severe disease signs based on quantitative assessment (e.g., hunched posture, lack of movement) or >20% weight loss.

RNA Extraction and Quantitative Reverse Transcription PCR

We homogenized lung tissues and extracted RNA by using the RNeasy method (QIAGEN, https://www.qiagen.com) according to the manufacturer's instructions. We added swab specimens to 1 mL of DMEM, vortexed them, and used 140 μL for RNA extraction by using the QiaAmp Viral RNA Kit and a QIAxtractor (QIAGEN).

We detected MERS-CoV viral RNA by using the UpE MERS-CoV assay (*25*) and the RotorGeneTM Probe Kit (QIAGEN). Primers in this assay target a highly conserved region upstream of MERS-CoV envelope gene. Sequences of MERS-CoV strains used in this study are identical in this region. MERS-CoV dilutions with known genome copies were run in parallel to enable calculation of genome copies in samples.

Histologic and Immunohistochemical Analysis

We fixed harvested tissues for ≥7 days in 10% neutral-buffered formalin, processed them by using a VIP-6 Tissue Tek Tissue Processor (Sakura Finetek, https://www.sakuraus.com), and embedded them in Ultraffin Paraffin Polymer (Cancer Diagnostics, https://www.cancerdiagnostics.com). We stained 5-μm sections with hematoxylin and eosin and detected coronavirus immunoreactivity by using MERS-CoV nucleocapsid protein rabbit antibody (diluted 1:4,000; Sino Biological Inc, https://www.sinobiological.com).

We processed tissues for immunohistochemical analysis by using the Discovery ULTRA Automated IHC/ISH Staining Instrument (and a Discovery ChromoMap DAB Kit (both from Ventana Medical Systems, https://diagnostics.roche.com). For morphometric analysis, we scanned slides by using the Aperio ScanScope AT2 (Aperio Technologies, Inc., https://www.aperio.com) and analyzed the entire section by using ImageScope Positive Pixel Count Algorithm version 9.1 (Aperio Technologies, Inc.). All tissue slides were evaluated by a board-certified veterinary anatomic pathologist.

Statistical Analyses

We performed analyses by using GraphPad Prism version 7.05 for Windows (https://www.graphpad.com). All strains were compared with EMC/12. For aerosol stability data analysis, we determined linear regression for the mean value of 3 runs/virus. We determined statistical significance in deviation from MERS-CoV/EMC12 results by using 1-way analysis of variance, followed by the Bonferroni multiple comparisons test or a 2-way unpaired Student's t-test. We used simple linear regression to evaluate slopes of decay. Survival of mice compared with mice inoculated with EMC/12 was performed by using the log-rank (Mantel-Cox) test. To calculate the amount of virus shedding per mouse in in vivo comparisons, we calculated the area under the curve for a plot of the viral load measured in oropharyngeal swab specimens.

Results

Stability of MERS-CoV Strains in Aerosols or as Fomites Compared with SARS-CoV-2

We selected 8 MERS-CoV strains and 1 SARS-CoV-2 strain (SARS-CoV-2/WA1-2020) to be used in this study (Table; Figure 1). Five MERS-CoV strains were isolated from human cases and 3 strains were isolated from dromedary camels. Strains were isolated during 2012–2018 and originated from the Middle East (*5*), Africa (*2*) or South Korea (*1*) (Table). All originally obtained viruses were passaged once in Vero E6 cells, and virus stocks were deep sequenced (Table). We used MERS-CoV sequences to construct a phylogenetic maximum-likelihood tree, which showed a wide distribution of MERS-CoV strains selected. Thus, our panel represents a broad sample of known genetic variation within currently circulating MERS-CoV strains.

We first investigated the stability of MERS-CoV as fomites on polypropylene, stainless-steel, copper, and silver surfaces, which we selected because they represent commonly encountered surfaces in hospital environments or have virocidal properties (*23*). For comparison with a pandemic human coronavirus, we also included SARS-CoV-2. Back-titrations of all virus strains showed comparable starting virus titers. Stability of MERS-CoV on polypropylene and stainless-steel surfaces, maintained at 21°C–22°C and a relative humidity of 45%–55% under standard laboratory light conditions, was similar to that reported for MERS-CoV and SARS-CoV-2 stability on surfaces (*21*,*26*). We found major differences in decay rates when comparing EMC/12 to SK/15, KSA/18, C/KSA/13, and C/BF/15 on polypropylene. These differences were not found for the other surfaces (Figure 2; Appendix Figure, https://wwwnc.cdc.gov/EID/article/27/12/21-0344-App1.pdf). Infectious virus titers were low for all strains on copper and silver surfaces at 24 hours. We analyzed data by using linear regression for the first 24 hours for each surface and each virus. Decay, averaged between all virus strains, was higher for copper (−0.11576 $\log_{10}$ $TCID_{50}$/h) and silver (−0.08744 $\log_{10}$ $TCID_{50}$/h) surfaces than for polypropylene (−0.0529 $\log_{10}$ $TCID_{50}$/h) and stainless-steel (−0.0469 $\log_{10}$ $TCID_{50}$/h) surfaces.

We aerosolized all MERS-CoV strains in a Goldberg drum at 21°C and a relative humidity of 60%–70% in the dark. We then tested samples at 0, 30, 60, 120 and 180 min after aerosolization, titrated them, and compared results with those for SARS-CoV-2. We detected no major differences in linear regression of loss of infectious virus in aerosols between strains. For all

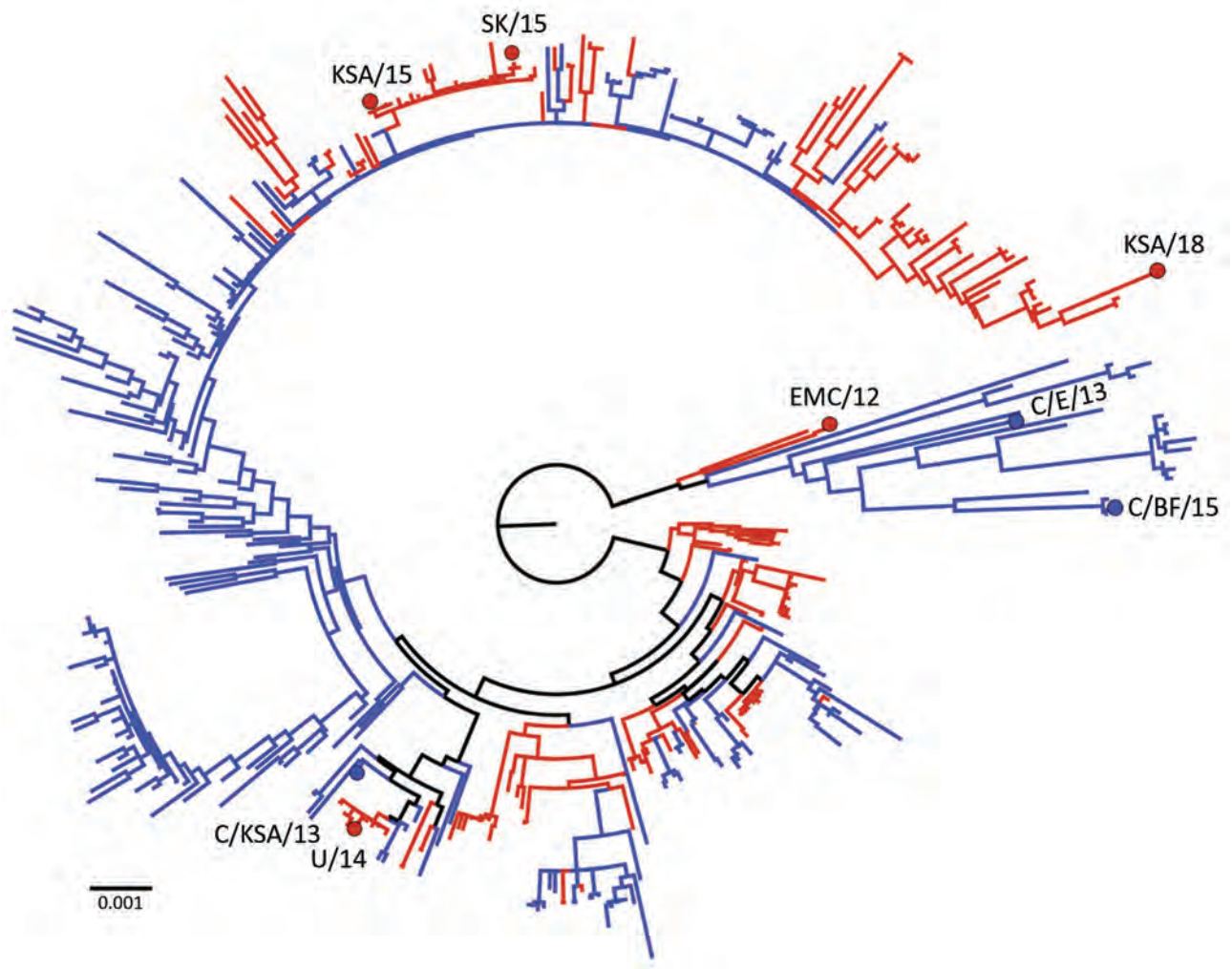

Figure 1. Phylogenetic tree of 446 full Middle East respiratory syndrome coronavirus (MERS-CoV) genomes showing distribution of human-derived (red) and camel-derived (blue) isolates. The tree was constructed with PhyML (https://www.atgc-montpellier.fr) and rooted at the midpoint. Strain EMC/12 was obtained from Erasmus Medical Center (Rotterdam, the Netherlands); U/14, KSA/15, and KSA/18 from the Centers for Disease Control and Prevention (Atlanta, GA, USA); SK/15 from Chungbuk National University (Cheongju, South Korea); and C/KSA/13, C/E/13, and C/BF/15 from Hong Kong University (Hong Kong, China). Scale bar indicates nucleotide substitutions per site. KSA, Kingdom of Saudi Arabia.

MERS-CoV strains, infectious virus could still be detected at 180 min after aerosolization (Figure 2, panel B).

In Vitro Replication of MERS-CoV Strains

To investigate any in vitro growth differences, we grew strains in 2 cell systems, Vero E6 cells and HAE cultures, in comparison to the reference strain EMC/12. At 48 hpi, C/KSA/13 and KSA/15 showed higher titers than EMC/12 in Vero E6 cells. At 72 hpi, C/KSA/13 and C/BF/15 showed lower titers than EMC/12 in HAE cultures. We observed no other major differences in either culture type. Although differences were not always statistically significant, all camel-derived viruses had reduced replication kinetics compared with those for EMC/12 in HAE cells at 24–72 hpi (Figure 3).

Disease Progression for MERS-CoV Strains in hDPP4 Transgenic Mice

MERS-CoV enters cells expressing the receptor human dipeptidyl peptidase IV (hDPP4). Our laboratory developed hDPP4 transgenic mice to test MERS-CoV vaccine efficacy (*20*). We intranasally inoculated 10 mice/group with 10^3 $TCID_{50}$ MERS-CoV/mouse. Mice started to lose weight on days 2–5 postchallenge; weight continued to decrease for all groups, except for mice inoculated with C/BF/15, in which only 1 mouse continued to lose weight (Figure 4,

panel A). For all groups, including C/BF/15, weight loss was also associated with other signs: ruffled coat, increased breathing rate, reluctance to move, and hunched posture. Only animals in the groups inoculated with SK/15 (1/6) and the group inoculated with C/BF/15 (5/6) survived. Average time to death was similar for all groups, excluding C/BF/15: EMC/12, 7.33 days; U/14, 6.5 days; KSA/15. 7 days; SK/15. 7.6 days; KSA/18. 7.67 days; C/KSA/13, 7.5 days; and C/E/13, 8 days (Figure 4, panel B).

We measured viral RNA in oral swab specimens obtained during days 1–7 postchallenge and found no

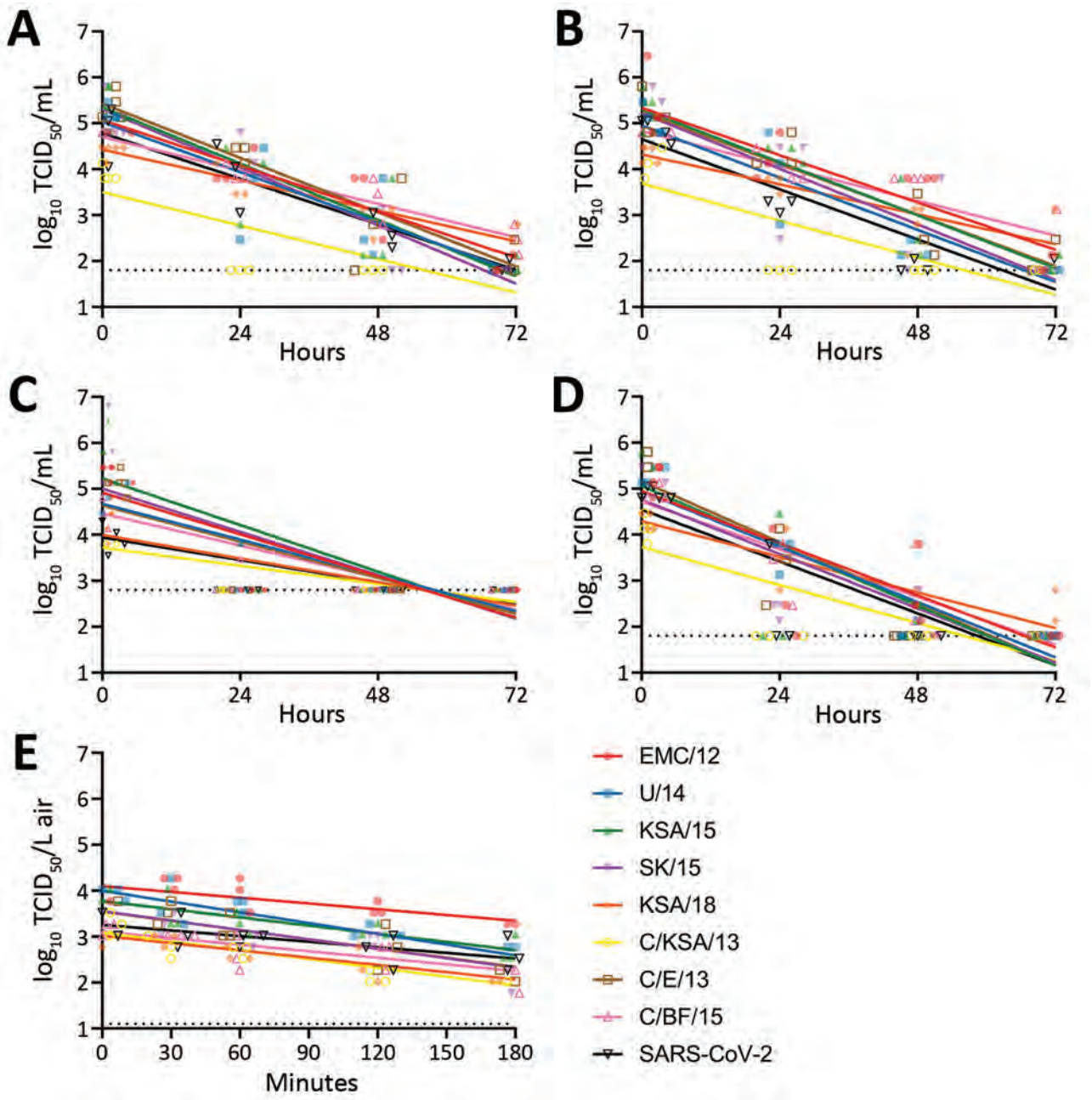

Figure 2. Stability of MERS-CoV strains on surfaces and in aerosols compared with those for SARS-CoV-2. Simple linear regression of virus was used for different surfaces and in aerosols. For surface stability, 50 μL of MERS-CoV or SARS-CoV-2 was spread on a surface, either polypropylene, stainless steel, copper, or silver; 1 mL of Dulbecco's modified Eagle medium was added at times 0, 1, 24, 48, or 72 hours, and samples were titrated. For aerosol stability, MERS-CoV– or SARS-CoV-2–containing aerosols were sprayed into a Goldberg drum; samples were taken at times 0, 30, 60, 120, and 180 min and then titrated. Linear regression was calculated per virus and indicated as lines. Dotted lines indicate limits of detection. Strain sources are listed in the legend for Figure 1. MERS-CoV, Middle East respiratory syndrome coronavirus; SARS-CoV-2, severe acute respiratory syndrome coronavirus 2; $TCID_{50}$, median tissue culture infectious dose.

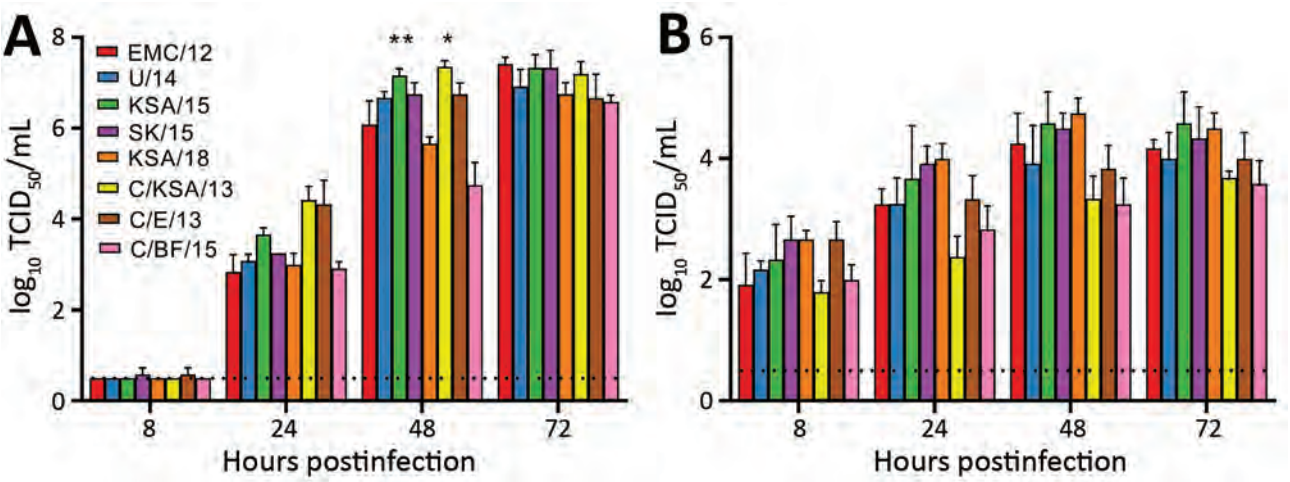

Figure 3. Middle East respiratory syndrome coronavirus replication in Vero E6 cells (A) and human airway epithelium (B). Replication is shown as geometric means; error bars indicate SDs. Vero E6 cells were infected with a multiplicity of infection of 0.01, and human airway epithelium were infected with a multiplicity of infection of 0.1. Samples of supernatants were obtained at 8, 24, 48 and 72 hours postinoculation and titrated. Statistically significant differences compared with those for the prototypical strain, EMC/12, were calculated by using ordinary 1-way analysis of variance, followed by a Bonferroni multiple comparisons test. Dotted lines indicate limits of detection. Strain sources are listed in the legend for Figure 1. $TCID_{50}$, median tissue culture infectious dose. *p<0.05; **p<0.01.

major differences in the amount of shedding between different groups (Figure 4, panels C, D). Viral genome RNA was lower in lung tissue collected on day 3 from mice inoculated with SK/15, C/E/15, and C/BF/15. Subgenomic RNA was lower to a major degree only in lung tissue of mice inoculated with C/BF/15 (Figure 4, panels E, F).

We observed no differences in pathology between different groups. Animals rarely showed pulmonary pathology at day 3. However, animals that had lesions showed only a minimal and random lymphocytic infiltrate. Immunohistochemical analysis showed that MERS-CoV antigen was expressed rarely or randomly in type I and II pneumocytes and not located in areas of inflammation. Morphometric analysis of pulmonary tissue that had immunoreactivity showed no major differences between groups (Figure 4, panel G).

Discussion

The ongoing MERS-CoV endemic in the Middle East and subsequent discovery of the virus in camel herds across Africa has resulted in a wealth of publicly available genetic data for various viral strains and isolates. In this study, we assessed several of these isolates for viral phenotypes related to public health in an attempt to better inform public health policy making with regards to MERS-CoV and other human coronaviruses that cause respiratory diseases, such as SARS-CoV-2.

Because nosocomial spread is at the center of MERS-CoV outbreaks, we assessed the stability of the virus on various surface material types commonly found in hospitals (polypropylene plastic and stainless steel), as well as materials that had potential antiviral and known antimicrobial properties (silver and copper) (*27*,*28*). Our experiments were performed at environmental conditions similar to those in hospitals, in which there is high risk for human-to-human, nosocomial transmission. Regardless of the surface material tested, strain C/KSA/13 was the least stable over time and was below detectable levels by 24 hours (Figures 2, 4). This strain had the lowest starting titer in these experiments, which might explain this difference in stability. In addition, our C/KSA/13 stock contains 2 nonsynonymous mutations in the viral structural proteins, spike and matrix, not found in our other strains, which might also play a role in this difference, either directly or indirectly (Table). These findings warrant further studies on how specific MERS-CoV polymorphisms in structural proteins affect viral growth.

As shown by Doremalen et al. (*21*), all virus strains tested had notably reduced stability on copper and silver surfaces (Figure 2, panel A). Copper has been shown to also have antiviral properties against influenza A(H1N1) virus and SARS-CoV-2 (*29*–*31*). The exact antiviral mechanism for copper is still unclear, but might be related to formation of hydroxyl radicals by copper ions when in aqueous solution (*31*). Silver-based nanoparticles have been shown to be antiviral for HIV-1 (*32*), herpes simplex virus 2 (*33*), hepatitis B virus (*34*), respiratory syncytial virus (*35*), and

monkeypox virus (*36*). Taking advantage of the antiviral properties of copper and silver might help decrease nosocomial transmission. Both silver and copper can be used for coating medical tools (*37*) and commonly touched items, such as bed rails, door handles, and intravenous poles (*38*). These findings appear to be more broadly applicable for other coronaviruses because we observed similar results for SARS-CoV-2 (Figure 2) (*21*). Further research should be invested in determining coronavirus susceptibility to metal ion inactivation.

MERS-CoV transmission might occur through aerosols and fomites (*39*), although the role of each route is not known. Transmission often occurs in hospitals; thus, aerosol-generating medical procedures might play a major role (*40*). MERS-CoV transmission has occurred over distances of >6 feet (*41*), and evidence of MERS-CoV on surfaces and in air in hospitals has been found (*39*). Studies have suggested that a hospital air-handling system might have contributed to nosocomial spread during the 2015 MERS-CoV outbreak in South Korea (*14*,*39*), and our group has shown that the virus can remain viable suspended in air for ≤10 min (*26*). We tested aerosol stability of viral isolates and observed that all viruses remained viable for a minimum of 180 min with an ≈10-fold

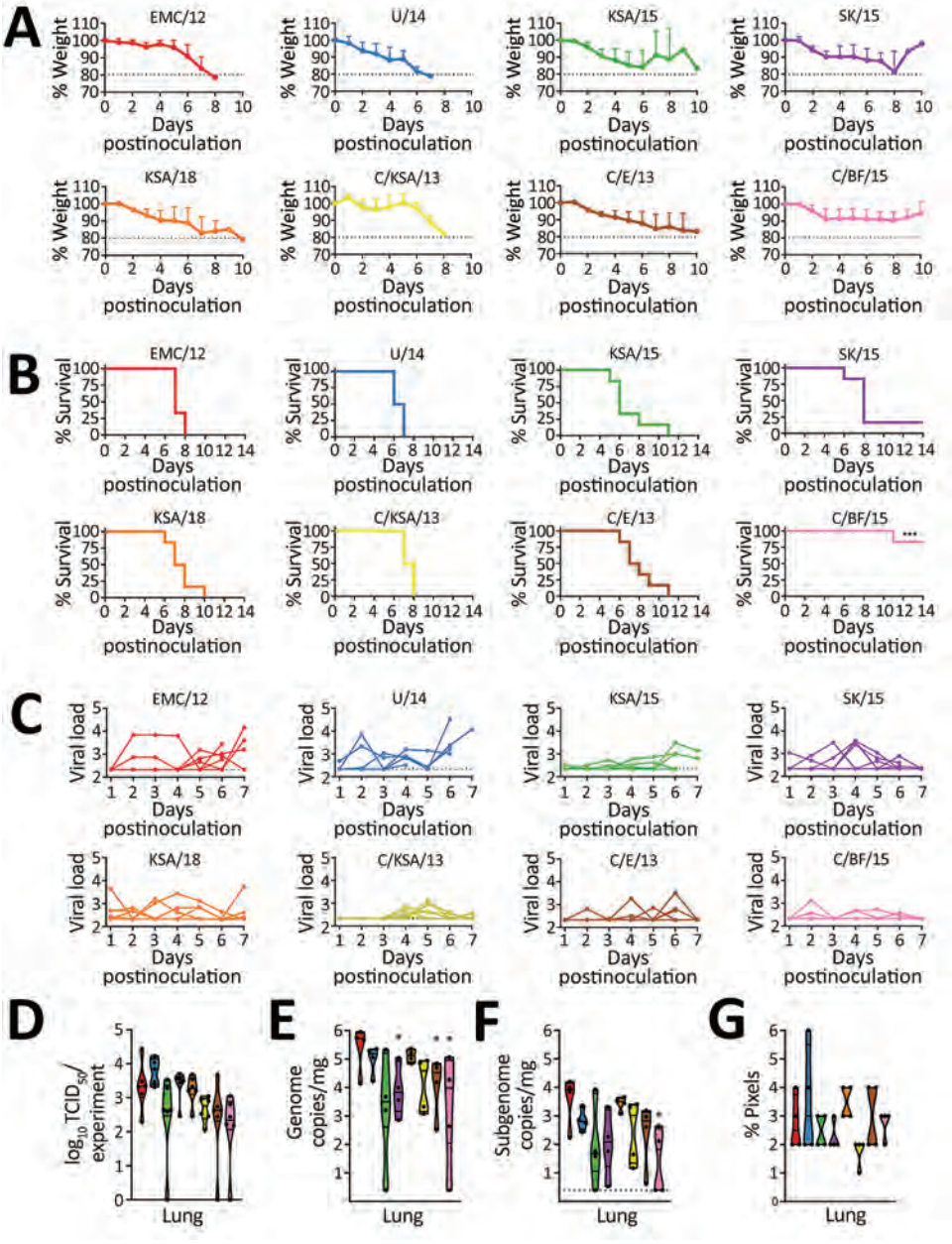

Figure 4. In vivo replication of different Middle East respiratory syndrome coronavirus (MERS-CoV) strains. hDPP4 mice were inoculated intranasally with 10^3 $TCID_{50}$ of MERS-CoV. Four mice were euthanized on day 3, and the remaining 6 mice were monitored for survival. A) Relative weight loss of hDPP4 mice. B) Survival of hDPP4 mice. C) Oropharyngeal shedding of MERS-CoV as measured by using an UpE quantitative reverse transcription PCR. D) Amount of shedding per experiment per mouse calculated by using area under the curve (AUC) analysis of viral load in oropharyngeal swab specimens. Results are displayed per mouse per virus strain. E) Viral load in lung tissue obtained from mice euthanized at day 3. F) Viral mRNA load in lung tissue obtained from mice euthanized at day 3. G) Percentage of positive pixels quantified from lung tissues stained for MERS-CoV antigen. Colors in panels D–F match those for strains in panels A–-C; strain sources are listed in the legend for Figure 1. Statistical significance was compared by using 1-way analysis of variance, followed by a Bonferroni multiple comparisons test. Dotted lines indicate limits of detection. $TCID_{50}$, median tissue culture infectious dose. *p<0.05.

reduction in viral titer observed on average within the collected aerosols (Figure 2, panel B).

Although we did not observe major differences in this study, strain stability is an useful phenotype to continue monitoring because mutations in viral capsid proteins have been shown to enhance environmental stability of bacteriophages, dengue virus, and transmissible gastroenteritis virus (*42*–*44*). Because MERS-CoV isolates contain polymorphisms throughout the entire viral genome, including the structural proteins that form virions, mutations might arise that influence overall virus particle stability. C/KSA/13, which showed reduced stability on surfaces in our experiments, contains polymorphisms in open reading frame 1b, the spike glycoprotein, and the virion matrix protein in comparison to the other strains tested. Recent studies have further demonstrated the influence of various external factors on environmental stability for SARS-CoV-2, including experimental ambient conditions and matrix in which the virus is suspended (*45*,*46*). Our experiments were performed in standard, indoor laboratory settings and with virus suspended in culture media, which enabled us to observe intrinsic differences determined solely at the viral level. Tracking and assessing the stability of coronavirus strains will improve our understanding of coronavirus variant spread.

We tested viral replication kinetics in Vero E6 cells and primary HAE cells (Figure 3). All viruses replicated to similar titers on Vero E6 cells by 72 hours. However, KSA/15 and C/KSA/13 had higher titers than EMC/12 by 48 hpi. Albeit the difference is not significant, C/BF/15 has a lower viral titer than EMC/12 at 48 hpi and 72 hpi. These results are consistent with those of a previous study, which showed that C/BF/15 has impaired replication (*18*). In primary HAE cultures, all camel-derived viral isolates had reduced replication kinetics compared with that for EMC/12 (Figure 3, panel B). More studies are needed with these camel-derived isolates to determine whether their differences in replication kinetics results from a comparison with EMC12, which has well-described tissue culture adaptations, or to see if MERS-CoV might adapt in humans after transmission from camels. Sequence analysis of the viral variants did not identify any obvious mutation patterns in any single viral protein that would explain the differences in replication kinetics. Thus, we speculate that these differences are the result of cumulative effects across ≥1 types of genetic variation.

We have shown that MERS-CoV replicates in type I and II pneumocytes in the lower respiratory tract of an animal model (*20*). Although disease progression after infection with this virus does not involve the central nervous system in humans, this small animal model is suitable for vaccine candidate testing, using animal survival or viral-induced death as a binary readout for vaccine efficacy. MERS-CoV C/BF/15 contains a deletion in open reading frame 4b, which has been shown in a similar mouse model to result in impaired suppression of the host interferon response and increased type I and type III interferon signaling (*18*). Taken together, these results pave the way for testing MERS-CoV vaccine candidates for broadly neutralizing potential in this animal model (*20*,*47*).

Our results with MERS-CoV C/KSA/13 suggest there might be a potential tradeoff between environmental surface stability and replication kinetics. This tradeoff was observed for a camel-derived isolate, and we did not observe similar phenotypic relationships for the other strains tested (Figures 2, 3). Future research efforts with camel-derived viruses and more closely related human-derived viruses could show whether adaptations are likely to occur after zoonosis. Our previous viral stability results with SARS-CoV-2 and the findings of this study with MERS-CoV suggest copper should be incorporated more in hospital settings, particularly in materials in areas of high contact between hospital workers and MERS patients, such as door handles, bed rails, and medical tools (*21*). Overall, we observed a range of stability, replication, and pathogenesis phenotypes between different MERS-CoV isolates, underscoring the need for continued surveillance of this virus and other coronaviruses, including SARS-CoV-2.

Acknowledgments

We thank the animal caretakers for providing assistance during the animal studies.

This study was supported by the Intramural Research Program of the National Institute of Allergy and Infectious Diseases, National Institutes of Health (grant 1ZIAAI001179-01).

About the Authors

Dr. van Doremalen is an associate scientist in the Virus Ecology Section, National Institutes of Health Rocky Mountain Laboratories, Hamilton, MT. Her primary research interests are development of coronavirus animal models and next-generation vaccines for emerging infectious diseases, including the Oxford/Astrazeneca COVID-19 vaccine.

Dr. Letko is an assistant professor at the Paul G. Allen School of Global Health, Washington State University, Pullman, WA. His primary research interests are virus–host molecular interactions and zoonotic transmission of novel, animal-derived viruses.

References

1. Zaki AM, van Boheemen S, Bestebroer TM, Osterhaus AD, Fouchier RA. Isolation of a novel coronavirus from a man with pneumonia in Saudi Arabia. N Engl J Med. 2012;367:1814–20. https://doi.org/10.1056/NEJMoa1211721
2. World Health Organization. MERS situation update, October 2019 [cited 2021 Aug 26]. http://www.emro.who.int/pandemic-epidemic-diseases/mers-cov/mers-situation-update-october-2019.html
3 Zhang W, Zheng XS, Agwanda B, Ommeh S, Zhao K, Lichoti J, et al. Serological evidence of MERS-CoV and HKU8-related CoV co-infection in Kenyan camels. Emerg Microbes Infect. 2019;8:1528–34. https://doi.org/10.1080/22221751.2019.1679610
4. van Doremalen N, Hijazeen ZS, Holloway P, Al Omari B, McDowell C, Adney D, et al. High prevalence of Middle East respiratory coronavirus in young dromedary camels in Jordan. Vector Borne Zoonotic Dis. 2017;17:155–9. https://doi.org/10.1089/vbz.2016.2062
5. Shirato K, Melaku SK, Kawachi K, Nao N, Iwata-Yoshikawa N, Kawase M, et al. Middle East respiratory syndrome coronavirus in dromedaries in Ethiopia is antigenically different from the Middle East isolate EMC. Front Microbiol. 2019;10:1326. https://doi.org/10.3389/fmicb.2019.01326
6. Kandeil A, Gomaa M, Nageh A, Shehata MM, Kayed AE, Sabir JSM, et al. Middle East respiratory syndrome coronavirus (MERS-CoV) in dromedary camels in Africa and Middle East. Viruses. 2019;11:11. https://doi.org/10.3390/v11080717
7. Farag E, Sikkema RS, Mohamedani AA, de Bruin E, Munnink BB, Chandler F, et al. MERS-CoV in camels but not camel handlers, Sudan, 2015 and 2017. Emerg Infect Dis. 2019;25:2333–5. https://doi.org/10.3201/eid2512.190882
8. Chu DK, Poon LL, Gomaa MM, Shehata MM, Perera RA, Abu Zeid D, et al. MERS coronaviruses in dromedary camels, Egypt. Emerg Infect Dis. 2014;20:1049–53. https://doi.org/10.3201/eid2006.140299
9. Alagaili AN, Briese T, Mishra N, Kapoor V, Sameroff SC, Burbelo PD, et al. Middle East respiratory syndrome coronavirus infection in dromedary camels in Saudi Arabia. MBio. 2014;5:e00884–14. https://doi.org/10.1128/mBio.01002-14
10. Miguel E, Chevalier V, Ayelet G, Ben Bencheikh MN, Boussini H, Chu DK, et al. Risk factors for MERS coronavirus infection in dromedary camels in Burkina Faso, Ethiopia, and Morocco, 2015. Euro Surveill. 2017;22:22. https://doi.org/10.2807/1560-7917.ES.2017.22.13.30498
11. Chu DK, Oladipo JO, Perera RA, Kuranga SA, Chan SM, Poon LL, et al. Middle East respiratory syndrome coronavirus (MERS-CoV) in dromedary camels in Nigeria, 2015. Euro Surveill. 2015;20:20. https://doi.org/10.2807/1560-7917.ES.2015.20.49.30086
12. Hui DS, Azhar EI, Kim YJ, Memish ZA, Oh MD, Zumla A. Middle East respiratory syndrome coronavirus: risk factors and determinants of primary, household, and nosocomial transmission. Lancet Infect Dis. 2018;18:e217–27. https://doi.org/10.1016/S1473-3099(18)30127-0
13. Assiri A, McGeer A, Perl TM, Price CS, Al Rabeeah AA, Cummings DA, et al.; KSA MERS-CoV Investigation Team. Hospital outbreak of Middle East respiratory syndrome coronavirus. N Engl J Med. 2013;369:407–16. https://doi.org/10.1056/NEJMoa1306742
14. Cho SY, Kang JM, Ha YE, Park GE, Lee JY, Ko JH, et al. MERS-CoV outbreak following a single patient exposure in an emergency room in South Korea: an epidemiological outbreak study. Lancet. 2016;388:994–1001. https://doi.org/10.1016/S0140-6736(16)30623-7
15. Chowell G, Abdirizak F, Lee S, Lee J, Jung E, Nishiura H, et al. Transmission characteristics of MERS and SARS in the healthcare setting: a comparative study. BMC Med. 2015;13:210. https://doi.org/10.1186/s12916-015-0450-0
16. Hunter JC, Nguyen D, Aden B, Al Bandar Z, Al Dhaheri W, Abu Elkheir K, et al. Transmission of Middle East respiratory syndrome coronavirus infections in healthcare settings, Abu Dhabi. Emerg Infect Dis. 2016;22:647–56. https://doi.org/10.3201/eid2204.151615
17. Kim KH, Tandi TE, Choi JW, Moon JM, Kim MS. Middle East respiratory syndrome coronavirus (MERS-CoV) outbreak in South Korea, 2015: epidemiology, characteristics and public health implications. J Hosp Infect. 2017;95:207–13. https://doi.org/10.1016/j.jhin.2016.10.008
18. Chu DK, Hui KPY, Perera RA, Miguel E, Niemeyer D, Zhao J, et al. MERS coronaviruses from camels in Africa exhibit region-dependent genetic diversity. Proc Natl Acad Sci U S A. 2018;115:3144–9. https://doi.org/10.1073/pnas.1718769115
19. Letko M, Miazgowicz K, McMinn R, Seifert SN, Sola I, Enjuanes L, et al. Adaptive evolution of MERS-CoV to species variation in DPP4. Cell Rep. 2018;24:1730–7. https://doi.org/10.1016/j.celrep.2018.07.045
20. Munster VJ, Wells D, Lambe T, Wright D, Fischer RJ, Bushmaker T, et al. Protective efficacy of a novel simian adenovirus vaccine against lethal MERS-CoV challenge in a transgenic human DPP4 mouse model. NPJ Vaccines. 2017;2:28. https://doi.org/10.1038/s41541-017-0029-1
21. van Doremalen N, Bushmaker T, Morris DH, Holbrook MG, Gamble A, Williamson BN, et al. Aerosol and surface stability of SARS-CoV-2 as compared with SARS-CoV-1. N Engl J Med. 2020;382:1564–7. https://doi.org/10.1056/NEJMc2004973
22. Karber G. Article on the collective handling of pharmacological array effort. Naunyn Schmiedebergs Arch Exp Pathol Pharmakol. 1931;162:480–3.
23. Katoh K, Standley DM. MAFFT multiple sequence alignment software version 7: improvements in performance and usability. Mol Biol Evol. 2013;30:772–80. https://doi.org/10.1093/molbev/mst010
24. Fischer RJ, Bushmaker T, Judson S, Munster VJ. Comparison of the aerosol stability of 2 strains of Zaire ebolavirus from the 1976 and 2013 outbreaks. J Infect Dis. 2016;214(suppl 3):S290–3. https://doi.org/10.1093/infdis/jiw193
25. Corman VM, Eckerle I, Bleicker T, Zaki A, Landt O, Eschbach-Bludau M, et al. Detection of a novel human coronavirus by real-time reverse-transcription polymerase chain reaction. Euro Surveill. 2012;17:17. https://doi.org/10.2807/ese.17.39.20285-en
26. van Doremalen N, Bushmaker T, Munster VJ. Stability of Middle East respiratory syndrome coronavirus (MERS-CoV) under different environmental conditions. Euro Surveill. 2013;18:18. https://doi.org/10.2807/1560-7917.ES2013.18.38.20590
27. Grass G, Rensing C, Solioz M. Metallic copper as an antimicrobial surface. Appl Environ Microbiol. 2011;77:1541–7. https://doi.org/10.1128/AEM.02766-10
28. Galdiero S, Falanga A, Vitiello M, Cantisani M, Marra V, Galdiero M. Silver nanoparticles as potential antiviral agents. Molecules. 2011;16:8894–918. https://doi.org/10.3390/molecules16108894
29. Noyce JO, Michels H, Keevil CW. Inactivation of influenza A virus on copper versus stainless steel surfaces. Appl Environ Microbiol. 2007;73:2748–50. https://doi.org/10.1128/AEM.01139-06

30. Minoshima M, Lu Y, Kimura T, Nakano R, Ishiguro H, Kubota Y, et al. Comparison of the antiviral effect of solid-state copper and silver compounds. J Hazard Mater. 2016;312:1–7. https://doi.org/10.1016/j.jhazmat.2016.03.023
31. Fujimori Y, Sato T, Hayata T, Nagao T, Nakayama M, Nakayama T, et al. Novel antiviral characteristics of nanosized copper (I) iodide particles showing inactivation activity against 2009 pandemic H1N1 influenza virus. Appl Environ Microbiol. 2012;78:951–5. https://doi.org/10.1128/AEM.06284-11
32. Lara HH, Ayala-Nuñez NV, Ixtepan-Turrent L, Rodriguez-Padilla C. Mode of antiviral action of silver nanoparticles against HIV-1. J Nanobiotechnology. 2010;8:1. https://doi.org/10.1186/1477-3155-8-1
33. Hu RL, Li SR, Kong FJ, Hou RJ, Guan XL, Guo F. Inhibition effect of silver nanoparticles on herpes simplex virus 2. Genet Mol Res. 2014;13:7022–8. https://doi.org/10.4238/2014.March.19.2
34. Lu L, Sun RW, Chen R, Hui CK, Ho CM, Luk JM, et al. Silver nanoparticles inhibit hepatitis B virus replication. Antivir Ther. 2008;13:253–62.
35. Yang XX, Li CM, Huang CZ. Curcumin modified silver nanoparticles for highly efficient inhibition of respiratory syncytial virus infection. Nanoscale. 2016;8:3040–8. https://doi.org/10.1039/C5NR07918G
36. Rogers J, Parkinson C, Choi YW, Speshock JL, Hussain SM. A preliminary assessment of silver nanoparticle inhibition of monkeypox virus plaque formation. Nanoscale Res Lett. 2008;3:129–33. https://doi.org/10.1007/s11671-008-9128-2
37. Cyphert EL, von Recum HA. Emerging technologies for long-term antimicrobial device coatings: advantages and limitations. Exp Biol Med (Maywood). 2017;242:788–98. https://doi.org/10.1177/1535370216688572
38. Salgado CD, Sepkowitz KA, John JF, Cantey JR, Attaway HH, Freeman KD, et al. Copper surfaces reduce the rate of healthcare-acquired infections in the intensive care unit. Infect Control Hosp Epidemiol. 2013;34:479–86. https://doi.org/10.1086/670207
39. Kim SH, Chang SY, Sung M, Park JH, Bin Kim H, Lee H, et al. Extensive viable Middle East respiratory syndrome (MERS) coronavirus contamination in air and surrounding environment in MERS isolation wards. Clin Infect Dis. 2016;63:363–9. https://doi.org/10.1093/cid/ciw239
40. Judson SD, Munster VJ. Nosocomial transmission of emerging viruses via aerosol-generating medical procedures. Viruses. 2019;11:11. https://doi.org/10.3390/v11100940
41. Park YS, Lee C, Kim KM, Kim SW, Lee KJ, Ahn J, et al. The first case of the 2015 Korean Middle East respiratory syndrome outbreak. Epidemiol Health. 2015;37:e2015049. https://doi.org/10.4178/epih/e2015049
42. Figueira-Mansur J, Aguilera EA, Stoque RM, Ventura GT, Mohana-Borges R. Mutations in the dimer interfaces of the dengue virus capsid protein affect structural stability and impair RNA-capsid interaction. Sci Rep. 2019;9:2829. https://doi.org/10.1038/s41598-019-39185-3
43. Escors D, Ortego J, Laude H, Enjuanes L. The membrane M protein carboxy terminus binds to transmissible gastroenteritis coronavirus core and contributes to core stability. J Virol. 2001;75:1312–24. https://doi.org/10.1128/JVI.75.3.1312-1324.2001
44. Lee KH, Miller CR, Nagel AC, Wichman HA, Joyce P, Ytreberg FM. First-step mutations for adaptation at elevated temperature increase capsid stability in a virus. PLoS One. 2011;6:e25640. https://doi.org/10.1371/journal.pone.0025640
45. Schuit M, Ratnesar-Shumate S, Yolitz J, Williams G, Weaver W, Green B, et al. Airborne SARS-CoV-2 is rapidly inactivated by simulated sunlight. J Infect Dis. 2020;222:564–71. https://doi.org/10.1093/infdis/jiaa334
46. Matson MJ, Yinda CK, Seifert SN, Bushmaker T, Fischer RJ, van Doremalen N, et al. Effect of environmental conditions on SARS-CoV-2 stability in human nasal mucus and sputum. Emerg Infect Dis. 2020;26:26. https://doi.org/10.3201/eid2609.202267
47. Alharbi NK, Padron-Regalado E, Thompson CP, Kupke A, Wells D, Sloan MA, et al. ChAdOx1 and MVA based vaccine candidates against MERS-CoV elicit neutralising antibodies and cellular immune responses in mice. Vaccine. 2017;35:3780–8. https://doi.org/10.1016/j.vaccine.2017.05.032

Address for correspondence: Michael Letko, Paul G. Allen School of Global Animal Health, Washington State University Pullman, WA 99164, USA; email: michael.letko@wsu.edu; or Vincent J. Munster, Rocky Mountain Laboratories, National Institute of Allergy and Infectious Diseases, National Institutes of Health, 903S 4th St, Hamilton, MT 59840, USA; email: vincent.munster@nih.gov

Novel Use of Capture-Recapture Methods to Estimate Completeness of Contact Tracing during an Ebola Outbreak, Democratic Republic of the Congo, 2018–2020

Jonathan A. Polonsky, Dankmar Böhning, Mory Keita, Steve Ahuka-Mundeke, Justus Nsio-Mbeta, Aaron Aruna Abedi, Mathias Mossoko, Janne Estill, Olivia Keiser, Laurent Kaiser, Zabulon Yoti, Patarawan Sangnawakij, Rattana Lerdsuwansri, Victor J. Del Rio Vilas

Despite its critical role in containing outbreaks, the efficacy of contact tracing, measured as the sensitivity of case detection, remains an elusive metric. We estimated the sensitivity of contact tracing by applying unilist capture-recapture methods on data from the 2018–2020 outbreak of Ebola virus disease in the Democratic Republic of the Congo. To compute sensitivity, we applied different distributional assumptions to the zero-truncated count data to estimate the number of unobserved case-patients with any contacts and infected contacts. Geometric distributions were the best-fitting models. Our results indicate that contact tracing efforts identified almost all (n = 792, 99%) of case-patients with any contacts but only half (n = 207, 48%) of case-patients with infected contacts, suggesting that contact tracing efforts performed well at identifying contacts during the listing stage but performed poorly during the contact follow-up stage. We discuss extensions to our work and potential applications for the ongoing coronavirus pandemic.

Contact tracing is the process by which persons who are believed to have come into contact with a confirmed case-patient with an infectious disease during the infectious period are located and checked for the presence of the infection or disease. Under traditional approaches, contact tracing involves 3 distinct steps: contact identification, in which potential contacts are identified through interview with the primary case-patient; contact listing, in which those identified contacts are listed and communication established with them; and contact follow-up, in which those listed contacts are monitored for presence of infection or onset of disease over a predefined period (*1*).

Because of its important role in case detection to monitor and curtail chains of transmission, contact tracing often forms part of the public health response to directly transmitted infectious diseases (*2*). Recently, contact tracing has received widespread attention because of its critical role in the response to outbreaks of diphtheria (*3*), Ebola virus disease (EVD) (*4*–*6*), and the ongoing coronavirus disease (COVID-19) pandemic (*7*,*8*).

During 2018–2020, the Democratic Republic of the Congo (DRC) experienced its 10th and largest EVD outbreak, the second largest ever experienced globally (*9*). EVD is a disease caused by viruses of the genus *Ebolavirus*, family *Filoviridae*. Zoonotic spillover events from the animal reservoir have led to large, explosive outbreaks in West and Central Africa in recent years (*9*–*12*). Owing to the high pathogenicity and virulence of Ebola virus, an elimination control strategy is always adopted, aiming to ensure that all case-patients are identified, isolated, and treated promptly after disease onset, thereby limiting the opportunity for onward community spread. Although contact tracing is a central pillar of control (*13*), no standardized methods have been established to assess a critical aspect of performance, its sensitivity

Author affiliations: World Health Organization, Geneva, Switzerland (J.A. Polonsky); Institute of Global Health, University of Geneva, Geneva (J.A. Polonsky, M. Keita, J. Estill, O. Keiser, L. Kaiser); University of Southampton, Southampton, UK (D. Böhning); World Health Organization Regional Office for Africa, Brazzaville, Republic of the Congo (M. Keita, Z. Yoti); Institut National de Recherche Biomédicale, Kinshasa, Democratic Republic of the Congo (S. Ahuka-Mundeke, M. Mossoko); Ministere de la Santé Publique, Kinshasa (J. Nsio-Mbeta, A. Aruna Abedi); Thammasat University, Bangkok, Thailand (P. Sangnawakij, R. Lerdsuwansri); World Health Organization South East Asia Regional Office, New Delhi, India (V.J. Del Rio Vilas)

DOI: https://doi.org/10.3201/eid2712.204958

(i.e., the ability to detect all contacts and secondary infections resulting from case-patients).

One approach to quantifying this metric is to employ capture-recapture (CRC) methods (*14*,*15*). Broadly, this family of methodologic approaches enables researchers to quantify any unit of interest missing from lists and subsequently estimate the sensitivity of the surveillance effort and the probability of detection. Although CRC has previously been used to estimate the number of unobserved cases of disease (*16*,*17*), such approaches typically rely on comparison of multiple lists, which are generally not available for contact lists. Therefore, we describe the application of a unilist capture-recapture approach (*15*) to quantifying the number of unobserved case-patients and contacts and describe their sociodemographic profile, helping to identify plausible risk factors that can be used to target limited resources at those unobserved case-patients most likely to generate onward transmission. More precisely, we aimed to address 2 questions, from which we can derive contact tracing sensitivity estimates: how many case-patients with any contacts did contact tracing miss, and how many case-patients with infected contacts did contact tracing miss?

Materials and Methods

Study Participants

We included all confirmed and probable EVD case-patients and contacts (classified according to standardized case definitions [*18*,*19*]) identified in Beni Health Zone, DRC, during July 31, 2018–April 26, 2020. Case-patients were principally detected through 3 identification mechanisms: passive detection at healthcare facilities from persons manifesting symptoms consistent with EVD, house-to-house active case-finding by community health workers, and tracing the contacts of EVD case-patients. Contact tracing was coordinated by the DRC Ministry of Public Health, with support from the World Health Organization, and conducted by locally recruited teams of contact-tracers. Upon detection of a case, efforts to identify and list the case-patient's contacts were undertaken.

For case-patients, our data contain basic information on sociodemographic characteristics (e.g., age, sex, and DRC Health Area of residence) and dates of disease onset and isolation. For contacts, our data contain similar sociodemographic information and information on the daily follow-up and final status of the contact (either "completed the 21 days follow-up," "confirmed as EVD case-patient," "lost to follow-up," "never seen," or "died during follow-up"). Contacts recorded as "confirmed as EVD case-patients" were those identified by the contact tracing teams during the course of their work. EVD was assumed to be the cause of death for contacts recorded as "died during follow-up" because of the short interval between their contact with an EVD case-patient and their death.

Exploratory Data Analysis

We determined the distribution of case-patients according to age, sex, and timing of disease onset. We used the Wilcoxon test to explore differences in continuous variables and the χ^2 test for categoric variables to determine the distribution of the number of contacts per case-patient between 2 distinct epidemic waves. Overdispersion (i.e., superspreading) in the offspring distribution of secondary case-patients arising from infectious persons may have profound effects on control strategies in low-resource settings (*20*,*21*), and we describe the extent of this phenomenon in 2 ways: first, by assessing the proportion of infectious persons linked to 80% of onward transmission using methods described by Endo et al. (*22*); and second, by estimating the dispersion parameter (k) using methods described by Althaus (*23*).

We used a multivariable logistic regression model to explore risk factors associated with loss to follow-up, in which previously successfully traced contacts (i.e., those identified, listed, and among whom follow-up has begun) become untraceable at some point during the 21-day follow-up period. In such instances, contacts unable to be traced for 3 consecutive days are recorded as having been lost to follow-up, and no further attempts at tracing are made. To explore characteristics of case-patients with infected contacts, we calculated the mean number of contacts, mean age, and sex ratio of case-patients with $\geq$1 listed contact (among whom we can be confident that at least a minimal investigation was conducted), according to 3 categories: those with no infected contacts identified, those with exactly 1 contact, and those with $\geq$2 contacts.

CRC Modeling

We classified the observed case-patients according to their number of listed contacts (either exactly 0 or $\geq$1 contact), further classifying this latter category according to the number of infected contacts observed (either exactly 0 or $\geq$1 contact). For each detected case, the contact tracing process generates a list of persons fitting the definition for a contact (Appendix, https://wwwnc.cdc.gov/EID/article/27/12/20-4958-App1.pdf), some of whom may themselves have been infected and will eventually become secondary

case-patients. From this list, frequency distributions of case-patients with any listed contacts, and of case-patients with infected contacts, can be generated by first excluding (truncating) those case-patients with 0 contacts. For example, the data can be binned into the number of case-patients with exactly 1 contact (f_1), 2 contacts (f_2), and so on, to the number of case-patients with the maximum number of contacts (f_m). Statistically, this process leads to a 0-truncated observed count distribution of case-patients with ≥1 contact. By applying a unilist CRC approach designed to estimate unobserved population sizes using the distribution of count data within single lists (*15*), we can infer f_0, the number of unobserved case-patients with ≥1 contact. Associated with the observed frequencies (f_1, f_2,…, f_m) and unobserved f_0 are probabilities p_1, p_2,…, p_m and p_0 that inform the probability of identifying a case-patient with exactly 1, 2,…, m and 0 contacts, respectively. A conventional approach assumes that the frequencies arise from a discrete distribution such as the Poisson, where

$$p_0 = e^{-\lambda}, p_1 = \frac{e^{-\lambda}\lambda}{1!}, p_2 = \frac{e^{-\lambda}\lambda^2}{2!}, \ldots, p_m = \frac{e^{-\lambda}\lambda^m}{m!}.$$

Other common distributions are the negative binomial and the geometric distribution. The geometric distribution has probabilities $p_0 = p$, $p_1 = p(1-p)$, $p(1-p)^2 \ldots p_m = p(1-p)^m$, where p is a probability parameter. Poisson and geometric are special cases of the negative binomial distribution, which provides a flexible model family (Appendix). Because the observed distribution contains only positive numbers of contacts, we need to consider the associated zero-truncated distribution $p_1/(1-p_0)$, $p_2/(1-p_0)$,…$p_m/(1-p_0)$. In other words, we assume that the number of observed contacts among case-patients who actually had contacts follows a parametric distribution (although nonparametric approaches are possible [*15*,*24*,*25*]), find the best-fitting zero-truncated distribution of case-patients with ≥1 observed contact (we explore the zero-truncated Poisson, negative binomial, and geometric distributions [Appendix]), and use the estimated probability p_0 of not observing a case-patient with contacts (calculated from the best-fitting distribution) to inform standard population estimators. We use the Horvitz–Thompson estimator to estimate f_0, the unobserved number of case-patients:

$$\widehat{f_0} = n\frac{p_0}{1-p_0}$$

where n is the number of observed case-patients with ≥1 observed contact and p_0 is as previously defined. The Horvitz–Thompson estimator provides an unbiased estimate of f_0, provided that p_0 is correctly specified; hence, using a correctly-specified distribution for the number of observed contacts is important. We use maximum likelihood for model fitting, selecting the model with the smallest Akaike information criteria (AIC) and Bayesian information criteria (BIC) (Appendix).

To estimate 95% CIs, we use a parametric bootstrap, described as follows. Suppose that N is the estimated size of the (observed and unobserved) population under a fitted model. We generate B samples of size N_b using the fitted model and its estimated parameter or parameters. For each sample, all zeros are truncated and the size estimate N_b computed, for each of the samples $b = 1, \ldots, B$. We chose B = 10,000 to minimize bootstrap simulation random error. We constructed 95% CIs by using the 2.5th percentile of the distribution of N_b as the lower end and the 97.5th percentile as the upper end.

Results

Exploratory Data Analysis

We identified 913 confirmed and 10 probable EVD case-patients in Beni Health Zone. The contact tracing process listed 80,556 contacts, of whom 6,375 were duplicates, having been listed as the contact of >1 case-patient, resulting in 74,181 contacts to trace. In discussion with contact tracing teams, duplicates were identified by matching name and residential location; for operational reasons, these persons were recorded as a contact of only the earliest-identified primary case-patient with whom they were associated. More than half of case-patients for whom sex and age information were available were women and girls (n = 515 [55.8%]); median age for all case-patients was 25 years (interquartile range [IQR] 13–38 years). Most contacts (64,545 [87.0%]) were successfully traced, leading to the detection of 396 secondary case-patients. The median delay between last contact with the primary case-patient and first contact by the contact tracing teams was 4 days (IQR 3–6 days).

Disease onset dates spanned the period from July 31, 2018, to April 26, 2020, and was bimodally distributed, showing 2 waves that peaked in October 2018 and June 2019 (Figure 1, panel A). The second wave followed a period of insecurity in this conflict-affected area that severely hampered response activities (*26*).

The median number of contacts among all case-patients was 61 (IQR 18–120), but this number was significantly lower during the first wave than the second (34 vs. 80; p<0.001). Case-patients infected in the first wave were more likely to have 0 listed contacts than those in the second wave (31.3% vs. 9.6%; p<0.001

by χ^2 test), and second-wave case-patients were more likely to have a large number (>100) of contacts (Figure 1, panel B). A total of 792 case-patients (85.8%) reported ≥1 contact (Figure 2, 3), among whom the median number of contacts was 74 (IQR 36–134) and the mean number of contacts was 102.

A total of 64,545 contacts (87.0%) were successfully traced, of whom 308 were confirmed as EVD case-patients and 88 died during follow-up. Therefore, the inferred total number of infected contacts was 396 (308 + 88), or 0.7% of the contacts successfully traced to completion of the follow-up period. Precise detail on the mechanism of identification of confirmed case-patients among contacts is not available; although we assume these infected contacts were identified by contact tracers during follow-up, the role of other surveillance activities cannot be excluded.

We observed substantial overdispersion in the offspring distribution of secondary case-patients; 80% of onward transmission was linked to only 13.9% (95% CI 11.4%–16.2%) of primary case-patients, and all secondary case-patients concentrated among the contacts of 207 (22.4%) primary case-patients. Further, only 99 (10.7%) primary case-patients led to >1 secondary case-patient (Figure 2, 4). We estimated k as 0.27 (95% CI 0.20–0.33).

Male contacts had slightly (but statistically significantly) greater odds of being lost to follow-up (odds ratio [OR] 1.06, 95% CI 1.01–1.11) (Table 1). Contacts in older age groups had significantly greater odds of being lost to follow-up compared with contacts in the youngest age group (0–15 years). We observed the greatest effect among contacts ≥60 years of age (OR 1.65, 95% CI 1.47–1.86) and a marginally smaller effect among contacts 45–59 years of age (OR 1.55, 95% CI 1.43–1.69). Conversely, contacts traced during the second wave had lower odds of being lost to follow-up (OR 0.83, 95% CI 0.79–0.88).

CRC Modeling

Completeness of Contract Tracing for Case-Patients with >1 Listed Contact

Among case-patients with ≥1 contact listed, the best-fitting distribution of the count of case-patients with any contacts was given by the zero-truncated geomet-

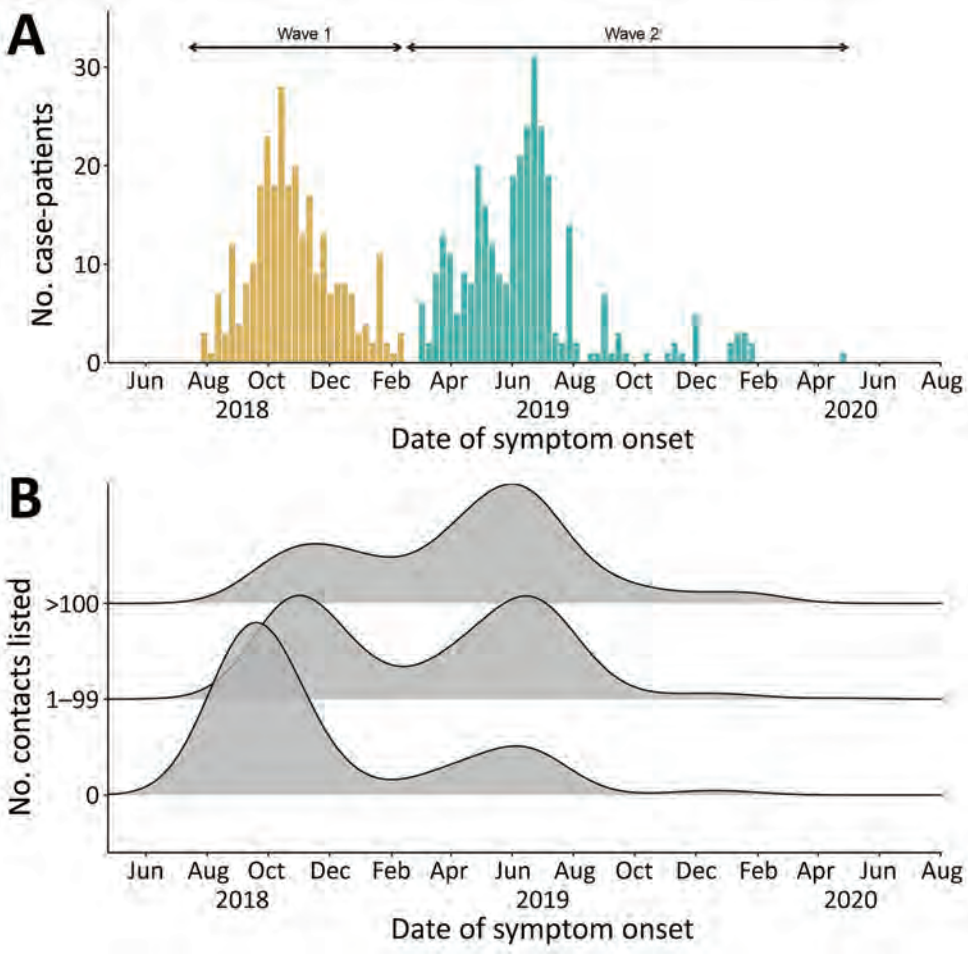

Figure 1. Epidemic curve and symptom onset dates among Ebola virus disease case-patients, Beni Health Zone, Democratic Republic of the Congo, July 31, 2018–April 26, 2020. A) Epidemic curve by date of symptom onset. Case-patients and contacts were divided into 2 epidemic waves, according to the date of symptom onset among case-patients (first wave, July 31, 2018–February 28, 2019; second wave, March 1, 2019–April 26, 2020). B) Distribution of dates of symptom onset among case-patients, by number of listed contacts. Data were smoothed by using a nonparametric (Gaussian) kernel-based estimate, with automatic bandwidth selection (37.6 days).

ric model, which produced the lowest AIC and BIC (Appendix Table 1). This distribution was very long-tailed (Figure 5), indicating that most case-patients with contacts were successfully detected, given that with an increasing mean of any count distribution, the probability for a zero count becomes smaller. This pattern is observed from the expression of the geometric distribution, described previously, where for $x = 0$ (i.e., the zero count), its estimated probability p_0 resolves the equation

$$\frac{1}{1+\mu}\left(\frac{\mu}{1+\mu}\right)^x$$

to return

$$\frac{1}{1+\mu},$$

where μ is the mean of the geometric model; the larger the mean, the smaller the probability of $x = 0$.

We estimated f_0 (the unobserved number of case-patients with any contacts) = 8 (95% CI = 8–10), where sample size (n) was 792 and p_0 was found as 0.01. The sensitivity of contact tracing to detect case-patients with any contacts was therefore 792/(792 + 8) = 0.99% (95% CI 0.99%–0.99%). We observed no difference in sensitivity by epidemic wave (wave 1 = 0.99% [95% CI 0.99%–0.99%]; wave 2 = 0.99 [95% CI 0.99–0.99]).

Completeness of Contact Tracing for Case-Patients with Infected Contacts

Among case-patients with infected contacts, the best-fitting distribution of the count of case-patients with infected contacts was again given by the zero-truncated geometric model, which produced the lowest AIC and BIC (Appendix Table 1). This distribution is concentrated on the lower counts from 1 to 4 (Figure 6), indicating that a substantial proportion of case-patients with infected contacts may not have been detected.

We estimated f_0 (the unobserved number of case-patients with infected contacts) = 227 (95% CI 171–241), where sample size (n) was 207 and p_0 was found as 0.52. The sensitivity of contact tracing to detect case-patients with infected contacts was therefore 207/(207 + 227) = 0.49% (95% CI 0.43%–0.55%). We observed a statistically significant difference in sensitivity by epidemic wave, with lower sensitivity

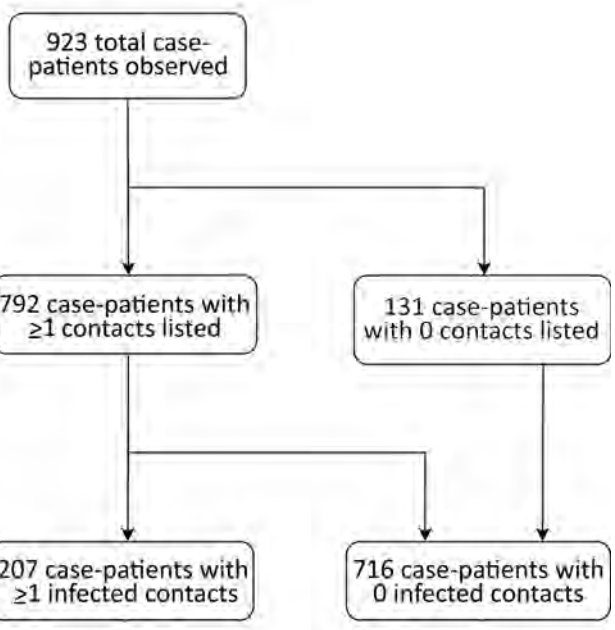

Figure 2. Flowchart showing breakdown of observed case-patients by number of listed and infected contacts among Ebola virus disease case-patients, Beni Health Zone, Democratic Republic of the Congo, July 31, 2018–April 26, 2020.

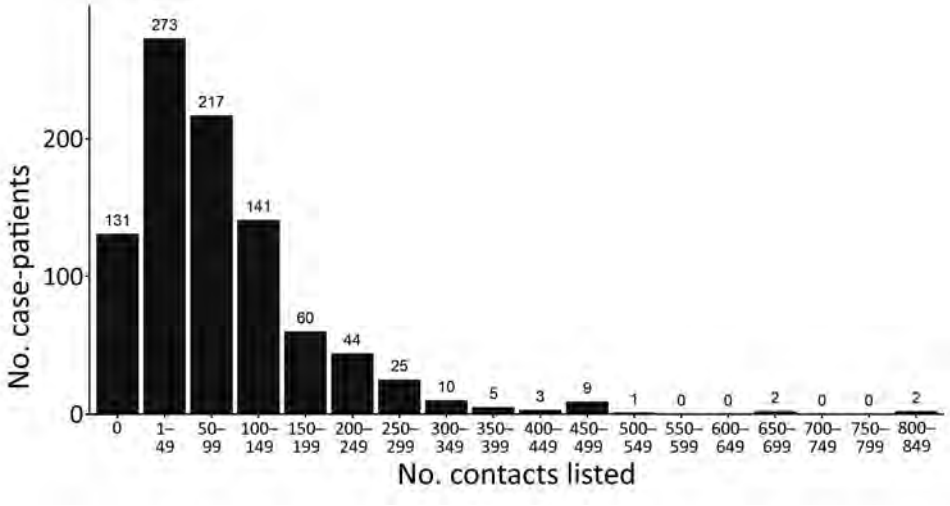

Figure 3. Frequency distribution of Ebola virus disease case-patients, by number of listed contacts, Beni Health Zone, Democratic Republic of the Congo, July 31, 2018–April 26, 2020.

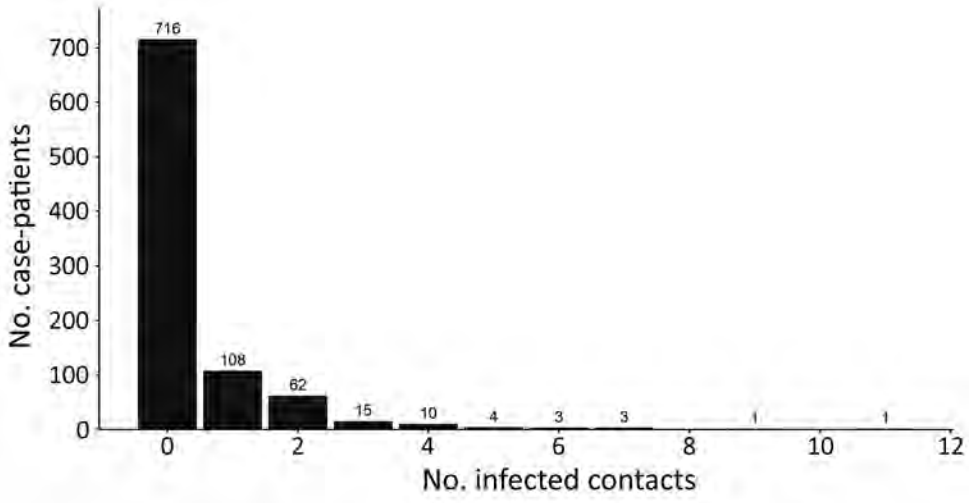

Figure 4. Frequency distribution of Ebola virus disease case-patients, by number of infected contacts, Beni Health Zone, Democratic Republic of the Congo, July 31, 2018–April 26, 2020.

during wave 1 (0.24% [95% CI = 0.11%–0.38%]) than during wave 2 (0.48% [95% CI = 0.40%–0.56%]). Among the 792 case-patients with ≥1 listed contact, those with 0 infected contacts had fewer contacts overall, were slightly older, and were slightly more likely to be women or girls compared with the other groups (Table 2).

Discussion

Our findings suggest that contract tracing efforts were very successful at identifying case-patients with ≥1 contact but much less successful at identifying case-patients with contacts who later had EVD symptoms. This finding is unsurprising, given that the investigation component (typically by interview with case-patients under treatment, their caregivers, or both) is easier to conduct than the tracing component (typically requiring daily visits to a large number of difficult-to-locate and mobile persons). This difference has important implications, because infected contacts contribute to ongoing chains of transmission when case investigation and contract tracing is inadequate; to prioritize scarce resources, control efforts should target those case-patients among whose contacts secondary infections arise (*20*,*21*,*27*). A high proportion of case-patients listed ≥1 contact (≈85%), compared with 27% during an EVD outbreak in Liberia (*28*) and 44% during an EVD outbreak in Sierra Leone (*27*), suggesting that lessons about enhancing the quality of contract tracing were learned from previous EVD outbreaks (*4*,*5*,*27*,*28*).

Case-patients with infected contacts had more contacts on average, which may result from 3 possible explanations. First, case-patients with more contacts are more likely to have ≥1 infected contact among these. Second, fewer overall listed contacts may be the result of poorly conducted case investigations. We found some evidence in support of this; the mean number of contacts increased as the

Table 1. Multivariable logistic regression for predictors of loss to follow-up of contacts of Ebola virus disease case-patients, Beni Health Zone, Democratic Republic of the Congo, July 31, 2018–April 26, 2020*

		Unadjusted		Adjusted	
Independent variable	No. contacts	OR (95% CI)	p value	OR (95% CI)	p value
Sex					
F	41,349	Referent		Referent	
M	37,296	1.07 (1.02–1.12)	0.003	1.06 (1.01–1.11)	0.013
Age group, y					
0–14	20,616	Referent		Referent	
15–29	26,142	1.18 (1.11–1.25)	<0.001	1.19 (1.12–1.27)	<0.001
30–44	17,665	1.16 (1.09–1.24)	<0.001	1.18 (1.10–1.26)	<0.001
45–59	6,157	1.56 (1.43–1.70)	<0.001	1.55 (1.43–1.69)	<0.001
≥60	2,599	1.64 (1.46–1.84)	<0.001	1.65 (1.47–1.86)	<0.001
Epidemic wave†					
First wave	14,374	Referent		Referent	
Second wave	66,182	0.85 (0.81–0.90)	<0.001	0.83 (0.79–0.88)	<0.001

*OR, odds ratio.
†Contacts were divided into 2 epidemic waves according to the date of symptom onset of their associated primary case-patient (first wave, July 31, 2018–February 28, 2019; second wave, March 1, 2019–April 26, 2020).

Table 2. Distribution of Ebola virus disease case-patients, their median age and sex ratio, and mean total number of contacts, grouped by number of infected contacts, among case-patients with ≥1 listed contact, Beni Health Zone, Democratic Republic of the Congo, July 31, 2018–April 26, 2020

No. infected contacts	No. case-patients	Median age of case-patients, y	% Women and girls among case-patients	Mean (95% CI) total number of contacts
0	585	28.2	59.5	85.7 (79.1–92.4)
1	108	23.6	56.7	122 (102.0–141.0)
≥2	99	25.6	54.6	174 (144.0–204.0)

epidemic progressed, indicating possible improvements in case investigation quality over time as staff became more accustomed to the procedure and community trust and engagement in the response improved (*29*). Third, case-patients with infected contacts may differ from other case-patients; in this study, such case-patients were younger and more likely to be men or boys, which are demographic factors previously shown to affect transmission of EVD and other diseases (*30*–*32*). Case-patients with more contacts have been shown to play a greater role in disease transmission and are more likely to have infected contacts (*33*,*34*). This tendency is particularly true of diseases that demonstrate heterogeneous transmission, including EVD and COVID-19, and our results suggest a high degree of overdispersion and superspreading, consistent with what has previously been reported during large EVD outbreaks (*23*). Overdispersion can lead to rapid expansion, particularly among hidden chains of transmission, and a promising area of research is to identify correlates of superspreading to better target limited resources for greatest impact. Previous research suggests that if highly infectious persons can be predictively identified and targeted, the efficiency of control can be greatly enhanced, such that focusing half of all control effort on the most infectious 20% of case-patients can improve effectiveness up to 3-fold (*20*,*21*).

Although estimating the number of unobserved case-patients with (infected) contacts is possible, identifying whether these case-patients have been misclassified as having 0 (infected) contacts or if they were undetected by the surveillance system in general is not possible. However, the greater probability of having 0 contacts listed during the first epidemic wave suggests substantial misclassification and suboptimal performance in the period during which surveillance activities were being established, as reported during previous EVD outbreaks (*4*,*27*,*28*). The sensitivity of contact tracing to detect case-patients with infected contacts was lower, and loss to follow-up greater, during the first epidemic wave, indicating quality improvements of this activity over time, either because the ability to conduct contact follow-up was hampered by the insecurity experienced during the first wave or because of greater familiarity with, and acceptance of, the process among contact tracing staff and the local population during later efforts.

Although the method we describe proposes a robust framework to assess the sensitivity of contact tracing, limitations include that no standard list of contacts against which to validate this method exists. However, the method itself has been validated to estimate actual population size in various other settings (*25*). The dataset does not permit the distinction between case-patients who were confirmed to have no contacts after a thorough case investigation and case-

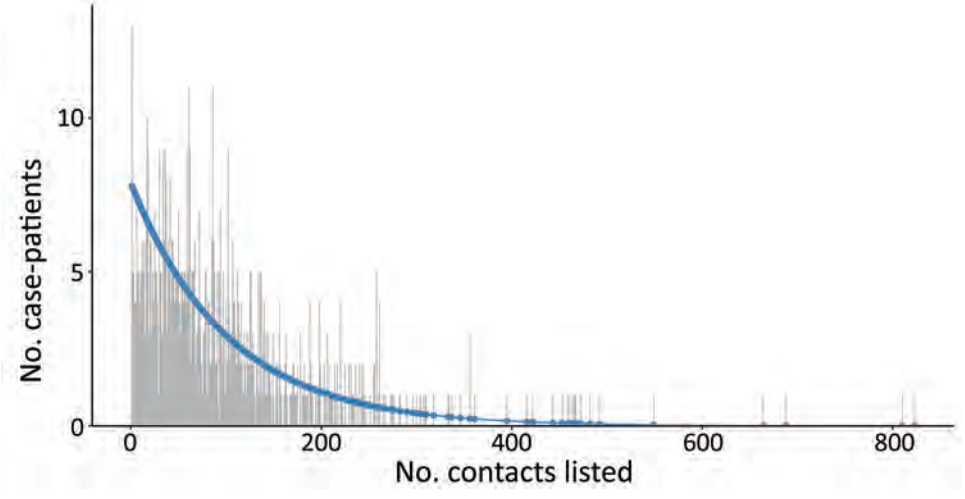

Figure 5. Observed (gray) and fitted (geometric; blue) zero-truncated distribution of the total number of contacts for case-patients with ≥1 contact listed, Beni Health Zone, Democratic Republic of the Congo, July 31, 2018–April 26, 2020..

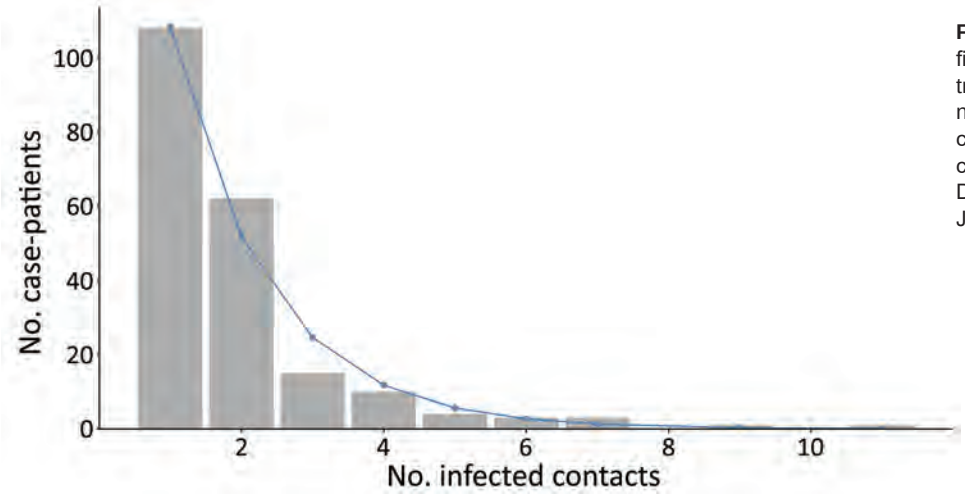

Figure 6. Observed (gray) and fitted (geometric; blue) zero-truncated distribution of the total number of infected contacts for case-patients with ≥1 infected contact listed, Beni Health Zone, Democratic Republic of the Congo, July 31, 2018–April 26, 2020.

patients having no listed contacts because of no (or inadequate) case investigation. However, our method may help to identify the magnitude of the misclassification arising from this limitation. The inferences made are exclusively informed by the definition of case-patients as defined by contact tracing protocols; for example, our results would not inform the sensitivity of contact tracing as applied to asymptomatic EVD case-patients if these persons are not part of the testing strategy.

Differences in performance between contact tracers could result in strong heterogeneity in the count distribution, which might be detectable. For this reason, we applied Chao's estimator (which allows for heterogeneity), and only if this was significantly different from the model-based estimate would we consider that an issue exists. In our results, we did not observe such a difference (Appendix Tables 2, 3). Finally, we have not adjusted for observed heterogeneity, such as age, sex, profession, geographic location of the case-patients, and delays in the contact tracing process. Further work is planned to incorporate such considerations.

In conclusion, contact tracing is crucial to containing certain disease outbreaks. However, as with many surveillance activities, contact tracing has the potential to suffer reduced effectiveness from underreporting and poor sensitivity (*4*,*27*,*28*). The consequences of poor ascertainment and misclassification can be disastrous, potentially creating explosive expansion among hidden chains of transmission, particularly during containment and de-escalation phases.

We have described a novel application of CRC models to estimate a crucial yet elusive performance indicator of a key component of the public health response to epidemics, namely the sensitivity of contact tracing, as applied to a recent outbreak of EVD. The method demonstrated that most case-patients with any contacts were observed, suggesting that the case investigation component of contact tracing performed well, whereas less than half of case-patients with infected contacts were observed, suggesting that the contact follow-up component of contact tracing performed poorly in this setting. The approach described can be used to assess the sensitivity of contact tracing for any disease, including COVID-19, for which contact tracing has been identified as a crucial component of response activities.

Acknowledgments

We thank the people of the DRC's Beni Health Zone for their participation in conducting this study. We acknowledge the enormous dedication of the various organizations and persons that responded and provided healthcare to this population and supported the public health response during this outbreak.

The authors received no specific funding for this work. The authors alone are responsible for the views expressed in this article, and they do not necessarily represent the views, decisions, or policies of the institutions with which they are affiliated.

About the Author

Mr. Polonsky is an epidemiologist with the World Health Organization, Geneva, Switzerland. His research interests include various aspects of public health response in humanitarian and emergency settings, with a primary focus on infectious disease outbreaks and monitoring the health impact of crises.

References

1. World Health Organization. Infection prevention and control: contact tracing [cited 2021 May 10]. https://www.who.int/news-room/q-a-detail/contact-tracing
2. Polonsky JA, Baidjoe A, Kamvar ZN, Cori A, Durski K, Edmunds WJ, et al. Outbreak analytics: a developing data science for informing the response to emerging pathogens. Philos Trans R Soc Lond B Biol Sci. 2019;374:20180276. https://doi.org/10.1098/rstb.2018.0276
3. Polonsky JA, Ivey M, Mazhar MKA, Rahman Z, le Polain de Waroux O, Karo B, et al. Epidemiological, clinical, and public health response characteristics of a large outbreak of diphtheria among the Rohingya population in Cox's Bazar, Bangladesh, 2017 to 2019: a retrospective study. PLoS Med. 2021;18:e1003587. https://doi.org/10.1371/journal.pmed.1003587
4. Swanson KC, Altare C, Wesseh CS, Nyenswah T, Ahmed T, Eyal N, et al. Contact tracing performance during the Ebola epidemic in Liberia, 2014–2015. PLoS Negl Trop Dis. 2018;12: e0006762. https://doi.org/10.1371/journal.pntd.0006762
5. Polonsky J, Mboussou F, Haskew C, le Polain de Waroux O, Belizaire MRD, Mondonge V, et al. Lessons learnt from Ebola virus disease surveillance in Équateur Province, May–July 2018. Wkly Epidemiol Rec. 2019;5 [cited 2020 Dec 28]. https://apps.who.int/iris/handle/10665/279754
6. Sikakulya FK, Mulisya O, Munyambalu DK, Bunduki GK. Ebola in the eastern Democratic Republic of Congo: One Health approach to infectious disease control. One Health. 2019;9:100117. https://doi.org/10.1016/j.onehlt.2019.100117
7. Keeling MJ, Hollingsworth TD, Read JM. Efficacy of contact tracing for the containment of the 2019 novel coronavirus (COVID-19). J Epidemiol Community Health. 2020;74:861–6.
8. Althoff KN, Coburn SB, Nash D. Contact tracing: essential to the public health response and our understanding of the epidemiology of coronavirus disease 2019. Clin Infect Dis. 2020;71:1960–1. https://doi.org/10.1093/cid/ciaa757
9. Ilunga Kalenga O, Moeti M, Sparrow A, Nguyen V-K, Lucey D, Ghebreyesus TA. The ongoing Ebola epidemic in the Democratic Republic of Congo, 2018–2019. N Engl J Med. 2019;381:373–83. https://doi.org/10.1056/NEJMsr1904253
10. Aylward B, Barboza P, Bawo L, Bertherat E, Bilivogui P, Blake I, et al.; WHO Ebola Response Team. Ebola virus disease in West Africa—the first 9 months of the epidemic and forward projections. N Engl J Med. 2014;371:1481–95. https://doi.org/10.1056/NEJMoa1411100
11. Polonsky JA, Wamala JF, de Clerck H, Van Herp M, Sprecher A, Porten K, et al. Emerging filoviral disease in Uganda: proposed explanations and research directions. Am J Trop Med Hyg. 2014;90:790–3. https://doi.org/10.4269/ajtmh.13-0374
12. Barry A, Ahuka-Mundeke S, Ahmed YA, Allarangar Y, Anoko J, Archer BN, et al.; Ebola Outbreak Epidemiology Team. Outbreak of Ebola virus disease in the Democratic Republic of the Congo, April–May, 2018: an epidemiological study. Lancet. 2018;392:213–21. https://doi.org/10.1016/S0140-6736(18)31387-4
13. World Health Organization. Implementation and management of contact tracing for Ebola virus disease [cited 2021 Oct 6]. https://www.who.int/publications/i/item/WHO-EVD-Guidance-Contact-15.1
14. Vergne T, Del Rio Vilas VJ, Cameron A, Dufour B, Grosbois V. Capture-recapture approaches and the surveillance of livestock diseases: a review. Prev Vet Med. 2015;120:253–64. https://doi.org/10.1016/j.prevetmed.2015.04.003
15. Bohning D, Heijden PGM, Bunge J, editors. Capture-recapture methods for the social and medical sciences. London: Chapman and Hall/CRC; 2017.
16. Gignoux E, Idowu R, Bawo L, Hurum L, Sprecher A, Bastard M, et al. Use of capture-recapture to estimate underreporting of Ebola virus disease, Montserrado County, Liberia. Emerg Infect Dis. 2015;21:2265–7. https://doi.org/10.3201/eid2112.150756
17. Isanaka S, Hedt-Gauthier BL, Salou H, Berthé F, Grais RF, Allen BGS. Active and adaptive case finding to estimate therapeutic program coverage for severe acute malnutrition: a capture-recapture study. BMC Health Serv Res. 2019;19:967. https://doi.org/10.1186/s12913-019-4791-9
18. Medley AM, Mavila O, Makumbi I, Nizeyemana F, Umutoni A, Balisanga H, et al. Case definitions used during the first 6 months of the 10th Ebola virus disease outbreak in the Democratic Republic of the Congo—four neighboring countries, August 2018–February 2019. MMWR Morb Mortal Wkly Rep. 2020;69:14–9. https://doi.org/10.15585/mmwr.mm6901a4
19. World Health Organization. Case definition recommendations for Ebola or Marburg virus diseases. 2014 [cited 2021 Oct 6]. https://www.who.int/csr/resources/publications/ebola/ebola-case-definition-contact-en.pdf
20. Woolhouse MEJ, Dye C, Etard J-F, Smith T, Charlwood JD, Garnett GP, et al. Heterogeneities in the transmission of infectious agents: implications for the design of control programs. Proc Natl Acad Sci U S A. 1997;94:338–42. https://doi.org/10.1073/pnas.94.1.338
21. Lloyd-Smith JO, Schreiber SJ, Kopp PE, Getz WM. Superspreading and the effect of individual variation on disease emergence. Nature. 2005;438:355–9. https://doi.org/10.1038/nature04153
22. Endo A, Abbott S, Kucharski AJ, Funk S; Centre for the Mathematical Modelling of Infectious Diseases COVID-19 Working Group. Estimating the overdispersion in COVID-19 transmission using outbreak sizes outside China. Wellcome Open Res. 2020;5:67. https://doi.org/10.12688/wellcomeopenres.15842.3
23. Althaus CL. Ebola superspreading. Lancet Infect Dis. 2015; 15:507–8. https://doi.org/10.1016/S1473-3099(15)70135-0
24. Böhning D, Rocchetti I, Maruotti A, Holling H. Estimating the undetected infections in the Covid-19 outbreak by harnessing capture-recapture methods. Int J Infect Dis. 2020;97:197–201. https://doi.org/10.1016/j.ijid.2020.06.009
25. Alfò M, Böhning D, Rocchetti I. Upper bound estimators of the population size based on ordinal models for capture-recapture experiments. Biometrics. 2021;77:237–48. https://doi.org/10.1111/biom.13265
26. Jombart T, Jarvis CI, Mesfin S, Tabal N, Mossoko M, Mpia LM, et al. The cost of insecurity: from flare-up to control of a major Ebola virus disease hotspot during the outbreak in the Democratic Republic of the Congo, 2019. Euro Surveill. 2020;25:1900735. https://doi.org/10.2807/1560-7917.ES.2020.25.2.1900735
27. Senga M, Koi A, Moses L, Wauquier N, Barboza P, Fernandez-Garcia MD, et al. Contact tracing performance during the Ebola virus disease outbreak in Kenema district, Sierra Leone. Philos Trans R Soc Lond B Biol Sci. 2017;372:372. https://doi.org/10.1098/rstb.2016.0300
28. Olu OO, Lamunu M, Nanyunja M, Dafae F, Samba T, Sempiira N, et al. Contact tracing during an outbreak of Ebola virus disease in the Western Area Districts of Sierra Leone: lessons for future Ebola outbreak response. Front Public Health. 2016;4:130. https://doi.org/10.3389/fpubh.2016.00130
29. Masumbuko Claude K, Underschultz J, Hawkes MT. Social resistance drives persistent transmission of Ebola virus

disease in eastern Democratic Republic of Congo: a mixed-methods study. PLoS One. 2019;14:e0223104. https://doi.org/10.1371/journal.pone.0223104
30. Kiti MC, Kinyanjui TM, Koech DC, Munywoki PK, Medley GF, Nokes DJ. Quantifying age-related rates of social contact using diaries in a rural coastal population of Kenya. PLoS One. 2014;9:e104786. https://doi.org/10.1371/journal.pone.0104786
31. Johnstone-Robertson SP, Mark D, Morrow C, Middelkoop K, Chiswell M, Aquino LDH, et al. Social mixing patterns within a South African township community: implications for respiratory disease transmission and control. Am J Epidemiol. 2011;174:1246–55. https://doi.org/10.1093/aje/kwr251
32. le Polain de Waroux O, Cohuet S, Ndazima D, Kucharski AJ, Juan-Giner A, Flasche S, et al. Characteristics of human encounters and social mixing patterns relevant to infectious diseases spread by close contact: a survey in Southwest Uganda. BMC Infect Dis. 2018;18:172. https://doi.org/10.1186/s12879-018-3073-1
33. Kangbai JB. Social network analysis and modeling of cellphone-based syndromic surveillance data for Ebola in Sierra Leone. Asian Pac J Trop Med. 2016;9:851–5. https://doi.org/10.1016/j.apjtm.2016.07.005
34. Hagel C, Weidemann F, Gauch S, Edwards S, Tinnemann P. Analysing published global Ebola virus disease research using social network analysis. PLoS Negl Trop Dis. 2017;11:e0005747. https://doi.org/10.1371/journal.pntd.0005747

Address for correspondence: Victor J. Del Rio Vilas, World Health Organization, South East Asia Regional Office, World Health House, Indraprastha Estate, Mahatma Gandhi Marg, New Delhi 110 002, India; email: delriov@who.int

Novel Assay to Measure Seroprevalence of Zika Virus in the Philippines

Cameron Adams, Ramesh Jadi, Bruno Segovia-Chumbez, Jedas Daag, Michelle Ylade, Freddy A. Medina, Tyler M. Sharp, Jorge L. Munoz-Jordan, In-Kyu Yoon, Jacqueline Deen, Anna Lena Lopez,[1] Aravinda M. de Silva, Lakshmanane Premkumar

Zika virus (ZIKV) is a member of the *Flaviviridae* family, which includes other clinically notable viruses such as the 4 dengue virus serotypes (DENV-1–4). Distinguishing DENVs from ZIKV using the established serologic assays widely used for monitoring DENV transmission is difficult because of antibody cross-reactivity between these closely related flaviviruses. We describe a modified and improved recombinant envelope domain III–based serologic assay for detecting ZIKV type-specific antibodies in regions with endemic DENV transmission. When the assay was used to measure ZIKV seroprevalence in 2017 among children 9–14 years of age living in a region of the Philippines with endemic DENV transmission, we observed a ZIKV seroprevalence of 18%. Investigators should consider using the ZIKV envelope domain III–based assay, which is simple and readily adaptable for use in standard clinical and public health laboratories, to assess ZIKV seroprevalence in areas with endemic DENV transmission.

Zika virus (ZIKV) is a positive sense RNA virus of the *Flaviviridae* family, which includes several medically notable arboviruses such as dengue (DENV), yellow fever, Japanese encephalitis virus, and West Nile virus. Before the 2015 epidemic in the Americas that spread to >40 countries and infected >1 million people (*1*), ZIKV was considered rare and responsible for minor epidemics in East Africa and parts of Asia. Although most ZIKV infections are asymptomatic or clinically mild, the epidemic in the Americas revealed that the virus can cause serious neurologic problems in some persons and severe teratogenic effects in pregnant women (*2*–*4*). Because ZIKV and DENV-1–4 share the same *Aedes* mosquito vectors, areas in the Americas most affected by ZIKV also experience endemic DENV transmission. The ZIKV pandemic in the Americas led to novel observations and questions about its epidemiology and pathogenesis in regions with endemic DENV transmission. Recent studies indicate that cross-reactive immunity between ZIKV and DENV can lead to protection or to more severe disease depending on the context (*5*–*7*).

Although sporadic transmission of Asian lineages of ZIKV in Southeast Asia and Pacific islands is well-documented (*8*,*9*), its prevalence in the region has been difficult to estimate using current serologic assays because of intense transmission of multiple DENV serotypes and antibody cross-reactivity between DENV and ZIKV. Most serologic assays for flaviviruses measure antibodies binding to viral-envelope glycoprotein (E protein) because this antigen is a major target of human antibodies. The *Flavivirus* E protein contains immunodominant antibody epitopes that are conserved (cross-reactive) between different flaviviruses or unique to each virus (type-specific) (*10*–*12*).

Traditional *Flavivirus* serologic assays exhibit poor specificity in distinguishing DENV from ZIKV infections because these assays use whole virions or E proteins containing conserved epitopes as antigens (*13*–*15*). More recently, the ZIKV epidemic in the Americas spurred the development of recombinant viral antigens and serologic assays for distinguishing ZIKV from DENV (*16*–*18*). We previously described a serologic assay using domain III of the ZIKV E

Author affiliations: University of North Carolina School of Medicine, Chapel Hill, North Carolina, USA (C. Adams, R. Jadi, B. Segovia-Chumbez, A.M. de Silva, L. Premkumar); University of the Philippines, Manila, Philippines (J. Daag, M. Ylade, J. Deen, A.L. Lopez); Centers for Disease Control and Prevention, San Juan, Puerto Rico, USA (F.A. Medina, T.M. Sharp, J.L. Munoz-Jordan); Coalition for Epidemic Preparedness Innovations, Washington, DC, USA (I.-K. Yoon)

DOI: https://doi.org/10.3201/eid2712.211150

[1]Deceased..

protein (EDIII) to detect ZIKV type-specific antibodies among persons in areas with DENV and ZIKV cocirculation (*19*). Here we describe development of a second-generation ZIKV EDIII–based serologic assay and its use to measure the seroprevalence of ZIKV among children 9–14 years of age in the Cebu Province of the Philippines.

Materials and Methods

ZIKV EDIII Antigen Production

We expressed a codon-optimized gene encoding for EDIII from ZIKV strain H/PF/2013 in Expi293 cells as a fusion protein containing a human serum albumin signal peptide for secretion, a polyhistidine tag (his-tag) for affinity purification, and a HaloTag (Promega, https://www.promega.com) for biotinylation (*20*). We deposited the nucleotide sequence of the construct into Genbank (accession no. MZ592925). HaloTag enables single, site-specific biotinylation distant from the folded EDIII protein. We purified recombinant EDIII antigen from the culture supernatant using nickel-nitrilotriacetic acid agarose (QIAGEN, https://www.qiagen.com) and biotinylated it using HaloTag PEG biotin ligand (Promega), according to manufacturer protocol. We analyzed the identity and purity of the biotinylated EDIII antigen using SDS-PAGE (sodium dodecylsulfate polyacrylamide gel electrophoresis) mobility-shift analysis.

ZIKV EDIII ELISA

We coated a 96-well high binding microtiter plate (Greiner Bio-One, https://www.gbo.com) with 50 μL of streptavidin at 4 μg/mL in tris-buffered saline (TBS, pH 7.4) for 1 h at 37°C. We captured the biotinylated EDIII at 2 μg/mL in TBS, washed the plate 3 times with wash buffer (TBS containing 0.2% Tween 20), and then blocked it with 100 μL of blocking solution (3% milk in TBS containing 0.05% Tween 20) for 1 h at 37°C. After removing the blocking solution, we added 50 μL of heat-inactivated (56°C for 30 min) serum sample at 1:20 or indicated dilutions in blocking buffer and incubated for 1 hour at 37°C. After washing the plate in the wash buffer, we added 50 μL of alkaline phosphatase-conjugated secondary goat anti-human secondary IgG (Sigma) at 1:2,500 dilution for 1 hour at 37°C. We washed the plate, added 50 μL of p-nitrophenyl phosphate substrate (Sigma, https://www.sigmaaldrich.com), and measured absorbance at 405 nm using an Epoch plate reader (Biotek, https://www.biotek.com). For analyzing the 547 serum samples from the Cebu cohort using ELISA assays performed over several days, we used human monoclonal antibody ZKA190 (*21*), which binds to highly accessible regions of ZIKV EDIII as a control to standardize EDIII ELISA optical density (OD) values across assays. Each plate was developed until wells with ZKA190 generated an OD value within a 1.0–1.3 range. If the signal was outside this range, we considered the assay invalid and repeated the process. We divided all OD values for human samples by the ZKA190 OD value on the same plate before determining the ZIKV-immune status of each participant (≥0.34 cutoff).

Human Serum Panel Used to Validate the EDIII Assay

To validate the EDIII assay as described elsewhere (*19*), we used a panel of 142 archived convalescent serum samples from 15 participants who received a licensed *Flavivirus* (yellow fever/Japanese encephalitis virus) vaccine, 27 serum samples from *Flavivirus*-naive participants, 33 from participants with immunity to ZIKV (including some with both ZIKV and DENV immunity), and 67 from participants with DENV immunity but no immunity to ZIKV. The DENV- and ZIKV-immunity status of convalescent specimens in the panel was based on participants in febrile illness study cohorts in Nicaragua and Sri Lanka with laboratory-confirmed acute DENV or ZIKV infections or tests for the presence of neutralizing DENV or ZIKV antibodies in single serum samples from healthy persons. We designated samples with no detectable neutralizing DENV and ZIKV antibodies or 50% plaque reduction neutralization test ($PRNT_{50}$) results <10 as naive. Collection, storage, and use of these convalescent serum samples for research was approved by the Institutional Review Board of the University of North Carolina at Chapel Hill (protocol 08–0895).

Centers for Disease Control and Prevention ZIKV Persistence Samples

The Centers for Disease Control and Prevention (CDC) and the Ponce Medical School Foundation monitored DENV and ZIKV patients seeking treatment at 2 hospitals in southern Puerto Rico. During triage, we identified case-patients with ≥1 signs or symptoms: fever (temperature ≥38.0°C or ≥100.5°F) or reporting fever lasting ≤7 days, rash, arthralgia or arthritis, or conjunctivitis and offered them participation in the study. We identified ZIKV cases through test results from the CDC Dengue Branch laboratory in San Juan, Puerto Rico, where reverse transcription (RT) PCR testing for DENV, ZIKV, CHIKV, and other respiratory infectious diseases is performed and

followed ZIKV cases longitudinally as described elsewhere (*22*). For our study, we selected and prospectively followed 27 ZIKV RT-PCR–positive cases for up to 2.5 years. Specimen collection was approved by institutional review boards at CDC and Ponce Medical School Foundation.

Pediatric Samples from Cebu Province

We published the Cebu study protocol and approvals elsewhere (*23*). In brief, our study used baseline serum samples that were collected from 2,996 children 9–14 years of age enrolled in a postlicensure DENV vaccine study. Cohort residence was equally split between Bogo and Balamban, both semiurban areas. We collected samples and demographic information before participants were vaccinated at the same visit.

DENV and ZIKV Focus Reduction Neutralization Test

We determined neutralization titers against DENV and ZIKV by focus-reduction neutralization test (FRNT) in a 96-well format described elsewhere (*24*). Serially diluted serum was mixed with 50–100 focus-forming units of the virus in Dulbecco modified Eagle medium with 2% fetal bovine serum. We incubated the antibody and virus complexes (1 h, 37°C), then transferred them to a monolayer of Vero-81 cells for infection. After 1 additional hour of incubating antibody and virus complex on Vero-81 monolayer, we overlaid cells with GIBCO Opti-MEM (https://www.thermofisher.com), a modified Eagle medium containing 2% fetal bovine serum and 1% carboxymethylcellulose. After allowing the predetermined time required to form viral foci, we fixed Vero-81 cells and immunostained them with *Flavivirus*-specific monoclonal antibodies. For neutralization assays, we calculated 50% inhibitory concentration by using the sigmoidal dose-response (variable slope) equation in Prism 6 (GraphPad Software, https://www.graphpad.com). For the study, we included only reported values with an R^2 (coefficient of determination) >0.75, hill slope >0.5, and 50% inhibitory concentration within the assay range. We performed FRNT for *Flavivirus* strains WP74 (DENV-1), S16803 (DENV-2), CH53489 (DENV-3), TVP-376 (DENV-4), and H/PF/2013 (ZIKV).

Depletion of DENV binding Antibodies

We obtained purified viral antigens for antibody depletions by infecting Vero-81 cell cultures in 850 cm^2 roller bottles (Greiner Bio-One, https://www.gbo.com) as described elsewhere (*25*). We conjugated *Flavivirus*-specific antibody 1M7 to Tosyl-activated Dynabeads (Thermo Fisher) magnetic beads and incubated purified DENV-1–4 viral antigens (1 h at 37°C) with the beads. To deplete DENV-specific antibodies, we incubated serum samples (3 h at 37°C) with DENV-conjugated Dynabeads and incubated serum samples with Dynabeads conjugated to an equivalent bovine serum albumin concentration. We confirmed cross-reactive and DENV antibody depletion using whole virion capture ELISA against DENV-1–4. We measured serotype-specific ZIKV antibodies in serum samples using ZIKV whole-virion capture ELISA after depletion, as described elsewhere (*24*).

Receiver Operator Characteristic Analysis

We used SPSS Statistics for Macintosh version 27.0 (https://www.ibm.com) to report the performance of the EDIII ELISA based on the receiver operating characteristic (ROC) curve, which presents test performance as true-positive (sensitivity) versus false-positive (1 – specificity). We calculated the optimal assay cutoff value, which maximizes sensitivity and specificity, from the ROC curve using the same software. According to the test, sensitivity is the fraction of total confirmed positive samples with true positives, and specificity is total confirmed negative samples with true negatives.

Results

Development of Immunoassay for Detecting ZIKV Antibodies in Patient Serum

We previously demonstrated that a serologic assay using the ZIKV EDIII fused to maltose-binding protein (MBP) reliably differentiated persons with past ZIKV infections from those with DENV infections (*19*). However, we observed a high background signal in some specimens, originating from human antibodies binding to MBP or the mouse antigen capture antibody used in the assay. To overcome this problem in the earlier version of the assay, we produced the ZIKV EDIII antigen fused to a HaloTag (Figure 1, panel A), derived from the haloalkane dehalogenase enzyme from *Rhodococcus rhodochrous* bacteria (*26*). By using a biotin HaloTag ligand (*27*), we added a single biotin molecule for each protein molecule at a site distant from the EDIII antigen (Figure 1, panel B). Using streptavidin-coated ELISA plates to capture the antigen, we established an assay for detecting ZIKV EDIII–binding antibodies in human clinical samples (Figure 1, panel C).

Performance of the Second-Generation ZIKV EDIII ELISA

We performed an ROC analysis to determine the diagnostic performance of the new EDIII-capture

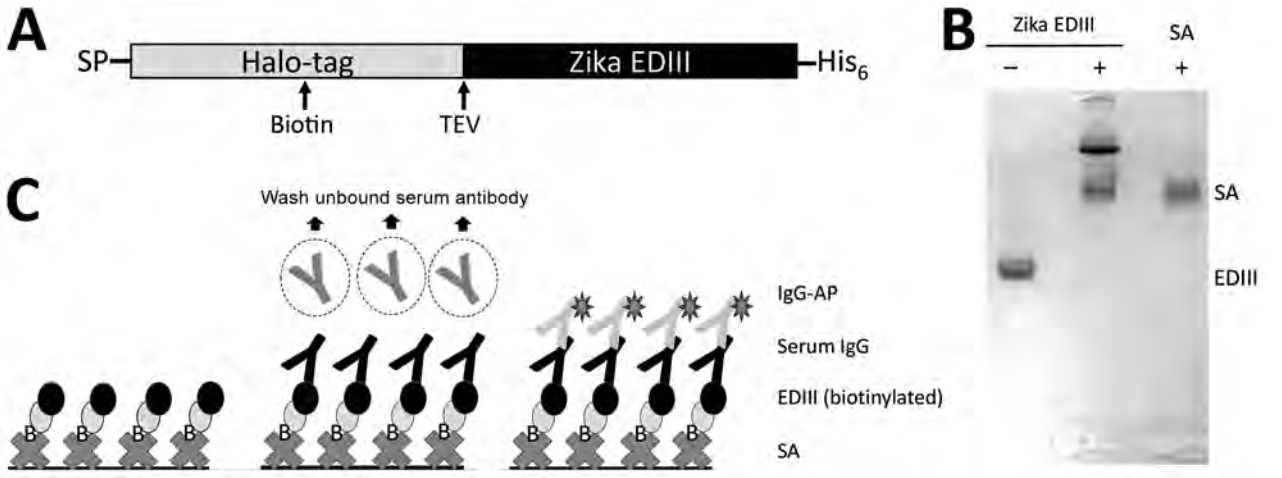

Figure 1. ZIKV Biotinylated-EDIII antigen capture ELISA in study of novel assay to measure ZIKV seroprevalence in the Philippines. A) Schematic of the ZIKV EDIII construct with an N-terminal human albumin secretion signal, a HaloTag (Promega, https://www.promega.com) for site-specific biotinylation and a C-terminal 6-histidine residue tag for affinity purification. The EDIII construct design also included a TEV protease cleavage site between HaloTag and EDIII. B) Biotinylated ZIKV EDIII displays an electrophoretic mobility shift with streptavidin. A site-specific biotinylated ZIKV EDIII was prepared using HaloTag biotin ligand. Electrophoretic gel shift analysis was performed in sodium dodecyl sulphate–polyacrylamide gel electrophoresis with biotinylated EDIII antigen in the presence and absence of streptavidin. C) Schematic of second-generation ZIKV EDIII ELISA using streptavidin-biotin interaction. Biotinylated EDIII antigen is captured by plate immobilized streptavidin. The antibody bound to EDIII is detected by a secondary anti–human IgG conjugated to alkaline phosphatase. EDIII, E protein domain III; IgG-AP, secondary IgG antibody conjugated to alkaline phosphatase; SA, streptavidin; SP, N terminal human albumin secretion signal; TEV, tobacco etch virus protease cleavage site; ZIKV, Zika virus.

ELISA in a panel of serum samples collected >12 weeks after symptom onset among persons with laboratory-confirmed ZIKV or DENV infections or who received a licensed *Flavivirus* vaccine. The panel included serum samples from DENV-naive and DENV-immune participants who received positive ZIKV RT-PCR test results, archived serum samples from persons who had primary (only 1 serotype) or secondary (≥2 serotypes) DENV infections, control samples from persons who had not experienced DENV or ZIKV infections, and samples from travelers who had received Japanese encephalitis virus vaccine or yellow fever virus vaccine or both. The EDIII assay was positive for 32 of 33 ZIKV-immune, 7 of 67 DENV-immune, and 2 of 42 DENV- and ZIKV-naive or yellow fever/Japanese encephalitis virus vaccine recipients (Figure 2, panel A). The ROC analysis demonstrated an area under the curve of 0.97 (95% CI of 0.94–0.99) (Figure 2, panel B). At a cutoff value of OD 0.34, the sensitivity of the EDIII-capture ELISA was 97% and the specificity was 92%.

Durability of ZIKV EDIII Antibodies in Persons Exposed to ZIKV Infections

Next, we assessed the durability of EDIII antibodies using a panel of 98 longitudinal samples collected 1–600 days after symptom onset from 27 residents of Puerto Rico with PCR-confirmed ZIKV infections. By testing the acute specimens for DENV-specific antibodies, we stratified the DENV-immune status at the time of ZIKV infection as 12 DENV-naive and 15 DENV-immune cases. We measured endpoint titers at each time point to follow the kinetics of serum ZIKV EDIII antibodies (Figure 3). The ZIKV EDIII antibody titers reached peak levels by 1 month after initial infection and stayed well above detection level for ≥20 months in DENV- naive and DENV-immune participants.

Seroprevalence of ZIKV in Cebu Province

Having established the performance of the ZIKV EDIII ELISA among participants exposed to multiple DENV serotypes, we used the assay to estimate the seroprevalence of ZIKV among children living in Balamban and Bogo City in Cebu Province. In 2017, we collected baseline blood samples from a DENV vaccine study of 2,996 children 9–14 years of age. Elsewhere we reported that 89.3% of the children were DENV-immune at baseline, demonstrating the high endemicity of the virus in this population (*23*). We selected a representative sample of 547 children on the basis of DENV-immune status from the baseline cohort to determine the seroprevalence of ZIKV (Table 1). The children selected for the study

consisted of 60 (11%) with no immunity to DENV, 43 (8%) with immunity to 1 DENV serotype, and 444 (81%) with immunity to ≥2 serotypes (Table 1; Figure 4, panel B) (*23*). We observed that 98/547 (18%) children were ZIKV antibody positive in the ZIKV EDIII assay (Figure 4, panel A). The number of children who tested positive or negative for ZIKV antibodies did not differ by sex, location, or prior DENV-immune status (Table 1).

Comparison of ZIKV EDIII ELISA and Virus Neutralizing Antibody Assays

The current standard for estimating the seroprevalence of a particular flavivirus is based on measuring virus neutralizing antibodies in cell culture systems. Although neutralizing antibody assays are more specific than assays that measure antibody binding to flaviviruses or whole recombinant proteins, persons exposed to multiple DENV serotypes can develop ZIKV cross-neutralizing antibodies as reported elsewhere (*10*,*24*,*28*,*29*). Given the large number of children in our cohort with a history of ≥2 DENV serotype infections, we compared the performance for estimating ZIKV seroprevalence of the EDIII ELISA using FRNT.

From the 547 baseline samples tested by ZIKV EDIII assay, we tested 495 samples in a single dilution (1:40) ZIKV neutralization assay. We have demonstrated elsewhere that at 1:40 dilution, neutralization of ≥70% of the input virus is a reliable screening criterion for previous DENV infection (*23*). When we used the same criterion for the single-dilution ZIKV neutralization assay, we observed a much higher seroprevalence (39%) compared with the estimate (18%) based on the EDIII ELISA (Appendix Table 1, https://wwwnc.cdc.gov/EID/article/27/12/21-1150-App1.pdf). Most of the discordant samples (positive in the ZIKV neutralization assay and negative in the ZIKV EDIII assay) were from children with preexisting multitypic immunity to DENVs (105/110 participants) (Appendix Table 1), raising the possibility that high levels of DENV antibodies cross-neutralize ZIKV.

To evaluate whether the discordant results were because of the poor specificity of the ZIKV neutralization assay or poor sensitivity of the ZIKV EDIII ELISA, we selected 24 samples that had been classified by full curve neutralization testing against the 4 DENV serotypes and ZIKV as primary DENV-immune only (n = 3), primary ZIKV-immune only (n = 4), both primary DENV- and primary ZIKV-immune (n = 6), multitypic DENV-immune only (n = 2), or both multitypic DENV- and ZIKV-immune (n = 9) participants (Appendix Table 2, Figure 2) for further study. By selectively removing all antibodies to DENVs in a sample before testing for ZIKV binding antibodies, it is possible to detect ZIKV type-specific antibodies indicative of a past ZIKV infection (*11*). We incubated all 24 samples with magnetic beads coated with the 4 DENV serotypes to remove all DENV-binding antibodies. After

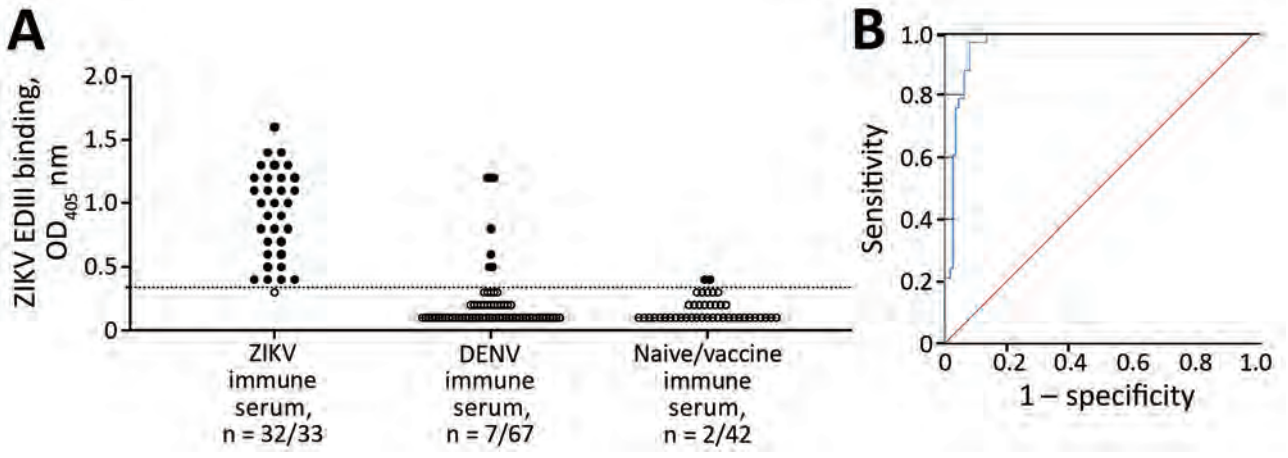

Figure 2. Performance evaluation of ZIKV EDIII assay in study of novel assay to measure ZIKV seroprevalence in the Philippines. Shown are the binding (A) and ROC (B) curve analysis of ZIKV EDIII ELISA using human convalescent serum samples. A panel of convalescent serum samples collected >12 weeks after onset of symptoms from primary and secondary ZIKV infections (n = 33), primary and multitypic DENV infections (n = 67), and serum samples collected >12 weeks after vaccination with a licensed *Flavivirus* vaccine or serum samples from *Flavivirus*-naive participants (n = 42) were tested by ZIKV EDIII ELISA. ROC demonstrated 0.966 (95% CI 0.94–0.99) area under the curve. The sensitivity of the EDIII capture ELISA was 97% (32/33) and the specificity 92% (100/109) at a cutoff value of 0.34. Red line indicates a random classifier and represents data points with equal true-positive rate and false-positive rate. The blue line is the ROC curve showing high performance of the ZIKV EDIII assay because the blue line is above and further away from a random classifier. DENV, dengue virus; EDIII, E protein domain III; OD_{405}, optical density at 405 nm; ROC, receiver operating characteristic; ZIKV, Zika virus.

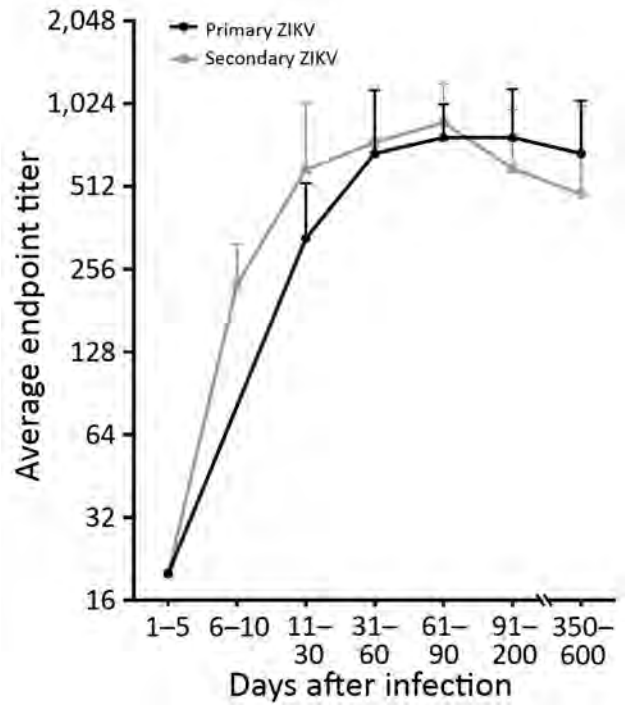

Figure 3. Durability of ZIKV EDIII antibodies in study of novel assay to measure ZIKV seroprevalence in the Philippines. Longitudinal samples from patients with PCR-confirmed ZIKV infections were collected 1–600 days after symptom onset and tested for ZIKV EDIII–binding antibodies. DENV serostatus was determined by DENV focus reduction neutralization test. Primary ZIKV serostatus indicates ZIKV infection in DENV-naive participants; secondary ZIKV serostatus indicates ZIKV infection in participants previously infected with DENV. DENV, dengue virus; EDIII, E protein domain III; ZIKV, Zika virus.

confirming removal of all DENV-binding antibodies, we tested the samples for ZIKV-binding antibodies. After depleting DENV-binding antibodies, we observed ZIKV-binding antibodies for the participants designated as immune to primary Zika only and primary DENV and primary ZIKV (Appendix Table 2, Figure 1, panel A). In contrast, 6/9 participants designated by neutralization testing as multitypic DENV- and ZIKV-immune showed no ZIKV-binding antibodies (Appendix Figure 1, panel A). All participants that retained ZIKV-binding antibodies after DENV-binding antibody depletion also tested positive in the ZIKV EDIII ELISA and all participants with no detectable ZIKV-specific antibodies tested negative in the EDIII assay (Appendix Table 2, Figure 1, panel B). These results suggest that the ZIKV EDIII ELISA is more reliable than neutralization testing for estimating ZIKV seroprevalence independent of DENV status.

Discussion

The 2015 ZIKV pandemic in the Americas mostly affected communities with high DENV endemicity because these viruses share the same mosquito vector. Efforts to monitor the spread of ZIKV and the effect of cross-reactive immunity on viral pathogenesis were severely hampered by the inability of conventional serologic assays to accurately distinguish DENV from ZIKV seropositivity. Several groups developed ZIKV recombinant antigen–based assays or antigen-antibody competition assays to improve the specificity of serologic assays (*16*–*18*).

In a previous study, we documented development of an ELISA to detect antibodies in persons who had recovered from ZIKV infections, using ZIKV EDIII fused to *Escherichia coli* MBP as an antigen (*19*). We observed in some persons high background levels of antibodies to the MBP fusion protein alone, most likely from natural exposure to bacterial proteins, highlighting the need for modifying the fusion

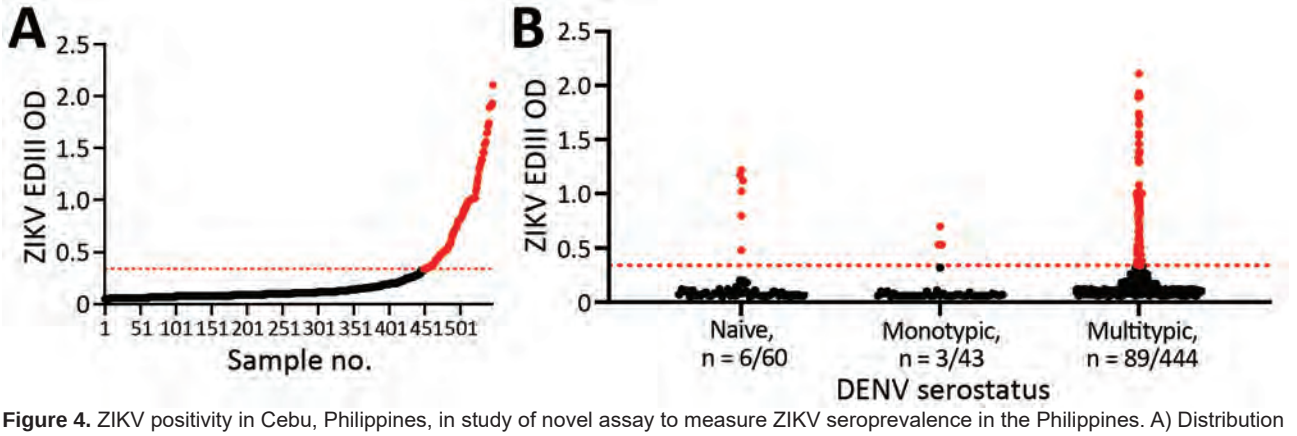

Figure 4. ZIKV positivity in Cebu, Philippines, in study of novel assay to measure ZIKV seroprevalence in the Philippines. A) Distribution of ZIKV EDIII antibody reactivity among the 547 participants tested; 18% of the participants tested positive. B) Distribution of ZIKV EDIII–positive participants by DENV serostatus. Horizontal dotted red lines indicate positive threshold of EDIII assay. DENV, dengue virus; EDIII, E protein domain III; OD, optical density; ZIKV, Zika virus.

protein used for antigen production. We describe a ZIKV EDIII antigen improved by replacing the MBP fusion tag with a HaloTag amenable to site-specific biotinylation. Using streptavidin-biotin chemistry to capture the antigen, we developed an ELISA with 97% sensitivity and 92% specificity for detecting past ZIKV infections.

A strength of our study was the use of serum samples from participants living in *Flavivirus*-endemic regions with well-defined exposures to DENVs or ZIKV or both to determine the performance of the assay when testing specimens with high levels of cross-reactive antibodies. A potential problem with using modular domains such as EDIII instead of the full-length envelope protein is a loss in assay sensitivity over time. However, our analysis of the longitudinal samples from patients with documented ZIKV infection demonstrated that ZIKV EDIII antibodies robustly developed and remained at high levels even after 2.7 years. This finding suggests that serologic assays based on EDIII will have the necessary sensitivity to characterize past ZIKV circulation at individual and population levels.

The severity of the epidemic in the Americas renewed interest in the epidemiology and pathogenesis of ZIKV in Asia. Asian lineages of the virus have been circulating for decades if not longer. The virus has been detected by molecular methods or virus isolation by cell culture in many countries, including Thailand, the Philippines, Vietnam, Malaysia, Cambodia, and India (*30*–*35*). One study of 600 migrant workers in Taiwan (predominantly from Indonesia, the Philippines, Thailand, and Vietnam) reported 37% seroprevalence using a ZIKV IgG assay (*36*,*37*). A similar study of Taiwan residents (n = 212) identified 4.2% of all participants with ZIKV IgG but confirmed only 1 participant by neutralization test (*36*). Investigators tested a cohort of children 1–4 years of age (n = 662) in Indonesia and estimated 9.1% seroprevalence using 90% neutralization as a cutoff value (*38*). A 2017 study of healthy adults (n = 801) in Vietnam estimated 1.1% seroprevalence using a ZIKV neutralization assay (*39*). An additional study in Guangxi Province, China, in March 2019 found 6% of 273 participants bound to ZIKV NS1 using IgG ELISA testing and neutralized ZIKV in cell cultures (*40*). Those past studies, especially those relying on tests of whole Zika virions and full-length antigens, had poor specificity, mainly because of antibodies induced by DENV infections cross-reacting with ZIKV antigens. In our study, we used a recombinant ZIKV antigen with a high specificity for distinguishing ZIKV-induced from DENV-induced antibodies; results showed that 18% of children 9–14 years of age living in Cebu Province had previously experienced a ZIKV infection. Although ZIKV is currently not considered by public health agencies to be a common infection in the Philippines, our results indicate otherwise.

Table. Demographics of study cohort and number of participants with ZIKV EDIII type-specific antibody in study of novel assay to measure ZIKV seroprevalence in the Philippines

Category	Total no. (%)	No. (%) ZIKV positive	p value*
All participants	547	98 (18)	
Sex			0.50
M	218 (40)	35 (16)	
F	329 (60)	63 (19)	
Location			0.90
Balamban	145 (27)	25 (17)	
Bogo	402 (73)	73 (18)	
Specific type			0.06
Naive	60 (11)	6 (10)	
Monotypic	43 (8)	3 (7)	
Multitypic	444 (81)	89 (20)	

*Association between ZIKV serostatus and sex or location measured by Fisher exact test. Association between ZIKV serostatus and DENV-type serostatus measured by χ^2 test.

Our results also highlight a problem with using accepted standards for neutralizing antibody testing to identify ZIKV infections in populations heavily exposed to DENVs. We observed ZIKV neutralizing antibodies in 39% of the children in this study, which was more than double the estimate based on the EDIII assay results. By depleting all DENV-binding antibodies from a subset of samples and then measuring ZIKV antibodies, we demonstrated that some children exposed to ≥2 DENV serotypes have low levels of ZIKV cross-neutralizing antibodies that can lead to false-positive results. In contrast, the ZIKV EDIII assay was not impacted by DENV-immune status because, even after removing all DENV-binding antibodies, the children maintained ZIKV EDIII–binding antibodies.

The novel assay we describe, which uses a biotinylated EDIII antigen to detect ZIKV type-specific antibodies, is simple and readily adaptable for use in standard clinical and public health laboratories to monitor ZIKV transmission at both the individual and population levels. Given that the 2015 ZIKV epidemic spread to >40 countries and infected more than a million people, many in regions with endemic transmission of DENVs, and that DENVs demonstrate cross-reactive immunity with ZIKV, the improved specificity of this assay provides a necessary resource for accurately monitoring ZIKV transmission in regions with high DENV endemicity.

Acknowledgments

We thank the children and their families in Balamban and Bogo City who volunteered for this study and the field staff who assisted with the study. We also thank Laura White and Alena Markmann for providing specimens for validating the assay and for supervising sample processing, inventory, and storage and Matt Collins for providing clinical samples for validating the assay.

The field component of the study in the Philippines was supported by the Department of Health (Philippines), the Hanako Foundation, the World Health Organization, and the Swedish International Development Cooperation Agency in partnership with the International Vaccine Institute in Seoul, South Korea. The laboratory studies at the University of North Carolina were supported by grants from the US Centers for Disease Control and Prevention (BAA 2017-N-18041; PI AdeS) and the US National Institutes of Health (U24 AI152170-01 and R21 AI134073 PIs: Ades and LP). C.A. was supported by NIH Predoctoral Training Grant T32 AI007419: "Molecular Biology of Viral Disease." US patent application no. 20200300855 on the method incorporating the EDIII antigen for serodiagnosis of Zika infection has been filed under the title "Methods and Compositions for Zika Virus Detection."

About the Author

Mr. Adams is an MD/PhD student at the University of North Carolina School of Medicine. His main research and clinical interests involve global health, infectious diseases, and vaccinology.

References

1. Hills SL, Fischer M, Petersen LR. Epidemiology of Zika virus infection. J Infect Dis. 2017;216(suppl_10):S868–74. https://doi.org/10.1093/infdis/jix434
2. Ventura CV, Maia M, Bravo-Filho V, Góis AL, Belfort R Jr. Zika virus in Brazil and macular atrophy in a child with microcephaly. Lancet. 2016;387:228. https://doi.org/10.1016/S0140-6736(16)00006-4
3. Johansson MA, Mier-y-Teran-Romero L, Reefhuis J, Gilboa SM, Hills SL. Zika and the risk of microcephaly. N Engl J Med. 2016;375:1–4. https://doi.org/10.1056/NEJMp1605367
4. Hoen B, Schaub B, Funk AL, Ardillon V, Boullard M, Cabié A, et al. Pregnancy outcomes after ZIKV infection in French territories in the Americas. N Engl J Med. 2018;378:985–94. https://doi.org/10.1056/NEJMoa1709481
5. Borchering RK, Huang AT, Mier-Y-Teran-Romero L, Rojas DP, Rodriguez-Barraquer I, Katzelnick LC, et al. Impacts of Zika emergence in Latin America on endemic dengue transmission. Nat Commun. 2019;10:5730. https://doi.org/10.1038/s41467-019-13628-x
6. Gordon A, Gresh L, Ojeda S, Katzelnick LC, Sanchez N, Mercado JC, et al. Prior dengue virus infection and risk of Zika: A pediatric cohort in Nicaragua. PLoS Med. 2019;16:e1002726. https://doi.org/10.1371/journal.pmed.1002726
7. Katzelnick LC, Narvaez C, Arguello S, Lopez Mercado B, Collado D, Ampie O, et al. Zika virus infection enhances future risk of severe dengue disease. Science. 2020;369:1123–8. https://doi.org/10.1126/science.abb6143
8. Duong V, Dussart P, Buchy P. Zika virus in Asia. Int J Infect Dis. 2017;54:121–8. https://doi.org/10.1016/j.ijid.2016.11.420
9. Hu T, Li J, Carr MJ, Duchêne S, Shi W. The Asian lineage of Zika virus: transmission and evolution in Asia and the Americas. Virol Sin. 2019;34:1–8. https://doi.org/10.1007/s12250-018-0078-2
10. Priyamvada L, Quicke KM, Hudson WH, Onlamoon N, Sewatanon J, Edupuganti S, et al. Human antibody responses after dengue virus infection are highly cross-reactive to Zika virus. Proc Natl Acad Sci U S A. 2016;113:7852–7. https://doi.org/10.1073/pnas.1607931113
11. Andrade P, Gimblet-Ochieng C, Modirian F, Collins M, Cárdenas M, Katzelnick LC, et al. Impact of pre-existing dengue immunity on human antibody and memory B cell responses to Zika. Nat Commun. 2019;10:938. https://doi.org/10.1038/s41467-019-08845-3
12. Rogers TF, Goodwin EC, Briney B, Sok D, Beutler N, Strubel A, et al. Zika virus activates de novo and cross-reactive memory B cell responses in dengue-experienced donors. Sci Immunol. 2017;2:eaan6809. https://doi.org/10.1126/sciimmunol.aan6809
13. Chua CL, Chan YF, Andu ESGS, Rovie-Ryan JJ, Sitam FT, Verasahib K, et al. Little evidence of Zika virus infection in wild long-tailed Macaques, peninsular Malaysia. Emerg Infect Dis. 2019;25:374–6. https://doi.org/10.3201/eid2502.180258
14. Beck C, Leparc-Goffart I, Desoutter D, Debergé E, Bichet H, Lowenski S, et al. Serological evidence of infection with dengue and Zika viruses in horses on French Pacific Islands. PLoS Negl Trop Dis. 2019;13:e0007162. https://doi.org/10.1371/journal.pntd.0007162
15. Netto EM, Moreira-Soto A, Pedroso C, Höser C, Funk S, Kucharski AJ, et al. High Zika virus seroprevalence in Salvador, Northeastern Brazil limits the potential for further outbreaks. MBio. 2017;8:e01390–17. https://doi.org/10.1128/mBio.01390-17
16. Balmaseda A, Stettler K, Medialdea-Carrera R, Collado D, Jin X, Zambrana JV, et al. Antibody-based assay discriminates Zika virus infection from other flaviviruses. Proc Natl Acad Sci U S A. 2017;114:8384–9. https://doi.org/10.1073/pnas.1704984114
17. Rockstroh A, Moges B, Barzon L, Sinigaglia A, Palù G, Kumbukgolla W, et al. Specific detection of dengue and Zika virus antibodies using envelope proteins with mutations in the conserved fusion loop. Emerg Microbes Infect. 2017;6:e99. https://doi.org/10.1038/emi.2017.87
18. Denis J, Attoumani S, Gravier P, Tenebray B, Garnier A, Briolant S, et al. High specificity and sensitivity of Zika EDIII-based ELISA diagnosis highlighted by a large human reference panel. PLoS Negl Trop Dis. 2019;13:e0007747. https://doi.org/10.1371/journal.pntd.0007747
19. Premkumar L, Collins M, Graham S, Liou GA, Lopez CA, Jadi R, et al. Development of envelope protein antigens to serologically differentiate Zika virus infection from dengue virus infection. J Clin Microbiol. 2018;56:e01504–17. https://doi.org/10.1128/JCM.01504-17
20. Los GV, Encell LP, McDougall MG, Hartzell DD, Karassina N, Zimprich C, et al. HaloTag: a novel protein labeling technology for cell imaging and protein analysis. ACS Chem Biol. 2008;3:373–82. https://doi.org/10.1021/cb800025k

21. Wang J, Bardelli M, Espinosa DA, Pedotti M, Ng TS, Bianchi S, et al. A human bi-specific antibody against Zika virus with high therapeutic potential. Cell. 2017;171:229–241.e15. https://doi.org/10.1016/j.cell.2017.09.002
22. Paz-Bailey G, Rosenberg ES, Sharp TM. Persistence of Zika virus in body fluids—final report. N Engl J Med. 2019;380:198–9. https://doi.org/10.1056/NEJMc1814416
23. Lopez AL, Adams C, Ylade M, Jadi R, Daag JV, Molloy CT, et al. Determining dengue virus serostatus by indirect IgG ELISA compared with focus reduction neutralisation test in children in Cebu, Philippines: a prospective population-based study. Lancet Glob Health. 2021;9:e44–51. https://doi.org/10.1016/S2214-109X(20)30392-2
24. Collins MH, McGowan E, Jadi R, Young E, Lopez CA, Baric RS, et al. Lack of durable cross-neutralizing antibodies against Zika virus from dengue virus infection. Emerg Infect Dis. 2017;23:773–81. https://doi.org/10.3201/eid2305.161630
25. Putnak R, Barvir DA, Burrous JM, Dubois DR, D'Andrea VM, Hoke CH, et al. Development of a purified, inactivated, dengue-2 virus vaccine prototype in Vero cells: immunogenicity and protection in mice and rhesus monkeys. J Infect Dis. 1996;174:1176–84. https://doi.org/10.1093/infdis/174.6.1176
26. Benink HA, Urh M. HaloTag technology for specific and covalent labeling of fusion proteins. Methods Mol Biol. 2015;1266:119–28. https://doi.org/10.1007/978-1-4939-2272-7_8
27. Dubey M, Emoto K, Takahashi H, Castner DG, Grainger DW. Affinity-based protein surface pattern formation by ligand self-selection from mixed protein solutions. Adv Funct Mater. 2009;19:3046–55. https://doi.org/10.1002/adfm.200900809
28. Dussupt V, Sankhala RS, Gromowski GD, Donofrio G, De La Barrera RA, Larocca RA, et al. Potent Zika and dengue cross-neutralizing antibodies induced by Zika vaccination in a dengue-experienced donor. Nat Med. 2020;26:228–35. https://doi.org/10.1038/s41591-019-0746-2
29. Fernandez E, Dejnirattisai W, Cao B, Scheaffer SM, Supasa P, Wongwiwat W, et al. Human antibodies to the dengue virus E-dimer epitope have therapeutic activity against Zika virus infection. [Erratum in Nat Immunol. 2020;21:354.] Nat Immunol. 2017;18:1261–9. https://doi.org/10.1038/ni.3849
30. Woon YL, Lim MF, Tg Abd Rashid TR, Thayan R, Chidambaram SK, Syed Abdul Rahim SS, et al. Zika virus infection in Malaysia: an epidemiological, clinical and virological analysis. BMC Infect Dis. 2019;19:152. https://doi.org/10.1186/s12879-019-3786-9
31. Ho ZJM, Hapuarachchi HC, Barkham T, Chow A, Ng LC, Lee JMV, et al.; Singapore Zika Study Group. Outbreak of Zika virus infection in Singapore: an epidemiological, entomological, virological, and clinical analysis. Lancet Infect Dis. 2017;17:813–21. https://doi.org/10.1016/S1473-3099(17)30249-9
32. Buathong R, Hermann L, Thaisomboonsuk B, Rutvisuttinunt W, Klungthong C, Chinnawirotpisan P, et al. Detection of Zika virus infection in Thailand, 2012–2014. Am J Trop Med Hyg. 2015;93:380–3. https://doi.org/10.4269/ajtmh.15-0022
33. Ruchusatsawat K, Wongjaroen P, Posanacharoen A, Rodriguez-Barraquer I, Sangkitporn S, Cummings DAT, et al. Long-term circulation of Zika virus in Thailand: an observational study. [Erratum in Lancet Infect Dis. 2019;19:e109.] Lancet Infect Dis. 2019;19:439–46. https://doi.org/10.1016/S1473-3099(18)30718-7
34. Alera MT, Hermann L, Tac-An IA, Klungthong C, Rutvisuttinunt W, Manasatienkij W, et al. Zika virus infection, Philippines, 2012. Emerg Infect Dis. 2015;21:722–4. https://doi.org/10.3201/eid2104.141707
35. Buerano CC, Pangilinan LS, Dimamay MTA, Mapua CA, Dimamay MPS, Matias RR, et al. Zika virus infection, Philippines, 2012. Emerg Infect Dis. 2020;26:2300–1. https://doi.org/10.3201/eid2609.190896
36. Chien YW, Ho TC, Huang PW, Ko NY, Ko WC, Perng GC. Low seroprevalence of Zika virus infection among adults in Southern Taiwan. BMC Infect Dis. 2019;19:884. https://doi.org/10.1186/s12879-019-4491-4
37. Perng GC, Ho TC, Shih HI, Lee CH, Huang PW, Chung CH, et al. Seroprevalence of Zika and dengue virus antibodies among migrant workers, Taiwan, 2017. Emerg Infect Dis. 2019;25:814–6. https://doi.org/10.3201/eid2504.181449
38. Sasmono RT, Dhenni R, Yohan B, Pronyk P, Hadinegoro SR, Soepardi EJ, et al. Zika virus seropositivity in 1–4-year-old children, Indonesia, 2014. Emerg Infect Dis. 2018;24:1740–3. https://doi.org/10.3201/eid2409.180582
39. Nguyen CT, Moi ML, Le TQM, Nguyen TTT, Vu TBH, Nguyen HT, et al. Prevalence of Zika virus neutralizing antibodies in healthy adults in Vietnam during and after the Zika virus epidemic season: a longitudinal population-based survey. BMC Infect Dis. 2020;20:332. https://doi.org/10.1186/s12879-020-05042-2
40. Zhou CM, Liu JW, Qi R, Fang LZ, Qin XR, Han HJ, et al. Emergence of Zika virus infection in China. PLoS Negl Trop Dis. 2020;14:e0008300. https://doi.org/10.1371/journal.pntd.0008300

Address for correspondence: Aravinda de Silva or Lakshmanane Premkumar, Department of Microbiology and Immunology, University of North Carolina School of Medicine, Chapel Hill, NC 27599-7292, USA; email: aravinda_desilva@med.unc.edu or prem@med.unc.edu

Novel Filoviruses, Hantavirus, and Rhabdovirus in Freshwater Fish, Switzerland, 2017

Melanie M. Hierweger, Michel C. Koch, Melanie Rupp, Piet Maes, Nicholas Di Paola, Rémy Bruggmann, Jens H. Kuhn, Heike Schmidt-Posthaus,[1] Torsten Seuberlich[1]

European perch (*Perca fluviatilis*) are increasingly farmed as a human food source. Viral infections of European perch remain largely unexplored, thereby putting farm populations at incalculable risk for devastating fish epizootics and presenting a potential hazard to consumers. To address these concerns, we applied metatranscriptomics to identify disease-associated viruses in European perch farmed in Switzerland. Unexpectedly, in clinically diseased fish we detected novel freshwater fish filoviruses, a novel freshwater fish hantavirus, and a previously unknown rhabdovirus. Hantavirus titers were high, and we demonstrated virus in macrophages and gill endothelial cells by using in situ hybridization. Rhabdovirus titers in organ samples were low, but virus could be isolated on cell culture. Our data add to the hypothesis that filoviruses, hantaviruses, and rhabdoviruses are globally distributed common fish commensals, pathogens, or both. Our findings shed new light on negative-sense RNA virus diversity and evolution.

Aquaculture is the fastest growing sector in food production worldwide (*1*); innovative intensive production technologies, such as recirculating aquaculture systems (RAS), are becoming increasingly valuable for commercial fish production (*2*). Attempts are continually made to introduce new types of fish into aquaculture, to reduce overfishing of wild fish populations, and to satisfy the progressing consumer demand for diverse supply (*3*). One example is the adaptation of European perch (*Perca fluviatilis*; order Perciformes, family Percidae) to farming and the growing consumer interest in this fish (*4*). European perch are actinopterygiids that naturally inhabit slow-flowing rivers, lakes, or ponds in Europe and northern Asia. During the 19th century, they were introduced into Australia as angling fish, where they are now considered invasive, competing with native fish for food and space, preying on other fish, and breeding to overpopulation (*5*).

Although little is known about diseases affecting European perch in the wild, infectious diseases lead to high mortality among these fish in aquaculture, making farming of these fish economically challenging. One of the main threats is infection with perch rhabdovirus (PRV; family *Rhabdoviridae*, genus *Perhabdovirus*), leading to the central nervous system (CNS) signs of loss of equilibrium and aberrant swimming behavior and to higher mortality (*2*,*6*–*10*). Lack of investigation of the occurrence and diversity of other pathogenic virus infections of European perch that result in disease impairs the treatment, control, and prevention of disease outbreaks in farm populations. To address this knowledge gap, we applied virus diagnostics, including metatranscriptomics (virus discovery by high-throughput RNA sequencing and bioinformatics), to a set of samples collected from sick juvenile European perch at a perch farm in Switzerland in 2017. Although we did not find PRV in these fish, our investigation led to the discovery of 5 novel negative-sense RNA viruses, belonging to the negarnaviricot families *Rhabdoviridae*, *Filoviridae*, and *Hantaviridae*, that could possibly contribute to disease development.

Methods

European Perch Origin

The European perch used in this study were raised in a private pond in Saxony, Germany, and were exported to a farm that uses RAS in Bernese Oberland,

Author affiliations: University of Bern, Bern, Switzerland (M.M. Hierweger, M.C. Koch, M. Rupp, R. Bruggmann, H. Schmidt-Posthaus, T. Seuberlich); KU Leuven, Leuven, Belgium (P. Maes); US Army Medical Research Institute of Infectious Diseases, Frederick, Maryland, USA (N. Di Paola); Integrated Research Facility at Fort Detrick, Frederick (J. H. Kuhn)

DOI: https://doi.org/10.3201/eid2712.210491

[1]These authors contributed equally to this article.

Switzerland, at 16 g (≈11,200 fish) and 33 g (≈4,800 fish). Eleven live juvenile European perch were sent to the Centre for Fish and Wildlife Health (FIWI), University of Bern (Bern, Switzerland), where they were euthanized and subjected to microbiological (including parasitologic, bacteriologic, mycologic, and virologic) and pathologic (including histopathologic) examination. Because the remaining fish at the farm exhibited clinical signs of disease, they were kept in quarantine for an additional 2 months and subsequently euthanized.

Cell Culture

We used bluegill (*Lepomis macrochirus*) fry cells (BF-2) and fathead minnow (*Pimephales promelas*) epithelioma papulosum cyprini (EPC) cells. These cells were originally obtained from the Friedrich-Loeffler-Institute, Federal Research Institute for Animal Health (Greifswald-Insel Riems, Germany; Collection of Cell Lines in Veterinary Medicine, catalog nos. CCLV-RIE 290 and CCLV-RIE 173 are maintained at FIWI).

We inoculated the cells with small pieces of pooled CNS or spleen, kidney, heart, and pyloric ceca tissue from 5 of the 11 euthanized European perch (in total <5 g) and incubated at 15°C. We monitored the cell cultures for CPE daily for 7 days by using light microscopy and then monitored subcultures for another 7 days. We harvested supernatants from cell cultures showing CPE and tested by reverse transcription PCR (RT-PCR) for the common European perch pathogen PRV, targeting the glycoprotein (*G*) gene of PRV isolate 9574.1 (GenBank accession no. JF502613), according to a previously published protocol, by using the primer pair oPVP116/118 and oPVP126/Rha2 (*11*).

High-Throughput Sequencing and Bioinformatics

We extracted total RNA from fresh-frozen pooled visceral organs and CNS tissue, originally taken for cell culture inoculation by using TRI Reagent (Sigma Life Sciences, https://www.sigmaaldrich.com), according to the manufacturer's instructions. We then prepared a high-throughput sequencing (HTS) library with the TruSeq Stranded Total RNA kit (Illumina, https://www.illumina.com) and performed HTS on a HiSeq 3000 machine (Illumina), generating paired-end reads of 2 × 150 bp. We performed bioinformatic analysis as described previously (*12*) (Appendix, https://wwwnc.cdc.gov/EID/article/27/12/21-0491-App1.pdf).

Reverse Transcription PCR, Rapid Amplification of cDNA Ends, and Sanger Sequencing

To fill gaps between HTS scaffolds, we reverse-transcribed extracted RNA to cDNA, performed PCRs, and subjected the amplicons to Sanger sequencing (Appendix). We performed 3′ and 5′ rapid amplification of cDNA ends (RACE), as described previously, on RNA extracted from pooled organs and CNS tissue as well as cell culture supernatants (*13*) (Appendix).

Taxonomic Analyses

We performed taxonomic analyses by using protein or nucleic acid sequences, following precedents established by the International Committee on Taxonomy of Viruses (ICTV) *Filoviridae* (*14*,*15*), *Hantaviridae* (*16*), and *Rhabdoviridae* (*17*) Study Groups. New filovirus-like genome sequences were analyzed by using pairwise sequence comparison (*18*) and maximum-likelihood phylogenetics. Filovirus phylogenetic estimations were inferred in FastTree version 2.1 (*19*) by using a general time-reversible model with 20 gamma-rate categories, 5,000 bootstrap replicates, and exhaustive search parameters (-slow) and pseudocounts (-pseudo). The new rhabdovirus-like sequence was taxonomically placed via analysis of its full-length large protein gene (*L*) sequence using maximum-likelihood phylogenetics. We applied the maximum-likelihood method in MEGA X (*20*) with 1,000 bootstraps for rhabdovirus and hantavirus phylogenetic estimations.

Histopathology and In Situ Hybridization

During a complete necropsy of the 11 fish, we used 3 whole perch for histologic examination. We fixed these fish in 10% buffered formalin for 24 hours and embedded cut sections of the gills, longitudinal head sections, and longitudinal cut sections of the body cavity in paraffin. We prepared 3-μm sections and stained them with hematoxylin and eosin according to standard protocols. We conducted chromogenic in situ hybridization on all formalin-fixed paraffin-embedded (FFPE) tissues used for histopathology. We performed staining with the RNAscope system (Advanced Cell Diagnostics, https://acdbio.com) (Appendix).

Results

Clinical and Pathologic Findings

In December 2016, a total of 16,000 juvenile European perch were imported from Saxony, Germany, to a farm using RAS in Bernese Oberland, Switzerland. After arrival, the fish were routinely quarantined. Shortly after arrival, because of a high death rate of 1% per day (reference range 0.01%–0.03% per day), 11 randomly selected live fish were sent to FIWI for microbiological and pathologic examination. Clinical signs included

anorexia, lethargy, skin ulcerations, multifocal hemorrhages, and eroded tail fins. Culture and PCR indicated that skin ulcerations were caused by oomycete (*Saprolegnia parasitica*) infection (*21*). Histopathology revealed mild to moderate gill epithelial proliferation and epithelial cell hypertrophy. Additional findings included necrotizing dermatitis with hemorrhage and intralesional oomycete hyphi and bacterial colonies. The newly arrived fish were treated with flubendazole, formalin, and peracetic acid, but death increased to 1.8%–4.2% per day. Two months after importation, deaths for the quarantined fish reached 22%–27% in total. All remaining fish were euthanized and discarded, thereby preventing these fish from entering the food chain.

Virus Isolation

For routine virus investigation, we exposed standard fish cell cultures (BF-2 and EPC) to suspensions of pooled perch CNS and pooled visceral organs. We selected these cell lines because of their high susceptibility to diverse fish viruses (*22*). CPE developed 10 days after inoculation of CNS suspension into BF-2 cells and 13 days after inoculation into EPC cells. Affected cell supernatants were harvested and tested preliminarily positive for PRV infection by RT-PCR. The sequence of the detected amplicon was, however, only 78% identical to the sequence of the perhabdovirus lake trout rhabdovirus (LTRV; GenBank accession no. AF434991), indicating the presence of a perhabdovirus distinct from PRV/LTRV.

Novel Perhabdovirus

To further characterize the putative novel perhabdovirus, we performed metatranscriptomics by using HTS and bioinformatic analysis of pooled CNS tissue and visceral organ RNA extracts of 5 fish. We found 16 sequence scaffolds 247–1,454-nt long with mean k-mer coverages of 1.0–5.9 and nucleotide sequence identities of 62%–98% to perhabdovirus genomes (Appendix Table 1). We mapped these scaffolds to LTRV (GenBank accession no. AF434991) and PRV (GenBank accession no. JX679246) as references and closed sequence gaps by RT-PCR and RACE followed by Sanger sequencing. The resulting complete genome of the novel virus was 11,595-nt long and had the characteristic genomic organization of (pe)rhabdoviruses (Figure 1, panel A). Each of the open reading frames (ORFs) is flanked by conserved transcriptional initiation (3′-UUGUUC) and termination/polyadenylation (3′-AURC$[U]_7$) signals with inverse complementarity of 13 nt of the 3′ and 5′ terminal genome sequences.

Phylogenetic comparison of the *L* gene confirmed a close relationship of the new virus to the 2 members of the species *Sea trout perhabdovirus* (i.e., LTRV and Swedish sea trout virus; GenBank accession no. AF434992) (Figure 1, panel B) and a recently described and thus far unclassified virus from a percid (sea trout rhabdovirus isolate 18/203; GenBank accession no. MN963997). This relationship is also reflected in phylogenetic comparisons of the nucleoprotein (*N*), phosphoprotein (*P*), matrix protein (*M*), and *G* genes (Appendix Figure 1). The current perhabdovirus sequence-based species demarcation criterion is a minimum divergence of 15% in the *L* gene (*17*). The *L* gene sequence of the novel virus is most closely related to that of the isolate 18/203 (divergence 10%); *L* genes of both viruses are ≈19% divergent from the next closest related perhabdovirus, sea trout perhabdovirus isolate R6146 (GenBank accession no. MN963999), thus indicating that we discovered a novel perhabdovirus that should be assigned to a new species along with isolate 18/203. We named the new virus Egli virus (EGLV) after a local Swiss-German word for European perch and deposited the complete viral genome sequence into GenBank (accession no. MN510774). Detection of EGLV in European perch FFPE tissue sections by RNA in situ hybridization was unsuccessful.

Four Novel Filoviruses

In addition to scaffolds that ultimately led us to identify EGLV, we found 41 scaffolds 240–4,726-nt long with low k-mer coverage (0.8–4.8×). The deduced amino acid sequences were 28%–30% identical to proteins of Huángjião virus (HUJV), a recently identified virus of marine greenfin horse–faced filefish (*Thamnaconus septentrionalis*) captured in the East China Sea (*23*) (Appendix Table 1). Alignment of these scaffolds to the HUJV genome (GenBank accession no. MG599981) and the deduced amino acid sequences to those of HUJV-encoded proteins revealed a complex scenario suggesting the presence of several distinct thamnoviral genomes, however with numerous gaps between the scaffolds. To obtain complete or coding-complete viral genome sequences, we resequenced the HTS library to generate ≈10 times more paired-end reads (2,051,046,671) than during the initial HTS run, reassembled the sequences, and performed RT-PCR and Sanger sequencing to bridge sequence gaps. This effort resulted in 3 long scaffolds of 13,764 nt (k-mer coverage 24×), 14,593 nt (k-mer coverage 15×), and 13,066 nt (k-mer coverage 5×), corresponding to 3 novel viruses.

We named these viruses Fiwi virus (FIWIV; GenBank accession no. MN510772), after FIWI; Oberland virus (OBLV;) GenBank accession no. MN510773), after Bernese Oberland; and Kander virus (KNDV;

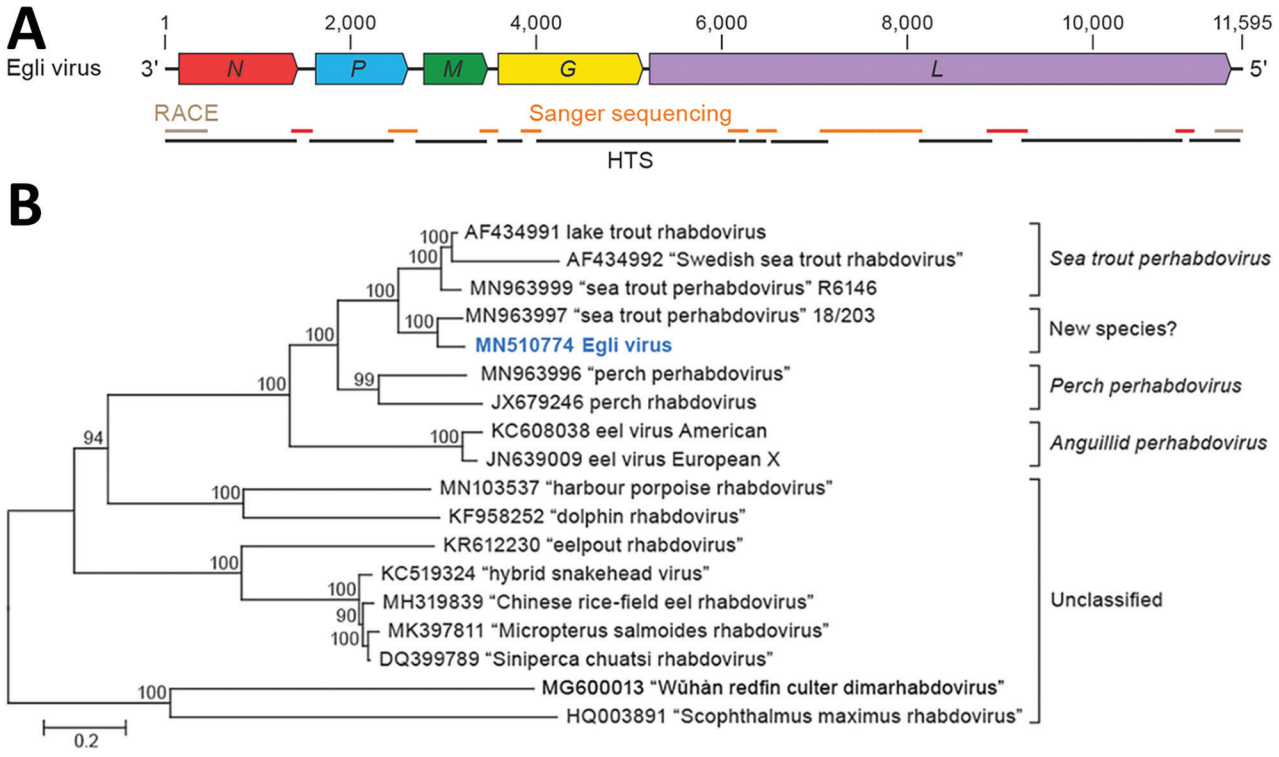

Figure 1. Identifying a novel rhabdovirus in European perch. A) Schematic representation of the Egli virus genome organization; open reading frames are indicated by colored arrows. B) Maximum-likelihood phylogenetic tree of the nucleotide sequence of the Egli virus *L* gene (bold blue) and representative classified and unclassified members of the genus *Perhabdovirus.* Numbers near nodes on the trees indicate bootstrap values. Branches are labeled by GenBank accession number, and virus name. Names of unclassified likely perhabdoviruses are placed in quotation marks. Scale bar indicates number of substitutions per site, reflected by branch lengths. *G*, glycoprotein gene; HTS, high-throughput sequencing; *L*, large protein gene; *M*, matrix protein gene; *N*, nucleoprotein gene; *P*, phosphoprotein gene; RACE, rapid amplification of cDNA ends.

GenBank accession no. MW093492), after the Kander River, which flows through Bernese Oberland. Whereas the FIWIV genome appears to be coding complete, the sequences of OBLV are coding incomplete at the 5′ terminus and of KNDV at both the 5′ and the 3′ termini. All attempts to determine the authentic 3′ and 5′ termini by RACE were unsuccessful, most likely because of low viral RNA loads. However, all 3 sequences have the genomic features of HUJV, encoding the filovirus-typical proteins nucleoprotein (NP), polymerase cofactor (VP35), glycoprotein ($GP_{1,2}$), transcriptional activator (VP30), and large protein (L) containing an RNA-directed RNA polymerase (RdRp) domain, as well as 1–2 novel proteins (*14*,*23*,*24*) (Figure 2, panel A). Phylogenetic comparison of the FIWIV, OBLV, and KNDV genomic sequences (Figure 2, panel B) and *L* gene sequences with those of representative classified viruses of the family *Filoviridae* (Figure 2, panel C) confirmed the genetic relationship of all 3 viruses to HUJV. The current demarcation criteria for filovirus sequence-based genus and species are ≥55% and ≥23% sequence divergence over complete genome sequences determined by using pairwise sequence comparison (*14*,*15*). We found a pairwise divergence of 49% compared with HUJV by using the FIWIV genome sequence (Table), indicating that FIWIV is a member of a new thamnovirus species ("*Thamnovirus percae*"). The available KNDV genome sequence is 49% divergent from HUJV and 37% divergent from FIWIV (Table), suggesting that KNDV represents yet another novel thamnovirus species ("*Thamnovirus kanderense*"). In contrast, OBLV was >62% divergent from HUJV, FIWIV, and KNDV viruses and thus represents a new species ("*Oblavirus percae*") within a new genus ("*Oblavirus*"). All attempts to detect FIWIV or OBLV viruses in 3 European perch FFPE tissue sections were unsuccessful.

In addition to FIWIV, OBLV, and KNDV, we found 4 shorter scaffolds (573–3,259 nt; Appendix Figure 2) similar to various HUJV genes, but attempts to demonstrate a physical linkage of these sequences by RT-PCR were not successful. Still, the

presence of these scaffolds is indicative of at least 1 additional novel filovirus, which we were not able to further characterize.

Novel Hantavirus

In the same RNA extract of pooled organs, we found 3 scaffolds, of which the deduced amino acid sequences

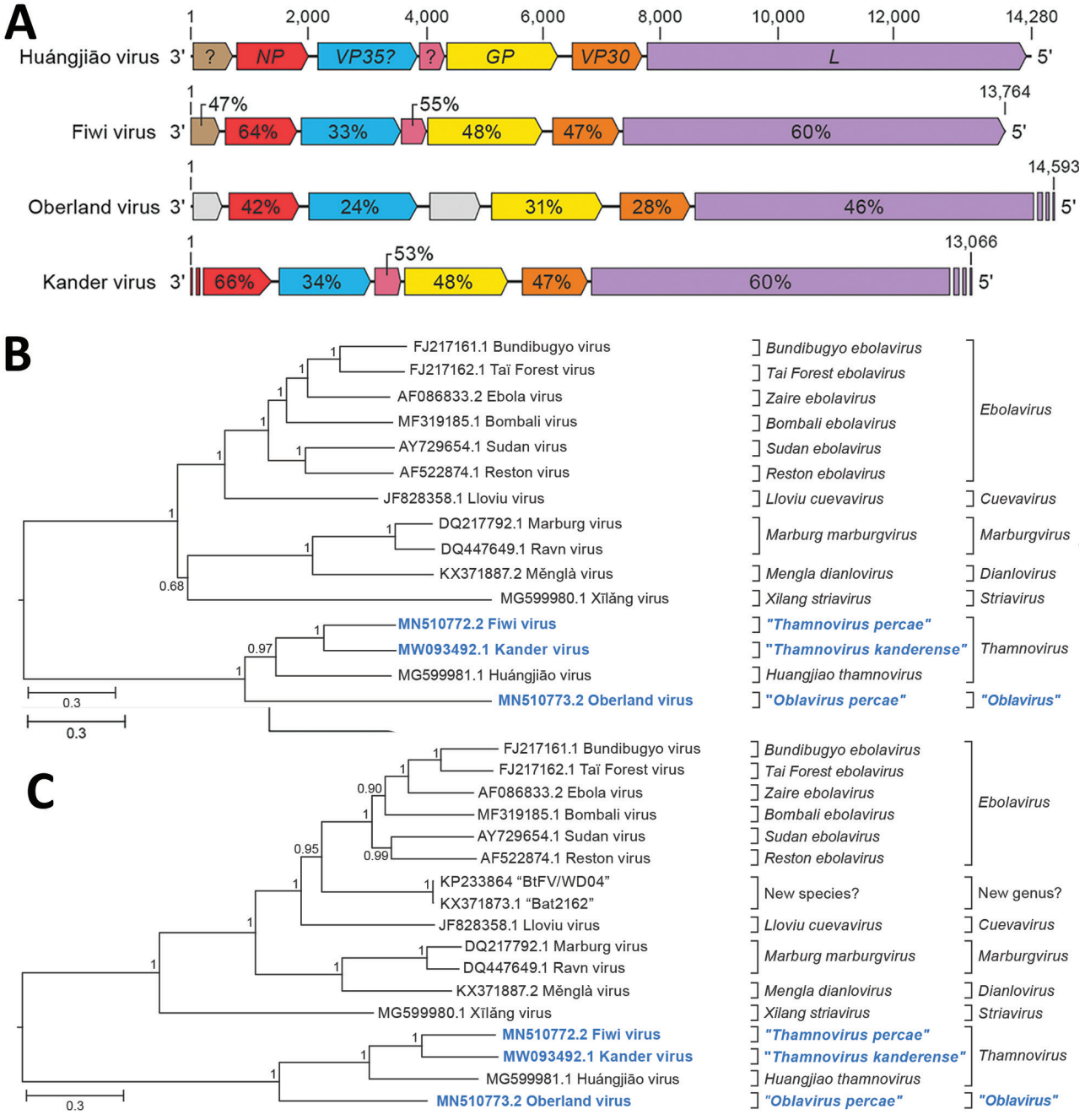

Figure 2. Identifying 3 novel filoviruses in European perch. A) Schematic representation of the genome organization of Fiwi virus, Oberland virus, and Kander virus compared with Huángjiāo virus (HUJV). Open reading frames (ORFs) are indicated by colored arrows. ORFs encoding HUJV-like proteins are depicted by the same color and sequence similarities are indicated as percentages. Undetermined ORF starts and ends are shown as stripes. B, C) Maximum-likelihood phylogenetic trees of the new filovirus genome sequences (bold blue) generated by using coding-complete and near-complete genome sequences (B) or only *L* gene sequences (C) of representative members of the family *Filoviridae*. Numbers near nodes on the trees indicate bootstrap values. Branches are labeled by GenBank accession number and virus names. Scale bar indicates number of substitutions per site, reflected by branch lengths. *GP*, glycoprotein gene; *L*, large protein gene; *NP*, nucleoprotein gene; *VP30*, transcriptional activator gene; *VP35*, polymerase cofactor gene.

were 25%–35% similar to those of the large (L), medium (M), and small (S) segments of Wēnlǐng minipizza batfish virus (WEMBV) and Wēnlǐng red spikefish virus (WERSV). WEMBV was recently identified in apparently healthy minipizza batfish (*Halieutaea stellate*) and WERSV in red spikefish (*Triacanthodes anomalus*) captured in the East China Sea (Appendix Table 1) (*23*). The mean k-mer coverage of these scaffolds ranged from 3×10^3 to 1.5×10^4, indicating a high viral RNA load. Using Sanger sequencing and RACE, we determined the complete sequences of the genomic L (GenBank accession no. MN510769), M (GenBank accession no. MN510770), and S (GenBank accession no. MN510771) segments of a novel virus, here named Bern perch virus (BPV). Similar to WEMBV and WERSV, the BPV L segment (6,372 nt) was deduced to encode the L protein including an RdRp domain, the M segment (3,804 nt) was deduced to encode the glycoprotein precursor, and the S segment (2,435 nt) was deduced to encode the nucleocapsid protein (Figure 3, panel A). The S and M segments contain 2 additional ORFs encoding putative proteins not represented in current protein databases in antisense (S segment) and sense (M segment) orientation. Alignment of the 3′ and 5′ sequences of all 3 segments revealed that the 8 terminal nucleotides are complementary within and conserved among segments (Figure 3, panel B), a known feature of members of the order *Bunyavirales* (*25*). However, these terminal sequences differ from those of members of the genus *Orthohantavirus* and are similar to those of members of the genus *Orthobunyavirus* (Appendix Table 1). Phylogenetic analysis of the L protein confirmed the close relationship ofw BPV to all currently classified actinoviruses (Figure 3, panel C; Appendix Figure 3) but indicated the need for a novel species to accommodate this virus. This need was confirmed by DEmARC (Diversity Partitioning by Hierarchical Clustering) analysis (*26*); on the basis of this evidence, the ICTV officially established this species as *Perch actinovirus* in 2021 (*27*,*28*).

Using in situ hybridization on FFPE tissue sections, we were able to detect BPV genomic RNA in gills with histopathologic lesions of 2 fish (Figure 4, panels A, B; Appendix Figure 4) and in a granuloma in the perivisceral fat tissue of 1 of these animals. Morphologically, we identified the affected cells in the gills and the perivisceral fat tissue as putative macrophages. In addition, putative endothelial cells were labeled positively in the gills (Figure 4, panel B).

Discussion

The diversity of fish viruses, in particular that of RNA viruses, remains poorly understood (*29*). Recent initial studies indicate that this diversity is enormous and that many viral taxa that have been established for pathogens of humans and other mammals need to be redefined (*23*,*30*–*32*). Husbandry conditions in huge tanks used on farms may favor the emergence and rapid intraspecies and interspecies transmission of fish viruses, potentially resulting in high economic loss for the fish industry. Also of concern is the introduction of novel viruses from fish farms into native fauna, which could have disastrous ecologic consequences. In addition, viruses of unknown pathogenicity in food animals may have zoonotic potential of yet unpredictable importance.

Table. Pairwise distances of complete or coding-complete genome nucleotide sequences between the newly identified Fiwi virus, Huángjiāo virus, and the closest related mammalian filovirus, Bombali virus*

Virus	Virus			
	Fiwi	Oberland	Kander	Huángjiāo
Oberland	66%			
Kander	37%	62%		
Huángjiāo	49%	64%	49%	
Bombali	86%	87%	87%	86%

*Fiwi virus, GenBank accession no. MN510772; Oberland virus, GenBank accession no. MN510773; Kander virus, GenBank accession no. MW093492; Bombali virus, GenBank accession no.MK340750. Oberland and Kander virus sequences are not coding complete and were compared on the basis of the available incomplete sequences.

In this study, we identified 1 novel rhabdovirus, 4 novel filoviruses (3 confirmed and 1 likely), and 1 novel hantavirus in morbid farmed European perch. The discovery of a novel rhabdovirus was not surprising and adds to the role of rhabdoviruses in fish health; rhabdoviruses, in particular those of the genera *Novirhabdovirus*, *Perhabdovirus*, *Sprivivirus*, and *Vesiculovirus*, are notorious marine and freshwater fish pathogens, causing diseases characterized by high lethality (*33*,*34*). Thus, these viruses pose a considerable threat to aquaculture. The European perch examined in this study exhibited signs compatible with rhabdovirus infection (*7*). Using HTS and exposing cell cultures to CNS tissue suspensions, we discovered a novel perhabdovirus, Egli virus. Although the viral RNA loads in tissues were low and we could not detect RNA by in situ hybridization in tissue sections, we were able to isolate the virus from brain tissue. Rhabdoviruses in perch are usually associated with disease and not known as commensals. The host range of Egli virus is unknown, but genetically it is more closely related to viruses identified in trout than to those infecting perch, suggesting the possibility of cross-species transmission, highlighting a concern for farms that raise fish other than perch and for native fish populations. Discovery of a lake trout rhabdovirus

as a probable cause of disease in European perch in Ireland (*7*) supports the hypothesis of high potential for interspecies transmission of these viruses.

Unexpectedly, we were able to assemble near-complete viral genomes of 3 novel filoviruses (Fiwi, Oberland, and Kander viruses) and detected a likely fourth filovirus in the diseased perch. Until recently, filoviruses, notorious for causing disease in humans with extremely high lethality (*35*), were thought to exclusively infect mammals. This view changed with the discovery of Xīlǎng virus (the only member of genus *Striavirus*) in striated frogfish (*Antennarius striatus*) and HUJV in greenfin horse–faced filefish captured in the East China Sea (*23*) as well as apparent thamnoviruses John Dory filovirus in John Dory (*Zeus faber*) and blue spotted goatfish filovirus in blue spotted goatfish (*Upeneichthys lineatus*) purchased at a fish market in Sydney, New

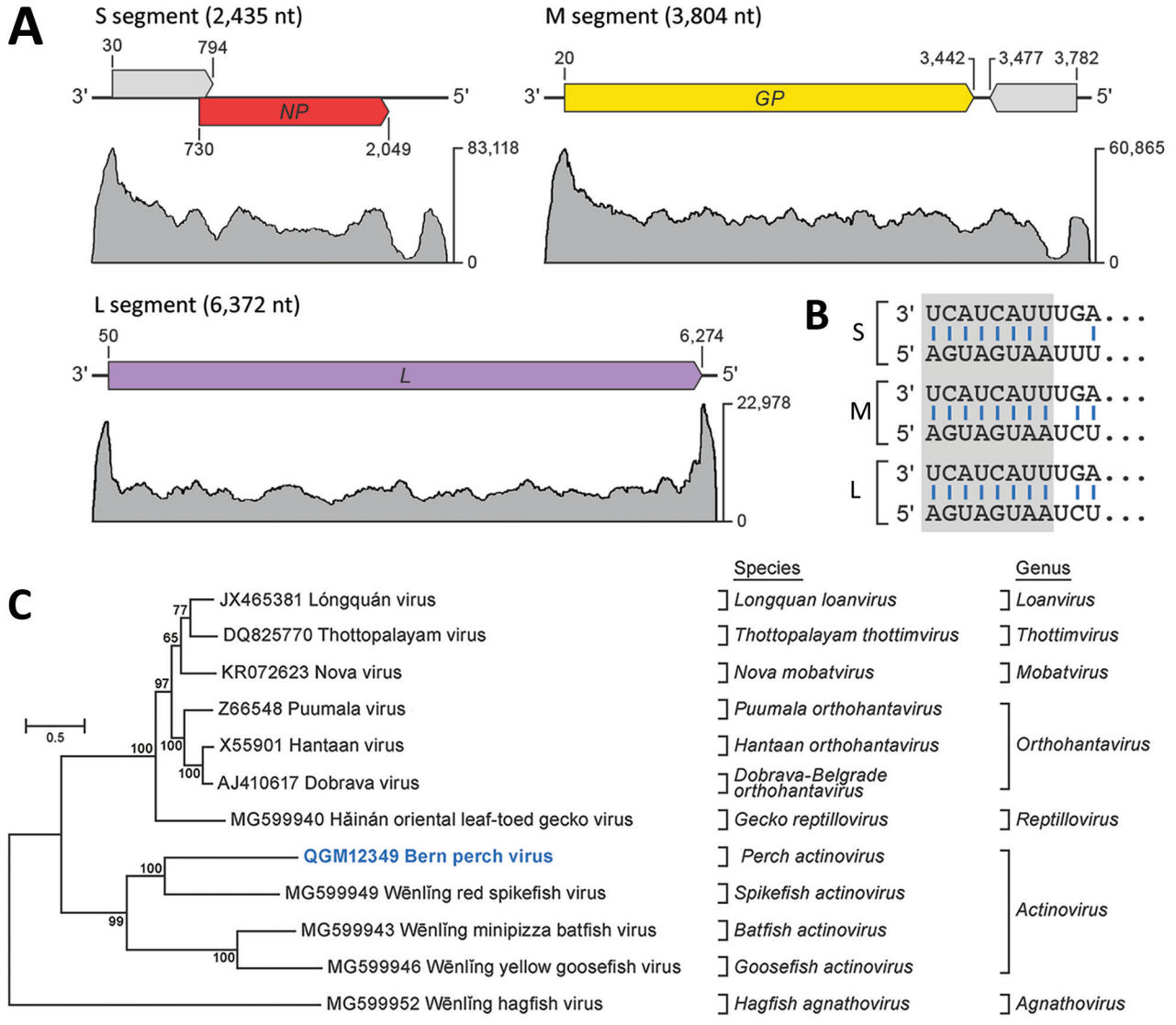

Figure 3. Identifying a novel hantavirus in European perch. A) Schematic representation of the 3 genome segments of Bern perch virus; open reading frames are indicated as colored arrows. Coverage plots of high-throughput sequencing reads are shown for each segment, and maximum-read coverages are indicated on the right. B) Alignment of the terminal sequences (11 nt) of the 3 segments. The terminal 8 nucleotides (gray box) are complementary within and conserved among segments. C) Maximum-likelihood phylogenetic tree of the Bern perch virus RNA-directed RNA-polymerase amino-acid sequence (bold blue) with RNA-directed RNA-polymerase amino-acid sequences of representative members of the family *Hantaviridae.* Numbers near nodes on the trees indicate bootstrap values. Branches are labeled by GenBank accession number, and virus name. Scale bar indicates number of substitutions per site, reflected by branch lengths. *GP*, glycoprotein gene; L, large; M, medium; *NP*, nucleocapsid protein gene; S, small.

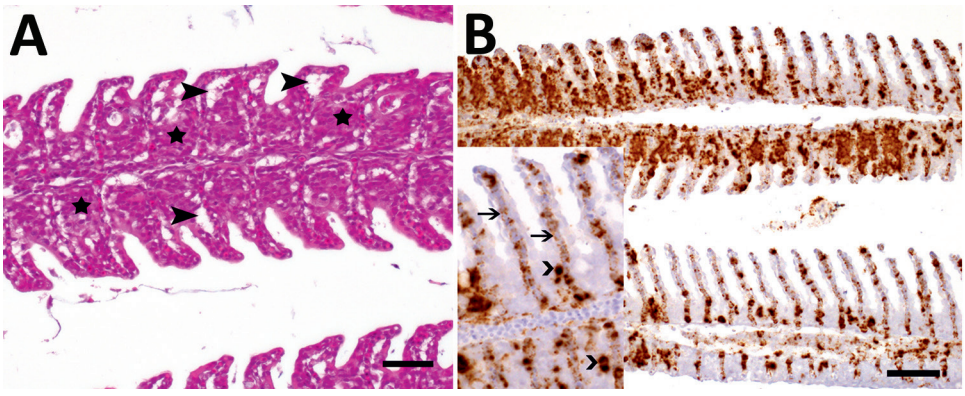

Figure 4. Histopathologic lesions and viral RNA in European perch infected with Bern perch virus. A) Histopathologic lesions in gills (hematoxylin and eosin stain) showing epithelial hypertrophy and hyperplasia, multifocally leading to lamellar fusion (stars) and multifocal epithelial lifting due to edema (closed arrowheads). Scale bar indicates 25 μm. B) In situ hybridization detection of RNA in gills (brown labeling): brown perch virus positive macrophages, more pronounced in proliferated areas, and endothelial cells. Inset: higher magnification showing positive macrophages (open arrowheads) and endothelial cells (arrows with open heads). Scale bar indicates 50 μm.

South Wales, Australia (*31*). However, currently, <300 nt contigs are known from John Dory fish and blue spotted goatfish filoviruses; hence, their true taxonomic affiliation remains to be determined. In contrast to Xīlǎng virus, HUJV, John Dory filovirus, and blue spotted goatfish filovirus (all of which were found in marine fish in China and Australia), FIWIV, OBLV, and KNDV apparently infect freshwater fish in Europe. This geographic and ecologic distribution indicates that filoviruses are broadly dispersed fish commensals or potential pathogens that probably number in the hundreds or thousands. Although on the basis of our data we cannot attribute filovirus infection to individual fish, a possible scenario includes co-infection with FIWIV, OBLV, KNDV, EGLV, or BPV or any combination of these viruses. Thamnovirus abundance was low in the sampled European perch, and detection of thamnoviral genomic RNA proved impossible in FFPE tissues. This low abundance, together with the unsuccessful attempt to demonstrate viral RNA in the tissue, suggests that infection in the investigated fish was subclinical rather than the cause of the observed clinical signs.

We also identified a novel hantavirus, BPV. Hantaviruses are best known as rodent-borne viruses of the mammantavirin genus *Orthohantavirus*, which cause hemorrhagic fever with renal syndrome or hantavirus pulmonary syndrome in humans (*36*) but have also been found in bats and eulipotyphla. Reptile hantaviruses (family *Repantavirinae*, genus *Reptillovirus*) and fish hantaviruses (family *Actantavirinae*, genus *Actinovirus*, and family *Agantavirinae*, genus *Agnathovirus*) (*32*) have only recently been discovered. The fish viruses include the actinoviruses WEMBV, WERSV (*23*), and Wēnlǐng yellow goosefish virus (detected in yellow goosefish [*Lophius litulon*] captured in China [*23*]); the likely actinovirus Aronnax virus, found in pygmy goby (*Eviota zebrina*) purchased at a fish market in Sydney (*31*); and the agnathovirus Wēnlǐng hagfish virus, detected in inshore hagfish (*Eptatretus burgeri*) captured in China (*23*). Similar to our filovirus findings, the discovery of BPV is remarkable because this actinovirus was found in freshwater fish from Europe rather than in marine fish from China or Australia. Actinoviruses have not yet been associated with disease in fish. Using in situ hybridization, we demonstrated, however, high concentrations of BPV RNA in macrophages and endothelial cells in the gills as well as in macrophages in the perivisceral fat tissue of morbid European perch. Other cell types tested negative. Human pathogenic orthohantaviruses predominantly infect macrophages and microvascular endothelial cells of a variety of organs, which leads to increased vascular permeability and severe disease (*11*). It is therefore tempting to speculate that the pathology observed in the gills of the European perch may have resulted in dyspnea, contributing to elevated mortality. In conclusion, our identification of new rhabdoviruses, filoviruses, and hantaviruses in farmed European perch in Switzerland raises concerns about the global distribution, host spectrum, and risks to human and animal health for these viruses.

Acknowledgments

We thank Pamela Nicholson and the HTS platform, University of Bern, for performing the HTS runs, Elsbeth Keller-Gautschi and Regula Hirschi for excellent technical assistance, and Laurent Bigarré for scientific exchange and advice. We are grateful to Anya Crane for editing the manuscript.

This work was supported by the Swiss National Science Foundation (grant no. 31003A_163438 to R.B. and T.S.), the Swiss Food Safety and Veterinary Office (grant no. MON-108 to T.S.), and the Swiss Innovation Agency (Innossuisse, grant no. 25178.1 PFLS-LS to H.S.-P). This work was supported in part through Laulima Government Solutions, LLC, prime contract with the US National Institute of Allergy and Infectious Diseases under contract no. HHSN272201800013C. J.H.K. performed this work as an employee of Tunnell Government Services, a subcontractor of Laulima Government Solutions, LLC, under contract no. HHSN272201800013C.

HTS raw data from this study have been deposited into the Sequence Read Archive (https://www.ncbi.nlm.nih.gov/sra) as SRR12586223.

About the Author

Dr. Hierweger works as a postdoctoral researcher at the Division of Neurological Sciences, Vetsuisse Faculty, University of Bern. Her main research interest is the discovery of emerging viruses and their involvement in disease.

References

1. Food and Agriculture Organization of the United Nations. The state of world fisheries and aquaculture 2018. Meeting the sustainable development goals [cited 2021 Jul 10]. http://www.fao.org/3/i9540en/I9540EN.pdf
2. Martins CIM, Eding EH, Verdegem MCJ, Heinsbroek LTN, Schneider O, Blancheton JP, et al. New developments in recirculating aquaculture systems in Europe: a perspective on environmental sustainability. Aquacult Eng. 2010;43:83–93. https://doi.org/10.1016/j.aquaeng.2010.09.002
3. Naylor RL, Hardy RW, Buschmann AH, Bush SR, Cao L, Klinger DH, et al. A 20-year retrospective review of global aquaculture. Nature. 2021;591:551–63. https://doi.org/10.1038/s41586-021-03308-6
4. Policar T, Schaefer FJ, Panana E, Meyer S, Teerlinck S, Toner D, et al. Recent progress in European percid fish culture production technology—tackling bottlenecks. Aquacult Int. 2019;27:1151–74. https://doi.org/10.1007/s10499-019-00433-y
5. Morgan DL, Gill HS, Maddern MG, Beatty SJ. Distribution and impacts of introduced freshwater fishes in Western Australia. N J Mar Freshwater Res. 2004;38:511–23. https://doi.org/10.1080/00288330.2004.9517257
6. Caruso C, Gustinelli A, Pastorino P, Acutis PL, Prato R, Masoero L, et al. Mortality outbreak by perch rhabdovirus in European perch (*Perca fluviatilis*) farmed in Italy: clinical presentation and phylogenetic analysis. J Fish Dis. 2019;42:773–6. https://doi.org/10.1111/jfd.12975
7. Ruane NM, Rodger HD, McCarthy LJ, Swords D, Dodge M, Kerr RC, et al. Genetic diversity and associated pathology of rhabdovirus infections in farmed and wild perch *Perca fluviatilis* in Ireland. Dis Aquat Organ. 2014;112:121–30. https://doi.org/10.3354/dao02801
8. Rupp M, Knüsel R, Sindilariu P-D, Schmidt-Posthaus H. Identification of important pathogens in European perch (*Perca fluviatilis*) culture in recirculating aquaculture systems. Aquacult Int. 2019;27:1045–53. https://doi.org/10.1007/s10499-019-00382-6
9. Dorson M, Torchy C, Chilmonczyk S, Kinkelin P, Michel C. A rhabdovirus pathogenic for perch, *Perca fluviatilis* L.: isolation and preliminary study. J Fish Dis. 1984;7:241–5. https://doi.org/10.1111/j.1365-2761.1984.tb00929.x
10. Dannevig BH, Olesen NJ, Jentoft S, Kvellestad A, Taksdal T, Håstein T. The first isolation of a rhabdovirus from perch (*Perca fluviatilis*) in Norway. Bull Eur Assoc Fish Pathol. 2001;21:186–94.
11. Talbi C, Cabon J, Baud M, Bourjaily M, de Boisséson C, Castric J, et al. Genetic diversity of perch rhabdoviruses isolates based on the nucleoprotein and glycoprotein genes. Arch Virol. 2011:156:2133–44. https://doi.org/10.1007/s00705-011-1103-z
12. Kauer RV, Koch MC, Hierweger MM, Werder S, Boujon CL, Seuberlich T. Discovery of novel astrovirus genotype species in small ruminants. PeerJ. 2019;7:e7338. https://doi.org/10.7717/peerj.7338
13. Hierweger MM, Werder S, Seuberlich T. Parainfluenza virus 5 infection in neurological disease and encephalitis of cattle. Int J Mol Sci. 2020;21:498. https://doi.org/10.3390/ijms21020498
14. Kuhn JH, Amarasinghe GK, Basler CF, Bavari S, Bukreyev A, Chandran K, et al.; ICTV Report Consortium. ICTV virus taxonomy profile: *Filoviridae*. J Gen Virol. 2019;100:911–2. https://doi.org/10.1099/jgv.0.001252
15. Bào Y, Amarasinghe GK, Basler CF, Bavari S, Bukreyev A, Chandran K, et al. Implementation of objective PASC-derived taxon demarcation criteria for official classification of filoviruses. Viruses. 2017;9:106. https://doi.org/10.3390/v9050106
16. Laenen L, Vergote V, Calisher CH, Klempa B, Klingström J, Kuhn JH, et al. *Hantaviridae*: current classification and future perspectives. Viruses. 2019;11:788. https://doi.org/10.3390/v11090788
17. Walker PJ, Blasdell KR, Calisher CH, Dietzgen RG, Kondo H, Kurath G, et al.; ICTV Report Consortium. ICTV virus taxonomy profile: *Rhabdoviridae*. J Gen Virol. 2018;99:447–8. https://doi.org/10.1099/jgv.0.001020
18. National Center for Biotechnology Information. Pairwise Sequence Comparison (PASC) [cited 2021 Jul 10]. https://www.ncbi.nlm.nih.gov/sutils/pasc/viridty.cgi?textpage=overview
19. Price MN, Dehal PS, Arkin AP. FastTree 2—approximately maximum-likelihood trees for large alignments. PLoS One. 2010;5:e9490. https://doi.org/10.1371/journal.pone.0009490
20. Kumar S, Stecher G, Li M, Knyaz C, Tamura K. MEGA X: Molecular Evolutionary Genetics Analysis across computing platforms. Mol Biol Evol. 2018;35:1547–9. https://doi.org/10.1093/molbev/msy096
21. Ravasi D, De Respinis S, Wahli T. Multilocus sequence typing reveals clonality in *Saprolegnia parasitica* outbreaks. J Fish Dis. 2018;41:1653–65. https://doi.org/10.1111/jfd.12869
22. World Organisation for Animal Health. Aquatic | Manual online access [cited 2021 Jul 10]. https://www.oie.int/|standard-setting/aquatic-manual/access-online
23. Shi M, Lin X-D, Chen X, Tian J-H, Chen L-J, Li K, et al. The evolutionary history of vertebrate RNA viruses. Nature. 2018;556:197–202. https://doi.org/10.1038/s41586-018-0012-7
24. Hume AJ, Mühlberger E. Distinct genome replication and transcription strategies within the growing filovirus family. J Mol Biol. 2019;431:4290–320. https://doi.org/10.1016/j.jmb.2019.06.029
25. Barr JN, Weber F, Schmaljohn CS. *Bunyavirales*: the viruses and their replication. In: Howley PM, Knipe DM,

Whelan SPJ, editors. Fields virology. 7th ed. Philadelphia: Wolters Kluwer/Lippincott Williams & Wilkins; 2020. p. 706–49.
26. Lauber C, Gorbalenya AE. Partitioning the genetic diversity of a virus family: approach and evaluation through a case study of picornaviruses. J Virol. 2012;86:3890–904. https://doi.org/10.1128/JVI.07173-11
27. International Committee on Taxonomy of Viruses [cited 2021 Jul 10]. https://talk.ictvonline.org/taxonomy
28. Walker PJ, Siddell SG, Lefkowitz EJ, Mushegian AR, Adriaenssens EM, Alfenas-Zerbini P, et al. Changes to virus taxonomy and to the International Code of Virus Classification and Nomenclature ratified by the International Committee on Taxonomy of Viruses (2021). Arch Virol. 2021;166:2633–48. https://doi.org/10.1007/s00705-021-05156-1
29. Kibenge FSB, Godoy MG, editors. Aquaculture virology. Amsterdam: Elsevier; 2016. p. 568.
30. Geoghegan JL, Di Giallonardo F, Cousins K, Shi M, Williamson JE, Holmes EC. Hidden diversity and evolution of viruses in market fish. Virus Evol. 2018;4:vey031. https://doi.org/10.1093/ve/vey031
31. Geoghegan JL, Di Giallonardo F, Wille M, Ortiz-Baez AS, Costa VA, Ghaly T, et al. Virome composition in marine fish revealed by meta-transcriptomics. Virus Evol. 2021;7:veab005.
32. Kuhn JH, Adkins S, Alioto D, Alkhovsky SV, Amarasinghe GK, Anthony SJ, et al. 2021 taxonomic update for phylum *Negarnaviricota* (*Riboviria: Orthornavirae*), including the large orders *Bunyavirales* and *Mononegavirales*. Arch Virol. 2021 Aug 31 [Epub ahead of print]. https://doi.org/10.1007/s00705-021-05143-6
33. Kurath G, Stone D. Fish rhabdoviruses (*Rhabdoviridae*). In: Bamford D, Zuckerman M, editors. Encyclopedia of Virology. 4th ed. Amsterdam: Elsevier; 2021. p. 324–31.
34. LaPatra S, Misk E, al-Hussinee L, Lumsden JS. Rhabdoviruses of fish. In: Kibenge FSB, Godoy MG, editors. Aquaculture virology. Amsterdam: Elsevier; 2016. p. 276–97.
35. Kuhn JH, Amarasinghe GK, Perry DL. *Filoviridae*. In: Howley PM, Knipe DM, Whelan SPJ, editors. Fields virology. 7th ed. Philadelphia: Wolters Kluwer/Lippincott Williams & Wilkins; 2020. p. 449–503.
36. Kuhn JH, Charrel RN. Arthropod-borne and rodent-borne virus infections. In: Jameson JL, Fauci AS, Kasper DL, Hauser SL, Longo DL, Loscalzo J, editors. Harrison's principles of internal medicine. 20th ed. Columbus (OH): McGraw-Hill Education; 2018. p. 1489–509.

Address for correspondence: Torsten Seuberlich, Divison of Neurological Sciences, Vetsuisse Faculty, University of Bern, Bremgartenstrasse 109a, CH-3012 Bern, Switzerland; email: torsten.seuberlich@vetsuisse.unibe.ch

Mammarenaviruses of Rodents, South Africa and Zimbabwe

Antoinette A. Grobbelaar, Jocelyn Jardine,[1] Felicity J. Burt,[2] Alasdair J. Shepherd, Susan P. Shepherd, Patricia A. Leman, Alan Kemp, Lawrence E.O. Braack,[3] Jacqueline Weyer, Janusz T. Paweska, Robert Swanepoel[3]

We conducted a survey for group-specific indirect immunofluorescence antibody to mammarenaviruses by using Lassa fever and Mopeia virus antigens on serum specimens of 5,363 rodents of 33 species collected in South Africa and Zimbabwe during 1964–1994. Rodents were collected for unrelated purposes or for this study and stored at −70°C. We found antibody to be widely distributed in the 2 countries; antibody was detected in serum specimens of 1.2%–31.8% of 14 species of myomorph rodents, whereas 19 mammarenavirus isolates were obtained from serum specimens and viscera of 4 seropositive species. Phylogenetic analysis on the basis of partial nucleoprotein sequences indicates that 14 isolates from *Mastomys natalensis*, the Natal multimammate mouse, were Mopeia virus, whereas Merino Walk virus was characterized as a novel virus in a separate study. The remaining 4 isolates from 3 rodent species potentially constitute novel viruses pending full characterization.

In response to the emergence of Lassa fever, Marburg virus, and Ebola virus in Africa, a Biosafety Level 4 laboratory was constructed at the National Institute for Communicable Diseases (NICD) in Johannesburg, South Africa, and became operational in 1980 (1). To establish which known viral hemorrhagic fevers in Africa occurred in South Africa and neighboring countries, antibody surveys were conducted on selected human, livestock, and wild animal populations. Findings for Crimean-Congo hemorrhagic fever were reported (2,3), but subsequent engagement of the laboratory in the investigation of a series of hemorrhagic fever outbreaks in Africa led to the suspension of survey publication. We present the results of a survey of 5,363 rodents for evidence of infection with mammarenaviruses and details of the isolation of mammarenaviruses from seropositive species. This project was undertaken with approval of the Ethics Committee of the National Institute for Virology, subsequently incorporated into NICD.

Author affiliations: National Institute for Communicable Diseases, Johannesburg, South Africa (A.A. Grobbelaar, J. Jardine, F.J. Burt, A.J. Shepherd, S.P. Shepherd, P.A. Leman, A. Kemp, J. Weyer, J.T. Paweska, R. Swanepoel); South African National Parks Board, Skukuza, South Africa (L.E.O. Braack).

DOI: https://doi.org/10.3201/eid2712.211088

Materials and Methods

Viruses, Antigens, Antiserum, and Antibody Tests

We prepared antigen slides to screen for group-specific antibody activity to mammarenaviruses by indirect immunofluorescence (IF) with Mopeia virus (MOPV) AN20410 and Lassa virus (LASV) Josiah (Table 1) grown in Vero 76 cells as described previously (*4*). The tests were performed with commercially available antimouse immunoglobulin fluorescein conjugate or recombinant protein A/G conjugate (both ThermoFisher Scientific, https://www.thermofisher.com) for nonmyomorph species. Polyclonal control antiserum was prepared by intraperitoneal inoculation of mice with live virus and exsanguination 6 weeks later. We screened serum specimens at dilutions of 1:8 and 1:16, titrated positive samples to endpoint, and confirmed the result by ELISA with MOPV antigen.

Cell lysate antigen for the ELISA was prepared and assays conducted as described previously for Ebola virus (*5*), by using antimouse horseradish peroxidase–conjugated IgG (SeraCare Life Sciences, Inc., https://www.seracare.com). In the absence of control data, we recorded reactions as positive where the net optical density of test serum specimens at 1:100 was ≥2.5 times the mean optical density of a panel of serum specimens from specific pathogen-free laboratory mice. Monoclonal antibodies to LASV and MOPV were obtained from the US Centers for Disease Control and Prevention (CDC; Atlanta, GA,

[1]Current affiliation: EduVos, Midrand, South Africa.

[2]Current affiliation: University of the Free State, Bloemfontein, South Africa.

[3]Current affiliation: University of Pretoria, Pretoria, South Africa..

USA) or prepared at NICD as described elsewhere for Crimean-Congo hemorrhagic fever virus (Table 2) (*6*).

Rodent Samples and Virus Isolation Studies

Most samples were opportunistically derived from material collected for unrelated surveys and stored at NICD. The initial 213 samples were collected at NICD during 1964–1981 for arbovirus surveys, 3,542 samples were collected and submitted by the Department of Health of South Africa during 1971–1988 for plague surveillance in the central part of the country, 831 rodents (with an emphasis on *Mastomys natalensis* mice) were collected in northeastern South Africa during 1984–1994 specifically for the investigation of mammarenaviruses, 764 rodent samples collected in Zimbabwe in 1974 were remnants of a study on Rift Valley fever virus (*7*), and 13 samples were collected in 1982 on a farm in south-central Zimbabwe where there had been a suspected but unconfirmed case of viral hemorrhagic fever in a patient admitted to a hospital in South Africa. Live-trapped rodents were euthanized and exsanguinated; serum samples and visceral organ (lung, heart, liver, spleen, and kidney) samples were conveyed to NICD with ice packs and stored at −70°C. Coordinates of sample collection sites were recorded as quarter-degree grid cells.

We confirmed identities of rodent species yielding virus isolates by determining partial cytochrome b gene sequences for 8 selected samples (*8*). Skull and skin preparations of rodents from plague surveillance were deposited in the Ditsong National Museum of Natural History (Pretoria, South Africa), and selected materials from other surveys were preserved at NICD.

We attempted isolation of mammarenaviruses for rodent species at locations where antibody was found. We inoculated serum and 10% clarified suspensions of pooled viscera onto Vero 76 monolayer cultures in replicate Lab-Tek 8-chamber slides (ThermoFisher Scientific) and examined after incubation for 7–10 days at 37°C by IF with pooled mouse antiserum to MOPV and LASV. We passed samples 3 times before recording them as negative. The 5 original isolates of MOPV from *M. natalensis* rodents from Mozambique were taken to CDC in 1977 (*9*); we used duplicate organ samples stored at NICD to reisolate the viruses. We screened antigen cell spots prepared from cultures infected with selected known mammarenaviruses plus isolates from this study by IF against mammarenavirus monoclonal antibodies at doubling dilutions from 1:100. We tested all isolates for intracerebral pathogenicity for 1-day-old mice by inoculation of 2 litters (8 infant mice/litter) for each virus.

Molecular Characterization and Phylogenetic Analysis of Mammarenavirus Isolates

We performed phylogenetic analysis on 48 isolates by using an ≈912-nt (299–304-aa) fragment of the nucleocapsid protein (NP) gene, consisting of 15 isolates from this study, 5 MOPV isolates from Mozambique (*9*) that were reisolated during this study, 3 mammarenaviruses received from other laboratories—namely, LASV 331 and MOPV isolates SPB801478 and SPB801480 from Zimbabwe (*10*)—and 25 viruses for which nucleotide sequences were retrieved from GenBank, including 3 New World arenaviruses as outgroup taxa (Table 1, https://wwwnc.cdc.gov/EID/article/27/12/21-1088-T1.htm). We omitted from analysis 4 isolates from this study with identical sequences to Mopeia virus isolate SPU84/491/40 (Table 1). We excluded potential related viruses for which inadequate information was available, such as Kodoko virus from Guinea (*11*) and Lemniscomys virus from Tanzania (*12*).

Table 2. Pairwise comparison of partial nucleocapsid protein amino acid sequence (299–304 aa) percentage difference between 5 selected southern Africa Old World mammarenavirus isolates from current study and closest relatives, South Africa and Zimbabwe*

Isolate name	MOPV AN20616	IPPYV DakAnB188	LASV Josiah	MOBV 3080	LCMV WE	LUJO ZAM	LUNK NKS1	LUNA NMW1	MRTV NR27	OKAV NR73	BITU ANG0070	SPU 86/415/2	SPU 86/415/4	SPU 86/485	SPU 84/491/406	SPU 85/353
SPU 86/415/2	30	29	29.6	31.3	37.7	43.4	34.7	30	33	15.5	14.2	0	3.7	15.2	32	19.9
SPU 86/415/4	30	28.3	29	31.3	37	43.3	34.3	29.6	32	15.2	14.2	3.7	0	14.8	31.3	19.2
SPU 86/485	27.6	27.6	29.6	29.3	33	39.4	31	28.3	29.3	8.4	9.3	15.2	15	0	29.3	20.5
SPU 84/491/106	24	22	25	25	34	44	35	26	13	30	35.3	32	31.3	29.3	0	27.3
SPU 85/353	26.6	27.6	28.3	29.6	33	42.8	32	28.3	28.3	20.9	19.4	19.9	19.2	20.5	27.3	0

*BITU, Bitu virus; IPPYV, Ippy virus; LASV, Lassa virus; LCMV, lymphocytic choriomeningitis virus; LUJO, Lujo virus; LUNA, Luna virus; LUNK, Lunk virus; MRTV, Mariental virus; MOBV, Mobala virus; MOPV, Mopeia virus; OKAV, Okahandja virus.

Table 3. Summary of rodent samples, serologic test results, and virus isolation studies in study of mammarenaviruses, South Africa and Zimbabwe*

Rodent species scientific name	Rodent species common name	Mammarenavirus IF antibody tests			Mammarenavirus isolation attempts			
		Tested	No. (%) positive	Titer range (GMT)	Serum samples	Organs	Total	Isolations
Aethomys chrysophilus	Red veld rat	135	10 (7.4)	8–4,096 (207.8)	23	75	77	1
A. ineptus	Tete veld rat	103	0		0	0	0	0
Dasymys incomtus	Water rat	2	0		0	1	1	0
Dendromus melanotis	Grey climbing mouse	1	0		0	1	1	0
Desmodillus auricularis	Short-tailed gerbil	69	0		0	3	3	0
Gerbilliscus afra	Cape gerbil	26	0		6	10	13	0
G. brantsii	Highveld gerbil	529	4 (0.8)	8–256 (26.9)	0	14	14	0
G. leucogaster	Bushveld gerbil	378	14 (3.7)	8–1,024 (57.9)	8	42	42	0
G. paeba	Hairy-footed gerbil	8	0		2	1	2	0
Lemniscomys rosalia	Single-striped mouse	21	0		2	8	8	0
Mastomys coucha	Cape multimammate mouse	664	11 (1.7)	8–512 (56.4)	14	63	73	0
M. natalensis	Natal multimammate mouse	1165	370 (31.8)	8–16,384 (219.5)	151	307	380	14
Micaelamys namaquensis	Namaqua rock mouse	273	20 (7.3)	8–2,048 (132.4)	44	85	101	1
Mus minutoides	Pygmy mouse	16	0		0	28	28	0
M. musculus	House mouse	25	0		0	23	23	0
Mystromys albicaudatus	White-tailed mouse	11	0		0	1	1	0
Otomys angoniensis	Angoni vlei rat	30	1 (3.3)	16	0	3	3	0
O. irroratus	Vlei rat	266	67 (25.2)	8–8,192 (127.9)	315	59	346	0†
O. unisulcatus	Bush vlei rat	178	28(21.3)	8–2,048 (99.1)	17	19	28	3
Parotomys brantsii	Brant's whistling rat	10	1 (10.0)	256	0	0	0	0
P. littledalei	Littledale's whistling rat	3	0	0	0	0	0	0
Rattus norvegicus	Brown rat	125	6 (4.8)	8–8,192 (644.6)	8	47	48	0
R. rattus	House rat	211	1 (0.5)	512	6	38	38	0
Rhabdomys pumilio s.l.	Four-striped mouse	933	11 (1.2)	8–64 (19.3)	73	59	118	0
Saccostomus campestris	Pouched mouse	82	6 (7.3)	8–1,024 (25.4)	11	24	28	0
Steatomys pratensis	Fat mouse	3	0		0	2	2	0
Thallomys paedulcus	Tree mouse	31	0		11	27	27	0
Zelotomys woosnami	Woosnam's desert rat	1	0		0	0	0	0
Cryptomys hottentotus	Common mole rat	6	0					
Graphiurus murinus	Woodland doormouse	8	0					
Paraxerus cepapi	Tree squirrel	6	0					
Xerus inauris	Ground squirrel	36	0					
Pedetes capensis	Springhare	8	0					
Totals		5,363	560		691	940	1,405	19

*IF, immunofluorescence.
†Organ pool from 1 *O. irroratus* rat was positive in mammarenavirus IF on first pass in culture but the potential isolate was lost on subculture.

We extracted total RNA from cultures by using the High Pure RNA isolation kit (Roche Diagnostics, https://www.roche.com) and performed reverse transcription PCR with primers 19C (5′-CGCACAGTGGATCCTAGGC-3′) (*13*) and OWA_2 (5′-TTCTTCATAAGGGTTCCTTTCACC-3′) (J.C.S. Clegg, Centre for Applied Microbiology and Research, pers. comm., 1991) by using the Titan One Tube reverse transcription PCR kit (Roche) to amplify an ≈1,000-bp fragment of the NP gene. The 19C primer is complementary to a conserved sequence at the 3′ terminus of the S RNA segment and the OWA_2 primer corresponds to nucleotide positions 2402–2424 relative to LASV 391 (GenBank accession no. X52400). We designed a degenerate reverse primer, Arena A (5′-ATRTARGGCCAWCCSTCTCC-3′), corresponding to nucleotide positions 2357–2376 relative to LASV 391 and 2401–2420 relative to MOPV AN20410 (GenBank accession no. NC006575), to amplify the region of interest for isolates SPU94/88/235 and SPU86/485. Cycling conditions were 50°C for 30 min, 94°C for 2 min, 30 cycles of 94°C for 30 s, 47°C for 30 s, and 68°C for 90 s, plus extension at 68°C for 7 min. We purified PCR products with the Wizard SV Gel and PCR clean-up kit (Promega Corporation, https://www.promega.com), sequenced with the BigDye Terminator v3.1 Cycle Sequencing Kit (ThermoFisher Scientific), purified on Centrisep columns (Princeton Separations Inc., https://www.prinsep.com), and ran testing on an ABI Prism 377 DNA Sequencing Unit. We aligned nucleotide and predicted amino acid

sequences using ClustalW (http://www.clustal.org/clustal2) incorporated inMEGA7 (https://www.megasoftware.net), performed phylogenetic analysis by the neighbor-joining method with 1,000 bootstrap iterations, and calculated sequence diversities (p-distances) (*14*).

Results

We tested a total of 5,363 rodents of 33 species from collection sites throughout South Africa and Zimbabwe for antibody to mammarenaviruses (Table 3; Figures 1–4). Antibody was found to be widely distributed in the 2 countries (Figures 1–4) and was detected in serum samples of 1.2%–31.8% of 14 species of myomorph rodents; 19 mammarenavirus isolates were obtained from serum and viscera of 4 seropositive species (Table 3).

Identities of the 4 myomorph species that yielded mammarenavirus isolates—*M. natalensis* mice and *Aethomys chrysophilus*, *Micaelamys namaquensis*, and *Otomys unisulcatus* rats—were confirmed from partial cytochrome b gene sequences (*8*) (GenBank accession nos. MK531528–35). However, the genus *Micaelamys* has subsequently proved to be polyphyletic and due for revision (*16*), whereas there is debate about inclusion of *O. unisulcatus* in the genus *Myotomys* (*17*). Furthermore, *O. unisulcatus* tissue remained available only for the Omdraaivlei isolates and not for the Merino Walk isolate. Most of the other myomorph rodents were identified from morphologic features and distribution patterns (*18*), but new species and subspecies with partially overlapping distributions have since been recognized in the genus *Rhabdomys* (*19*–*21*). No organs remained available, and serum specimens failed to yield DNA for phylogenetic studies; thus, the samples are recorded as *R. pumilio* sensu lato (Table 3).

No mammarenavirus antibody or virus was found in 14 of the myomorph rodent species (Table 3), and although these rodents were relatively poorly represented in the collection, they tend to be rare

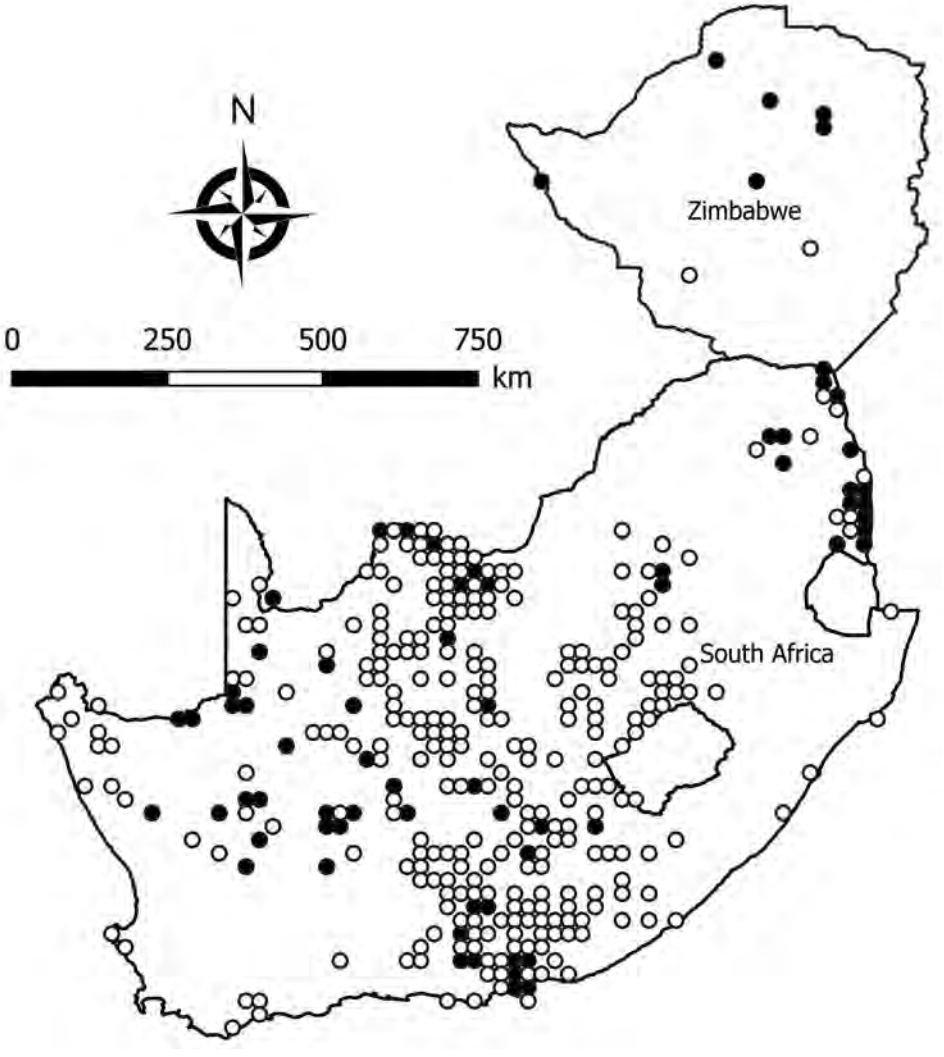

Figure 1. Locations where samples from 5,363 rodents of 33 species were collected and tested for evidence of infection with mammarenaviruses, South Africa and Zimbabwe. White circles indicate sites where no evidence of infection was found; black circles indicate sites where antibody to mammarenaviruses was detected by indirect immunofluorescence.

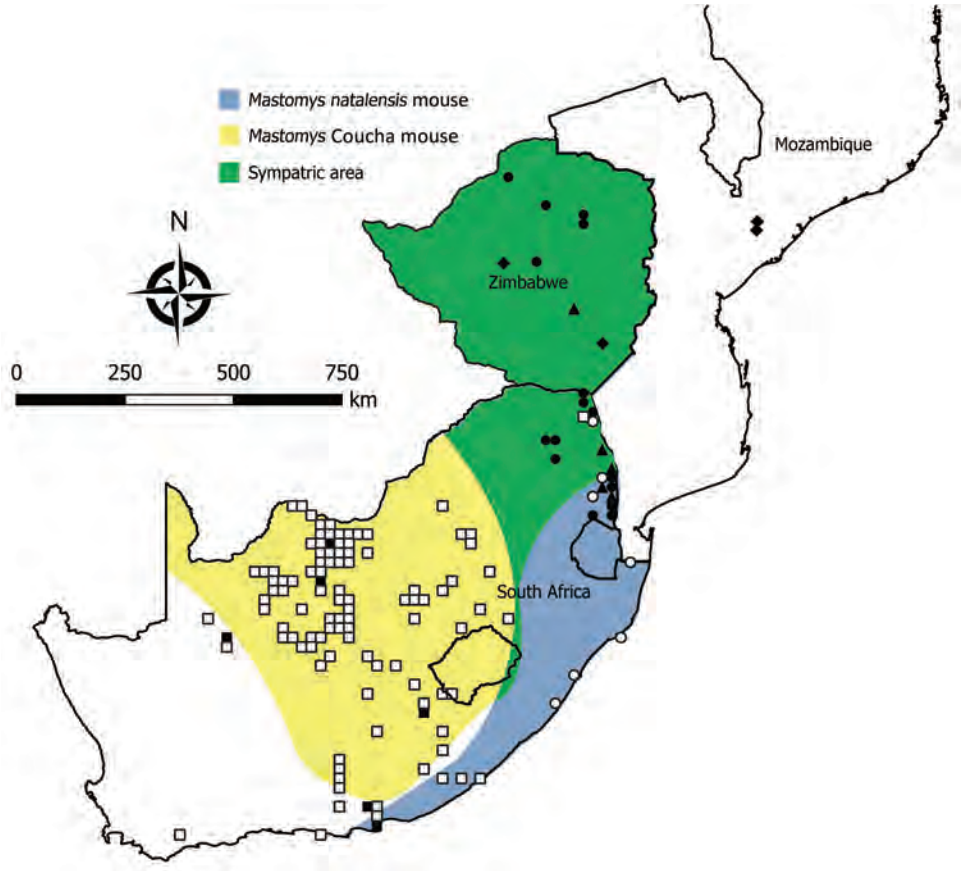

Figure 2. Locations where samples were collected from *Mastomys* spp. rodents, South Africa and Zimbabwe. White squares indicate sites where no antibody to mammarenaviruses was found in *M. coucha* mouse serum specimens; black squares,where antibody was detected in *M. coucha* mouse serum specimens; white circles, where no antibody to mammarenaviruses was found in *M. natalensis* mouse serum specimens; black circles, where antibody was detected in *M. natalensis* mouse serum specimens; black triangles, where Mopeia virus was isolated from *M. natalensis* mouse samples during this study; black diamonds, where Mopeia virus was isolated from *M. natalensis* mouse samples during previous studies, including the original isolations in Mozambique (*9*,*10*).

species or occur in specialized habitats, such as deserts. A further 9 species of rodents—*M. coucha*, *O. angoniensis*, *Parotomys brantsii*, *Rattus norvegicus*, *R. rattus*, *R. pumilio* s.l., *Saccostomus campestris*, *Gerbilliscus brantsii*, and *G. leucogaster*—had low prevalence (0.5%–7.3%) of IF antibody to mammarenaviruses; no clear tendency to cluster was noted, except that the reactions were detected in locations where antibody was prevalent in other species. Although IF titers were generally low in these species (geometric mean titers [GMT] 19.3–57.9), the few ≥16 tended to be supported by ELISA reactions, but samples cultured yielded no virus. Anomalous high IF titers of 8,192 supported by ELISA reactions were recorded in 2 serum samples from *R. norvegicus* rats collected from a location where antibody prevalence of 29.1% was recorded in serum specimens from *O. irroratus* rats, but no isolates were obtained.

The remaining 5 species of myomorph rodents—*A. chrysophilus*, *M. namaquensis*, *M. natalensis*, *O. unisulcatus*, and *O. irroratus*—had mammarenavirus IF antibody prevalence of 4.2%–31.8%; positive reactions tended to cluster and reached 30%–50% prevalence at some trapping sites. The IF titers ranged from 8–16,384 (GMT 99.1–219.5), and titers ≥16 were supported by positive ELISA reactions. A total of 19 mammarenavirus isolates were obtained from 4 of these species (Table 3), but a single sample of *O. irroratus* rat produced an IF reaction on first pass in cell cultures that was lost during subculture and could not be repeated in further attempts to isolate virus. In addition, attempts to reisolate MOPV from 5 sets of *M. natalensis* organs from Mozambique (*9*) held in storage at NICD were successful (Table 1). All isolates were pathogenic for day-old mice inoculated intracerebrally.

A total of 6 isolates from this study plus 1 reisolated MOVP from Mozambique demonstrated 4 patterns of reactivity in IF screening tests with monoclonal antibodies and selected mammarenavirus isolates (Table 2). Deduced NP amino acid distances between selected isolates and closest relatives were calculated (Table 4). We determined the phylogenetic relationships of 48 mammarenavirus isolates, including 15/19 isolates from this study and the 5 reisolated MOPV isolates from Mozambique (Table 1), on the basis of neighbor-joining analysis of partial NP sequences (≈912 nt), together with host relationships (Figure 5).

The *M. natalensis* isolates from Mozambique and from this study grouped with 2 earlier isolates from Zimbabwe as Mopeia virus, whereas 5 isolates from this study fell into 4 groups; isolate Bobomene from South Africa grouped with more recent isolates Mariental from Namibia and isolate Witsand from South Africa grouped with Okahandja from Namibia and with isolate Bitu from Angola (Figure 5). We determined phylogenetic relationships on the basis of neighbor-joining analysis of a 136 bp cytochrome b barcode sequence for 8 selected rodents from which mammarenavirus isolates were obtained in this study and reference taxonomic voucher sequences from GenBank (Figure 6).

Discussion

The main impetus for this rodent survey came from the isolation of the mammarenavirus MOPV at NICD from *M. natalensis* rodents collected in a village in Mozambique during an arbovirus study in 1972; within months, the same rodent species was identified as the host of LASV in West Africa (*9*,*22*,*23*). As a consequence, work ceased on Mopeia virus at NICD and the isolates were transferred to CDC, where the relationship to LASV was confirmed (*9*). Although MOPV proved to be nonpathogenic for nonhuman primates (*24*), investigating the possible occurrence and role of mammarenaviruses as causes of human infection in South Africa was considered necessary.

Our survey detected widespread presence of antibody activity to mammarenaviruses in myomorph rodent serum specimens within the study area. Because *M. natalensis* mice have an eastern distribution in South Africa (*18*), rodents were trapped along the northeastern border and MOPV was successfully isolated. However, a mammarenavirus isolated from another rodent species, *A. chrysophilus*, within the

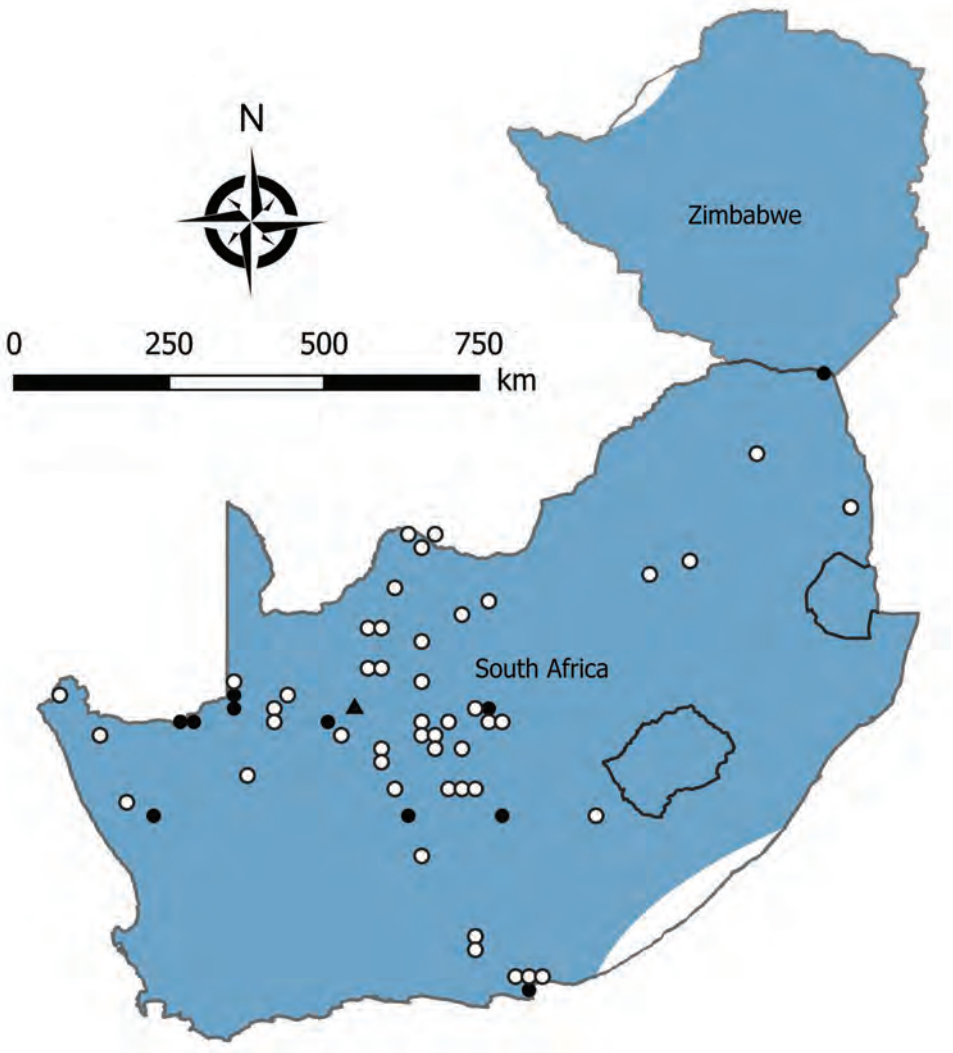

Figure 3. Locations where samples were collected from *Micaelamys namaquensis* rodents, South Africa and Zimbabwe. White circles indicate sites where no antibody to mammarenaviruses was found in *M. namaquensis* rat serum specimens; black circles, where antibody was detected in *M. namaquensis* rat serum specimens; black triangle, where a mammarenavirus isolate was obtained from an *M. namaquensis* rat sample.

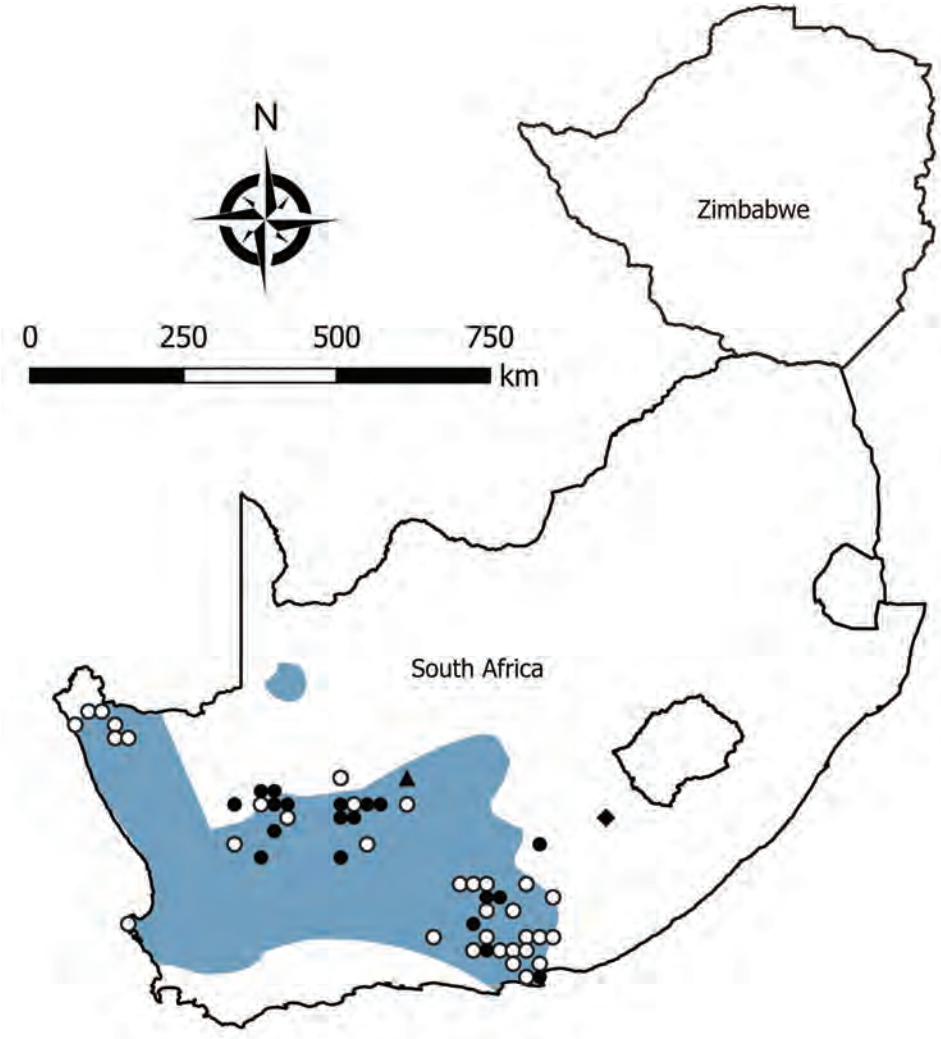

Figure 4. Locations where samples were collected from *Otomys unisulcatus* rodents, South Africa and Zimbabwe. White circles indicate sites where no antibody to mammarenaviruses was found in *O. unisulcatus* rat serum specimens; black circles, where antibody was detected in *O. unisulcatus* rat serum specimens; black triangle, where Omdraaivlei mammarenavirus isolates were obtained from *O. unisulcatus* rat samples; black diamond, where Merino Walk virus was isolated from *O. unisulcatus* rat. Shading indicates distribution range of *O. unisulcatus* rats. Adapted from Chimimba and Bennett (*15*).

distribution range of *M. natalensis* mice was found to be distinct from MOPV; 4 isolates obtained from 2 other rodent species further to the west also differed from MOPV (Tables 1–4; Figure 5).

Unpublished serosurveys conducted on humans in South Africa during 1984–1988 in parallel with the rodent survey included a study of 7,665 long-term (≥5 years) healthcare workers from 66 secondary

Table 4. Reactivity of selected mammarenavirus isolate-infected cell antigens in indirect immunofluorescence tests with monoclonal antibodies to Lassa fever and Mopeia viruses, South Africa and Zimbabwe*

	Monoclonal antibody titer†						
Virus antigen	CDC 5254–6 Lassa N	CDC 5293–4 Lassa N	CDC 5273–8 Lassa N	CDC 5285–6 Lassa G	CDC 5329–1 Mopeia N	NICD 4E9 Mopeia N	NICD 3G9 Mopeia N
LCM Armstrong	≥12,800	–	–	1,600	–	–	–
Lassa Josiah	≥12,800	≥12,800	≥12,800	3,200	–	≥12,800	–
Ippy DakAnB 188d	≥12,800	–	–	3,200	3,200	≥12,800	–
Mobala A11/3076	≥12,800	–	–	6,400	–	≥12,800	–
Mopeia AN 20410	≥12,800	≥12,800	–	400	≥12,800	≥12,800	≥12,800
Mopeia SPU82/30/1	≥12,800	≥12,800	400	800	≥12,800	≥12,800	≥12,800
Mopeia SPU84/491/73	≥12,800	≥12,800	400	200	≥12,800	≥12,800	≥12,800
Bobomene SPU84/491/106	≥12,800	≥12,800	–	1,600	≥12,800	≥12,800	≥12,800
Witsand SPU86/485	≥12,800	≥12,800	≥12,800	–	≥12,800	≥12,800	–
Omdraaivlei SPU86/415/2	≥12,800	≥12,800	≥12,800	–	≥12,800	≥12,800	–
Merino Walk SPU85/353	≥12,800	–	–	–	≥12,800	–	–

*G, antiglycoprotein; N, antinucleoprotein; –, none.
†Antibody titers shown as reciprocals of serum dilution.

hospitals that receive patient referrals from district hospitals who were tested for evidence of nosocomial infection, plus a study of 2,041 long-term (≥5 years) rural residents and workers in the livestock and wildlife industries who were investigated for evidence of exposure to zoonotic viruses (R. Swanepoel, unpub. data). An overall prevalence of 1.0% (93/9,704) of IF antibody to MOPV antigen was recorded at titers of 8–2,048, gmt 33.0; higher prevalences of 10%–15% occurred in a few widely separated locations near the eastern border, but no histories of disease considered indicative of mammarenavirus infection were obtained. To the west, in Free State, Northern Cape, North West, and Gauteng Provinces, no antibody to mammarenaviruses was detected in rural residents and workers in the livestock industry despite the isolation of mammarenaviruses from rodents. Aliquots of human serum samples collected during the original investigations in Mopeia village, Mozambique, in 1972 remained available at NICD, and IF antibody to

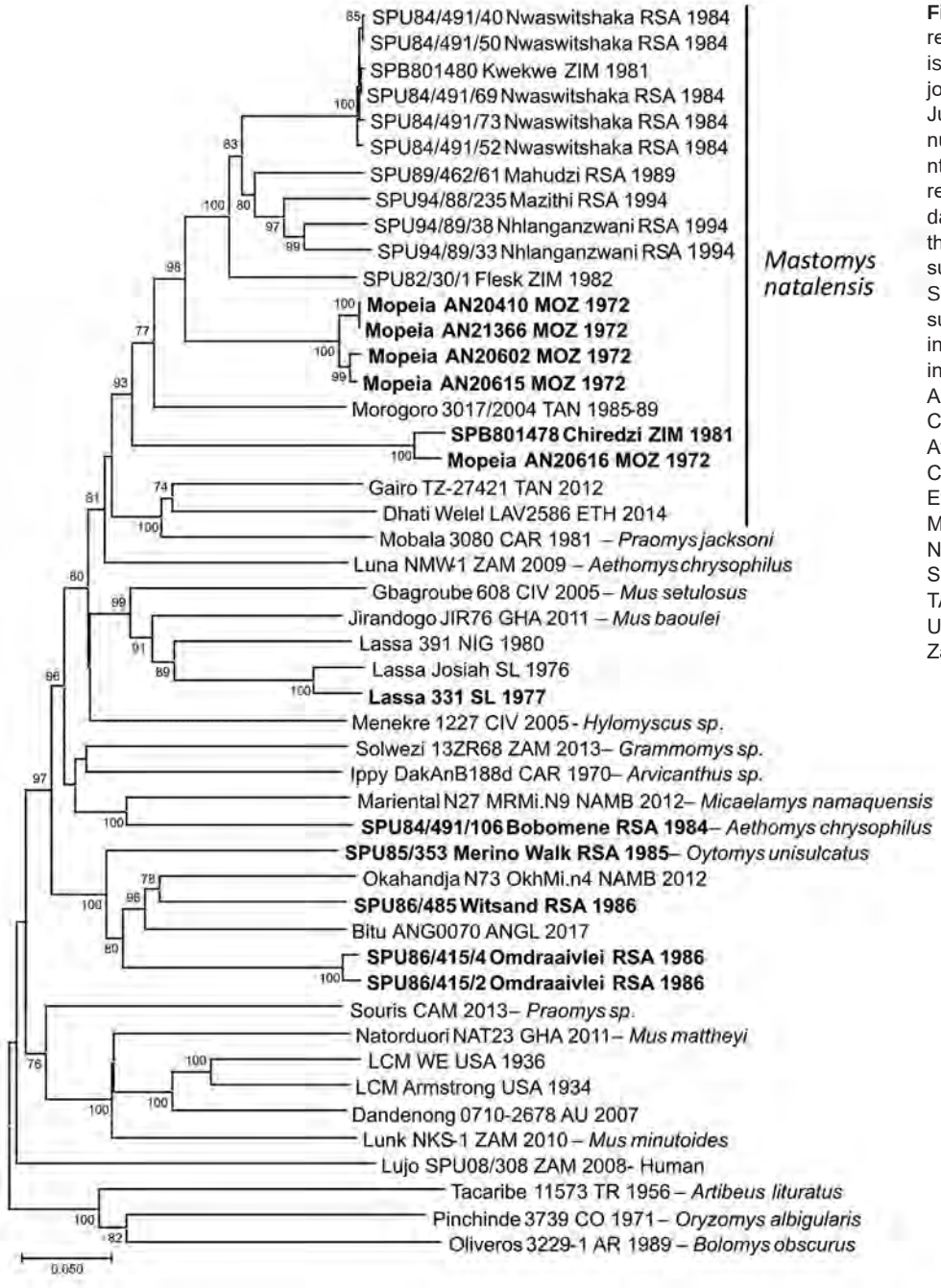

Figure 5. Phylogenetic relationships of 48 arenavirus isolates based on neighbor-joining analysis applying a Jukes-Cantor model of partial nucleoprotein sequences (≈912 nt), together with known host relationships and collection dates. Values at nodes indicate the level (%) of bootstrap support from 1,000 replicates. Scale bar indicates base substitutions per site. Bold indicates sequences determined in this study. ANGL, Angola; AR, Argentina; AU, Australia; CAM, Cameroon; CAR, Central Africa Republic; CO, Colombia; CIV, Côte d'Ivoire; ETH, Ethiopia; GHA, Ghana; MOZ, Mozambique; NAMB, Namibia; NIG, Nigeria; RSA, Republic of South Africa; SL, Sierra Leone; TAN, Tanzania; TR, Trinidad; USA, United States; ZAM, Zambia; ZIM, Zimbabwe.

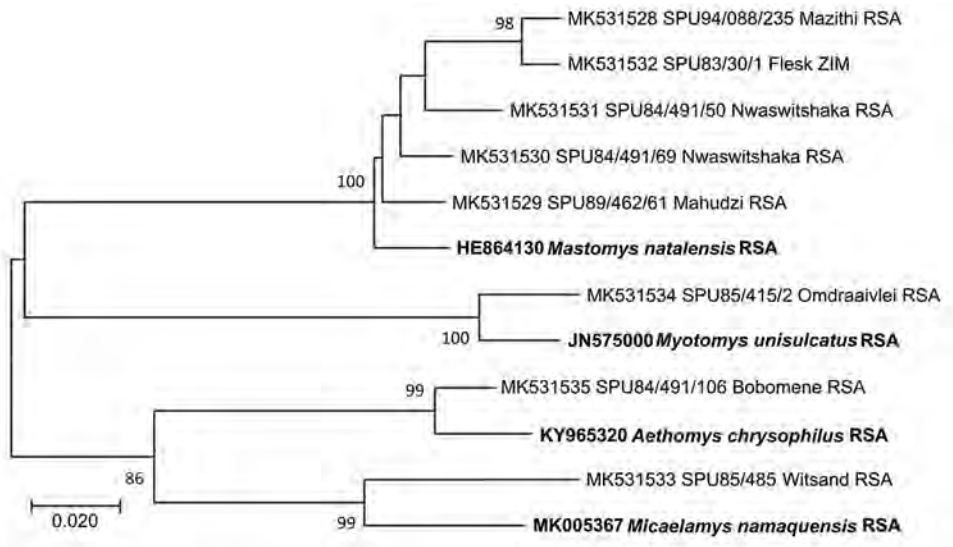

Figure 6. Phylogenetic relationships of 8 rodents from which mammarenavirus isolates were obtained in this study (bold) and reference taxonomic voucher sequences from GenBank. Tree was constructed based on neighbor-joining analysis of a 136-bp cytochrome b barcode sequence. Values at nodes indicate the level of bootstrap support from 1,000 replicates. Scale bar indicates base substitutions per site. GenBank accession numbers, rodent reference number, and country of collection are indicated. RSA, Republic of South Africa; ZIM, Zimbabwe.

MOPV antigen was detected at a prevalence of 16.1% (32/199) with titers ranging from 8 to 8,192, gmt 229.6, similar to the findings initially recorded when no disease associations were identified (R. Swanepoel, unpub. data).

In further checks on the possible occurrence of mammarenavirus-associated disease, 379 patients experiencing febrile illness in 4 district hospitals along the northeastern coast of KwaZulu-Natal Province, South Africa, were monitored for evidence of MOPV infection or seroconversion in 1985 without positive result. No antibody was detected in 100 chronic renal failure patients on dialysis in Gauteng Province, South Africa, in 1993 (R. Swanepoel, unpub. data).

Among routine diagnostic samples submitted to NICD, resting IF titers of 128 and 256 of IgG to MOPV antigen were detected in 2 patients from South Africa, but no etiologic significance could be attached to these findings. A single case of fatal LASV infection was diagnosed in a patient from Nigeria who was evacuated to a hospital in South Africa in 2007 (R. Swanepoel, unpub. data). The only other human arenavirus infections diagnosed within South Africa were in 2 patients referred successively from Zambia in 2008 who were infected with the novel Lujo virus and 3 local healthcare workers who acquired nosocomial infection from those patients (*25*). At the time of the Lujo virus outbreak, involvement of any of the mammarenaviruses isolated from rodents during the current study was ruled out; in the process, the Merino Walk isolate was characterized as a novel mammarenavirus (*26*).

The widely distributed *M. natalensis* mouse of sub-Saharan Africa consists of 6 matrilineages that fall into 2 clades, AI-III and BIV-VI, on the basis of the mitochondrial cytochrome b marker (*27*,*28*). Each lineage is associated with ≥1 mammarenavirus, ranging from LASV in lineage AI in West Africa to MOPV and Luna virus in lineage BVI in southern Africa (*28*,*29*). Our findings confirm the association of MOPV with *M. natalensis* mice in southern Africa, where this rodent is sympatric with *M. coucha* mice in northeastern South Africa and in Zimbabwe. However, the distribution of *M. coucha* mice extends westwards into the drier interior of South Africa; the low prevalence of MOPV antibody found in this species could represent spillover of infection from other rodents, rather than the harboring of a mammarenavirus (Table 3). Whereas *M. natalensis* mice in the mesic east are peridomestic, indigenous rodents tend to be sylvatic and less closely associated with human dwellings in the xeric west, where no evidence of infection was detected in humans.

The isolates from this study are provisionally named for their locations of origin (Table 1; Figure 5), but the isolates obtained from *M. natalensis* mice represent exemplar isolates of MOPV, and Merino Walk virus is clearly distinct. Although the apparent sharing of rodent hosts mitigates against species recognition within the mammarenaviruses (*30*), clarifying the interrelationships between the Bobomene, Witsand, and Omdraaivlei isolates and their relationship to the Mariental and Okahandja viruses from Namibia (*31*) and Bati virus from Angola (*32*) anticipates complete genomic characterization of the isolates.

The phylogenetic relationships between 8 rodents from which mammarenaviruses were isolated in this study and reference taxonomic voucher sequences from

GenBank are compatible with the concept of cospeciation of arenaviruses and their rodent hosts (Figure 6), except that the interrelationships between Witsand, Okahandja, and Bitu isolates await clarification as previously noted. Moreover, the unavailability of rodent host tissue for Merino Walk virus precluded comparison with ostensibly the same host species, the *O. unisulcatus* rat, of the Omdraaivlei isolates. However, *O. unisulcatus* rats reportedly comprise a coastal lowland group that is located where the host of Merino Walk virus was collected and a central interior group that covers the area where the hosts of the Omdraaivlei isolates were obtained, although the low sequence divergences did not warrant recognition of subspecies (*33*). The observations on rodents from Zimbabwe were limited, and the single isolation of Mopeia virus obtained from *M. natalensis* mice from a farm near Masvingo was not related to the nonfatal illness of a former farm resident who was hospitalized in South Africa.

Further research on mammarenaviruses in rodents in South Africa should include attempts to isolate virus from *O. irroratus* rats and possibly *Lemniscomys rosalia* mice, which were underrepresented in this survey; the presence of Luna-related and Lunk-related viruses that were identified in Zambia in *M. natalensis* and *M. minutoides* rodents should also be investigated (*34*). Furthermore, the reservoir host and distribution range of Lujo virus in southern Africa have not been determined. A greater knowledge of the occurrence and diversity of mammarenaviruses in Africa is foundational to understanding the possible health risks associated with these viruses and preparedness for the emergence of such viruses in the future.

Acknowledgments

We thank Anthony Craig for preparing the maps used in this manuscript.

About the Author

Ms. Grobbelaar is a medical scientist at the National Institute for Communicable Diseases in Johannesburg. Her interests include the laboratory diagnosis and research (in particular molecular epidemiology) of zoonotic viral pathogens.

References

1. Swanepoel R. Viral haemorrhagic fevers in South Africa: history and national strategy. S Afr J Sci. 1987;83:80–8.
2. Swanepoel R, Shepherd AJ, Leman PA, Shepherd SP, McGillivray GM, Erasmus MJ, et al. Epidemiologic and clinical features of Crimean-Congo hemorrhagic fever in southern Africa. Am J Trop Med Hyg. 1987;36:120–32. https://doi.org/10.4269/ajtmh.1987.36.120
3. Shepherd AJ, Swanepoel R, Shepherd SP, McGillivray GM, Searle LA. Antibody to Crimean-Congo hemorrhagic fever virus in wild mammals from southern Africa. Am J Trop Med Hyg. 1987;36:133–42. https://doi.org/10.4269/ajtmh.1987.36.133
4. Johnson KM, Elliott LH, Heymann DL. Preparation of polyvalent viral immunofluorescent intracellular antigens and use in human serosurveys. J Clin Microbiol. 1981; 14:527–9. https://doi.org/10.1128/jcm.14.5.527-529.1981
5. Ksiazek TG, West CP, Rollin PE, Jahrling PB, Peters CJ. ELISA for the detection of antibodies to Ebola viruses. J Infect Dis. 1999;179(Suppl 1):S192–8. https://doi.org/10.1086/514313
6. Blackburn NK, Besselaar TG, Shepherd AJ, Swanepoel R. Preparation and use of monoclonal antibodies for identifying Crimean-Congo hemorrhagic fever virus. Am J Trop Med Hyg. 1987;37:392–7. https://doi.org/10.4269/ajtmh.1987.37.392
7. Swanepoel R, Blackburn NK, Efstratiou S, Condy JB. Studies on Rift Valley fever in some African murids (Rodentia: Muridae). J Hyg (Lond). 1978;80:183–96. https://doi.org/10.1017/S0022172400053535
8. Galan M, Pagès M, Cosson J-F. Next-generation sequencing for rodent barcoding: species identification from fresh, degraded and environmental samples. PLoS One. 2012;7:e48374. https://doi.org/10.1371/journal.pone.0048374
9. Wulff H, McIntosh BM, Hamner DB, Johnson KM. Isolation of an arenavirus closely related to Lassa virus from Mastomys natalensis in south-east Africa. Bull World Health Organ. 1977;55:441–4.
10. Johnson KM, Taylor P, Elliott LH, Tomori O. Recovery of a Lassa-related arenavirus in Zimbabwe. Am J Trop Med Hyg. 1981;30:1291–3. https://doi.org/10.4269/ajtmh.1981.30.1291
11. Lecompte E, ter Meulen J, Emonet S, Daffis S, Charrel RN. Genetic identification of Kodoko virus, a novel arenavirus of the African pigmy mouse (Mus Nannomys minutoides) in West Africa. Virology. 2007;364:178–83. https://doi.org/10.1016/j.virol.2007.02.008
12. de Bellocq JG, Borremans B, Katakweba A, Makundi R, Baird SJ, Becker-Ziaja B, et al. Sympatric occurrence of 3 arenaviruses, Tanzania. Emerg Infect Dis. 2010;16:692–5. https://doi.org/10.3201/eid1604.091721
13. Bowen MD, Peters CJ, Nichol ST. The phylogeny of New World (Tacaribe complex) arenaviruses. Virology. 1996;219:285–90. https://doi.org/10.1006/viro.1996.0248
14. Kumar S, Stecher G, Tamura K. MEGA7: Molecular Evolutionary Genetics Analysis version 7.0 for bigger datasets. Mol Biol Evol. 2016;33:1870–4. https://doi.org/10.1093/molbev/msw054
15. Chimimba CT, Bennett NC. 2005. Order Rodentia. In: Skinner JD and Chimimba CT, editors. The mammals of the southern African subregion, 3rd edition. Cape Town: Cambridge University Press; 2005. p. 77–209.
16. Russo IR, Chimimba CT, Bloomer P. Bioregion heterogeneity correlates with extensive mitochondrial DNA diversity in the Namaqua rock mouse, *Micaelamys namaquensis* (Rodentia: Muridae) from southern Africa—evidence for a species complex. BMC Evol Biol. 2010;10:307. https://doi.org/10.1186/1471-2148-10-307
17. Do Linh San E, Babu N, Xalu M, Le Gars S, Perquin J-C, Baxter RM, et al. A conservation assessment of Otomys unisulcatus. In: Child MF, Roxburgh L, Do Linh San E, Raimondo D, Davies-Mostert HT, editors. The red list of mammals of South Africa, Swaziland and Lesotho 2016. Pretoria, South Africa: South African National Biodiversity

Institute and Endangered Wildlife Trust; 2017.
18. Monadjem A, Taylor PJ, Denys C, Cotterill FPD. Rodents of sub-Saharan Africa: a biogeographic and taxonomic synthesis. Berlin: Walter de Gruyter GmbH; 2015.
19. Castiglia R, Solano E, Makundi RH, Hulselmans J, Verheyen E, Colangelo P. Rapid chromosomal evolution in the mesic four-striped grass rat *Rhabdomys dilectus* (Rodentia, Muridae) revealed by mtDNA phylogeographic analysis. J Zool Syst Evol Res. 2011;50:165–72. https://doi.org/10.1111/j.1439-0469.2011.00627.x
20. du Toit N, van Vuuren BJ, Matthee S, Matthee CA. Biome specificity of distinct genetic lineages within the four-striped mouse *Rhabdomys pumilio* (Rodentia: Muridae) from southern Africa with implications for taxonomy. Mol Phylogenet Evol. 2012;65:75–86. https://doi.org/10.1016/j.ympev.2012.05.036
21. Ganem G, Dufour C, Avenant N, Caminade P, Eiseb S, Tougard C, et al. An update on the distribution and diversification of *Rhabdomys sp*. (Muridae, Rodentia). J Vert Biol. 2020;69:1. https://doi.org/10.25225/jvb.20013
22. McIntosh BM, Dickinson DB, Meenehan GM, Dos Santos IS. *Culex (Eumelanomyia) rubinotus* Theobald as vector of Banzi, Germiston and Witwatersrand viruses. II. Infections in sentinel hamsters and wild rodents. J Med Entomol. 1976;12:641–4. https://doi.org/10.1093/jmedent/12.6.641
23. Monath TP, Newhouse VF, Kemp GE, Setzer HW, Cacciapuoti A. Lassa virus isolation from *Mastomys natalensi*s rodents during an epidemic in Sierra Leone. Science. 1974;185:263–5. https://doi.org/10.1126/science.185.4147.263
24. Walker DH, Johnson KM, Lange JV, Gardner JJ, Kiley MP, McCormick JB. Experimental infection of rhesus monkeys with Lassa virus and a closely related arenavirus, Mozambique virus. J Infect Dis. 1982;146:360–8. https://doi.org/10.1093/infdis/146.3.360
25. Paweska JT, Sewlall NH, Ksiazek TG, Blumberg LH, Hale MJ, Lipkin WI, et al.; Outbreak Control and Investigation Teams. Nosocomial outbreak of novel arenavirus infection, southern Africa. Emerg Infect Dis. 2009;15:1598–602. https://doi.org/10.3201/eid1510.090211
26. Palacios G, Savji N, Hui J, Travassos da Rosa A, Popov V, Briese T, et al. Genomic and phylogenetic characterization of Merino Walk virus, a novel arenavirus isolated in South Africa. J Gen Virol. 2010;91:1315–24. https://doi.org/10.1099/vir.0.017798-0
27. Colangelo P, Verheyen E, Leirs H, Tatard C, Denys C, Dobigny G, et al. A mitochondrial phylogeographic scenario for the most widespread African rodent, Mastomys natalensis. Biol J Linn Soc Lond. 2013;108:901–16. https://doi.org/10.1111/bij.12013
28. Göuy de Bellocq J, Bryjová A, Martynov A, Lavrenchenko L. Dhati Welel virus, the missing mammarenavirus of the widespread Mastomys natalensis. J Vert Biol. 2020;69:20018.
29. Gryseels S, Baird SJE, Borremans B, Makundi R, Leirs H, Goüy de Bellocq J. When viruses don't go viral: the importance of host phylogeographic structure in the spatial spread of arenaviruses. PLoS Pathog. 2017;13:e1006073. https://doi.org/10.1371/journal.ppat.1006073
30. Radoshitzky SR, Buchmeier MJ, Charrel RN, Clegg JCS, Gonzalez JJ, Günther S, et al.; Ictv Report Consortium. ICTV virus taxonomy profile: Arenaviridae. J Gen Virol. 2019;100:1200–1. https://doi.org/10.1099/jgv.0.001280
31. Witkowski PT, Kallies R, Hoveka J, Auste B, Ithete NL, Šoltys K, et al. Novel arenavirus isolates from Namaqua rock mice, Namibia, Southern Africa. Emerg Infect Dis. 2015;21:1213–6. https://doi.org/10.3201/eid2107.141341
32. Těšíková J, Krásová J, Goüy de Bellocq J. Multiple mammarenaviruses circulating in Angolan rodents. Viruses. 2021;13:982. https://doi.org/10.3390/v13060982
33. Edwards S, Claude J, Van Vuuren BJ, Matthee CA. Van Vuuren Bj, Matthee Ca. Evolutionary history of the Karoo bush rat, Myotomys unisulcatus (Rodentia: Muridae): disconcordance between morphology and genetics. Biol J Linn Soc Lond. 2011;102:510–26. https://doi.org/10.1111/j.1095-8312.2010.01583.x
34. Ishii A, Thomas Y, Moonga L, Nakamura I, Ohnuma A, Hang'ombe BM, et al. Molecular surveillance and phylogenetic analysis of Old World arenaviruses in Zambia. J Gen Virol. 2012;93:2247–51. https://doi.org/10.1099/vir.0.044099-0

Address for correspondence: Jacqueline Weyer, National Institute for Communicable Diseases, 1 Modderfontein Rd, Sandringham 2292, South Africa; email: jacquelinew@nicd.ac.za

Potential Use for Serosurveillance of Feral Swine to Map Risk for Anthrax Exposure, Texas, USA

Rachel M. Maison, Courtney F. Pierce, Izabela K. Ragan, Vienna R. Brown, Michael J. Bodenchuk, Richard A. Bowen, Angela M. Bosco-Lauth

Anthrax is a disease of concern in many mammals, including humans. Management primarily consists of prevention through vaccination and tracking clinical-level observations because environmental isolation is laborious and bacterial distribution across large geographic areas difficult to confirm. Feral swine (*Sus scrofa*) are an invasive species with an extensive range in the southern United States that rarely succumbs to anthrax. We present evidence that feral swine might serve as biosentinels based on comparative seroprevalence in swine from historically defined anthrax-endemic and non–anthrax-endemic regions of Texas. Overall seropositivity was 43.7% (n = 478), and logistic regression revealed county endemicity status, age-class, sex, latitude, and longitude were informative for predicting antibody status. However, of these covariates, only latitude was statistically significant (β = –0.153, p = 0.047). These results suggests anthrax exposure in swine, when paired with continuous location data, could serve as a proxy for bacterial presence in specific areas.

Anthrax, caused by *Bacillus anthracis*, is a zoonotic disease of global importance because of its ecologic effects on wildlife and free-ranging livestock and resulting economic impact on farmers and herders, its worldwide distribution, and its ability to cause disease even after decades of lying dormant in the environment. Known risks of exposure, considered together with unconfirmed environmental distribution in most regions and unidentified or evolving epidemiologic risk factors, make *B. anthracis* a pathogen of continuing human and animal health concern.

B. anthracis is a gram-positive, endospore-forming bacterium. Anthrax cases have been clinically described since the 1700s, but symptomatic descriptions of the disease have been recorded as early as 1000 BCE (*1*,*2*). Genetic studies however, suggest that the geographic origin of *B. anthracis* was in sub-Saharan Africa; subsequent environmental spread followed the migration of humans and domesticated animals (*3*,*4*). Current case report data indicate that enzootic anthrax correlates with warmer climates, although some cases have been documented above the arctic circle, in Canada, and in northern Siberia (*5*). The true incidence of the disease remains unknown in many countries, although it is assumed that the bacterium resides in most regions (*6*). Extensive ecologic modeling efforts now offer some ability to predict outbreak risks spatially and temporally in several countries (*7*–*10*). Of note, recent modeling efforts have indicated that, in the United States, landscapes most capable of supporting *B. anthracis* span a north–south corridor encompassing most of the central United States and southwestern Texas (*11*).

Thought to affect all mammals to varying degrees, *B. anthracis* infection generally causes the highest levels of illness and death in herbivorous species (*12*,*13*). Exposure most commonly occurs when an animal ingests the dormant spore form of the bacterium, but cutaneous and inhalational infections also occur (*14*). Once inside a susceptible host, bacteria transform into a vegetative form that secretes a combination of lethal and edema factor proteins as well as the cell receptor–binding protein-protective antigen (PA), which mediates their entry into host cells and activates them to produce lethal factor and edema factor toxins, contributing to the ultimate death of susceptible hosts. Upon host death, exposure of vegetative bacilli to atmospheric oxygen, typically

Author affiliations: Colorado State University, Fort Collins, Colorado, USA (R.M. Maison, I.K. Ragan, R.A. Bowen, A.M. Bosco-Lauth); US Department of Agriculture National Wildlife Research Center, Fort Collins (C.F. Pierce); US Department of Agriculture National Feral Swine Damage Management Program, Fort Collins (V.R. Brown); US Department of Agriculture Animal and Plant Health Inspection Service, San Antonio, Texas, USA (M.J. Bodenchuk)

DOI: https://doi.org/10.3201/eid2712.211482

through carcass manipulation by scavengers, initiates the sporulation process, in which bacteria return to their dormant form. Sporulated *B. anthracis* is highly resistant to environmental degradation; some environmental isolations have detected viable spores up to 200 years old (*4*). Humans and other animals that encounter infected carcasses or animal materials are therefore at increased risk of exposure because infected carcasses that are manipulated or opened can initiate sporulation and consequently perpetuate the environmental persistence of infectious *B. anthracis*.

Current preventive management for domestic herbivores is primarily vaccine-based (*12*), but vaccination is not a requirement for livestock owners, who instead commonly use it reactively to control outbreaks (*11*,*15*). Outbreaks of anthrax in wild and domestic animals today are defined by the detection of carcasses, often from otherwise healthy animals. Unlike among domestic populations however, observation of anthrax is extremely difficult among wild or free-ranging herbivores, because detecting carcasses over large landscapes is an imperfect and likely inaccurate method for reporting true incidence, and wildlife usually cannot be observed for clinical signs of disease (*16*–*18*).

Humans, suids, and carnivores are considered incidental hosts and considerably less susceptible to lethal infection than herbivores (*19*). Although the causes of these variations in susceptibility remain largely unknown, it is likely they are a combination of differences in physiology, behavior, dosage, and transmission routes (*20*). For example, carnivores, omnivores, and scavengers all have lower stomach pH than herbivores, likely killing *B. anthracis* spores or vegetative cells incidentally ingested while foraging (*12*,*21*). In addition, some evidence indicates that necrophilic and hemophagic arthropods can contribute to infection (*19*,*22*), suggesting that transmission routes might also differ by a regions' competent vector species. In endemic regions such as Africa, there appears to be little evidence of predators and scavengers dying of anthrax; those animals instead exhibit a high prevalence of antibodies against the bacterium (*20*). On the basis of these observations, it has previously been proposed that anthrax-resistant suid species, such as the Eurasian wild boar (*Sus scrofa*) in Ukraine and feral hog in the United States, might be used as biosentinels for anthrax (*23*). Of note, although a previous study (*23*) described serologic evidence of exposure in wild boars Ukraine, no studies to date have formally evaluated exposure in taxonomically identical feral swine (also *S. scrofa*) present in the United States. Introduced initially in the 1500s to states bordering the Gulf of Mexico, populations of feral swine have exploded since the 1980s and have become established throughout most suitable habitats in the southern United States (*24*).

In addition to known pathways of transmission, the shared presence of *B. anthracis* and anthrax-resistant wildlife species might contribute to anthrax epidemiology under certain conditions by increasing the risk for exposure to humans or more susceptible herbivorous species. Resistant species may also help to disseminate infectious spores to new landscapes through mechanical transmission or bacterial shedding (*6*,*25*). Feral swine are known to be opportunistic omnivores that occasionally scavenge carcasses, as well as routinely root in soils for food (*26*). These behaviors, coupled with their documented resistance to anthrax, suggest that feral swine might be a good indicator of bacterial presence on the landscapes they occupy. We report the potential biosentinel utility of feral swine for measuring anthrax distribution by examining antibody prevalence in confirmed endemic and nonendemic regions of Texas, USA.

Materials and Methods

Study Area

We conducted our investigation in Texas because anthrax is a reportable disease and is relatively predictable in select regions of the state. Feral swine populations are also present in most counties, offering a unique opportunity to evaluate the species as a biosentinel for *B. anthracis*. In addition, observations by residents of the state's endemic region have described resurgences in anthrax in areas recently colonized by feral swine, anecdotally suggesting the 2 events might be related.

Outbreaks of anthrax occur regularly in portions of Crockett, Val Verde, Sutton, Edwards, Kinney, Uvalde, and Maverick Counties, colloquially referred to as the Anthrax Triangle, usually in dry summer months following heavy spring rains (*27*,*28*). Conversely, eastern Texas does not experience regular outbreaks, despite also being heavily populated with domestic livestock (*29*). Furthermore, populations of ranched white-tailed deer in areas of Val Verde, Uvalde, and Webb Counties are also regularly affected, suggesting wild herbivores in the same region might become infected at similar rates. We binarily defined areas as either endemic for anthrax for those 7 counties on the western side of the state comprising the historic Anthrax Triangle (Figure 1) or nonendemic if outside of this region, because these counties do not experience regular, seasonal cases.

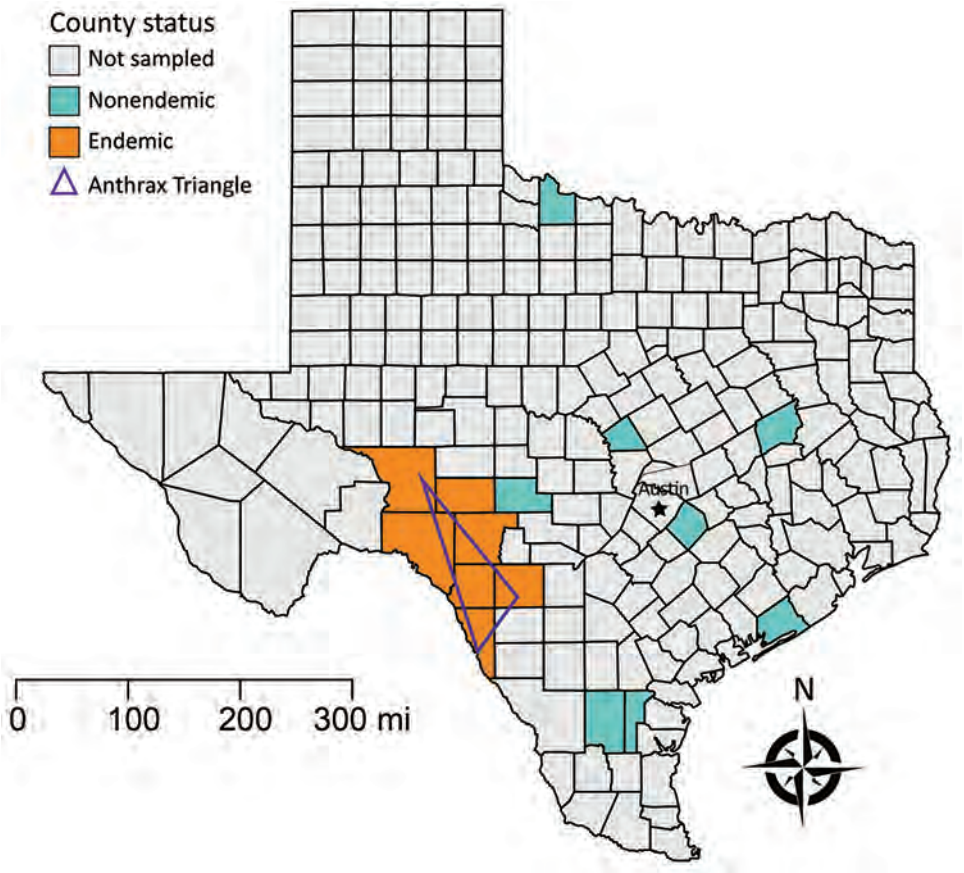

Figure 1. Field sampling designations for feral swine serum samples collected in Texas, USA. The Anthrax Triangle designates a region that experiences semiregular outbreaks of anthrax in both domestic and wildlife species. All other Texas counties are considered nonendemic, but we serosampled only 7 of those counties.

Field Sampling

Wildlife Services, a branch within the US Department of Agriculture (USDA), routinely removes feral swine from the landscape for damage control and invasive species management, and as part of these efforts, collect serum samples from a subset of swine for disease surveillance. Samples not used for routine surveillance are archived and can be used for select retrospective studies. Through these efforts, we obtained 478 serum samples collected during 2007–2019 from feral swine removed from areas throughout Texas and tested them to determine the prevalence of feral swine exposure to *B. anthracis* by measuring antibodies against PA. We illustrated spatial data on the geographic origins of the feral swine serum samples (Table 1; Figure 1) at the county level to protect personally identifiable information because many samples were collected on private property. Approximately half (n = 243) of the serum samples originated in the 7 endemic counties within the Anthrax Triangle and the rest (n = 235) from 7 nonendemic counties outside of it. We randomly selected the 7 nonendemic counties from the 246 Texas counties located outside of the Anthrax Triangle; 7 counties were selected so that the sampling effort was equal between endemic and nonendemic regions. Sampling events took place year-round.

Serum samples were taken from male and female feral swine classified as either adult, estimated by Wildlife Services field personnel to be >1 year of age, or subadult, estimated as 2 months–1 year of age (Table 1). We did not collect samples from juveniles (<2 months of age) to avoid confounding serology that could result from the presence of maternal antibodies (*30*). All blood samples were collected postmortem and serum extracted within 12 hours of clotting and shipped overnight on ice to the National Wildlife Research Center (Fort Collins, CO, USA), where they were stored at –80°C until testing.

Serology

We used an indirect ELISA platform similar to those described elsewhere (*31*–*34*), with slight modifications to target antibodies of swine origin. We assayed samples blindly relative to the origin, sex, and age-class of individual animals until all results were finalized. We coated high binding polystyrene 96-well flat-bottom microtiter plates (ThermoFisher Scientific, https://www.thermofisher.com) with recombinant protective antigen (rPA) from *B. anthracis* (American

Table 1. Sampling distribution of feral swine serum samples collected from endemic and nonendemic regions of Texas, USA.

	Male		Female		
Region type	Adult	Subadult	Adult	Subadult	Total
Endemic	90	16	121	16	243
Nonendemic	113	12	101	9	235
Total	203	28	222	25	478

Type Culture Collection, https://www.atcc.org) diluted in carbonate buffer solution at a concentration of 5 μg/mL per well and incubated plates overnight at 4°C. The following day, we discarded the coating buffer and washed the wells 5× with phosphate-buffered saline containing 0.05% Tween 20 washing buffer. We blocked wells by adding 300 μL of 10% skim milk in phosphate-buffered saline and allowed plates to incubate for 1.5 h at room temperature. We again washed wells, then added 100 μL of test serum diluted 1:100 in blocking buffer and incubated plates for 1 h with shaking at room temperature. After additional washing, we added 100 μL/well of protein A/G-horseradish peroxidase (ThermoFisher Scientific) diluted 1:1,000 in blocking buffer, and further incubated plates with shaking for 30 min. After 1 final washing step, we added 150 μL of one-step ABTS (ThermoFisher Scientific), incubated for 15 min, and then added 100 μL of 1% sodium dodecyl sulfate solution to stop the reaction. We measured absorbance at 25°C and 405 nm using a BioTek microplate reader paired with Gen5 version 3.09 microplate reader and imager software (https://www.biotek.com). We considered samples positive for rPA antibodies if their mean absorbance measurements were >3 times the SD above the mean of the negative controls. We ran individual samples in triplicate.

Because of their inherent resistance to anthrax infection, domestic pigs are not as routinely vaccinated as ruminant livestock species. As such, swine serum samples were unavailable for use as antibody-positive and -negative controls for this assay. Instead, we obtained control serum samples included in each assay from one male domestic goat (*Capra aegagrus hircus*) before and after vaccination with Anthrax Vaccine Adsorbed (BioThrax, https://www.beiresources.org). Protein A/G is known to bind to the constant region of both goat and swine IgG with comparable affinity (*35*–*37*).

Statistics

We examined how the probability of an individual animal being positive for anthrax antibodies varied by region (endemic vs. nonendemic), sex, age-class (adult vs. subadult), latitude, and longitude using logistic regression and mixed-effects models implemented in R version 4.0.2 (R Foundation for Statistical Computing, https://www.r-project.org). We examined region, sex, age-class, latitude, and longitude as fixed effects and evaluated sampling year as a random effect to account for temporal variation in anthrax prevalence and sampling. Since most anthrax cases in Texas originate from the Anthrax Triangle (*27*,*28*), we included region as a fixed effect to evaluate whether feral swine residing in known contaminated environments are more likely to be antibody positive than those outside. We used county centroids as a proxy for sampling locations and considered latitude and longitude fixed effects to account for spatial trends in anthrax prevalence. Interaction between age-class and sex was also examined to account for potential impacts of age variations by sex.

We evaluated support for including a random effect (sampling year) using Akaike's information criterion (AIC) and likelihood ratio test (LRT) in R. As recommended elsewhere (*38*), we first examined whether sample year should be included by comparing AIC and LRT with and without its addition from a fully parameterized fixed effects model. If the random effect was supported (ΔAIC >2 compared with the model excluding the random effect), then it was retained in all models and the fixed effects compared. Using LRT as an additional method of evaluating the inclusion of sampling year, we calculated the difference in the log likelihoods of the 2 nested models (i.e., fully parameterized fixed effect model with or without the addition of the random effect) and if the difference was statistically significant ($\alpha = 0.05$), we included the random effect in all models.

We compared all combinations of fixed effects covariates using AIC implemented in the R package MuMIn (R Foundation for Statistical Computing); the lowest AIC value represented the most parsimonious model. If model uncertainty existed (i.e., >1 competing model <2 ΔAIC of the top model), we examined the relative support for each covariate by calculating cumulative covariate weights; we considered weights >0.5 supported (*39*). We selected the final model based on the supported covariate regression coefficients used to calculate odds ratios and 95% CI for the probability of having anthrax antibodies by covariate. Finally, to assess model fit we calculated area under the curve (AUC) for the receiver operating characteristic (ROC) (*40*) curve using the pROC (partial receiver operating characteristic) curve package in R (*41*); the ROC curve enabled us to assess the performance of the binary classification model for identifying individual animals as positive or negative. To summarize

the ROC curve, we calculated the AUC, an aggregated measure of binary classification model performance, in which the model AUC = 0.5 for no predictive power, >0.5–<0.7 for poor predictive power, ≥0.7–<0.8 for acceptable predictive power, and ≥0.8–<0.9 for excellent predictive power (*40*).

Results

Serology

Negative control goat serum collected before vaccination exhibited absorbance readings of 0.018–0.11 (mean 0.08, SD 0.022). Pooled positive serum taken 3 and 5 weeks after anthrax vaccination exhibited an absorbance range of 0.26–3.42 (mean 1.62, SD 1.27). We calculated the assay cutoff of +3 SD above the mean of the negative controls at 0.15. Of the 478 samples examined, we identified 209 (43.7%) as positive and 269 (56.3%) as negative for PA antibodies. From the entire sample pool, we recorded a minimum absorbance value of –0.006 and maximum value of 3.9.

Statistics

Basic data structure, including anthrax antibody status stratified by covariate and apparent seroprevalence (Table 2), includes raw data confirming that more swine from the endemic region (49.49%) compared with the nonendemic region (37.45%) were seropositive; we also illustrate individual sample absorbance by region (Figure 2). Seroprevalence was higher among female (48.18%) than male (38.96%) swine and among adult (44.71%) than subadult (35.85%) swine. The fully parametrized model failed to converge, so we excluded longitude and the interaction term (age-class*sex) from the fully parameterized model to evaluate inclusion of sampling year as a random effect. Sampling year did not improve the predictive power of the model (fixed effects model AIC = 649.87 and mixed-effects model AIC = 648.59; LRT p = 0.070); probability of an individual animal being seropositive was therefore best predicted by a fixed effects model. There was uncertainty about the optimal model (7 models were <2 ΔAIC). To determine their relative importance, we examined cumulative covariate weights and found that county endemicity status, age-class, sex, latitude, and longitude were informative for predicting antibody status, and therefore included them in the final model. We calculated odds ratios and 95% CI for each predictor variable (Table 3), but only latitude was statistically significant (β = –0.153; p = 0.047). The final model had poor predictive ability (AUC = 0.613) suggesting the presence of unexplained variance in anthrax antibody status.

Table 2. Distribution of anthrax seroprevalence in feral swine by region, sex, and age group.

Predictor	No. tested	No. positive	Apparent seroprevalence, %
Region			
Endemic	243	121	49.49
Nonendemic	235	88	37.45
Sex			
M	231	90	38.96
F	247	119	48.18
Age group			
Subadult	53	19	35.85
Adult	425	190	44.71

Discussion

Serologic surveillance in various anthrax-resistant species has assisted wildlife managers and health officials in identifying areas of high outbreak risk (*20*) and the surprisingly high seroprevalence we identified in feral swine supports this strategy. *B. anthracis* spores exist in soil and the carcasses of animals that have died from anthrax, but the sampling efforts required to identify contaminated environments and subsequent outbreak risks are often too laborious or expensive to use, making the use of biosentinels an appealing option. In addition, human and animal case reports and mortality data likely underestimate

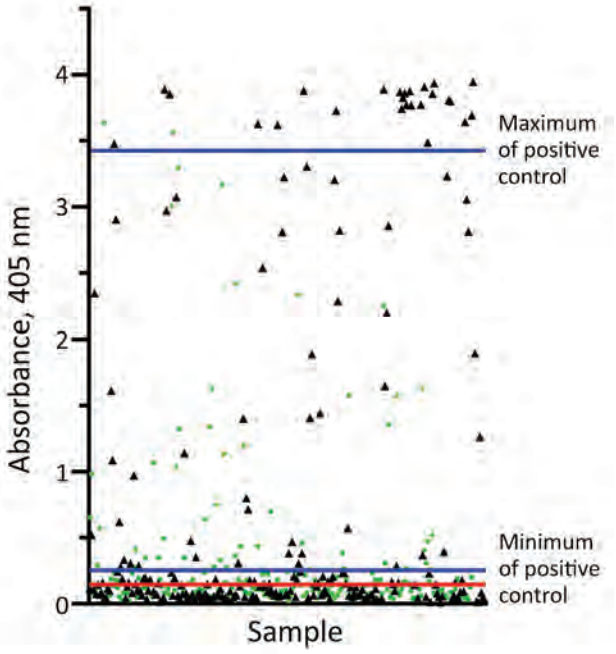

Figure 2. Sample absorbance values measured by ELISA at 405 nm for 478 feral swine serum samples collected from defined endemic and nonendemic regions of Texas, USA. The red cutoff line represents the calculated assay cutoff between seropositive and seronegative animals (e.g., +3 SD above the mean of the negative control), equal to 0.15 absorbance units. Blue lines delineate the absorbance unit range of the positive assay control. Black triangles represent samples taken in endemic counties; green boxes represent samples taken in nonendemic counties.

Table 3. Odds ratios and 95% CIs of the probability of having anthrax antibodies by fixed effects covariates

Covariate	Odds ratio (95% CI)
County status: endemic	1.035 (0.523–2.054)
Age class: adult	1.641 (0.903–3.059)
Sex: female	1.398 (0.966–2.026)
Latitude	0.858 (0.737–0.997)
Longitude	0.877 (0.702–1.092)

the geographic extent of this pathogen, while exposure data obtained through serosurveillance might enable acquisition of multidimensional biologic information, such as environmental range and relative time of exposure. Because swine are resistant to anthrax (*19*) and there is serologic evidence of exposure in taxonomically identical species such as wild boar in Ukraine, feral swine might be good indicators of bacterial presence throughout their range in the United States. Feral swine also exhibit relatively small home ranges, 1–5 km^2 (*41*,*42*), potentially enabling high resolution in estimating the geographic extent of contaminated environments.

Data presented here demonstrate that the overall odds of feral swine in Texas with anthrax antibodies differ between those inhabiting broadly defined endemic and nonendemic regions; animals originating within the Anthrax Triangle exhibit higher odds of being seropositive than those outside. This finding is not surprising given the regularity of outbreaks in domestic herbivores within this region and supports our preliminary hypothesis that feral swine are being exposed in regions experiencing regular occurrences of the disease. However, ≈37% of individual animals from nonendemic counties were also seropositive, so county status alone proved not to be a significant predictor covariate, and the size of that proportion suggests that bacteria might be present and therefore swine exposed beyond the confines of the Anthrax Triangle. This possibility is further supported by latitude but not county status being a statistically significant covariate in our top-performing model.

Although the role that feral swine might play in the overall epidemiology of anthrax is unknown, swine do exhibit close relationships with soil (*26*) and thus likely experience higher rates of exposure than humans and perhaps some domestic and wild ruminants; therefore, they might contribute to bacterial spread through biologic or mechanical dissemination. However, the level of exposure might simply reflect bacterial presence irrespective of swine involvement in dissemination, because outbreaks outside of the Anthrax Triangle are reported occasionally (*28*). Although our statistical analysis was unable to distinguish anthropogenically defined endemic and nonendemic regions, the high apparent seroprevalence observed in feral swine across the state of Texas is still useful information, because exposure data are further indicative of bacterial distribution occurring beyond the confines of the Anthrax Triangle, as has been predicted by the ecologic modeling efforts of others (*8*,*11*).

Of note, female and adult swine tended to have higher seropositivity than male and subadult swine, although the measures were not statistically significant. Higher odds by sex might be because of the inherent dynamics of swine sounders; groups typically are composed of several females and their offspring, whereas adult and subadult males are often solitary, only associating with females during breeding (*26*). The likelihood then of observing seropositive female swine in a *B. anthracis*–contaminated region might be higher simply because female swine traveling together are experiencing the same environmental exposures compared with their solitary male counterparts. The potential age-class bias observed could be explained in part by the unequal sample sizes between these covariates; more extensive data might be necessary to confirm this association. Finally, feral swine have been observed to opportunistically feed on carcasses of other animals, as well as prey on some livestock (*43*–*45*). Thus, feral swine might be contributing to anthrax epidemiology through a variety of mechanisms, including carrying and depositing spores or vegetative cells acquired from rooting in soil or by feeding on the carcasses of animals who have died from anthrax.

As with any retrospective, opportunistic serosurvey, the data and subsequent findings presented here are not without limitations. First, the fact that we broadly defined regions as endemic and nonendemic solely on the basis of whether a county was located in the Anthrax Triangle likely does not account for the contiguous or disjointed presence of this bacterium predicted in soils throughout the state (*11*), and counties that were sampled on the border of the Anthrax Triangle, such as Kimble, might have skewed results with some antibody-positive animals originating from this region. Also, in conjunction with the regions we defined, we did not examine any environmental conditions or weather patterns, which likely are substantial factors influencing bacterial distribution and infectivity rates between the sampling years examined and could be the source of the unexplained variance suggested during model evaluation.

In conclusion, feral swine are a fecund invasive species that often encounter people and domestic animals, as well as other wildlife species. Past investigations have identified myriad pathogens that can

be transmitted or carried by these animals (*46*), and national programs supported by the USDA regularly survey populations for diseases of national concern to humans or related to agriculturally important species (*24*). Despite the amount of attention feral swine receive for harboring some pathogens, future investigations are needed to fully define the role feral swine play in anthrax epidemiology, particularly whether they are contributing to bacterial dissemination. However, our investigation suggests that levels of anthrax exposure in feral swine, when paired with continuous location data, could serve as a proxy for identifying *B. anthracis* presence in a specific area.

Acknowledgments

We thank the staff and field personnel of USDA's National Feral Swine Damage Management Program for collecting and providing the field samples and corresponding animal data for this study. We also thank Terry Nett and Eric Weber for their guidance in developing and troubleshooting ELISAs and the American Type Culture Collection for providing the recombinant protective antigen used for our assays. Finally, we thank Amy Davis, Ryan Miller, and Tim Smyser for their helpful suggestions on statistical analysis and assistance during manuscript revision.

This research was supported by the US Department of Agriculture, Animal and Plant Health Inspection Service, Wildlife Services. The findings and conclusions in this manuscript are those of the authors and should not be interpreted to represent any official USDA or US Government determination or policy, nor should the materials used herein indicate endorsement by the US Government.

About the Author

Ms. Maison is a graduate student at Colorado State University in Fort Collins, Colorado. Her primary research interests include how invasive species such as feral swine impact the health of native wildlife populations as well as how they contribute to human health dynamics.

References

1. Sternbach G. The history of anthrax. J Emerg Med. 2003; 24:463–7. https://doi.org/10.1016/S0736-4679(03)00079-9
2. Zasada AA. Detection and identification of *Bacillus anthracis*: from conventional to molecular microbiology methods. Microorganisms. 2020;8:125. https://doi.org/10.3390/microorganisms8010125
3. Keim P, Kalif A, Schupp J, Hill K, Travis SE, Richmond K, et al. Molecular evolution and diversity in Bacillus anthracis as detected by amplified fragment length polymorphism markers. J Bacteriol. 1997;179:818–24. https://doi.org/10.1128/jb.179.3.818-824.1997
4. Smith KL, DeVos V, Bryden H, Price LB, Hugh-Jones ME, Keim P. *Bacillus anthracis* diversity in Kruger National Park. J Clin Microbiol. 2000;38:3780–4. https://doi.org/10.1128/JCM.38.10.3780-3784.2000
5. Turnbull, PCB, editor. Anthrax in humans and animals. 4th ed. Geneva: World Health Organization; 2008.
6. Mongoh MN, Dyer NW, Stoltenow CL, Khaitsa ML. Risk factors associated with anthrax outbreak in animals in North Dakota, 2005: a retrospective case-control study. Public Health Rep. 2008;123:352–9. https://doi.org/10.1177/003335490812300315
7. Bezymennyi M, Bagamian KH, Barro A, Skrypnyk A, Skrypnyk V, Blackburn JK. Spatio-temporal patterns of livestock anthrax in Ukraine during the past century (1913–2012). Appl Geogr. 2014;54:129–38. https://doi.org/10.1016/j.apgeog.2014.07.016
8. Blackburn JK, McNyset KM, Curtis A, Hugh-Jones ME. Modeling the geographic distribution of Bacillus anthracis, the causative agent of anthrax disease, for the contiguous United States using predictive ecological niche modeling. Am J Trop Med Hyg. 2007;77:1103–10. [Erratum in Am J Trop Med Hyg. 2008;78:358]. https://doi.org/10.4269/ajtmh.2007.77.1103
9. Hampson K, Lembo T, Bessell P, Auty H, Packer C, Halliday J, et al. Predictability of anthrax infection in the Serengeti, Tanzania. J Appl Ecol. 2011;48:1333–44. https://doi.org/10.1111/j.1365-2664.2011.02030.x
10. Steenkamp PJ, van Heerden H, van Schalkwyk OL. Ecological suitability modeling for anthrax in the Kruger National Park, South Africa. PLoS One. 2018;13:e0191704. https://doi.org/10.1371/journal.pone.0191704
11. Yang A, Mullins JC, Van Ert M, Bowen RA, Hadfield TL, Blackburn JK. Predicting the geographic distribution of the *Bacillus anthracis* A1.a/Western North American sub-lineage for the continental United States: new outbreaks, new genotypes, and new climate data. Am J Trop Med Hyg. 2020;102:392–402. https://doi.org/10.4269/ajtmh.19-0191
12. Beyer W, Turnbull PCB. Anthrax in animals. Mol Aspects Med. 2009;30:481–9. https://doi.org/10.1016/j.mam.2009.08.004
13. Fasanella A, Galante D, Garofolo G, Jones MH. Anthrax undervalued zoonosis. Vet Microbiol. 2010;140:318–31. https://doi.org/10.1016/j.vetmic.2009.08.016
14. Spickler AR. Anthrax. 2017 [cited 2021 May 1]. https://www.cfsph.iastate.edu/Factsheets/pdfs/anthrax.pdf
15. Blackburn JK, Hadfield TL, Curtis AJ, Hugh-Jones ME. Spatial and temporal patterns of anthrax in white-tailed deer, *Odocoileus virginianus*, and hematophagous flies in West Texas during the summertime anthrax risk period. Ann Assoc Am Geogr. 2014;104:939–58. https://doi.org/10.1080/00045608.2014.914834
16. Welkos S, Bozue J, Twenhafel N, Cote C. Animal models for the pathogenesis, treatment and prevention of infection by *Bacillus anthracis*. Microbiol Spectr. 2015;3:TBS-0001–2012. https://doi.org/10.1128/microbiolspec.TBS-0001-2012
17. Bellan SE, Gimenez O, Choquet R, Getz WM. A hierarchical distance sampling approach to estimating mortality rates from opportunistic carcass surveillance data. Methods Ecol Evol. 2013;4:361–9. https://doi.org/10.1111/2041-210x.12021
18. Huso MMP. An estimator of wildlife fatality from observed carcasses. Environmetrics. 2011;22:318–29. https://doi.org/10.1002/env.1052
19. Hugh-Jones ME, de Vos V. Anthrax and wildlife. Rev Sci Tech. 2002;21:359–83. https://doi.org/10.20506/rst.21.2.1336
20. Bagamian KH, Alexander KA, Hadfield TL, Blackburn JK. Ante- and postmortem diagnostic techniques for anthrax:

rethinking pathogen exposure and the geographic extent of the disease in wildlife. J Wildl Dis. 2013;49:786–801. https://doi.org/10.7589/2013-05-126
21. Beasley DE, Koltz AM, Lambert JE, Fierer N, Dunn RR. The evolution of stomach acidity and its relevance to the human microbiome. PLoS One. 2015;10:e0134116. https://doi.org/10.1371/journal.pone.0134116
22. Hugh-Jones M, Blackburn J. The ecology of *Bacillus anthracis*. Mol Aspects Med. 2009;30:356–67. https://doi.org/10.1016/j.mam.2009.08.003
23. Bagamian KH, Skrypnyk A, Rodina Y, Bezymennyi M, Nevolko O, Skrypnyk V, et al. Serological anthrax surveillance in wild boar (*Sus scrofa*) in Ukraine. Vector Borne Zoonotic Dis. 2014;14:618–20. https://doi.org/10.1089/vbz.2013.1521
24. Animal and Plant Health Inspection Service, United States Department of Agriculture. Feral swine damage. 2021 [cited 2021 May 1]. https://www.aphis.usda.gov/aphis/ourfocus/wildlifedamage/operational-activities/feral-swine/feral-swine-damage
25. Saggese MD, Noseda RP, Uhart MM, Deem SL, Ferreyra H, Romano MC, et al. First detection of *Bacillus anthracis* in feces of free-ranging raptors from central Argentina. J Wildl Dis. 2007;43:136–41. https://doi.org/10.7589/0090-3558-43.1.136
26. Graves HB. Behavior and ecology of wild and feral swine (*Sus scrofa*). J Anim Sci. 1984;58:482–92. https://doi.org/10.2527/jas1984.582482x
27. Texas parks and wildlife. Frequently asked questions. 2019 [cited 2021 May 1]. https://tpwd.texas.gov/landwater/land/habitats/faq/diseases/disease7.phtml
28. Sidwa T, Salzer JS, Traxler R, Swaney E, Sims ML, Bradshaw P, et al. Control and prevention of anthrax, Texas, USA, 2019. Emerg Infect Dis. 2020;26:2815–24. https://doi.org/10.3201/eid2612.200470
29. United States Department of Agriculture, National Agricultural Statistics Service, USA. County estimate map—cattle, Texas [cited 2021 May 20]. https://www.nass.usda.gov/Statistics_by_State/Texas/Publications/County_Estimates/ce_maps/ce_catt.php
30. Poonsuk K, Zimmerman J. Historical and contemporary aspects of maternal immunity in swine. Anim Health Res Rev. 2018;19:31–45. https://doi.org/10.1017/S1466252317000123
31. Grunow R, Porsch-Ozcürümez M, Splettstoesser W, Buckendahl A, Hahn U, Beyer W, et al. Monitoring of ELISA-reactive antibodies against anthrax protective antigen (PA), lethal factor (LF), and toxin-neutralising antibodies in serum of individuals vaccinated against anthrax with the PA-based UK anthrax vaccine. Vaccine. 2007;25:3679–83. https://doi.org/10.1016/j.vaccine.2007.01.056
32. Lembo T, Hampson K, Auty H, Beesley CA, Bessell P, Packer C, et al. Serologic surveillance of anthrax in the Serengeti ecosystem, Tanzania, 1996-2009. Emerg Infect Dis. 2011;17:387–94. https://doi.org/10.3201/eid1703.101290
33. Mukarati NL, Ndumnego O, van Heerden H, Ndhlovu DN, Matope G, Caron A, et al. A serological survey of anthrax in domestic dogs in Zimbabwe: a potential tool for anthrax surveillance. Epidemiol Infect. 2018;146:1526–32. https://doi.org/10.1017/S0950268818001577
34. Turnbull PC, Broster MG, Carman JA, Manchee RJ, Melling J. Development of antibodies to protective antigen and lethal factor components of anthrax toxin in humans and guinea pigs and their relevance to protective immunity. Infect Immun. 1986;52:356–63. https://doi.org/10.1128/iai.52.2.356-363.1986
35. Sjöbring U, Falkenberg C, Nielsen E, Akerström B, Björck L. Isolation and characterization of a 14-kDa albumin-binding fragment of streptococcal protein G. J Immunol. 1988;140:1595–9.
36. Richman DD, Cleveland PH, Oxman MN, Johnson KM. The binding of staphylococcal protein A by the sera of different animal species. J Immunol. 1982;128:2300–5.
37. Hage DS, Bian M, Burks R, Karle E, Ohnmacht C, Wa C. Bioaffinity chromatography. In: Hage DS, Cazes J, editors. Handbook of affinity chromatography. Boca Raton (FL): CRC Press; 2005. p. 101–104.
38. Zuur AF, Ieno EN, Walker NJ, Saveliev AA, Smith GM. Mixed effects models and extensions in ecology with R. In: Gail M, Samet JM, editors. Statistics for biology and health. New York: Springer; 2009. p. 101–42.
39. Doherty PF, White GC, Burnham KP. Comparison of model building and selection strategies. J Ornithol. 2012;152(S2):317–23. https://doi.org/10.1007/s10336-010-0598-5
40. Hosmer DW, Lemeshow S, Sturdivant RX. Assessing the fit of the model. In: Applied logistic regression. Hoboken (NJ): Wiley; 2013. p. 153–225.
41. Gaston WD, Armstrong JB, Arjo WM, Stribling HL. Home range and habitat use of feral hogs (*Sus scrofa*) on Lowndes County WMA, Alabama. Presented at: 2008 National Conference on Feral Hogs; 2008 Apr 13–15; St. Louis, Missouri, USA.
42. Kurz JC, Marchinton RL. Radiotelemetry studies of feral hogs in South Carolina. J Wildl Manage. 1972;36:1240–8. https://doi.org/10.2307/3799254
43. Seward NW, VerCauteren KC, Witmer GW, Engeman RM. Feral swine impacts on agriculture and the environment. Sheep Goat Res J. 2004;12:34–40.
44. Hanson RP, Karstad L. Feral swine in the southeastern United States. J Wildl Manage. 1959;23:64–74. https://doi.org/10.2307/3797747
45. Nichols L Jr. Ecology of the wild pig. Job completion report. July 1, 1961–June 30, 1962. Federal Aid in Wildlife Restoration Final Report Project W-5-R-13. Honolulu (HI): Hawaii Department of Land and Natural Resources, Division of Fish and Game; , 1962.
46. Bevins SN, Pedersen K, Lutman MW, Gidlewski T, Deliberto T. Consequences associated with the recent range expansion of nonnative feral swine. Bioscience. 2014;64:291–9. https://doi.org/10.1093/biosci/biu015
47. Fawcett T. An introduction to ROC analysis. Pattern Recognit Lett. 2006;27:861–74. https://doi.org/10.1016/j.patrec.2005.10.010
48. Robin X, Turck N, Hainard A, Tiberti N, Lisacek F, Sanchez JC, et al. pROC: an open-source package for R and S+ to analyze and compare ROC curves. BMC Bioinformatics. 2011;12:77. https://doi.org/10.1186/1471-2105-12-77

Address for correspondence: Angela Bosco-Lauth, Department of Biomedical Sciences, Colorado State University, 1683 Campus Delivery, Fort Collins, CO 80523, USA; email: Angela.Bosco-Lauth@colostate.edu.

Detection of SARS-CoV-2 in Wastewater at Residential College, Maine, USA, August–November 2020

Yolanda M. Brooks, Bailey Gryskwicz, Shawn Sheehan, Sheri Piers, Parag Mahale, Susan McNeil, Jenna Chase, Doreen Webber, David Borys, Michael Hilton, Dion Robinson, Stephen Sears, Emer Smith, Emily K. Lesher, Robert Wilson, Matthew Goodwin,[1] Michael Pardales

We used wastewater surveillance to identify 2 coronavirus disease outbreaks at a college in Maine, USA. Cumulative increases of >1 $\log_{10}$ severe acute respiratory syndrome coronavirus 2 RNA in consecutive 24-hour composite samples preceded the outbreaks. For 76% of cases, RNA was identified in grab samples from residence halls ≤7 days before case discovery.

Wastewater surveillance can indicate the presence and temporal trends of coronavirus disease (COVID-19) cases in a sewershed (*1*,*2*). Large universities have used wastewater surveillance to identify residence halls at high risk for transmission of severe acute respiratory syndrome coronavirus 2 (SARS-CoV-2), the causative agent of COVID-19 (*3*,*4*). We demonstrate that wastewater surveillance using grab samples collected from residential halls and 24-hour composite samples from lift stations can detect COVID-19 outbreaks at a small residential college.

The Study

During August 21–November 20, 2020 (days 0–92), we collected weekly grab samples of flowing untreated wastewater from 6 residence halls at a residential college in Maine, USA. The residence halls served 605 students; hall A housed 64 students, hall B housed 127 students, hall C housed 80 students, hall D housed 109 students, hall E housed 87 students, and hall F housed 138 students. During days 13–92 we also collected 24-hour composite samples approximately twice a week from 2 lift stations (i.e., L1 and L3) where wastewater from various buildings on campus was consolidated in holding tanks and pumped to septic tanks; these composite samples represented the total population in the residence halls. L1 contained effluent from halls E–F and L3 contained effluent from halls A–D. Both lift stations also contained effluent from other campus buildings. The wastewater was collected and stored at 4°C for <72 hours before we assayed 105-mL samples using the Water SARS-CoV-2 RT-PCR test (IDEXX Laboratories, Inc., https://www.idexx.com) according to the manufacturer's instructions. The 2019-nCoV_N_Positive Control plasmid (Integrated DNA Technologies, Inc., https://www.idtdna.com) had a limit of quantification of 2 (average cycle threshold [C_t] 39.42) copies per reaction, and the purified 2019-nCoV_N_Positive Control plasmid cloned into *Escherichia coli* had a limit of quantification of 20 (average C_t 35.95) copies per reaction. The theoretical limit of detection in all samples was 1 copy per reaction. We included a negative extraction control, no-template control, and a step from the standard curve (2×10^3 or 2×10^4 copies/reaction) in each run. We calculated SARS-CoV-2 RNA concentrations as copies per day per person for 24-hour composite samples and copies per liter per person for grab samples. Nondetectable samples were reported at one half the theoretical limit of detection (*5*).

Author affiliations: Saint Joseph's College of Maine, Standish, Maine, USA (Y.M. Brooks, B. Gryskwicz, S. Sheehan, S. Piers, S. McNeil, J. Chase, D. Webber, D. Borys, M. Hilton, D. Robinson, E.K. Lesher, R. Wilson, M. Goodwin, M. Pardales); Centers for Disease Control and Prevention, Atlanta, Georgia, USA (P. Mahale); Maine Center for Disease Control and Prevention, Augusta, Maine, USA (P. Mahale, S. Sears, E. Smith); University of Southern Maine, Portland, Maine, USA (E. Smith)

DOI: https://doi.org/10.3201/eid2712.211199

[1]Current affiliation: St. Catherine University, St. Paul, Minnesota, USA.

Each week, ≈100 students were randomly selected for individual surveillance testing by reverse transcription PCR. We instituted expanded surveillance testing for students living in residence halls with detectable RNA in grab samples or served by lift stations that had increased RNA concentrations.

Affected students were isolated or quarantined according to guidelines from the Centers for Disease Control and Prevention (*6*,*7*). COVID-19 outbreak investigations by the Maine Center for Disease Control and Prevention (Augusta, Maine, USA) end 28 days (2 infectious periods) after the specimen collection date of the last identified case. All residential students were tested for SARS-CoV-2 upon outbreak identification, beginning on day 25 for the first outbreak and day 81 for the second outbreak. Widespread testing among students continued weekly until all students had negative test results for 2 successive rounds during the outbreak period.

On day 18, we detected SARS-CoV-2 RNA from the wastewater discharge of hall F and both lift stations, preceding an outbreak on days 21–58 (Figure, panels A, B). By day 22, RNA concentrations in both lift stations increased by >1 $\log_{10}$; subsequently, concentrations decreased by >1 $\log_{10}$ by day 33 for L3 and day 40 for L1 (Figure, panel B). On day 21, expanded individual surveillance testing of half of the students living in hall F identified 2 COVID-19 cases (Figure, panels C, D). Widespread surveillance testing beginning on day 22 identified 6 additional cases in hall F, 1 case in hall D, and 1 case in hall E (Figure, panel C). In response, the college implemented remote learning during days 22–36.

Students returned to their residence halls from quarantine or isolation on days 21–45; we observed an increase of SARS-CoV-2 RNA in L3 on days 40–46 (Figure, panel B). We detected RNA in grab samples from hall D on days 45 and 53 and hall F on days 50 and 53 (Figure, panel A); however, concentrations were undetectable in L3 on days 49–70 (Figure, panel B). On day 53, individual surveillance testing of all students in hall F did not identify any COVID-19 cases (Figure, panels C, D).

From days 70 to 82, SARS-CoV-2 RNA concentrations in L3 increased by >1 $\log_{10}$. A second outbreak occurred during days 78–92. Expanded surveillance testing of all students in hall B identified 3 COVID-19 cases, prompting an outbreak investigation. During days 83–89, widespread testing of all students detected 7 additional COVID-19 cases in hall B, 1 case in hall C, and 1 case in hall E (Figure, panel C). The first COVID-19 case in hall E was discovered on day

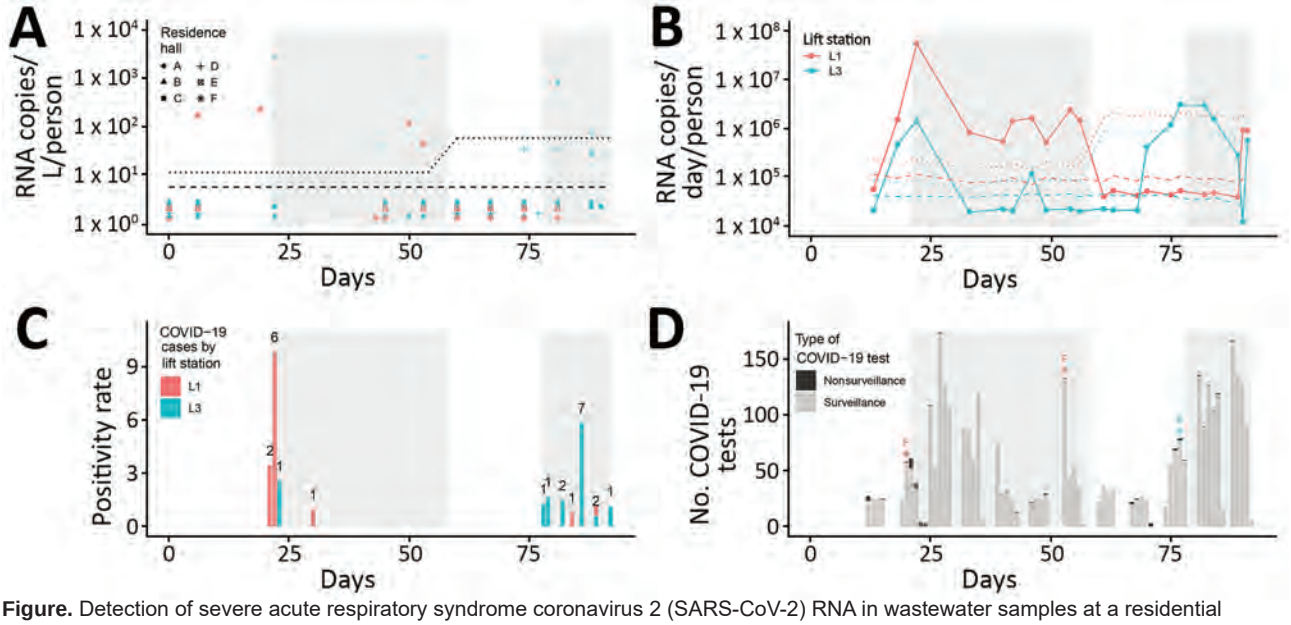

Figure. Detection of severe acute respiratory syndrome coronavirus 2 (SARS-CoV-2) RNA in wastewater samples at a residential college, Maine, USA, August–November 2020. A) Grab samples from 6 residence halls (i.e., A–F). B) 24-hour composite samples from 2 lift stations: L1 for halls E–F and L3 for halls A–D. Dashed lines indicate theoretical limit of detection; dotted lines indicate limit of quantification. These limits were dependent on flow rate (B only) and population served for each sample. Data points below dashed lines indicate undetected concentrations of SARS-CoV-2 RNA and are recorded at one-half the limit of quantification (*5*). Data points between dashed and dotted lines indicates detectable but nonquantifiable concentrations of SARS-CoV-2 RNA and are recorded at one half the limit of quantification. C) Daily positivity rate of COVID-19 tests. The number above the bar indicates the number of positive cases. Positive results were typically received within 24 hours after administration of the diagnostic test. D) Total COVID-19 diagnostic tests, including surveillance and nonsurveillance tests. Letter and symbol indicate resident hall of affected student. Shaded areas indicate the days during which the college declared an active outbreak. COVID-19, coronavirus disease.

84, when SARS-CoV-2 RNA was undetectable in L1 (Figure, panel B). The discovery of 7 cases in hall B on day 86 indicated that transmission might be widespread. During days 88–92, the college instituted an exit strategy comprising remote learning and widespread surveillance testing of all students 48 hours before departing campus. On day 91, we detected SARS-CoV-2 RNA in L1 and identified 3 COVID-19 cases (1 in hall A, 1 in hall B, and 1 in hall E; Figure, panels B, C). We detected RNA in grab samples from hall D 4 days before the outbreak as well as during the outbreak and staged dismissal but did not identify any cases in hall D.

Conclusions

We found that a >1 $\log_{10}$ increase of SARS-CoV-2 RNA concentrations in composite samples from a lift station preceded 2 COVID-19 outbreaks at a college campus. RNA concentrations did not substantially increase during the outbreak even as more cases were discovered (Figure, panels B, C). Thus, wastewater surveillance is best used to discover the onset of outbreaks at a small college campus.

We hypothesized that detectable concentrations of SARS-CoV-2 RNA in the wastewater discharge in L1 on days 40–56 (Figure, panel B) were caused by residual shedding among recovering students who were no longer infectious, as described in clinical data (*8*,*9*). In addition, a study in Utah, USA, documented evidence of residual shedding in municipal wastewater systems after a decrease in reported cases (*2*). In L1, SARS-CoV-2 RNA was undetectable 26 days in the wastewater system after the last known case was identified. The decrease of RNA to undetectable levels was consistent with the previously reported median fecal shedding time of 25 days among hospitalized COVID-19 patients (*9*).

In total, 9 of 10 confirmed patients during the first outbreak and 10 of 15 patients during the second outbreak lived in residence halls where RNA was present in grab samples collected ≤7 days before diagnosis. Similarly, a study at a large college campus found the presence of RNA in grab samples from residence halls had 79.9% positive predictive value of COVID-19 cases within 4 days of collection (*10*). The RNA in 4 grab samples from halls D and F during days 45–53 could be from visitors recovering or actively infectious with SARS-CoV-2; this ambiguity is a limitation of wastewater surveillance. We did not evaluate the magnitude of the RNA concentrations in the grab samples because those samples represent RNA loading in the wastewater flow only at the time of sampling.

In conclusion, wastewater surveillance can indicate changes in SARS-CoV-2 transmission in the student population at a small residential college. Wastewater surveillance can quickly identify outbreaks, localize the detection of COVID-19 cases, and inform the management of resources for clinical surveillance testing.

Acknowledgments

We thank Eilidh Sidaway and Brianna Shelley for laboratory support.

The Saint Joseph's College of Maine Pandemic Response team financially supported this project.

About the Author

Dr. Brooks is an assistant professor at Saint Joseph's College of Maine, Standish, Maine, USA. Her research interests include the sources and persistence of fecal pollution in drinking water, recreational waters, and wastewater, as well as its potential effects on human health.

References:

1. Ahmed W, Angel N, Edson J, Bibby K, Bivins A, O'Brien JW, et al. First confirmed detection of SARS-CoV-2 in untreated wastewater in Australia: a proof of concept for the wastewater surveillance of COVID-19 in the community. Sci Total Environ. 2020;728:138764. https://doi.org/10.1016/j.scitotenv.2020.138764
2. Weidhaas J, Aanderud ZT, Roper DK, VanDerslice J, Gaddis EB, Ostermiller J, et al. Correlation of SARS-CoV-2 RNA in wastewater with COVID-19 disease burden in sewersheds. Sci Total Environ. 2021;775:145790. https://doi.org/10.1016/j.scitotenv.2021.145790
3. Gibas C, Lambirth K, Mittal N, Juel MAI, Barua VB, Roppolo Brazell L, et al. Implementing building-level SARS-CoV-2 wastewater surveillance on a university campus. Sci Total Environ. 2021;782:146749. https://doi.org/10.1016/j.scitotenv.2021.146749
4. Scott LC, Aubee A, Babahaji L, Vigil K, Tims S, Aw TG. Targeted wastewater surveillance of SARS-CoV-2 on a university campus for COVID-19 outbreak detection and mitigation. Environ Res. 2021;200:111374. https://doi.org/10.1016/j.envres.2021.111374
5. Centers for Disease Control and Prevention. Wastewater surveillance data reporting and analytics. 2021 [cited 2020 Sep 5]. https://www.cdc.gov/healthywater/surveillance/wastewater-surveillance/data-reporting-analytics.html
6. Centers for Disease Control and Prevention. Ending home isolation for persons with COVID-19 not in healthcare settings. 2021 [cited 2020 Sep 20]. https://www.cdc.gov/coronavirus/2019-ncov/hcp/disposition-in-home-patients.html
7. Centers for Disease Control and Prevention. If you are sick or caring for someone. 2020 [cited 2020 Sep 20]. https://www.cdc.gov/coronavirus/2019-ncov/if-you-are-sick/index.html
8. Wölfel R, Corman VM, Guggemos W, Seilmaier M, Zange S, Müller MA, et al. Virological assessment of hospitalized

patients with COVID-2019. Nature. 2020;581:465–9. https://doi.org/10.1038/s41586-020-2196-x
9. Wang X, Zheng J, Guo L, Yao H, Wang L, Xia X, et al. Fecal viral shedding in COVID-19 patients: clinical significance, viral load dynamics and survival analysis. Virus Res. 2020;289:198147. https://doi.org/10.1016/j.virusres.2020.198147
10. Betancourt WQ, Schmitz BW, Innes GK, Prasek SM, Pogreba Brown KM, Stark ER, et al. COVID-19 containment on a college campus via wastewater-based epidemiology, targeted clinical testing and an intervention. Sci Total Environ. 2021;779:146408. https://doi.org/10.1016/j.scitotenv.2021.146408

Address for correspondence: Yolanda M. Brooks, Saint Joseph's College of Maine, 278 Whites Bridge Rd, Standish, ME 04084, USA; email: ybrooks@sjcme.edu

SARS-CoV-2–Specific Antibodies in Domestic Cats during First COVID-19 Wave, Europe

Claudia Schulz,[1] Byron Martina,[1] Monica Mirolo, Elisabeth Müller, Ruth Klein, Holger Volk, Herman Egberink, Mariana Gonzalez-Hernandez, Franziska Kaiser, Maren von Köckritz-Blickwede, Albert Osterhaus

We conducted a severe acute respiratory syndrome coronavirus 2 antibody seroprevalence study among >2,000 domestic cats from 4 countries during the first coronavirus disease wave in Europe. We found 4.4% seroprevalence using a virus neutralization test and 4.3% using a receptor-binding domain ELISA, demonstrating probable human-to-cat transmission.

Severe acute respiratory syndrome coronavirus 2 (SARS-CoV-2), the cause of the ongoing coronavirus disease (COVID-19) pandemic, causes high rates of illness and death among humans. SARS-CoV-2 is a newly recognized member of the genus *Betacoronavirus*, family *Coronaviridae*, that infects humans. An early serosurvey among domestic cats in Wuhan, China, during January–March 2020 reported 14.7% seropositivity (*1*). Experimental infections demonstrated susceptibility to SARS-CoV-2 infection in cats and other carnivore species, such as ferrets (*Mustela putorius furo*), minks (*Neovison vison*), and to a lesser extent domestic dogs (*2*,*3*), and confirmed anecdotal observations of naturally occurring human-to-animal transmissions (*4*,*5*). Respiratory and gastrointestinal signs were observed in SARS-CoV-2–infected cats (*6*–*8*). We conducted a seroprevalence study for SARS-CoV-2–specific antibodies among domestic cats in Europe during and after the first COVID-19 pandemic wave, using a plaque-reduction virus neutralization test (VNT) and a SARS-CoV-2 receptor-binding domain–specific ELISA (RBD-ELISA).

Author affiliations: University of Veterinary Medicine Hannover, Hannover, Germany (C. Schulz, M. Mirolo, H. Volk, M. Gonzalez-Hernandez, F. Kaiser, M. von Köckritz-Blickwede, A. Osterhaus); Artemis One Health Research Foundation, Delft, the Netherlands (B. Martina, M. Mirolo); LABOklin, Kissingen, Germany (E. Müller, R. Klein); Utrecht University Faculty of Veterinary Medicine, Utrecht, the Netherlands (H. Egberink)

DOI: https://doi.org/10.3201/eid2712.211252

The Study

We analyzed serum samples collected from 2,160 domestic cats during April–June 2020. Samples had been sent to a veterinary diagnostic laboratory (LABOklin; Kissingen, Germany) for diagnostic purposes unrelated to suspicion of SARS-CoV-2 infection (*9*). Samples were from 1,136 cats in Germany, 331 in the United Kingdom, 333 in Italy, and 360 in Spain. Among 1,799 samples with demographic data, cats ranged from 0.1–23 years of age (median and mean age 11 years). We estimated a minimum of 300 total samples per location to enable a realistic estimation for each location. To confirm specificity of the assays to detect SARS-CoV-2–specific antibodies, we included 25 prepandemic cat serum samples and 25 serum samples from cats that tested positive for feline coronavirus/feline infectious peritonitis (FCoV/FIP) by NovaTec VetLine (Novatec Immundiagnostica GmbH, https://www.novatec-id.com), a commercial antibody test, in the screening.

We tested all serum samples by VNT, as previously described (*10*). We considered serum samples positive when titers were >20, expressed as the reciprocal of the dilution that gave >80% reduction of stained cells in the plaque reduction neutralization test ($PRNT_{80}$) (Appendix, https://wwwnc.cdc.gov/EID/article/27/12/21-1252-App1.pdf).

We also tested serum samples with an indirect ELISA we developed and validated inhouse. We used an ELISA previously used for detecting SARS-CoV-2 RBD antibodies in human serum (*11*) and replaced the anti-human IgG conjugate with an anti-cat IgG conjugate (Appendix).

We evaluated performance characteristics of the cat ELISA-RBD by using Pearson correlation of the results obtained by ELISA-RBD and Gaussian distribution analyses for the VNT. We also calculated

[1]These authors contributed equally to this article.

Table 1. Overall VNT SARS-CoV-2 seroprevalence in cats by country during the first pandemic wave, Europe, April–August 2020*

Location	No. tested	No. positive	% Positive (95% CI†)
Germany	1,136	48	4.2 (3.1–5.6)
United Kingdom	331	11	3.3 (1.7–5.9)
Italy	333	14	4.2 (2.3–7.0)
Spain	360	23	6.4 (4.1–9.4)
Total	2,160	96	4.4 (3.6–5.4)

*Seroprevalence determined by virus neutralization test (VNT). Similar results were found with RBD-ELISA, 4.3% (96/2,160; 95% CI 3.6%–5.4%) were seropositive (Table 2). RBD-ELISA, receptor-binding domain–specific ELISA; SARS-CoV-2, severe acute respiratory syndrome coronavirus 2; VNT, virus neutralization test.
†Calculated by using 2-sided exact binomial test in R (R Foundation for Statistical Computing, https://www.r-project.org).

diagnostic sensitivity and specificity of the ELISA-RBD compared with VNT. We conducted data analyses using R (R Foundation for Statistical Computing, https://www.r-project.org) and Prism version 9 (GraphPad Software Inc., https://www.graphpad.com). We calculated SARS-CoV-2 seroprevalence in cats separately for each country.

We found overall SARS-CoV-2 seroprevalence among cats was 4.2% in Germany, 3.3% in the United Kingdom, 4.2% in Italy, and 6.4% in Spain (Table 1; Figure). Among all 2,160 cat serum samples tested, 96 (4.4%, 95% CI 3.6%–5.4%) were positive by VNT and 92 (4.3%, 95% CI 3.4%–5.2%) by RBD-ELISA. The RBD-ELISA showed a diagnostic sensitivity of 90.6% (95% CI 90.0%–91.2%) and specificity of 99.8% (95% CI 99.8%–99.8%) compared with VNT (Table 2). Furthermore, correlation (r = 0.9, 95% CI 0.9–0.9) and Gaussian distribution analyses (r^2>0.7) revealed high agreement between VNT and RBD-ELISA sensitivities. All 25 prepandemic serum samples and 25 FCoV/FIP-positive samples tested SARS-CoV-2–negative in both the VNT and RBD-ELISA (data not shown), confirming the specificity of the assay for measuring SARS-CoV-2–specific antibodies.

Our study of domestic cat serum from 4 selected countries showed that during the first COVID-19 wave in Europe, >4% of domestic cats had been infected with SARS-CoV-2, probably through their contacts with infected humans. Because serum samples were sent to the veterinary diagnostic laboratory for conditions unrelated to a suspected SARS-CoV-2 infection, our data might not fully represent the overall seropositivity of the domestic cat population in Europe.

We used a VNT and an RBD-ELISA based on the original SARS-CoV-2 wild-type isolate (Wuhan-Hu-1, GenBank accession no. MN908947.3). The RBD-ELISA proved to have a high sensitivity and specificity compared with the VNT (Table 2), but 5 low-titer (titer = 20) VNT-positive samples remained undetected by the RBD-ELISA. These samples might have remained undetected because of the high specificity of RBD-ELISA, which detects antibodies toward the single spike protein ectodomain. Unlike RBD-ELISA, VNT might identify a broader range of virus neutralizing antibodies, including those directed against other domains of the spike protein. Of note, the only correlation of virus protection we have to date is virus neutralization, which apparently correlates well with RBD-ELISA positivity. For serologic screening and for individual diagnostic testing of domestic cats, the RBD-ELISA could replace the VNT, thus avoiding

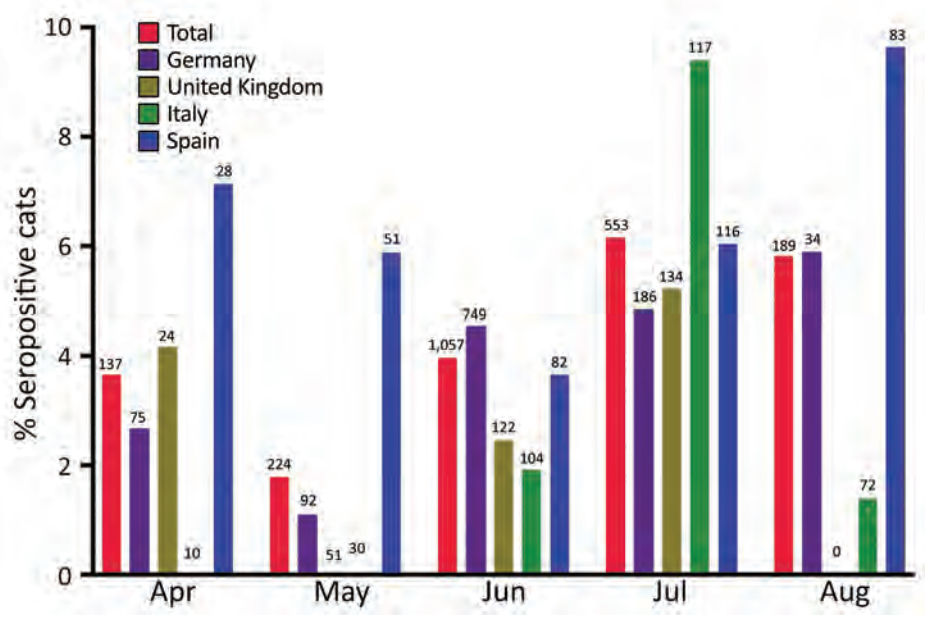

Figure. Overall seroprevalence of severe acute respiratory syndrome coronavirus 2 neutralizing antibodies in 2,160 domestic cats, by month and country, during the first coronavirus disease pandemic wave, Europe, April–August 2020. Numerals at the top of each column represent the number of samples collected. Seroprevalence rates peaked in July or August at ≤9.6% (95% CI 4.25%–18.11%) in Spain (Tables 1, 2).

the use of live SARS-CoV-2 under Biosafety Level 3 laboratory conditions. We further confirmed specificities of the VNT and RBD-ELISA by showing that prepandemic and FCoV/FIP-positive cat serum samples were negative in both assays. This finding excluded the detection of cross-reactive antibodies against feline alphacoronaviruses (*4*) and alphacoronaviruses of other animal species that might infect cats (*4*,*12*). Our data contrast a heavily affected area in China at the onset of the pandemic from which seropositivity levels of domestic cats ranged ≤15% (*1*), although those results were from relatively fewer tested cats and used a different assay.

Conclusions

During the first COVID-19 pandemic wave, reported seroprevalence levels in domestic cats ranged from 0.4% in the Netherlands (*4*) to 23% among cats in COVID-19–positive households in France (*13*). Similar seroprevalence levels in cats and humans in the same areas found by us and others suggest that in the absence of another known source (*4*,*13*; C. Schulz, unpublished data) (Appendix Table), SARS-CoV-2 infections in cats are most likely due to human-to-cat contact transmission.

Most natural SARS-CoV-2 infections of cats appear to run a mild or subclinical course, with respiratory or gastrointestinal clinical signs reported in confirmed natural infections (*6*–*8*). Evidence from experimental studies suggests that cats are susceptible to SARS-CoV-2 infection and can maintain the virus within a cat population and spill the infection backward or forward to other species (*2*,*3*,*14*). However, no evidence of cat-to-human transmission, nor of cat-specific mutations or variants of SARS-CoV-2, has been detected thus far (*8*,*12*,*15*). This finding contrasts reports on minks kept in farms, where mink-to-human spillback infections and mink-specific mutations have been reported (*5*). Although no evidence currently suggests that domestic cats play a role in the epidemiology of human SARS-CoV-2 infection, clinicians and veterinary practitioners should recommend that SARS-CoV-2–infected persons avoid close contact with their domestic cats and practice the same nonpharmaceutical prevention measures toward cats as they do to prevent human-to-human infection.

This study was supported in part by the Ministry of Science and Culture of Lower Saxony in Germany (grant no. 14-76103-184 CORONA-15/20). This publication was supported by the DFG and the University of Veterinary Medicine Hannover Foundation within the funding program Open Access Publishing.

Table 2. Comparison of diagnostic sensitivity and specificity of the RBD-ELISA and VNT in a study of SARS-CoV-2 seroprevalence among domestic cats during the first pandemic wave, Europe, April–August 2020*

Test results	Value
RBD-ELISA sensitivity, % (95% CI)	90.6 (90.0–91.2)
RBD-ELISA specificity, % (95% CI)	99.8 (99.8–99.8)
No. positive (%; 95% CI), n = 2,160	
RBD-ELISA and VNT	87 (4.0; 3.2–4.9)
RBD-ELISA only	92 (4.3; 3.5–5.2)
VNT only	96 (4.4; 3.6–5.4)

*A total of 5 samples were positive with RBD-ELISA and negative with VNT; 9 samples were positive with VNT but negative with RBD-ELISA. RBD-ELISA, receptor-binding domain–specific ELISA; SARS-CoV-2, severe acute respiratory syndrome coronavirus 2; VNT, virus neutralization test.

About the Author

Dr. Schulz is a postdoctoral researcher at University of Veterinary Medicine Hannover, Hannover, Germany. Her research interests include the pathogenesis and epidemiology of emerging and vectorborne diseases. Dr. Martina is a senior researcher at Artemis One Health Research Foundation, Delft, the Netherlands. His research interests include the pathogenesis of and intervention strategies against emerging virus infections.

References

1. Zhang Q, Zhang H, Gao J, Huang K, Yang Y, Hui X, et al. A serological survey of SARS-CoV-2 in cat in Wuhan. Emerg Microbes Infect. 2020;9:2013–9. https://doi.org/10.1080/22221751.2020.1817796
2. Bosco-Lauth AM, Hartwig AE, Porter SM, Gordy PW, Nehring M, Byas AD, et al. Experimental infection of domestic dogs and cats with SARS-CoV-2: pathogenesis, transmission, and response to reexposure in cats. Proc Natl Acad Sci U S A. 2020;117:26382–8. https://doi.org/10.1073/pnas.2013102117
3. Shi J, Wen Z, Zhong G, Yang H, Wang C, Huang B, et al. Susceptibility of ferrets, cats, dogs, and other domesticated animals to SARS–coronavirus 2. Science. 2020;368:1016–20. https://doi.org/10.1126/science.abb7015
4. Zhao S, Schuurman N, Li W, Wang C, Smit LAM, Broens EM, et al. Serologic screening of severe acute respiratory syndrome coronavirus 2 infection in cats and dogs during first coronavirus disease wave, the Netherlands. Emerg Infect Dis. 2021;27:1362–70. https://doi.org/10.3201/eid2705.204055
5. European Centre for Disease Prevention and Control. Detection of new SARS-CoV-2 variants related to mink–12 November 2020 [cited 2021 May 28]. https://www.ecdc.europa.eu/sites/default/files/documents/RRA-SARS-CoV-2-in-mink-12-nov-2020.pdf
6. Sailleau C, Dumarest M, Vanhomwegen J, Delaplace M, Caro V, Kwasiborski A, et al. First detection and genome sequencing of SARS-CoV-2 in an infected cat in France. Transbound Emerg Dis. 2020;67:2324–8. https://doi.org/10.1111/tbed.13659
7. Garigliany M, Van Laere AS, Clercx C, Giet D, Escriou N, Huon C, et al. SARS-CoV-2 natural transmission from human to cat, Belgium, March 2020. Emerg Infect Dis. 2020;26:3069–71. https://doi.org/10.3201/eid2612.202223

8. Hosie MJ, Epifano I, Herder V, Orton RJ, Stevenson A, Johnson N, et al.; COVID-19 Genomics UK (COG-UK) consortium Detection of SARS-CoV-2 in respiratory samples from cats in the UK associated with human-to-cat transmission. Vet Rec. 2021;188:e247. https://doi.org/10.1002/vetr.247
9. Nørgaard SK, Vestergaard LS, Nielsen J, Richter L, Schmid D, Bustos N, et al. Real-time monitoring shows substantial excess all-cause mortality during second wave of COVID-19 in Europe, October to December 2020. Euro Surveill. 2021;26:2002023. PubMed https://doi/org/10.2807/1560-7917.ES.2021.26.1.2002023
10. Wang C, Li W, Drabek D, Okba NMA, van Haperen R, Osterhaus ADME, et al. A human monoclonal antibody blocking SARS-CoV-2 infection. Nat Commun. 2020;11:2251. PubMed https://doi.org/10.1038/s41467-020-16256-y
11. Okba NMA, Müller MA, Li W, Wang C, GeurtsvanKessel CH, Corman VM, et al. Severe acute respiratory syndrome coronavirus 2–specific antibody responses in coronavirus disease patients. Emerg Infect Dis. 2020;26:1478–88. https://doi.org/10.3201/eid2607.200841
12. Hosie MJ, Hofmann-Lehmann R, Hartmann K, Egberink H, Truyen U, Addie DD, et al. Anthropogenic infection of cats during the 2020 COVID-19 pandemic. Viruses. 2021;13:185. https://doi.org/10.3390/v13020185
13. Fritz M, Rosolen B, Krafft E, Becquart P, Elguero E, Vratskikh O, et al. High prevalence of SARS-CoV-2 antibodies in pets from COVID-19+ households. One Health. 2021;11:100192. https://doi.org/10.1016/j.onehlt.2020.100192
14. Halfmann PJ, Hatta M, Chiba S, Maemura T, Fan S, Takeda M, et al. Transmission of SARS-CoV-2 in domestic cats. N Engl J Med. 2020;383:592–4. https://doi.org/10.1056/NEJMc2013400
15. Barrs VR, Peiris M, Tam KWS, Law PYT, Brackman CJ, To EMW, et al. SARS-CoV-2 in quarantined domestic cats from COVID-19 households or close contacts, Hong Kong, China. Emerg Infect Dis. 2020;26:3071–4. https://doi.org/10.3201/eid2612.202786

Address for correspondence: Albert Osterhaus, Research Center for Emerging Infections and Zoonoses, University of Veterinary Medicine Hannover, Buenteweg 17, 30559 Hannover, Germany; email: albert.osterhaus@tiho-hannover.de

etymologia revisited

Zika [zēkə] Virus

Originally published in June 2014

Zika virus is a mosquito-borne positive-sense, single-stranded RNA virus in the family *Flaviviridae*, genus *Flavivirus* that causes a mild, acute febrile illness similar to dengue. In 1947, scientists researching yellow fever placed a rhesus macaque in a cage in the Zika Forest (*zika* meaning "overgrown" in the Luganda language), near the East African Virus Research Institute in Entebbe, Uganda. A fever developed in the monkey, and researchers isolated from its serum a transmissible agent that was first described as Zika virus in 1952. It was subsequently isolated from a human in Nigeria in 1954. From its discovery until 2007, confirmed cases of Zika virus infection from Africa and Southeast Asia were rare. In 2007, however, a major epidemic occurred in Yap Island, Micronesia. More recently, epidemics have occurred in Polynesia, Easter Island, the Cook Islands, and New Caledonia.

Sources

1. Dick GW, Kitchen SF, Haddow AJ. Zika virus. I. Isolations and serological specificity. Trans R Soc Trop Med Hyg. 1952;46:509–20. http://dx.doi.org/10.1016/ 0035-9203(52)90042-4
2. Hayes EB. Zika virus outside Africa. Emerg Infect Dis. 2009; 15:1347–50. http://dx.doi.org/10.3201/eid1509.090442
3. MacNamara FN. Zika virus: a report on three cases of human infection during an epidemic of jaundice in Nigeria. Trans R Soc Trop Med Hyg. 1954;48:139–45. http://dx.doi.org/10.1016/0035-9203(54)90006-1
4. Murphy JD. Luganda–English dictionary. Washington (DC): The Catholic University of America Press; 1972.

https://wwwnc.cdc.gov/eid/article/20/6/et-2014_article

Increased Incidence of Melioidosis in Far North Queensland, Queensland, Australia, 1998–2019

Simon Smith, Peter Horne, Sally Rubenach, Richard Gair, James Stewart, Lee Fairhead, Josh Hanson

During January 1998–December 2019, the annual incidence of melioidosis in Far North Queensland, Queensland, Australia, more than doubled. Because climate and prevalence of predisposing medical conditions remained stable during that time, we hypothesize that the increased incidence was caused by urban expansion and increased construction, resulting in greater exposure to *Burkholderia pseudomallei*.

Burkholderia pseudomallei, an environmental gram-negative bacterium, causes the disease melioidosis. Although infection is frequently asymptomatic, melioidosis may be rapidly fatal for patients with underlying conditions that increase the risk for invasive disease. Modeling suggests that *B. pseudomallei* is ubiquitous in the tropics and that the global burden of disease is expected to rise (*1*). Indeed, increased melioidosis incidence has been documented in some countries (*2*). Although this increase may be associated with improved diagnostic capacity, it may also be explained by a growing burden of predisposing concurrent medical conditions or by greater *B. pseudomallei* exposure from environmental disruption (*3*,*4*). Changing weather patterns also have the potential to increase melioidosis incidence (*5*).

B. pseudomallei is endemic to Far North Queensland (FNQ), a region in the northernmost part of the state of Queensland, Australia (Figure 1). Incidence of melioidosis in the Torres Strait Islands in the region's north is among the highest reported in published series of melioidosis cases in Australia (*4*,*6*). During the past 20 years, the FNQ population has grown rapidly, predominantly in the city of Cairns, the region's major industrial hub, and in the nearby towns (Cairns area, in and around Cairns). This growth has necessitated substantial expansion of local infrastructure, including 2-phase development of a large motorway on the city's southern outskirts during 2011–2017. Surveillance data suggest that this development coincided with a marked increase in the local incidence of melioidosis, primarily in the Cairns area. We aimed to determine if there was any temporospatial association between the motorway construction and the increasing incidence of melioidosis in the region or if there were other possible explanations for any observed change, with a particular focus in the Cairns area.

Author affiliations: Cairns Hospital, Cairns, Queensland, Australia (S. Smith, J. Stewart, L. Fairhead, J. Hanson); Tropical Public Health Services, Cairns (P. Horne, S. Rubenach, R. Gair); University of New South Wales, Sydney, New South Wales, Australia (J. Hanson)

DOI: https://doi.org/10.3201/eid2712.211302

The Study

Cairns Hospital is the sole public microbiological service provider for FNQ, a region of >380,000 km^2 (*7*). We reviewed all culture-confirmed cases of *B. pseudomallei* infection identified in the hospital's laboratory during January 1, 1998–December 31, 2019. Clinical details of each case were recorded as described by J.D. Stewart et al. (*4*); predisposing conditions were diabetes mellitus (glycated hemoglobin ≥6.5%), hazardous alcohol use, chronic lung disease, chronic renal disease, and immunosuppression. We used data from the Australian Bureau of Statistics to calculate disease incidence and from the Australian Bureau of Meteorology to record local climatic factors including rainfall, temperatures, cloud cover, dew points, and cyclones. For our analyses we used Stata version 14.2 statistical software (https://www.stata.com) and determined trends over time by using an extension of the Wilcoxon rank-sum test and using year of presentation as a continuous variable (*8*). We constructed maps by using MapInfo Pro 2019 Geographic Information System software

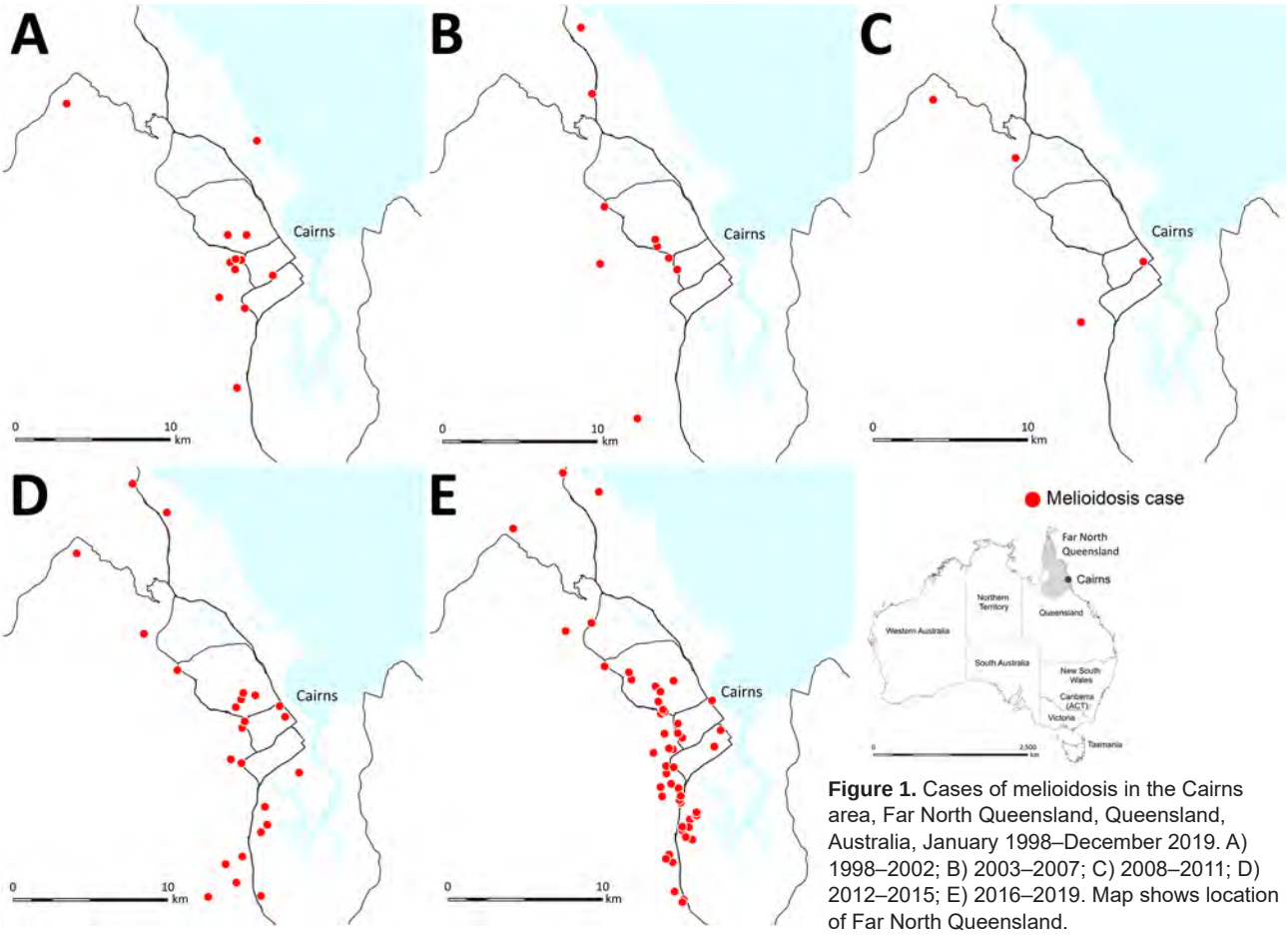

Figure 1. Cases of melioidosis in the Cairns area, Far North Queensland, Queensland, Australia, January 1998–December 2019. A) 1998–2002; B) 2003–2007; C) 2008–2011; D) 2012–2015; E) 2016–2019. Map shows location of Far North Queensland.

(https://support.precisely.com); in the absence of a clear occupational or recreational exposure, we used participants' residential addresses as the site of *B. pseudomallei* exposure. The study was approved by the Far North Queensland Human Research Ethics Committee (HREC/15/QCH/46-977).

A total of 297 cases of melioidosis were diagnosed during the study period, of which 284 were acquired from FNQ and included in our analysis. The mean annual incidence in FNQ increased from 4.0 (95% CI 2.7–5.2) cases/100,000 population during 1998–2002 to 9.9 (95% CI 4.9–14.9) cases/100,000 population

Table 1. Incidence, predisposing conditions, and outcomes of locally acquired melioidosis cases in Far North Queensland, Queensland, Australia, January 1998–December 2019

Variable	1998–2002	2003–2007	2008–2011	2012–2015	2016–2019	p value*
Far North Queensland population, mean	220,814	232,598	256,852	272,055	283,178	<0.001
No. cases	44	41	31	56	112	<0.001
Annual incidence, cases/100,000 population, mean (95% CI)	4.0 (2.7–5.2)	3.5 (1.8–5.2)	3.0 (0–6.2)	5.1 (0.6–9.7)	9.9 (4.9–14.9)	<0.001
Age, y, median (interquartile range)	46 (32–58)	52 (40–63)	51 (38–62)	49 (42–64)	55 (47–65)	0.001
Predisposing condition, %						
Any†	73	85	84	82	90	0.02
Diabetes mellitus	50	56	58	44	58	0.59
Hazardous alcohol use	34	39	45	46	31	0.60
Chronic lung disease	7	12	16	14	16	0.13
Chronic kidney disease	16	15	3	23	17	0.48
Immunosuppression	7	12	16	20	13	0.21
Bacteremia, %	70	68	77	77	68	0.85
Case-fatality rate, %	27	15	3	11	9	0.004

*p value for trend calculated by using annual data with year as a continuous variable.
†Incomplete access to patient charts from early in the study period is likely to lead to overestimation of the proportion of cases with no predisposing factor.

Table 2. Incidence, predisposing conditions, and outcomes of melioidosis cases near Cairns, Queensland, Australia, January 1998–December 2019

Variable	1998–2002	2003–2007	2008–2011	2012–2015	2016–2019	p value*
Cairns area population, mean	200,351	206,342	228,504	243,389	253,841	<0.001
No. cases	6	9	4	25	67	<0.001
Annual incidence, cases/100,000 population, mean (95% CI)	0.6 (0.1–1.1)	0.9 (0.1–1.6)	0.4 (0–0.9)	2.5 (0–5.8)	6.6 (3.0–10.2)	<0.001
Age, y, median (interquartile range)	45 (30–62)	65 (55–69)	49 (39–58)	56 (43–66)	56 (49–66)	0.56
Predisposing condition, %						
Any†	100	89	75	84	87	0.38
Diabetes mellitus	67	44	50	40	47	0.69
Hazardous alcohol use	67	22	75	40	28	0.046
Chronic lung disease	0	22	25	24	18	0.86
Chronic kidney disease	17	22	0	32	18	0.99
Immunosuppression	33	44	0	24	19	0.25
Bacteremia, %	67	100	100	84	72	0.18
Case-fatality rate, %	0	33	0	8	10	0.60

*p value for trend value calculated using annual data with year as a continuous variable
†Limited access to charts is likely to result in incomplete documentation of risk factors from early in the study period.

during 2016–2019 (p<0.001) (Table 1). In the Cairns area, incidence rose from 0.6 (95% CI 0.1–1.1) cases/100,000 population during 1998–2002 to 6.6 (95% CI 3.0–10.2) cases/100,000 population during 2016–2019 (p<0.001) (Table 2; Figure 1).

During the study period, the proportion of patients in FNQ with different predisposing conditions for melioidosis did not change. The proportion of bacteremic patients also remained stable (Table 1). The case-fatality rate declined during the study period (Table 1).

In the Cairns area, where increased incidence was more marked, the small increases in mean temperature, cloud cover, and dew points in the final period of the study did not reach statistical significance. During the study period, 14 cyclones came within 200 km of Cairns, but only 1 occurred during 2016–2019 (p = 0.86) (Appendix, https://wwwnc.cdc.gov/EID/article/27/12/21-1302-App1.pdf).

Of the 284 cases included in the study, 111 (39%) were in the Cairns area; only 3 of these patients reported having an occupation in construction. Before commencement of the southern motorway expansion in the Cairns area in 2011, only 1/19 (5%) cases in the Cairns area were within 1,000 m of the existing road and 2/19 (11%) were within 2,000 m. However, after January 2012, a total of 92/168 (55%) cases occurred in the Cairns area, of which 15/92 (16%) were within 1,000 m of the highway construction and 27/92 (29%) within 2,000 m (Figure 2).

Conclusions

The incidence of melioidosis in FNQ is rising, increasing during the study period by ≈10-fold in the Cairns area. The proportion of bacteremic patients has not changed, suggesting improved diagnosis. Similarly, we found no statistically significant change in climate or frequency of cyclones. The proportion of patients who had the common predisposing conditions remained similar. However, urban expansion may be contributing because almost a third of cases in the past 8 years of the study period occurred within 2,000 m of development of a large motorway. Of note, the motorway is built predominantly through alluvial plain soils with moderate clay content and poor drainage, which favor *B. pseudomallei* growth (*9*).

Increased rainfall, dew points, cloud cover, and temperatures have been associated with increased melioidosis cases; however, these climatic factors were stable over our study period (*5*). Cyclones have been linked to increased melioidosis cases; however, we did not observe that association in FNQ (*10*). Indeed, since 2015 when melioidosis incidence in the Cairns area sharply increased, there has been only 1 cyclone within 200 km of the area.

Why the rates of bacteremic melioidosis remain higher in FNQ than in other parts of Australia remains unclear (*11*). The higher rates may be partly explained by fewer diagnoses of cutaneous disease in rural and remote communities; however, skin swab samples are frequently taken to identify other pathogens, and skin and soft tissue *B. pseudomallei* infections are uncommon in urban areas, where most new cases have been identified (*12*). Virulence factors in local *B. pseudomallei* strains may contribute (*13*). Despite the increasing incidence, the overall case-fatality rate from melioidosis in FNQ decreased significantly during the study period, which can probably be explained by early recognition and prompt access to multimodal intensive care unit support.

Among the limitations of our study, data collection was predominantly retrospective; in addition, in the absence of clear inoculation with *B. pseudomallei*, we assumed residential addresses to be the sites of

exposure. Domestic gardens are a source of melioidosis in Australia, but it is possible that unrecorded patient movements may have resulted in exposure to *B. pseudomallei* elsewhere (*14*). Additional confounding factors that increase the risk for melioidosis (e.g., socioeconomic disadvantage) may help explain regional variations in incidence, although the local geographic distribution of this socioeconomic disadvantage has not substantially changed in the past 20 years (*15*). In conclusion, although host factors and climate continue to influence the risk of acquiring melioidosis, we hypothesize that urban expansion and construction in soils harboring *B. pseudomallei* may explain the recent rapid increase in Far North Queensland, Australia.

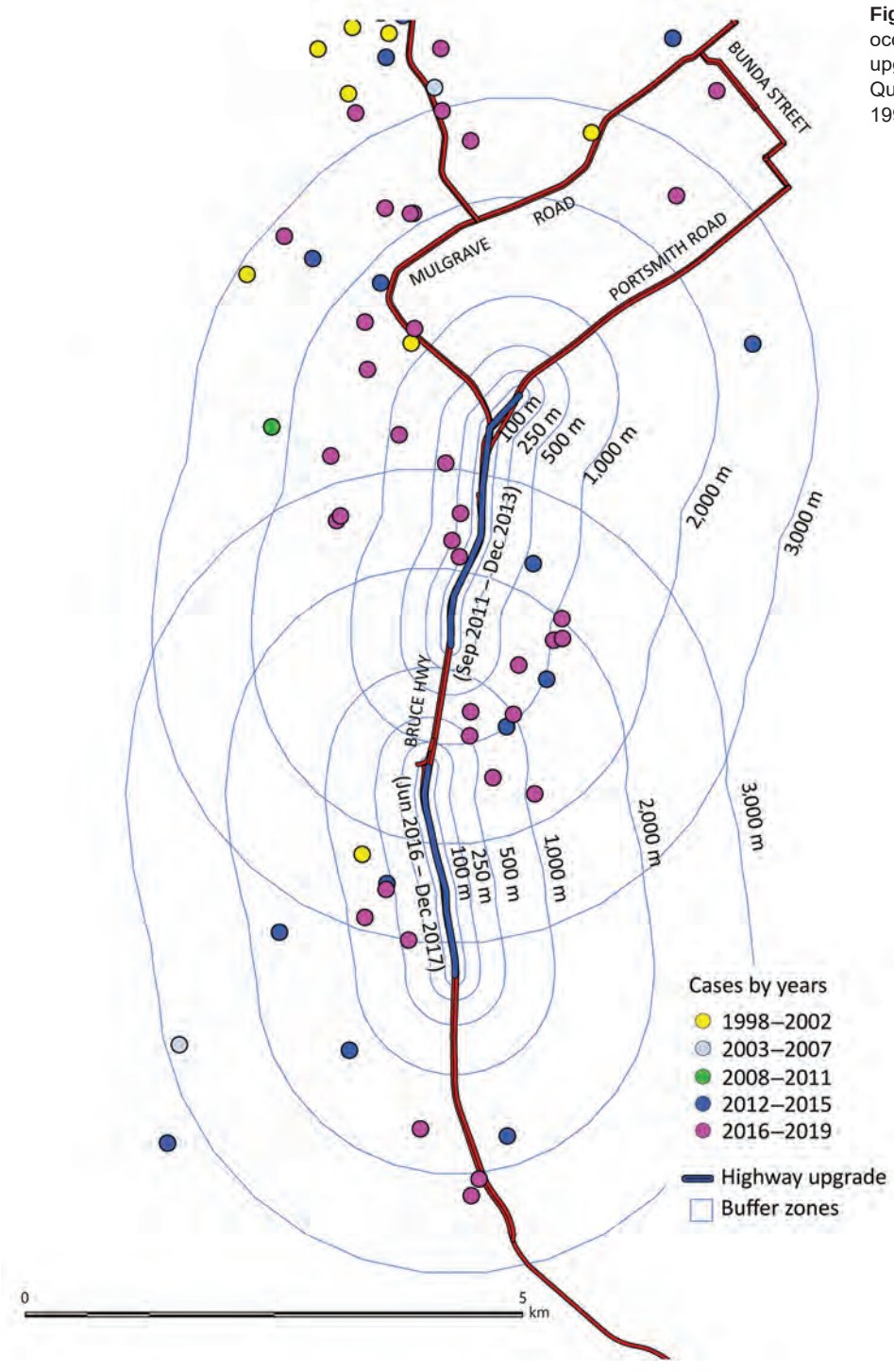

Figure 2. Cases of melioidosis occurring near to a motorway upgrade in southern Cairns, Far North Queensland, Queensland, Australia, 1998–2019.

About the Author

Dr. Smith is an infectious diseases and general internal medicine physician in Cairns, Queensland, Australia. His research interests include melioidosis, leptospirosis, and management of severe clinical manifestations of tropical diseases.

References

1. Limmathurotsakul D, Golding N, Dance DA, Messina JP, Pigott DM, Moyes CL, et al. Predicted global distribution of *Burkholderia pseudomallei* and burden of melioidosis. Nat Microbiol. 2016;1:15008. https://doi.org/10.1038/nmicrobiol.2015.8
2. Limmathurotsakul D, Wongratanacheewin S, Teerawattanasook N, Wongsuvan G, Chaisuksant S, Chetchotisakd P, et al. Increasing incidence of human melioidosis in northeast Thailand. Am J Trop Med Hyg. 2010;82:1113–7. https://doi.org/10.4269/ajtmh.2010.10-0038
3. Rachlin A, Mayo M, Webb JR, Kleinecke M, Rigas V, Harrington G, et al. Whole-genome sequencing of *Burkholderia pseudomallei* from an urban melioidosis hot spot reveals a fine-scale population structure and localised spatial clustering in the environment. Sci Rep. 2020;10:5443. https://doi.org/10.1038/s41598-020-62300-8
4. Stewart JD, Smith S, Binotto E, McBride WJ, Currie BJ, Hanson J. The epidemiology and clinical features of melioidosis in Far North Queensland: implications for patient management. PLoS Negl Trop Dis. 2017;11:e0005411. https://doi.org/10.1371/journal.pntd.0005411
5. Kaestli M, Grist EPM, Ward L, Hill A, Mayo M, Currie BJ. The association of melioidosis with climatic factors in Darwin, Australia: a 23-year time-series analysis. J Infect. 2016;72:687–97. https://doi.org/10.1016/j.jinf.2016.02.015
6. Hempenstall AJ, Smith S, Stanton D, Hanson J. Melioidosis in the Torres Strait Islands, Australia: exquisite interplay between pathogen, host, and environment. Am J Trop Med Hyg. 2019;100:517–21. https://doi.org/10.4269/ajtmh.18-0806
7. Queensland Government. 2019–2020 annual report [cited 2021 Jul 18]. https://www.parliament.qld.gov.au/documents/tableOffice/TabledPapers/2020/5720T394.pdf
8. Cuzick J. A Wilcoxon-type test for trend. Stat Med. 1985;4:87–90. https://doi.org/10.1002/sim.4780040112
9. Goodrick I, Todd G, Stewart J. Soil characteristics influencing the spatial distribution of melioidosis in Far North Queensland, Australia. Epidemiol Infect. 2018;146:1602–7. https://doi.org/10.1017/S0950268818001188
10. Stewart JD, Smith S, Hanson J. Melioidosis in Far North Queensland is not correlated with severe weather events. Med J Aust. 2017;207:394. https://doi.org/10.5694/mja16.01332
11. Currie BJ, Ward L, Cheng AC. The epidemiology and clinical spectrum of melioidosis: 540 cases from the 20 year Darwin prospective study. PLoS Negl Trop Dis. 2010;4:e900. https://doi.org/10.1371/journal.pntd.0000900
12. Guthridge I, Smith S, Horne P, Hanson J. Increasing prevalence of methicillin-resistant *Staphylococcus aureus* in remote Australian communities: implications for patients and clinicians. Pathology. 2019;51:428–31. https://doi.org/10.1016/j.pathol.2018.11.015
13. Young A, Tacon C, Smith S, Reeves B, Wiseman G, Hanson J. Case report: fatal pediatric melioidosis despite optimal intensive care. Am J Trop Med Hyg. 2017;97:1691–4. https://doi.org/10.4269/ajtmh.17-0650
14. Kaestli M, Harrington G, Mayo M, Chatfield MD, Harrington I, Hill A, et al. What drives the occurrence of the melioidosis bacterium *Burkholderia pseudomallei* in domestic gardens? PLoS Negl Trop Dis. 2015;9:e0003635. https://doi.org/10.1371/journal.pntd.0003635
15. Hanson J, Smith S, Stewart J, Horne P, Ramsamy N. Melioidosis-a disease of socioeconomic disadvantage. PLoS Negl Trop Dis. 2021;15:e0009544. https://doi.org/10.1371/journal.pntd.0009544

Address for correspondence: Simon Smith, Department of Medicine, Cairns Hospital, Cairns, QLD 4870, Australia; email: simon.smith2@health.qld.gov.au

Large-Scale Screening of Asymptomatic Persons for SARS-CoV-2 Variants of Concern and Gamma Takeover, Brazil

Douglas Adamoski,[1] Jaqueline Carvalho de Oliveira, Ana Claudia Bonatto, Roseli Wassem, Meri Bordignon Nogueira, Sonia Mara Raboni, Edvaldo da Silva Trindade, Emanuel Maltempi de Souza, SCB-UFPR COVID-19 team,[2] Daniela Fiori Gradia[1]

We performed a large-scale severe acute respiratory syndrome coronavirus 2 screening campaign using 2 PCR-based approaches, coupled with variant genotyping, aiming to provide a safer environment for employees of Federal University in Curitiba, Brazil. We observed the rapid spread of the Gamma variant of concern, which replaced other variants in <3 months.

Ongoing screening for active severe acute respiratory syndrome coronavirus 2 (SARS-CoV-2) infections, coupled with contact tracing, can efficiently reduce viral transmission within the community (*1*). However, as new and more transmissible variants emerge, an increased number of cases can be observed across affected regions. This increase demands immediate action, such as consistent, uninterrupted genomic surveillance for regular evaluation of vaccination approaches (*2*), to curb virus spread.

Brazil has reaped the consequences of lack of genomic surveillance in a context of high seroprevalence. The variant of concern (VOC) Gamma (B.1.1.28/P.1) emerged in the city of Manaus, Brazil, at a time when three quarters of the population had tested positive for antibodies; it proceeded to spread across the city (*3*). The Gamma variant was able to replace its predecessor, the variant of interest (VOI) B.1.1.28/P.2, previously the dominant lineage in the region (*4*).

Author affiliations: Brazilian Biosciences National Laboratory, Brazilian Center for Research in Energy and Materials, Campinas, Brazil (D. Adamoski); Universidade Federal do Paraná, Curitiba, Brazil (D. Adamoski, J. Carvalho de Oliveira, A.C. Bonatto, R. Wassem, M.B. Nogueira, S.M. Raboni, E.S. Trindade, E.M. de Souza, D.F. Gradia)

DOI: https://doi.org/10.3201/eid2712.211326

Routine SARS-CoV-2 mass screening programs of asymptomatic persons and follow-up genotyping of samples are necessary measures to control the number of cases and prevent further infection surges (*5*,*6*). Simplified approaches, such as multiplex quantitative PCR, provide a feasible, cost-effective way to discriminate samples and prioritize whole-genome sequencing efforts (*5*,*7*). To provide a safer environment for the university community, we performed a large-scale screening for SARS-CoV-2 infections and VOCs in the Federal University of Paraná (Curitiba, Brazil) community. The study was approved by the University Research Ethics Committee (approval no. CAAE: 31687620.2.0000.0096).

The Study

During October 10, 2020–May 24, 2021, asymptomatic and mildly symptomatic persons within the community of the Federal University of Paraná were called for voluntary participation through social media and email. Eligible participants were members of the academic community (students, technicians, professors, or outsourced employees) or their relatives (grandparents, parents, siblings, or children) or household members. Saliva samples were self-collected by using an individually wrapped plastic drinking straw, transferred to a prelabeled 2.0 mL microtube, and stored at 4°C. Samples were transported to the laboratory in <1 h; total turnaround time to results was <48 h.

Samples were homogenized and allowed to settle for 30 min or centrifuged for 2 min (2,000 × *g*). A quantity of 200 μL from each specimen was

[1]These authors were co–principal investigators.

[2]Members of the group are listed at the end of this article.

then pooled (*8*) in groups of 5. We performed RNA extraction by using an automated magnetic EXTRACTA–RNA and DNA Viral kit (Loccus Biotecnologia, https://loccus.com.br). We performed amplification in 2 ways: on a QuantStudio5 instrument (Thermo Fisher Scientific, https://www.thermofisher.com) using AllPlex nCov-2019 reverse transcription PCR Master Mix Kit (SeeGene, https://www.seegene.com) (*1*) or Molecular SARS-CoV-2 EDx (Bio-Manguinhos/FioCruz, https://www.bio.fiocruz.br) (*2*). If the pool rendered a positive result, we reprocessed samples individually.

We further evaluated positive samples by using 2 probe-based genotyping systems to detect VOCs. The first one was the Vogels et al. (*7*) multiplex approach to detect Spike Δ69–70 and Orf1a Δ3675–3677 deletions as an outcome for distinguishing Alpha, Beta, or Gamma and wild-type or other lineages (*7*). For this approach, we also included the Centers for Disease Control and Preventon N1 target and defined a cycle threshold (C_t) of <28 on this particular target to evaluate the gene dropouts.

The second approach involved 3 allelic discrimination TaqMan assays (Thermo Fisher Scientific). The proposed readout was P.1 (K417T, N501Y, and E484K), P.2 (only E484K), B.1.1.7 (only N501Y), B.1.351 (N501Y and E484K, failure for K417T assay), and wild-type or others for the absence of mutated alleles (*9*). The discriminating power of this second assay made it possible to distinguish the B1.1.28/P.2 from the wild-type and the Beta/Gamma variants. We performed both assays by using GoTaq Probe 1-Step reverse transcription quantitative PCR System (Promega, https://www.promega.com) in the same instrument.

A total of 16 collection dates were recorded; 12,558 examinations were processed (Table) from the 7,249 persons who attended because some participants engaged in >1 day of collection. The number of attendees per collection date ranged from 162 to 1,737. The overall prevalence rate was 1.28% (161/12,558). Comparing these numbers to cases in the state of Paraná by the epidemiologic week of diagnosis (Figure 1, panel A), we found prevalence similar to the prevalence rate at the beginning of the state's second wave of SARS-CoV-2 infections (Figure 1, panel A).

We also evaluated all SARS-CoV-2–positive cases by using multiplex and singleplex genotyping approaches (Figure 2). From all 161 positive cases evaluated, the Vogels et al. (*7*) multiplex assay was invalidated in 46 (28.6%) against 50 (31.1%) in a Thermo Fisher 3-assay allelic detection approach because of the high C_t values. Comparing the original C_t value of detection, performance depreciated in samples with C_t >30 (Figure 2, panel B), as stated in the Thermo Fisher manual. Nevertheless, all genotyped cases were concordant between the 2 assays, considering that the Vogels et al. (*7*) assay alone does not discriminate between wild-type and B1.1.28/P.2 VOI.

Table. Collection dates, engagement, and positivity rates for severe acute respiratory syndrome coronavirus 2 infection, Curitiba, Brazil

Date	Total tested	No. (%) positive
2020 Oct 2	275	0
2020 Oct 19	279	0
2020 Nov 6	510	6 (1.18)
2020 Nov 24	1,265	34 (2.69)
2020 Dec 8	1,070	17 (1.59)
2021 Jan 12	1,692	23 (1.36)
2021 Jan 26	1,737	14 (0.81)
2021 Feb 9	1,615	16 (0.99)
2021 Mar 29	196	1 (0.51)
2021 Apr 12	157	4 (2.55)
2021 Apr 20	872	2 (0.23)
2021 Apr 26	162	4 (2.47)
2021 May 4	884	12 (1.36)
2021 May 10	177	1 (0.56)
2021 May 18	1,431	20 (1.4)
2021 May 24	236	7 (2.97)
Total	12,558	161 (1.28)

Detection of the Gamma variant occurred on January 21, 2021, <2 weeks after the collapse of the healthcare system in Manaus. Prevalence of the Gamma variant was 9.1% on this date and increased to 42.9% 2 weeks later (Figure 1, panel B). A possible explanation for this scenario is the increased transmission of this variant in ≥20% compared with the wild-type transmission rate (*10*), which is supported by the observation of a reproduction number of 1.5 in Paraná (http://shiny.leg.ufpr.br/elias/covid19time) in the weeks before the death peak, the highest reproduction number observed during the pandemic. This increase in cases could be correlated with the subsequent collapse of the Curitiba city healthcare system and a surge of coronavirus disease deaths in the Paraná state, reaching values >5% in the subsequent weeks. A similar scenario was also observed in Manaus, the origin of the Gamma variant; both SARS-CoV-2 cases and excess of burials in the city reached their highest levels during the pandemic to that point (*4*). Two factors could explain those observed surges: increased lethality of the Gamma variant—which is not yet defined (*10*)—and the actual collapse of healthcare systems, leading to poorer patient support. When testing activities resumed after the healthcare collapse, all cases became Gamma variant, completely displacing B1.1.28/P.2 VOI and wild-type cases in 3 months.

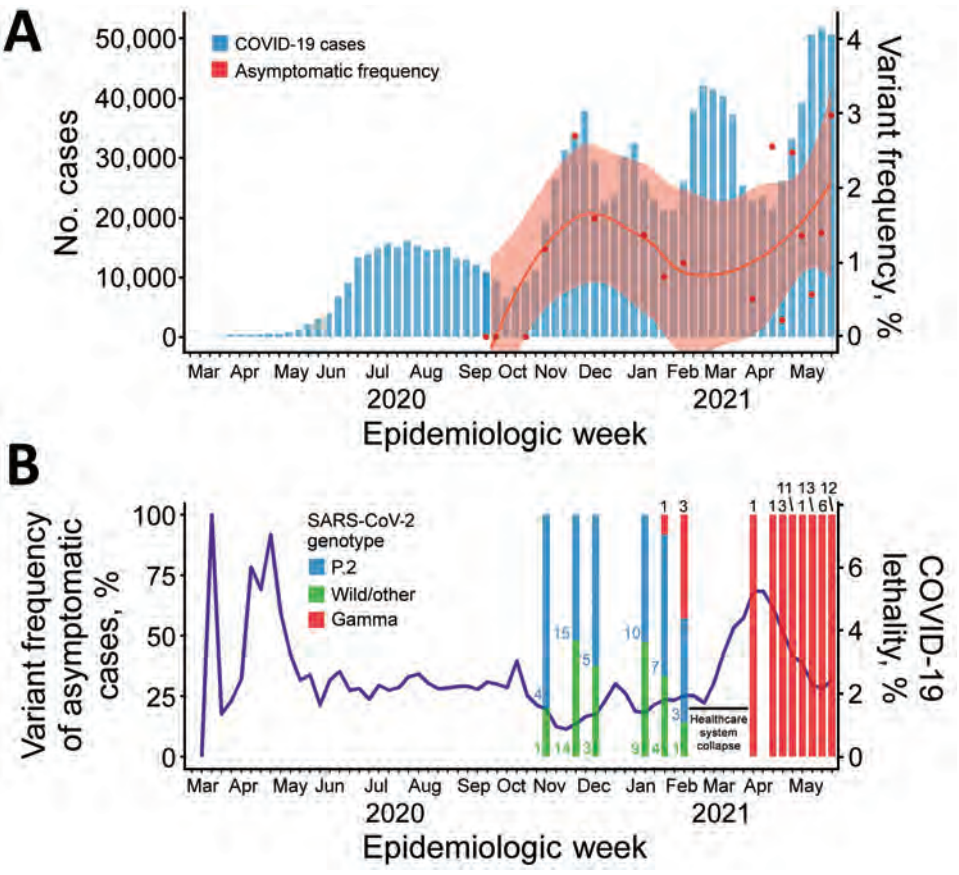

Figure 1. COVID-19 diagnoses asymptomatic and variant frequency, and lethality, Paraná state, Brazil. A) COVID-19 diagnoses in Paraná and Federal University of Paraná (Curitiba, Brazil) mass testing program positivity rates by epidemiologic week. Blue bars summarize positive cases in Paraná by diagnosis day notified to state surveillance system through February 15, 2021. Red dots represent the fraction of positive cases in all samples from mass screening collection at Federal University of Paraná, smoothed by locally estimated scatterplot smoothing in the red line; pink shading indicates SE from locally estimated scatterplot smoothing fit. B) Overall lethality of COVID-19 in Paraná (purple line) and variant prevalence among asymptomatic and mildly symptomatic cases, by epidemiologic week. Numbers represent the absolute quantity of cases for each variant. Scales for the y-axes differ substantially to underscore patterns but do not permit direct comparisons. COVID-19, coronavirus disease; SARS-CoV-2, severe acute respiratory syndrome coronavirus 2.

Conclusions

Analysis of saliva in pools as described in this study offers an inexpensive and easy-to-implement asymptomatic screening strategy. Thus, given the high rates of SARS-CoV-2 transmission, the risk for asymptomatic coronavirus disease spread and the importance of social distancing should continue to be stressed to the public until the vaccine is viable for large-scale application. Our mass testing program was intended to be accessible (every test was free-of-charge for the participant), reliable (all participants received their results and positive persons had a follow-up opportunity), and aimed to reach all social strata within the academic community (from professors to outsourced employees, which consisted mainly of socially, economically, and ethnically vulnerable groups), which are key characteristics of a strong mass testing system (*11*).

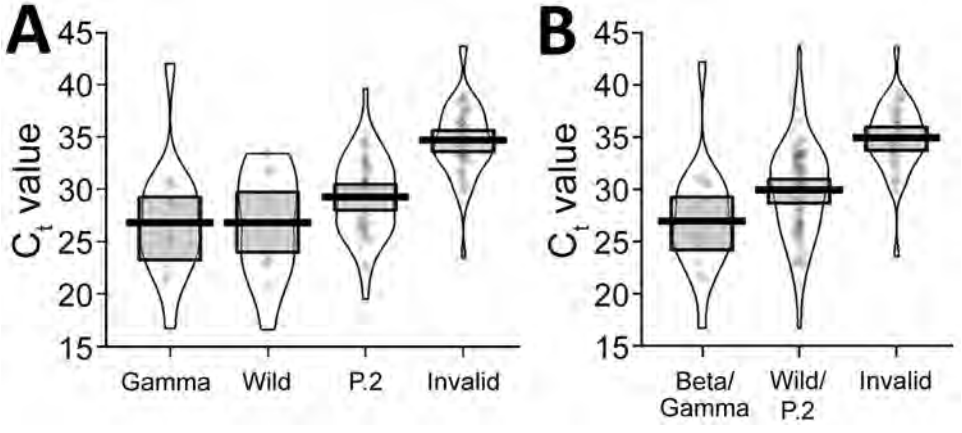

Figure 2. Violin plots of diagnostic C_t values for severe acute respiratory syndrome coronavirus 2–positive cases in Paraná state, Brazil, and detection performance for singleplex (A) and multiplex (B) genotyping methods. Violin plots are made by kernel-smoothed density plots from the actual data (represented by the dots). Horizonal lines within boxes indicate medians; upper and lower box limits indicate interquartile ranges. C_t, cycle threshold.

We found that both multiplex PCR and singleplex PCR approaches were valuable tools to evaluate the proportion of variants within genomic surveillance and were faster and less expensive than whole-genome sequencing approaches. Although those methods do not serve as substitutes for whole-genome sequencing, they could be an essential method to screen and select samples for further variant classification. Nevertheless, those approaches could demonstrate rapid spread of new variants and predict surges of SARS-CoV-2 infections, acting as a lighthouse for far-reaching public health decisions.

This article was preprinted at https://www.medrxiv.org/content/10.1101/2021.06.18.21258649v1.

SCB-UFPR (Setor de Ciências Biológicas-Universidade Federal do Paraná) COVID-19 team members: Altina Bruna de Souza Barbosa, Beatriz Bocatte de Mattos, Bruna da Silva Soley, Carla Adriane Royer, Cibele Batina Rabelo, Cristina Kaehler, Diego Candido de Abreu, Guilherme Antonio Vendramin, Helyn Priscila de Oliveira Barddal, Letícia Dalla Vechia Henschel, Madson Silveira de Melo, Nathalie Carla Cardoso, and Rachel dos Santos de Sena de Vasconcelos.

Acknowledgments

We are grateful to Centro de Assessoria de Publicação Acadêmica (CAPA) from Federal University of Paraná for English revision. We are also grateful to Maria da Graça Bicalho for her support. We give special thanks to the team of volunteers; this job would not be possible without your help.

This work was supported by the PROPLAN/Federal University of Parana, Curitiba, Paraná, Brazil; FINEP-Funder of Studies and Projects, Ministry of Science, Technology and Innovation, Brazil, Institutional Network Project: Laboratories for Diagnostic tests for COVID-19 (0494/20).

About the Author

Dr. Adamoski is a substitute professor of genetics at the Curitiba Campus from Federal University of Paraná, now positioned as Researcher at National Laboratory of Biosciences. His primary research interests include mRNA binding proteins, splicing regulation, and genomics.

References

1. Mercer TR, Salit M. Testing at scale during the COVID-19 pandemic. Nat Rev Genet. 2021;22:415–26. https://doi.org/10.1038/s41576-021-00360-w
2. Fontanet A, Autran B, Lina B, Kieny MP, Karim SSA, Sridhar D. SARS-CoV-2 variants and ending the COVID-19 pandemic. Lancet. 2021;397:952–4. https://doi.org/10.1016/S0140-6736(21)00370-6
3. Buss LF, Prete CA Jr, Abrahim CMM, Mendrone A Jr, Salomon T, de Almeida-Neto C, et al. Three-quarters attack rate of SARS-CoV-2 in the Brazilian Amazon during a largely unmitigated epidemic. Science. 2021;371:288–92. https://doi.org/10.1126/science.abe9728
4. Faria NR, Mellan TA, Whittaker C, Claro IM, Candido DDS, Mishra S, et al. Genomics and epidemiology of the P.1 SARS-CoV-2 lineage in Manaus, Brazil. Science. 2021;372:815–21. https://doi.org/10.1126/science.abh2644
5. Matic N, Lowe CF, Ritchie G, Stefanovic A, Lawson T, Jang W, et al. Rapid detection of SARS-CoV-2 variants of concern, including B.1.1.28/P.1, British Columbia, Canada. Emerg Infect Dis. 2021;27:1673–6. https://doi.org/10.3201/eid2706.210532
6. Hamilton WL, Fieldman T, Jahun A, Warne B, Illingworth CJR, Jackson C, et al.; Cambridge COVID-19 group. Applying prospective genomic surveillance to support investigation of hospital-onset COVID-19. Lancet Infect Dis. 2021;21:916–7. https://doi.org/10.1016/S1473-3099(21)00251-6
7. Vogels CBF, Breban MI, Ott IM, Alpert T, Petrone ME, Watkins AE, et al.; Brazil-UK CADDE Genomic Network; Network for Genomic Surveillance in South Africa. Multiplex qPCR discriminates variants of concern to enhance global surveillance of SARS-CoV-2. PLoS Biol. 2021;19:e3001236. https://doi.org/10.1371/journal.pbio.3001236
8. Garg J, Singh V, Pandey P, Verma A, Sen M, Das A, et al. Evaluation of sample pooling for diagnosis of COVID-19 by real time-PCR: A resource-saving combat strategy. J Med Virol. 2021;93:1526–31. https://doi.org/10.1002/jmv.26475
9. Naveca FG, Nascimento V, de Souza VC, Corado AL, Nascimento F, Silva G, et al. COVID-19 in Amazonas, Brazil, was driven by the persistence of endemic lineages and P.1 emergence. Nat Med. 2021;27:1230–8. https://doi.org/10.1038/s41591-021-01378-7
10. Silva SJRD, Pena L. Collapse of the public health system and the emergence of new variants during the second wave of the COVID-19 pandemic in Brazil. One Health. 2021;13:100287. https://doi.org/10.1016/j.onehlt.2021.100287
11. Raffle AE, Pollock AM, Harding-Edgar L. Covid-19 mass testing programmes. BMJ. 2020;370:m3262. https://doi.org/10.1136/bmj.m3262

Address for correspondence: Douglas Adamoski, Brazilian Biosciences National Laboratory (LNBio), Brazilian Center for Research in Energy and Materials (CNPEM), Zip Code 13083-970, Campinas, Brazil; email: douglas.adamoski@gmail.com

Heartland Virus Transmission, Suffolk County, New York, USA

Alan P. Dupuis II,[1] Melissa A. Prusinski,[1] Collin O'Connor, Joseph G. Maffei, Kiet A. Ngo, Cheri A. Koetzner, Michael P. Santoriello, Christopher L. Romano, Guang Xu, Fumiko Ribbe, Scott R. Campbell, Stephen M. Rich, P. Bryon Backenson, Laura D. Kramer, Alexander T. Ciota

During 2018, Heartland virus RNA was detected in an *Amblyomma americanum* tick removed from a resident of Suffolk County, New York, USA. The person showed seroconversion. Tick surveillance and white-tailed deer (*Odocoileus virginianus*) serosurveys showed widespread distribution in Suffolk County, emphasizing a need for disease surveillance anywhere *A. americanum* ticks are established or emerging.

Heartland virus (HRTV; *Phenuviridae*, *Bandavirus*) is an emerging human pathogen initially isolated from patients in Missouri, USA, during 2009 (*1*). Since then, ≥50 known human cases have been identified in Arkansas, Georgia, Illinois, Indiana, Iowa, Kansas, Kentucky, Missouri, North Carolina, Oklahoma, and Tennessee (*2*–*5*). *Amblyomma americanum*, the lone star tick, has been implicated in HRTV transmission and maintenance (*6*–*8*). Small-sized and medium-sized mammals and ground dwelling birds, such as wild turkeys (*Meleagris gallopavo*), serve as hosts for immature ticks. Adult ticks feed primarily on large mammals, such as coyotes (*Canis latrans*) and white-tailed deer (*Odocoileus virginianus*). Ticks at all 3 active developmental stages will bite humans (*9*). Serologic evidence in mammal hosts, including white-tailed deer, indicates that HRTV is distributed primarily in the Midwest and southeast United States, as well as the northeastern Atlantic coast (*10*–*12*).

Author affiliations: New York State Department of Health, Slingerlands, New York, USA (A.P. Dupuis II, J.G. Maffei, K.A. Ngo, C.A. Koetzner, L.D. Kramer, A.T. Ciota); New York State Department of Health, Albany, New York, USA (M.A. Prusinski, C. O'Connor, P.B. Backenson); Suffolk County Department of Health Services, Yaphank, New York, USA (M.P. Santoriello, C.L. Romano, S.R. Campbell); University of Massachusetts, Amherst, Massachusetts, USA (G. Xu, F. Ribbe, S.M. Rich); State University of New York at Albany School of Public Health, Albany (L.D. Kramer, A.T. Ciota)

DOI: https://doi.org/10.3201/eid2712.211426

During August 2018, New York State Department of Health (NYSDOH) epidemiologists were notified that HRTV RNA was detected in an *A. americanum* nymph removed from a resident of Long Island, New York, USA. This infected tick was tested at the University of Massachusetts (https://www.tickreport.com).

In response, the NYSDOH and Suffolk County Department of Health Services conducted tick surveillance and performed HRTV serologic analysis on the person from whom the tick was removed. Analysis was also performed for a hunter-harvested white-tailed deer in Suffolk County.

The Study

Officials with the NYSDOH and Suffolk County Department of Health Services contacted a Long Island, New York, resident for a follow-up investigation after receiving notification that a tick removed from the resident and submitted for comprehensive pathogen testing was positive for HRTV RNA. The resident, a man in his 60s, removed the tick on August 8, 2018, and recalled having a low-grade fever (maximum temperature 100.5°F) and fatigue for 5 days beginning on August 15, 2018. He noted no other symptoms.

Serum was provided at multiple time points for serologic analysis. We tested serum samples by using a standard 90% plaque reduction neutralization test ($PRNT_{90}$) for HRTV (strain M12-66) (*8*), provided by the Centers for Disease Control and Prevention. We tested samples at Wadsworth Center, NYSDOH, and results were confirmed by the Centers for Disease Control and Prevention. Neutralizing antibody titers were 1:20, 1:160, and 1:160 for samples collected at 8, 50, and 96 days after symptom onset (15, 57, and 103 days after removal of the tick), respectively, indicative of a recent infection with HRTV.

[1]These authors contributed equally to this article.

We initiated standardized drag and flag sampling of host-seeking *A. americanum* ticks on public lands for arbovirus surveillance during 2016, before HRTV detection. We found that 132 pools (containing 475 nymphs and 437 adults) from 4 Suffolk County locations were negative for HRTV by real-time reverse transcription PCR using established protocols (*8*). During 2018, tick surveillance at 5 locations yielded 102 pools (969 adults); all were negative for HRTV.

Increased efforts during the public health investigation conducted on August 23 and 24, 2018, yielded an additional 113 *A. americanum* ticks (92 larvae and 21 nymphs) from a location where tick exposure potentially occurred. All ticks collected during the investigation were negative for HRTV. No ticks were found during sampling of the property surrounding the residence of the case-patient.

During 2019 and 2020, tick surveillance in the towns of Brookhaven and Riverhead yielded 1,123 pools of *A. americanum* ticks (2,788 adults and 6,728 nymphs) (Figure 1). We found that 3 pools of unengorged nymphs collected from the Brookhaven site on June 14 (n = 1) and June 24 (n = 2), 2019, and 2 pools of unengorged nymphs collected from the same location on July 25 and August 5, 2020, were positive for HRTV RNA. We isolated virus from 2 tick pools after incubation on Vero cells. We found that testing of >1,100 *Ixodes scapularis* ticks (199 pools) collected during the surveillance campaign in Suffolk County, during 2018–2020, were negative for HRTV.

We extracted RNA from isolates by using established protocols (*13*). We developed primer pairs to amplify the small, medium, and large RNA segments by using a One-Step Superscript III Reverse Transcription PCR with Platinum Taq (Life Technologies, https://www.thermofisher.com) (Table 1). We performed 3 separate reactions using 5 μL of RNA, 1 μL of polymerase, and 0.2 μmol/L final concentration of primer pairs in a total reaction volume of 50 μL. We amplified products with the following thermocycler

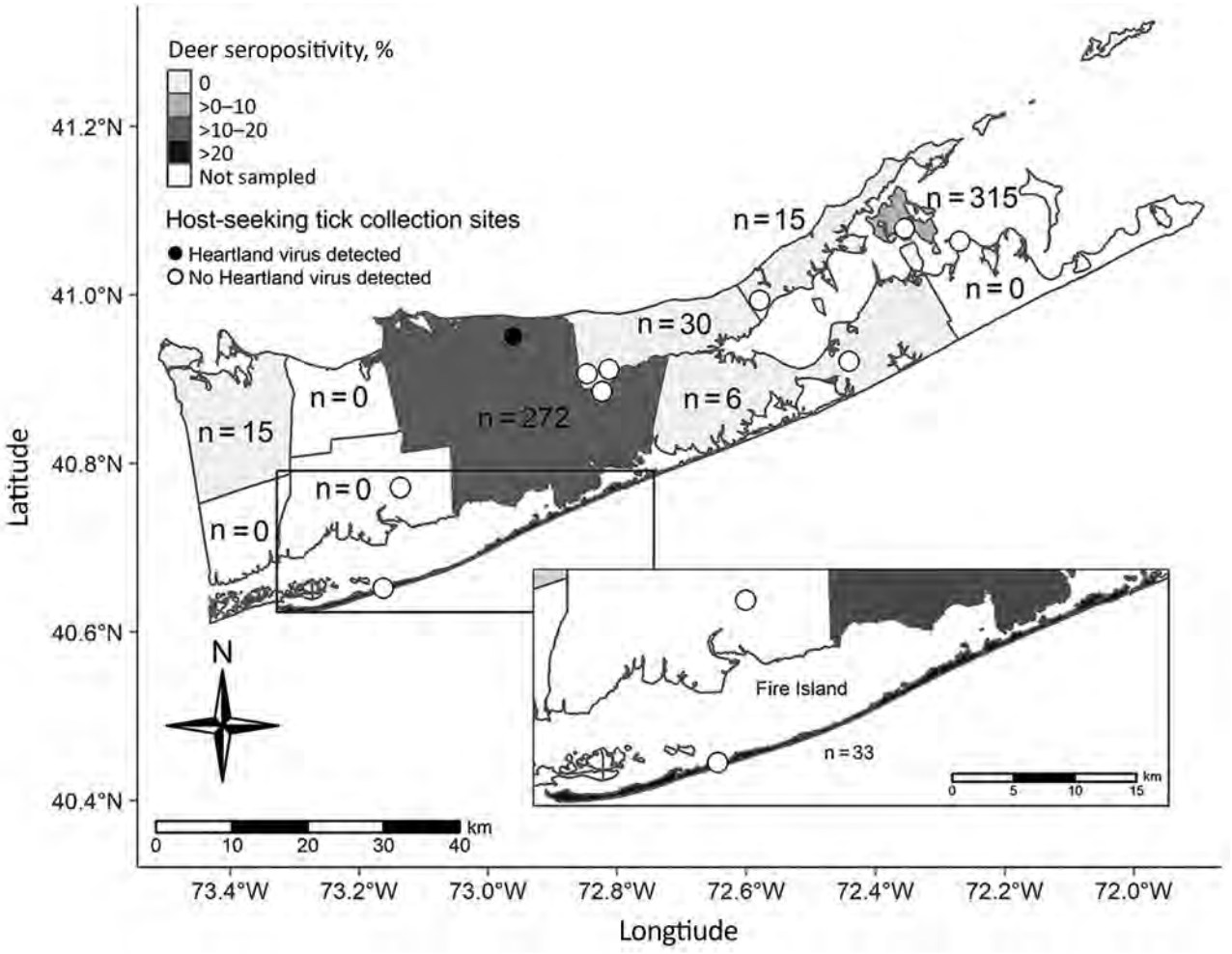

Figure 1. Tick collection sites in study of heartland virus transmission, Suffolk County, New York, USA. Numbers within townships indicate sample size of deer tested for neutralizing antibody.

Table 1. Primer pairs for amplifying small, medium, and large RNA segments of Heartland virus genome

Name	Sequence, 5′→3′	Target
HRTV_S_F	TTACACAAAGAACCCCTTGAATTATCA	Small
HRTV_S_R	CATCAAGCATGACTGACTGGTCTGCAAT	Small
HRTV_M_F	AAGTAGAGGTAAACCGTAATCCACTGAGAT	Medium
HRTV_M_R	ACAAAGACCGGCTATACAAATTGAAAAC	Medium
HRTV_L1_F	GACGTCCAGATGAATTTAGAAGCTCTT	Large
HRTV_L1_R	CTATAGCTGCCTTGATGGTTCTGC	Large
HRTV_L2_F	TGCAAGAAGATGATGATGGACCTC	Large
HRTV_L2_R	AAGACCGTCCAGATATCAACCTTTAGG	Large

conditions: 55°C for 30 min; 94°C for 2 min; 40 cycles at 94°C for 30 s, 57°C for 45 s, and 68°C for 4 min; and a final extension at 68°C for 10 min. Amplicons were visualized by electrophoresis on a 1% agarose gel. Products were pooled and purified for next-generation sequencing at the Wadsworth Center, NYSDOH, Applied Genomics Core. We prepared libraries by using the Nextera XT Kit (Illumina, https://www.illumina.com) and performed sequencing using the MiSeq Illumina platform; we analyzed sequences by using Geneious Prime Software (https://www.geneious.com) (Table 2; Figure 2).

We conducted serologic testing of hunter-harvested white-tailed deer blood submitted for arbovirus serosurveys by using $PRNT_{90}$, as described (*14*). We screened 686 serum samples at a dilution of 1:20 for neutralizing antibodies to HRTV (Figure 1) and serially diluted positive serum samples for endpoint titers. Overall, 9.8% of the deer were seropositive and had titers ranging from 1:20 to >1:640; 76% of the seropositive deer had titers >1:20. We tested 1,641 *A. americanum* ticks collected from 145 sampled deer for HRTV RNA but did not detect any virus.

Conclusions

Evidence of widespread HRTV transmission was demonstrated throughout Suffolk County, New York. Consistent with previous studies, *A. americanum* ticks were implicated in local transmission of HRTV. All positive pools were nymphal stage ticks, including the tick originally submitted for testing at the University of Massachusetts. Tick minimal infection rates ranged from 0% to 1.1%. It is unclear whether flat nymphs had acquired the virus as larvae feeding on viremic hosts, through cofeeding transmission, or transovarially because each of these modes has been demonstrated in the laboratory (*7*).

The lack of HRTV detection in adult ticks is notable if one considers that collections occurred at the same site across 3 seasons. Higher numbers of positive nymph pools were observed in Missouri, where 53/60 HRTV-positive tick pools collected at sites near the first described human cases were nymphs (*6*). Complete genome sequence analysis of the HRTV strains isolated during this study showed >98% amino acid and >93% nucleotide identities to the original strains isolated from patients in Missouri during 2009 (*1*) and a strain isolated in Tennessee during 2013 (*2*).

White-tailed deer are a sensitive sentinel model for many arboviruses, given their abundance, limited home range, and the frequency on which they are fed upon by hematophagous arthropods (*10,11,14*). Approximately 10% of the deer sampled during this study were seropositive against HRTV. Our serologic testing strategy differed from those of previous studies by using a more stringent $PRNT_{90}$. Suffolk County deer seropositive rates were similar to those reported in Vermont (10%), Maine (11%), and Florida (4%) deer (*12*). The rates are lower than those reported for deer tested in midwestern and southeastern states, areas with burgeoning populations of *A. americanum* ticks (*10,11*). To date, no competent vertebrate host, including deer, has been implicated in HRTV amplification (*15*).

Table 2. Pairwise genetic distance (% of variable positions) among fully sequenced isolates of Heartland virus, by segment (small/medium/large), for nucleotide (below diagonal) and amino acid (above diagonal) sequences

Isolate (reference)	NY20-1782	NY20-1820	MO 2009-P1	MO 2009-P2	TN 2013
NY20-1782, MZ440344/MZ440346 /MZ440345*		0/0/0	0.54/0.46/0.43	0.72/1.67/0.34	1.26/0.46/0.19
NY20-1820, MZ440341/MZ440343/ MZ440342*	0/0.03/0.61		0.54/0.46/0.43	0.72/0.43/0.34	1.26/0.46/0.19
MO 2009-P1 (*1*), JX005842.1/JX005844.1/ JX005846.1*	1.41/1.43/1.84	1.41/1.46/2.45		0.54/1.77/0.77	1.26/0.37/0.62
MO 2009-P2 (*1*), JX005843.1/JX005845.1/ JX005847.1*	1.69/4.32/1.88	1.69/4.35/2.49	1.45/4.52/1.90		1.44/0.77/0.53
TN 2013 (*2*), KJ740146.1/KJ740147.1/ KJ740148.1*	2.34/2.45/1.98	2.34/2.48/2.50	2.06/2.22/2.00	2.57/4.91/1.95	

*GenBank accession numbers.

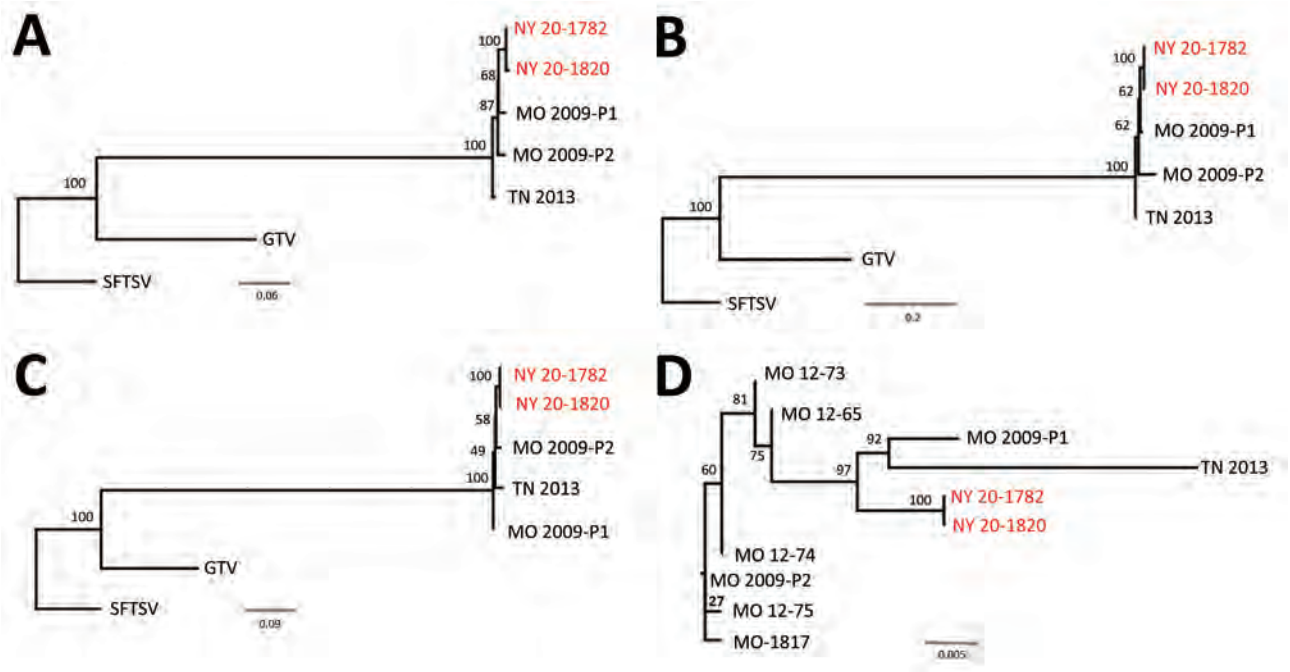

Figure 2. Phylogenetic relationship among Heartland virus isolates, Suffolk County, Long Island, New York, USA. Separate alignments of large segments (A), medium segments (B), small segments (C), and partial nonstructural sequences (D) were created with MAFFT in Geneious version 11.1.5 (https://www.geneious.com). Maximum-likelihood analyses were completed with RAxML (https://cme.h-its.org) using 1,000 bootstraps. Bootstrap values are indicated at each node. Phylogenetic trees for each segment were rooted to SFTSV strain HB154 (GenBank accession nos. JQ733560–62). Guerta virus strain DXM was included as an additional outgroup (GenBank accession nos. 328591–93). New York isolates from this study (red text), together with the 3 previously available full-genome sequences (MO 2009-P1 [patient 1, GenBank accession nos. JX005842, 4, 6]; MO 2009-P2 [patient 2, GenBank accession nos. X005843, 5, and 7]; and TN 2013 [TN, GenBank accession nos. J740146–8]), were included in these analyses (panels A, B, and C). Six additional partial sequences available for a 606-nt region of the nonstructural protein gene (GenBank accession nos. C466555, KC466560, KC466561, KC466562, KC466563, and MT052710) are indicated in an unrooted maximum-likelihood tree in panel D. Scale bars indicate nucleotide substitutions per site. GTV; Guerta virus; SFTSV, severe fever with thrombocytopenia syndrome virus.

Results from this study emphasize the need to include HRTV in surveillance programs wherever *A. americanum* ticks are distributed. Furthermore, clinicians should be aware of this pathogen and the potential for overlapping symptomologies (fever, fatigue, and loss of appetite) with other tickborne infections. Providers should request HRTV testing for patients who have clinical symptoms, including leukopenia and thrombocytopenia, and a history of tick exposure or travel to regions where *A. americanum* ticks are reported.

Acknowledgments

We thank Lauren Barlow and the Suffolk County Public Health staff for obtaining patient blood and submitting specimens and Dylan Bartlett, Lauren Rose, Anna Perry, and Jessica Stout for assisting with tick surveillance, processing, and testing. Cells for serologic assays and media production were provided by the Wadsworth Center Media and Tissue Culture Core. Genetic sequencing was conducted at the Wadsworth Center Applied Genomics Technology Core.

This study was supported by cooperative agreement U01CK000509 funded by the Centers for Disease Control and Prevention.

About the Author

Mr. Dupuis is a research scientist at the Wadsworth Center, New York State Department of Health, Albany, NY. His research interests include the role of the vertebrate host in the ecology of mosquitoborne and tickborne viruses.

References

1. McMullan LK, Folk SM, Kelly AJ, MacNeil A, Goldsmith CS, Metcalfe MG, et al. A new phlebovirus associated with severe febrile illness in Missouri. N Engl J Med. 2012;367:834–41. https://doi.org/10.1056/NEJMoa1203378
2. Muehlenbachs A, Fata CR, Lambert AJ, Paddock CD, Velez JO, Blau DM, et al. Heartland virus-associated death in Tennessee. Clin Infect Dis. 2014;59:845–50. https://doi.org/10.1093/cid/ciu434
3. Pastula DM, Turabelidze G, Yates KF, Jones TF, Lambert AJ, Panella AJ, et al.; Centers for Disease Control and Prevention (CDC). Notes from the field: heartland virus

disease—United States, 2012–2013. MMWR Morb Mortal Wkly Rep. 2014;63:270–1.
4. Stubbs AM, Steele MT. Heartland virus disease—United States, 2012–2013. Ann Emerg Med. 2014;64:314. https://doi.org/10.1016/j.annemergmed.2014.06.012
5. Centers for Disease Control and Prevention. Heartland virus disease cases by state, as of January 2021. April 23, 2021 [cited 2021 Aug 10]. https://www.cdc.gov/heartland-virus/statistics/index.html
6. Savage HM, Godsey MS Jr, Panella NA, Burkhalter KL, Ashley DC, Lash RR, et al. Surveillance for Heartland virus (Bunyaviridae: Phlebovirus) in Missouri during 2013: first detection of virus in adults of *Amblyomma americanum* (Acari: Ixodidae). J Med Entomol. 2016;53:607–12. https://doi.org/10.1093/jme/tjw028
7. Godsey MS Jr, Savage HM, Burkhalter KL, Bosco-Lauth AM, Delorey MJ. Transmission of Heartland virus (Bunyaviridae: Phlebovirus) by experimentally infected *Amblyomma americanum* (Acari: Ixodidae). J Med Entomol. 2016;53:1226–33. https://doi.org/10.1093/jme/tjw080
8. Savage HM, Godsey MS, Lambert A, Panella NA, Burkhalter KL, Harmon JR, et al. First detection of heartland virus (Bunyaviridae: Phlebovirus) from field collected arthropods. Am J Trop Med Hyg. 2013;89:445–52. https://doi.org/10.4269/ajtmh.13-0209
9. Means RG, White DJ. New distribution records of *Amblyomma americanum* (L.) (Acari: Ixodidae) in New York State. J Vector Ecol. 1997;22:133–45.
10. Riemersma KK, Komar N. Heartland virus neutralizing antibodies in vertebrate wildlife, United States, 2009–2014. Emerg Infect Dis. 2015;21:1830–3. https://doi.org/10.3201/eid2110.150380
11. Clarke LL, Ruder MG, Mead DG, Howerth EW. Heartland virus exposure in white-tailed deer in the southeastern United States, 2001–2015. Am J Trop Med Hyg. 2018;99:1346–9. https://doi.org/10.4269/ajtmh.18-0555
12. Bosco-Lauth AM, Panella NA, Root JJ, Gidlewski T, Lash RR, Harmon JR, et al. Serological investigation of heartland virus (Bunyaviridae: Phlebovirus) exposure in wild and domestic animals adjacent to human case sites in Missouri 2012–2013. Am J Trop Med Hyg. 2015;92:1163–7. https://doi.org/10.4269/ajtmh.14-0702
13. Bialosuknia SM, Tan Y, Zink SD, Koetzner CA, Maffei JG, Halpin RA, et al. Evolutionary dynamics and molecular epidemiology of *West Nile virus* in New York State: 1999–2015. Virus Evol. 2019;5:vez020. https://doi.org/10.1093/ve/vez020
14. Dupuis AP, Prusinski MA, Russell A, O'Connor C, Maffei JG, Oliver J, et al. Serologic survey of mosquito-borne viruses in hunter-harvested white-tailed deer (*Odocoileus virginianus*), New York State. Am J Trop Med Hyg. 2020. https://doi.org/10.4269/ajtmh.20-1090
15. Clarke LL, Ruder MG, Mead D, Howerth EW. Experimental infection of white-tailed deer (*Odocoileus virginanus*) with Heartland virus. Am J Trop Med Hyg. 2018;98:1194–6. https://doi.org/10.4269/ajtmh.17-0963

Address for correspondence; Alan P. Dupuis II, The Arbovirus Laboratory, New York State Department of Health, 5668 State Farm Rd, Slingerlands, NY 12159, USA; email: alan.dupuis@health.ny.gov

SARS-CoV-2 Variants, South Sudan, January–March 2021

Daniel Lule Bugembe, My V.T. Phan, Abe G. Abias, James Ayei, Lul Lojok Deng, Richard Lino Loro Lako, John Rumunu, Pontiano Kaleebu, Joseph Francis Wamala, Juma John HM, Dennis Kenyi Lodiongo, Sudhir Bunga, Matthew Cotten

As the coronavirus pandemic continues, severe acute respiratory syndrome coronavirus 2 (SARS-CoV-2) sequence data are required to inform vaccine efforts. We provide SARS-CoV-2 sequence data from South Sudan and document the dominance of SARS-CoV-2 lineage B.1.525 (Eta variant) during the country's second wave of infection.

As of August 2021, coronavirus disease (COVID-19) had caused >199 million cases and >4.2 million deaths worldwide (*1*). Severe acute respiratory syndrome coronavirus 2 (SARS-CoV-2), the virus that causes COVID-19, is being sequenced to document virus evolution and to inform vaccine efforts. In South Sudan, the COVID-19 index case was confirmed on April 4, 2020 (*2*); it was followed by 2 infection waves, in May–July 2020 and in February–March 2021 (Appendix Figure 1, https://wwwnc.cdc.gov/EID/article/27/12/21-1488-App1.pdf). As of August 3, 2021, a total of 11,063 cases and 119 deaths (*1*) had been reported in South Sudan. An earlier study from South Sudan reported that, after the second wave, 28% of the population showed serologic evidence of infection (*3*).

Chronic underdevelopment caused by prolonged conflicts has left South Sudan with a weak health system and population displacement. Large populations live in camps that may promote rapid spread and amplification of SARS-CoV-2, and poor socioeconomic conditions limit community-based COVID-19 prevention efforts. Monitoring the circulating viral genomic lineages in South Sudan is crucial, especially as vaccination is implemented and novel virus variants appear globally.

Author affiliations: Medical Research Council/Uganda Virus Research Institute and London School of Hygiene & Tropical Medicine Uganda Research Unit, Entebbe, Uganda (D.L. Bugembe, M.V.T. Phan, P. Kaleebu, M. Cotten); National Public Health Laboratory—Ministry of Health, Juba, South Sudan (A.G. Abias, J. Ayei, L.L. Deng, R.L.L. Lako, J. Rumunu); World Health Organization, Juba (J.F. Wamala, J.J. HM); US Centers for Disease Control and Prevention, Juba, South Sudan (D.K. Lodiongo, S. Bunga); University of Glasgow Centre for Virus Research, Glasgow, Scotland, UK (M. Cotten)

DOI: https://doi.org/10.3201/eid2712.211488

The Study

As part of South Sudan COVID-19 surveillance, samples were collected from community surveillance, point-of-entry screening, and sentinel site surveillance and tested for SARS-CoV-2 by real-time reverse transcription PCR (RT-PCR) at the National Public Health Laboratory (Juba, South Sudan) (*4*). During the second COVID-19 wave in February–March 2021 (Appendix Figure 1), we tested 56,014 samples for SARS-CoV-2; 6,645 samples tested positive (12% positivity). We selected a set of 70 (1%) of these positive samples for genomic sequencing with these inclusion criteria: diagnostic RT-PCR cycle threshold (C_t) values <31, from multiple locations (Figure 1), from new arrivals, from death cases, and from sites showing community transmission. We extracted nucleic acid from swab material and generated SARS-CoV-2 genome as previously described (*5*). A total of 45 complete genomes generated from samples collected in January–March 2021 showed a prevalence of 2 lineages: B.1.525 (Eta) and A.23.1 (Figure 1). The A.23.1 lineage, which was observed in October 2020 in Uganda (*6*) and has now spread globally to 26 countries, was one we observed in Juba and Nimule in early January 2021. The A.23.1 case-patients in Nimule, a South Sudan town on the border with Uganda (Figure 1), were travelers returning from Uganda. In Juba, the earliest-reported A23.1 case was in a traveler returning to South Sudan from Uganda. We detected A23.1 for only a short period; from the end of January to the end of March, we detected only B.1.525 genomes (Appendix Table). The B.1.525 lineage, reported earliest in

the United Kingdom and Nigeria, has spread to 44 countries and is considered a variant of interest (*7*).

Phylogenetic analyses of the South Sudan genomes combined with the available global A.23.1 or B.1.525 genomes were performed to gain insight into the virus movement. The maximum-likelihood trees of both A.23.1 and B.1.525 genome sequences (Figure 2) suggested multiple importations of the strains into South Sudan; South Sudan strains belonged to several sublineages, rather than a single sublineage.

Both A.23.1 and B.1.525 lineages encoded changes in their spike protein (Appendix Figure 2) as well as other parts of the genome and substitutions or deletions in the nonstructural protein 6, open reading frame 3a and 8, and nucleocapsid genes (data not shown), which might be associated with higher transmission or immune evasion. Especially relevant, the A.23.1 genomes encoded spike P681R, which is adjacent to the small (S) 1/S2 furin cleavage site and is also present in the variant of concern B.1.617.2 (Delta) lineage, which is spreading in India and globally and may increase S1/S2 cleavage (*10,11*; B. Lubinski et al., unpub. data. http://biorxiv.org/lookup/doi/10.1101/2021.06.30.450632). A related P681H substitution is present in variants of concern B.1.1.7 (Alpha) and P.1 (Beta). The South Sudan B.1.525 genomes encoded a deletion in the N-terminal domain (NTD) at spike positions 69 and 79, which is also present in B.1.1.7 and many other global variants, and a deletion in the spike NTD in positions 141–146, which may help in evasion of host immune responses. The spike D614G substitution may alter the spike protein conformation; the Q677H substitution is near the furin cleavage site and may alter spike processing.

Conclusions

We describe the patterns of SARS-CoV-2 virus genomics in South Sudan in the second wave of infections during February–March 2021, showing circulation of B.1.525 (Eta) as well as the variant A.23.1. South Sudan faced high transmission of SARS-CoV-2 during this reporting period; our data suggest that the B.1.525 lineage spread widely and progressively increased in frequency in the country during the period. Data from Uganda and Rwanda retrieved from GISAID (https://www.gisaid.org) also showed the appearance of B.1.525 at this time.

A limitation of our study is that sample numbers are low and were limited by the challenges of procurement, shipment, and testing in a harsh and

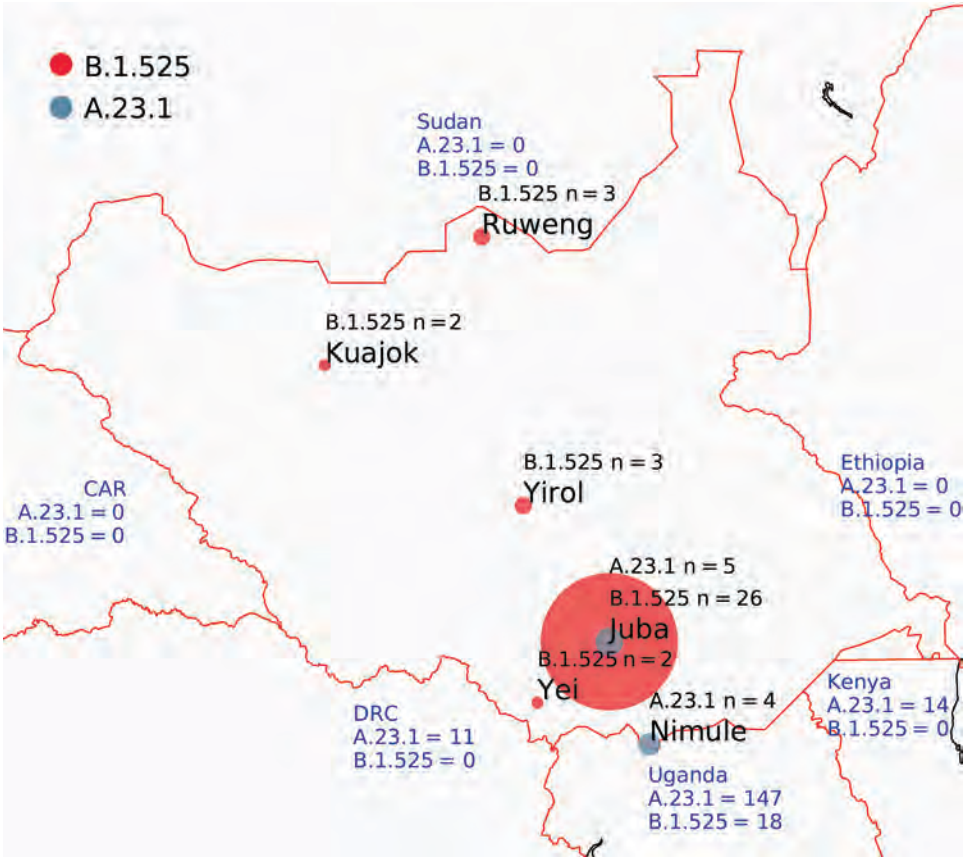

Figure 1. Locations of severe acute respiratory syndrome coronavirus 2 infection case-patients from whom genomes were isolated, South Sudan. Red circles indicate viruses of lineage B.1.525; dark gray circles indicate lineage A.23.1. Circle size is proportional to number of genomes. Blue text shows the number of A.23.1 and B.1.525 genomes reported from neighboring countries. CAR, Central African Republic; DRC, Democratic Republic of the Congo.

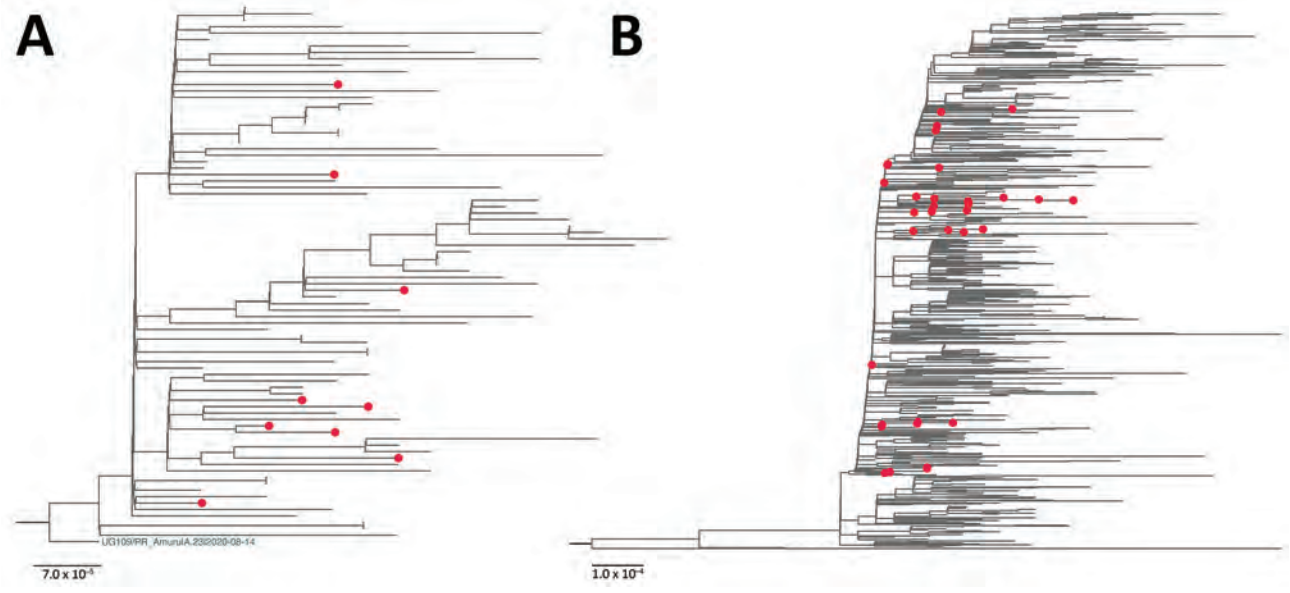

Figure 2. Maximum-likelihood phylogenetic tree of severe acute respiratory syndrome coronavirus 2 viruses from South Sudan (red dots) and reference sequences. A) Lineage A.23.1. All sequences from South Sudan were combined with a subset of all available global A.23.1 genomes, algorithmically thinned. All available global A.23.1 genomes were retrieved from GISAID (https://www.gisaid.org) and aligned, and for the first genome, all genomes closer than 5 hamming distance were removed. This process was continued until the entire set was thinned. This global, thinned A.23.1 set was combined with all South Sudan A.23.1 genomes and used to infer the A.23.1 maximum-likelihood tree. The tree was rooted with the A.23 strain (UG109/PR_Amuru|A.23|2020–08–14). B) Lineage B.1.525. The B.1.525 genome sequences were prepared in the same manner as those for A.23.1 except the hamming distance of 20. Maximum-likelihood phylogenetic trees were constructed in RaxML-NG (*8*) under the general time reversible plus gamma 4 plus invariate sites model as the best-fit model of substitution according to the Akaike information criterion determined by modeltestNG (*9*) and run for 100 pseudoreplicates and visualized using FigTree version 1.4.4 (http://tree.bio.ed.ac.uk/software/figtree). For B.1.525, the tree was midpoint rooted for clarity. Scale bar indicates nucleotide substitutions per site.

resource-poor environment. Careful sample selection was performed to provide an unbiased description of the epidemic; however, not all positive samples yielded genome sequences. This lack of data could introduce bias in the reported genomes. Nonetheless, the study accurately describes SARS-CoV-2 lineages during the second wave of epidemic in South Sudan.

Substantial land-based traffic with neighboring countries makes it imperative to document the viruses circulating in this region. Careful monitoring of locally circulating viruses as vaccination becomes widespread is essential for interpreting vaccine function and for informing the healthcare systems whether the current vaccines are still a good match for the circulating viruses. We recommend continued genomic surveillance in South Sudan to help with public health responses, especially as new waves of infections come to the country and continent.

D.L.B., M.V.T.P., and M.C. were funded by the Medical Research Council/United Kingdom Research and Innovation (grant no. NC_PC_19060) and Wellcome Trust (grant no. 220977/Z/20/Z).

About the Author

Dr. Bugembe is a scientist at the Medical Research Council/Uganda Virus Research Institute and London School of Hygiene and Tropical Medicine Research Unit in Entebbe, Uganda. His research interests are virus evolution and the computational analysis of viral genetic data to predict infectious disease trends.

References

1. Center for Systems Science and Engineering (CSSE) at Johns Hopkins University. COVID-19 dashboard. 2020 [cited 2021 Jan 24]. https://www.arcgis.com/apps/opsdashboard/index.html#/bda7594740fd40299423467b48e9ecf6
2. World Health Organization. South Sudan confirms first case of COVID-19. 2020 [cited 2021 Sep 3]. https://www.afro.who.int/news/south-sudan-confirms-first-case-covid-19
3. Wiens KE, Mawien PN, Rumunu J, Slater D, Jones FK, Moheed S, et al. Seroprevalence of severe acute respiratory syndrome coronavirus 2 IgG in Juba, South Sudan, 2020. Emerg Infect Dis. 2021;27:1598–1606. https://doi.org/10.3201/eid2706.210568
4. World Health Organization. South Sudan joint external evaluation report 2018. 2018 [cited 2021 Sep 3]. https://www.afro.who.int/publications/south-sudan-joint-external-evaluation-report2018

5. Cotten M, Bugembe DL, Kaleebu P, Phan, MVT. Alternate primers for whole-genome SARS-CoV-2 sequencing. Virus Evol. 2021; 27:veab006. https://doi.org/10.1093/ve/veab006
6. Bugembe DL, Phan MVT, Ssewanyana I, Semanda P, Nansumba H, Dhaala B, et al. Emergence and spread of a SARS-CoV-2 lineage A variant (A.23.1) with altered spike protein in Uganda. Nat Micronbiol. 2021; 6:1094–1101. https://doi.org/10.1038/s41564-021-00933-9
7. World Health Organization. Tracking SARS-CoV-2 variants. 2021 [cited 2021 Sep 3]. https://www.who.int/en/activities/tracking-SARS-CoV-2-variants
8. Kozlov, AM, Darriba D, Flouri, T, Morel, B, Stamatakis A. RAxML-NG: a fast, scalable and user-friendly tool for maximum-likelihood phylogenetic inference. Bioinformatics. 2019;35:4453–55. https://doi.org/10.1093/bioinformatics/btz305
9. Darriba D, Posada D, Kozlov AM, Stamatakis A, Morel B, Flouri T. ModelTest-NG: a new and scalable tool for the selection of DNA and protein evolutionary models. Molecular Biology and Evolution. 2020; 37:291–294. https://doi.org/10.1093/molbev/msz189
10. Johnson BA, Xie X, Bailey AL, Kalveram B, Lokugamage KG, Muruato A, et al. Loss of furin cleavage site attenuates SARS-CoV-2 pathogenesis. Nature. 2021;591:293–9 https://doi.org/10.1038/s41586-021-03237-4
11. Hoffmann M, Kleine-Weber H, Pöhlmann S. A multibasic cleavage site in the spike protein of SARS-CoV-2 is essential for infection of human lung cells. https://doi.org/10.1016/j.molcel.2020.04.022

Address for correspondence: Matthew Cotten, M RC/UVRI & LSHTM Uganda Research Unit, PO Box 49, Plot 51-59 Nakiwogo Rd, Entebbe, Uganda; email: matthew.cotten@lshtm.ac.uk

Incidence Trends for SARS-CoV-2 Alpha and Beta Variants, Finland, Spring 2021

Ravi Kant,[1] Phuoc Truong Nguyen,[1] Soile Blomqvist, Mert Erdin, Hussein Alburkat, Maija Suvanto, Fathiah Zakham, Veera Salminen, Viktor Olander, Minna Paloniemi, Leena Huhti, Sara Lehtinen, Bruno Luukinen, Hanna Jarva, Hannimari Kallio-Kokko, Satu Kurkela, Maija Lappalainen, Hanna Liimatainen, Sari Hannula, Jani Halkilahti, Jonna Ikonen, Niina Ikonen, Otto Helve, Marianne Gunell, Tytti Vuorinen, Ilya Plyusnin, Erika Lindh, Pekka Ellonen, Tarja Sironen, Carita Savolainen-Kopra, Teemu Smura, Olli Vapalahti

Severe acute respiratory syndrome coronavirus 2 Alpha and Beta variants became dominant in Finland in spring 2021 but had diminished by summer. We used phylogenetic clustering to identify sources of spreading. We found that outbreaks were mostly seeded by a few introductions, highlighting the importance of surveillance and prevention policies.

Several new variants of severe acute respiratory syndrome coronavirus 2 (SARS-CoV-2) have emerged globally, most notably variants of concern Alpha (B.1.1.7) (*1*), Beta (B1.351) (*2*), Gamma (P.1) (*3*), and most recently, Delta (B.1.617.2). Each variant is thought to pose an increased public health risk compared with the earlier wild-type strains that were circulating in 2020 because of ≥1 epidemiologic characteristics, such as higher transmissibility (*4*), greater immune escape properties toward antibodies from previous SARS-CoV-2 infection (*5*), lower response to current vaccines (*6*), or more severe outcomes or increased mortality rates (*7*). Detecting and monitoring these novel variants is essential in SARS-CoV-2 surveillance.

The Study

To assess the temporal epidemiologic dynamics among different variants of concern and identify spreading events and sources of SARS-CoV-2 cases detected in Finland, we began sequencing 400–1,000 virus samples per week collected during December 2020–May 2021 and analyzed the resulting genomes (n = 14,080), which are now available in the GISAID (https://www.gisaid.org) database. For quality control purposes, we removed all sequences with ≥2.0% gaps.

We analyzed the resulting dataset (n = 9,160) with Pangolin (https://cov-lineages.org) (*8*) to identify lineages, from which we filtered Alpha and Beta variants for phylogenetic analyses. Each phylogenetic tree was computed from the filtered sequences and a global reference dataset consisting of 5 representative sequences, 1 sequence from the country of origin (England for Alpha, South Africa for Beta) and 4 randomly chosen from other countries containing the same lineage, for each date during December 2020–May 2021. The reference datasets included 841 genomes for Alpha variant and 775 genomes for Beta variant trees. We aligned sequences using MAFFT (https://mafft.cbrc.jp) (*9*) and removed gaps in the resulting alignments by trimming 50 characters from both the 5′ and 3′ ends.

We then used the aligned sequences to compute the trees with a SARS-CoV-2–specific version of IQ-TREE 2 (*10*) using ModelFinder to identify and use the optimal nucleotide substitution model,

Author affiliations: University of Helsinki, Helsinki, Finland (R. Kant, P. Truong Nguyen, M. Erdin, H. Alburkat, M. Suvanto, F. Zakham, V. Salminen, V. Olander, H. Jarva, I. Plyusnin, T. Sironen, T. Smura, O. Vapalahti); Finnish Institute for Health and Welfare (THL), Helsinki (S. Blomqvist, J. Halkilahti, J. Ikonen, N. Ikonen, O. Helve, E. Lindh, C. Savolainen-Kopra); Fimlab Laboratories Ltd., Tampere, Finland (M. Paloniemi, L. Huhti, S. Lehtinen, B. Luukinen); HUS Diagnostic Center, University of Helsinki and Helsinki University Hospital, Uusimaa, Finland (H. Jarva, H. Kallio-Kokko, S. Kurkela, M. Lappalainen, H. Liimatainen, T. Smura, O. Vapalahti); Institute for Molecular Medicine Finland (FIMM), Helsinki (S. Hannula, P. Ellonen); Turku University Hospital, Turku, Finland (M. Gunell, T. Vuorinen)

DOI: https://doi.org/10.3201/eid2712.211631

[1]These authors contributed equally to this article.

performing 1,000 ultrafast bootstraps. We set the initial wild-type reference strain (GenBank accession no. NC_045512.2) as the outgroup. We assigned sequences to clusters using TreeCluster (*11*) based on an arbitrary branch length of 0.001 to identify major transmission chains. We collapsed clusters with ≤5 sequences for visualization purposes.

By May 2021, there had been 93,393 laboratory-confirmed SARS-CoV-2 infections reported in Finland (*12*); incidence peaks occurred in April and December 2020 and March 2021 (Appendix Figure 1, panel A, https://wwwnc.cdc.gov/EID/article/27/12/21-1631-App1.pdf). During this period, the weekly number of cases was as high as 4,900. National vaccinations began in late December 2020, and within 7 months, 3.5 million (62.8% of total population) persons had received first doses and 1.4 million (24.5% of total population) second doses (*13*). Seroprevalence remained low (<2%) until February 2021 (*14*) but increased because of growing vaccination coverage (Appendix Figure 1, panel B).

Throughout 2020, sequencing-based surveillance of the virus was conducted in the Hospital District of Helsinki and Uusimaa (HUS; Helsinki, Finland), which had the highest number of COVID-19 cases in the country (n = 21,742). Until December 18, 2020, only wild-type strains of SARS-CoV-2 had been detected, but the emergence of Alpha and Beta variants led to increased sequencing and sampling efforts at points of entry into Finland (i.e.,

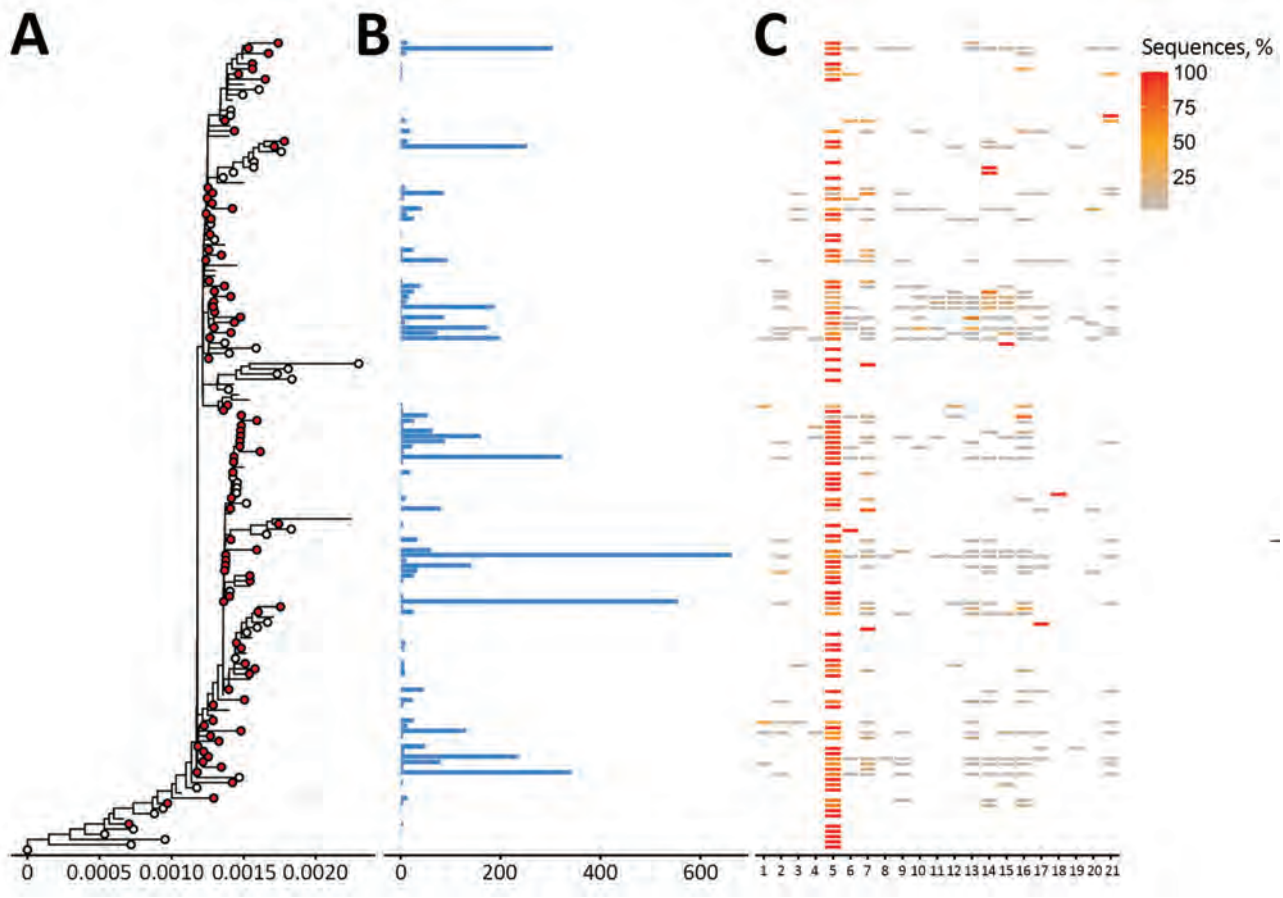

Figure 1. Phylogenetic tree of severe acute respiratory syndrome coronavirus 2 Alpha (B.1.1.7) variant clusters from Finland and sequence distribution. The tree (A) shows 86 clusters with ≥5 sequences (red circles), of which 84 contain 5,270 sequences sampled in Finland using TreeCluster, and 32 Finland singletons (white circles). The tree was constructed by using IQ-TREE 2 (*10*) with 1,000 ultrafast bootstraps. Each row in subsequent graphs is equivalent to a cluster and shows the number of sequences from Finland (B) and the proportion of sequences per region of Finland (C). Regions of Finland: 1, Åland Islands; 2, Central Finland Health Care District; 3, Central Ostrobothnia Hospital District; 4, East Savo Hospital District; 5, Hospital District of Helsinki and Uusimaa; 6, Hospital District of South Ostrobothnia; 7, Hospital District of Southwest Finland; 8, Kainuu Social and Health Care Joint Authority; 9, Kanta-Häme Hospital District; 10, Länsi-Pohja Healthcare District; 11, Lapland Hospital District; 12, North Karelia Hospital District; 13, North Ostrobothnia Hospital District; 14, North Savo Hospital District; 15, Päijät-Häme Hospital District; 16, Pirkanmaa Hospital District; 17, Satakunta Hospital District; 18, Social and Health Services in Kymenlaakso; 19, South Karelia Social and Health Care District; 20, South Savo Hospital District; 21, Vaasa Hospital District.

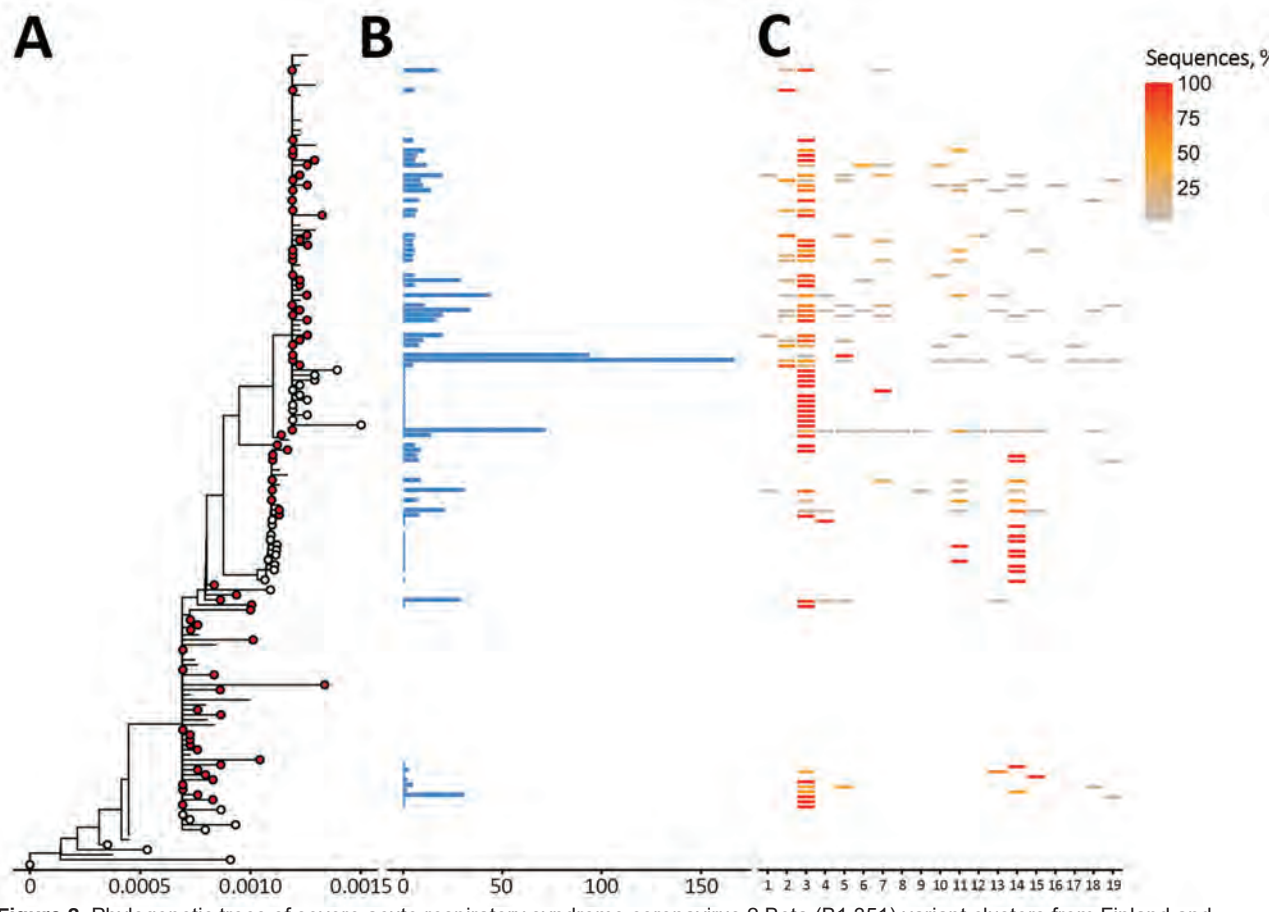

Figure 2. Phylogenetic trees of severe acute respiratory syndrome coronavirus 2 Beta (B1.351) variant clusters from Finland and sequence distribution. The tree (A) shows 76 clusters with ≥5 sequences (red circles), of which 48 contain 898 sequences sampled in Finland using TreeCluster (*11*), and 23 Finland singletons (white circles) from 33. The tree was constructed by using IQ-TREE 2 (*10*) with 1,000 ultrafast bootstraps. Each row in subsequent panels is equivalent to a cluster and shows the number of sequences from Finland (B) and the proportion of sequences per region of from Finland (C). Regions of Finland: 1, Central Finland Health Care District; 2, East Savo Hospital District; 3, Hospital District of Helsinki and Uusimaa; 4, Hospital District of South Ostrobothnia; 5, Hospital District of Southwest Finland; 6, Kainuu Social and Health Care Joint Authority; 7, Kanta-Häme Hospital District; 8, Länsi-Pohja Healthcare District; 9, Lapland Hospital District; 10, North Karelia Hospital District; 11, North Ostrobothnia Hospital District; 12, North Savo Hospital District; 13, Päijät-Häme Hospital District; 14, Pirkanmaa Hospital District; 15, Satakunta Hospital District; 16, Social and Health Services in Kymenlaakso; 17, South Karelia Social and Health Care District; 18, South Savo Hospital District; 19, Vaasa Hospital District.

airports, harbors, land border crossing sites) starting in week 51 of 2020.

During December 2020–May 2021, a total of 14,080 SARS-CoV-2 genomes representing ≈20.4% of the PCR-confirmed SARS-CoV-2 infections (n = 65,921) were sequenced. During this period, the Alpha variant (5,370 total detections) comprised 58.6% of all cases, and its proportion in weekly counts rapidly increased from 3 (6.0%) of 50 in week 51 of 2020 to 602 (69.1%) of 871 in week 11 of 2021 (Appendix Figure 2). The highest proportion of Alpha variant cases was 240 (82.2%) of 292 detections in week 17. Beta variant incidence rose later and at a slower rate (1,049 total detections, 19.5% of all cases); the proportion in weekly case counts rose from 2 (1.7%) in week 2 of 2021 to 181 (23.1%) by week 12. The proportions of Alpha and Beta variants started to diminish in week 13. Only 1 Gamma variant case was recorded, in week 10, and the first Delta variant samples in Finland were collected during week 17. In addition, several variants of interest (*15*) were detected beginning in early January 2021: B.1.429 (2 detections), B.1.525 (25 detections), B.1.526 (1 detection), B.1.617.1 (6 detections), and P.2 (1 detection). Of the variants being monitored (*15*), 18 cases of AT.1 and 29 of B.1.1.318 lineages were detected during this period.

The clustering analysis of Alpha variants (Figure 1) showed 86 distinct clusters, of which 84 contained 5,270 sequences from Finland (57.5% of all sequences). The 13 largest clusters from Finland (total n =

3,669, 69.6%) had 132–663 sequences each. We detected 32 singletons (0.6% of Alpha detections) from Finland, suggesting that the epidemic was largely seeded from a few introductions, which aligns with the super-spreading properties of SARS-CoV-2 epidemiology. Most Alpha sequences were from the HUS district (n = 3,476, 64.7% of cases). We included all available high-quality sequences from random populations from Finland and thus included data from both mild and severe cases. However, a proportion of the samples from the HUS region came from points of entry into Finland and other hospital districts. The proportions of these imported samples varied over the sampling period depending on travel restrictions and hospitalized case-patients, which may have led to nonrandomized sampling from the HUS region.

Beta variants formed 76 distinct clusters, of which 56 contained 910 sequences from Finland (9.9% of all sequences from Finland) (Figure 2). We also identified 33 singletons, of which 23 were from Finland (2.2% of Beta detections). In total, there might have been 79 introductions from other countries, which seeded 1 major cluster (≥100 Finland sequences) containing 167 sequences (15.9% of cases). Most Beta sequences were also from the HUS hospital district (n = 505, 48.1% of cases). Hospital district reports were based on data from the Finnish Institute for Health and Welfare (https://sampo.thl.fi), HUS, and Fimlab (https://fimlab.fi).

Conclusions

Altogether, our study shows both Alpha and Beta variants emerging early and rapidly beginning in December 2020. Most (98.2% Alpha, 86.8% Beta) formed clusters, and only a small proportion (0.6% Alpha, 2.2% Beta) were singletons. Because the singletons represent a small fraction of the sequences and many were transmitted directly from travelers, it is likely that a few introductions were able to seed the epidemic.

The Alpha and Beta variants dominated detected SARS-CoV-2 cases, although at lower numbers for Beta, during early 2021. Despite the rapid emergence of these variants, their incidence fell sharply (Appendix Figure 1, panel A). Incidence in Finland has been low compared with other countries in Europe, permitting use of more moderately restrictive prevention measures. Incidence, and therefore seroprevalence, remained relatively low until vaccines became available. Practices and policies enacted in Finland, including frequent testing, contact tracing, isolation, quarantine, and other nonpharmaceutical interventions, helped effectively interrupt chains of transmission, and ongoing national efforts have resulted in most of the population of Finland receiving at least the first vaccine dose. These findings suggest that with proper surveillance and preventative measures, along with moderate restriction compliance, the spread SARS-CoV-2 could be mitigated effectively.

Acknowledgments

We acknowledge CSC–IT Center for Science, Finland, for providing computational resources.

This study was supported by the Academy of Finland (grant number 336490), VEO European Union's Horizon 2020 (grant number 874735), Finnish Institute for Health and Welfare, Jane and Aatos Erkko Foundation, and Helsinki University Hospital Funds (TYH2018322 and TYH2021343).

About the Authors

Dr. Kant is a postdoctoral researcher in the Department of Virology and Veterinary Bioscience at the University of Helsinki, Finland. His research interests include virus evolution and genomics, as well as bioinformatics. Mr. Truong Nguyen is a doctoral candidate in the Department of Virology in the University of Helsinki, Finland. His research interests include evolution of viruses and computational biology.

References

1. Public Health England. Investigation of SARS-CoV-2 variants of concern [cited 2021 Feb 16]. https://www.gov.uk/government/publications/investigation-of-novel-sars-cov-2-variant-variant-of-concern-20201201
2. Tegally H, Wilkinson E, Giovanetti M, Iranzadeh A, Fonseca V, Giandhari J, et al. Detection of a SARS-CoV-2 variant of concern in South Africa. Nature. 2021;592:438–43. https://doi.org/10.1038/s41586-021-03402-9
3. Faria NR, Mellan TA, Whittaker C, Claro IM, Candido DDS, Mishra S, et al. Genomics and epidemiology of the P.1 SARS-CoV-2 lineage in Manaus, Brazil. Science. 2021;372:815–21. https://doi.org/10.1126/science.abh2644
4. Campbell F, Archer B, Laurenson-Schafer H, Jinnai Y, Konings F, Batra N, et al. Increased transmissibility and global spread of SARS-CoV-2 variants of concern as at June 2021. Euro Surveill. 2021;26:2100509. https://doi.org/10.2807/1560-7917.ES.2021.26.24.2100509
5. Virtanen J, Uusitalo R, Korhonen EM, Aaltonen K, Smura T, Kuivanen S, et al. Kinetics of neutralizing antibodies of COVID-19 patients tested using clinical D614G, B.1.1.7, and B 1.351 isolates in microneutralization assays. Viruses. 2021;13:996. https://doi.org/10.3390/v13060996
6. Jalkanen P, Kolehmainen P, Häkkinen HK, Huttunen M, Tähtinen PA, Lundberg R, et al. COVID-19 mRNA vaccine induced antibody responses against three SARS-CoV-2

variants. Nat Commun. 2021;12:3991. https://doi.org/10.1038/s41467-021-24285-4
7. Davies NG, Jarvis CI, CMMID COVID-19 Working Group, Edmunds WJ, Jewell NP, Diaz-Ordaz K, et al. Increased mortality in community-tested cases of SARS-CoV-2 lineage B.1.1.7. Nature. 2021;593:270–4. https://doi.org/10.1038/s41586-021-03426-1
8. O'Toole A, Scher E, Underwood A, Jackson B, Hill V, McCrone JT, et al. Assignment of epidemiological lineages in an emerging pandemic using the Pangolin tool. Virus Evol. 2021;7:veab064.
9. Katoh K, Standley DM. MAFFT multiple sequence alignment software version 7: improvements in performance and usability. Mol Biol Evol. 2013;30:772–80. https://doi.org/10.1093/molbev/mst010
10. Minh BQ, Schmidt HA, Chernomor O, Schrempf D, Woodhams MD, von Haeseler A, et al. IQ-TREE 2: new models and efficient methods for phylogenetic inference in the genomic era. [Erratum in Mol Biol Evol. 2020;37:2461]. Mol Biol Evol. 2020;37:1530–4. https://doi.org/10.1093/molbev/msaa015
11. Balaban M, Moshiri N, Mai U, Jia X, Mirarab S. TreeCluster: clustering biological sequences using phylogenetic trees. PLoS One. 2019;14:e0221068. https://doi.org/10.1371/journal.pone.0221068
12. Finnish Institute for Health and Welfare (THL). COVID-19 cases in the infectious diseases registry [cited 2021 Feb 17]. https://sampo.thl.fi/pivot/prod/en/epirapo/covid19case/fact_epirapo_covid19case
13. Finnish Institute for Health and Welfare (THL). COVID-19 vaccinations in Finland: vaccinations over time in hospital care districts per age group [cited 2021 Jul 12]. https://sampo.thl.fi/pivot/prod/en/vaccreg/cov19cov/summary_cov19covareatime
14. Finnish Institute for Health and Welfare (THL). Report of the population serology survey of the coronavirus epidemic [Finnish] [cited 2021 Jun 30]. https://www.thl.fi/roko/cov-vaestoserologia/sero_report_weekly.html
15. European Centre for Disease Prevention and Control. SARS-CoV-2 variants of concern as of 15 July 2021 [cited 2021 Jul 16]. https://www.ecdc.europa.eu/en/covid-19/variants-concern

Address for correspondence: Teemu Smura, Department of Virology, University of Helsinki, Haartmaninkatu 3, 00014, Helsinki, Uusimaa, Finland; email: teemu.smura@helsinki.fi; Olli Vapalahti, Department of Virology, University of Helsinki, Haartmaninkatu 3, 00014, Helsinki, Uusimaa, Finland; email: olli.vapalahti@helsinki.fi

etymologia revisited

Originally published in June 2019

***Neospora caninum* [ne-os′ pə-rə ca-nin′ um]**

From the *neo-* (Latin, "new") + *spora* (Greek, "seed") and *canis* (Latin, "dog"), *Neospora caninum* is a sporozoan parasite that was first described in 1984. It is a major pathogen of cattle and dogs but can also infect horses, goats, sheep, and deer. Antibodies to *N. caninum* have been found in humans, predominantly in those with HIV infection, although the role of this parasite in causing or exacerbating illness is unclear.

Sources:

1. Bjerkås I, Mohn SF, Presthus J. Unidentified cyst-forming sporozoon causing encephalomyelitis and myositis in dogs. Z Parasitenkd. 1984;70:271–4. http://dx.doi.org/10.1007/BF00942230
2. Dubey JP. Review of *Neospora caninum* and neosporosis in animals. Korean J Parasitol. 2003; 41:1–16. http://dx.doi.org/10.3347/kjp.2003.41.1.1
3. Lobato J, Silva DA, Mineo TW, Amaral JD, Segundo GR, Costa-Cruz JM, et al. Detection of immunoglobulin G antibodies to *Neospora caninum* in humans: high seropositivity rates in patients who are infected by human immunodeficiency virus or have neurological disorders. Clin Vaccine Immunol. 2006;13:84–9. http://dx.doi.org/10.1128/CVI.13.1.84-89.2006

https://wwwnc.cdc.gov/eid/article/25/6/et-2506_article

Potential Mosquito Vectors for Shuni Virus, South Africa, 2014–2018

Milehna Mara Guarido, Thopisang Motlou, Megan A. Riddin, Caitlin MacIntyre, Sontaga Cris Manyana, Todd Johnson, Maarten Schrama, Erin E. Gorsich, Basil D. Brooke, A. Paulo G. Almeida, Marietjie Venter

Shuni virus is associated with neurologic and febrile illness in animals and humans. To determine potential vectors, we collected mosquitoes in South Africa and detected the virus in species of the genera *Mansonia*, *Culex*, *Aedes*, and *Anopheles*. These mosquitoes may be associated with Shuni virus outbreaks in Africa and emergence in other regions.

The genus *Orthobunyavirus* (family *Peribunyaviridae*) includes emerging arthropodborne viruses associated with human and animal disease worldwide (*1*). In 1966, orthobunyavirus Shuni virus (SHUV) was isolated from a cow, *Culicoides* midges, and a febrile child in Nigeria (*2*); SHUV recently emerged in Israel, where it has been associated with birth defects in ruminants (*3*). SHUV has been associated with neurologic disease in horses and wildlife (*4*,*5*) and was recently implicated in human cases of neurologic disease in South Africa (*6*). SHUV was detected in field-caught *Culex theileri* mosquitoes in the 1970s (*5*), and *Culicoides* midges have been suggested as vectors (*7*). We investigated mosquitoes collected in northeastern parts of South Africa to identify their potential as vectors of orthobunyaviruses in the Simbu serogroup of arboviruses, including SHUV.

The Study

We collected mosquitoes across 5 provinces of South Africa (Figure 1). Site selection was based on historical outbreaks of arboviruses, including SHUV, in animals (*4*,*5*) and humans (*6*). During January 2014–May 2017, we collected mosquitoes monthly; we performed additional collections in 2017 in and around the Kruger National Park (*8*). In 2018, we performed 1 collection per site during January–May.

We used multiple types of dry ice (carbon dioxide) baited traps: nets, CDC miniature light traps (https://www.johnwhock.com), and BG-Sentinel traps (https://www.bg-sentinel.com). We set traps during 3:30–6:00 PM and emptied them during 5:00–8:00 AM. We killed mosquitoes by freezing and then morphologically identified them to the species level. We pooled females (≤50 individuals) by species, collection site, and month. We selected mosquitoes for screening from pools collected during January–June, which represents late summer and autumn, when arbovirus infections in animals and humans in South Africa increase. We obtained climate data from the South African Weather Service (http://www.weathersa.co.za).

For the virus assays, we produced homogenate pools by placing 5 sterile glass beads in microcentrifuge tubes containing 2 mL of reconstituted minimum essential medium, which we then vigorously shook and clarified. The resulted supernatant was stored at −80°C. To extract viral RNA from 200 µL homogenate, we used an RNeasy mini kit (QIAGEN, https://www.qiagen.com) according to the manufacturer's instructions. We screened extracted RNA by using 2 PCRs, each targeting the nucleocapsid (NP) gene on the small (S) segment: a Simbu serogroup/orthobunyavirus–specific one-step TaqMan real-time reverse transcription PCR targeting a 152-bp fragment (*4*) and an SHUV nested real-time RT-PCR targeting a 460-bp fragment (*9*). In an attempt to obtain larger fragments, we performed an SHUV conventional PCR with published primers (*10*).

For mosquito barcoding (species identification), we extracted DNA from 50 µL of the homogenate by using a QIAGEN DNeasy Blood & Tissue Kit according

Author affiliations: University of Pretoria, Pretoria, South Africa (M.M. Guarido, T. Motlou, M.A. Riddin, C. MacIntyre, S.C. Manyana, T. Johnson, A.P.G. Almeida, M. Venter); Copperbelt University, Kitwe, Zambia (T. Johnson); Leiden University, Leiden, the Netherlands (M. Schrama); University of Warwick, Coventry, UK (E.E. Gorsich); National Institute for Communicable Diseases/NHLS, Johannesburg, South Africa (B.D. Brooke); University of the Witwatersrand, Johannesburg (B.D. Brooke); NOVA University of Lisbon, Lisbon, Portugal (A.P.G. Almeida)

DOI: https://doi.org/10.3201/eid2712.203426

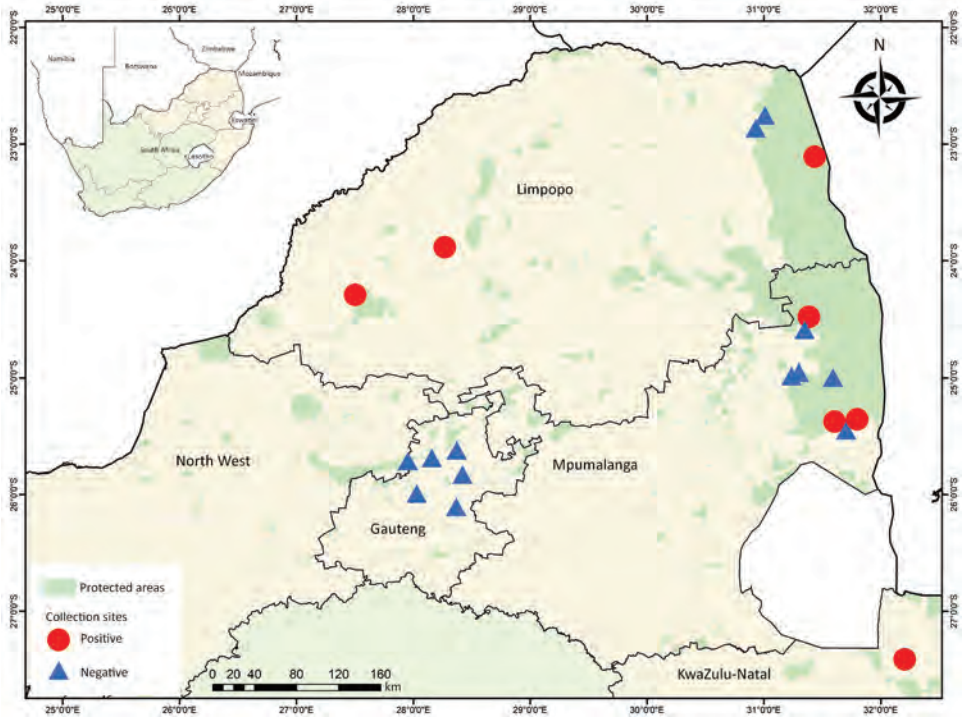

Figure 1. Mosquito collection sites indicating collection locations of Shuni virus–positive (circles) and negative (triangles) mosquito pools, South Africa, January 2014–May 2018. Inset map shows location of South Africa in Africa.

to the manufacturer's instructions. The subunit I of the cytochrome oxidase gene was amplified by using universal primers (*11*).

All products of the expected size were sequenced by Sanger sequencing at the Forestry Agriculture Bioinformatics Institute, University of Pretoria (Pretoria, South Africa). We compared the resulting sequences by using BLAST (https://blast.ncbi.nlm.nih.gov/Blast.cgi) with sequences available from GenBank, including SHUV strains from South Africa, Nigeria, and Israel and other representative members of Simbu serogroup. For the cytochrome oxidase gene, we selected representative mosquito sequences from GenBank and BOLD (https://v3.boldsystems.org). We compiled multiple sequence alignments by using MAFFT (https://mafft.cbrc.jp/alignment/software), produced maximum-likelihood trees by using MEGA 7.0 (https://www.megasoftware.net), and calculated maximum-likelihood estimates of mosquito infection rates by using PooledInfRate (https://www.cdc.gov/ncidod/dvbid/westnile/software.htm).

Of the 64,603 adult mosquitoes collected as described (*8*,*12*), we tested 39,035 females. A total of 11 pools were positive for SHUV (Table 1). No other orthobunyaviruses were detected. Positive pools for SHUV were detected in conservation areas (6/11, 54.5%) and rural areas (5/11, 45.5%) (Figure 1). Populations of the SHUV-positive mosquito species peaked with the heavy rains and with the highest mean air temperatures (Appendix Figure 1, https://wwwnc.cdc.gov/EID/article/27/12/20-3426-App1.pdf), which promote establishment of breeding sites and favorable habitats for developing stages and subsequent population growth.

The maximum-likelihood phylogeny based on the genus *Orthobunyavirus* PCR fragment of 152-bp of the S segment showed that all SHUV viruses from the mosquitoes clustered with the Simbu serogroup (Appendix Figures 1, 2) and were closest to SHUV on the basis of p-distance analyses (data not shown). For 5 samples, a larger region of the S segment could be amplified to confirm the clustering with SHUV strains previously identified in horses and wildlife from South Africa (Figure 2) and p-distances of 94%–100% with strains previously identified in South Africa, Israel, and Nigeria. Mosquito barcodes consisting of 517-bp were used to build a maximum-likelihood tree (Appendix Table 1, Figures 1–3). The barcoding confirmed all morphologic identifications except for a pool of damaged *Aedes* spp. mosquitoes and for *Ae. subargenteus* mosquitoes (for which no other sequence was available in the databases).

Of the 11 pools of SHUV-positive mosquitoes, species belonged to the genera *Mansonia* (5 pools), *Aedes* (3 pools), *Culex* (2 pools), and *Anopheles* (1 pool) (Table 2). Previously, SHUV had been detected in

Table 1. Mosquito species positive for Shuni virus, South Africa, January 2014–May 2018

Species	No. assayed	No. pools positive/no. pools tested	Infection rate, % (95% CI)*
Anopheles pharoensis	27	1/4	39.0 (2.4–212.0)
Culex theileri	508	1/22	1.9 (0.1–9.0)
Cx. annulioris	120	1/7	6.7 (0.5–33.6)
Mansonia africana	340	3/13	8.7 (2.6–23.3)
Ma. uniformis	2,428	2/62	0.8 (0.1–2.7)
Aedes subargenteus	1	1/1	Not applicable†
Ae. mcintoshi	3,653	1/87	0.3 (0.0–1.3)
Aedes spp.	273	1/25	3.6 (0.2–17.2)
Total	7,350	11/221	

*Maximum-likelihood estimation: no. positive/no. mosquitoes assayed × 1,000.
†When all pools tested were positive for Shuni virus, the likelihood methods failed.

Cx. theileri mosquitoes collected in the 1970s near Johannesburg, South Africa (*5*). In that study, 2 pools of SHUV-positive *Cx. theileri* mosquitoes were also identified, although mosquitoes of this species were not abundant in the sites detected.

The highest rate of SHUV detection was in *Mansonia uniformis* mosquitoes, which were found in high numbers at the Shuni virus–positive pool collection sites. Three other arboviruses have been isolated from *M. uniformis* mosquitoes in South Africa: Wesselsbron, Ndumu, and Spondeweni (*13*). *M. africana* mosquitoes tested positive, but only small numbers of these mosquitoes were collected. *Mansonia* spp. mosquitoes can feed readily on humans and animals (*13*) and could have a potential epidemiologic role as bridge species for transmission between animals and humans.

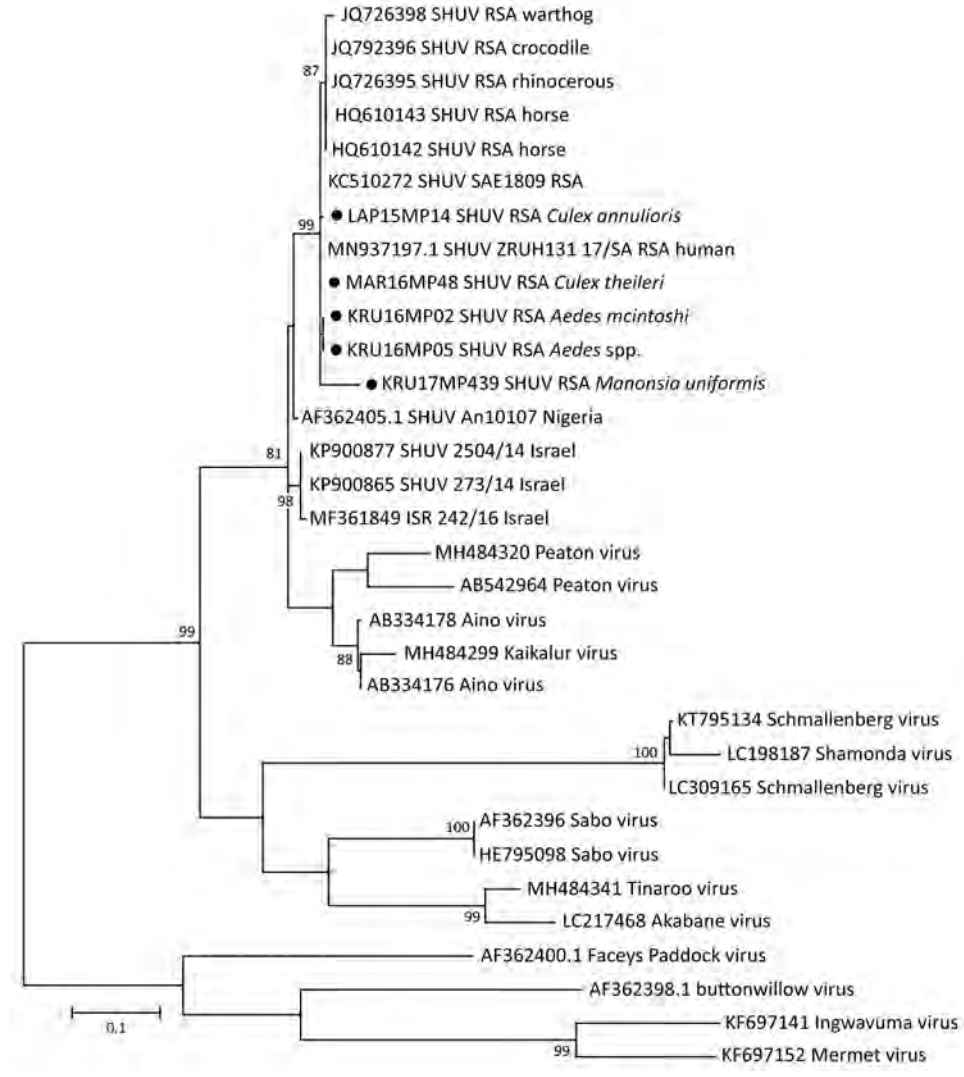

Figure 2. Phylogenetic tree of SHUV-positive homogenate mosquito pools, South Africa, January 2014–May 2018 (black dots), based on 32 sequences and 328 bp of the nucleocapsid gene on the small segment. The tree was constructed with MEGA 7 software (https://www.megasoftware.net) by using the maximum-likelihood method and the Kimura 2-parameter model with 1,000 bootstrap replicates and includes members of the Simbu serogroup. The tree with the highest log likelihood (−299.13) is shown. GenBank accession numbers are indicated for the new and reference strains, which were selected from SHUV strains identified in South Africa among horses and wildlife (*4*,*9*) as well as strains from Nigeria and Israel available in GenBank. Numbers on internal branches indicate bootstrap values. RSA, South Africa; SHUV, Shuni virus.

Table 2. Mosquitoes positive for Shuni virus, South Africa, January 2014–May 2018*

Species	Site	ID no.	Pool size	GenBank SHUV accession no.	GenBank COI accession no.†
Anopheles. pharoensis	Marakele	Mar16mp59	12	NA	MT428079
Culex theileri	Marakele	Mar16mp48	3	MN914125	MT428080
Cx. annulioris	Lapalala	Lap15mp15	4	MN914124	MT428086
Mansonia uniformis	KNP	Knp17mp758	9	NA	MT428087
Ma. africana	KNP	Knp17mp761	41	NA	MT428089
Ma. uniformis	KNP	Knp17mp755	2	NA	MT428088
Ma. africana	KNP	Knp17mp753	1	NA	MT434140
Aedes subargenteus	Jozini	Kzn17mp108	2	NA	MT428082
Ae. mcintoshi	Mnisi	Kru16mp02	4	MT433095	MT428081
Aedes spp.	Mnisi	Kru16mp05	8	MT433096	MT428085
Ma. uniformis	Mnisi	Kru17mp439	50	MT433097	MT428083

*COI, subunit I of the cytochrome oxidase gene; ID, identification; KNP, Kruger National Park; NA, not available because of sequence <200 bp; SHUV, Shuni virus.
†These sequences are available upon request.

Mosquitoes of other species that tested positive included *Aedes mcintoshi* and *Ae. subargenteus.* Positive *Ae. mcintoshi* mosquitoes were collected from Mnisi, where they were the most abundant *Aedes* spp. at that site. They are considered nonspecific/opportunistic feeders and have a broad range of mammal hosts (*14*). *Ae. subargenteus* mosquitoes are tree hole mosquitoes and are either rare in South Africa (*14*) or are not attracted to the traps used in our study. Although little information about those mosquitoes is available, they might have a strong preference for biting humans (*14*).

Although SHUV has been detected in mosquitoes, recent studies have also implicated *Culicoides* spp. midges as potential competent vectors (*15*). An investigation of the vector competence of *Culicoides* midges and laboratory-reared *Cx. pipiens* and *Ae. aegypti* mosquitoes for SHUV (*7*) indicated that neither species of mosquito was susceptible but that *Culicoides* midges demonstrated the capacity to transmit SHUV. No *Ae. aegypti* and *Cx. pipiens* field-caught mosquitoes tested positive for SHUV in this or other studies. Vector competence studies that used SHUV-positive species of mosquitoes identified in our study may define appropriate mosquito vectors and their role in the transmission of SHUV to animals and humans in Africa and the risk to areas where they are found outside the continent.

Conclusions

Entomologic surveillance for orthobunyaviruses revealed a wide range of potential mosquito vectors for SHUV. We identified SHUV in different species of mosquitoes in South Africa, where cases with neurologic signs have been detected in animals (*4*,*5*) and humans (*6*). The identified mosquito species have also been associated with other arboviruses across Africa. SHUV recently emerged in Israel, where it is associated with neurologic disease and birth defects in animals (*3*). Mosquitoes of the identified species are potential vectors of SHUV and may be associated with SHUV outbreaks in Africa and further emergence in new regions.

Acknowledgments

We are grateful to Lapalala Wilderness, Marataba Conservation, South African National Park, for logistical assistance and permission to collect mosquitoes. We acknowledge Leo Braack and Danny Govender for their valuable contribution to mosquito collection. We are grateful to the South Africa Weather Service for providing data for this study.

This study was supported by Cooperative Agreement no. 5 NU2GGH001874-02-00, funded by the Centers for Disease Control and Prevention. It was also funded in part through scholarships from the National Research Foundation and The World Academy of Sciences. A.P.G.A. has been a recipient of the Visiting Professor Programme by the University of Pretoria, South Africa, and acknowledges the Global Health and Tropical Medicine unit. This study was also funded by the Gratama Fund (grant no. 2016.08), the Uyttenboogaart-Eliasen foundation (SUB.2016.12.08), and the RCN-IDEAS travel grant to M.S. and E.E.G.

About the Author

Dr. Guarido completed her PhD degree and performs postdoctoral work at the Faculty of Veterinary Sciences, University of Pretoria. Her primarily research interest is the study of mosquitoborne viruses, with a focus on the entomology aspects of arbovirus transmission cycles.

References

1. Hughes HR, Adkins S, Alkhovskiy S, Beer M, Blair C, Calisher CH, et al.; ICTV Report Consortium. ICTV virus taxonomy profile: *Peribunyaviridae.* J Gen Virol. 2020;101:1–2. https://doi.org/10.1099/jgv.0.001365
2. Causey OR, Kemp GE, Causey CE, Lee VH. Isolations of Simbu-group viruses in Ibadan, Nigeria 1964-69, including

the new types Sango, Shamonda, Sabo and Shuni. Ann Trop Med Parasitol. 1972;66:357–62. https://doi.org/10.1080/00034983.1972.11686835
3. Golender N, Brenner J, Valdman M, Khinich Y, Bumbarov V, Panshin A, et al. Malformations caused by Shuni virus in ruminants, Israel, 2014–2015. Emerg Infect Dis. 2015;21:2267–8. https://doi.org/10.3201/eid2112.150804
4. Steyn J, Motlou P, van Eeden C, Pretorius M, Stivaktas VI, Williams J, et al. Shuni virus in wildlife and non-equine domestic animals in South Africa. Emerg Infect Dis. 2020;26:1521–5. https://doi.org/10.3201/eid2607.190770
5. van Eeden C, Williams JH, Gerdes TG, van Wilpe E, Viljoen A, Swanepoel R, et al. Shuni virus as cause of neurologic disease in horses. Emerg Infect Dis. 2012;18:318–21. https://doi.org/10.3201/eid1802.111403
6. Motlou T, Venter M. Shuni virus in cases of neurological diseases in humans, South Africa. Emerg Infect Dis. 2020;27:567–9.
7. Möhlmann TWR, Oymans J, Wichgers Schreur PJ, Koenraadt CJM, Kortekaas J, Vogels CBF. Vector competence of biting midges and mosquitoes for Shuni virus. PLoS Negl Trop Dis. 2018;12:e0006993. https://doi.org/10.1371/journal.pntd.0006993
8. Gorsich EE, Beechler BR, van Bodegom PM, Govender D, Guarido MM, Venter M, et al. A comparative assessment of adult mosquito trapping methods to estimate spatial patterns of abundance and community composition in southern Africa. Parasit Vectors. 2019;12:462. https://doi.org/10.1186/s13071-019-3733-z
9. Van Eeden C, Zaayman D, Venter M. A sensitive nested real-time RT-PCR for the detection of Shuni virus. J Virol Methods. 2014;195:100–5. https://doi.org/10.1016/j.jviromet.2013.10.008
10. Bowen MD, Trappier SG, Sanchez AJ, Meyer RF, Goldsmith CS, Zaki SR, et al.; RVF Task Force. A reassortant bunyavirus isolated from acute hemorrhagic fever cases in Kenya and Somalia. Virology. 2001;291:185–90. https://doi.org/10.1006/viro.2001.1201
11. Folmer O, Black M, Hoeh W, Lutz R, Vrijenhoek R. DNA primers for amplification of mitochondrial cytochrome c oxidase subunit I from diverse metazoan invertebrates. Mol Mar Biol Biotechnol. 1994;3:294–9.
12. Guarido MM, Riddin MA, Johnson T, Braack LEO, Schrama M, Gorsich EE, et al. *Aedes* species (Diptera: Culicidae) ecological and host feeding patterns in the north-eastern parts of South Africa, 2014-2018. Parasit Vectors. 2021;14:339. https://doi.org/10.1186/s13071-021-04845-9
13. Sharp BL, Appleton CC, Thompson DL, Meenehan G. Anthropophilic mosquitoes at Richards Bay, Natal, and arbovirus antibodies in human residents. Trans R Soc Trop Med Hyg. 1987;81:197–201. https://doi.org/10.1016/0035-9203(87)90214-8
14. Muspratt J. The *Stegomyia* mosquitoes of South Africa and some neighbouring territories. Memoirs of the Entomological Society of Southern Africa. 1956;4:1–138.
15. Snyman J, Venter GJ, Venter M. An investigation of *Culicoides* (Diptera: Ceratopogonidae) as potential vectors of medically and veterinary important arboviruses in South Africa. Viruses. 2021;13:1978. https://doi.org/10.3390/v13101978

Address for correspondence: Marietjie Venter, Zoonotic Arbo- and Respiratory Virus Program, Centre for Viral Zoonosis, Department Medical Virology, Pathology Building, Prinshof Campus South, University of Pretoria, Private Bag X323, Gezina 0031, South Africa; email: marietjie.venter@up.ac.za

Incubation Period for Neuroinvasive Toscana Virus Infections

Lison Laroche,[1] Frédéric Jourdain,[1] Nazli Ayhan, Anne-Laure Bañuls, Rémi Charrel, Jorian Prudhomme

Toscana virus (TOSV) is an emerging pathogen in the Mediterranean area and is neuroinvasive in its most severe form. Basic knowledge on TOSV biology is limited. We conducted a systematic review on travel-related infections to estimate the TOSV incubation period. We estimated the incubation period at 12.1 days.

Toscana virus (TOSV) is an arthropodborne virus transmitted to humans through a bite from an infected sand fly (*1*). An RNA virus, it belongs to the genus *Phlebovirus*, species (*Sandfly fever Naples phlebovirus* family *Phenuiviridae*, order Bunyavirales) (*2*). TOSV infections are endemic to the Mediterranean basin and are considered frequent even though they are neglected (*3*). TOSV can be neuroinvasive and is a major cause of meningitis and encephalitis during summer months in areas to which it is endemic (*4*). However, most infections are asymptomatic or produce mild symptoms (*5*). Thus, TOSV cases are massively underestimated and unreported. Cases are mainly diagnosed by reverse transcription PCR in cerebrospinal fluid, blood, and, rarely, urine or by detecting virus-specific IgM or IgG (*6*). A total of 3 different TOSV lineages (A, B, and C) have been identified, but no clear evidence of a link between clinical manifestation and lineages exists (*7*).

In this study, we considered the incubation period (IP) of an infectious disease as the delay between infection and symptom onset; this definition differs from the latent period, which is defined as the time from infection to infectiousness. For arthropodborne viruses, the infectious bite represents the date of infection (*8*). The potential period of exposure is represented by the length of stay in the country of infection before symptom onset. We therefore focused on imported cases.

Determining the IP is primordial for disease surveillance, outbreak investigation, public health interventions, infectious disease control, and modeling (*9*). However, IP estimates are often unsourced, imprecise, and based on limited evidence, as illustrated by the heterogeneous values proposed (Appendix Table 1, https://wwwnc.cdc.gov/EID/article/27/12/20-3172-App1.pdf). In this context, we conducted a systematic review of symptomatic travel-related neuroinvasive forms of TOSV to provide an evidence-based estimate of the IP.

The Study

We used PubMed and ISI Web of Knowledge search engines with no restriction on language and the phrase "Toscana AND virus AND (case report OR case-report OR travel* OR import*)." We conducted a systematic search on ProMed and Google Scholar, as well as cross-reference checking. The inclusion criteria were laboratory-documented acute TOSV infection, indication of a travel-related infection in a TOSV-endemic area, and number of days between travel return and symptom onset. Two reviewers screened titles, abstracts, and full-text articles independently.

We extracted clinic and biologic elements from neuroinvasive TOSV case reports. For each patient, data related to the duration of travel and the time of symptom onset, gender, age, country in which case was reported, and country of infection were reported.

To estimate the IP, we used censored time-to-event models (*10*). Interval-censored observations related to travel duration represented the exposure time. Absence of a departure date was treated as left-censored data, whereas onset of illness during the travel period was considered right-censored. We performed data analysis by using R with the icenReg

Author affiliations: Université de Montpellier, Institut de Recherche pour le Développement, Centre National de la Recherche Scientifique, Montpellier, France (L. Laroche, F. Jourdain, A.-L. Bañuls, J. Prudhomme); Santé Publique France, Saint-Maurice, France (F. Jourdain); Aix-Marseille Université, Institut de Recherche pour le Développement, Institut national de la santé et de la recherche médicale, Marseille, France (N. Ayhan, R. Charrel)

DOI: https://doi.org/10.3201/eid2712.203172

[1]These authors contributed equally to this article.

package (R Foundation for Statistical Computing, https://www.r-project.org). We defined the data distribution with 4 parametric models (log-normal, log-logistic, Gamma, and Weibull). To determine the best model for our distribution, we calculated the Akaike information criterion. We used the nonparametric log-rank test from the interval package to assess the effect of age and gender as covariates. To check the result stability, we performed an additional Bayesian approach, fitting with the Weibull distribution.

Regarding imported case reports, 142 documents were identified on PubMed and 133 on Web of Knowledge. We removed 79 duplicates and excluded 118 records after screening titles and abstracts. A total of 42 articles were eligible after full-text reading. We then selected 22 documents for data extraction. A total of 24 cases were selected (Appendix Table 2, Figure). All travel-associated cases fulfilling the inclusion criteria were neuroinvasive; these cases were diagnosed in a non–TOSV-endemic area after a stay in a proven TOSV-endemic area (Figure 1).

We selected Weibull distribution because it presented the lower Akaike information criterion (Figure 2; Appendix Table 3). The median IP for neuroinvasive forms is estimated to be 12.1 (95% CI 10.2–14.4) days. In 5% of neuroinvasive cases, symptoms will develop by 6.8 (95% CI 3.8–9.9) days after an infectious bite; symptoms will develop in 95% of cases by 16.8 (95% CI 13.9–21.7) days after the infectious bite. We found no evidence of age or gender effect on the length of the IP (p value >0.05 by log-rank test). By using Bayesian analysis, we found an IP of 12.1 (95% CI 9.9–14.4) days (data not shown; results same as Figure 2).

Conclusions

In the literature, the IP values of TOSV are often heterogeneous, unsourced, or without evidence and therefore do not constitute a valid estimate for clinical or infection control decisions. Our literature review identified 24 neurologic cases of TOSV infection. Some travel durations were reported approximately in case reports and were not included in the analysis. All the data used were based on severe neurologic forms of the disease, which required hospitalization soon after the exposure period.

We estimated the median IP of TOSV at 12 (95% CI 10.2–14.4) days. Considering the delay from infection to symptom onset, this value is greater than that for most other arboviruses (*11*). Our estimate of the IP is evidence-based and relies on data from well-characterized cases. However, cases that cause mildersymptoms, as opposed to neuroinvasive forms of the disease, might have a shorter IP (similar to

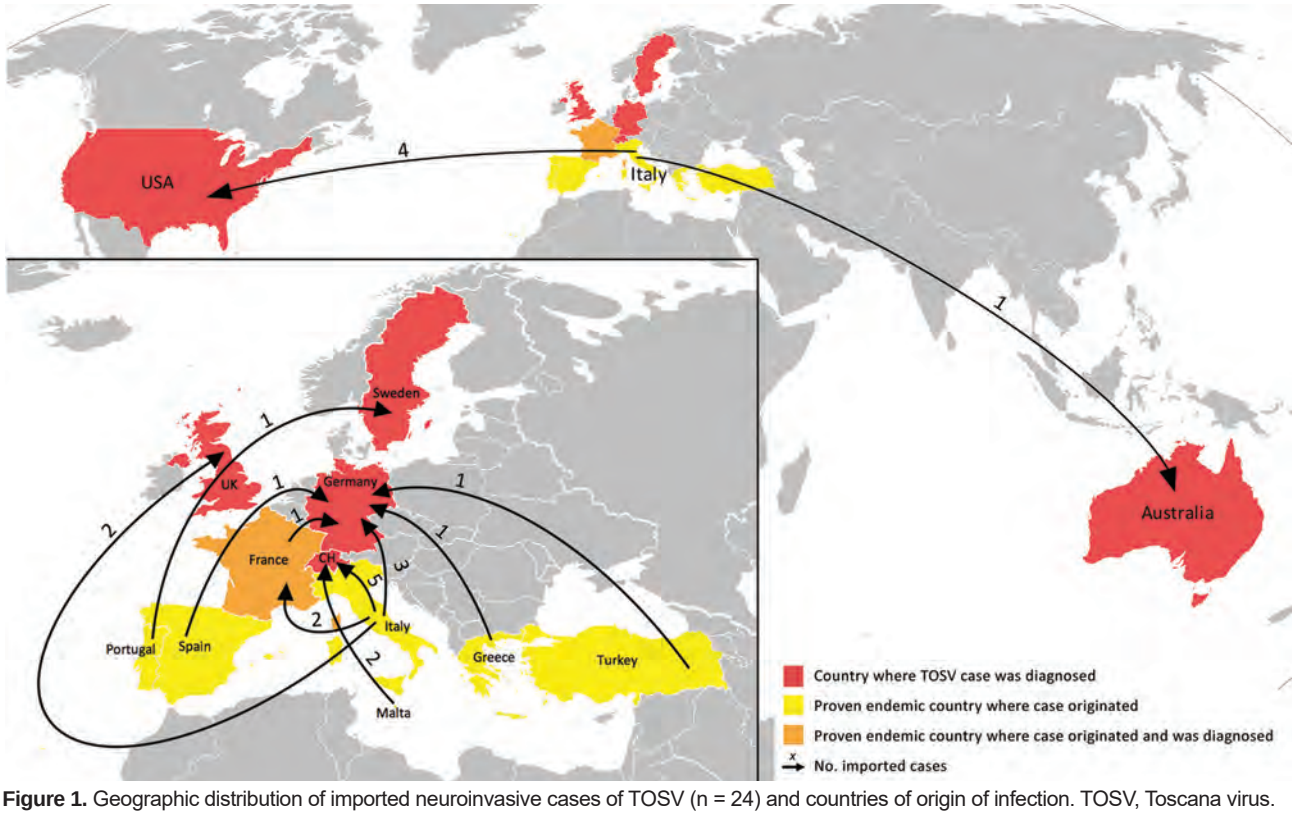

Figure 1. Geographic distribution of imported neuroinvasive cases of TOSV (n = 24) and countries of origin of infection. TOSV, Toscana virus.

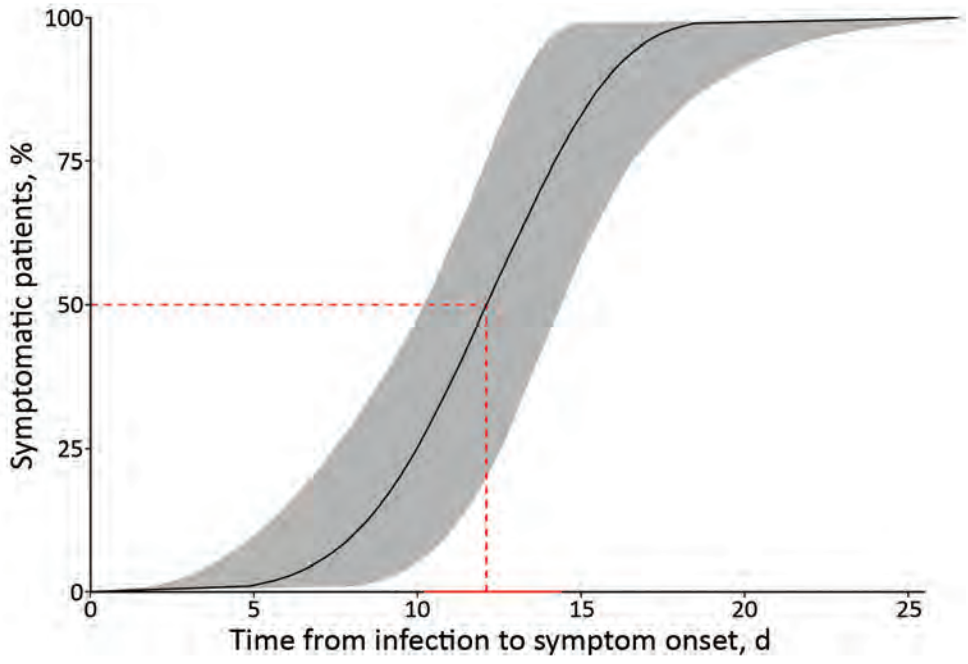

Figure 2. Cumulative percentage of Toscana virus cases manifesting with neurologic symptoms by a given day under the estimates for the Weibull parametric distribution (n = 24). Red dashed line represents the median estimation of the incubation period. Solid red horizontal line represents the 95% CI of the median. Gray shading indicates the 95% CI of the values.

other arboviruses). Other symptoms associated with paucisymptomatic forms of TOSV might not have been described yet and should be further investigated to improve case definition and diagnosis.

We also cannot exclude infections by other sandfly fever Naples phleboviruses because of cross-reaction risk in serologic analyses due to their close genetic relationships (*12*). However, the incidence in the population of other genetically similar phleboviruses is lower than TOSV, and TOSV remains the most common cause of neuroinvasive symptoms (*3*). Knowledge of TOSV genotypes and their aptitude to cause different clinical forms is limited (*12*). Analyzing this hypothesis was not possible because of the limited amount of available data. In addition to the genotype, other parameters may influence the IP, such as viral strain, patient's immune status, or viremia (*9*). The amount of virus transmitted during bites (viral load) could also influence the IP and should be further investigated.

In addition, all other cases were diagnosed in countries or regions to which TOSV is not endemic (United States, United Kingdom, Sweden, Germany, Switzerland, Australia, and France). These imported cases represent a risk for emergence in these areas when vectors are established (*13*), as has been observed for other vectorborne diseases (*14*). Moreover, sand flies are known to spread in countries or regions to which TOSV is not endemic (*15*).

Currently, information on TOSV infections is lacking (*12*). Precise definitions of the IP should provide more information on the disease epidemiology and on its development in the human host. Moreover, because the IP is a key parameter for disease modeling (*9*), it would improve our understanding of the disease transmission dynamics. More reports of travel-related cases and standardization of data collection with reliable information (e.g., location and duration of the trips and precise dates of symptom onset) are clearly needed. The IP estimation will be improved with addition of new data.

Acknowledgments

We thank Julian Wei-Tze Tang, James Farrugia, Jonas Schmidt-Chanasit, Josef Georg Heckmann, and David Breen for answering our questions by email to clarify information regarding the TOSV case reports. We also thank Eric Elguero for his support in statistical analysis, Heïdi Lançon for the English revision of the manuscript, and Jérôme Depaquit for reviewing the manuscript.

This research was funded by the IRD (Institut de Recherche pour le Développement), CNRS (Centre National de la Recherche Scientifique), UM (Université de Montpellier) and by the by the European Virus Archive Global (EVA-GLOBAL) project that has received funding from the European Union's Horizon 2020-INFRAIA-2019 research and innovation program under grant agreement No 871029. F.J. is financially supported by the SPF (Santé Publique France) through a doctoral fellowship, J.P. by the INFRAVEC2 project (https://infravec2.eu), L.L. by a UM doctoral fellowship, and N.A. by a postdoctoral fellowship from the AMU (Aix Marseille University).

About the Author

Ms. Laroche is a doctoral student at the French National Research Institute for Sustainable Development and the University of Montpellier, France. Her primary research interests are medical entomology, especially the interactions between pathogens (*Phlebovirus, Leishmania*), and their vector (the sand fly).

References

1. Depaquit J, Grandadam M, Fouque F, Andry PE, Peyrefitte C. Arthropod-borne viruses transmitted by Phlebotomine sandflies in Europe: a review. Euro Surveill. 2010;15:19507. https://doi.org/10.2807/ese.15.10.19507-en
2. Ayhan N, Prudhomme J, Laroche L, Bañuls AL, Charrel RN. Broader geographical distribution of toscana virus in the Mediterranean region suggests the existence of larger varieties of sand fly vectors. Microorganisms. 2020;8:e114. https://doi.org/10.3390/microorganisms8010114
3. Charrel RN, Bichaud L, de Lamballerie X. Emergence of Toscana virus in the Mediterranean area. World J Virol. 2012;1:135–41. https://doi.org/10.5501/wjv.v1.i5.135
4. Charrel RN, Gallian P, Navarro-Marí JM, Nicoletti L, Papa A, Sánchez-Seco MP, et al. Emergence of Toscana virus in Europe. Emerg Infect Dis. 2005;11:1657–63. https://doi.org/10.3201/eid1111.050869
5. Braito A, Corbisiero R, Corradini S, Marchi B, Sancasciani N, Fiorentini C, et al. Evidence of Toscana virus infections without central nervous system involvement: a serological study. Eur J Epidemiol. 1997;13:761–4. https://doi.org/10.1023/A:1007422103992
6. Ergunay K, Kaplan B, Okar S, Akkutay-Yoldar Z, Kurne A, Arsava EM, et al. Urinary detection of toscana virus nucleic acids in neuroinvasive infections. J Clin Virol. 2015;70:89–92. https://doi.org/10.1016/j.jcv.2015.07.297
7. Ayhan N, Charrel RN. Of phlebotomines (sandflies) and viruses: a comprehensive perspective on a complex situation. Curr Opin Insect Sci. 2017;22:117–24. https://doi.org/10.1016/j.cois.2017.05.019
8. Pingen M, Bryden SR, Pondeville E, Schnettler E, Kohl A, Merits A, et al. Host inflammatory response to mosquito bites enhances the severity of arbovirus infection. Immunity. 2016;44:1455–69. https://doi.org/10.1016/j.immuni.2016.06.002
9. Chan M, Johansson MA. The incubation periods of Dengue viruses. PLoS One. 2012;7:e50972. https://doi.org/10.1371/journal.pone.0050972
10. Cowling BJ, Muller MP, Wong IOL, Ho LM, Louie M, McGeer A, et al. Alternative methods of estimating an incubation distribution: examples from severe acute respiratory syndrome. Epidemiology. 2007;18:253–9. https://doi.org/10.1097/01.ede.0000254660.07942.fb
11. Rudolph KE, Lessler J, Moloney RM, Kmush B, Cummings DAT. Incubation periods of mosquito-borne viral infections: a systematic review. Am J Trop Med Hyg. 2014;90:882–91. https://doi.org/10.4269/ajtmh.13-0403
12. Maes P, Adkins S, Alkhovsky SV, Avšič-Županc T, Ballinger MJ, Bente DA, et al. Taxonomy of the order Bunyavirales: second update 2018. Arch Virol. 2019;164:927–41. https://doi.org/10.1007/s00705-018-04127-3
13. Knechtli R, Jenni L. Distribution and relative density of three sandfly (Diptera: Phlebotominae) species in southern Switzerland [in French]. Ann Parasitol Hum Comp. 1989;64:53–63. https://doi.org/10.1051/parasite/198964153
14. Liang G, Gao X, Gould EA. Factors responsible for the emergence of arboviruses; strategies, challenges and limitations for their control. Emerg Microbes Infect. 2015;4:e18. https://doi.org/10.1038/emi.2015.18
15. Maroli M, Feliciangeli MD, Bichaud L, Charrel RN, Gradoni L. Phlebotomine sandflies and the spreading of leishmaniases and other diseases of public health concern. Med Vet Entomol. 2013;27:123–47. https://doi.org/10.1111/j.1365-2915.2012.01034.x

Address for correspondence: Lison Laroche, UMR MIVEGEC, IRD–CNRS–Université de Montpellier, 911 avenue Agropolis, F34394 Montpellier, France; email: lisonlaroche14@gmail.com

Uptake, Retention, and Excretion of Infectious Prions by Experimentally Exposed Earthworms

Sandra Pritzkow, Rodrigo Morales, Manuel Camacho, Claudio Soto

Prions are proteinaceous infectious agents that can be transmitted through various components of the environment, including soil particles. We found that earthworms exposed to prion-contaminated soil can bind, retain, and excrete prions, which remain highly infectious. Our results suggest that earthworms potentially contribute to prion disease spread in the environment.

Prions are unique infectious agents composed exclusively of a misfolded form of the prion protein (PrP^{Sc}) (*1*). Among prion diseases, chronic wasting disease, affecting cervids, and scrapie, affecting sheep, are highly contagious. Studies conducted in natural and experimental conditions suggest that these diseases likely are transmitted via environmental contamination and that soil is a primary vector (*2*–*4*). We examined whether earthworms contribute to environmental spread of infectious prions.

The Study

To investigate whether earthworms can act as carriers of infectious prions, we exposed groups of worms (*Eisenia fetida*) to soil previously mixed with brain homogenate (BH) from clinically diseased 263K Syrian golden hamsters (*Mesocricetus auratus*) (Harlan Envigo, https://www.envigo.com). For experiments, we homogenously mixed 375 g of Elliot soil (kindly provided by Joel Pedersen, Johns Hopkins University) with 25 mL of 10% wt/vol 263K brain homogenate. We assessed whether prions bind to worms or worm-associated soil by using protein misfolding cyclic amplification (PMCA) technology (*5*,*6*), which can detect prions down to the level of a single particle (*7*). Because PMCA efficiency can be severely affected by components in the inoculum (*6*), we first analyzed the effect of worm homogenate (WH) with or without soil on the efficiency of in vitro prion replication by PMCA (Appendix Figure 1, https://wwwnc.cdc.gov/EID/article/27/12/20-4236-App1.pdf). Our results indicated that whole WH does interfere with the reaction, but we could still obtain maximum amplification after 3 rounds of PMCA (Appendix Figure 1).

After verifying PMCA efficiency, we tested worms exposed to contaminated soil for different lengths of time. We collected worms from contaminated soil after 1, 3, 7, 14, and 28 days of exposure (Figure 1, panel A). PMCA results showed that worms exposed to prions take up PrP^{Sc} and efficiently sustain prion replication at all exposure times tested (Figure 1, panel B). We observed no PrP^{Sc} uptake in any worms exposed to control soil.

To study whether contaminated worms can transmit disease, we intraperitoneally injected hamsters with WH obtained from worms exposed to prion-soil mix for 28 days. To assess reproducibility, we used 3 different worms for this assay. Our results showed that worms exposed to prion-contaminated soil can transmit prion disease, albeit with variable efficiencies (Appendix Figure 2). Of the 3 worm extracts, 2 caused an attack rate of 4/5 and mean incubation periods of 237 (SE ±39) and 255 (SE ±25) days. A third WH transmitted disease to only 1/5 injected hamsters, which showed an incubation period of 272 days (Appendix Figure 2). For positive controls, we intraperitoneally injected groups of hamsters directly with 10% 263K BH. Terminal disease developed in all animals; the median incubation period was 151.4 (SE ±30) days (Appendix Figure 2). We confirmed prion disease by biochemical detection of protease-resistant PrP (Figure 1, panel C). We did not detect a PrP^{Sc} signal in hamsters that did not show clinical signs, suggesting the absence of preclinical prion disease in

Author affiliations: University of Texas Health Science Center at Houston, Houston, Texas, USA (S. Pritzkow, R. Morales, M. Camacho, C. Soto); CIBQA, Universidad Bernardo O'Higgins, Santiago, Chile (R. Morales); Case Western Reserve University, Cleveland, Ohio, USA (M. Camacho)

DOI: https://doi.org/10.3201/eid2712.204236

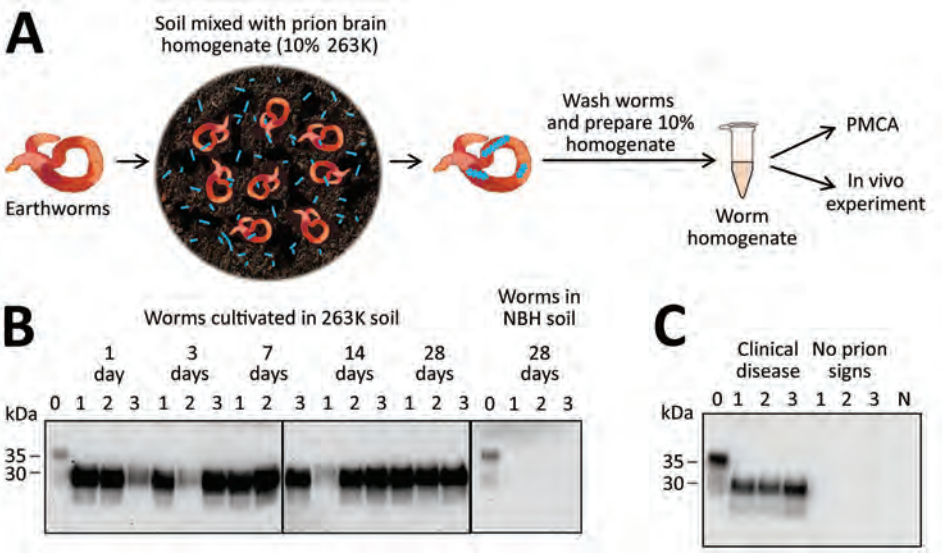

Figure 1. Detection of prion protein (PrP^{Sc}) attached to earthworms by PMCA and infectivity bioassay. A) Process for exposing earthworms to infected soil. Earthworms were placed in soil mixed with 10% wt/vol infected 263K hamster brain homogenate for 1, 3, 7, 14, or 28 days; worms were washed thoroughly, then prepared into a 10% homogenate for analysis. B) Results of PMCA on earthworms exposed to contaminated soil. As a control, earthworms also were exposed to soil mixed with NBH for 28 days and analyzed with the same methods. For each measurement, 3 worms were analyzed per time point in 3 different gels but blotted in the same membrane. Lane 0 is NBH used as a positive control for electrophoretic migration of the normal prion protein (PrP^{C}); lanes 1–3 indicate 3 different worms. Vertical lines between images depict membrane splicing. Numbers on the left indicate molecular weight markers. C) Biochemical analysis of brains of hamsters infected with worm homogenate. Groups of hamsters were injected with homogenates from 3 different worms exposed to prion contaminated soil; many of the animals developed prion disease (Appendix Figure 2, https://wwwnc.cdc.gov/EID/article/27/12/20-4236-App1.pdf). Brains were collected and homogenized and samples were digested with proteinase K (Sigma Aldrich, https://www.sigmaaldrich.com) at 50 μg/mL for 1 h at 37°C, except NBH (lane labeled N) used as a migration control. Numbers on the left indicate molecular weight markers. Results confirmed the presence of PrP^{Sc} accumulation in the brain of animals showing clinical signs of prion disease. NBH, normal hamster brain homogenate; PMCA, protein misfolding cyclic amplification.

those animals. Comparing incubation time and attack rate data obtained with WH and different dilutions of infected brain material suggests that the number of prions in each worm is equivalent to 1×10^{-5} to 1×10^{-6} dilution of infected brain. This estimation also is supported by analysis of the data by using a semiquantitative PMCA technique (*8*).

To investigate whether earthworms can retain infectious prions when exposed for different lengths of time to a prion-free environment, we exposed experimental subjects to prion-containing soil and subsequently transferred worms to naive soil (Figure 2, panel A). We collected worms from prion-containing soil after 7 days of exposure, thoroughly cleaned soil attached to the worms' surface, and cultivated worms in naive soil for another 1, 3, 7, 14, and 28 days; we collected and analyzed 4 worms at each time point. PMCA results showed PrP^{Sc}–positive signal for all 4 worms immediately after exposure to prion-contaminated soil (Figure 2, panel B). We found that 25%–50% of worms exposed to prion-free naive soil retained PMCA-detectable PrP^{Sc} (Figure 2, panel B). We observed no clear trend with the time of incubation in naive soil, and even animals exposed to prion-free soil for 28 days retained prions in their bodies (Figure 2, panel B).

To evaluate whether prion-contaminated earthworms excrete PrP^{Sc} back into the environment, we analyzed worm castings by using PMCA. We collected 2 worms exposed to prion-contaminated soil for 7 days and thoroughly washed worms with water. For casting collection, we placed animals in petri dishes and collected 8 pieces of casting from the petri dish to analyze PrP^{Sc} content by PMCA (Figure 2, panel C). The results showed 6/8 casting samples were positive for PrP^{Sc} (Figure 2, panel D). Of note, 3 samples had large amounts of PrP^{Sc} detectable by just 2 rounds of PMCA, indicating that earthworms exposed to prions in soil can take up and release PrP^{Sc} competent for prion replication.

Finally, to study whether some PrP^{Sc} molecules taken up from the soil remain attached to the body of the animal, we contaminated 6 worms by exposure to contaminated soil for 7 days. After washing to remove outside soil, we dissected animals to completely remove all soil particles inside the animal. We thoroughly washed worm bodies, homogenized them, and then used the homogenate for PrP^{Sc} detection by PMCA. Of the 6 six soil-void worms, 5 were positive for PrP^{Sc} after only 2 rounds of PMCA (Figure 2, panel E). The sixth worm became positive in the third PMCA round, as did control worms from which we

did not remove internal soil (Figure 2, panel E). These results suggest that a substantial part of PrP^{Sc} taken up by worms from soil remained attached to the body of the animal and not merely in the soil particles that the worm acquired.

Conclusions

The mechanisms implicated in the natural spread of infectious prions are not completely known. Some prion diseases, such as chronic wasting disease and scrapie, are thought to be highly transmissible through

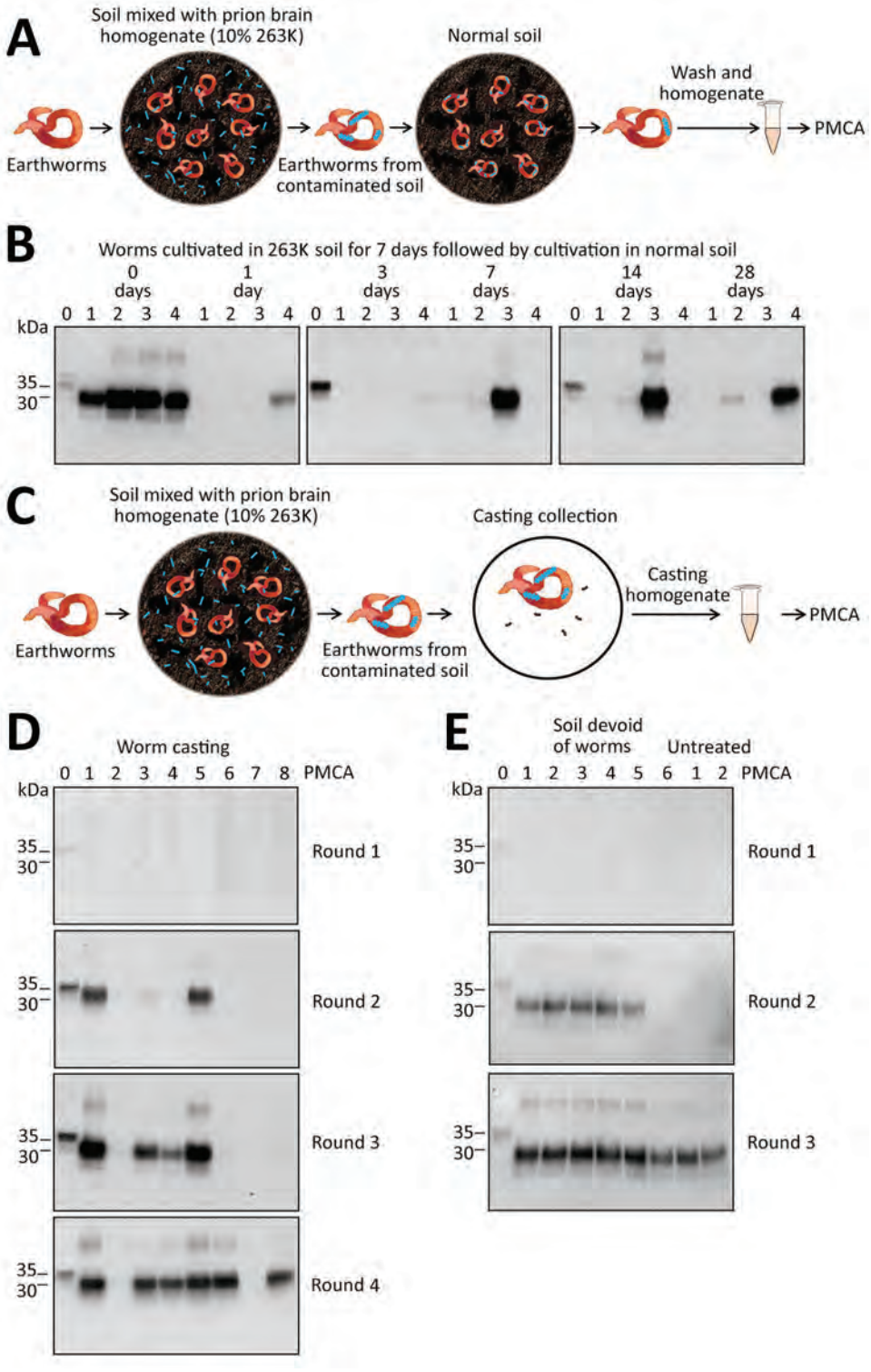

Figure 2. Detection of pathological prion protein (PrP^{Sc}) retention and dispersion by earthworms. A) Process for exposing earthworms to PrP^{Sc}–contaminated soil and analyzing for PrP^{Sc} retention. Worms were kept in PrP^{Sc}–contaminated soil for 7 days, then transferred to normal, prion-free soil and collected at various times. After collection, worms were thoroughly washed, homogenized, and used for PrP^{Sc} detection. B) Western blot analysis of PMCA of worm samples after cultivation in 263K-contaminated soil for 7 days and exposure to normal soil for 0, 1, 3, 7, 14, and 28 days. Lane 0 is normal brain homogenate (NBH) used as positive control; lanes 1–4 indicate 4 different worms for each time point. C) Process for collecting castings excreted by prion-contaminated worms to analyze for PrP^{Sc}. D) PMCA results for castings collected from earthworms exposed to 263K-soil for 7 days. Samples 1–8 were harvested and subjected to 4 PMCA rounds. E) Detection of PrP^{Sc} attached to 6 earthworms after exposure to prion-contaminated soil for 7 days. After collection and thorough washing, worms were dissected, and soil was carefully removed from the inside of the animal (soil-devoid worms). Worm carcasses were homogenized and used for PMCA detection of $PrPS^{c}$. As controls, we used 2 untreated worms, that is, worms for which no soil was removed. In panels B, D, and E, all samples were digested with proteinase K (Sigma Aldrich, https://www.sigmaaldrich.com) at 50 μg/mL for 1 h at 37°C, except the NBH used as a migration control of PrP^{C}. Numbers on the left indicate molecular weight markers. PMCA, protein misfolding cyclic amplification.

exposure to prion-contaminated environments (*2*,*3*). We previously demonstrated that infectious prions can attach to various components of the environment, including soil, plants, wood, and rock, and to several man-made surfaces, such as metals, plastic, and glass (*9*,*10*). However, little is known about how organisms living in the prion-exposed environment contribute to the spread of prions. In this study, we focused on earthworms (*E. fetida*) that live in close contact with known sources of prion infectivity in the environment, soil and diseased carcasses, and can move at a rate of 20–70 m/h (*11*,*12*). Our results demonstrate that earthworms can efficiently take up prions and act as vectors of prion disease transmission. In worms exposed to prion-contaminated soil, we noted PrP^{Sc} competent for both in vitro prion replication and in vivo infectivity. Even a relatively short exposure of 1 day was enough to contaminate all exposed worms. Of note, within 1 day after moving contaminated worms into prion-free soil, many earthworms were free of infectious particles. However, 25%–50% of worms retained PMCA-detectable PrP^{Sc} even 28 days after living in noncontaminated soil. Dissection of the worm's bodies to separate tissue from soil inside the animal showed that a substantial amount of PrP^{Sc} was in the worm bodies. Furthermore, analysis of the casting excreted by contaminated worms showed that 75% of the animal feces contained a relatively large quantity of PrP^{Sc} detectable by PMCA. These results suggest that earthworms exposed to prions remain potentially infectious for long periods and release prions back into the soil, therefore possibly contributing to the spread of infectious prions in nature.

Acknowledgments

We thank Joel Pedersen for providing Elliot soil used for these studies.

This study was supported in part by grants from the National Institute of Health (no. P01AI077774 to C.S. and no. R01AI132695 to R.M.) and the US Department of Agriculture Animal and Plant Health Inspection Service (grant no. AP20VSSPRS00C143 to R.M.). The funders had no role in study design, data collection and analysis, decision to publish, or preparation of the manuscript.

C.S. is inventor on several patents related to the protein misfolding cyclic amplification (PMCA) technology and is currently founder, chief scientific officer, and member of the board of directors of Amprion, Inc. (https://amprionme.com), a biotech company focusing on the commercial utilization of PMCA for prion diagnosis. R.M. is listed as an inventor in a patent associated with the PMCA technology. S.P. also has a conflict of interest related to the PMCA technology and Amprion, Inc. The University of Texas System has licensed intellectual property to Amprion, Inc.

About the Author

Dr. Pritzkow is an assistant professor in the Department of Neurology, University of Texas McGovern Medical School in Houston, Texas, USA. Her research interest is in the development of biochemical techniques for detecting prion-like neurodegenerative diseases.

References

1. Prusiner SB. Prions. Proc Natl Acad Sci U S A. 1998;95:13363–83. https://doi.org/10.1073/pnas.95.23.13363
2. Escobar LE, Pritzkow S, Winter SN, Grear DA, Kirchgessner MS, Dominguez-Villegas E, et al. The ecology of chronic wasting disease in wildlife. Biol Rev Camb Philos Soc. 2020;95:393–408. https://doi.org/10.1111/brv.12568
3. Saunders SE, Bartelt-Hunt SL, Bartz JC. Prions in the environment: occurrence, fate and mitigation. Prion. 2008;2:162–9. https://doi.org/10.4161/pri.2.4.7951
4. Giachin G, Narkiewicz J, Scaini D, Ngoc AT, Margon A, Sequi P, et al. Prion protein interaction with soil humic substances: environmental implications. PLoS One. 2014;9:e100016. https://doi.org/10.1371/journal.pone.0100016
5. Saborio GP, Permanne B, Soto C. Sensitive detection of pathological prion protein by cyclic amplification of protein misfolding. Nature. 2001;411:810–3. https://doi.org/10.1038/35081095
6. Morales R, Duran-Aniotz C, Diaz-Espinoza R, Camacho MV, Soto C. Protein misfolding cyclic amplification of infectious prions. Nat Protoc. 2012;7:1397–409. https://doi.org/10.1038/nprot.2012.067
7. Saá P, Castilla J, Soto C. Ultra-efficient replication of infectious prions by automated protein misfolding cyclic amplification. J Biol Chem. 2006;281:35245–52. https://doi.org/10.1074/jbc.M603964200
8. Chen B, Morales R, Barria MA, Soto C. Estimating prion concentration in fluids and tissues by quantitative PMCA. Nat Methods. 2010;7:519–20. https://doi.org/10.1038/nmeth.1465
9. Pritzkow S, Morales R, Lyon A, Concha-Marambio L, Urayama A, Soto C. Efficient prion disease transmission through common environmental materials. J Biol Chem. 2018;293:3363–73. https://doi.org/10.1074/jbc.M117.810747
10. Pritzkow S, Morales R, Moda F, Khan U, Telling GC, Hoover E, et al. Grass plants bind, retain, uptake, and transport infectious prions. Cell Rep. 2015;11:1168–75. https://doi.org/10.1016/j.celrep.2015.04.036
11. Zirbes L, Brostaux Y, Mescher M, Jason M, Haubruge E, Deneubourg JL. Self-assemblage and quorum in the earthworm *Eisenia fetida* (Oligochaete, Lumbricidae). PLoS One. 2012;7:e32564. https://doi.org/10.1371/journal.pone.0032564
12. Venter JM, Reinecke AJ. The life-cycle of the compost worm *Eisenia fetida* (Oligochaeta). S Afr J Zool. 1988;23:161–5. https://doi.org/10.1080/02541858.1988.11448096

Address for correspondence: Claudio Soto, University of Texas McGovern Medical School, 6431 Fannin St, Houston, TX 77030, USA; email: Claudio.Soto@uth.tmc.edu

Trichinella spiralis [tri·kuh·neh′·luh spr·a′·luhs]

Monika Mahajan

Trichinella is derived from the Greek words *trichos* (hair) and *ella* (diminutive); *spiralis* means spiral. In 1835, Richard Owen (1804–1892) and James Paget (1814–1899) described a spiral worm (*Trichina spiralis*)–lined sandy diaphragm of a cadaver. In 1895, Alcide Raillet (1852–1930) renamed it as *Trichinella spiralis* because *Trichina* was attributed to an insect in 1830. In 1859, Rudolf Virchow (1821–1902) described the life cycle. The genus includes many distinct species, several genotypes, and encapsulated and nonencapsulated clades based on the presence/absence of a collagen capsule.

Figure 1. Sir James Paget (January 11, 1814–December 30, 1899), English surgeon and pathologist who observed a spiral encysted nematode in a cadaver. Source: http://resource.nlm.nih.gov/101425853

The smallest, viviparous nematode or pig parasite has sylvatic and domestic cycles and causes trichinellosis or trichinosis. Transmission occurs through the consumption of meat infected with pathogenic cysts, encasing larvae. Human-to-human transmission has not been reported.

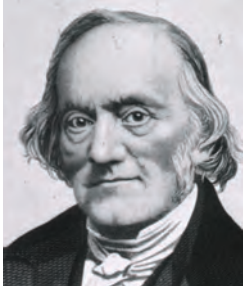

Figure 2. Sir Richard Owen (July 20, 1804–December 18, 1892), English biologist, comparative anatomist, and paleontologist who did not share the credit of discovery of *Trichina spiralis* with Paget. Source: http://resource.nlm.nih.gov/101424684.

Figure 3. Photomicrograph of an intestinal mucosa tissue specimen showing a *Trichinella spiralis* parasitic nematode, which had burrowed itself into the columnar epithelial intestinal lining, in a case of trichinosis. Source: CDC/Dr. Robert Kaiser (https://phil.cdc.gov/Details.aspx?pid=14931).

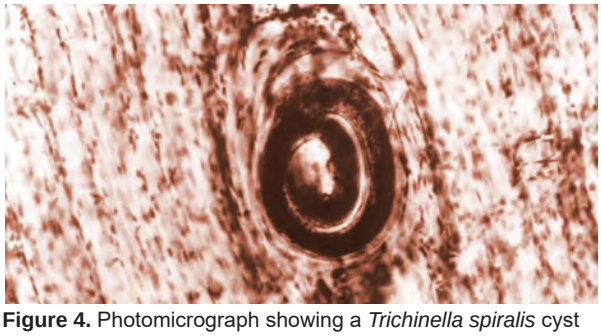

Figure 4. Photomicrograph showing a *Trichinella spiralis* cyst that was embedded in a muscle tissue specimen, in a case of trichinellosis, acquired by ingesting meat containing cysts (encysted larvae) of *Trichinella* sp. Source: CDC/Dr. Irving Kagan (https://phil.cdc.gov/Details.aspx?pid=10180).

Sources

1. Campbell WC. History of trichinosis: Paget, Owens and the discovery of *Trichinella spiralis*. Bull Hist Med. 1979;53:520–52.
2. Centers for Disease Control and Prevention. Trichinellosis: general information [cited 2021 May 11]. https://www.cdc.gov/parasites/trichinellosis/gen_info/faqs.html
3. Gottstein B, Pozio E, Nöckler K. Epidemiology, diagnosis, treatment, and control of trichinellosis. Clin Microbiol Rev. 2009;22:127–45. https://doi.org/10.1128/CMR.00026-08
4. Observations on *Trichina spiralis*. Boston Med Surg J. 1860; 63:294–8. https://doi.org/10.1056/NEJM186011080631504
5. Zarlenga D, Thompson P, Pozio E. *Trichinella* species and genotypes. Res Vet Sci. 2020;133:289–96. https://doi.org/10.1016/j.rvsc.2020.08.012

Address for correspondence: Monika Mahajan, Medical Microbiology, Postgraduate Institute of Medical Education and Research, Research Block A, Sector 12, Chandigarh 160012, India; email: monideepmj@yahoo.com

DOI: https://doi.org/10.3201/eid2712.211230

Author affiliation: Postgraduate Institute of Medical Education and Research, Chandigarh, India

Experimental Oronasal Transmission of Chronic Wasting Disease Agent from White-Tailed Deer to Suffolk Sheep

Eric D. Cassmann, S. Jo Moore, Justin J. Greenlee

Chronic wasting disease (CWD) is a fatal prion disease of cervids. We examined host range of CWD by oronasally inoculating Suffolk sheep with brain homogenate from a CWD-positive white-tailed deer. Sixty months after inoculation, 1/7 sheep had immunoreactivity against the misfolded form of prion protein in lymphoid tissue. Results were confirmed by mouse bioassay.

Transmissible spongiform encephalopathies (TSEs), also known as prion diseases, are a group of fatal neurologic diseases caused by a misfolded form of the prion protein (PrP^{Sc}). Several TSEs affect livestock, including scrapie in sheep and chronic wasting disease (CWD) in cervids.

Susceptibility of sheep to the agent of scrapie is determined by the host prion protein genotype. Three polymorphisms at codons 136, 154, and 171 of the prion protein gene occur in sheep. The haplotype $A_{136}R_{154}R_{171}$ is associated with resistance to scrapie, whereas VRQ is linked with susceptibility. Likewise, the deer prion protein genotype GG_{96} is overrepresented in cases of CWD.

CWD was identified in captive mule deer in Colorado, USA, in 1967 (*1*). Since then, CWD has been reported in ≥24 states in the United States, 2 provinces in Canada, and South Korea (*2*,*3*). During 2016, CWD was reported in Europe, and it has since been detected in 3 Nordic countries (Norway, Sweden, and Finland), although CWD strains in Europe were recently shown to be distinct from strains in North America (*4*). Because of human consumption of cervid meat products and intermingling of various livestock species with wild cervid populations, there is major interest in characterizing the possible host range of CWD.

Scrapie has been implicated as the possible source of CWD in cervids (*5*). This finding is supported by in vitro conversion of sheep prion protein by infectious CWD prions (*6*) and glycoprofile similarities between scrapie and CWD prions (*7*). Another similarity between scrapie and CWD is prominent lymphoid accumulation of PrP^{Sc} in both species affected (*5*). Experimental transmission of mule deer CWD to Suffolk sheep by intracranial inoculation, a highly artificial route of transmission, has been performed (*8*). Widespread peripheral lymphoid accumulation of PrP^{Sc} is retained in intracranially CWD inoculated sheep.

The objective of this study was to test the oronasal susceptibility of sheep to the agent of CWD. We report the preliminary findings of an ongoing multiyear study.

The Study

Initially, we oronasally inoculated (*9*) seven Suffolk lambs (3–4 months of age) with the $V_{136}R_{154}Q_{171}$/ARQ (n = 2), ARQ/ARQ (n = 4), or ARQ/ARR (n = 1) prion protein genotype and 0.1 g of 10% (wt/vol) brain homogenate from a GG_{96} white-tailed deer that had CWD. The sheep were housed indoors in a Biosafety Level 2 agriculture facility separate from scrapie-affected sheep. At 60 months postinoculation, the initial experimental endpoint, sheep were asymptomatic, and all 7 sheep were culled.

We performed a postmortem examination on each sheep and collected a full spectrum of tissues, which we froze and stored in 10% neutral-buffered formalin. To evaluate lymphoinvasion and neuroinvasion, we tested tissues from the brainstem at the obex and pons, third eyelid, palatine tonsil, lymph nodes (mesenteric and retropharyngeal), spleen, and ileum. We processed the formalin-fixed tissues, embedded in paraffin, and sectioned at optimal thickness (brain, 4 μm; lymphoid, 3 μm; and other tissues, 5 μm) for subsequent staining with hematoxylin and eosin and immunohistochemical (IHC) analysis. We used a

Author affiliation: US Department of Agriculture, Ames, Iowa, USA

DOI: https://doi.org/10.3201/eid2712.204978

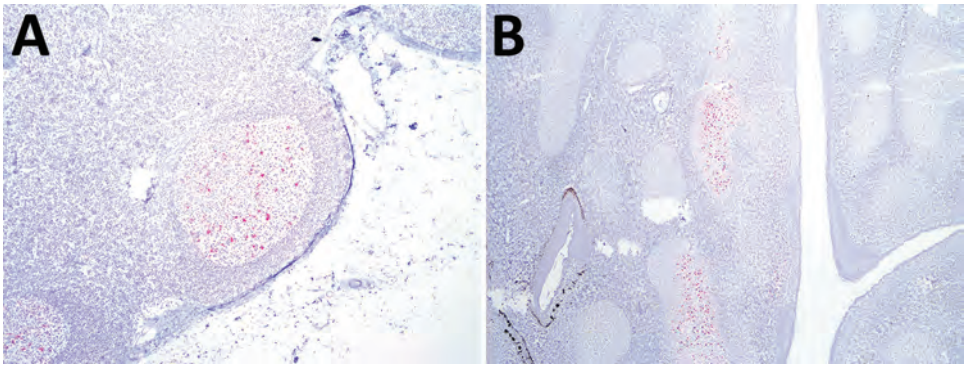

Figure 1. Immunoreactivity against misfolded form of the prion protein (red) in lymphoid tissue from a sheep oronasally inoculated with the agent of chronic wasting disease from white-tailed deer. A) Retropharyngeal lymph node (original magnification ×100.) B) Palatine tonsil (original magnification ×40). We used a cocktail of monoclonal antibodies (F89/160.1.5 and F99/97.6.1).

cocktail of PrP^{Sc} monoclonal antibodies (F89/160.1.5 and F99/97.6.1; 5 μg/mL) for IHC.

Examination of IHC-stained tissues showed PrP^{Sc} in the retropharyngeal lymph node (Figure 1, panel A) and palatine tonsil (Figure 1, panel B) of 1 sheep inoculated with the ARQ/ARQ genotype. The retropharyngeal lymph node was also positive by enzyme immunoassay (EIA) (HerdChek; IDEXX Laboratories, https://www.idexx.com) at initial (optical density 0.99; negative cutoff value 0.186) and repeat (optical density 0.559; negative cutoff value 0.178) tests. The palatine tonsil was negative by EIA.

To confirm prion disease infectivity in the retropharyngeal lymph node, we performed bioassays in Tg12 cervidized (*10*) and Tg338 ovinized (*11*) transgenic mice. Mice expressed the transgene for the elk prion protein polymorphism MM_{132} (Tg12) and the ovine prion protein polymorphisms $V_{136}R_{154}Q_{171}$ (Tg338). We homogenized fresh frozen lymph nodes to 10% (wt/vol) and enriched them by repeated rounds of differential centrifugation; we intracranially inoculated mice with 20 μL of 10% (wt/vol) equivalent enriched homogenate. The Tg12 bioassay had a partial attack rate of 5/9 mice. Most (4/5) dead Tg12 mice were strongly positive by EIA (optical density 4.0) and had an average incubation period of 511 days.

Western blots of these 4 Tg12 mice confirmed the presence of proteinase K–resistant PrP^{Sc} in the brains (Figure 2). The positive EIA results were obtained from brain homogenates in Tg12 mice; the spleens were negative for PrP^{Sc}. For the Tg338 bioassay (n = 15), brains and spleens were negative by EIA. Four Tg338 mice that died or were euthanized because of intercurrent disease at 254, 462, 629, and 657 days postinoculation were negative by EIA. The rest of the Tg338 mice were negative at the study endpoint, 700 days postinoculation.

Conclusions

The oronasal susceptibility of sheep to the agent of CWD is a major finding in light of its possible effect on risk assessment and understanding possible transmission of CWD to noncervid species in field conditions. Interspecies transmission of TSEs is less likely when the experimental species barrier between hosts is strong (*12*). One study demonstrated that the CWD agent does not readily transmit to transgenic ovinized mice (*13*). However, another study reported lifelong replication of PrP^{Sc} in the spleen after intracranial inoculation of the CWD agent in Tg338 ovinized mice (*14*). The finding of extraneuronal PrP^{Sc} in 1 sheep 5 years after oral inoculation suggests that sheep are unlikely to develop neurologic disease after natural exposure to the agent of CWD, but they might serve as asymptomatic carriers under the right conditions.

In this study, we used a relatively low dose (0.1 g) of brain homogenate. These results are intriguing, but they do not assess potential modes of transmission that could occur in the field, such as nose-to-nose contact or

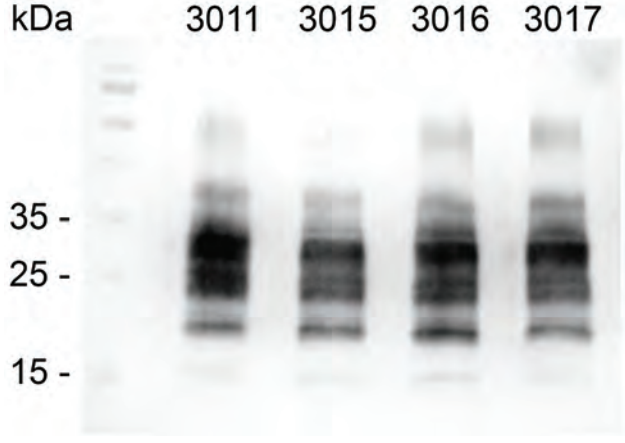

Figure 2. Western blot analysis showing proteinase K–resistant misfolded form of the prion protein (PrP^{Sc}) in brains of 4 Tg12 mice. Mice were intracranially inoculated with a homogenate made from retropharyngeal lymph node of a sheep oronasally inoculated with the agent of chronic wasting disease. Tg12 brain was prepared as a 10% (wt/vol) homogenate with phosphate-buffered saline. A total of 1 mg of tissue equivalent was treated with proteinase K (90 μg/mL) before electrophoresis. Immunodetection of PrP^{Sc} was performed overnight at 4°C with monoclonal antibody Sha31 (dilution 1:10,000). Left lane, molecular mass ladder. kDa, kilodaltons.

environmental contamination. In our ongoing multiyear study, 1 sheep had PrP^{Sc}-positive lymphoid tissue but no evidence of neuroinvasion 5 years postinoculation. This time interval is an extremely protracted incubation period. Had we continued this experiment, it is unknown how long the sheep would have remained asymptomatic or whether they would have eventually developed clinical disease. Because PrP^{Sc} was detected in lymphoid tissues of the head, the possibility that this sheep might have been shedding infectivity into the environment cannot be ruled out.

Positive bioassay results in Tg12 mice confirm CWD infectivity in the lymph node. Negative results in Tg338 mice could be explained by a donor/host mismatch between the ARQ donor sheep and VRQ expressing mice. Pursuing bioassays in A_{136}-expressing transgenic mice could be more fruitful.

Interspecies transmission events might increase the pathogenicity of an infectious prion on subsequent transmission to other species (*15*). Thus, exploration of potential new host ranges of this CWD isolate and performing human health risk assessments will provide useful information for this prion.

Acknowledgments

We thank Quazetta Brown, Rylie Frese, Kevin Hassall, Zoe Lambert, Joe Lesan, Leisa Mandell, and Trudy Tatum for providing excellent technical support; Qingzhong Kong for providing Tg12 mice; and Hubert Laude for providingTg338 mice.

This study was supported by the US Department of Agriculture, Agricultural Research Service. S.J.M. was appointed to the Agricultural Research Service Research Participation Program administered by the Oak Ridge Institute for Science and Education through an interagency agreement between the US Department of Energy and the US Department of Agriculture. The Oak Ridge Institute for Science and Education is managed by Oak Ridge Associated Universities under Department of Energy contract no. DE-SC0014664.

About the Author

Dr. Cassmann is a research veterinary medical officer at the National Animal Disease Center, Ames, IA. His primary research interests are veterinary pathology, animal prion diseases, interspecies transmission, host ranges, host genetic susceptibility, and diagnostics.

References

1. Williams ES, Young S. Spongiform encephalopathies in Cervidae. Rev Sci Tech. 1992;11:551–67. https://doi.org/10.20506/rst.11.2.611
2. Carlson C, Hopkins C, Nguyen N, Richards B, Walsh D, Walter WD. Chronic wasting disease: status, science, and management support by the US Geological Survey. US Geological Survey; March 2018. Report no. Open-File Report 2017–1138 [cited 2021 Aug 23]. https://pubs.er.usgs.gov
3. Haley NJ, Hoover EA. Chronic wasting disease of cervids: current knowledge and future perspectives. Annu Rev Anim Biosci. 2015;3:305–25. https://doi.org/10.1146/annurev-animal-022114-111001
4. Nonno R, Di Bari MA, Pirisinu L, D'Agostino C, Vanni I, Chiappini B, et al. Studies in bank voles reveal strain differences between chronic wasting disease prions from Norway and North America. Proc Natl Acad Sci U S A. 2020;117:31417–26. https://doi.org/10.1073/pnas.2013237117
5. Williams ES. Chronic wasting disease. Vet Pathol. 2005;42:530–49. https://doi.org/10.1354/vp.42-5-530
6. Raymond GJ, Bossers A, Raymond LD, O'Rourke KI, McHolland LE, Bryant PK III, et al. Evidence of a molecular barrier limiting susceptibility of humans, cattle, and sheep to chronic wasting disease. EMBO J. 2000;19:4425–30. https://doi.org/10.1093/emboj/19.17.4425
7. Race RE, Raines A, Baron TG, Miller MW, Jenny A, Williams ES. Comparison of abnormal prion protein glycoform patterns from transmissible spongiform encephalopathy agent-infected deer, elk, sheep, and cattle. J Virol. 2002;76:12365–8. https://doi.org/10.1128/JVI.76.23.12365-12368.2002
8. Hamir AN, Kunkle RA, Cutlip RC, Miller JM, Williams ES, Richt JA. Transmission of chronic wasting disease of mule deer to Suffolk sheep following intracerebral inoculation. J Vet Diagn Invest. 2006;18:558–65. https://doi.org/10.1177/104063870601800606
9. Moore SJ, Smith JD, Greenlee MHW, Nicholson EM, Richt JA, Greenlee JJ. Comparison of two US sheep scrapie isolates supports identification as separate strains. Vet Pathol. 2016;53:1187–96. https://doi.org/10.1177/0300985816629712
10. Kong Q, Huang S, Zou W, Vanegas D, Wang M, Wu D, et al. Chronic wasting disease of elk: transmissibility to humans examined by transgenic mouse models. J Neurosci. 2005;25:7944–9. https://doi.org/10.1523/JNEUROSCI.2467-05.2005
11. Vilotte JL, Soulier S, Essalmani R, Stinnakre MG, Vaiman D, Lepourry L, et al. Markedly increased susceptibility to natural sheep scrapie of transgenic mice expressing ovine prp. J Virol. 2001;75:5977–84. https://doi.org/10.1128/JVI.75.13.5977-5984.2001
12. Torres JM, Espinosa JC, Aguilar-Calvo P, Herva ME, Relaño-Ginés A, Villa-Diaz A, et al. Elements modulating the prion species barrier and its passage consequences. PLoS One. 2014;9:e89722. https://doi.org/10.1371/journal.pone.0089722
13. Tamgüney G, Giles K, Bouzamondo-Bernstein E, Bosque PJ, Miller MW, Safar J, et al. Transmission of elk and deer prions to transgenic mice. J Virol. 2006;80:9104–14. https://doi.org/10.1128/JVI.00098-06
14. Béringue V, Herzog L, Jaumain E, Reine F, Sibille P, Le Dur A, et al. Facilitated cross-species transmission of prions in extraneural tissue. Science. 2012;335:472–5. https://doi.org/10.1126/science.1215659
15. Espinosa JC, Andréoletti O, Castilla J, Herva ME, Morales M, Alamillo E, et al. Sheep-passaged bovine spongiform encephalopathy agent exhibits altered pathobiological properties in bovine-PrP transgenic mice. J Virol. 2007;81:835–43. https://doi.org/10.1128/JVI.01356-06

Address for correspondence: Justin Greenlee, National Animal Disease Center, Agricultural Research Service, US Department of Agriculture, 1920 Dayton Ave, PO Box 70, Ames, IA 50010, USA; email: justin.greenlee@usda.gov

Rift Valley Fever Virus Seroprevalence among Humans, Northern KwaZulu-Natal Province, South Africa, 2018–2019

Janusz T. Pawęska, Veerle Msimang, Joe Kgaladi, Orienka Hellferscee, Jacqueline Weyer, Petrus Jansen van Vuren

We detected Rift Valley fever virus (RVFV) IgM and IgG in human serum samples collected during 2018–2019 in northern KwaZulu-Natal Province, South Africa. Our results show recent RVFV circulation and likely RVFV endemicity in this tropical coastal plain region of South Africa in the absence of apparent clinical disease.

Geographic expansion of Rift Valley fever virus (RVFV) associated with health and socioeconomic losses is of great concern for veterinary and public health professionals worldwide (*1*). In South Africa, major human Rift Valley fever (RVF) epidemics occurred in 1950–1951, 1974–1975, and 2010–2011 (*2*–*4*), but single outbreaks are reported only sporadically (*5*). RVF outbreaks in South Africa primarily have occurred on the temperate central plateau of the country (*6*), but historic data suggest circulation of RVFV in both humans and animals in the northern, tropical part of KwaZulu-Natal Province (*7*–*9*). Results of recent studies in this region show high RVFV seroprevalence in domestic goats (31.7%) and cattle (34%) (*10*) and in wild ruminants (35%) (*11*), without reported epizootics. To investigate the possibility of undetected RVFV infections in humans, we tested patients visiting healthcare facilities in northern KwaZulu-Natal for RVFV antibodies.

Author affiliations: National Institute for Communicable Diseases of the National Health Laboratory Service, Johannesburg, South Africa (J.T. Pawęska, V. Msimang, J. Kgaladi, O. Hellferscee, J. Weyer, P. Jansen van Vuren); University of Pretoria, Pretoria, South Africa (J.T. Pawęska, J. Weyer); Rand Water, Vereeniging, South Africa (J. Kgaladi); Australian Centre for Disease Preparedness, CSIRO-Health and Biosecurity, Geelong, Victoria, Australia (P. Jansen van Vuren)

DOI: https://doi.org/10.3201/eid2712.210643

The Study

Because of recent active circulation of RVFV in livestock and wildlife (*10*,*11*), we selected the uMkhanyakude Health District for active RVFV surveillance during April 2018–August 2019. Many households keep livestock composed of indigenous Nguni chickens, cattle, goats, or ducks. Participating locations were 4 hospitals, Manguzi, Bethesda, and Mseleni, and Ndumo clinic attached to Mosvold hospital, and associated clinics, Mahlungulu, Makathini, and Mbazwana (Figure). The study was performed in accordance with protocols approved by the Human Research Ethics Committee of the University of Witwatersrand (Johannesburg, South Africa; approval nos. HREC M170606, M160667, and M161005) and provincial department of health (reference no. KZ_201709–037).

Enrolled participants comprised persons ≥5 years of age of either sex who had measured axillary temperature of ≥37.5°C at examination or history of symptoms ≤7 days before examination, or at the time of examination, such as rash, headache, myalgia, arthralgia, and conjunctivitis. Study controls were persons from the same selected health facilities who were seeking healthcare for noninfectious conditions or for chronic care, and who had no history of fever ≤7 days. Case-controls were matched to age groups of enrolled participants as much as possible. Nurses conducted interviews and collected and recorded survey data on a case investigation form at the time the blood was drawn. Data were transferred into data gathering tool built on a tablet computer by using REDCap software (https://projectredcap.org), which is powered by Vanderbilt University (Nashville, Tennessee, USA). For analysis, we downloaded data from respective servers into Excel software (Microsoft, https://www.microsoft.com).

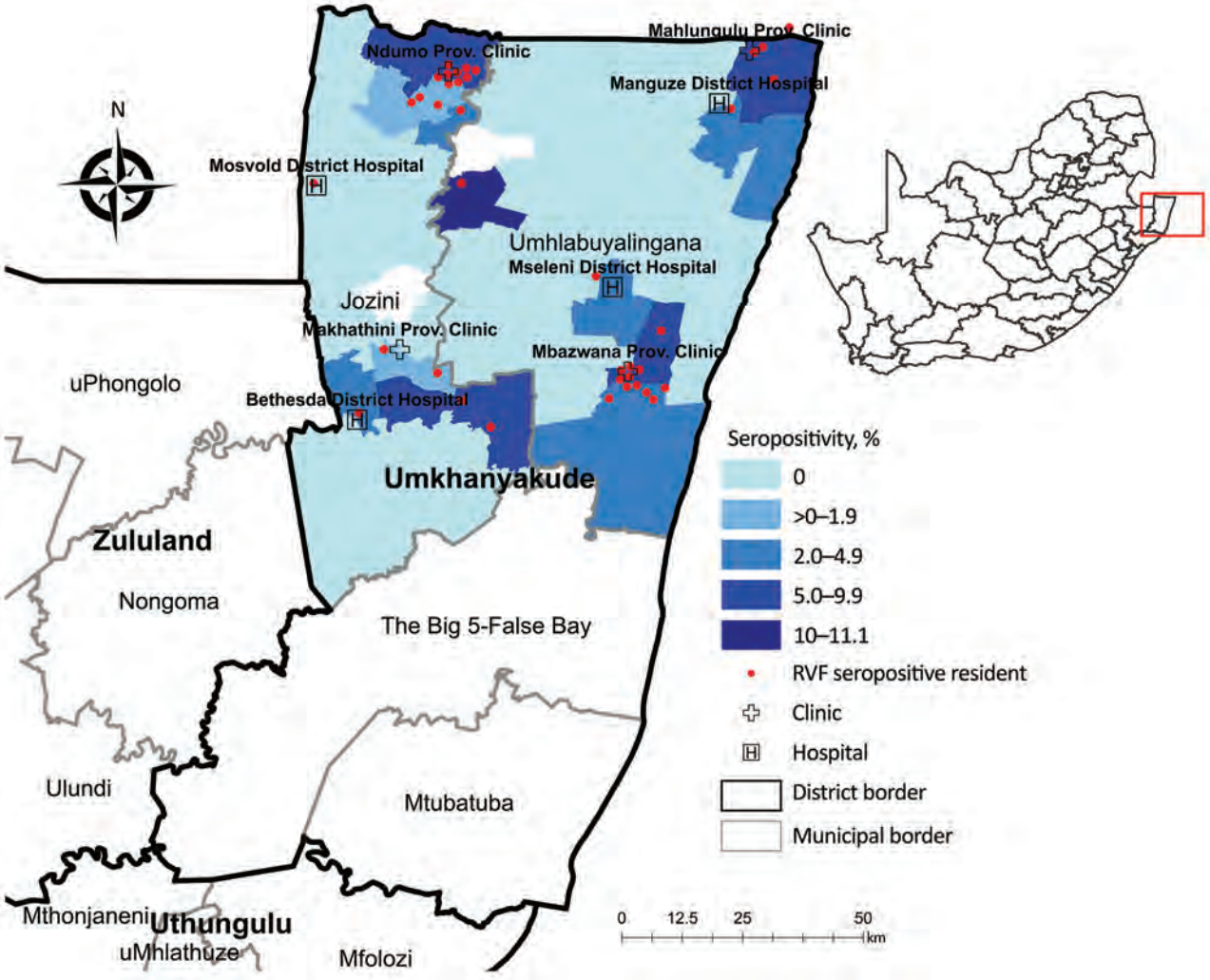

Figure. Distribution of human Rift Valley fever virus seropositivity and ward-specific seropositivity in northern municipalities of the uMkhanyakude District, KwaZulu-Natal Province, South Africa, April 2018–August 2019. Inset shows location of uMkhanyakude District (red box) in South Africa. Map was constructed in ArcGIS 10.2 (Esri, https://www.esri.com) using district, municipal, and ward boundaries, facilities, and participants' residential coordinates collected during the study. Data are available under CC-BY 4.0 (Creative Commons Attribution, https://creativecommons.org) license.

Nurses drew 5 mL of whole blood from participants 5–12 years of age and 10 mL from participants >12 years of age. Blood specimens were transported daily from clinics to their associated hospital laboratory for processing and temporary storage until transported for testing to the National Institute for Communicable Diseases of the National Health Laboratory Service (Johannesburg). We enrolled and collected samples from a total of 1,395 volunteers during April 2018–August 2019.

We first tested serum samples by inhibition RVFV ELISA (*12*), then tested all positive samples by IgG sandwich ELISA and IgM capture ELISA, as previously described (*13*). We tested IgM-positive serum samples by using real-time reverse transcription PCR (rRT-PCR) (*14*). Of note, RVF and malaria can have similar clinical manifestations in patients, such as fever, arthralgia, and headache. Thus, we also tested specimens collected during April 2018–January 2019 for malaria antigen by using an ICT Malaria Combo Cassette Test (ICT International, https://www.ictdiagnostics.com), according to manufacturer instructions. We performed statistical analyses by using Stata version 13 (StataCorp LLC, https://www.stata.com) and Excel. We determined univariable statistics by using Fisher exact test for variables associated with RVFV seropositivity, such as sex, age, time outdoors, and agriculture activities. We used ArcGIS ArcMap 10.2 (Esri, https://www.esri.com) to create distribution and choropleth maps of RVF occurrence.

Among participants, 72.6% (997) were female and 27.4% (377) were male; no sex was recorded for

Table 1. Rift Valley fever virus IgG and IgM seropositivity in survey participants by healthcare facility and uMkhanyakude district, northern Kwazulu-Natal, South Africa, 2018–2019

Healthcare facility	No. tested	No. (%) seropositive*	No. (%) IgG positive†	No. (%) IgM positive‡
Mbazwana	185	8 (4.3)	7 (3.8)	1 (0.5)
Ndumo-Mosvold	377	16 (4.2)	14 (3.7)	7 (1.9)
Bethesda	178	5 (2.8)	5 (2.8)	1 (0.6)
Manguzi-Mahlungulu	207	5 (2.4)	5 (2.4)	1 (0.5)
Mseleni	178	4 (2.3)	4 (2.3)	1 (0.6)
Makhathini	270	1 (0.4)	1 (0.4)	0
Total	1,395	39 (2.8)	36 (2.6)	11 (0.8)

*Serum tested by an inhibition ELISA with 99.47% diagnostic sensitivity, 99.66% diagnostic specificity. This assay measures total Rift Valley fever virus antibody but does not discriminate between IgG and IgM (*12*).
†Serum tested by an IgG-sandwich ELISA with 100% diagnostic sensitivity, 99.95% diagnostic specificity (*13*).
‡Serum tested by an IgM-capture ELISA with 96.47% diagnostic sensitivity, 99.44% diagnostic specificity (*13*).

21 participants. The average age among participants was 35.3 (SD 17.0, range 5–96) years, and median was 33 (interquartile range 22–46) years.

Of 1,395 volunteers tested, 39 tested RVFV positive by inhibition ELISA, of which 11 were positive for RVFV IgM and 9 for RVFV IgG (Table 1). The overall seropositivity adjusted for facility clustering was 2.8% (95% CI 1.45%–5.34%), and seropositivity differed significantly between facilities (p = 0.03) (Table 1). RVFV seropositivity was higher among groups ≥10 years of age compared with those 5–9 years old (p = 0.001) but was not significantly associated with sex (p = 0.481), spending time outdoors (p = 0.263), or working in agriculture (p = 0.161). None of the 11 IgM seropositive persons tested positive by RVFV rRT-PCR; 6 had fever at clinical examination at the healthcare facility. The most frequently observed symptoms were headache, myalgia, and arthralgia, and 3 participants had conjunctivitis (Table 2). Among IgM-positive participants, 3 were tested for malaria infection, and 2 tested positive.

The east coast, the border with Mozambique, the Ndumo area in the north, Ubombo towards the south of the district where Bethesda is located, and the southeast near the iSimangaliso had higher RVFV seroprevalence, suggesting that more favorable conditions for RVFV circulation and human exposure exist in these areas. Of 11 IgM seropositive participants, 7 were seen in the Ndumo clinic, located in the northern section of the Jozini municipality and at the southern edge of Ndumo Game reserve and adjacent Tembe Elephant Park, part of the Lubombo Transfrontier Conservation and Resource area with Mozambique.

Conclusions

Our serosurvey confirms recent exposure and indicates endemic circulation of RVFV in humans residing in the tropical coastal plain of northern KwaZulu-Natal Province in South Africa. The RVFV seropositivity we noted in our study is lower than that reported in the temperate inland of South Africa (*15*). The central plateau of South Africa is prone to RVF outbreaks, and more frequent and intense RVF outbreaks have occurred in the central plateau than the eastern coastal area (*6*). The inland of South Africa has the largest and most concentrated sheep farming regions. Sheep farms are not common in northern KwaZulu-Natal, and households keep livestock comprised mostly of indigenous cattle and goats. Among livestock, sheep, particularly newborn lambs, are most susceptible to RVFV infection (*1*,*6*). Most confirmed cases during the 2008–2011 RVF outbreak in South Africa were caused by physical contact with infected animals, either through disposal of dead animals or aborted fetuses, or slaughtering (*4*,*15*). No RVF outbreaks have been reported in northern KwaZulu-Natal, either in humans or animals, but recent findings suggest year-round virus transmission in cattle, goats (*10*), and wild antelopes (*11*) are associated with high RVFV seroconversion rates in domestic ruminants (*10*).

Table 2. Symptoms and signs in Rift Valley fever virus in IgM-positive participants by health care facility, uMkhanyakude district, northern Kwazulu-Natal, South Africa, 2018–2019*

Healthcare facility	Age, y/sex	Fever	Rash	Headache	Myalgia	Arthralgia	Conjunctivitis	Vomiting	Malaria
Mbazwana	30/M	Y	N	Y	N	Y	Y	N	Y
Ndumo-Mosvold	55/F	N	N	Y	N	Y	N	N	N
	39/F	Y	Y	Y	Y	N	N	N	Y
	50/F	N	N	N	N	N	N	N	NT
	71/F	N	N	N	N	Y	N	N	NT
	27/M	Y	N	Y	Y	N	N	N	NT
	72/F	Y	N	Y	Y	Y	Y	N	NT
	25/F	N	N	Y	Y	Y	N	Y	NT
Bethesda	67/M	Y	N	N	Y	N	Y	N	NT
Manguzi-Mahlungulu	15/F	Y	N	N	N	Y	N	N	NT
Mseleni	47/F	N	N	Y	N	N	N	N	NT

*NT, not tested.

Study participants had detectable IgG and IgM to RVFV, and most IgM-positive samples were collected from participants with no recent history of travel beyond the study area. Our study indicates that RVFV infections in northern KwaZulu-Natal could be misdiagnosed or underreported, highlighting the urgent need for improved diagnostic testing and awareness of RVF and other arbovirus diseases in this part of South Africa. Moreover, our results suggest the possible role of the northern KwaZulu-Natal wildlife-livestock-vector host reservoir system in maintaining RVFV endemicity, including the potential to drive large-scale emergence and spread of the virus to other parts of the country. Because clinical manifestations of RVF in humans mimic those of malaria, RVFV surveillance can reduce potential misuse of antimalaria treatments. Our findings underscore the need for improved and active arbovirus biosurveillance in humans, wildlife, livestock, and mosquito vectors to mitigate associated transmission risk and potential RVF epidemics.

Acknowledgments

We thank the healthcare workers of the facilities and the uMkhanyakude community in KwaZulu-Natal Province for supporting the study. We also thank the staff of the Center for Emerging Zoonotic and Parasitic Diseases, NICD/NHLS for the technical and laboratory assistance for testing of the samples.

This work was supported by the Division of Global Migration and Quarantine, National Center for Emerging and Zoonotic Infectious Diseases, US Centers for Disease Control and Prevention Division under grant no. U19GH000622-05.

About the Author

Dr. Pawęska is head of the Centre for Emerging Zoonotic and Parasitic Diseases at the National Institute for Communicable Diseases, Johannesburg, South Africa. His research interests include diagnostics, epidemiology, and ecology of zoonotic and arthropodborne risk group 3 and 4 viral agents.

References

1. Pawęska JT, Jansen van Vuren P. Rift Valley fever: a virus with potential for global emergence. In: Johnson N, editor. The role of animals in emerging viral diseases. London: Elsevier Academic Press; 2013. p. 169–200.
2. Joubert JD, Fergusson AL, Gear J. Rift Valley fever in South Africa. The occurrence of human cases in the Orange Free State, the north-western Cape Province, the western and southern Transvaal. Epidemiological and clinical findings. S Afr Med J. 1951;25:890–1.
3. McIntosh BM, Russell D, dos Santos I, Gear JH. Rift Valley fever in humans in South Africa. S Afr Med J. 1980;58:803–6.
4. Archer BN, Thomas J, Weyer J, Cengimbo A, Landoh DE, Jacobs C, et al. Epidemiologic investigations into outbreaks of Rift Valley fever in humans, South Africa, 2008–2011. Emerg Infect Dis. 2013;19:1918–25. https://doi.org/10.3201/eid1912.121527
5. Jansen van Vuren P, Kgaladi J, Msimang V, Pawęska JT. Rift Valley fever reemergence after 7 years of quiescence, South Africa, May 2018. Emerg Infect Dis. 2019;25:338–41. https://doi.org/10.3201/eid2502.181289
6. Swanepoel R, Coetzer JAW. Rift Valley fever. In: Coetzer JAW, Thomson GR, Tustin RC, editors. Infectious diseases of livestock with special reference to Southern Africa. Cape Town: Oxford University Press; 2004. p. 1, 688–717.
7. Smithburn KC, Kokernot RH, Heymann CS, Weinbren MP, Zentkowsky D. Neutralizing antibodies for certain viruses in the sera of human beings residing in Northern Natal. S Afr Med J. 1959;33:555–61.
8. McIntosh BM. Rift Valley fever. 1. Vector studies in the field. J S Afr Vet Med Assoc. 1972;43:391–5.
9. McIntosh BM, Jupp PG, dos Santos I, Rowe AC. Field and laboratory evidence implicating *Culex zombaensis* and *Aedes circumluteolus* as vectors of Rift Valley fever virus in coastal South Africa. S Afr J Sci. 1983;79:61–4.
10. van den Bergh C, Venter EH, Swanepoel R, Thompson PN. High seroconversion rate to Rift Valley fever virus in cattle and goats in far northern KwaZulu-Natal, South Africa, in the absence of reported outbreaks. PLoS Negl Trop Dis. 2019;13:e0007296. https://doi.org/10.1371/journal.pntd.0007296
11. Van den Bergh C, Venter EH, Swanepoel R, Hanekom CC, Thompson PN. Neutralizing antibodies against Rift Valley fever virus in wild antelope in far northern KwaZulu-Natal, South Africa, indicate recent virus circulation. Transbound Emerg Dis. 2020;67:1356–63. https://doi.org/10.1111/tbed.13479
12. Pawęska JT, Mortimer E, Leman PA, Swanepoel R. An inhibition enzyme-linked immunosorbent assay for the detection of antibody to Rift Valley fever virus in humans, domestic and wild ruminants. J Virol Methods. 2005;127:10–8. https://doi.org/10.1016/j.jviromet.2005.02.008
13. Pawęska JT, Burt FJ, Swanepoel R. Validation of IgG-sandwich and IgM-capture ELISA for the detection of antibody to Rift Valley fever virus in humans. J Virol Methods. 2005;124:173–81. https://doi.org/10.1016/j.jviromet.2004.11.020
14. Drosten C, Göttig S, Schilling S, Asper M, Panning M, Schmitz H, et al. Rapid detection and quantification of RNA of Ebola and Marburg viruses, Lassa virus, Crimean-Congo hemorrhagic fever virus, Rift Valley fever virus, dengue virus, and yellow fever virus by real-time reverse transcription-PCR. J Clin Microbiol. 2002;40:2323–30. https://doi.org/10.1128/JCM.40.7.2323-2330.2002
15. Msimang V, Thompson PN, Jansen van Vuren P, Tempia S, Cordel C, Kgaladi J, et al. Rift Valley fever virus exposure amongst farmers, farm workers, and veterinary professionals in central South Africa. Viruses. 2019;11:140. https://doi.org/10.3390/v11020140

Address for correspondence: Janusz T. Pawęska, Center for Emerging Zoonotic and Parasitic Diseases, National Institute for Communicable Diseases of the National Health Laboratory Service, 1 Modderfontein Road, Sandringham 2131, Johannesburg, South Africa; email: januszp@nicd.ac.za

Surge of Typhoid Intestinal Perforations as Possible Result of COVID-19–Associated Delays in Seeking Care, Madagascar

Hyon Jin Jeon,[1] Florian Marks,[1] Jonathan Sugimoto, Justin Im, Sophie S.Y. Kang, Andrea Haselbeck,[1] Raphael Rakotozandrindrainy[1]

During the coronavirus disease pandemic, we observed a 6.4-fold increase in typhoid intestinal perforation incidence in Antananarivo, Madagascar. Thirteen perforations and occurred within 6 months (February 2020–July 2020) compared with 13 perforations during the previous 41 months (August 2016–January 2020). The increase may be attributable to delayed healthcare seeking during the pandemic.

In an effort to understand the health impacts of endemic typhoid, the Severe Typhoid Fever Surveillance in Africa Program (SETA) detects and records cases of surgically confirmed intestinal perforations, a relatively rare but severe complication of *Salmonella enterica* serovar Typhi infection (*1*). Since the beginning of the coronavirus disease (COVID-19) global pandemic in early 2020, SETA surveillance has found an alarming increase in surgically confirmed intestinal perforations cases in Madagascar. This increase, which does not correlate with an increase in blood culture–confirmed typhoid cases found through SETA surveillance, may insinuate the serious effects on healthcare-seeking behavior and healthcare quality that the COVID-19 pandemic has had in the country.

Typhoid intestinal perforation is a severe complication of untreated or mismanaged infection that disproportionately affects low-income countries (*2*). Delay in diagnosis and proper antibiotic treatment of typhoid is frequently cited as a major factor contributing to typhoid intestinal perforation incidence and associated deaths (*3*–*6*). As such, increases in intestinal perforation cases may suggest deterioration in the quality of healthcare or changes in the healthcare-seeking behavior of the community.

SETA sentinel sites represent both primary and tertiary healthcare facilities, where all incoming patients are screened for febrile illness, clinically suspected typhoid, and gastrointestinal perforations. Once a patient is enrolled in the study, cultures of their blood, stool, and (in the case of surgery) tissue are used to detect *Salmonella* Typhi and other bacteremia. Over a 4-year period of SETA observation, we detected a marked increase in the rate of surgically confirmed typhoid intestinal perforations after the onset of the COVID-19 pandemic in early 2020 (Figure, panel A).

SETA Madagascar enrolled case-patients with suspected typhoid intestinal perforations in the town of Imerintsiatosika, 43 km from the capital city of Antananarivo, as well as case-patients from tertiary care facilities in Antananarivo (*1*) (Figure). Clinical and demographic data were systematically collected from enrolled participants at entry into the study. We observed participants daily until their hospital discharge. We detected a total of 26 intestinal perforation cases of any etiology during August 2016–September 2020. The mean age of the patients was 28.5 years (SD $\pm$ 19.1 years); men and boys accounted for 69% of the total patients. Of the 26 patients with perforation, 9 died and 17 were discharged. The overall case-fatality rate was 50% among women and girls and 28% among men and boys. Of note, all 4 deaths among women and girls occurred during the prepandemic period, and all 5 deaths among men and boys occurred during the

Author affiliations: University of Cambridge School of Clinical Medicine, Cambridge Biomedical Campus, Cambridge, UK (H.J. Jeon, F. Marks); International Vaccine Institute, Seoul, South Korea (H.J. Jeon, F. Marks, J. Sugimoto, J. Im, S.Y. Kang, A. Haselbeck,); University of Antananarivo, Antananarivo, Madagascar (F. Marks, R. Rakotozandrindrainy)

DOI: https://doi.org/10.3201/eid2712.210516

[1]These authors contributed equally to this article.

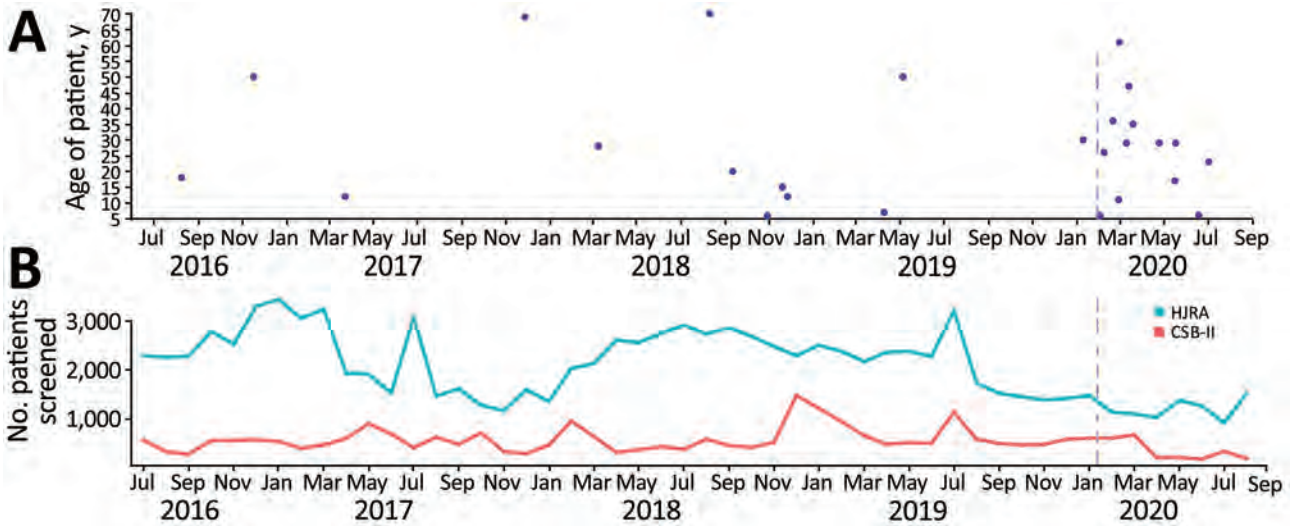

Figure. Typhoid intestinal perforation cases and number of patients screened in hospitals participating in the Severe Typhoid Fever Surveillance in Africa Program (SETA), Madagascar, July 2016–September 2020. A) Intestinal perforation cases recorded by SETA at 3 hospitals, by age of patient and date of hospitalization. B) Number of patients screened monthly by SETA at Hospital Joseph Ravoahangy Andrianavalona, the largest hospital in the capital city of Antananarivo, and its tertiary care center, and at the Centres Santé de Bases II, a primary care facility in the town of Imerintsiatosika in the rural region west of Antananarivo. Vertical purple lines indicate date first case of COVID-19 reported in Africa. CSB-II, Centres Santé de Bases II; HJRA, Hospital Joseph Ravoahangy Andrianavalona.

pandemic period. During August 1, 2016–January 31, 2020, the pre–COVID-19 pandemic period, 13 perforations (2.1/100,000 person-years of observation [PYO]) and 4 deaths (0.6/100,000 PYO) occurred. These incidence rates contrast with the remainder of 2020, the COVID-19 pandemic period, during which 13 perforations (13.2/100,000 PYO) and 5 deaths (5.1/100,000 PYO) occurred. This change represents a 6.4-fold (95% CI 3.0–13.7-fold) increase in the incidence of intestinal perforations during the COVID-19 pandemic period ($p<0.05$). Although we noted no statistically significant difference in mean age of onset for intestinal perforation patients detected before versus after the onset of the pandemic (30 vs. 27 years; $p = 0.75$ by t-test), intestinal perforation patients identified during the pandemic seem more likely to be middle-aged (20–50 years of age) (Figure, panel A).

We suspect that the immediate increase in incident intestinal perforations observed since February 2020 may be an externality of delayed treatment for mild typhoid fever because of changes in healthcare-seeking behavior, healthcare quality, or both during the initial COVID-19 pandemic outbreak. However, COVID-19 investigations to date indicate that COVID-19 can affect various organs, including the gastrointestinal tract; hence, the possibility of SARS-CoV-2 having a direct effect on the risk for perforations cannot be ruled out at this stage and warrants further research.

As of Oct 19, 2021, a total of 42,898 COVID-19 cases and 958 COVID-19–related deaths had been reported in Madagascar (*7*). Well before the first 3 cases of COVID-19 were reported in-country on March 20, 2020, media coverage of the global pandemic was substantial (*8*,*9*). Like the rest of the international community, Madagascar watched with collective anxiety and apprehension as the novel coronavirus outbreak unfolded. Although the surge of reported perforation cases predates regional lockdowns, which were first imposed in July 2020 (*10*), we cannot rule out ad hoc closures of healthcare centers affecting the community's ability to seek regular care in addition to the unknowns of potential social stigma that raises barriers to the already low levels of healthcare-seeking observed during nonpandemic conditions in the community (*11*,*12*).

Before future in-depth qualitative research can provide a comprehensive picture of healthcare in Madagascar during the COVID-19 pandemic, SETA screening records may provide the first hint at a disruption of individual healthcare-seeking behavior as shown by a reduction in the number of overall patient hospital visitations beginning in January 2020 (Figure, panel B). SETA records all patients who visit any of the sentinel health centers for any concern and screens those patients for study eligibility; consequently, SETA screening numbers can be understood as a proxy for hospital visitation numbers.

The COVID-19 pandemic is likely having broad impacts on other preventable diseases in an already struggling healthcare system; widespread availability of COVID-19 vaccines in Madagascar is expected only in 2023 (*13*). The observed increase in illness and deaths from treatable diseases and disruption of routine primary care should not be neglected (*14*,*15*). Although the SETA program has only investigated intestinal perforations in the capital city, delayed healthcare-seeking might be an even larger problem in more remote areas of the country. The public health community must remain vigilant about maintaining routine healthcare services and ensuring that healthcare facilities are safe and usable. In particular, public trust in the healthcare system amidst the pandemic is essential for encouraging persons with potentially life-threatening conditions to seek healthcare.

The SETA Program is funded by the Bill and Melinda Gates Foundation (grant no. OPP1127988).

About the Author

Ms. Jeon is Project Manager in the Department of Medicine at the University of Cambridge and Senior Program Administrator at the International Vaccine Institute. Her research interests include disease surveillance for bacterial and viral infections. Ms. Jeon is currently working on her PhD investigating field site analysis of invasive Salmonellosis in sub-Saharan Africa.

Dr. Marks is the Deputy Director General at the International Vaccine Institute, Principal Research Associate at the Department of Medicine, University of Cambridge and holds an appointment at the University of Antananarivo. His research interest includes vaccine-preventable diseases epidemiology and vaccine impact assessments.

References

1. Park SE, Toy T, Cruz Espinoza LM, Panzner U, Mogeni OD, Im J, et al. The Severe Typhoid Fever in Africa Program: study design and methodology to assess disease severity, host immunity, and carriage associated with invasive salmonellosis. Clin Infect Dis. 2019;69(Suppl 6):S422–34. https://doi.org/10.1093/cid/ciz715
2. Contini S. Typhoid intestinal perforation in developing countries: still unavoidable deaths? World J Gastroenterol. 2017;23:1925–31. https://doi.org/10.3748/wjg.v23.i11.1925
3. Ameh EA. Typhoid ileal perforation in children: a scourge in developing countries. Ann Trop Paediatr. 1999;19:267–72. https://doi.org/10.1080/02724939992356
4. Ekenze SO, Ikefuna AN. Typhoid intestinal perforation under 5 years of age. Ann Trop Paediatr. 2008;28:53–8. https://doi.org/10.1179/146532808X270680
5. Sümer A, Kemik O, Dülger AC, Olmez A, Hasirci I, Kişli E, et al. Outcome of surgical treatment of intestinal perforation in typhoid fever. World J Gastroenterol. 2010;16:4164–8. https://doi.org/10.3748/wjg.v16.i33.4164
6. Bitar R, Tarpley J. Intestinal perforation in typhoid fever: a historical and state-of-the-art review. Rev Infect Dis. 1985;7:257–71. https://doi.org/10.1093/clinids/7.2.257
7. Worldometer. Madagascar coronavirus cases: 42,898; deaths: 958 [cited 2021 Oct 19]. https://www.worldometers.info/coronavirus/country/madagascar
8. Rasolo F. Suspension temporaire des vols Antananarivo-Guangzhou. Madagascar Tribune. 2021 Jan 31 [cited 2021 Oct 19]. https://www.madagascar-tribune.com/Suspension-temporaire-des-vols-Antananarivo-Guangzhou.html
9. Madagascar: country confirms first cases of COVID-19 March 20 /update 3. GardaWorld. 2020 Mar 20 [cited 2021 Oct 19]. https://www.garda.com/crisis24/news-alerts/325126/madagascar-country-confirms-first-cases-of-covid-19-march-20-update-3
10. Anadolu Agency. Madagascar imposes lockdown amid rise in COVID-19 cases. 2020 Jul 6 [cited 2021Oct 19]. https://www.aa.com.tr/en/africa/madagascar-imposes-lockdown-amid-rise-in-covid-19-cases/1900940
11. Logie CH. Lessons learned from HIV can inform our approach to COVID-19 stigma. J Int AIDS Soc. 2020;23:e25504. https://doi.org/10.1002/jia2.25504
12. World Health Organization Regional Office for Africa. Combattre la peur et la stigmatisation liées à la COVID-19. 2020 Jul 23 [cited 2021 Oct 19]. https://www.afro.who.int/fr/news/combattre-la-peur-et-la-stigmatisation-liees-la-covid-19
13. More than 85 poor countries will not have widespread access to coronavirus vaccines before 2023. Economist Intelligence Unit. 2021 Jan 27 [cited 2021 Oct 19]. https://www.eiu.com/n/85-poor-countries-will-not-have-access-to-coronavirus-vaccines
14. Ansumana R, Sankoh O, Zumla A. Effects of disruption from COVID-19 on antimalarial strategies. Nat Med. 2020;26:1334–6. https://doi.org/10.1038/s41591-020-1047-5
15. Barach P, Fisher SD, Adams MJ, Burstein GR, Brophy PD, Kuo DZ, et al. Disruption of healthcare: will the COVID pandemic worsen non-COVID outcomes and disease outbreaks? Prog Pediatr Cardiol. 2020;59:101254. https://doi.org/10.1016/j.ppedcard.2020.101254

Address for correspondence: Florian Marks, International Vaccine Institute, SNU Research Park, 1 Gwanak-ro, Gwanak-gu, Seoul 08826, South Korea; email: fmarks@ivi.int

Evidence of Human Exposure to Tamdy Virus, Northwest China

Abulimiti Moming,[1] Shu Shen,[1] Yaohui Fang, Jingyuan Zhang, Yanfang Zhang, Shuang Tang, Tianxian Li, Zhihong Hu, Hualin Wang, Yujiang Zhang, Surong Sun, Lin-Fa Wang, Fei Deng

We report the isolation of Tamdy virus from *Hyalomma asiaticum* ticks in northwest China and serologic evidence of human Tamdy virus infection in the same region. These findings highlight the need to further investigate a potential causal relationship between Tamdy virus and febrile illnesses of unknown etiology in that region.

The species *Tamdy orthonairovirus* (genus *Orthonairovirus*, family *Nairoviridae*) includes 5 viruses: Tamdy virus (TAMV), Burana virus (BURV), Tǎchéng tick virus 1 (TcTV-1), Huángpí tick virus 1 (HpTV-1), and Wēnzhōu tick virus (WzTV) (*1*). TAMV and BURV were initially isolated from ticks in countries in central Asia (*2*–*4*), but little is known about their medical and veterinary importance. TcTV-1, HpTV-1, and WzTV were putative viruses identified by virome sequencing from ticks in China (*5*); however, their virologic properties and pathogenesis potential remain unclear. One study (*6*) reported TcTV-1 isolated from a febrile patient in northwest China, providing evidence of the potential public health threat from these viruses. We report TAMV isolated from ticks in northwest China and demonstrate serologic evidence of infection in humans.

The Study

During April and May of 2016 and 2017, we collected *Hyalomma asiaticum* ticks (n = 4,123) from Xinjiang in northwest China and divided the ticks into 55 groups according to the sampling location (n = 50–100 ticks/group) (Figure 1; Appendix Table 1, https://wwwnc.cdc.gov/EID/article/27/12/20-3532-App1.pdf). We isolated the virus from homogenates of each tick group in suckling mice. After the first inoculation, we observed symptoms in mice including loss of balance, limb paralysis, tremors, and articulo mortis from 4 (36.37%) of 11 pooled samples from Yuli County, 1 (14.29%) of 7 from the city of Karamay, 3 (60%) of 5 from Luntai County, and 17 (53.13%) of 32 from the city of Wujiaqu (Appendix Table 1). We performed a second inoculation using brain samples from diseased mice from Luntai and Wujiaqu Counties, in which >50% of the mice experienced illness onset after first inoculation. Similar symptoms were reproducibly observed in 1 group from Luntai and 4 groups from Wujiaqu (Appendix Table 1).

Subsequently, we prepared 3 RNA pools of diseased mouse brains and obtained a total of 196,946,814 reads by RNA sequencing. We found TAMV contigs in all 3 pools (Appendix Table 2), confirming findings using real-time reverse transcription PCR (rRT-PCR) (data not shown). We used homogenates of 2 TAMV RNA-positive brain samples from the A-M6 pool (Appendix Table 2) to isolate viruses in Vero E6 cells. As indicated by immunofluorescence assays (IFA) (Appendix), we observed increasing TAMV infection from first to fourth passages in Vero E6 cells, suggesting successful isolation (Appendix Figure 1).

Negative-stain electron microscopy revealed an enveloped spherical viral morphology with a diameter of ≈90–110 nm (Figure 2, panel A). We observed viral particles in cytoplasm and vesicles of infected cells (Figure 2, panel B). Although this screening was not exhaustive, IFAs showing varied susceptibility of different cells lines indicate that TAMV seems to have a broad host range, including humans, monkeys, sheep, dogs, and mice (Appendix Figure 2).

Author affiliations: Wuhan Institute of Virology, Chinese Academy of Sciences, Wuhan, China (A. Moming, S. Shen, Y. Fang, J. Zhang, Y. Zhang, S. Tang, T. Li, Z. Hu, H. Wang, F. Deng); College of Life Science and Technology, Xinjiang University, Urumqi, China (A. Moming, S. Sun); National Virus Resource Center, Wuhan (S. Shen, Y. Zhang, S. Tang, F. Deng); Center for Disease Control and Prevention of Xinjiang Uygur Autonomous Region, Urumqi, China (Y. Zhang); Programme in Emerging Infectious Diseases, Duke-NUS Medical School, Singapore (L-F.. Wang)

DOI: https://doi.org/10.3201/eid2712.203532

[1]These authors contributed equally to this article.

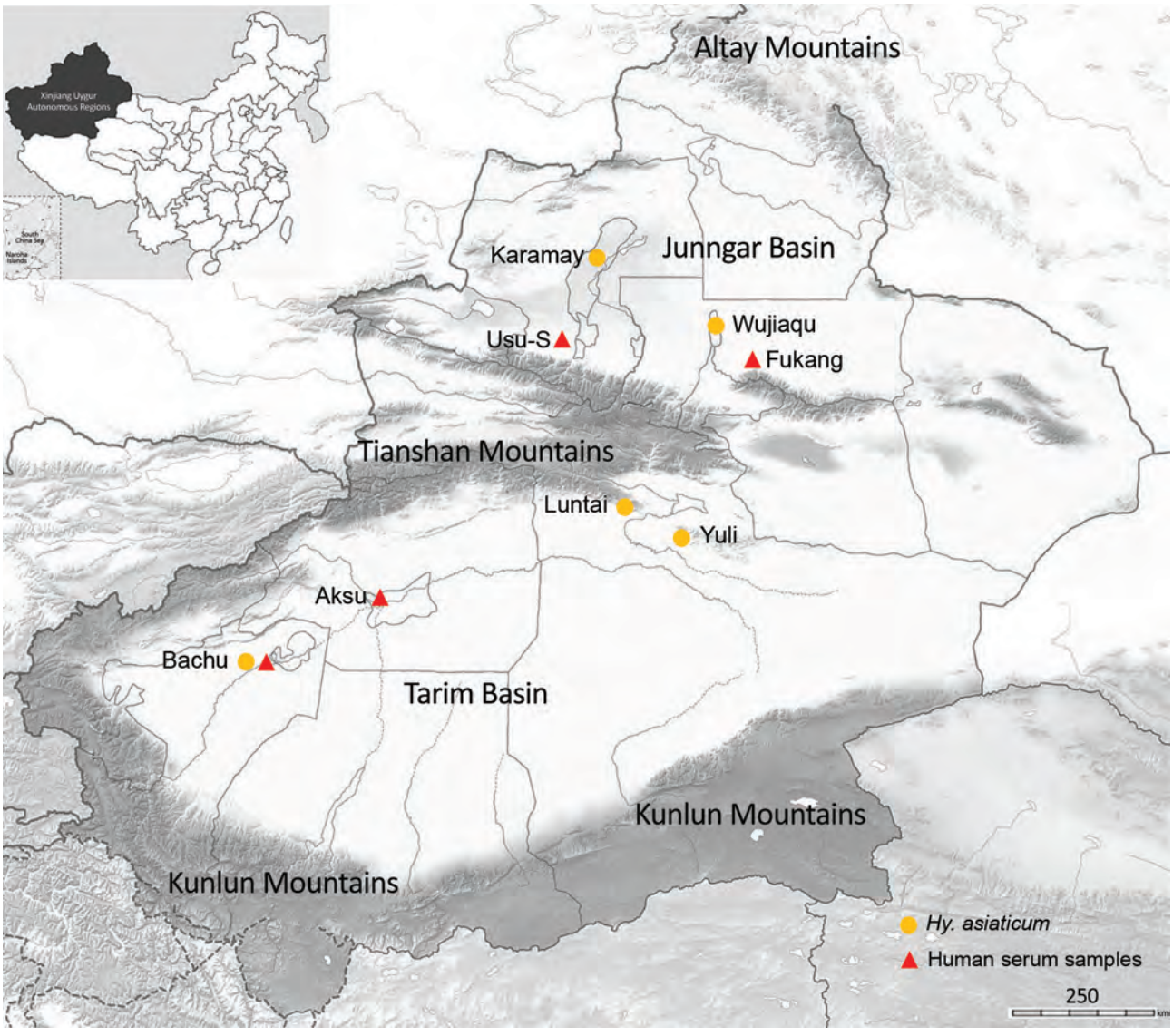

Figure 1. Collection locations for *Hyalomma asiaticum* ticks and human serum samples used in study of human exposure to Tamdy virus, Xinjiang, China. Usu-S, southern area of Usu City.

The 2 TAMV isolates shared very high sequence similarities (99.96% for large, 100% for medium, and 99.95% for small segments). We named the 2 TAMV strains YL16082 and YL16083, including an abbreviation (YL) for the geographic location (Yuli County) where the original tick samples were collected. TAMV genome sequences (YL16082) shared 37%–59% identity with other members of the *T. orthonairovirus* species and 34%–49% identity with Crimean-Congo hemorrhagic fever virus (CCHFV), another *Orthonairovirus* species. Protein sequences shared 44%–62% identity with other members of the *T. orthonairovirus* species and 33%–40% with CCHFV (Table 1). Phylogenetic trees based on nucleotide sequences of RNA-dependent RNA polymerase, glycoprotein, and nucleoprotein (NP) genes all confirmed the close taxonomic relationships with currently known TAMV strains and other members of the species *T. orthonairovirus* (Appendix Figure 3).

To investigate potential human infection by TAMV in northwest China, we conducted a seroprevalence study using archived serum samples from 725 healthy persons (collected in 2005 from Fukang City, 2014 from Aksu City, and 2017 from Usu City) and 87 febrile patients (collected in 2007 from Bachu County, which has a history of CCHFV prevalence) (Appendix). Of the 87 febrile patients, 21 (24.14%) were TAMV IgG positive and 17 (19.54%)

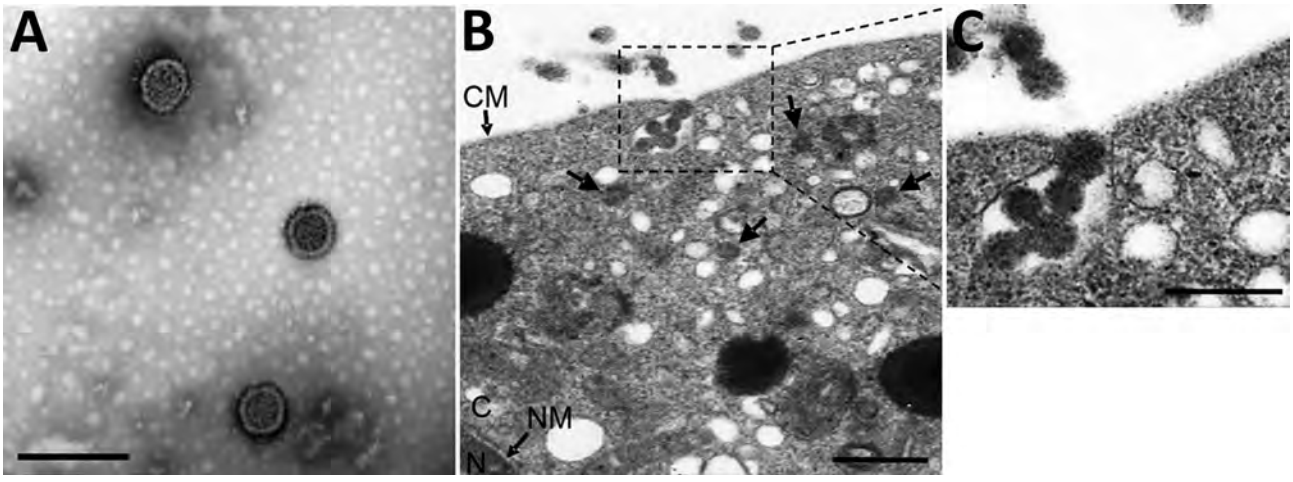

Figure 2. Visualization and subcellular localization of Tamdy virus (TAMV) virions by electron microscopy. A) Negative-staining image of purified TAMV virions. Scale bar indicates 200 nm. B) Image of Vero E6 cells infected with TAMV; arrows indicate TAMV virions in the cytoplasm. Scale bar indicates 500 nm. C) The enlarged image of interest from B. scale bar indicates 200 nm. CM, cell membrane; C, cytoplasm; NM, nuclear membrane; N, nucleus

IgM positive (Table 2; Appendix Table 4), whereas only 1 (0.13%) of the 725 healthy participants we tested IgG positive (data not shown). Neutralization (titers 16–64) was demonstrated in serum samples from 6 febrile patients (6.9%) (Table 2). Moreover, of the 24 tick groups from the same locations as the febrile patients, 10 groups (41.76%, 6 identified in sheep and 4 in fields) tested positive for TAMV RNA by rRT-PCR (data not shown). Partial sequences of large segments from these positive groups clustered together with TAMV strains (Appendix Figure 4). These results showed serologic evidence of human exposure to TAMV and evidence of TAMV presence in *Hy. asiaticum* ticks in northwest China as early as 2007, which warranted more in-depth investigation to establish the potential causal relationship between TAMV and febrile illnesses of unknown etiology in regions where TAMV is present.

Finally, because another *T. orthonairovirus*, TcTV-1, had been identified in a febrile patient in northwest China (*6*), we thought it important to determine the potential serologic cross-reactivity between these 2 viruses. However, TAMV and TcTV-1 shared limited protein sequence identity (49%–60%) (Table 1), suggesting limited cross-reactivity, if any. This result was confirmed by conducting serologic testing using recombinant NP proteins from the 2 viruses. As shown by both IFA and Western blot analyses, TAMV NP antibodies had no cross-reaction with TcTV-1 NP (Appendix Figure 5, panels A, B). In addition, human serum samples that were positive for TAMV IgM or IgG, or both, showed reactivity with TAMV NP, but not with TcTV-1 NP (Appendix Figure 5, panel C).

Conclusions

TAMV was initially found in ticks in countries in central Asia, including Kazakhstan, Kyrgyzstan, Uzbekistan, and Turkmenistan (*3*,*4*). Its infection status in humans and livestock animals was not well characterized. Our data, together with reports of TAMV isolated from ticks in Xinjiang, China (*7*), and identified in Turkey (*8*), shows that the geographic distribution of TAMV is much wider than originally recognized. In addition, we provide strong serologic evidence of human exposure in TAMV-affected regions.

Findings of a potential role of TcTV-1 in causing human febrile disease (*6*) suggest that >1 virus in this species group may have the potential to cause

Table 1. Sequence identity of TAMV isolate YL16082 from China compared with other members of the species *Tamdy orthonairovirus* and Crimean-Congo hemorrhagic fever virus*

Virus	Nucleotide identity, %			Amino acid identity, %		
	L segment	M segment	S segment	RdRp	G	NP
Wēnzhōu tick virus	59	50	42	62	51	44
Tǎchéng tick virus 1	57	46	44	60	51	49
Huángpí tick virus 1	55	45	42	58	47	46
Burana virus†	59	47	37	62	50	44
Crimean-Congo hemorrhagic fever virus	49	34	39	40	33	36

*G, glycoprotein; L, large; M, medium; NP, nucleoprotein; RdRp, RNA-dependent RNA polymerase; S, small; TAMV, Tamdy virus.
†Partial sequences were available for analyses.

Table 2 Seroprevalence of TAMV among 87 febrile patients with samples collected in 2007 from Bachu County, Xinjiang, China*

Patient characteristics	Serum samples, no.	TAMV IgG positive, %	TAMV IgM positive, %	Neutralization activity, %	Neutralization titers
Sex					
M	20	3 (15.0)	7 (35.0)	1 (5.0)	64
F	29	6 (20.7)	5 (17.2)	3 (10.3)	16, 32, 32
NA	38	12 (31.6)	5 (13.6)	2 (5.3)	16, 16
Age, y†					
<18	6	2 (33.3)	1 (16.7)	0	
18–30	20	1 (5.0)	8 (40.0)	1 (5.0)	16
31–45	7	2 (28.6)	1 (14.3)	0	
46–60	11	2 (18.2)	0	1 (9.1)	32
>60	5	2 (40.0)	2 (40.0)	2 (40.0)	32, 64
Total	87	21 (24.1)	17 (19.5)	6 (6.9)	16–64

*NA, not available; TAMV, Tamdy virus.
†Age stratification based on 49 patients with recorded age information

diseases in humans. However, our data did suggest the possibility of such a relationship because the TAMV-positive ratio was much higher among febrile patients than healthy persons in the study from the same region. In addition, at least 2 febrile patients had both TAMV IgM and IgG at the time of sampling, during or not long after acute illness; 1 of them had neutralization to TAMV (Appendix Table 3).

Among study limitations, the nature of using archived samples limited our ability to provide direct evidence of a causal relationship between TAMV and human febrile illnesses. Also, it is possible that the high TAMV antibody-positive ratio might have resulted not from the recent cases but from a small outbreak of human TAMV infection in northwest China in 2007.

In summary, our study strongly suggests the potential of TAMV as a human pathogen and supports an urgent need to conduct more in-depth epidemiologic and pathogenesis investigations into this group of viruses in China, central Asia, and beyond. While the world's attention is currently on coronavirus disease and batborne viruses, our study highlights the need to pay attention at the same time to emerging zoonoses of tick origin to prevent future outbreaks.

Acknowledgments

We thank the core facility and technical support groups of Wuhan Institute of Virology for providing technical support for electron microscopy analysis, animal experiments, and experimental activities in a Biosafety Level 3 laboratory.

This work was mainly supported by the Science and Technology Basic Work Program (2013FY113500) from the Ministry of Science and Technology of China, the Intergovernmental Special Program of State Key Research and Development Plan from the Ministry of Science and Technology of China (2016YFE0113500), the National R&D Infrastructure and Facility Development Program of China, "Fundamental Science Data Sharing Platform" (Y706061YZ1), Science Foundation of China (81690369, 81760365), and the Science Research Key Project of Xinjiang Education Department (XJEDU2019I002). Work in L.-F.W.'s group is supported in part by NRF grants NRF2016NRF-NSFC002-013 and NRF2018NRF-NSFC003SB-002, CD-PHRG grant CDPHRG/0006/2014, NMRC grant ZRRF16006, and MINDEF grant DIRP2015-9016102060.

About the Author

Mr. Moming is a doctoral student in a joint training project at the College of Life Science and Technology, Xinjiang University, and Wuhan Institute of Virology, Chinese Academy of Sciences. His main research interests include epidemiologic investigation, identification, and characterization of tick-borne viruses.

References

1. Abudurexiti A, Adkins S, Alioto D, Alkhovsky SV, Avšič-Županc T, Ballinger MJ, et al. Taxonomy of the order *Bunyavirales*: update 2019. Arch Virol. 2019;164:1949–65. https://doi.org/10.1007/s00705-019-04253-6
2. L'vov DK, Al'khovskiĭ SV, Shchelkanov MI, Shchetinin AM, Deriabin PG, Gitel'man AK, et al. Taxonomic status of the Burana virus (BURV) (*Bunyaviridae, Nairovirus,* Tamdy group) isolated from the ticks *Haemaphysalis punctata* Canestrini et Fanzago, 1877 and *Haem. concinna* Koch, 1844 (*Ixodidae, Haemaphysalinae*) in Kyrgyzstan [in Russian]. Vopr Virusol. 2014;59:10–5.
3. L'vov DK, Sidorova GA, Gromashevskiĭ VL, Skvortsova TM, Aristova VA. Isolation of Tamdy virus (*Bunyaviridae*) pathogenic for man from natural sources in Central Asia, Kazakhstan and Transcaucasia [in Russian]. Vopr Virusol. 1984;29:487–90.
4. Lvov DK, Sidorova GA, Gromashevsky VL, Kurbanov M, Skvoztsova LM, Gofman YP, et al. Virus "Tamdy"—a new arbovirus, isolated in the Uzbee S.S.R. and Turkmen S.S.R. from ticks *Hyalomma asiaticum asiaticum* Schulee et Schlottke, 1929, and *Hyalomma plumbeum plumbeum* Panzer, 1796. Arch Virol. 1976;51:15–21. https://doi.org/10.1007/BF01317830
5. Li CX, Shi M, Tian JH, Lin XD, Kang YJ, Chen LJ, et al.

Unprecedented genomic diversity of RNA viruses in arthropods reveals the ancestry of negative-sense RNA viruses. eLife. 2015;4:e05378. https://doi.org/10.7554/eLife.05378
6. Liu X, Zhang X, Wang Z, Dong Z, Xie S, Jiang M, et al. A tentative Tamdy orthonairovirus related to febrile illness in northwestern China. Clin Infect Dis. 2020;70:2155–60. https://doi.org/10.1093/cid/ciz602
7. Zhou H, Ma Z, Hu T, Bi Y, Mamuti A, Yu R, et al. Tamdy virus in *Ixodid* ticks infesting bactrian camels, Xinjiang, China, 2018. Emerg Infect Dis. 2019;25:2136–8. https://doi.org/10.3201/eid2511.190512
8. Brinkmann A, Dinçer E, Polat C, Hekimoğlu O, Hacıoğlu S, Földes K, et al. A metagenomic survey identifies Tamdy orthonairovirus as well as divergent phlebo-, rhabdo-, chu- and flavi-like viruses in Anatolia, Turkey. Ticks Tick Borne Dis. 2018;9:1173–83. https://doi.org/10.1016/j.ttbdis.2018.04.017

Address for correspondence: Linfa Wang, Programme in Emerging Infectious Diseases, Duke-NUS Medical School, 169857, Singapore; email: linfa.wang@duke-nus.edu.sg; Fei Deng, Wuhan Institute of Virology, Chinese Academy of Sciences, Xiaohongshan 44, Wuchang District, Wuhan City, Hubei Province, 430071, China; email: df@wh.iov.cn

SARS-CoV-2 B.1.1.7 Variant Infection in Malayan Tigers, Virginia, USA

Patrick K. Mitchell, Mathias Martins, Tara Reilly, Leonardo C. Caserta, Renee R. Anderson, Brittany D. Cronk, Julia Murphy, Erin L. Goodrich, Diego G. Diel

Author affiliations: Cornell University, Ithaca, New York, USA (P.K. Mitchell, M. Martins, L.C. Caserta, R.R. Anderson, B.D. Cronk, E.L. Goodrich, D.G. Diel); Virginia Zoo, Norfolk, Virginia, USA (T. Reilly); Virginia Department of Health, Richmond, Virginia (J. Murphy)

DOI: https://doi.org/10.3201/eid2712.211234

We report infection of 3 Malayan tigers with severe acute respiratory syndrome coronavirus 2 (SARS-CoV-2) B.1.1.7 (Alpha) variant at a zoologic park in Virginia, USA. All tigers exhibited respiratory signs consistent with SARS-CoV-2 infection. These findings show that tigers are susceptible to infection with the SARS-CoV-2 B.1.1.7 variant.

On April 4, 2021, a 5-year-old male Malayan tiger (*Panthera tigris jacksoni*) at the Virginia Zoo (Norfolk, VA, USA) began exhibiting lethargy, labored breathing, coughing, intermittent upper respiratory sounds, hyporexia, and mucoid nasal discharge. On April 7, another 5-year-old male Malayan tiger began experiencing labored breathing, cough, clear nasal discharge, and hyporexia. On April 10, a third Malayan tiger, a 10-year-old male, had cough and later clear nasal discharge. The tigers' clinical signs resolved by April 15, eleven days after the outbreak began.

Zoo staff collected nasal swab and fecal samples from the 5-year-old tigers on April 9 and the 10-year-old tiger on April 13 and submitted these to Cornell University's Animal Health Diagnostic Center (AHDC; Ithaca, NY, USA). AHDC tested samples for *Bordetella* sp., *Chlamydia felis*, *Mycoplasma cynos*, *M. felis*, *Streptococcus equi* subspecies *zooepidemicus*, influenza virus, pneumovirus, feline calicivirus, and feline herpesvirus; all results were negative. All samples tested positive for severe acute respiratory syndrome coronavirus 2 (SARS-CoV-2) by EZ-SARS-CoV-2 Real-Time RT-PCR Test (Tetracore, Inc., https://tetracore.com). We isolated SARS-CoV-2 from respiratory and fecal specimens from the first tiger. Testing at the US Department of Agriculture National Veterinary Services Laboratories (Ames, IA, USA) confirmed SARS-CoV-2 infection. We screened the tiger samples using TaqPath COVID-19 RT-PCR Kit (Thermo Fisher Scientific, https://www.thermofisher.com), which revealed a spike gene dropout in samples from all 3 tigers; only the nucleoprotein and open reading frame 1ab gene targets were detected, suggesting B.1.1.7 variant infection.

We performed whole-genome sequencing on all samples by using MinION (Oxford Nanopore Technologies, https://nanoporetech.com), as previously described (*1*). We assembled reads using the ARTIC ncov-2019 protocol (ARTIC Network, https://artic.network) and Medaka (Oxford Nanopore Technologies) for variant calling. We obtained near-complete (29,702–29,710-bp) assemblies from all nasal swab specimens (GenBank accession nos. MZ305031–3) but no assemblies from fecal samples. We identified respiratory specimen genomes as lineage B.1.1.7 (Alpha variant) by using Pangolin version 2.4.2 (https://github.com/cov-lineages/pangolin). We used Nextstrain (https://nextstrain.org) for phylogenetic analysis of tiger-derived sequences and other B.1.1.7 sequences downloaded from GISAID (https://www.gisaid.org) on April 15, 2021 (*2*,*3*). Tiger-derived sequences all were identical, except 1 manually corrected homopolymer repeat error, and fell into a clade defined by a C4900T mutation containing other samples collected primarily in the United States. Tiger-derived sequences differed from others in the clade by 1 single-nucleotide polymorphism in the spike gene (K558N) (Figure, panel A). Using the vdb tool (*4*), we found 46 additional B.1.1.7 sequences that had the K558N mutation in GISAID on July 22, 2021; all were collected from Virginia during March 27–July 7, 2021. However, phylogenetic analysis of these sequences and the tiger-derived sequences showed divergence of 11 single-nucleotide polymorphism, minus the divergence producing the K558N mutation (Figure, panel B), indicating the sequences are not related epidemiologically.

The source of the tigers' infection is unknown. The zoo has been open to the public, but transmission from a visitor is unlikely because tiger exhibit areas are separated from visitors by either a glass enclosure or ≥9 m distance. The most plausible explanation is that ≥1 tiger acquired the virus from a keeper because they had close contact. However, no employees tested positive for SARS-CoV-2 nor had symptoms during the 4 weeks before the tigers' symptom onset. Nine keepers were responsible for the animals' daily care; 2 other persons prepared animal diets daily. Employees were required to wear facemasks always, indoors and outdoors; everyone wore standard 2-ply surgical masks or homemade cloth facemasks. Staff also were required to wear gloves when handling and preparing food and when servicing animal areas. Furthermore, staff were

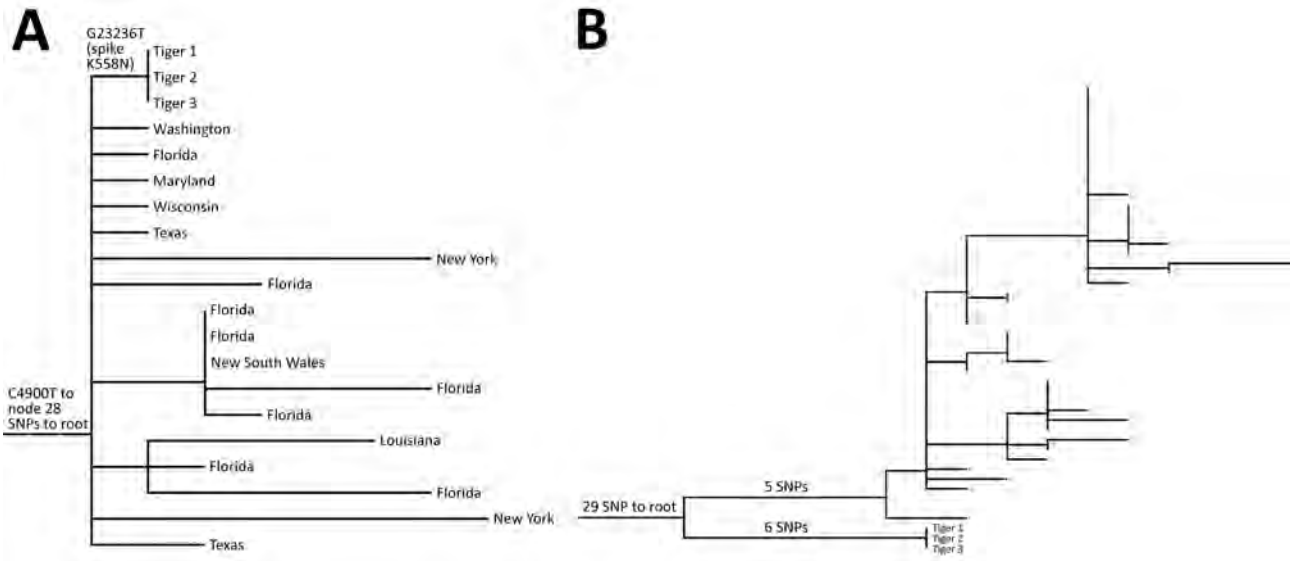

Figure. Maximum-likelihood phylogenetic trees of severe acute respiratory syndrome coronavirus 2 from 3 Malayan tigers, Virginia, USA. Tiger samples are numbered in order of symptom onset. A) Subset of phylogenetic tree showing parent (G23236T) and grandparent (C4900T) nodes of the tiger sequences, with tips labeled as states of origin in the United States or Australia. B) Phylogenetic tree showing that other B.1.1.7 viruses detected in Virginia that contain the K558N mutation are not epidemiologically related to the sequences detected in tigers 1, 2, and 3. SNP, single-nucleotide polymorphism.

required to step into an accelerated hydrogen peroxide disinfectant footbath when entering the tiger building and diet kitchen. The 3 tigers might have been infected by an employee, or 1 tiger was infected, then transmission occurred to the others. Two tigers lived in the same enclosure and had no direct contact with the third, but all 3 rotated through common enclosure spaces.

After identification of the tiger infections, 4 additional zoo animals were tested: 1 lion (*Panthera leo*) with lethargy and hyporexia ≈1 week after SARS-CoV-2 diagnosis in the tigers; another asymptomatic lion because of age and proximity to the first lion; and 2 degus (*Octodon degus*) that died in late March and had interstitial pneumonia on necropsy. AHDC tested nasal swab samples from the lions and frozen spleen and cecum samples from the degus by reverse transcription PCR; all results were negative for SARS-CoV-2.

Our findings underscore felid susceptibility to SARS-CoV-2, which also has been detected in captive snow leopards (*Panthera uncia*) and pumas (*Puma concolor*) (*5*). Other nonhuman species, including gorillas (*Gorilla gorilla*), minks (*Neovison vison*), and ferrets (*Mustela putorius furo*), have acquired SARS-CoV-2; additional species have been shown to be susceptible experimentally (*5*–*7*). Domestic cats and dogs in the United Kingdom and United States reportedly had B.1.1.7 infections, suggesting that mutations characterizing this lineage are not constrained to a host range (*8*; L. Ferasin et al., unpub. data, https://doi.org/10.1101/2021.03.18.435945). Monitoring animals for SARS-CoV-2 infection is critical to determining potential host range, particularly as new virus variants emerge and spread.

This article was preprinted at https://doi.org/10.21203/rs.3.rs-618448/v1.

Acknowledgments

We gratefully acknowledge the originating and submitting laboratories of the sequence data submitted to GISAID (https://www.gisaid.org) used in this manuscript.

The sequencing infrastructure at the Animal Health Diagnostic Center, Cornell University, used in this study, is funded through grants from the National Animal Health Network to D.G.D. (grant nos. AP20VSD and B000C020).

About the Author

Dr. Mitchell is a research associate in the Department of Population Medicine and Diagnostic Sciences at Cornell University. His primary research interest is molecular epidemiology of infectious diseases.

References

1. Caserta LC, Mitchell PK, Plocharczyk E, Diel DG. Identification of a SARS-CoV-2 lineage B1.1.7 virus in New York following return travel from the United Kingdom. Microbiol Resour Announc. 2021;10:e00097-21. https://doi.org/10.1128/MRA.00097-21

2. Hadfield J, Megill C, Bell SM, Huddleston J, Potter B, Callender C, et al. Nextstrain: real-time tracking of pathogen evolution. Bioinformatics. 2018;34:4121–3. https://doi.org/10.1093/bioinformatics/bty407
3. Sagulenko P, Puller V, Neher RA. TreeTime: maximum-likelihood phylodynamic analysis. Virus Evol. 2018;4:vex042. https://doi.org/10.1093/ve/vex042
4. West AP, Wertheim JO, Wang JC, Vasylyeva TI, Havens JL, Chowdhury MA, et al. Detection and characterization of the SARS-CoV-2 lineage B.1.526 in New York. Nat Comm. 2021;12:4886. https://doi/org/10.1038/s41467-021-25168-4
5. World Organisation for Animal Health. COVID-19 [cited 2021 May 19]. https://www.oie.int/en/what-we-offer/emergency-and-resilience/covid-19
6. US Department of Agriculture Animal and Plant Health Inspection Service. Cases of SARS-CoV-2 in animals in the United States [cited 2021 May 19]. https://www.aphis.usda.gov/aphis/dashboards/tableau/sars-dashboard
7. Delahay RJ, de la Fuente J, Smith GC, Sharun K, Snary EL, Flores Girón L, et al. Assessing the risks of SARS-CoV-2 in wildlife. One Health Outlook. 2021;3:7. https://doi.org/10.1186/s42522-021-00039-6
8. Hamer SA, Ghai RR, Zecca IB, Auckland LD, Roundy CM, Davila E, et al. SARS–CoV–2 B.1.1.7 variant of concern detected in a pet dog and cat after exposure to a person with COVID–19, USA. Transbound Emerg Dis. 2021 May 12 [Epub ahead of print] https://doi.org/10.1111/tbed.14122

Address for correspondence: Diego G. Diel, Animal Health Diagnostic Center, Cornell University, 240 Farrier Rd, Ithaca, NY 14853, USA; email: dgdiel@cornell.edu

Postmortem Stability of SARS-CoV-2 in Mouse Lung Tissue

Sophie A. Valkenburg, Samuel M.S. Cheng, Asmaa Hachim, Malik Peiris, John Nicholls

Author affiliations: The University of Hong Kong, Hong Kong, China

DOI: https://doi.org/10.3201/eid2712.211621

The infectivity of severe acute respiratory syndrome coronavirus 2 in deceased persons and organisms remains unclear. We studied transgenic K18 hACE2 mice to determine the kinetics of virus infectivity after host death. Five days after death, virus infectivity in the lung declined by >96% and RNA copies declined by 48.2%.

The safe handling and disposal of bodies of persons who have died of coronavirus disease (COVID-19) is vital for infection control. Although cremation or burial practices are mainly dictated by religious and societal customs, deaths associated with contagious illness warrant appropriate precautions. Severe acute respiratory syndrome coronavirus 2 (SARS-CoV-2), the causative agent of COVID-19, is rapidly inactivated (>2 $\log_{10}$) within hours on nonporous surfaces (*1*). In addition, several studies have detected viral RNA by reverse transcription PCR (RT-PCR) of nasopharyngeal and pharyngeal mucosal swab specimens, skin swab specimens, and tissue samples collected during autopsies at different times after death (*2*–*5*). Furthermore, infectious virus was isolated in 2 of 4 cases at 4–17 days postmortem; however, this study did not quantify virus titers to determine the loss of virus infectivity (*6*). A separate study found that infectious virus was undetectable after exhumation at 3–4 months postmortem (*7*). Overall, RNA detection by RT-PCR might not directly correlate with virus infectivity or duration of symptomatic disease.

Transgenic K18-hACE2 mice provide a surrogate model to study the kinetics of SARS-CoV-2 viral replication during infection (*8*) and after host death. In humans and K18-hACE2 mice, little evidence exists for extrapulmonary dissemination of SARS-CoV-2, except for neurotropism in younger mice, a finding that has not been demonstrated reliably in humans. We investigated the temporal decay of infectious SARS-CoV-2 in postmortem tissues of infected K18-hACE2 mice. All experimental procedures were conducted in accordance with the standards and approved by the Committee on the Use of Live Animals in Teaching and Research (approval no. 5511-20) at The University of Hong Kong (Hong Kong, China).

We infected twelve 14–20-week-old mice with 1×10^4 50% tissue culture infectious dose ($TCID_{50}$)/25μL SARS-CoV-2 by the intranasal route. Five days later, after the mice had lost 18.8% (SD 7.77%) of their body weight, we euthanized them by ketamine/xylazil anesthesia. We wrapped each carcass in a sealable plastic bag, similar to the storage of human corpses, and stored them intact at 4°C, which is standard mortuary temperature. On days 0, 1, 5, and 14 after death, we dissected 3 carcasses and tested the lung tissue for coronavirus nucleoprotein (N) by histologic and immunohistochemistry assays (*9*) (Appendix Figure, panels A–H, https://wwwnc.cdc.gov/EID/article/27/12/21-1612-App1.pdf). We quantified infectious virus by culture (Figure, panel A) and viral RNA by RT-PCR (Figure, panel B) (Appendix).

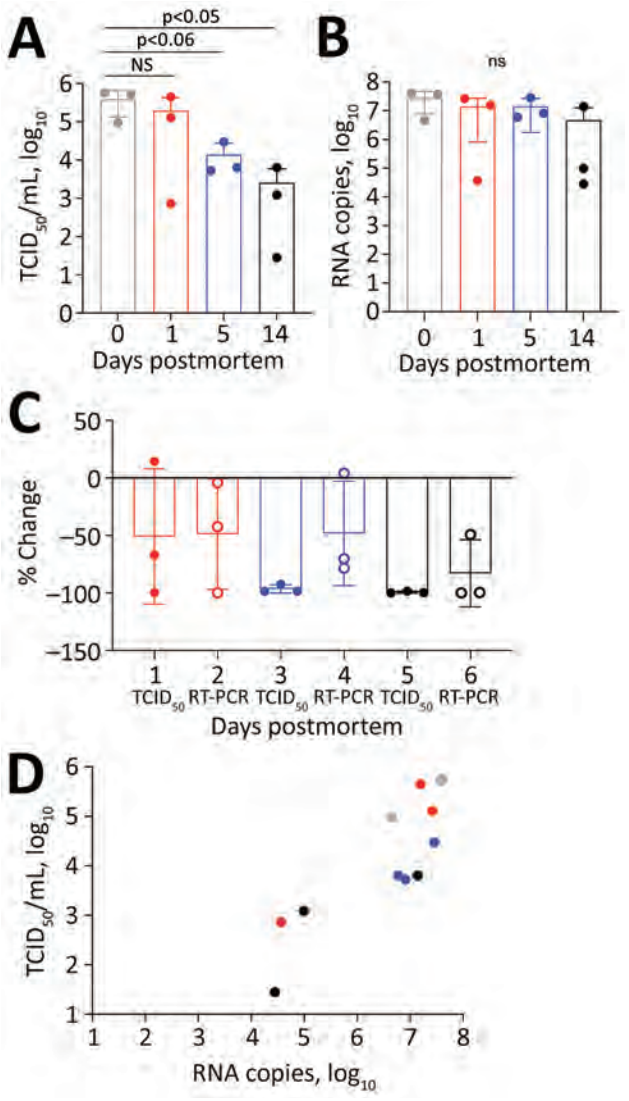

Figure. Postmortem stability of severe acute respiratory syndrome coronavirus 2 in mouse lung tissue. A) Infectious virus measured by $TCID_{50}$ of VeroE6 cells. B) Viral RNA measured by copies of N gene detected by RT-PCR. C) Percentage change compared with day 0. D) Correlation between infectious virus and viral RNA. $R^2 = 0.51$; $F = 0.005$ by analysis of variance. NS, not significant; RT-PCR, reverse transcription PCR; $TCID_{50}$, 50% tissue culture infectious dose.

Viral decay, measured using $TCID_{50}$ for infectious virus and RNA copies of the N gene detected by RT-PCR, occurred over a 14-day period (Table). At day 1 we observed a 50% reduction of infectious virus and 48.8% loss of viral RNA (Figure, panels A, B). By day 5, levels of infectious virus had fallen by 96.5%, whereas viral RNA remained at 48.2% compared with day 0 (Figure, panels C, D). At day 14 only 0.7% of the initial infectious virus and 17% of viral RNA remained. Plenzig et al. (*7*) detected viral RNA in 2 exhumed corpses at 3 months postmortem, despite an absence of infectious virus. We used hematoxylin and eosin staining to detect viral nucleoprotein in lung tissue. We observed persistent antigen staining until day 5; by day 14, only 1 of 3 samples had detectable staining (Appendix Figure).

We euthanized the mice 5 days after infection, when the lungs had a high viral load. However, COVID-19 deaths usually occur during later stages of disease, by which time infectious viral load has decreased from the peak usually seen early during the symptomatic phase of the illness (*10*). We detected virus antigen in the lungs of all mice at 5 days postmortem; infectious virus had declined by 96.48%, but viral RNA declined by only 48.21%. Our results shows that infectious virus declines earlier than viral RNA or antigen in postmortem tissues.

These findings have implications for the safe handling of deceased COVID-19 patients. Infectious virus can persist on inanimate surfaces for up to 14 days at lower temperatures (<4°C), but rapidly decays in postmortem tissue samples. We observed a 96.5% decrease in infectious virus by day 5 and a 99.3% decrease by day 14. Most published postmortem studies in humans have reported viral load at the time of death using cycle threshold values rather than N gene copies as we have done; results range from 17–36 for cycle threshold values and 0–5.49 log_{10} for N gene copies (*11*). Therefore, the maximum potential risk of transmission from an infected

Table. Postmortem viral loads in K18-hACE2 mice lung tissue after 5 days of infection with severe acute respiratory syndrome coronavirus 2*

Day	N gene copies, log_{10}	% Reduction of N gene copies†	$TCID_{50}$/mL, log_{10}	% Reduction of $TCID_{50}$/mL†	Lung inflammation score‡	SARS-CoV-2 N protein antigen score§	Positive for SARS N protein¶
0	7.28 ± 0.53	NA	5.48 ± 0.44	NA	9.33 ± 1.53	3.66 ± 1.15	3 (100.0)
1	6.39 ± 1.59	−48.85 ± 48.14	4.54 ± 1.48	−50.88 ± 58.82	7 ± 2	2.66 ± 2.31	2 (66.6)
5#	7.05 ± 0.36	−48.21 ± 45.43	4.00 ± 0.41	−96.48 ± 3.54	5.33 ± 4.61	4 ± 1.4	2 (100.0)
14	5.53 ± 1.43	−82.95 ± 29.13	2.78 ± 1.21	−99.35 ± 0.86	10.33 ± 1.53	1.66 ± 2.88	1 (33.3)

*Values are mean ±SD, except as indicated. NA, not applicable; $TCID_{50}$, 50% tissue culture infectious dose.
†Compared with day 0.
‡Scale of 0–16, in which 16 represents most severe inflammation.
§Scale of 0–5, in which 5 represents highest amount of antigen.
¶Values are no. (%).
#Days 0,1, and 14 values reflect 3 mice. Day 5 values reflect 2 mice for histology and 3 mice for $TCID_{50}$ and reverse transcription PCR.

corpse is during the first 24 hours after death. By day 5, the amount of infectious virus has decreased by 96.48%. If proper biosafety precautions and personal protective equipment are used to handle the corpse during autopsy or preparation for burial or cremation, we believe that the burial or cremation process is unlikely to spread disease.

This study was partly supported by the Health and Medical Research Fund (grant no. HMRF COVID-190115 to M.P. and S.A.V.), and Commissioned Research on Control of Infectious Diseases (phase III and IV) from the Health and Medical Research Fund (M.P.).

About the Author

Dr. Valkenburg is a viral immunologist at the HKU-Pasteur Research Pole, University of Hong Kong, Hong Kong, China. Her research interests include immune correlates for influenza and severe acute respiratory syndrome coronavirus 2.

References

1. Chin AWH, Chu JTS, Perera MRA, Hui KPY, Yen HL, Chan MCW, et al. Stability of SARS-CoV-2 in different environmental conditions. Lancet Microbe. 2020;1:e10. https://doi.org/10.1016/S2666-5247(20)30003-3
2. Heinrich F, Meißner K, Langenwalder F, Püschel K, Nörz D, Hoffmann A, et al. Postmortem stability of SARS-CoV-2 in nasopharyngeal mucosa. Emerg Infect Dis. 2021;27:329–331. https://doi.org/10.3201/eid2701.203112
3. Skok K, Stelzl E, Trauner M, Kessler HH, Lax SF. Post-mortem viral dynamics and tropism in COVID-19 patients in correlation with organ damage. Virchows Arch. 2021;478:343–53. https://doi.org/10.1007/s00428-020-02903-8
4. Sablone S, Solarino B, Ferorelli D, Benevento M, Chironna M, Loconsole D, et al. Post-mortem persistence of SARS-CoV-2: a preliminary study. Forensic Sci Med Pathol. 2021;17:403–410. https://doi.org/10.1007/s12024-021-00375-z
5. Schröder AS, Edler C, Ondruschka B, Püschel K, Schädler J, Heinemann A, et al. The handling of SARS-CoV-2 associated deaths—infectivity of the body. Forensic Sci Med Pathol. 2021;17:411–418. https://doi.org/10.1007/s12024-021-00379-9
6. Plenzig S, Bojkova D, Held H, Berger A, Holz F, Cinatl J, et al. Infectivity of deceased COVID-19 patients. Int J Legal Med. 2021;135:2055–60. https://doi.org/10.1007/s00414-021-02546-7
7. Plenzig S, Holz F, Bojkova D, Kettner M, Cinatl J, Verhoff MA, et al. Detection and infectivity of SARS-CoV-2 in exhumated corpses. Int J Legal Med. 2021 Jul 24 [Epub ahead of print]. https://doi.org/10.1007/s00414-021-02670-4
8. Zheng J, Wong LR, Li K, Verma AK, Ortiz ME, Wohlford-Lenane C, et al. COVID-19 treatments and pathogenesis including anosmia in K18-hACE2 mice. Nature. 2021;589:603–7. https://doi.org/10.1038/s41586-020-2943-z
9. Perera RAPM, Tso E, Tsang OTY, Tsang DNC, Fung K, Leung YWY, et al. SARS-CoV-2 virus culture and subgenomic RNA for respiratory specimens from patients with mild coronavirus disease. Emerg Infect Dis. 2020;26:2701–4. https://doi.org/10.3201/eid2611.203219
10. Zou L, Ruan F, Huang M, Liang L, Huang H, Hong Z, et al. SARS-CoV-2 viral load in upper respiratory specimens of infected patients. N Engl J Med. 2020;382:1177–9. https://doi.org/10.1056/NEJMc2001737
11. Nienhold R, Ciani Y, Koelzer VH, Tzankov A, Haslbauer JD, Menter T, et al. Two distinct immunopathological profiles in autopsy lungs of COVID-19. Nat Commun. 2020;11:5086. https://doi.org/10.1038/s41467-020-18854-2

Address for correspondence: John Nicholls, Block T, Queen Mary Hospital, The University of Hong Kong, Pokfulam, Hong Kong, China; email: nicholls@pathology.hku.hk

Guillain-Barré Syndrome Associated with COVID-19 Vaccination

Shih-Chieh Shao,[1] Chien-Ho Wang,[1] Kai-Cheng Chang, Ming-Jui Hung, Hui-Yu Chen, Shu-Chen Liao

Author affiliations: Keelung Chang Gung Memorial Hospital, Keelung, Taiwan (S.-C. Shao, C.-H. Wang, M.-J. Hung, S.-C. Liao); National Cheng Kung University College of Medicine, Tainan, Taiwan (S.-C. Shao, K-C, Chang); Linkou Chang Gung Memorial Hospital, Taoyuan, Taiwan (K.-C. Chang, H.-Y. Chen); Chang Gung University College of Medicine, Taoyuan (M.-J. Hung, S.-C. Liao)

DOI: https://doi.org/10.3201/eid2712.211634

We conducted a multi-institutional study in Taiwan and a systematic review of the literature for reports of Guillain-Barré syndrome after coronavirus disease vaccination. This condition, mostly the classic form and the acute inflammatory demyelinating polyneuropathy subtype, has been reported in 39 cases and has occurred within 2 weeks of vaccine administration.

Guillain-Barré syndrome (GBS), an immune-mediated polyradiculoneuropathy with a ≈5% mortality rate, has an incidence worldwide of 0.81–1.91 cases/100,000 person-years (*1*). GBS has been

[1]These authors contributed equally to this article.

reported to be associated with coronavirus disease (COVID-19) vaccination, but a comprehensive summary regarding this rare adverse event is still lacking. To determine clinical features of GBS associated with COVID-19 vaccination, we conducted hospital-based investigations in Taiwan along with a systematic review of published case reports.

We analyzed electronic medical records data from Taiwan's largest multi-institutional healthcare system, including 9 branches of Chang Gung Memorial Hospital (2), where healthcare workers received first-priority COVID-19 ChAdOx1-S vaccine (Oxford/AstraZeneca, https://www.astrazeneca.com) starting March 22, 2021. We included healthcare workers vaccinated during March 22–May 31 and followed them for 30 days after vaccination. We identified GBS cases on the basis of code G610 from the International Classification of Disease, 10th Revision, Clinical Modification, or spontaneous adverse drug reaction reporting systems within the hospitals. Two authors (C.H.W. and S.C.L.) confirmed diagnosis and classification of GBS cases through chart reviews (3,4). This study was approved by the Institutional Review Board of Chang Gung Medical Foundation (approval no. 202101087B0).

To summarize clinical features of published cases from literature, we searched PubMed and Embase for reports posted through August 17, 2021, using relevant key terms such as "COVID-19," "Guillain-Barré syndrome," and "vaccine" with suitable MeSH terms. Two independent reviewers (S.C.S., C.H.W.) performed the study selection and data extraction; a third-reviewer (S.C.L.) settled any differences between them. We excluded cases with coexisting COVID-19 or preexisting GBS. We included only publications with reports of clinical features related

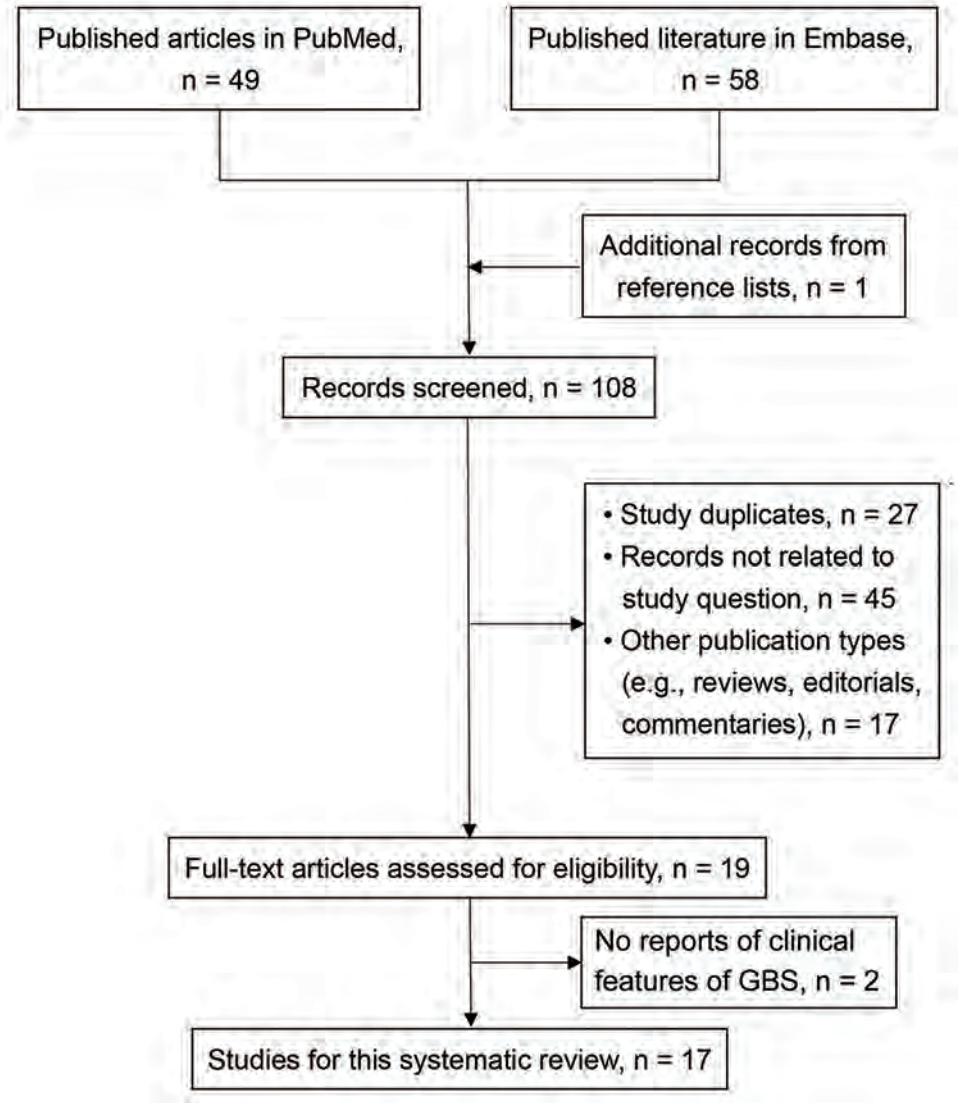

Figure. Systematic review of published literature in study of Guillain-Barré syndrome associated with coronavirus vaccination, 2021. GBS, Guillain-Barré syndrome.

to GBS. We described basic characteristics, laboratory data, pathologic reports, treatment patterns, and prognosis of GBS cases associated with COVID-19 vaccination. The study protocol of this systematic review is published on PROSPERO (https://www.crd.york.ac.uk/PROSPERO/display_record.php?RecordID=265479).

We included 18,269 healthcare workers (mean age 40.6 years, range 18–87 years; 67.5% were women) who received ChAdOx1-S vaccine during the study period. After these 18,257 first-dose and 544 second-dose vaccinations, we identified 1 GBS case after a first dose of ChAdOx1-S vaccine in 1 of the hospitals participating in the study.

After a systematic review of published literature (Figure), we included 17 publications reporting an additional 38 cases of GBS related to COVID-19 vaccination (India, 10 cases; United Kingdom, 11 cases; Mexico, 7 cases; United States, 3 cases; France, 1 case; Italy, 3 cases; Malta, 1 case; Turkey, 1 case; and Qatar, 1 case) (Appendix Table, https://wwwnc.cdc.gov/EID/article/27/12/21-1634-App1.pdf). Including the case in Taiwan, these 39 cases occurred in persons with a mean age of 57.8 (range 20–86) years; 56.4% were male. Most of the reported case-patients received ChAdOx1-S (25/39), followed by BNT162b2 (12/39) (Pfizer-BioNTech, https://www.pfizer.com), Ad26.COV2.S (1/39) (Johnson & Johnson, https://www.jnj.com), and CoronaVac (1/39) (Sinovac Biotech, http://www.sinovac.com). The GBS rate after COVID-19 vaccination ranged from 1.8 to 53.2 cases/1 million doses. The initial symptoms of GBS included myalgia (12/39), paraparesis (5/39), quadriparesis (22/39), paresthesia (28/39), and facial palsy (23/39), and symptoms of dysautonomia also were observed during hospitalizations (3/39). The average time from vaccination to symptom onset was 11.3 days. A total of 34 case-patients received lumbar puncture; 30 had manifestations of albuminocytologic dissociation in the cerebrospinal fluid.

On the basis of the clinical diagnostic classification of GBS, we found that most case-patients had the classic form (22/39), followed by bilateral facial palsy with paresthesia (12/39), the paraparetic form (4/39), and GBS–Miller Fisher syndrome overlap variant (1/39). We defined all classic and paraparetic forms of GBS (26/26) as level 1 or 2 on the basis of the Brighton criteria (*5*). We identified the GBS subtype in 33/39 cases by electrophysiological examination; most reported case-patients had a diagnosis of acute inflammatory demyelinating polyneuropathy (23/33), followed by acute motor and sensory axonal neuropathy (4/33) and acute motor axonal neuropathy (3/33). For GBS management, 33 case-patients received intravenous immunoglobulin and 2 received plasmapheresis. One case-patient died; 9 case-patients required mechanical ventilation during hospitalization. The scores on the GBS disability scale (*5*) were only available for 30 cases; 12 scored ≥4 (i.e., indicating bedridden or chair-bound status) during follow-up or after discharge.

Similar to previous reviews on GBS associated with COVID-19, we found that both COVID-19 and COVID-19 vaccination mostly cause the classic form of GBS (under the clinical diagnosis classification) and the acute inflammatory demyelinating polyneuropathy subtype (based on electrodiagnostic features) within 2 weeks of infection or vaccination (*6*–*8*). However, the bilateral facial palsy with paresthesia variant and initial onset symptoms of facial diplegia were more frequently found in GBS case-patients after COVID-19 vaccination.

Case series and reports can indicate safety issues and outline clinical features of diseases, but they cannot establish robust causal relationships between COVID-19 vaccination and GBS. Despite the benefits (e.g., increase in the number of persons not susceptible to infection and decrease in severe outcomes after infection) of COVID-19 vaccination far outweighing the potentially severe adverse events after infection (*9*), our findings highlight the need for vigilance in patients with neurologic symptoms after COVID-19 vaccination and for postvaccination surveillance programs to assess causality of GBS.

Acknowledgments

We thank Cheng-Yang Hsieh and Wen-Mei Cheng for their insightful opinions on this study.

About the Author

Dr. Shao is a clinical pharmacist at Keelung Chang Gung Memorial Hospital. His research interests include the use of systematic review and meta-analysis to summarize current best evidence on clinical topics, specifically in regard to complications in COVID-19 patients.

References

1. Shahrizaila N, Lehmann HC, Kuwabara S. Guillain-Barré syndrome. Lancet. 2021;397:1214–28. https://doi.org/10.1016/S0140-6736(21)00517-1
2. Shao SC, Chan YY, Kao Yang YH, Lin SJ, Hung MJ, Chien RN, et al. The Chang Gung Research Database—a multi-institutional electronic medical records database for real-world epidemiological studies in Taiwan. Pharmacoepidemiol Drug Saf. 2019;28:593–600. https://doi.org/10.1002/pds.4713
3. Uncini A, Vallat JM, Jacobs BC. Guillain-Barré syndrome in

SARS-CoV-2 infection: an instant systematic review of the first six months of pandemic. J Neurol Neurosurg Psychiatry. 2020;91:1105–10. https://doi.org/10.1136/jnnp-2020-324491
4. Leonhard SE, Mandarakas MR, Gondim FAA, Bateman K, Ferreira MLB, Cornblath DR, et al. Diagnosis and management of Guillain-Barré syndrome in ten steps. Nat Rev Neurol. 2019;15:671–83. https://doi.org/10.1038/s41582-019-0250-9
5. Fokke C, van den Berg B, Drenthen J, Walgaard C, van Doorn PA, Jacobs BC. Diagnosis of Guillain-Barré syndrome and validation of Brighton criteria. Brain. 2014;137:33–43. https://doi.org/10.1093/brain/awt285
6. Koike H, Chiba A, Katsuno M. Emerging infection, vaccination, and Guillain-Barré syndrome: a review. Neurol Ther. 2021. https://doi.org/10.1007/s40120-021-00261-4
7. Uncini A, Vallat JM, Jacobs BC. Guillain-Barré syndrome in SARS-CoV-2 infection: an instant systematic review of the first six months of pandemic. J Neurol Neurosurg Psychiatry. 2020;91:1105–10. https://doi.org/10.1136/jnnp-2020-324491
8. Abu-Rumeileh S, Abdelhak A, Foschi M, Tumani H, Otto M. Guillain-Barré syndrome spectrum associated with COVID-19: an up-to-date systematic review of 73 cases. J Neurol. 2021;268:1133–70. https://doi.org/10.1007/s00415-020-10124-x
9. Goodman JL, Grabenstein JD, Braun MM. Answering key questions about COVID-19 vaccines. JAMA. 2020;324:2027–8. https://doi.org/10.1001/jama.2020.20590

Address for correspondence to: Shu-Chen Liao, Department of Emergency Medicine, Keelung Chang Gung Memorial Hospital, 222 Maijin Rd, Keelung, Taiwan; email: ermdsusan@gmail.com

Limited Protection of Inactivated SARS-CoV-2 Vaccine against Wild-Type Strain and Variants of Concern

Taweewun Hunsawong, Stefan Fernandez, Rome Buathong, Naretrit Khadthasrima, Kamonthip Rungrojchareonkit, Jindarat Lohachanakul, Rungarun Suthangkornkul, Kedsara Tayong, Angkana T. Huang, Chonticha Klungthong, Piyawan Chinnawirotpisan, Yongyuth Poolpanichupatam, Anthony R. Jones, Eric D. Lombardini, Supaporn Wacharapluesadee, Opass Putcharoen

Author affiliations: Armed Forces Research Institute of Medical Sciences, Bangkok, Thailand (T. Hunsawong, S. Fernandez, K. Rungrojchareonkit, J. Lohachanakul, R. Suthangkornkul, K. Tayong, A.T. Huang, C. Klungthong, P. Chinnawirotpisan, Y. Poolpanichupatam, A.R. Jones, E.D. Lombardini); Ministry of Public Health, Nonthaburi, Thailand (R. Buathong); Ministry of Public Health, Samut Sakhon Province, Samut Sakhon, Thailand (N. Khadthasrima); Thai Red Cross Emerging Infectious Diseases Clinical Center, Bangkok (S. Wacharapluesadee);, Chulalongkorn University Faculty of Medicine, Bangkok (O. Putcharoen)

DOI: https://doi.org/10.3201/eid2712.211772

In vitro determination of severe acute respiratory syndrome coronavirus 2 neutralizing antibodies induced in serum samples from recipients of the CoronaVac vaccine showed a short protection period against the original virus strain and limited protection against variants of concern. These data provide support for vaccine boosters, especially variants of concern circulate.

Circulation of novel severe acute respiratory syndrome coronavirus 2 (SARS-CoV-2) variants capable of evading vaccine-derived protection is challenging the efficacy of coronavirus disease (COVID-19) vaccines (*1*). The inactivated SARS-CoV-2 vaccine CoronaVac (Sinovac Biotech, http://www.sinovac.com), 1 of 2 COVID-19 vaccines licensed in Thailand, has been widely administered to health care workers. Clinical studies show CoronaVac efficacy against symptomatic COVID-19 ranging from 51% (Brazil) to 65.9% (Chile) and 100% against severe illness and illness requiring hospitalization (*2*,*3*). However, data on CoronaVac efficacy against variants of concern are very limited. Our study was approved by the Research Ethics Review Committee, Faculty of Medicine, Chulalongkorn University (Bangkok, Thailand) and recorded in the Thai Clinical Trial Registry (TCTR20210325003). Investigators adhered to U.S. Department of Defense AR 70–25 policies for protection of human subjects.

For this study, we enrolled 207 health care workers in Thailand who were fully vaccinated with 2 doses of CoronaVac (0.5 mL/dose, 2–4 wk between doses); all had received their first dose during February 22–March 12, 2021. Median age was 39 (interquartile range 30–51) years of age; 67 (49.6%) were men. Among study participants, 58 (28%) provided blood samples only at baseline (when the first dose was administered), 93 (44.0%) both at baseline and 2–3 weeks after the second dose, and 56 (27.0%) at baseline and at 2–3 weeks and 10–12 weeks after the second dose. Using an in vitro system (Appendix, https://wwwnc.cdc.gov/EID/article/27/12/21-1772-App1.pdf), we evaluated the ability of the serum of CoronaVac

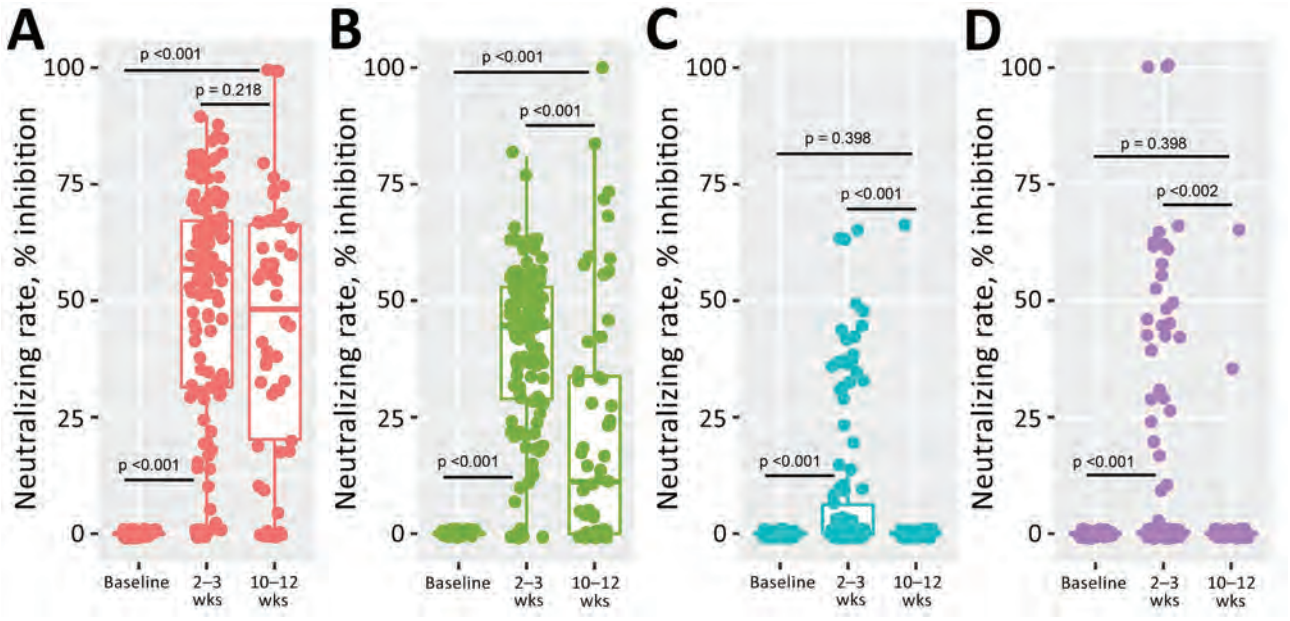

Figure. Results of in vitro testing by surrogate virus neutralization test ELISA and microneutralization assay of CoronaVac-induced neutralizing Wild-type strain and Alpha-, Beta-, and Delta-variant SARS-CoV-2 antibodies (n = 207). Overall vaccine-induced neutralizing antibodies shown at baseline, 2–3 weeks, and 10–12 weeks after second dose. Differences in mean inhibition rate were compared based on blood collection times. p value <0.05 indicates statistical significance.

recipients to neutralize SARS-CoV-2. We measured circulating serum neutralizing antibodies to the original SARS-CoV-2 wild-type strain by using a cPass receptor binding domain antigen-based surrogate virus neutralization test (sVNT) ELISA (GeneScript, https://www.genscript.com) and using a microneutralization assay (MNA) for SARS-CoV-2 wild-type strain and Alpha, Beta, and Delta neutralizing antibodies. Seroconversion rates for CoronaVac-vaccinated participants, determined by sVNT ELISA using 30% inhibition as cutoff, were 85.2% (78.2% mean inhibition level) at 2–3 weeks and 35% (25.4% mean inhibition level) at 10–12 weeks. The MNA seropositivity cutoff was set at ≥50%.

At 2–3 weeks after the second dose, 61.1% (91/149) of participants were seropositive against the wild-type strain, 35.6% (53/149) against Alpha variant, 3.4% (5/149) against Beta, and 8.7% (13/149) against Delta (Figure). Mean neutralizing rate at 2–3 weeks was 49.3% (95% CI 44.9%–53.6%) against the wild-type strain, 40.9% (95% CI 37.8%–43.9%) against Alpha variant, 9.0% (95% CI 6.1%–11.8%) against Beta, and 10.8% (95% CI 7.1%–14.5%) against Delta. At 10–12 weeks after the second dose, the proportion of seropositive participants fell to 50% (28/56) against Wild-type strain and was significantly reduced (p<0.001) to 17.9% (10/56) against Alpha variant, 1.8% (1/56) against Beta, and 1.8% (1/56) against Delta. Mean neutralizing rates at 10–12 weeks were 48.0% (95% CI 39.9%–56.1%) against the wild-type strain, 21.8% (95% CI 37.8%–43.9%) against Alpha variant, 1.2% (95% CI 3.5%–8.8%) against Beta, and 1.0% (95% CI 2.9%–7.5%) against Delta.

Comparing sVNT ELISA results between the 2 time points, Wild-type strain antibodies appear to have a half-life of 83.4 days (95% CI 76.6–90.3 days). However, when the MNA was used, neutralizing antibodies waned in a time- and variant-dependent manner. The half-life of neutralizing antibodies was as low as 47.2 days (95% CI 37.5–56.9 days) for the wild-type strain, 38.6 days (95%

Table. Results of in vitro testing by surrogate virus neutralization test ELISA and microneutralization assay of CoronaVac-induced neutralizing wild-type strain and Alpha, Beta, and Delta variants of severe acute respiratory syndrome coronavirus 2*

Neutralization test detection method	Slope coefficient (95% CI)	Half-time coefficient, d (95% CI)
Surrogate virus neutralization test ELISA	–0.645 (–0.751 to –0.538)	83.42 (76.55–90.29)
Microneutralization assay		
Wild-type	0.008 (–0.141 to 0.159)	47.17 (37.48–56.86)
Alpha	–0.187 (–0.302 to –0.072)	38.57 (31.16–45.99)
Beta	–0.063 (–0.121 to –0.006)	6.88 (3.20–10.57)
Delta	–0.125 (–0.211 to –0.040)	12.27 (6.78–17.77)

*CoronaVac vaccine by Sinovac Biotech (http://www.sinovac.com).

CI 31.2–45.9 days) for Alpha variant, 6.9 days (95% CI 3.2–10.6 days) for Beta, and 12.3 days (95% CI 6.8–17.8 days) for Delta (Table). These data indicate the possibility that SARS-CoV-2 variants are able to escape humoral induced by wild-type prototype inactivated vaccines, which is consistent with results of other recent studies (4,5). Our findings support administering vaccine boosters, especially where these variants circulate.

Acknowledgments

Our sincere thanks to all participants in this study.

We also thank Bassam Hallis, Alex Sigal, and Tulio de Oliveira of BEI resources of the National Institute of Allergy and Infectious Diseases, National Institutes of Health, who provided SARS-CoV-2 wild-type strain virus, and Alpha and Beta variants. Research was supported by NIH/NIAID award no. U01AI151797 and National Research Council of Thailand award no. N35A640037.

Research reported in this publication was supported by the National Institute of Allergy and Infectious Diseases of the National Institutes of Health (award no. U01AI151797). The content is solely the responsibility of the authors and does not necessarily represent the official views of the National Institutes of Health. This research was also partially funded by National Research Council of Thailand under Award Number N35A640037.

Material has been reviewed by the Walter Reed Army Institute of Research. There is no objection to its presentation or publication. The opinions or assertions contained herein are the private views of the authors, and are not to be construed as official, or as reflecting true views of the Department of the Army or the Department of Defense. The investigators have adhered to the policies for protection of human subjects as prescribed in AR 70–25.

About the Author

Dr. Hunsawong is a research scientist in the Department of Virology of the US Army Medical Directorate of the Armed Forces Research Institute of Medical Sciences in Bangkok, Thailand. Her research interests include host-immune response to arbovirus and respiratory virus infections, vaccine development and anti-viral drug testing.

References

1. Planas D, Veyer D, Baidaliuk A, Staropoli I, Guivel-Benhassine F, Rajah MM, et al. Reduced sensitivity of SARS-CoV-2 variant Delta to antibody neutralization. Nature. 2021;596:276–80. https://doi.org/10.1038/s41586-021-03777-9
2. Palacios R, Patiño EG, de Oliveira Piorelli R, Conde MTRP, Batista AP, Zeng G, et al. Double-blind, randomized, placebo-controlled phase III clinical trial to evaluate the efficacy and safety of treating healthcare professionals with the adsorbed COVID-19 (inactivated) vaccine manufactured by Sinovac—PROFISCOV: a structured summary of a study protocol for a randomised controlled trial. Trials. 2020;21:853. https://doi.org/10.1186/s13063-020-04775-4
3. Jara A, Undurraga EA, González C, Paredes F, Fontecilla T, Jara G, et al. Effectiveness of an inactivated SARS-CoV-2 vaccine in Chile. N Engl J Med. 2021;385:875–84. https://doi.org/10.1056/NEJMoa2107715
4. Wang GL, Wang ZY, Duan LJ, Meng QC, Jiang MD, Cao J, et al. Susceptibility of circulating SARS-CoV-2 variants to neutralization. N Engl J Med. 2021;384:2354–6. https://doi.org/10.1056/NEJMc2103022. PMID: 33822491
5. Al Kaabi N, Zhang Y, Xia S, Yang Y, Al Qahtani MM, Abdulrazzaq N, et al. Effect of 2 inactivated SARS-CoV-2 vaccines on symptomatic COVID-19 infection in adults: a randomized clinical trial. JAMA. 2021;326:35–45. https://doi.org/10.1001/jama.2021.8565

Address for correspondence: Opass Putcharoen, Emerging Infectious Diseases Clinical Center, Thai Red Cross, Faculty of Medicine, Chulalongkorn University, Bangkok, Thailand; email: opass.p@chula.ac.th

Breakthrough Infections of E484K-Harboring SARS-CoV-2 Delta Variant, Lombardy, Italy

Andreina Baj, Federica Novazzi, Renee Pasciuta, Angelo Genoni, Francesca Drago Ferrante, Marilena Valli, Michele Partenope, Rosalia Tripiciano, Andrea Ciserchia, Giuseppe Catanoso, Daniele Focosi, Fabrizio Maggi

Author affiliations: ASST SetteLaghi, Varese, Italy (A. Baj, F. Novazzi, R. Pasciuta, F. Drago Ferrante, F. Maggi); University of Insubria, Varese (A. Baj, A. Genoni, F. Maggi); St. Anna Hospital, Como, Italy (M. Valli, M. Partenope); ATS Insubria, Varese (R. Tripiciano, A. Ciserchia, G. Catanoso); Pisa University Hospital, Pisa, Italy (D. Focosi)

DOI: https://doi.org/10.3201/eid2712.211792

The Delta variant of concern of severe acute respiratory syndrome coronavirus 2 is dominant worldwide. We report a case cluster caused by Delta sublineage B.1.617.2 harboring the mutation E484K in Italy during July 11–July 29, 2021. This mutation appears to affect immune response and vaccine efficacy; monitoring its appearance is urgent.

Since the beginning of 2021, a severe acute respiratory syndrome coronavirus 2 (SARS-CoV-2) variant originally described in India has become the predominant circulating variant of the coronavirus disease pandemic. This variant of concern (VOC) was renamed Delta by the World Health Organization and consists to date of 5 different sublineages (B.1.617.2, AY.1, AY.2, AY.3, and AY.3.1, according to PANGOLIN phylogeny) that share T478K and L452R as the main mutations of concern (MOCs) within the spike protein. B.1.617.2 (also known as VUI-21APR-02) is by far the most represented Delta sublineage. None of the 5 sublineages are to date characterized by the occurrence of the other MOC E484K, which causes resistance to monoclonal antibodies and reduced vaccine efficacy. However, given the widespread convergent evolution of the spike protein observed across clades, the occurrence of MOC E484K and its widespread circulation is largely expected. A clade simultaneously harboring all such MOCs is likely to be of extreme concern because of theoretical increased immune escape. We report a cluster of B.1.617.2 and E484K occurring in Lombardy, Italy. All cases were first tested by real-time reverse transcription PCR and, if positive, sequenced as previously reported (*1*).

On July 11, 2021, a 41-year-old man from a small village in northern Lombardy (vaccinated with BNT162b2 [Pfizer-BioNTech, https://www.pfizer.com] on June 12 and July 12) began experiencing cough, fever, and malaise; a nasopharyngeal swab specimen tested positive on July 14 by the SARS-CoV-2 Variants Elite MGB Kit (EliTech Group, https://www.elitechgroup.com); cycle threshold (C_t) was 21 for open reading frame (ORF) 1ab gene and 21 for the nucleocapsid (N) gene. He fully recovered without need for hospital admission; whole-genome sequencing confirmed B.1.617.2 that harbored E484K. His 80-year-old mother (vaccinated with mRNA-1273 [Moderna, https://www.modernatx.com] on April 9 and May 7) experienced fatigue, headache, myalgia, and dyspnea beginning July 17 and tested positive on July 24 (C_t 22 for ORF1ab gene and C_t 21 for N gene). She likely further infected (while playing cards) a 77-year-old man (vaccinated with BNT162b2 on April 26 and May 17) who began experiencing fever July 21 and tested positive on July 23 (C_t 20 for ORF1ab gene and C_t 19 for N gene) and an 83-year-old woman (vaccinated with BNT162b2 on April 3 and April 24) who experienced fever, fatigue, ageusia, and anosmia beginning July 21 and tested positive July 24 (C_t 18 for both genes). None required hospital admission. An unrelated patient from the same village, an 81-year-old woman (vaccinated with mRNA-1273 on May 7 and June 9), experienced dyspnea, fever, myalgia, and fatigue beginning July 24. On July 29, she tested positive for SARS-CoV-2 RNA (C_t 23 for ORF1ab gene and C_t 21 for N gene), and she was admitted to the hospital. All sequences obtained in this study have been deposited into GISAID (https://www.gisaid.org; accession nos. EPI_ISL_3462078, EPI_ISL_3462074, EPI_ISL_3462072, EPI_ISL_346208).

E484K is the hallmark MOC of VOCs Beta and Gamma, in addition to having been reported in a minor sublineage of VOC Alpha, in variants of interest Eta and Iota, and at frequencies >50% in 38 more strains. E484K causes resistance to many class 2 RBD-directed antibodies (*2*), including bamlanivimab (*3*). The most potent mRNA vaccine–elicited monoclonal antibodies were ≥10-fold less effective against pseudotyped viruses carrying the E484K mutation (Z. Wang et al., unpub. data, https://www.biorxiv.org/content/10.1101/2021.01.15.426911v2). As of August 12, 2021, GISAID reported E484K in 52 of 408,781 B.1.617.2 sequences, 2 of 549 AY.1 sequences, and 32 of 19,996 AY.3 (Delta) sequences; none of these reports were in Italy. E484K has been additionally reported in 1 of 6,011 B.1.617.1 (Kappa variant) sequences (*4*).

Nasopharyngeal swab specimens positive for the Delta variant have ≈4-fold higher viral loads than non-VOC or Alpha variants (C. von Wintersdorff et al., unpub. data, https://www.researchsquare.com/article/rs-762916/v1) and a shorter incubation time of 4 days (B. Li et al., unpub. data, https://www.medrxiv.org/content/10.1101/2021.07.07.21260122v1). It is resistant to REGN10933 (T. Tada et al., unpub. data, https://www.biorxiv.org/content/10.1101/2021.07.19.452771v3) and bamlanivimab (M. Hoffman et al., unpub. data, https://www.biorxiv.org/content/10.1101/2021.05.04.442663v1; P. Arora et al., unpub. data, https://www.biorxiv.org/content/10.1101/2021.06.23.449568v1), whereas neutralization by antibodies derived from cyclic citrullinated peptide, BNT162b2, mRNA-1273, and Ad26.COV2.S are reduced by 3–5-fold (T. Tada et al., unpub. data).

E484K mutation represents a critical evolutionary event that leads to immune escape, although its consequences on viral fitness are unclear. Surveillance by genome sequencing should be maintained (T. Farinholt et al., unpub. data, https://www.medrxiv.org/content/10.1101/2021.06.28.21258780v4).

About the Author

Dr. Baj is a medical research scientist at University of Insubria, Varese, Italy. Her research interests include persistent and emerging viral infections.

References

1. Baj A, Novazzi F, Ferrante FD, Genoni A, Cassani G, Prestia M, et al. Introduction of SARS-COV-2 C.37 (WHO VOI lambda) from Peru to Italy. J Med Virol. 2021 Jul 27 [Epub ahead of print]. https://doi.org/10.1002/jmv.27235
2. Greaney AJ, Starr TN, Barnes CO, Weisblum Y, Schmidt F, Caskey M, et al. Mapping mutations to the SARS-CoV-2 RBD that escape binding by different classes of antibodies. Nat Commun. 2021;12:4196. https://doi.org/10.1038/s41467-021-24435-8
3. Starr TN, Greaney AJ, Dingens AS, Bloom JD. Complete map of SARS-CoV-2 RBD mutations that escape the monoclonal antibody LY-CoV555 and its cocktail with LY-CoV016. Cell Rep Med. 2021;2:100255. https://doi.org/10.1016/j.xcrm.2021.100255
4. Latif AA, Mullen JL, Alkuzweny M, Tsueng G, Cano M, Haag E, et al. S:E484K mutation report. 2021 [cited 2021 Aug 12]. https://outbreak.info/situationreports?pango&muts=S%3AE484K

Address for correspondence: Dr.ssa Andreina Baj, Dipartimento di Medicina e Chirurgia, Universita' degli Studi dell'Insubria, Laboratorio di Microbiologia Medica, Viale Borri 57, Varese, Italy; email: andreina.baj@uninsubria.it

Subclinical *Burkholderia pseudomallei* Infection Associated with Travel to the British Virgin Islands

Courtney M. Dewart, Francisco A. Almeida, Christine Koval, Scott Nowicki, Jay E. Gee, Mindy Glass Elrod, Christopher A. Gulvik, Johanna S. Salzer, Sietske de Fijter, Lindy Liu

Author affiliations: Centers for Disease Control and Prevention, Atlanta, Georgia, USA (C.M. Dewart, J.E. Gee, M.G. Elrod, C.A. Gulvik, J.S. Salzer, L. Liu); Ohio Department of Health, Columbus, Ohio, USA (C.M. Dewart, S. Nowicki, S. de Fijter); Cleveland Clinic, Cleveland, Ohio, USA (F.A. Almeida, C. Koval)

DOI: https://doi.org/10.3201/eid2712.211816

Phylogenetic analysis of a clinical isolate associated with subclinical *Burkholderia pseudomallei* infection revealed probable exposure in the British Virgin Islands, where reported infections are limited. Clinicians should consider this geographic distribution when evaluating possible infection among persons with compatible travel history.

Burkholderia pseudomallei is a gram-negative aerobic bacillus and the etiologic agent of melioidosis (*1*). The clinical signs and symptoms of melioidosis are varied, and subclinical infection can occur with or without latent clinical manifestation (*1*–*3*). Infection with *B. pseudomallei* typically is associated with environmental exposure through inhalation or direct contact with contaminated soil or water (*1*,*3*). The incubation period can vary from a few days in acute infection to months or years in latent infection, making identification of the exposure source challenging (*1*). Most melioidosis cases are reported in northern Australia and Southeast Asia; however, the known and predicted geographic distribution of *B. pseudomallei* continues to be characterized (*1*,*3*,*4*). We report identification of subclinical *B. pseudomallei* infection by endobronchial ultrasound–transbronchial needle aspiration. We show that phylogenetic analysis of the clinical isolate combined with patient interview were integral to determining a probable location of exposure because the patient traveled to multiple *B. pseudomallei*–endemic regions. This project was reviewed by the Centers for Disease Control and Prevention (CDC) and determined to be nonresearch.

In 2018, a female Ohio resident >65 years of age underwent tooth and torus mandibularis removal after several months of recurrent maxillary molar tooth pain and infections. An oral ulceration was noted, and a biopsy proved it was a squamous cell carcinoma. During her evaluation to undergo maxillectomy and hard palate resection, combined positron emission tomography–computed tomography imaging demonstrated a fluorodeoxyglucose-avid precarinal station 4R lymph node and fluorodeoxyglucose avidity in the right hard palate, consistent with her known malignancy. The patient reported some discomfort at the right upper palate and a sore throat but otherwise had a preserved appetite and weight and denied any chest pain, dyspnea, hemoptysis, fever, chills, or night sweats. She underwent an endobronchial ultrasound–transbronchial needle aspiration, at which time the 4R node was sampled a dozen times. Because a rapid onsite cytology examination failed to demonstrate any malignant cells, additional samples were obtained for routine gram, fungal, and acid-fast bacilli stains and cultures. Scant colonies of *B. pseudomallei* grew on culture media several days after the bronchoscopy, and preliminary identification was made by using VITEK 2 (bioMérieux, https://www.biomerieux.com).

Results from automated systems in clinical laboratories can misidentify *B. pseudomallei* as a variety of

other bacteria and are not confirmatory for this bacterium. Even 16S rRNA gene sequencing can be inadequate depending on the segment queried (*1*). The Ohio Department of Health Laboratory confirmed *B. pseudomallei* by using CDC's Laboratory Response Network algorithm (https://emergency.cdc.gov/lrn/index.asp).

Because the patient could not tolerate optimal eradication therapy (*5*), she received intensive therapy with intravenous meropenem for 14 days, then completed a 3-month course of oral doxycycline. Computed tomography images shortly after completing the treatment course showed no evidence of active infection.

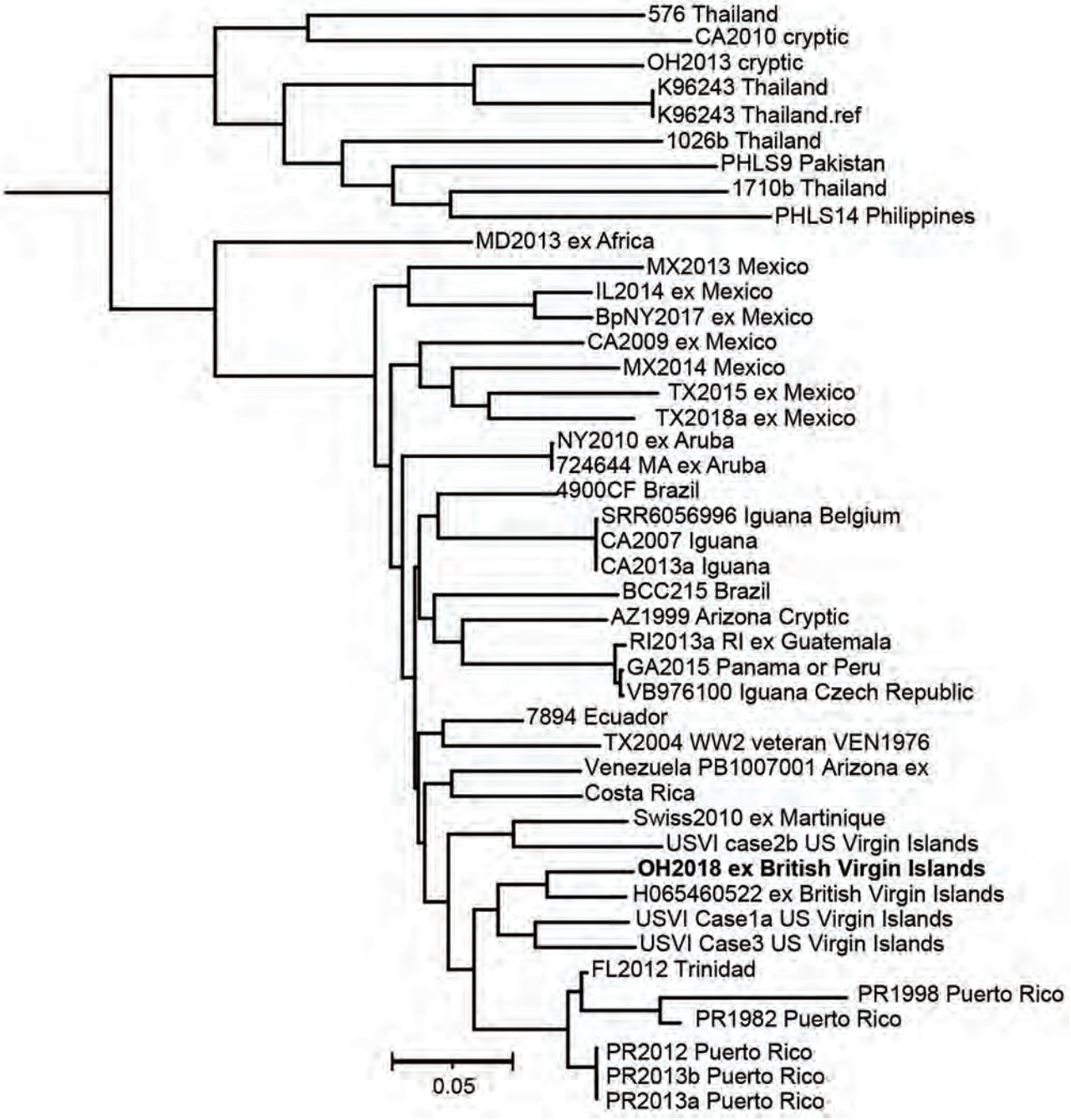

Figure. Dendrogram of *Burkholderia pseudomallei* isolated in a patient who traveled to the British Virgin Islands, 2018. Bold text indicates patient isolate; reference genomes predominantly are from the Western Hemisphere. The tree was generated by using MEGA 7.0 software (http://www.megasoftware.net). Single-nucleotide polymorphism analysis was performed by using Parsnp in the Harvest 1.3 package (https://github.com/marbl/harvest). Scale bar indicates nucleotide substitutions per site.

During interviews with public health officials, the patient reported traveling to the British Virgin Islands (BVI) twice a year for ≈3 weeks at a time and had visited 2–3 months before the identification of lymphadenitis. She also reported trips of <1 month duration to China and Singapore, where *B. pseudomallei* is endemic, within the previous 10 years (*1*,*3*). No known exposures to *B. pseudomallei* were reported. However, she recalled landscaping activities in BVI that resulted in noticeable dust in her residence, but she did not know on which BVI visit this exposure to aerosolized soil occurred.

CDC performed whole-genome sequencing of the patient's *B. pseudomallei* isolate, OH2018, for comparison to reference genomes that have well-established geographic origins. The isolate's genome sequence is available at the National Center for Biotechnology Information (https://www.ncbi.nlm.nih.gov) under Bioproject accession no. PRJNA575632. Multilocus sequence typing classified the isolate as sequence type 92, which previously has been observed in several isolates originating from the Western Hemisphere (*6*,*7*). Phylogenetic single-nucleotide polymorphism analysis demonstrated OH2018 groups with reference genomes from the Caribbean, especially the US Virgin Islands and BVI (Figure).

Whole-genome sequencing of the isolate was essential to determining potential exposure risk because the patient traveled to multiple regions where *B. pseudomallei* is endemic. The patient likely was exposed to *B. pseudomallei* in BVI 2–3 months before infection was identified, as ascertained through molecular epidemiology and supported by her report of travel and exposure to aerosolized soil in this location. The case provides additional evidence that *B. pseudomallei* is endemic to the Caribbean and, more specifically, BVI, where reported infections are limited. Only 1 other infection associated with BVI has been reported in the literature (*8*), and no environmental isolates have been reported. To support prompt identification and treatment for melioidosis, clinicians and public health officials should be aware of this geographic distribution when considering possible infection among persons with compatible travel history.

Acknowledgments

We thank Hillary Van Heule for providing information about patient isolates and the local health department and public health officials who assisted in the epidemiologic investigation.

About the Author

Dr. Dewart is a registered nurse and infectious disease epidemiologist. She served as a CDC Epidemic Intelligence Service officer during 2019–2021 and is currently a field assignee to the Ohio Department of Health, Columbus, Ohio, USA, through CDC's Center for Preparedness and Response. Her primary research interests include healthcare-associated infections and antimicrobial resistance.

References

1. Wiersinga WJ, Virk HS, Torres AG, Currie BJ, Peacock SJ, Dance DAB, et al. Melioidosis. Nat Rev Dis Primers. 2018;4:17107. https://doi.org/10.1038/nrdp.2017.107
2. Chakravorty A, Heath CH. Melioidosis: an updated review. Aust J Gen Pract. 2019;48:327–32. https://doi.org/10.31128/AJGP-04-18-4558
3. Currie BJ. Melioidosis: evolving concepts in epidemiology, pathogenesis, and treatment. Semin Respir Crit Care Med. 2015;36:111–25. https://doi.org/10.1055/s-0034-1398389
4. Limmathurotsakul D, Golding N, Dance DA, Messina JP, Pigott DM, Moyes CL, et al. Predicted global distribution of *Burkholderia pseudomallei* and burden of melioidosis. Nat Microbiol. 2016;1:15008. PubMed https://doi.org/10.1038/nmicrobiol.2015.8
5. Lipsitz R, Garges S, Aurigemma R, Baccam P, Blaney DD, Cheng AC, et al. Workshop on treatment of and postexposure prophylaxis for *Burkholderia pseudomallei* and *B. mallei* infection, 2010. Emerg Infect Dis. 2012;18:e2. https://doi.org/10.3201/eid1812.120638
6. Gee JE, Gulvik CA, Elrod MG, Batra D, Rowe LA, Sheth M, et al. Phylogeography of *Burkholderia psuedomallei* isolates, Western Hemisphere. Emerg Infect Dis. 2017;23:1133–8. https://doi.org/10.3201/eid2307.161978
7. Gee JE, Gulvik CA, Castelo-Branco DSCM, Sidrim JJC, Rocha MFG, Cordeiro RA, et al. Genomic diversity of *Burkholderia pseudomallei* in Ceara, Brazil. MSphere. 2021;6:e01259-20. https://doi.org/10.1128/mSphere.01259-20
8. Corral DM, Coates AL, Yau YC, Tellier R, Glass M, Jones SM, et al. *Burkholderia pseudomallei* infection in a cystic fibrosis patient from the Caribbean: a case report. Can Respir J. 2008;15:237–9. https://doi.org/10.1155/2008/290412

Address for correspondence: Courtney Dewart, Ohio Department of Health, 35 E Chestnut St, Columbus, Ohio 43215, USA; email: Courtney.Dewart@odh.ohio.gov

SARS-CoV-2 Sequence Analysis during COVID-19 Case Surge, Liberia, 2021

Bode Shobayo,[1] Mitali Mishra,[1] Stephen Sameroff, Alexandra Petrosov, James Ng, Alper Gokden, Jane MaCauley, Komal Jain, Courtney Renken, James Tanu Duworko, Moses Badio, Wilhemina Jallah, Lisa Hensley, Thomas Briese, W. Ian Lipkin, Nischay Mishra

Author affiliations: National Public Health Institute of Liberia, Monrovia, Liberia (B. Shobayo, J. MaCauley); Partnership for Research on Infectious Diseases in Liberia, Monrovia (B. Shobayo, C. Renken, J.T. Duworko, M. Badio, L. Hensley); Columbia University, New York, New York, USA (M. Mishra, S. Sameroff, A. Petrosov, J. Ng, A. Gokden, K. Jain, T. Briese, W.I. Lipkin, N. Mishra); National Institutes of Health, Bethesda, Maryland, USA (C. Renken, L. Hensley); Ministry of Health, Monrovia (W. Jallah)

DOI: https://doi.org/10.3201/eid2712.211818

In June 2021, severe acute respiratory syndrome coronavirus 2 (SARS-CoV-2) cases surged in Liberia. SARS-CoV-2 sequences from patients hospitalized during March–July 2021 revealed the Delta variant was in Liberia in early March and was dominant in June, irrespective of geography. Mutations and deletions suggest multiple SARS-CoV-2 Delta variant introductions.

Before May 2021, Liberia reported <10 coronavirus disease (COVID-19) cases per day among its population of ≈5 million (*1*). Thereafter, case numbers, hospitalizations, and deaths rapidly increased and peaked to >200 cases and 10–15 deaths per day in mid-July 2021 (Appendix Figure 1, https://wwwnc.cdc.gov/EID/article/27/12/21-1818-App1.pdf). To determine whether the rapid case surge was associated with the introduction of severe acute respiratory syndrome coronavirus 2 (SARS-CoV-2) variants of concern or newly emerging variants, we collected nasopharyngeal swab samples from 267 hospitalized patients countrywide during March–July 2021 for high-throughput sequencing.

We collected samples in viral transport media from Bomi, Bong, Grand Cape Mount, Lofa, Margibi, Maryland, Montserrado, and Nimba Counties (Appendix Figure 2). We noted sample collection date and site and sex and median age of patients from whom samples were obtained (Table; Appendix Table). We used Buffer AVL (QIAGEN, https://www.qiagen.com) lysis buffer to extract total nucleic acid and performed PCR by using the Triplex-CII-SARS-Cov-2 rRT PCR assay (*2*). We conducted further high-throughput sequencing on 89/267 (33.3%) samples that had cycle threshold values <33 (Appendix Table).

To prepare libraries, we used the Kapa Hyperplus Kit (Roche, https://www.roche.com) on first strand cDNA synthesized from 89 RNA samples (*3*), then we enriched for SARS-CoV-2 by using myBaits Custom RNA-Seq Kit (Daicel Arbor Biosciences, https://arborbiosci.com). We sequenced captured libraries on Nextseq 2000 or Nextseq 550 (Illumina, https://www.illumina.com), which yielded 5–8 million 220-bp reads per sample. We mapped reads to a SARS-CoV-2 reference sequence (GenBank accession no. NC_045512) to determine variants (Table; Appendix Table).

Of the 89 RNA samples, 77 (86.5%) yielded complete coding sequences with a minimum depth of ≈15× (GISAID accession nos. EPI_ISL_3547663–705, EPI_ISL_3560291, and EPI_ISL_4232122–52). Using high-throughput sequencing data, we generated consensus fasta sequences of 77 SARS-CoV-2 genomic sequences and further analyzed sequences by using Geneious R10 (https://www.geneious.com), NextStrain (*4*), and GISAID (*5*).

Among 77 genomes recovered, 4 (5.2%) were Alpha variant (B.1.1.7); 6 (7.8%) were Beta variant (B.1.351); 1 (1.3%) was Iota variant (B.1.526); 6 (7.8%) were Eta variant (B.1.525); and 56 (72.7%) were Delta variant (B.1.617.2) viruses (Table). We identified Delta variant viruses in samples collected in early March and in April and May 2021, from Bong County. Delta variant viruses were co-circulating with Alpha, Beta, Eta, Iota, and other 20B variant viruses in Liberia. All 44 sequences recovered during June–July 2021 were from Delta variant viruses (Table). We used complete polyprotein coding sequences from Liberia, other representative SARS-CoV-2 sequences, and variant reference sequences to create a maximum-likelihood, nucleotide-based phylogenetic tree in MEGA X (*6*) (Figure).

Using reference sequence NC_045512 as a baseline, we found 3 Alpha variant–specific amino acid deletions (H69del, V70del, Y144del) in the surface glycoprotein of all Alpha variant genomes and 3 Beta variant–specific amino acid deletions (L241del, L242del, A243del) in the surface glycoprotein of all Beta variant genomes. All 56 Delta variant genomes had the 2 variant-specific amino acid deletions, F157del and R158del, and 8 of 9 other Delta variant–

[1]These first authors contributed equally to this article.

Table. Characteristics of 77 clinical samples collected before and during COVID-19 case surge that yielded complete SARS-CoV-2 coding genomic sequences, Liberia, 2021

Month collected	Total no. samples	Patient sex, no.	Average age, y (SD)	County	No. samples/ county	SARS-CoV-2 variant, no. of samples/county/mo					
						Delta B.1.617.2	Alpha B.1.1.7	Beta B.1.351	Eta B.1.525	Iota B.1.526	20B other
Mar	4	2M, 2F	39.25 (6.05)	Montserrado	3			1	1	1	
				Bong	1	1					
Apr	11	10M, 1F	42.54 (11.52)	Montserrado	10	4	1	3	2		
				Grand Cape Mount	1			1			
May	18	9M, 9F	40.11 (16.82)	Bong	1	1					
				Margibi	1						
				Montserrado	14	6	3	2	2		1
				Nimba	2						2
Jun	36	13M, 23F	39.22 (18.36)	Lofa	5	5					
				Margibi	1	1					
				Maryland	1	1					
				Montserrado	29	29					
Jul	8	4M, 4F	51.25 (9.71)	Margibi	1	1					
				Montserrado	5	5					
				Nimba	2	2					

*Liberia experienced a surge in COVID-19 cases during June 2021. Blank cells indicate no variants detected. COVID-19, coronavirus disease; SARS-CoV-2, severe acute respiratory syndrome coronavirus 2.

specific amino acid substitutions in the surface glycoprotein (T19R, G142D, E156G, L452R, T478K, D614G, P681R, and D950N). The A222V surface glycoprotein mutation was absent in only 2/56 Delta variant genomes, LIB-0226 and LIB-0217, collected from Monteserrado County in May 2021 (*4*). We observed another mutation in the surface glycoprotein, V367L, in 14 sequences: 1 from Bong, 2 from Margibi, 1 from Maryland, 9 from Montserrado, and 1 from Nimba. No sequences recovered from Lofa County had the V367L mutation. We noted the R724K mutation in the open reading frame 1a region of 2 sequences from Lofa, LIB-0131 and LIB-0133. LIB-0073 and LIB-0093 sequences collected from Montserrado County had 2 amino acid deletions in the open reading frame 8 region (position 120–121).

Recent surges in COVID-19 in many countries have been associated with the emergence of highly transmissible Delta variant viruses (*7*,*8*). In March 2021, the National Public Health Institute of Liberia sequenced 10 random samples from hospitalized COVID-19 patients in Monteserrado; all sequences were Alpha variant viruses (B. Shobayo, unpub. data).

A limitation of our study is the small sample sets used for analysis; nonetheless, our findings suggest that Alpha and other circulating variant viruses were replaced by Delta variant viruses countrywide in Liberia in <3 months. Mutation and phylogenetic analyses further indicate that several Delta variant strains were circulating after March 2021 and suggest multiple separate introductions.

Before June 2021, only a small percentage of the population was vaccinated in Liberia. The infections we report occurred in unvaccinated persons. The Ministry of Health, Liberia, initiated a vaccination drive in August 2021. By September, ≈130,000 persons, >2% of the population, had received a single dose of the Johnson & Johnson/Janssen vaccine (https://www.jnj.com). The COVID-19 vaccination campaign is ramping up as <30 cases/day are reported in Liberia, but the currently circulating Delta variants are a concern because they contain mutations and deletions in the surface glycoprotein that might influence vaccine efficacy (*9*). Liberia should continued surveillance for SARS-CoV-2 variants of concern to determine whether additional vaccination or public health measures are needed to curb severe disease and future case surges in the country.

Acknowledgments

We thank Pryanka Sharma and Gilbert Smith; Melvin Johnson, John Fayiah and Julie Blie and all the members of Partnership for Research on Vaccines and Infectious Diseases in Liberia; Julius Teahton, Francis Jaryan, John Dogba, Fahn Taweh, and Joseph Tahyor; and National Public Health Institute of Liberia research and lab team members for their support in collection and transport of samples.

Financial support was provided by by the Skoll Foundation for the Global Alliance for Pandemic Prevention (GAPP grant no. 20-45017), the Tong Tsung and Wei Fong Chao Foundation (grant no. GT007457), and the Chau Hoi Sheun Foundation (grant no. GT007457).

The National Institute of Allergy and Infectious Diseases, National Institutes of Health, also participated in study design, analysis and interpretation of data, writing of the report, and decision to submit the article for publication.

About the Author

Dr. Shobayo is public health and medical research scientist and deputy director at National Public Health Institute of Liberia, Monrovia, Liberia, and member of Partnership for Research on Infectious Diseases in Liberia. His research interests include survillence and investigation of emerging and re-emerging viruses and their impacts on public health.

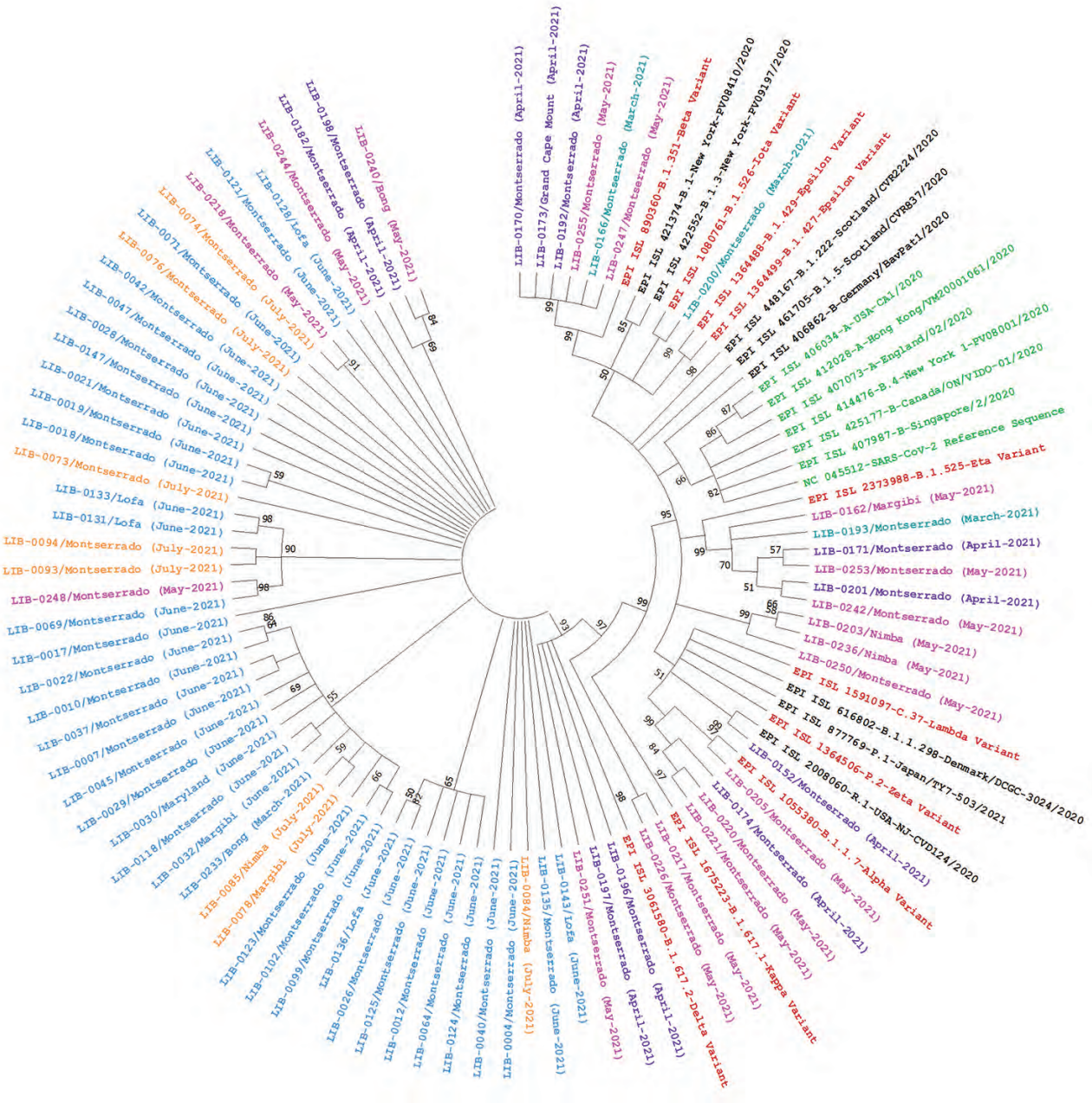

Figure. Phylogenetic analysis of 77 nasopharyngeal swab samples collected during coronavirus disease case surge, Liberia, March–July 2021, and reference sequences. We created a maximum-likelihood nucleotide phylogenetic tree of the complete polyprotein coding region by using MEGA X (https://www.megasoftware.net), with a bootstrap value of 100 and and used Tamura-Nei 93 (TN93) as a substitution model with a discrete gamma distribution (+G) for evolutionary rate; the rate variation model allowed some sites to be evolutionarily invariable (+I). Numbers along the branches are bootstrap values of 100 bootstrap resamplings. Teal indicates samples collected in March 2021; purple indicates samples collected in April 2021; pink indicates samples collected in May 2021; blue indicates samples collected in June 2021; orange indicates samples collected in July 2021; brown indicates variants of concern or variants of interest; black indicates other circulating variants; green indicates severe acute respiratory syndrome coronavirus 2 reference sequence and other early parental sequences from 2020.

References:

1. Worldometer. COVID-19 coronavirs disease data, Liberia [cited 2021 Sep 26]. https://www.worldometers.info/coronavirus/country/liberia
2. US Food and Drug Administration. Accelerated emergency use authorization (EUA) summary the Triplex CII-SARS-CoV-2 rRT-PCR test updated 9/14/2020 [cited 2021 Sep 15]. https://www.fda.gov/media/137983/download
3. Mishra N, Ng TFF, Marine RL, Jain K, Ng J, Thakkar R, et al. Antibodies to enteroviruses in cerebrospinal fluid of patients with acute flaccid myelitis. MBio. 2019;10:e01903-19. https://doi.org/10.1128/mBio.01903-19
4. GISAID. Tracking of variants [cited 2021 Sep 15]. https://www.gisaid.org/hcov19-variants
5. Next-Strain. Real-time tracking of pathogen evolution [cited 2021 Sep 15]. https://nextstrain.org
6. Kumar S, Stecher G, Li M, Knyaz C, Tamura K. MEGA X: Molecular Evolutionary Genetics Analysis across computing platforms. Mol Biol Evol. 2018;35:1547–9. https://doi.org/10.1093/molbev/msy096
7. Lopez Bernal J, Andrews N, Gower C, Gallagher E, Simmons R, Thelwall S, et al. Effectiveness of Covid-19 vaccines against the B.1.617.2 (Delta) variant. N Engl J Med. 2021;385:585–94. https://doi.org/10.1056/NEJMoa2108891
8. Alizon S, Haim-Boukobza S, Foulongne V, Verdurme L, Trombert-Paolantoni S, Lecorche E, et al. Rapid spread of the SARS-CoV-2 Delta variant in some French regions, June 2021. Euro Surveill. 2021;26.2100573. https://doi.org/10.2807/1560-7917.ES.2021.26.28.2100573
9. Creech CB, Walker SC, Samuels RJ. SARS-CoV-2 vaccines. JAMA. 2021;325:1318–20. https://doi.org/10.1001/jama.2021.3199

Address for correspondence: Nischay Mishra, Center for Infection and Immunity, Columbia University, 722 W 168th St, New York, NY 10032, USA; email: nm2641@cumc.columbia.edu

Real-Time Projections of SARS-CoV-2 B.1.1.7 Variant in a University Setting, Texas, USA

Kaitlyn E. Johnson,[1] Spencer Woody,[1] Michael Lachmann, Spencer J. Fox, Jessica Klima, Terrance S. Hines, Lauren Ancel Meyers

Author affiliations: University of Texas at Austin Department of Integrative Biology, Austin, Texas, USA (K.E. Johnson, S. Woody, S.J. Fox, L. Ancel Meyers); Santa Fe Institute, Santa Fe, New Mexico, USA (M. Lachmann); University of Texas at Austin Office of the Vice President for Research, Austin (J. Klima); University of Texas at Austin Department of Population Health, Austin (T.S. Hines)

DOI: https://doi.org/10.3201/eid2712.210652

We used the incidence of spike gene target failures identified during PCR testing to provide an early projection of the prevalence of severe acute respiratory syndrome coronavirus 2 variant B.1.1.7 in a university setting in Texas, USA, before sequencing results were available. Findings from a more recent evaluation validated those early projections.

Identification of the highly transmissible novel severe acute respiratory syndrome coronavirus 2 (SARS-CoV-2) variant B.1.1.7 (Alpha variant) in the United Kingdom raised concerns for renewed pandemic surges worldwide (*1*,*2*). B.1.1.7 likely arrived in the United States by October 2020 (*1*); it was first detected in December 2020 and declared the dominant strain in April 2021, as projected in January 2021 (*3*). However, the regional prevalence of B.1.1.7 was largely unknown in early 2021 because of limited molecular surveillance for SARS-CoV-2 (*4*). To provide local situational awareness at that pivotal moment in the coronavirus disease (COVID-19) pandemic, we estimated the prevalence of B.1.1.7 on the basis of 17,003 student SARS-CoV-2 PCR test results reported through the Proactive Community Testing Program at the University of Texas (UT; Austin, Texas, USA), a large public university located in a metropolitan area with a population >2 million, during January 16–February 12, 2021 (K.E. Johnson et al., unpub. data, https://doi.org/10.1101/2021.03.05.21252541. Those early estimates were subsequently validated by using PCR data through April 9, 2021.

Mutations in the B.1.1.7 spike protein result in a failure to detect the spike gene probe in standard SARS-CoV-2 quantitative reverse transcription PCR (qRT-PCR). In estimating the prevalence of B.1.1.7 from local quantitative PCR data, we initially assumed US estimates for the proportion of spike gene target failures (SGTF) attributable to B.1.1.7 (*4*) and, in our retrospective analysis, update that proportion on the basis of local sequencing data. We used a Bayesian model to estimate the local growth rate of B.1.1.7 among all SARS-CoV-2 infections and applied a compartmental susceptible-exposed-infected-recovered model of SARS-CoV-2 transmission to project the effect of B.1.1.7 on future COVID-19 prevalence.

[1]These authors contributed equally to this article.

We previously estimated that the relative frequency of B.1.1.7 among positive SARS-CoV-2 samples was growing logistically at a daily rate of 0.077 (95% CI 0.017–0.140), corresponding to an early doubling time of 9.0 days (95% CI 5.0–41.0 days) (K.E. Johnson et al., unpub. data, https://doi.org/10.1101/2021.03.05.21252541). At the time, we projected that B.1.1.7 would comprise most cases at UT by March 5 (95% predictive interval [PI] February 20–March 28) (Figure, panel A).

Subsequent estimates of B.1.1.7 prevalence based on quantitative PCR data from February 20 through April 9 fell within 95% PIs of the early projections (Figure, panel A) but suggested a lower daily growth rate of 0.037 (95% CI 0.026–0.048) and a corresponding doubling time of 18.7 days (95% CI 14.3–26.7 days). As of April 9, we estimated that B.1.1.7 comprised 61.2% (95% CI 48.5%–72.6%) of SARS-CoV-2 infections, consistent with our initial projections that B.1.1.7 would become the dominant variant by March 28 (95% CI March 20–April 10) and that B.1.1.7 is 24% (95% CI 17%–32%) more transmissible than the wild-type virus.

Based on those local estimates, scenario-based projections suggested that B.1.1.7 might cause 6.2%

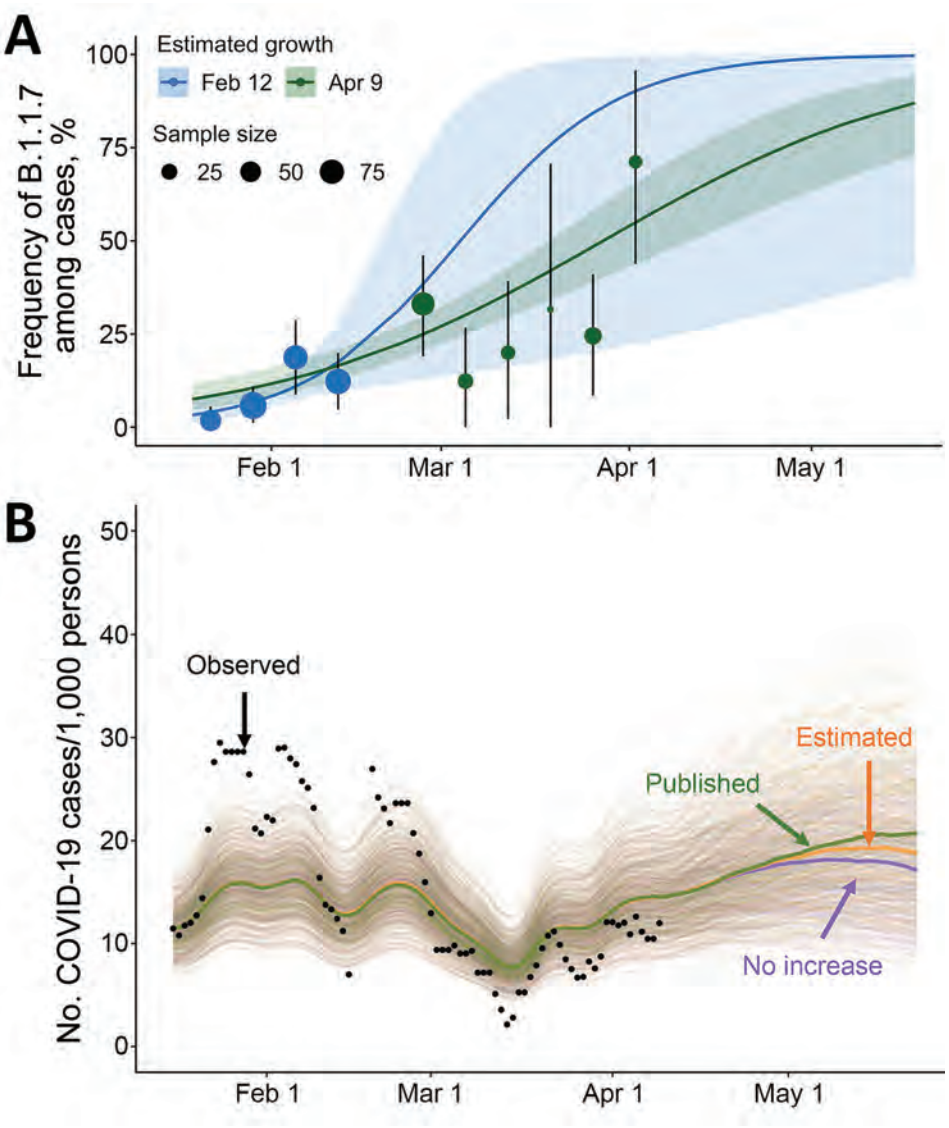

Figure. Estimated frequency of the B.1.1.7 variant among COVID-19 cases at the University of Texas and its projected impact on COVID-19 prevalence, Texas, USA, January 16–May 23, 2021. A) On the basis of the number of samples with spike gene target failures among severe acute respiratory syndrome coronavirus 2–positive samples reported by the University of Texas Proactive Community Testing Program (PCT), we estimated the weekly frequency of the B.1.1.7 variant (points); vertical error bars indicate 95% CIs. We fit a logistic growth model to data through February 12 (blue) and April 9 (green) to project the prevalence of the B.1.1.7 variant relative to the previously circulating wild-type virus through May 23. Shaded bands indicate 95% credible intervals, which reflect uncertainty in the percentage of cases that are spike gene dropouts, the percentage of spike gene dropouts that are B.1.1.7, and the fitted model parameters. The 95% credible interval of our initial projections (blue shading) contains the posterior median estimated from subsequent data (green line). B) Projected COVID-19 cases at the University of Texas through the end of the spring semester. Green, orange, and purple indicate projections with variant transmissibility from published literature, with the university-derived estimate, and with no transmissibility increase from the variant, respectively; black dots indicate the 7-day average reported positive cases per 1,000 persons detected through PCT. The projections assume a reproduction number (R_t) of 1.17 (95% CI 0.94–1.43) as of April 9, on the basis of a recent estimate from PCT data (*5*,*6*). Spaghetti lines display 500 simulations; bold lines indicate the median projected value on each day. A lower-transmission scenario is described in the Appendix (https://wwwnc.cdc.gov/EID/article/27/12/21-0652-App1.pdf). COVID-19, coronavirus disease.

(95% PI 3.7%–8.4%) more cumulative infections during April 9–May 23, 2021, than if it were not more transmissible than the wild-type virus (Figure, panel B). When we assume a higher published estimate for the relative transmissibility of B.1.1.7 of 59% (95% CI 56%–63%) (2), we projected that B.1.1.7 would increase overall incidence by 14.3% (95% CI 10.8%–18.0%) during this period (Figure, panel B; Appendix Figure 5, https://wwwnc.cdc.gov/EID/article/27/12/21-0652-App1.pdf). We provide projections as total infections, rather than hospitalizations or deaths, because the primary concerns of the university at the time of this analysis were anticipating increased demand for isolation facilities, testing, and contact tracing. In either scenario, if behavior stays constant for the remainder of the semester, then we would not expect B.1.1.7 to drive a major surge in infections in the university community during this period (Figure, panel B). The relatively small effect derives from 2 factors that constrained future growth of B.1.1.7. We estimated that, by April 9, 47% (95% CI 39%–57%) of the student community was immunized by prior infection (either viral variant providing complete immunity) and that B.1.1.7 already comprised most (61.2%) new cases. This result hinges on the assumption that previous infection from either viral variant confers immunity to both variants and therefore would not apply to any type able to evade vaccine- or infection-acquired immunity. Our projections, which do not consider future behavioral change or reflect the full range of uncertainty, were not intended as forecasts but rather as plausible guideposts to help the university anticipate the severity of B.1.1.7.

UT surveillance testing indicates that B.1.1.7 rapidly became the dominant variant during the spring 2021 semester. Our methodology enabled rapid detection of B.1.1.7 emergence from widely available quantitative PCR data when sequence confirmation was not available or delayed, while quantifying uncertainty in the variant growth rate and fraction of SGTF samples that were positive for B.1.1.7. During January 16–March 5, UT confirmed 22 of 23 sequenced SGTF SARS-CoV-2 specimens as the B.1.1.7 variant, corroborating our reliance on SGTF data (Appendix).

Our findings reinforce the urgent need for expanded molecular surveillance capacity. In the absence of widespread and rapid sequencing efforts, quantitative PCR data from large-scale testing efforts have provided sentinel warning of B.1.1.7 emergence in cities throughout the United States.

Acknowledgments

We thank Andreas Matouschek for his insightful comments on the manuscript. We also thank the Proactive Community Testing team at the University of Texas at Austin.

We received financial support from the National Institutes of Health (grant no. R01 AI151176) and the Centers for Disease Control and Prevention (grant no. U01IP001136).

About the Author

Dr. Johnson is a postdoctoral researcher in the Department of Integrative Biology at the University of Texas at Austin. She uses mathematical models to aid in decision-making for control of infectious diseases. Dr. Woody is a postdoctoral researcher in the Department of Integrative Biology at the University of Texas at Austin. He develops mathematical and statistical models to elucidate transmission dynamics, surveillance, and control of infectious diseases.

References

1. Du Z, Wang L, Yang B, Ali ST, Tsang TK, Shan S, et al. Risk for international importations of variant SARS-CoV-2 originating in the United Kingdom. Emerg Infect Dis. 2021;27:1527–9. https://doi.org/10.3201/eid2705.210050
2. Davies NG, Abbott S, Barnard RC, Jarvis CI, Kucharski AJ, Munday JD, et al.; CMMID COVID-19 Working Group. COVID-19 Genomics UK (COG-UK) Consortium. Estimated transmissibility and impact of SARS-CoV-2 lineage B.1.1.7 in England. Science. 2021;372:eabg3055. https://doi.org/10.1126/science.abg3055
3. Galloway SE, Paul P, MacCannell DR, Johansson MA, Brooks JT, MacNeil A, et al. Emergence of SARS-CoV-2 B.1.1.7 lineage—United States, December 29, 2020–January 12, 2021. MMWR Morb Mortal Wkly Rep. 2021;70:95–9. https://doi.org/10.15585/mmwr.mm7003e2
4. Washington NL, Gangavarapu K, Zeller M, Bolze A, Cirulli ET, Schiabor Barrett KM, et al. Emergence and rapid transmission of SARS-CoV-2 B.1.1.7 in the United States. Cell. 2021;184:2587–2594.e7. https://doi.org/10.1016/j.cell.2021.03.052
5. University of Texas at Austin. University of Texas Proactive Community Testing Program for COVID-19 [cited 2021 Feb 9]. https://healthyhorns.utexas.edu/coronavirus_proactive_testing.html
6. Cori A, Ferguson NM, Fraser C, Cauchemez S. A new framework and software to estimate time-varying reproduction numbers during epidemics. Am J Epidemiol. 2013;178:1505–12. https://doi.org/10.1093/aje/kwt133
7. Volz E, Mishra S, Chand M, Barrett JC, Johnson R, Geidelberg L, et al.; COVID-19 Genomics UK (COG-UK) Consortium. Assessing transmissibility of SARS-CoV-2 lineage B.1.1.7 in England. Nature. 2021;593:266–9. https://doi.org/10.1038/s41586-021-03470-x

Address for correspondence: Lauren Ancel Meyers, The University of Texas at Austin, Department of Integrative Biology, 1 University Station C0930, Austin, TX 78712, USA: email: laurenmeyers@austin.utexas.eduSubmitted: 7/4/2020

Correlation between Buruli Ulcer Incidence and Vectorborne Diseases, Southeastern Australia, 2000–2020

Jake Andrew Linke, Eugene Athan, N. Deborah Friedman

Author affiliations: Deakin University School of Medicine, Geelong, Victoria, Australia (J.A. Linke, E. Athan); Barwon Health, Geelong (E. Athan, N.D. Friedman)

DOI: https://doi.org/10.3201/eid2712.203182

Researchers have hypothesized that mosquitoes are vectors involved in *Mycobacterium ulcerans* transmission. Previous findings of a correlation between incidence of *M. ulcerans*, which causes Buruli ulcer, and locally acquired vectorborne diseases in southeastern Australia further strengthened this argument. However, our updated data indicate that this correlation has not continued beyond 2008.

Mycobacterium ulcerans infection causes skin and soft tissue destruction and is classified by the World Health Organization as a neglected tropical disease. Internationally, disease caused by *M. ulcerans* infection is known as Buruli ulcer (BU) and has been reported in 33 countries (*1*), mostly in central and western Africa. However, in southeastern Australia, the epidemic is worsening; disease incidence and severity of infection have increased rapidly since 2015 (*2*). Although the mode(s) of transmission of *M. ulcerans* remain(s) unclear, a study published in 2009 showed a correlation between BU incidence and locally acquired vectorborne diseases in southeastern Australia (*3*). This finding strengthened the hypothesis that mosquitoes may be involved in *M. ulcerans* transmission. We examined data to determine if this correlation continued beyond 2008.

In Africa, *M. ulcerans* is thought to be transmitted by water bugs, and a report of a case in southeastern Australia suggested that a BU lesion first appeared at the site of a mosquito bite (*4*). Subsequently, the probability of mosquitoes being *M. ulcerans* positive by PCR has been associated with the degree of BU endemicity in southeastern Australia (*4*,*5*). Furthermore, being bitten by a mosquito substantially increases the odds of BU developing, and using insect repellent and protective clothing reduces the odds (*6*). However, this association does not necessarily imply that mosquitoes are involved in *M. ulcerans* transmission because covering limbs with clothing would also help to protect against other potential environmental sources of *M. ulcerans*, such as possum excreta or soil contamination of wounds. Furthermore, mosquitoes rarely act as vectors for bacteria, and no other species of *Mycobacteria* are known to have arthropod vectors.

The apparent role of mosquitoes in the transmission of *M. ulcerans* may be explained by mechanical vectoring. Within *M. ulcerans*–endemic areas of southeastern Australia, the geographic locations of BU cases are highly focal. Cases are often clustered together, and adjoining communities only a few kilometers away may be spared (*7*). However, *Aedes camptorhynchus* mosquitoes, one of the main species thought to be involved in *M. ulcerans* transmission, are widespread within *M. ulcerans*–endemic and –nonendemic areas, and many species of mosquito may have the capacity to fly distances that would take them outside of BU-affected regions. Therefore, the transmission model for *M. ulcerans* may not be explained by mosquitoes alone.

In coastal regions of southeastern Australia, Ross River virus (RRV) and Barmah Forest virus (BFV) cause locally acquired vectorborne diseases. RRV and BFV are transmitted by *Ae. camptorhynchus* mosquitoes, which were the main species captured during an *M. ulcerans* outbreak in Point Lonsdale, southeastern Australia (*4*). The incidence of RRV and BFV peaks sporadically, especially during years of above average rainfall or La Niña events, as occurred during the 2020–21 summer in Australia (*8*). These environmental changes often favor increased mosquito population sizes, thus giving rise to RRV and BFV outbreaks (*9*). It is also thought that BU incidence is associated with environmental factors; increased incidence has lagged 12 months behind periods of greater rainfall (*10*). However, no association has been found between rainfall and BU cases on the Mornington Peninsula, the main *M. ulcerans*–endemic site driving the increased incidence of BU in southeastern Australia.

During 2002–2008, BU incidence correlated with combined RRV/BFV incidence in Victoria, southeastern Australia ($r^2 = 0.52$) (*3*). It was argued that this correlation strengthened the link between mosquitoes and *M. ulcerans* transmission in southeastern Australia. However, this observation was made over a short time. Using the square of the Pearson product-moment correlation coefficient (coefficient of determination) analysis over a 21-year period (2000–2020), we found little to no correlation between BU and combined RRV/BFV incidence in southeastern Australia ($r^2 = 0.05$; $p = 0.69$) (Figure) (Appendix, https://wwwnc.cdc.gov/EID/

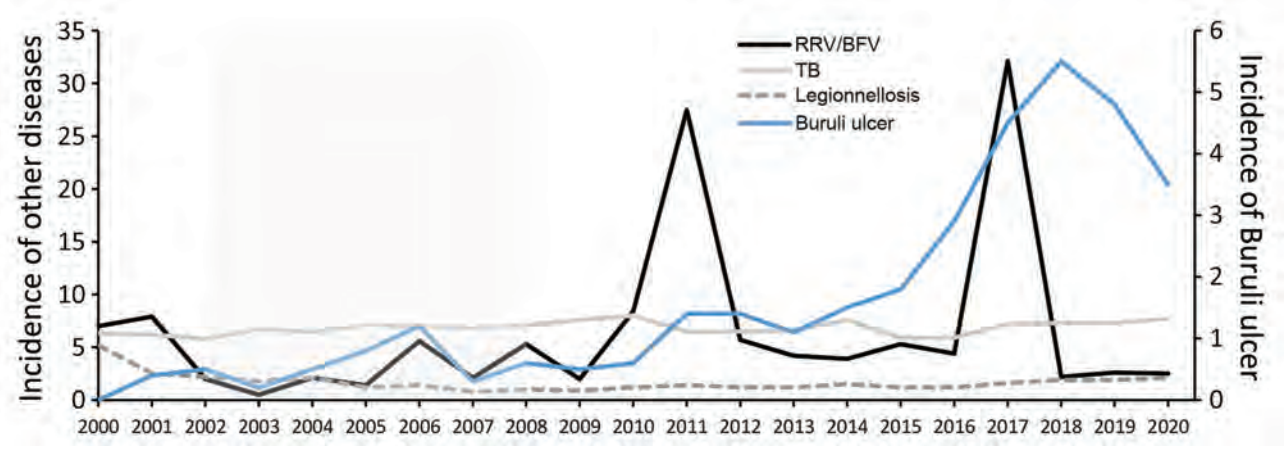

Figure. Incidence (cases/100,000 population) of Buruli ulcer compared with that of other notifiable diseases in Victoria, Australia, during 2000–2020. Victoria is located in southeastern Australia. "Other diseases" on left y-axis indicates TB, legionellosis, and RRV and BFV incidence combined. The shaded area (2002–2008) denotes a period when Buruli ulcer incidence correlated with RRV/BFV incidence (*3*). In Australia, these infections are notifiable and incidence rates are publicly available (*8*). BFV, Barmah Forest; RRV, Ross River virus; TB, tuberculosis.

article/27/12/20-3182-App1.pdf). For comparison, during this same period there was no correlation between BU and infection with *M. tuberculosis* (the other main mycobacterial disease in southeastern Australia) or *Legionella* (water-associated bacteria).

A lack of correlation between BU incidence and locally acquired vectorborne diseases does not disprove that mosquitoes are involved in *M. ulcerans* transmission. Nevertheless, this lack of correlation may suggest that the worsening BU epidemic in southeastern Australia is not caused by increased mosquito populations or other environmental changes that favor RRV and BFV outbreaks. We believe that other independent factors may be driving the increased BU incidence, although the effects of recent La Niña events on BU incidence in 2021 are not yet known. Planning and implementing successful public health interventions to control *M. ulcerans* are substantially hindered by lack of knowledge of the mechanism of disease transmission.

About the Author

Mr. Linke is a final-year doctor of medicine student at the Geelong Clinical School, Deakin University. His research interests include mosquitoborne flaviviruses and cellulitis.

References

1. World Health Organization. Number of new reported cases: data by country [cited 2020 Jun 24]. https://apps.who.int/gho/data/node.main.A1631
2. Tai AYC, Athan E, Friedman ND, Hughes A, Walton A, O'Brien DP. Increased severity and spread of *Mycobacterium ulcerans,* southeastern Australia. Emerg Infect Dis. 2018;24:58–64. https://doi.org/10.3201/eid2401.171070
3. Johnson PD, Lavender CJ. Correlation between Buruli ulcer and vector-borne notifiable diseases, Victoria, Australia. Emerg Infect Dis. 2009;15:614–5. https://doi.org/10.3201/eid1504.081162
4. Johnson PD, Azuolas J, Lavender CJ, Wishart E, Stinear TP, Hayman JA, et al. *Mycobacterium ulcerans* in mosquitoes captured during outbreak of Buruli ulcer, southeastern Australia. Emerg Infect Dis. 2007;13:1653–60. https://doi.org/10.3201/eid1311.061369
5. Lavender CJ, Fyfe JA, Azuolas J, Brown K, Evans RN, Ray LR, et al. Risk of Buruli ulcer and detection of *Mycobacterium ulcerans* in mosquitoes in southeastern Australia. PLoS Negl Trop Dis. 2011;5:e1305. https://doi.org/10.1371/journal.pntd.0001305
6. Quek TY, Athan E, Henry MJ, Pasco JA, Redden-Hoare J, Hughes A, et al. Risk factors for *Mycobacterium ulcerans* infection, southeastern Australia. Emerg Infect Dis. 2007;13:1661–6. https://doi.org/10.3201/eid1311.061206
7. Boyd SC, Athan E, Friedman ND, Hughes A, Walton A, Callan P, et al. Epidemiology, clinical features and diagnosis of *Mycobacterium ulcerans* in an Australian population. Med J Aust. 2012;196:341–4. https://doi.org/10.5694/mja12.10087
8. Department of Health and Human Services Victoria. Local government areas surveillance report [cited 2021 May 20]. https://www2.health.vic.gov.au/public-health/infectious-diseases/infectious-diseases-surveillance/interactive-infectious-disease-reports/local-government-areas-surveillance-report
9. Passmore J, O'Gardy K, Moran R, Wishart E. An outbreak of Barmah Forest virus disease in Victoria. Commun Dis Intell Q Rep. 2002;26:600–4.
10. Yerramilli A, Tay EL, Stewardson AJ, Fyfe J, O'Brien DP, Johnson PDR. The association of rainfall and Buruli ulcer in southeastern Australia. PLoS Negl Trop Dis. 2018;12:e0006757. https://doi.org/10.1371/journal.pntd.0006757

Address for correspondence: Jake Andrew Linke, Geelong Clinical School, c/o The University Hospital, Geelong, PO Box 281, Geelong, VIC 3220, Australia; email: jalinke@deakin.edu.au

Borrelia miyamotoi in Human-Biting Ticks, United States, 2013–2019

Guang Xu, Chu-Yuan Luo, Fumiko Ribbe, Patrick Pearson, Michel Ledizet, Stephen M. Rich

Author affiliations: University of Massachusetts–Amherst, Amherst, Massachusetts USA (G. Xu, C.-Y. Luo, F. Ribbe, P. Pearson, S.M. Rich); L2 Diagnostics, New Haven, Connecticut, USA (M. Ledizet)

During 2013–2019, *Borrelia miyamotoi* infection was detected in 19 US states. Infection rate was 0.5%–3.2%; of *B. miyamotoi*–positive ticks, 59.09% had concurrent infections. *B. miyamotoi* is homogeneous with 1 genotype from *Ixodes scapularis* ticks in northeastern and midwestern states and 1 from *I. pacificus* in western states.

DOI: https://doi.org/10.3201/eid2712.204646

Borrelia miyamotoi, a relapsing fever group spirochete (*1*), was first isolated from *Ixodes persulcatus* ticks in Japan in 1995 (*2*) and later detected in *Ixodes* ticks in the United States and Europe (*3*–*5*). Although *B. miyamotoi* bacteria have been mainly detected in *I. ricinus* species complex ticks that transmit *B. burgdorferi* worldwide, the vector specificity needs further study because investigators have found *B. miyamotoi* in multiple tick species (*6*). *B. miyamotoi* has 3 geographically distinct genotypes: Asian, European, and American. In the United States, *B. miyamotoi* bacteria have been found in field-collected *I. scapularis* ticks in the northeastern and northern midwestern regions, where the average infection rate is 1.9% (*7*). However, an expanded geographic study of the prevalence of *B. miyamotoi* in human-biting ticks, its genotypes, and concurrent infections with other tickborne pathogens is warranted.

Human-biting ticks were submitted to the public tick testing program at the University of Massachusetts (Amherst, Massachusetts, USA) during May 2013–December 2019. We extracted DNA from individual ticks using the Epicenter Master Complete DNA and RNA Purification Kits (Lucigen, https://www.lucigen.com). We performed a species-specific quantitative PCR (qPCR) for differentiation of *I. scapularis* and *I. pacificus* ticks (*8*). To detect *Borrelia* bacteria, we first applied a genus-specific detection assay, followed by specific qPCR assays for *B. burgdorferi* sensu lato and *B. miyamotoi*. We detected the tickborne pathogens *Anaplasma phagocytophilum*, *Babesia microti*, *B. mayonii,* and *Ehrlichia muris*–like agent (EMLA) by a multiplex qPCR assay targeting different genes. We used a qPCR assay targeting tick 16S mtDNA gene as an internal control (*8*). We sequenced 3 partial gene fragments, 16S rDNA (*16S*) (*9*), flagellin (*fla*) (*6*), and glycerophosphodiester phosphodiesterase (*glpQ*) (*6*), for *B. miyamotoi* samples that were positive by qPCR.

We received and tested 39,198 ticks found on humans for *B. miyamotoi* during May 2013–December 2019. Of those, 38,855 (99.12%) ticks originated from the continental United States, comprising 18 tick species (Table). Although *Ixodes* ticks are the main vectors for *B. miyamotoi*, we did not detect *B. miyamotoi* DNA in *I. affinis*, *I. angustus*, *I. cookei*, *I. dentatus*, *I. marxi*. *I. muris,* or *I. spinipalpis* ticks. We detected *B. miyamotoi* in *I. pacificus* (14/1,497, 0.94%) and *I. scapularis* (594/34,621, 1.72%) ticks.

B. miyamotoi was found in 19 states; infection rates were 0.5%–3.2% (Figure). In the western

Table. Human-biting tick species positive for *Borrelia miyamotoi* and *B. burgdorferi* sensu lato, United States, 2013–2019

Tick species	Total no. tested	No. *B. miyamotoi* positive	No. *B. burgdorferi* s.l. positive
Amblyomma americanum	1,167	0	0
A. cajennense	1	0	0
A. maculatum	8	0	0
Dermacentor andersoni	60	0	0
D. occidentalis	91	0	0
D. variabilis	1,060	0	0
Haemaphysalis leporispalustris	2	0	0
H. longicornis	7	0	0
Ixodes affinis	2	0	0
I. angustus	55	0	0
I. cookei	123	0	0
I. dentatus	48	0	7
I. marxi	26	0	0
I. muris	9	0	2
I. pacificus	1,497	14	25
I. scapularis	34,621	594	11,287
I. spinipalpis	63	0	3
Rhipicephalus sanguineus	15	0	0
Total	38,855	608	11.324

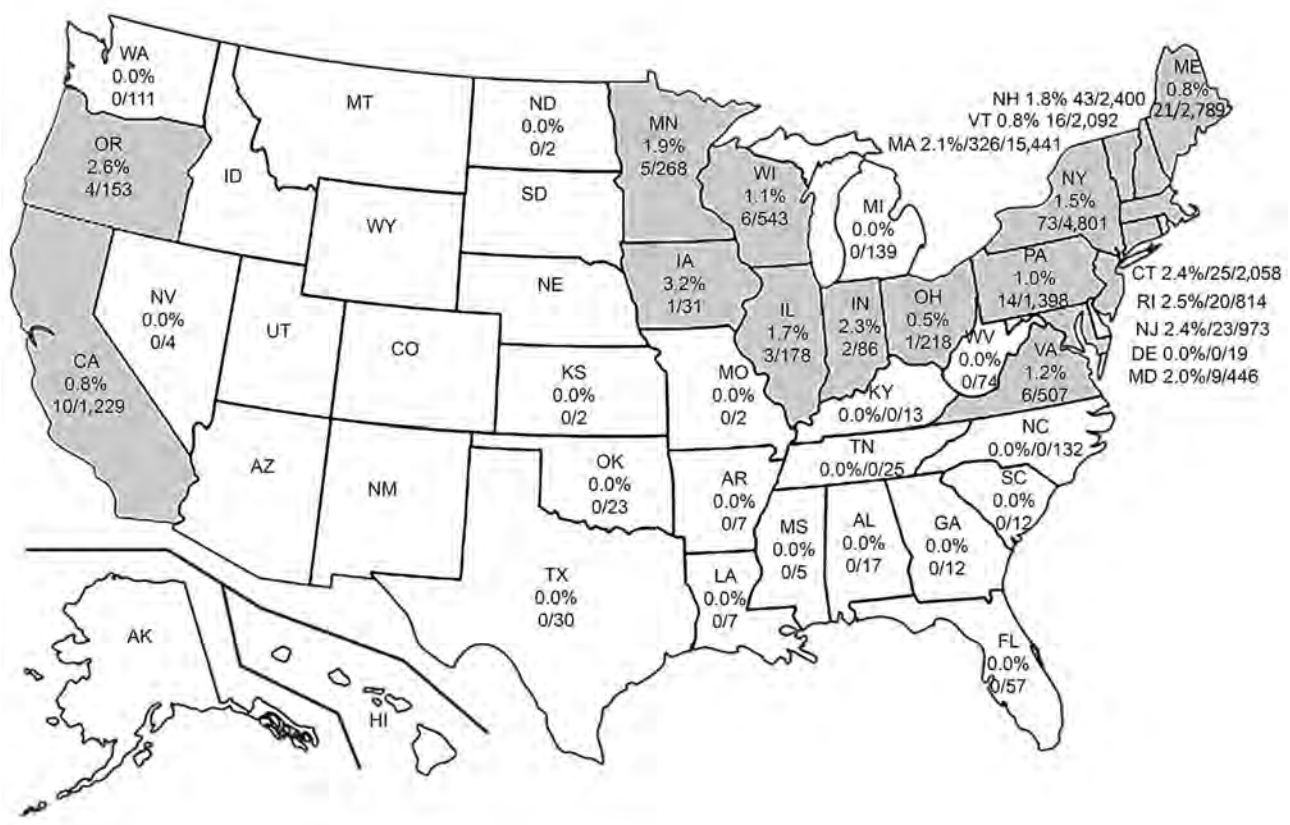

Figure. *Borrelia miyamotoi* positivity rates in human-biting *Ixodes scapularis* and *I. pacificus* ticks, United States, 2013–2019. Gray shading indicates states in which *B.miyamotoi* was detected in human-biting ticks.

United States, *B. miyamotoi* was found in *I. pacificus* ticks in Oregon and California (14/1,497, 0.94%). Although *I. scapularis* ticks are distributed across the eastern United States, no *B. miyamotoi*–positive ticks were detected south of Virginia. *B. miyamotoi*–positive ticks were concentrated in the Northeast and upper Midwest (594 of 34,621, 1.72%) (Figure). Lyme disease remains the principal public health concern; the causative agent, *B. burgdorferi* (11,287/34,621; 32.60%, 95% CI 32.1%–33.1%), was 19 times more prevalent than *B. miyamotoi* (594/34,621, 1.72%) in *I. scapularis* ticks.

On average, prevalence of *B. miyamotoi* infection in *I. scapularis* ticks (1.72%, 95% CI 1.58%–1.86%) was higher than in *I. pacificus* ticks (0.94%, 95% CI 0.51%–1.56%). The prevalence of *B. miyamotoi* in *I. pacificus* ticks was 1.00% (95% CI 0.53%–1.7%) in adults (13/1,300), 0.53% (95% CI 0.01%–2.9%) in nymphs (1/190), and 0.00% (95% CI 0%–40.1%) in larvae (0/7). The prevalence of *B. miyamotoi* in *I. scapularis* ticks was 1.80% (95% CI 1.64%–1.97%) in adults (456/25,376), 1.54% (95% CI 1.29−1.83%) in nymphs (133/8,615), and 0.79% (95% CI 0.26%–1.84%) in larvae (5/630).

Of 594 *B. miyamotoi*–positive *I. scapularis* ticks, 351 (59.09%) had concurrent infections. We found 293 (49.33%) *I. scapularis* ticks had a dual infection with *B. miyamotoi*: 220 (37.04%) were also infected with *B. burgdorferi* s.l., 43 (7.24%) with *A. phagocytophilum*, and 30 (5.05%) with *B. microti*. We further found 52 (8.75%) had a triple infection with *B. miyamotoi*: 23 (3.87%) were also infected with *B. burgdorferi* s.l. and *A. phagocytophilum*, 22 (3.70%) with *B. burgdorferi* s.l. and *B. microti*, and 7 (1.18%) with *A. phagocytophilum* and *B. microti*. Six (1.01%) of the *B. miyamotoi*–positive ticks had a quadruple infection with *B. miyamotoi*, *B. burgdorferi* s.l., *A. phagocytophilum*, and *B. microti*. No ticks with *B. mayonii* or EMLA were additionally infected with *B. miyamotoi*.

Multilocus sequence typing of the *16S*, *fla*, and *glpQ* genes revealed 2 distinct *B. miyamotoi* genotypes separated by their tick vectors, *I. scapularis* ticks in the Northeast and upper Midwest and *I. pacificus* ticks in the West (Appendix, https://wwwnc.cdc.gov/EID/article/27/12/20-4646-App1.pdf). Whereas the *16S* gene sequences were identical among all isolates, variable sites were found among *fla* and *glpQ* nucleotide sequences. Among 14 *I. pacificus* tick–borne

B. miyamotoi isolates, all *fla* and *glpQ* sequences were identical. A previously reported A/G substitution in *B. miyamotoi fla* sequences from *I. pacificus* ticks (*5*,*9*) was outside of our sequenced *fla* fragment (Appendix). The genetic identity between the 2 tick species–specific genotypes was 0.996 for *fla* and 0.986 for *glpQ*. Unlike heterogeneous *B. burgdorferi* populations, *B. miyamotoi* appears to be very homogeneous within its respective tick vectors.

About the Author

Dr. Xu is a research professor in the department of microbiology, University of Massachusetts–Amherst. His research interests include ticks and tickborne diseases.

References

1. Krause PJ, Fish D, Narasimhan S, Barbour AG. *Borrelia miyamotoi* infection in nature and in humans. Clin Microbiol Infect. 2015;21:631–9. https://doi.org/10.1016/j.cmi.2015.02.006
2. Fukunaga M, Takahashi Y, Tsuruta Y, Matsushita O, Ralph D, McClelland M, et al. Genetic and phenotypic analysis of *Borrelia miyamotoi* sp. nov., isolated from the ixodid tick *Ixodes persulcatus*, the vector for Lyme disease in Japan. Int J Syst Bacteriol. 1995;45:804–10. https://doi.org/10.1099/00207713-45-4-804
3. Scoles GA, Papero M, Beati L, Fish D. A relapsing fever group spirochete transmitted by *Ixodes scapularis* ticks. Vector Borne Zoonotic Dis. 2001;1:21–34. https://doi.org/10.1089/153036601750137624
4. Bunikis J, Tsao J, Garpmo U, Berglund J, Fish D, Barbour AG. Typing of *Borrelia* relapsing fever group strains. Emerg Infect Dis. 2004;10:1661–4. https://doi.org/10.3201/eid1009.040236
5. Mun J, Eisen RJ, Eisen L, Lane RS. Detection of a *Borrelia miyamotoi* sensu lato relapsing-fever group spirochete from *Ixodes pacificus* in California. J Med Entomol. 2006;43:120–3. https://doi.org/10.1093/jmedent/43.1.120
6. Jiang BG, Jia N, Jiang JF, Zheng YC, Chu YL, Jiang RR, et al. *Borrelia miyamotoi* infections in humans and ticks, northeastern China. Emerg Infect Dis. 2018;24:236–41. https://doi.org/10.3201/eid2402.160378
7. Barbour AG, Bunikis J, Travinsky B, Hoen AG, Diuk-Wasser MA, Fish D, et al. Niche partitioning of *Borrelia burgdorferi* and *Borrelia miyamotoi* in the same tick vector and mammalian reservoir species. Am J Trop Med Hyg. 2009;81:1120–31. https://doi.org/10.4269/ajtmh.2009.09-0208
8. Xu G, Pearson P, Dykstra E, Andrews ES, Rich SM. Human-biting *Ixodes* ticks and pathogen prevalence from California, Oregon, and Washington. Vector Borne Zoonotic Dis. 2019;19:106–14. https://doi.org/10.1089/vbz.2018.2323
9. Cook VJ, Fedorova N, Macdonald WP, Lane RS, Barbour AG. Unique strain of *Borrelia miyamotoi* in *Ixodes pacificus* ticks, California, USA. Emerg Infect Dis. 2016;22:2205–7. https://doi.org/10.3201/eid2212.152046

Address for correspondence: Guang Xu, University of Massachusetts—Microbiology, Fernald Hall Room B1, 270 Stockbridge Rd, University of Massachusetts, Amherst, MA 01003, USA; email: gxu@umass.edu

Wohlfahrtiimonas chitiniclastica Monomicrobial Bacteremia in a Homeless Man

Omar Harfouch, Paul M. Luethy, Mandee Noval, Jonathan D. Baghdadi

Author affiliation: University of Maryland Medical Center, Baltimore, Maryland, USA

DOI: https://doi.org/10.3201/eid2712.210327

We report a case of septic shock attributable to monomicrobial bloodstream infection secondary to *Wohlfahrtiimonas chitiniclastica* infection. This case suggests that *W. chitiniclastica* likely possesses the virulence to cause severe disease. Culture-independent techniques were essential in the identification of this organism, which enabled selection of appropriate therapy.

In August 2020, a 63-year-old homeless man with a history of deep vein thrombosis and chronic venous insufficiency was found in his truck, unconscious and covered in feces and maggots. He reportedly had been parked in a single parking spot in rural Maryland, USA, for 3 days. His blood pressure in the field was too low to be quantified, and he was admitted to a community hospital in septic shock. Blood cultures were drawn before establishing intravenous access for administration of vancomycin, piperacillin/tazobactam, and crystalloid. After being stabilized, he was transferred to our hospital, a tertiary care center in Baltimore, Maryland, USA, where surgeons performed superficial surgical debridement of his lower extremities and removed maggots by using a scrub brush with the patient under anesthesia in the operating room. We discarded the maggots, and they were not submitted for identification.

The patient's leukocyte count on arrival was 38.6 K/μL (reference range 4.5–11.0 K/μL), his creatinine 6.86 mg/dL (reference range 0.7–1.5 mg/dL), and his lactic acid 3.5 mmol/L (reference range 0.5–2.2 mmol/L). He had elevated transaminases, an aspartate aminotransferase level of 436 U/L (reference range 17–59 U/L) and alanine transaminase of 174 U/L (reference range 0–49 U/L). A computed tomography scan of the lower extremities showed ulceration of the anterior right lower leg with edema and fat stranding of the subcutaneous tissue without fluid collection or gas. A magnetic resonance imaging of his left foot showed no evidence of osteomyelitis.

On day 2 of hospitalization, transient hemodynamic instability necessitated initiation of

vasopressor support and continuous renal replacement therapy; however, these treatments were rapidly tapered off. We identified gram-negative rods in the anaerobic blood culture from the community hospital, and we narrowed the patient's antibiotics to piperacillin/tazobactam monotherapy. On hospital day 5, we identified the gram-negative rods as *W. chitiniclastica* by using matrix-assisted laser desorption/ionization time-of-flight (MALDI-TOF) mass spectrometry. We changed the patient's intravenous antibiotics to 2 g of ceftriaxone daily and then, on hospital day 9, changed the regimen to 750 mg of oral levofloxacin daily to complete a 21-day course of treatment. We were unable to follow up with the patient after his discharge, but we proceeded with reporting about his case after it was deemed to be exempt by the Institutional Review Board at the University of Maryland Baltimore.

In 2008, *W. chitiniclastica* was first isolated from larvae of the parasitic fly *Wohlfahrtia magnifica* (*1*). Since 2008, a total of 11 cases of *W. chitiniclastica* bloodstream infections have been described (*2*–*10*; Appendix references *11*,*12*, https://wwwnc.cdc.gov/EID/article/21/12/21-0327-App1.pdf)

Table. Published cases of *Wohlfahrtiimonas* chitiniclastica bloodstream infection*

Country of origin (reference)	Age, y/sex; housing status; presentation	Bacteria identified on blood cultures	Microbiology tools used	Antimicrobial agents and duration of treatment	Outcome
France (*2*)	60/F; homeless; fatigue and ulcers to the scalp	*W. chitiniclastica*	16S rRNA sequencing	Ceftriaxone; duration not defined	Survival
Argentina (*3*)	70/M; homeless; altered mental status, septic shock, and plaques in the inguinal region	*W. chitiniclastica*	16S rRNA sequencing	Ciprofloxacin and ampicillin/sulbactam; duration not defined	Death
Washington, USA (*4*)	57/M; stable home; wet gangrene of the ankle, septic shock, and multi-organ failure	Propionibacterium acnes, *Staphylococcus hominis*, and *Wohlfahrtiimonas* species	MALDI-TOF mass spectrometry and 16S rRNA sequencing	No mention of antimicrobials used	Death
Ohio, USA (*5*)	41/F; stable home; abdominal pain and sacral osteomyelitis	*Proteus mirabilis* and *W. chitiniclastica*	MALDI-TOF mass spectrometry	Vancomycin, cefepime, and metronidazole; duration of 6 wks	Death from *Clostridioides difficile* infection
Indiana, USA (*6*)	37/M; not specified; necrotizing infection of lower extremities	*W. chitiniclastica*, *Ignatzschineria Indica*, and *Providencia stuartii*	Not specified	Piperacillin/tazobactam, clindamycin and vancomycin, then cefepime; duration of 10 d	Survival
United Kingdom (*7*)	82/F; stable home; unconscious	*W. chitiniclastica*, *P. mirabilis*, *Providencia rettgeri*, and *Staphylococcus aureus*	MALDI-TOF mass spectrometry and 16S rRNA sequencing	Cefuroxime, metronidazole, and clarithromycin, then flucloxacillin; duration of 7 d	Survival
Australia (*8*)	54/M; stable home; unconscious, septic shock and myasis of the foot and toes	*W. chitiniclastica* and *Morganella morganii*	MALDI-TOF mass spectrometry	Piperacillin/tazobactam, then meropenem, then ciprofloxacin; duration of 3 wks	Survival
Hawaii, USA (*9*)	72/M; stable home; unconscious, septic shock, and myasis of the umbilical cord	*Escherichia coli* and *W. chitiniclastica*	16S rRNA sequencing	Piperacillin/tazobactam, clindamycin, and vancomycin; duration not specified	Death
Japan (*10*)	75/M; homeless; unconscious	*Peptoniphilus harei* on initial blood cultures. On day 20, *P. mirabilis*, *M. morganii*, *Streptococcus anginosus*, *Streptococcus agalactiae*, *Bacteroides fragilis*, and *W. chitiniclastica*	MALDI-TOF mass spectrometry and 16S rRNA sequencing	Cefazolin, then vancomycin, cefepime, and metronidazole; duration not specified	Survival
North Dakota, USA (Appendix reference *11*)	70/M; stable home; fall	*W. chitiniclastica*	Not specified	Levofloxacin; duration not specified	Survival
Pennsylvania, USA (Appendix reference *12*)	82/M; stable home; fall and confusion, myasis of the lower extremities and toes	*Staphylococcus aureus*, *W. chitiniclastica*, and *I. indica*	MALDI-TOF mass spectrometry	Daptomycin for 6 wks Ceftriaxone for 2 wks	Survival

*Appendix, https://wwwnc.cdc.gov/EID/article/21/12/21-0327-App1.pdf. MALDI-TOF, matrix-assisted laser desorption/ionization time-of-flight.

(Table). Our patient shares risk factors observed in other cases, including homelessness and chronic venous insufficiency (Appendix reference *13*). The pathogenicity of *W. chitiniclastica* has remained uncertain in previous case reports secondary to its identification in polymicrobial infections. This severe case of monomicrobial *W. chitiniclastica* BSI is similar to a previous report of a 70-year-old man in Argentina who had septic shock with multiorgan failure secondary to the same bacteria (*3*). Taken together, these 2 cases challenge the hypothesis that other bacteria present in polymicrobial infections are primarily responsible for the disease associated with BSI attributable to *W. chitiniclastica* infection (*9*) and instead suggest that this pathogen may cause severe disease.

For our patient, *W. chitiniclastica* was first identified on MALDI-TOF mass spectrometry from a positive anaerobic blood culture. In all 9 cases for which detailed microbiologic methods are reported, *W. chitiniclastica* was identified from blood or tissue cultures by using MALDI-TOF mass spectrometry (*5*,*8*; Appendix reference *12*), 16S rRNA sequencing (*2*,*3*,*9*), or both (*4*,*7*,*10*) (Table). This pattern demonstrates that *W. chitiniclastica* is extremely difficult to identify from clinical specimens without culture-independent techniques and highlights the utility of these techniques in clinical care.

Published case-reports demonstrate a heterogeneous approach to the clinical management of patients with *W. chitiniclastica* BSI. Often, selection of antibiotics was dictated by the other pathogens present in a polymicrobial infection. Generally, most studies report the use of β-lactams (*2*,*3*,*5*–*10*; Appendix reference *12*) as initial therapy, with fluoroquinolones available as second-line or step-down therapy (*3*,*7*,*8*). The duration of treatment ranges from 7 days to 6 weeks (*5*–*8*; Appendix reference *12*). Given that our patient rapidly improved and the presumed source of his infection had been controlled with debridement of his lower extremities, we opted for a 3-week course of treatment.

Acknowledgments

We thank the healthcare team that participated in this patient's care at the University of Maryland Medical Center and the University of Maryland Midtown Campus.

About the Author

Dr. Harfouch is an infectious diseases fellow at the University of Maryland Medical Center. His primary research interests include the epidemiology and prevention of HIV among lesbian, gay, bisexual, and transgender persons.

References:

1. Tóth EM, Schumann P, Borsodi AK, Kéki Z, Kovács AL, Márialigeti K. *Wohlfahrtiimonas chitiniclastica* gen. nov., sp. nov., a new gammaproteobacterium isolated from *Wohlfahrtia magnifica* (Diptera: Sarcophagidae). Int J Syst Evol Microbiol. 2008;58:976–81. https://doi.org/10.1099/ijs.0.65324-0
2. Rebaudet S, Genot S, Renvoise A, Fournier PE, Stein A. *Wohlfahrtiimonas chitiniclastica* bacteremia in homeless woman. Emerg Infect Dis. 2009;15:985–7. https://doi.org/10.3201/eid1506.080232
3. Almuzara MN, Palombarani S, Tuduri A, Figueroa S, Gianecini A, Sabater L, et al. First case of fulminant sepsis due to *Wohlfahrtiimonas chitiniclastica*. J Clin Microbiol. 2011;49:2333–5. https://doi.org/10.1128/JCM.00001-11
4. Bonwitt JH, Tran M, Dykstra EA, Eckmann K, Bell ME, Leadon M, et al. Fly reservoir associated with *Wohlfahrtiimonas* bacteremia in a human. Emerg Infect Dis. 2018;24:370–3. https://doi.org/10.3201/eid2402.170913
5. Chavez JA, Alexander AJ, Balada-Llasat JM, Pancholi P. A case of *Wohlfahrtiimonas chitiniclastica* bacteremia in continental United States. JMM Case Rep. 2017;4:e005134. https://doi.org/10.1099/jmmcr.0.005134
6. Lysaght TB, Wooster ME, Jenkins PC, Koniaris LG. Myiasis-induced sepsis: a rare case report of *Wohlfahrtiimonas chitiniclastica* and *Ignatzschineria indica* bacteremia in the continental United States. Medicine (Baltimore). 2018;97:e13627. https://doi.org/10.1097/MD.0000000000013627
7. Campisi L, Mahobia N, Clayton JJ. *Wohlfahrtiimonas chitiniclastica* bacteremia associated with myiasis, United Kingdom. Emerg Infect Dis. 2015;21:1068–9. https://doi.org/10.3201/eid2106.140007
8. Connelly KL, Freeman E, Smibert OC, Lin B. *Wohlfahrtiimonas chitiniclastica* bloodstream infection due to a maggot-infested wound in a 54-year-old male. J Glob Infect Dis. 2019;11:125–6. https://doi.org/10.4103/jgid.jgid_58_18
9. Nogi M, Bankowski MJ, Pien FD. *Wohlfahrtiimonas chitiniclastica* infections in 2 elderly patients, Hawaii, USA. Emerg Infect Dis. 2016;22:567–8. https://doi.org/10.3201/eid2203.151701
10. Katanami Y, Kutsuna S, Nagashima M, Takaya S, Yamamoto K, Takeshita N, et al. *Wohlfahrtiimonas chitiniclastica* bacteremia hospitalized homeless man with squamous cell carcinoma. Emerg Infect Dis. 2018;24:1746–8. https://doi.org/10.3201/eid2409.170080

Address for correspondence: Omar Harfouch, University of Maryland Medical Center, 725 W Lombard St, Baltimore MD 21211, USA; email: oharfouch@som.umaryland.edu

Septic Polyarthritis Caused by *Streptobacillus moniliformis*

Ali Uddin, Tung Phan, Mohamed Yassin

Author affiliation: University of Pittsburgh, Pittsburgh, Pennsylvania, USA

DOI: https://doi.org/10.3201/eid2712.210649

Streptobacillus moniliformis is a pleomorphic, fastidious gram-negative bacillus that colonizes rodent respiratory tracts and causes rat-bite fever in humans. Rat-bite fever is associated with septic arthritis, usually monoarticular or pauciarticular. We report a rare case of polyarticular septic arthritis caused by *S. moniliformis*; the disease was initially misdiagnosed as inflammatory arthritis.

Streptobacillus moniliformis is a pleomorphic, fastidious gram-negative bacillus commonly found in the nasopharynxes of rats and other rodents (*1*). It is transmitted to humans through rat bites, scratches, or ingestion of food or water contaminated with rat feces (*2*), as exemplified by a 1926 outbreak in Haverhill, Massachusetts, USA (*3*). Symptoms usually comprise fever, headache, pharyngitis, myalgia, migratory arthralgia, and vomiting, followed by a maculopapular rash on extensor surfaces. Arthralgia related to reactive polyarthritis develops in ≈50% of patients (*4*). Wang et al. (*5*) reported a well-documented case of septic arthritis and reviewed 11 cases in the literature; 5 of 12 cases had local signs of arthritis but not fever or general sepsis (*5*).

In January 2021, a 59-year-old cleaning woman sought treatment for 3 consecutive days at the emergency department before she was admitted for 2 months of progressively worsening left knee pain. She did not have a rash or fever. Her medical history included ovarian cancer, which was treated surgically 20 years before, and cervical stenosis after C2-T1 fusion. Radiographs of her knee showed mild arthritis; arthrocentesis conducted at the first emergency department visit produced synovial fluid with no organisms visible by Gram staining. The patient was prescribed steroids for inflammatory arthritis, but joint pain and swelling did not improve. At her third visit to the emergency department, she was afebrile and had tender, warm, and swollen knees, wrists, right shoulder, and left ankle; these joints also showed a decreased range of motion (Figure). She did not have a rash or lymphadenopathy. Seven days after admission, a second arthrocentesis produced synovial fluid with 40,000 leukocytes/mL^3, no organisms visible by Gram staining, and no crystals. Other rheumatic results were within reference ranges. On

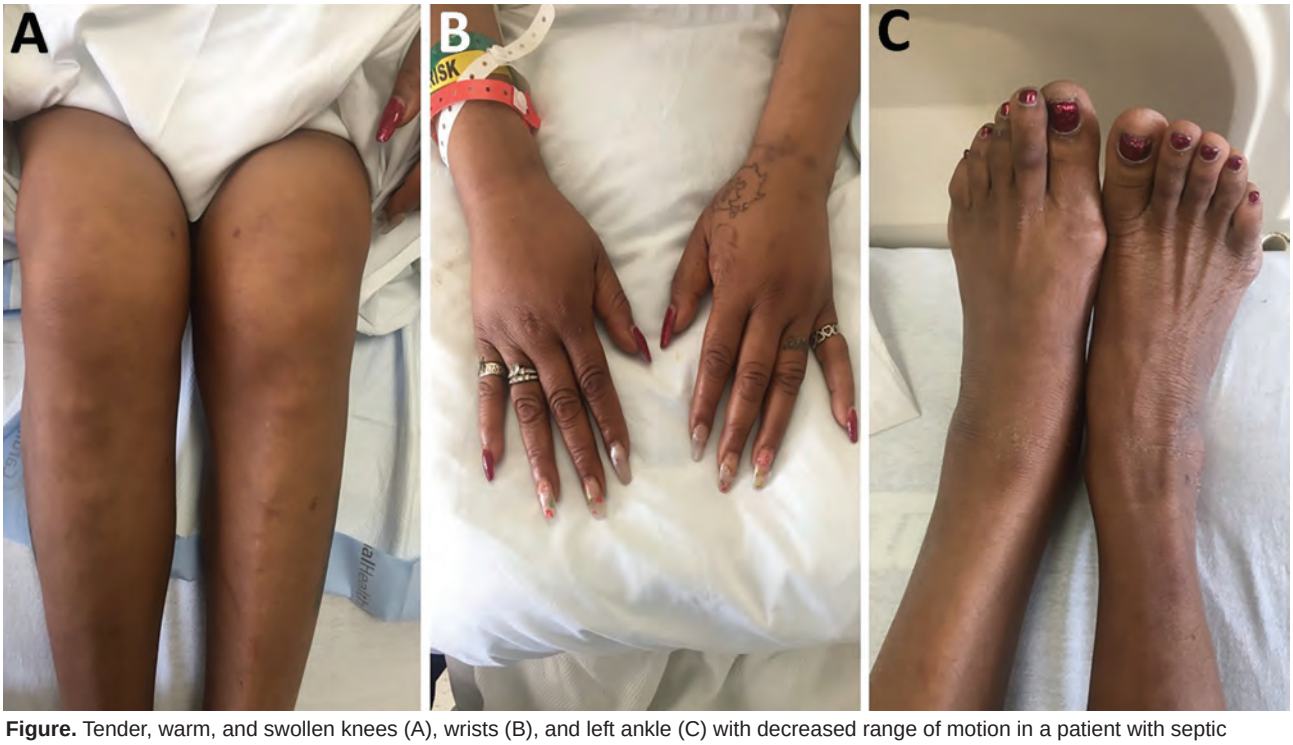

Figure. Tender, warm, and swollen knees (A), wrists (B), and left ankle (C) with decreased range of motion in a patient with septic polyarthritis caused by *Streptobacillus moniliformis* infection, United States.

day 11, tiny colonies grew poorly on sheep blood agar (Appendix Figure, https://wwwnc.cdc.gov/EID/article/27/12/21-0649-App1.pdf). We did not observe growth on chocolate, MacConkey, or Columbia colistin-nalidixic acid agars. Microscopic examination of a Gram-stained smear revealed gram-negative rods with bulbar swellings (Appendix Figure). We used matrix-assisted laser desorption/ionization time-of-flight mass spectrometry to confirm the colonies as *S. moniliformis* (score 2.35); we did not conduct susceptibility testing.

We diagnosed subacute polyarticular septic arthritis, which has a recommended treatment of penicillin G (200,000 units 2×/d for 5–7 days); the alternative option is a 4-week course of ceftriaxone. We stopped steroid treatment and prescribed ceftriaxone because the patient had a severe penicillin allergy. She responded very well to intravenous treatment, and her joint pain and swelling improved remarkably. Two months before symptom onset, she had cleaned a research laboratory housing rats and homes that had mousetraps. She was not aware of any bites or scratches. We obtained informed consent for her participation in this research.

S. moniliformis is the etiologic agent of rat-bite fever, which usually causes fever, rash, and arthralgia. However, this patient and others had polyarticular involvement without fever or rash (*5*,*6*). Previous case reports have described *S. moniliformis* as favoring synovial and serosal surfaces (*7*,*8*).

S. moniliformis is difficult to identify because of its fastidious nature and slow growth on culture; as a result, it is sometimes misdiagnosed as inflammatory arthritis. An informed diagnosis requires raised clinical awareness and attention to patient social history. Arthrocentesis should be conducted in any case of suspected septic arthritis. As shown in this case, matrix-assisted laser desorption/ionization time-of-flight mass spectrometry is a useful tool for diagnosing *S. moniliformis* infection.

Acknowledgment

We thank the staff of the clinical microbiology laboratory at UPMC Mercy for help with initial isolation and characterization of the isolate.

About the Author

Dr. Uddin is a resident in internal medicine at the University of Pittsburgh, Pittsburgh, Pennsylvania, USA. Her research interests include infectious disease.

References

1. Strangeways WI. Rats and carriers of *Streptobacillus moniliformis*. J Pathol Bacteriol. 1933;37:45–51. https://doi.org/10.1002/path.1700370106
2. Centers for Disease Control and Prevention. Fatal rat-bite fever—Florida and Washington, 2003. MMWR Morb Mortal Wkly Rep. 2005;53:1198–202.
3. Place EH, Sutton LE. Erythema arthriticum epidemicum (Haverhill fever). Arch Intern Med (Chic). 1934;54:659–84. https://doi.org/10.1001/archinte.1934.00160170002001
4. Stehle P, Dubuis O, So A, Dudler J. Rat bite fever without fever. Ann Rheum Dis. 2003;62:894–6. https://doi.org/10.1136/ard.62.9.894
5. Wang TK, Wong SS. *Streptobacillus moniliformis* septic arthritis: a clinical entity distinct from rat-bite fever? BMC Infect Dis. 2007;7:56. https://doi.org/10.1186/1471-2334-7-56
6. Dendle C, Woolley IJ, Korman TM. Rat-bite fever septic arthritis: illustrative case and literature review. Eur J Clin Microbiol Infect Dis. 2006;25:791–7. https://doi.org/10.1007/s10096-006-0224-x
7. Rumley RL, Patrone NA, White L. Rat-bite fever as a cause of septic arthritis: a diagnostic dilemma. Ann Rheum Dis. 1987;46:793–5. https://doi.org/10.1136/ard.46.10.793
8. Adams SH, Mahapatra R. Rat bite fever with osteomyelitis and discitis: case report and literature review. BMC Infect Dis. 2021;21:479–86. https://doi.org/10.1186/s12879-021-06172-x

Address for correspondence: Mohamed Yassin, Division of Infectious Diseases, University of Pittsburgh, Pittsburgh, PA 15219, USA; email: yassinm@upmc.edu

Coxiella burnetii in 3 Species of Turtles in the Upper Midwest, United States

William E. Sander, Richard King, William Graser, Joshua M. Kapfer, Aubrey I. Engel, Laura Adamovicz, Matthew C. Allender

Author affiliations: University of Illinois Urbana–Champaign, Urbana, Illinois, USA (W. E. Sander, A.I. Engel, L. Adamovicz, M.C. Allender); Northern Illinois University, DeKalb, Illinois, USA (R. King); Kane County Forest Preserve, Geneva, Illinois, USA (W. Graser); University of Wisconsin–Whitewater, Whitewater, Wisconsin, USA (J.M. Kapfer)

DOI: https://10.3201/eid/2712.211278

Coxiella burnetii, the causative bacterium of the zoonotic disease Q fever, has been documented in many different species. We describe documented turtles that were PCR positive for *C. burnetii* from multiple locations in Illinois and Wisconsin, USA. Assessing the conservation implications, reservoir potential, and zoonotic risk requires further research.

Two studies have identified *Coxiella burnetii* in poikilotherms (vertebrates that cannot regulate body temperature physiologically); both studies originated in India. Two tortoises had antibodies to *C. burnetii* by capillary agglutination testing of their serum samples in Uttar Pradesh (*1*). Additional reptiles, including snakes and skinks, had serum samples positive for *C. burnetii* in a separate study in Karnataka (*2*). Although both studies are useful in clarifying how this bacterium might interface with reptiles, there is no other evidence to support the role played by this large class of vertebrates (*3*). Furthermore, serologic assays applied to species that they were not designed for are difficult to interpret (Appendix, https://wwwnc.cdc.gov/EID/article/27/12/21-1278-App1.pdf).

Serologic testing, typically using indirect immunofluorescence assay, is the primary method used to diagnose *C. burnetii* infection, which causes Q fever in humans and coxiellosis in domestic ruminants (*4*). Additional serologic testing includes complement fixation and ELISA (*5*). Serologic assay benefits include commercial availability and insights into acute, treated, and chronic patients, depending on titers (*6*). Several PCR-based assays have been developed for detection of *C. burnetii* in samples from nontraditional mammals, birds, and arthropods (*7*). PCR provides a simple and reliable method for detection of the bacterium even retrospectively from tissues (*6*). Therefore, we tested turtles from multiple locations in Illinois and Wisconsin, USA, for *C. burnetii*.

This study was approved by the institutional animal care and use committees of the University of Illinois (20258), Northern Illinois University (LA16–0016), and University of Wisconsin–Whitewater (K145011020Q). The Wildlife Epidemiology Laboratory, based at the University of Illinois College of Veterinary Medicine, continually conducts long-term, prospective health assessments of several turtle species across Illinois and neighboring states in natural habitats. Reptiles can be an excellent proxy for the health of environments, and many turtle species have small home ranges with diverse diets reflecting local conditions (*8*).

As part of these annual surveys, turtle species collected have various morphometric data, blood samples, or oral and cloacal swab specimens obtained before being released. Several diagnostic tests are performed with these samples, such as PCR screening for several pathogens, including *C. burnetii*. Other pathogenic organisms include *Ambystoma tigrinum* virus, Bohle iridovirus, Terrapene herpesvirus 1, Terrapene herpesvirus 2, epizootic hematopoietic necrosis virus, *Emydomyces testavorans*, frog virus 3, Emydid herpesvirus 1, Emydoidea herpesvirus 1 (in Blanding's turtles), *Mycoplasma agassizii*, *M. testudineum*, *Salmonella* spp., and Testudinid herpesvirus 2 (*9*).

We extracted DNA from frozen, combined oral/cloacal swab specimens from each turtle by using the DNA Blood Mini Kit (QIAGEN, https://www.qiagen.com). We assessed spectrophotometrically DNA concentration and purity by using NanoDrop 1000 (Thermo Fisher Scientific Inc., https://www.thermofisher.com). We performed quantitative PCR by using a QuantStudio3 Real Time PCR System (Applied Biosystems, https://www.thermofisher.com) and a TaqMan primer–probe assay targeting the *C. burnetti icd* gene as described (*10*).

We assayed all samples, standards, and nontemplate controls in triplicate and quantified positive samples by using a 7-point standard curve (10^1–10^7 target copies). Samples were considered positive if all 3 replicates had a lower cycle threshold value than the lowest detected standard dilution. We used a highly sensitive and specific quantitative PCR for *C. burnetti.*

During 2019, samples from 5/605 turtles encountered across 8 counties showed positive results for quantitative PCRs, indicating presence of *C. burnetii* (Figure). We collected positive samples from 3 Blanding's turtles (*Emydoidea blandingii*), 1 painted turtle (*Chrysemys picta*), and 1 ornate box turtle (*Terrapene ornata*). These positive turtles were found in Kane and Lee Counties in Illinois and Sauk County in Wisconsin. We did not perform serologic analysis for these animals. One Blanding's turtle had a microchip and transmitter, was sampled again during 2020, and showed a negative PCR result. All of these turtles were found within a 1-hour drive to the Illinois–Wisconsin state border within protected preserves. However, the 3 locations in which the 5 turtles varied in proximity to farms, livestock, industry, residential areas, and major highways; we found no geographic associations. All other screening tests showed negative results for pathogenic organisms for these 5 animals.

C. burnetii is a ubiquitous bacterium that has been found in many different species, often

without pathogenicity (*4*). A variety of species of turtles are sampled annually in Illinois and surrounding areas through the Wildlife Epidemiology Laboratory. Over time, the testing for various organisms has expanded, especially as additional tests are validated. Screening for the bacterium that causes Q fever has been conducted for many species but infrequently in poikilotherms. These results show that the bacteria can be detected in these species and should be further researched to understand additional sources of this reportable disease, including potential management or regulatory decisions.

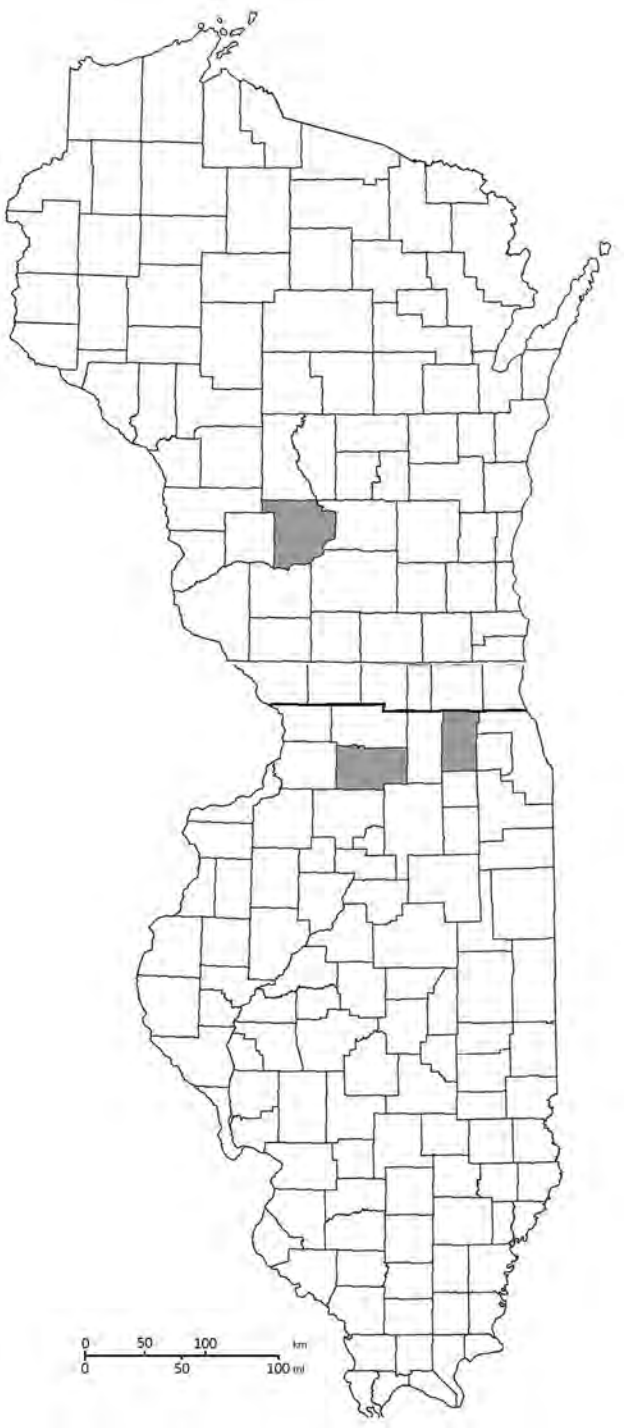

Figure. Location (gray areas) of turtles PCR positive for *Coxiella burnetii*, by county, Wisconsin (top) and Illinois (bottom), USA.

Continued investigation and screening in poikilotherms for zoonotic pathogens should be prioritized to understand the potential risk from additional hosts. The pet trade is a potential avenue of risk for exposure between humans and turtles. As these pathogens of concern are better characterized, the implications of different and varied hosts will drive the need for continued One Health research and dialogue between environmental, animal, and human health professionals.

Acknowledgments

We thank the students and employees of the Wildlife Epidemiology Laboratory at the University of Illinois College of Veterinary Medicine for providing assistance; and Joseph Mozuch, Jarod Lorenz, Jacquelyn Kincanon, and Kari Rebman for providing assistance with the Wisconsin fieldwork.

This study was supported by the State of Illinois (Wildlife grants (T-104-R-2 and T-111-R-1). Support for the Wisconsin fieldwork was provided by a donation to The Nature Conservancy by the family of Orie and Elinor Loucks.

About the Author

Dr. Sander is an assistant professor of preventive medicine and public health and director of the DVM/MPH joint degree program in the Department of Veterinary Clinical Medicine, University of Illinois College of Veterinary Medicine, Urbana, IL. His primary research interest is One Health approaches, including the interface of infectious disease and toxicities between humans and animals both domestically and internationally.

References

1. Yadav MP, Sethi MS. Poikilotherms as reservoirs of Q-fever (*Coxiella burnetii*) in Uttar Pradesh. J Wildl Dis. 1979;15:15–7. https://doi.org/10.7589/0090-3558-15.1.15
2. Stephen S, Rao KN. Coxiellosis in reptiles of South Kanara district, Karnataka. Indian J Med Res. 1979;70:937–41.
3. Marschang RE. Clinical virology. In: Mader DR, Divers JJ. Current therapy in reptile medicine and surgery. New York: Elsevier Inc.; 2013. p. 32–52.
4. Tissot-Dupont H, Raoult D. Q fever. Infect Dis Clin North Am. 2008;22:505–14, ix. https://doi.org/10.1016/j.idc.2008.03.002

5. Eldin C, Mélenotte C, Mediannikov O, Ghigo E, Million M, Edouard S, et al. From Q fever to *Coxiella burnetii* infection: a paradigm change. Clin Microbiol Rev. 2017;30:115–90. https://doi.org/10.1128/CMR.00045-16
6. Fournier P-E, Marrie TJ, Raoult D. Diagnosis of Q fever. J Clin Microbiol. 1998;36:1823–34. https://doi.org/10.1128/JCM.36.7.1823-1834.1998
7. Sahu R, Rawool DB, Vinod VK, Malik SV, Barbuddhe SB. Current approaches for the detection of *Coxiella burnetii* infection in humans and animals. J Microbiol Methods. 2020;179:106087. https://doi.org/10.1016/j.mimet.2020.106087
8. Way Rose BM, Allender MC. Health assessment of wild eastern box turtles (*Terrapene carolina carolina*) in east Tennessee. J Herpetological Med Surg. 2011;21:107. https://doi.org/10.5818/1529-9651-21.4.107
9. Archer GA, Phillips CA, Adamovicz L, Band M, Byrd J, Allender MC. Detection of copathogens in free-ranging eastern box turtles (*Terrapene carolina carolina*) in Illinois and Tennessee. J Zoo Wildl Med. 2017;48:1127–34. https://doi.org/10.1638/2017-0148R.1
10. Klee SR, Tyczka J, Ellerbrok H, Franz T, Linke S, Baljer G, et al. Highly sensitive real-time PCR for specific detection and quantification of *Coxiella burnetii*. BMC Microbiol. 2006;6:2. https://doi.org/10.1186/1471-2180-6-2

Address for correspondence: William E. Sander, Department of Veterinary Clinical Medicine, University of Illinois at Urbana–Champaign, 1008 W Hazelwood Dr, Urbana, IL 61801-3028, USA; email: wsander@illinois.edu

Reassortant Influenza A(H1N1)pdm09 Virus in Elderly Woman, Denmark, January 2021

Jakob N. Nissen, Sophie J. George, Charlotte K. Hjulsager, Jesper S. Krog, Xiaohui C. Nielsen, Tina V. Madsen, Klara M. Andersen, Tyra G. Krause, Lasse S. Vestergaard, Lars E. Larsen, Ramona Trebbien

Author affiliations: Statens Serum Institut, Copenhagen, Denmark (J.N. Nissen, C.K. Hjulsager, J.S. Krog, K.M. Andersen, T.G. Kause, L.S. Vestergaard, R. Trebbien); University of Copenhagen, Copenhagen (S.J. George, L.E. Larsen); Zealand University Hospital, Koege, Denmark (X.C. Nielsen, T.V. Madsen)

DOI: https://doi.org/10.3201/eid2712.211361

A case of human infection with influenza A(H1N1)pdm09 virus containing a nonstructural gene highly similar to Eurasian avian-like H1Nx swine influenza virus was detected in Denmark in January 2021. We describe the clinical case and report testing results of the genetic and antigenic characterizations of the virus.

Human infection with swine influenza A virus (IAV) had not previously been detected in Denmark, but sporadic cases have been reported from other countries (*1*). We report the identification of a case of zoonotic swine influenza infection in Denmark during a low-activity influenza season.

The variant IAV was detected by the National Influenza Center at Statens Serum Institut (Copenhagen, Denmark), as part of routine surveillance. A sputum sample was collected on January 21, 2021, in Zealand, Denmark, from a female patient in her 70s with various concurrent conditions, including a chronic respiratory disease, who was admitted to hospital after 2 days of moderate influenza-like symptoms: fever (39°C), coughing, sore throat, and difficulty breathing. The patient sample was positive for IAV in analyses at the local hospital microbiology laboratory; remaining sample material was submitted to the National Influenza Center, which confirmed it positive for influenza A(H1N1)pdm09 (Appendix, https://wwwnc.cdc.gov/EID/article/27/12/21-1361-App1.pdf).

We performed whole genome sequencing on the virus (*2*), and named it A/Denmark/1/2021 (vH1N1), and submitted to GISAID (https://www.gisaid.org; accession no. EPI_ISL_909652). BLAST (https://blast.ncbi.nlm.nih.gov/Blast.cgi) and phylogenetic analyses revealed that all segments except the nonstructural gene belonged to influenza A(H1N1)pdm09 clade 1A3.3.2 (*3*), which is most similar (97%–98% nt identity) to viruses collected from swine in France and Germany in 2014 and 2015 (Table; Figure). The nonstructural gene was most similar (95%) to Eurasian avian-like H1Nx swine viruses of clade 1C. No segments had a near-exact match to sequences in GenBank or GISAID, and all were distinct from the seasonal vaccine strain, A/Guangdong-Maonan/SWL1536/2019 (Table).

Because of the suspected swine origin of the case virus, we used whole-genome sequencing to retrospectively analyze 68 IAVs with a hemagglutinin (HA) gene belonging to clade 1A.3.3.2 sampled from swine herds in Denmark during 2020–2021. Nine of the samples, collected April 2020–January 2021 from ≥7 different herds in different parts of Denmark, including Zealand, contained the same

Table. Percentage identity similarity between gene and protein segments of influenza virus isolate A/Denmark/1/2021 (vH1N1) from a patient in Denmark and reference viruses from GISAID*

A/Denmark/1/2021 (vH1N1) segment	Identity, %			
	A/swine/Luedinghausen/ 21728/2015†	A/California/07/2009‡	A/Guangdong-Maonan/SWL1536/2019¶	A/swine/Denmark/ 3797–4/2020§
Amino acid				
PB2	98.7	97.5	97.6	100
PB1	99.5	99.3	98.7	99.9
PA	98.9	98.0	98.3	99.6
PA-X	98.7	97.4	97.0	99.6
HA	97.3	92.0	91.9	99.3
NP	99.0	99.0	98.2	100
NA	97.9	95.1	91.9	99.8
M1	98.8	98.4	97.6	100
M2	96.9	96.9	93.8	100
NS1	76.5	77.4	74.7	99.5
NEP	85.1	86.0	85.1	99.2
Nucleotide				
PB2	98.0	96.1	94.7	99.8
PB1	96.8	95.9	93.8	99.2
PA	98.0	96.7	95.4	99.4
HA	97.3	94.4	93.0	99.4
NP	97.4	96.4	94.5	99.4
NA	97.4	96.1	93.7	99.5
MP	97.8	97.4	95.9	99.9
NS	80.2	80.3	80.3	99.8

*GISIAD, https://www.gisaid.org. PB1/PB2, polymerase basic protein 1/2; PA, polymerase acidic protein; HA, hemagglutinin; NP, nucleoprotein; NA, neuraminidase; MP/M1/M2, matrix protein 1/2, NS/NS1; nonstructural protein; NEP, nuclear export protein
†GISAID accession no. EPI_ISL_504870.
‡GISAID accession no EPI_ISL_227813.
¶GISAID accession no. EPI_ISL_377080.
§GISAID accession no. EPI_ISL_1673668.

gene constellation as the case virus (98.9%–99.4% nt identity). This finding suggests that the virus from the human case originated from swine in Denmark.

The patient and her husband reside in the countryside, <2 km from a medium-sized farm with finisher pigs. Because of coronavirus disease pandemic restrictions, she had not been in close contact with other persons or been close to the pig farm. Both the patient and her husband, who had no signs of illness, were vaccinated against seasonal influenza in October or November 2020. European General Data Protection Regulation (https://gdpr.eu) restrictions on reporting personally identifiable information prevent revealing additional information about the patient or the farm.

Veterinary authorities in Denmark collected nose swab samples from 68 pigs at the neighboring farm on February 1, 2021, according to standard procedures. All samples tested negative by PCR for IAV. Because of the high prevalence of influenza-positive herds in Denmark, we could not be confident potential seropositive swine were infected by the virus in question, so we did not take blood samples. However, we therefore could not exclude previous virus circulation in the herd, because swabs were taken 11 days after virus detection in the patient. According to the Danish Meteorological Institute, the patient's residence was downwind of the pig herd most days preceding clinical symptoms.

Most of the case virus genes were derived from influenza A(H1N1)pdm09, which has been circulating in the human population of Denmark since 2009. However, the HA gene is different from that of the strains currently circulating (*4*), and it is therefore difficult to predict the level of immunity in the human population against this virus. Antigenic characterization (*5*) showed no or very poor cross-reactivity to all reference antiserum used for analysis (Appendix Table 1), and the HA gene contained several more mutations at antigenic sites compared with the seasonal vaccine strain (Appendix Figure). Therefore, vaccine effectiveness of the 2020–2021 seasonal influenza vaccine against the variant virus has been assessed as low.

Neuraminidase inhibition tests showed no reduction of oseltamivir or zanamivir inhibition, and the viral genome contains no known antiviral mutations except the V27A mutation in the M2 gene, known from most other H1N1 viruses circulating in human and swine (*6*,*7*). We identified no amino acid changes presumed to be related to increased risk of human infection (*8*), but further in vitro and in vivo analyses are planned to explore this possibility.

Because national coronavirus disease pandemic restrictions limited interpersonal contact, there

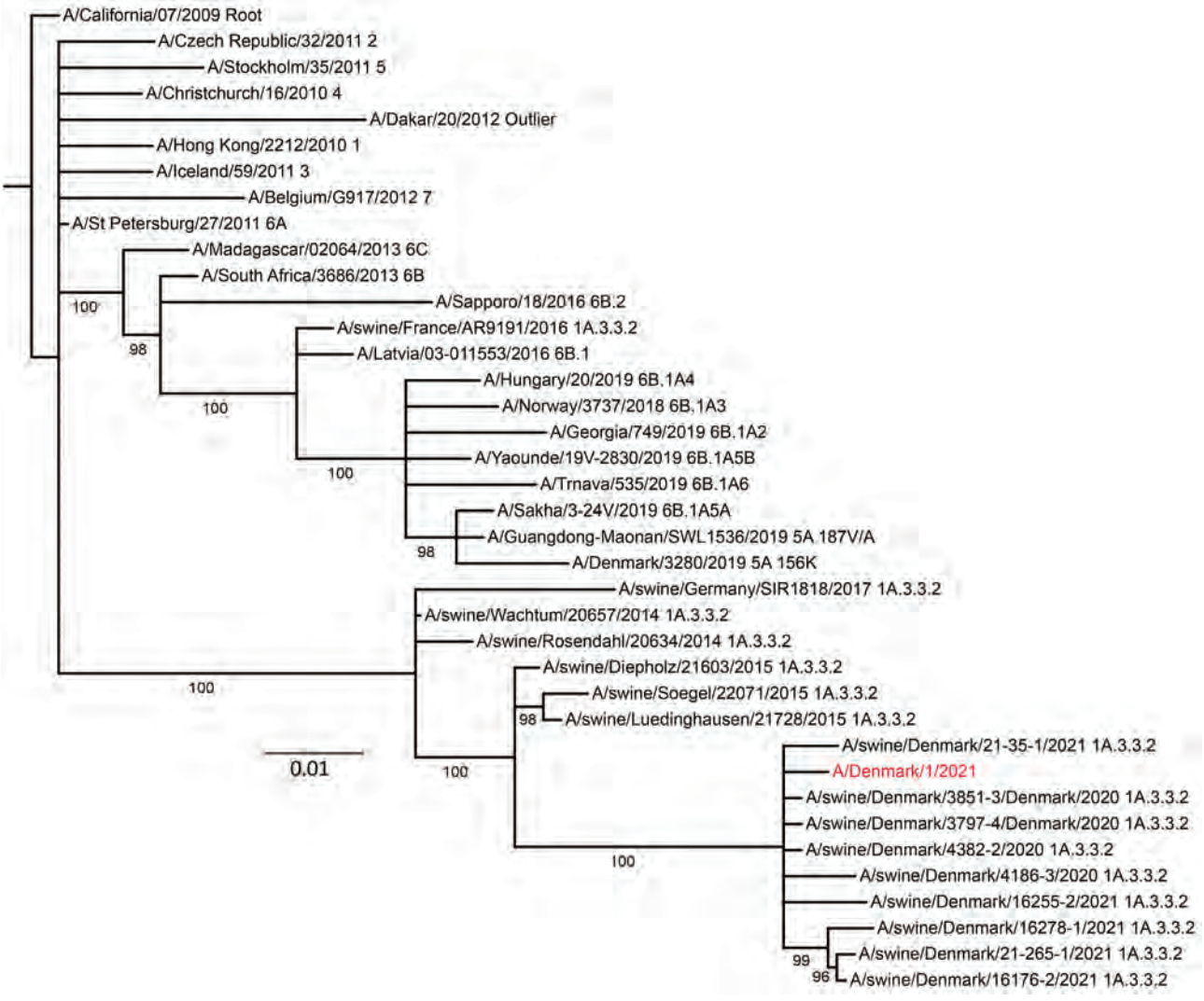

Figure. Maximum-likelihood phylogenetic tree of the hemagglutinin gene of influenza virus isolate A/Denmark/1/2021 (vH1N1) from a patient in Denmark (red) and reference viruses. The tree includes closest BLAST matches (https://blast.ncbi.nlm.nih.gov/Blast.cgi), the Denmark swine influenza virus with highest similarity to the case variant virus A/Denmark/1/2021 (indicated in red), and human seasonal reference viruses and is rooted on A/California/07/2009. Leaves are labeled by isolate name and clade designation. Branch labels indicate UFBoot2 bootstrap values. All uncertain branches (bootstrap <95%) have been removed. Scale bar indicates nucleotide substitutions per site.

were only 46 confirmed influenza cases in Denmark during the 2020–2021 season, and transmission of the variant virus was considered negligible. The Danish Patient Authority did not identify any person-to-person swine influenza transmission, and no further public health response measures were enacted.

The effects of the most recent swine influenza pandemic and the extensive diversity and reassortment in swine influenza viruses indicate the obvious zoonotic potential of these viruses (*9*,*10*). Therefore, more attention should be given to routine detection and control of swine influenza viruses.

Acknowledgments

We thank laboratory technicians Mille Weissman Poulsen, Carina Bøgh Folsing, Jesper Rønn, Sari Mia Dose, and Sophia Rasmussen for technical assistance in the laboratory.

This work was conducted as part of the national influenza surveillance in Denmark, which is funded by the government.

About the Author

Dr. Nissen is a postdoctoral researcher at the National Influenza Center, Statens Serum Institut, Copenhagen,

Denmark. With a background in genomics and bioinformatics, he focuses on bioinformatic tool development and the prediction of the zoonotic potential of influenza viruses.

References

1. Dürrwald R, Wedde M, Biere B, Oh D-Y, Heßler-Klee M, Geidel C, et al. Zoonotic infection with swine A/H1$_{av}$N1 influenza virus in a child, Germany, June 2020. Euro Surveill. 2020;25:2001638. https://doi.org/10.2807/1560-7917.ES.2020.25.42.2001638
2. Trebbien R, Pedersen SS, Vorborg K, Franck KT, Fischer TK. Development of oseltamivir and zanamivir resistance in influenza A(H1N1)pdm09 virus, Denmark, 2014. Euro Surveill. 2017;22:30445. https://doi.org/10.2807/1560-7917.ES.2017.22.3.30445
3. Anderson TK, Macken CA, Lewis NS, Scheuermann RH, Van Reeth K, Brown IH, et al. A phylogeny-based global nomenclature system and automated annotation tool for H1 hemagglutinin genes from swine influenza A viruses. MSphere. 2016;1:e00275–16. https://doi.org/10.1128/mSphere.00275-16
4. Melidou A, Pereyaslov D, Hungnes O, Prosenc K, Alm E, Adlhoch C, et al.; WHO European Region influenza surveillance network; WHO European Region Influenza Surveillance Network author list. Virological surveillance of influenza viruses in the WHO European Region in 2019/20—impact of the COVID-19 pandemic. Euro Surveill. 2020;25:2001822. https://doi.org/10.2807/1560-7917.ES.2020.25.46.2001822
5. World Health Organization Global Influenza Surveillance Network. Manual for the laboratory diagnosis and virological surveillance of influenza. Geneva: The Organization; 2011.
6. Krumbholz A, Schmidtke M, Bergmann S, Motzke S, Bauer K, Stech J, et al. High prevalence of amantadine resistance among circulating European porcine influenza A viruses. J Gen Virol. 2009;90:900–8. https://doi.org/10.1099/vir.2008.007260-0
7. Dong G, Peng C, Luo J, Wang C, Han L, Wu B, et al. Adamantane-resistant influenza a viruses in the world (1902–2013): frequency and distribution of M2 gene mutations. PLoS One. 2015;10:e0119115. https://doi.org/10.1371/journal.pone.0119115
8. GISAID. FluServer: real-time surveillance of influenza mutations [cited 2021 Mar 29]. https://flusurver.bii.a-star.edu.sg
9. Neumann G, Noda T, Kawaoka Y. Emergence and pandemic potential of swine-origin H1N1 influenza virus. Nature. 2009;459:931–9. https://doi.org/10.1038/nature08157
10. Henritzi D, Petric PP, Lewis NS, Graaf A, Pessia A, Starick E, et al. Surveillance of European domestic pig populations identifies an emerging reservoir of potentially zoonotic swine influenza A viruses. Cell Host Microbe. 2020;28:614–627.e6. https://doi.org/10.1016/j.chom.2020.07.006

Address for correspondence: Ramona Trebbien, Statens Serum Institut, Artillerivej 5, 2300 Copenhagen S, Denmark; email: ratr@ssi.dk

Correction: Vol. 27, No. 10

The name of author Xiaohui Wang was misspelled in *Emergomyces orientalis* Emergomycosis Diagnosed by Metagenomic Next-Generation Sequencing (D. He et al.). The article has been corrected online (https://wwwnc.cdc.gov/eid/article/27/10/21-0769_article).

Modern Epidemics: From the Spanish Flu to COVID-19

Salvador Macip; translated from Catalan by Julie Wark; Polity Press, Medford, Massachusetts, USA, 2020; Hardcover ISBN-10: 1509546561; ISBN-13: 978-1509546565; Pages: 288; Price: US $63.91

DOI: https://doi.org/10.3201/eid2712.211312

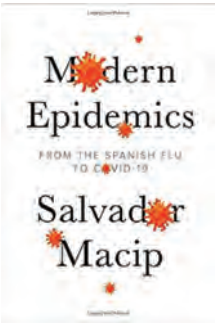

In Modern Epidemics: From the Spanish Flu to COVID-19, Salvador Macip presents an ambitiously comprehensive overview of human diseases. This updated version, translated into English by Julie Wark, provides an accessible introduction to the microbes that cause harm, the science behind treatment and prevention, and the challenges to successful disease control. The book begins, appropriately, with how bacteria have enabled humans to evolve and persist and then pivots to pathogenic microbes.

Modern Epidemics is written with lay readers in mind, so diseases are grouped by relevance to humans—for instance microbes with bioterrorist potential—rather than by pathogen relatedness. Macip guides readers through tools for prevention and treatment, and current knowledge for neglected and emerging diseases, including coronaviruses.

Unsurprisingly, coronavirus disease (COVID-19) information has become rapidly outdated, including the death toll, but that chapter maintains relevance as a time capsule of the early pandemic. Some uncertainties Macip relates also have been resolved; for instance, the promise of the Moderna vaccine has been borne out. Still, some uncertainties remain, such as whether COVID-19 will persist as a seasonal disease, like influenza or a mild cold-like illness, or as isolated outbreaks, damaging but limited in scope.

Macip describes the impossibility of predicting future pandemics, which could emerge from diverse microbes or, as he states, "a supervirus that doesn't even exist yet," but I suspect such predictions could become possible. Understanding why pathogens evolve to cause harm represents a major focus in evolutionary biology. Indeed, recent research investigates why pathogens evolve transmission before symptoms (*1*), a trait responsible for considerable COVID-19 spread. This perspective narrows the possibilities by examining whether harmful traits are unlikely to emerge or simply have not evolved yet (*2*). Macip instead addresses the more immediate question of how to plan for the worst and incorporate data as it becomes available.

Modern Epidemics ends with an overview of major ongoing epidemics, including influenza, HIV, tuberculosis, and malaria. Macip explains the mechanics of producing influenza vaccines, including why producing vaccines against certain strains can be difficult; the surprising reason is that some viruses replicate agonizingly slowly inside chicken eggs. Despite impressive scientific gains, these epidemics continue to impose an enormous health burden; discussing them last underscores the substantial challenges that remain even after the COVID-19 pandemic.

Throughout Modern Epidemics, Macip avoids idolizing preeminent scientists, past and present. For example, he points out that immunization had precedent in other cultures long before it was supposedly discovered by Edward Jenner. Crucially, Macip's narrative continues beyond the scientific discovery of effective treatments or preventative measures to outline the enormous political and economic barriers that persist despite scientific advances. Unfortunately, the comprehensiveness of Modern Epidemics precludes in-depth exploration of fascinating topics that arise during these narratives, such as the use of disease as a weapon of colonization and the economics of sustaining disease control. Nonetheless, Modern Epidemics serves as a broad-ranging introduction to the history, biology, and sociology of infectious diseases and will be useful to readers wishing to rapidly gain a sense of the field.

References

1. Saad-Roy CM, Wingreen NS, Levin SA, Grenfell BT. Dynamics in a simple evolutionary-epidemiological model for the evolution of an initial asymptomatic infection stage. Proc Natl Acad Sci U S A. 2020;117:11541–50. https://doi.org/10.1073/pnas.1920761117
2. Day T, Mideo N, Alizon S. Why is HIV not vector-borne? Evol Appl. 2008;1:17–27. https://doi.org/10.1111/j.1752-4571.2007.00014.x

Megan A. Greischar

Author affiliation: Cornell University, Ithaca, New York, USA

Address for correspondence: Megan A. Greischar, Cornell University, E315 Corson Hall, 215 Tower Rd, Ithaca, NY 14853, USA; email: megan.greischar@cornell.edu

Prepare and Protect: Safer Behaviors in Laboratories and Clinical Containment Settings

Sean G. Kaufman; ASM Press, Washington, DC, USA; and Wiley, Hoboken, NJ, USA, 2020; ISBN: 9781683670148 (hardcover); ISBN: 9781683673569 (e-book); Pages: 272; Price: $130.00 (hardcover); $104.00 (e-book)

DOI: https://doi.org/10.3201/eid2712.211866

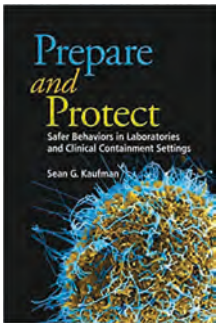

In the business of space exploration, it is said that the best spacecraft is the one that is on the rocket. Similarly, the best standard operating procedure is the one that produces the desired outcome and can be, and is, followed. By applying universal human behaviors and making safety engaging, in Prepare and Protect: Safer Behaviors in Laboratories and Clinical Containment Settings, the author, Sean G. Kaufman, encourages the reader to think about and promote biosafety in new, significant ways.

Kaufman speaks to his readers in an approachable manner, taking us on an honest journey on which he asks us to rethink many preconceived ideas about what truly makes us safe or unsafe in the laboratory. Breaking down near misses, accidents, and disasters into their most basic components to see where things went wrong and why, Kaufman helps the reader begin to see patterns emerge. Memorable lessons include the impact of safety culture, the importance of meaningful risk assessment, human risk factors, and the ways biosafety professionals can best serve their programs.

The book begins with basic biosafety principles such as containment, risk mitigation, and the primary controls of safety, always presented with interesting and important discussion and nuance. For example, the author presents a proposal for clinical containment levels, thoughts on risk assessment as a living process, and the concept that it is critical to teach the workforce why they are asked to do something. We are also introduced to the intriguing subject of human risk factors, where we discover how our mental, physical, and emotional states, capabilities, institutional culture, and experiences all affect safety when working in the laboratory. This chapter is a pleasure, highlighted by stories about behavioral evolution and the dangers of appealing to authority.

With the same unique insight and fresh approaches, later chapters consider effective plans, emergency preparedness and response, and standard operating procedures to address these challenges. We also read about the critical impact on safety culture of accountable leadership. One important contribution of note is that personal protective equipment must be matched with a corresponding and effective standard operating procedure for doffing, exemplified by the beaking method of glove removal. Some chapters could possibly have been reordered or combined to feel more intuitive, but their conciseness makes each topic easier to process. First-person narratives included are often compelling and give insight into personal journeys of biosafety practitioners, complementing didactic content with real-world experience and insight.

The ongoing pandemic illustrates how the lessons in this book apply far beyond the lab, underscoring the extent to which we all contribute to biosafety. Aspiring, new, and experienced biosafety practitioners will enjoy this timely, informative, and engaging journey, one that can lead us to safer labs and better health for all. Above all, Kaufman reminds us to treat each other with kindness, respect, and dignity in our journeys towards safer outcomes.

Kristy Jennings, Christopher E. Carr

Author affiliation: Georgia Institute of Technology, Atlanta, Georgia, USA

Address for correspondence: Kristy Jennings, Georgia Institute of Technology, Environmental Health and Safety, 793 Marietta St, Atlanta, GA 30318, USA; email: kristy.jennings@ehs.gatech.edu

Franz Marc (1880–1916), *The Tiger* (detail), 1912. Oil on canvas. 43.9 in x 40.0 in/111.7 cm x 101.8 cm. Städtische Galerie im Lenbachhaus and Kunstbau, Munich, Germany. Image source: Art Resource, New York, New York, USA.

"It Is a Tiger That Devours Me, But I Am the Tiger"

Byron Breedlove

On March 11, 2020, the World Health Organization declared COVID-19 to be a pandemic. Shortly thereafter, reports of animals becoming infected with SARS-CoV-2 appeared. Although the pandemic is being driven by person-to-person transmission, transmission from people to animals of multiple species has been documented. According to the Centers for Disease Control and Prevention, the animals known to have been infected with SARS-CoV-2 include otters, mink, white-tailed deer, dogs, ferrets, and felids, including domestic cats, lions, pumas, and tigers.

An April 2020 US Department of Agriculture statement concerning a New York zoo's lions and tigers showing clinical signs of respiratory illness was among the earliest such reports. Diagnostic samples taken from one tiger confirmed infection with SARS-CoV-2, and public health officials postulated that the source was exposure to a zoo employee positive for the virus. Stories about captive great cats with clinical signs of respiratory illness testing positive for SARS-CoV-2 have continued generating headlines from diverse locations around the globe.

Reports of animals becoming infected with SARS-CoV-2 through contact with humans may be in the spotlight, but humans are also disease vectors for numerous other pathogens. A 2014 literature review in *PLoS One* documents myriad cases in which humans transmitted influenza A virus, *Mycobacterium tuberculosis*, methicillin-resistant *Staphylococcus aureus,* and other pathogens to animals and stated

Author affiliation: Centers for Disease Control and Prevention, Atlanta, Georgia, USA

DOI: https://doi.org10.3201/eid2712.AC2712

that "transmission occurred in every continent except Antarctica therefore indicating a worldwide disease threat." A report by Iatta et al. in the *International Journal for Parasitology: Parasites and Wildlife* states, "Infectious diseases by pathogens, including those of zoonotic concern, may act as a primary or contributory cause of threat to wildlife conservation and may represent a risk for human health, mainly for people working at, or visiting the zoological parks."

That message is underscored by accounts of captive great cats becoming infected with SARS-CoV-2. More tigers now live in captivity than in their natural habitats, putting them at potential risk of acquiring infections from people. Actions that are based on One Health and that recognize that the health of humans, animals, and the environment is closely connected will be increasingly important for ensuring the survival of animals of keystone species, such as tigers, as well as in helping to disrupt the cycle of transmission for zoonotic pathogens, and in increasing understanding of One Health issues across disciplines and sectors.

This month's cover image, *The Tiger*, is by German Expressionist artist Franz Marc. He was the son of a landscape painter, and he studied at the Academy of Fine Arts, Munich. In 1903 and 1907, he traveled to Paris, where he learned about Japanese woodcuts and the art of the Impressionists, Cubists, and Expressionists. Marc, along with Russian artist Wassily Kandinsky, founded the avant-garde group *Der Blaue Reiter* (*The Blue Rider*). Many of Marc's works completed during his short life—he was killed during combat in World War I—vividly depict animals. The Brooklyn Museum notes that he "cultivated a dynamic Expressionist style that used rhythmic patterns of color and line to evoke movement." In Marc's own words, he wanted to "achieve a pantheistic empathy with the throbbing and racing of the blood in nature, in trees, in animals, in the air."

The Lenbachhaus Museum, which houses the painting, notes that the "almost square image format is dominated by the mighty, crouching form of a tiger, which, with angular outlines as if carved out of stone, turns its beautifully shaped head back in a bold swing." Marc used interlocking, bold blocks to form the tiger's yellow and black body. The tiger's diamond shaped eyes transfix the viewer. The landscape surrounding the tiger comprises angular, cubic forms that Marc imbues with rich, glowing shades of red, green, violet, and orange. The image bristles with tension and energy, as though its fractured components could suddenly coalesce and lunge snarling from the canvas.

The Lenbachhaus offers additional insight into Marc's tiger: "The facets of his glowing yellow body join with the transparent, cubic formations of his surroundings to form an indissoluble unit in which there is no longer any distinction between organic and inorganic substances." The viewer, captivated, gains some knowledge of the tiger's perspective, perhaps feeling both discomfort and connection. Argentine writer Jorge Luis Borges concludes his mid-1940s essay, "A New Refutation of Time," with the following lines that both evoke the One Health perspective on the interconnectedness of humans, animals, and nature and that, in recalling Marc's notion of pantheistic empathy, could serve as a caption for The Tiger: "Time is the substance from which I am made. Time is a river which carries me along, but I am the river; it is a tiger that devours me, but I am the tiger; it is a fire that consumes me, but I am the fire."

Bibliography

1. Borges JL. A new refutation of time. Labyrinths: selected stories and other writings. New York: New Directions Publishing Company; 1964. p. 234.
2. Brooklyn Museum. Tiger: Franz Marc [cited 2021 Oct 5]. https://www.brooklynmuseum.org/opencollection/objects/65730
3. Centers for Disease Control and Prevention. Animals and COVID-19 [cited 2021 Oct 10]. https://www.cdc.gov/coronavirus/2019-ncov/daily-life-coping/animals.html
4. Centers for Disease Control and Prevention. Zoonotic diseases [cited 2021 Oct 10]. https://www.cdc.gov/onehealth/basics/zoonotic-diseases.html
5. Iatta R, Natale A, Ravagnan S, Mendoza-Roldan J, Zatelli A, Cavalera MA, et al. Zoonotic and vector-borne pathogens in tigers from a wildlife safari park, Italy. Int J Parasitol Parasites Wildl. 2020;12:1–7 [cited 2021 Nov 18]. https://doi.org/10.1016/j.ijppaw.2020.03.006
6. Lenbachhaus Museum. Tiger [cited 2021 Oct 8]. https://www.lenbachhaus.de/entdecken/sammlung-online/detail/tiger-30019617
7. McAloose D, Laverack M, Wang L, Killian ML, Caserta LC, Yuan F, et al. From people to *Panthera*: natural SARS-CoV-2 infection in tigers and lions at the Bronx Zoo. MBio. 2020;11:e02220–20. https://doi.org/10.1128/mBio.02220-20
8. Messenger AM, Barnes AN, Gray GC. Reverse zoonotic disease transmission (zooanthroponosis): a systematic review of seldom-documented human biological threats to animals. PLoS One. 2014;9:e89055. https://doi.org/10.1371/journal.pone.0089055
9. Plowright RK, Parrish CR, McCallum H, Hudson PJ, Ko AI, Graham AL, et al. Pathways to zoonotic spillover. Nat Rev Microbiol. 2017;15:502–10. https://doi.org/10.1038/nrmicro.2017.45
10. US Department of Agriculture. USDA statement on the confirmation of COVID-19 in a tiger in New York [cited 2021 Oct 10]. https://www.aphis.usda.gov/aphis/newsroom/news/sa_by_date/sa-2020/ny-zoo-covid-19
11. US Fish and Wildlife Service Tigers [cited 2021 Oct 10]. https://www.fws.gov/international/animals/tigers.html

Address for correspondence: Byron Breedlove, EID Journal, Centers for Disease Control and Prevention, 1600 Clifton Rd NE, Mailstop H16-2, Atlanta, GA 30329-4027, USA; email: wbb1@cdc.gov

EMERGING INFECTIOUS DISEASES®

Emerging Infectious Diseases **thanks the following reviewers for their support through thoughtful, thorough, and timely reviews in 2021. Please contact us if your name is missing from this list.**

Joseph Abrams
Bahaa Abu-Raya
Anna Acosta
Douglas Adamoski
Kristina Adams-Waldorf
Toidi Adekambi
Atin Adhikari
Bishwa Adhikari
Jennifer Adjemian
Cornelia Adlhoch
Danielle R. Adney
Israel Agaku
Rakesh Aggarwal
Kamruddin Ahmed
Judd M. Aiken
Kaylynn Aiona
Andrei R. Akhmetzhanov
Lara J. Akinbami
Ana Alastruey-Izquierdo
Rachel Albalak
Nisha Alden
Afsar Ali
Sheikh Ali
Matthew T. Aliota
Abdelkafar Alkishe
Samantha E. Allen
Karen Alroy
Abeer Alshukairi
Arshad Altaf
Louis Altamura
Miriam Alter
Christian L. Althaus
Gerardo Alvarez
Ettore Amato
Avnika Amin
Sharon Amit
Alongkorn Amonsin
Shuchi Anand
Albert M. Anderson
Evan J. Anderson
Larry Anderson
Julien Andreani
Jason R. Andrews
Emmanouil Angelakis
Kristina Angelo
Joshua J. Anzinger
Abdel-Satar Arafa
Carmen Ardanuy
Alexandre Arenales
Paul M. Arguin
Aziza Arifkhanova
Sevtap Arikan Akdagli
George Armah
Philip M. Armstrong
Naomi Aronson
Rahul K. Arora
Nancy Arrospide
Ray R. Arthur
Ehsan Aryan
Benoit Assogba
Ali Ataya
Robert L. Atmar
Paul G. Auwaerter
Tatjana Avsic
Andrew S. Azman
Eduardo Azziz-Baumgartner
Annette Backhans
Nathan C. Bahr
Andreina Baj
Waheed Bajwa
Agoritsa Baka
Michael Ballesteros
Ashley Banyard
Philippe Barboza
Leslie Barclay
Sapha Barkati
Bridget Barker
Alex-Mikael Barkoff
John R. Barnes
Elizabeth Barnett
Sophie Baron
Ian Barr
Joel Barratt
Alan D.T. Barrett
Vanessa Barrs
Albert Barskey
Casey B. Behravesh
Sridhar Basavaraju
David Baud
Christina Baumbach
Daniel Bausch
Lauren Bayliss
Bernard Beall
Julien Beauté
Robert Bednarczyk
Emily S. Beeler
Martin Beer
Nancy Beerens
Ma Behr
Ermias Belay
Guido Beldi
Michael Bell
Jessica A. Belser
Kaitlin Benedict
Camilla Benfield
Albert Bensaid
Dennis Bente
Elizabeth Berkow
John Bernardo
Mabel Berois
Stephen Bertke
Kyle Bibby
Dorothee Bienzle
Dean Biggins
Megan Birkhold
Emma Birnie
Zeno Bisoffi
Aaron Bivins
Allison Black
Carina Blackmore
Stuart Blacksell
Carol D. Blair
Isobel M. Blake
Romain Blaizot
David D. Blaney
Lucas S. Blanton
Dean Blumberg
Matteo Boattini
Caitlin Bohannon
Sameh W. Boktor
Lakkana Boonyagars
Robert Booy
Andrew Borman
Benny Borremans
Ray Borrow
Eric Bortz
Albert Bosch
Angela Bosco-Lauth
Katrina L. Bosward
Amar Bouam
Yann F. Boucher
Valerie Bouchez
Daniel Bourque
Richard Bowen
Carol Bower
William A. Bower
Dwight Bowman
Richard S. Bradbury
Robert Bradsher
Mary E. Brandt
Aaron Brault
Byron Breedlove
James Brien
Thomas Briese
Tim Brooks
Yolanda Brooks
Philippe Brouqui
Corrie Brown
Heidi E. Brown
Joe Brown
Michael Brown
Peter Brown
James C.M. Brust
Udo Buchholz
Niccolo Buetti
Leslie Bulaga-Seraphin
Dora Buonfrate
Danilo Buonsenso
Brandy Burgess
Jeffrey Burton
Sarah Cahill
Renee M. Calanan
Rafael Calero-Bernal
Charles H. Calisher
Cyril Caminade
Fabricio Campos
Rafael K. Campos
Marta Canuti
Wuchun Cao
Ilaria Capua
Michael J. Carter
Jordi Casabona
Cynthia H. Cassell
Pamela K. Cassiday
Francesco Castelli
Godfred Cato

Catherine B. Cetre-Sossah
Thawatchai Chaijarasphong
Serafeim C. Chaintoutis
Jasper Chan
Martin Chi-Wai Chan
Paul K.S. Chan
Shu-Sen Chang
Rémi N. Charrel
Vishnu Chaturvedi
Hualan Chen
Jinping Chen
Liang Chen
Lin H. Chen
Hoa-Yuan Cheng
Harrell W. Chesson
Vera Lucia Pereira-Chioccola
Young J. Choe
Eun Hwa Choi
Mary Joung Choi
Won Suk Choi
Terence Chorba
Eric James Chow
Nancy Chow
Anuradha Chowdhary
Gerardo Chowell
Rebecca C. Christofferson
Daniel K.W. Chu
Hin Chu
Justin Jang Hann Chu
Victoria Chu
Carol Ciesielski
Alexander T. Ciota
Filip Claes
Andrew Clark
John D. Clemens
Brooke Clemons
Frank G.J. Cobelens
Steve L. Cochi
Kristen Cohen
Nived Collercandy
Sarah Collier
Philippe Colson
John Conly
Bruce Conn
Teresa M. Coque
Victor M. Corman
Oliver Cornely
Fatima Coronado
Irene Cortese
Caitlin Cossaboom
Matthew Cotten
Benjamin Cowling
Estee Cramer
Pascal Crépey
Julio Croda
Robert Cross
Bart J. Currie
Dustin W. Currie
Andrew Curtis
Juliana Da Silva
Laurent Dacheux
Ron Dagan
Janet Daly
Heath Damron
David Dance
Patrizia Danes
Alexandre Dasilva
Rachel Daniels
Michael David
Stephanie Davis
Charles T. Davis
William Davis
Bernard Davoust
Patrick Dawson
Marcos de Almeida
Mark G. de Boer
Marc de Chambrun
Kevin M. De Cock
Miranda de Graaf
Adela Gonzalez de la Campa
Daniele De Luca
Jesus de Pedro Cuesta
Rita De Sousa
Annabelle De St. Maurice
Anja De Weggheleire
Johnathan Dear
Nicola Decaro
Scott Dee
Arnaud Del Bello
Oscar H. Del Brutto
Eric Delaporte
Pascal Delaunay
Eric Delwart
Walter Demczuk
Erick Denamur
Xiangyu Deng
Benoït Desnues
Gregor Devine
Grant Dewell
Vijaykrishna Dhanasekaran
Georges Diatta
Maureen H. Diaz
Audrey Dionne
Thomas Dodson
Yohei Doi
Daryl Domman
Lu Dong
Van Do-Reynoso
Philip Dormitzer
Pierre Dorny
Jeff Doty
Christine J. Doyle
Chris Drakeley
Michel Drancourt
Steven Drews
Jan F. Drexler
Robert Drillien
Kirk M. Druey
Zhanwei Du
Grégory Dubourg
Mariette F. Ducatez
Priya Duggal
Roger Dumke
John S. Dumler
Ghinwa Dumyati
Herbert L. DuPont
Alan Dupuis
Ralf Dürrwald
Gregory Ebel
Hideki Ebihara
Isabella Eckerle
Michael Edelstein
Paul H. Edelstein
Chris Edens
Kathryn Edwards
Paul V. Effler
Andrea Egizi
Hanna Y. Ehrlich
Martin Eiden
Lars Eisen
Rebecca J. Eisen
Carole Eldin
Sascha Ellington
Ehud Elnekave
Esteban Engel
David M. Engelthaler
Dean D. Erdman
Mary K. Estes
Charles M. Evans
Álvaro A. Faccini-Martínez
Anna Fagre
Joseph O. Falkinham
Shufang Fan
Seamus Fanning
Nuno R. Faria
Joseph R. Fauver
Alyssa Fears
Ian Feavers
Amy K. Feehan
Heinz Feldmann
Leora R. Feldstein
Michelle Felicella
Mustapha Fellag
María del Pilar Fernández
Stefan Fernandez
Marcelo Ferreira
Alyssa Finlay
Anthony Fiore
Melanie Firestone
Kerstin Fischer
Leah Fischer
Julia Fitzner
Dana Flanders
Brendan Flannery
Shannon Fleck-Derderian
Katherine Fleming-Dutra
Min Whui Fong
Anthony R. Fooks
Andrea Forde
Brian Forde
Kimberly Fornace
Kaitlin Forsberg
Geoffrey Foster
Jeffrey T. Foster
Monique A. Foster
Rob Foster
Pierre-Edouard Fournier
Ashley L. Fowlkes
Mark Fox
Spencer J. Fox
Brian D. Foy
Joshua R. Francis
Mark R. Francis
Christina Frank
Neil Franklin
John Frean
David O. Freedman
Molly M. Freeman
Ana Friães
Thomas C. Friedrich
Norman K. Fry

Jonathan Frye
King-wa Fu
Hans-Peter Fuehrer
Takahisa Fujino
Richard M. Fulton
Isaac Chun-Hai Fung
Jennifer Furin
Nathan Woo Furukawa
Miklos Fuzi
Mauro Gacci
Lalitha Gade
Kenneth Gage
Mario Gajdacs
Eleni Galanis
Maria Galletti
Pushpa Gamalathge
Manoj Gambhir
Dario Garcia de Viedma
Richard Garfield
Mutien-Marie Garigliany
Philippe Gautret
Valentina Gazzaniga
Yang Ge
Kathleen Gensheimer
Jemma L. Geoghegan
Dale N. Gerding
Peter Gerner-Smidt
Lorenzo Giacani
Federica Gigliucci
Amy Gilbert
James R. Gilkerson
Emmanuelle Gilot-Fromont
Marta Giovanetti
Janet Glowicz
Sebastian Gnat
Lutz Goehring
Wil H.F. Goessens
Jeremy A.W. Gold
Jeremy D. Goldhaber-Fiebert
Paul N. Goldwater
Jonathan Golub
Aubree Gordon
Catherine Gordon
Richard Gorman
Rachel Gorwitz
Celine M. Gossner
Nicole Gottdenker
Frédérique Gouriet
Joelle Gouy de Bellocq
Nelesh P. Govender
Elena A. Govorkova
Erin Graf
Mark Graham
Gregor Grass
Stephen Gray
Chris Gregory
Daniel Griffin
Daniel Grint
Beate Grüner
Sophie Gryseels
Larisa Gubareva
Jonathan B. Gubbay
Jean-Luc Guérin
Alice Guh
Clair Guinat
Christopher A. Gulvik
Robert Gunn
Suman Das Gupta
Amanda Guthrie
Judith A. Guzman-Cottrill
Bart Haagmans
Nicole M. Hackman
Maryam B. Haddad
Stephen C. Hadler
Ferry Hagen
Nicholas Haley
Pete Halfmann
Carina M. Hall
Eric S. Halsey
Scott B. Halstead
Sarah A. Hamer
Nassim Hammoudi
Leah Hamner
Mi S. Han
Jennifer H. Harcourt
Timm Harder
Rafael Harpaz
Christopher J. Harrison
Heli H. Simmonds
Eric Harvill
Nabeeh A. Hasan
Yoshihisa Hashiguchi
Takehiro Hashimoto
Henrik Hasman
Ben M. Hause
Harry W. Haverkos
Hal Hawkins
Laura Hawks
Craig Hedberg
Fabian Heinrich
Robert Heinzen
Amy Heinzerling
Maged G. Hermida
Elizabeth Hemming-Schroeder
Emily Henkle
Thomas W. Hennessy
Christiane Herden
Jocelyn J. Herstein
David A. Hewitt
Roger Hewson
David L. Heymann
Janet E. Hill
Jonas Z. Hines
Wolfgang Hladik
Linda Hoang
Natasha S. Hochberg
Martin Hoenigl
Regina Hofmann-Lehmann
Catherine A. Hogan
Andrias Hojgaard
Mike Holbrook
David P. Holland
Steven M. Holland
F. Blaine Hollinger
NaTasha D. Hollis
Edward C. Holmes
Juan P. Horcajada
Heidie Hornstra
Harold Horowitz
Katja Hoschler
Margaret Hosie
Sasan Hosseini
Rein M.G.J. Houben
Jennifer A. House
Joppe W.R. Hovius
Jessica Howard-Anderson
Rosalind E. Howes
Daniela F. Hozbor
William T. Hu
Xinyi Hua
James Hughes
Ralph Huits
Klaus-Peter Hunfeld
Ivan Hung
Tine Huyse
Zsofia Igloi
M. Khalid Ijaz
Hon S. Ip
Malia Ireland
Seth Irish
Stuart N. Isaacs
John Iskander
Brendan R. Jackson
Chandra Jackson
Megan Jacob
Denise Jamieson
J. Michael Janda
Yunho Jang
Josep Jansa
Andrew Jardine
Agatha N. Jassem
Daniel Jeffares
Amy V. Jennison
Seonghye Jeon
Kwang C. Jeong
Kaitlyn E. Johnson
Nick Johnson
Paul Johnson
Stuart Johnson
Jefferson M. Jones
Martin H. Jones
T. Stephen Jones
Terry Jones
Somchai Jongwutiwes
Lim Jue Tao
Pallavi Kache
Wangeci Kagucia
Alexander J. Kallen
Everlyn Kamau
Saleem Kamili
Hajime Kamiya
Rui Kano
Rose Kantor
Bryan Kaplan
Jon Kaplan
Prashant Kapoor
Shanthi Kappagoda
Abraar Karan
Ruwandi Kariyawasam
Erik A. Karlsson
Morgan J. Katz
Leah Katzelnick
Charandeep Kaur
Ghazi Kayali
Felicia Keesing
Stefan Keller
Aubree Kelly
Bridget J. Kelly
Alyson Kelvin
Eben Kenah
Emma Kennedy
Tsuyoshi Kenri
Anusak Kerdsin
Janna Kerins
Andrew Kerkhoff
Ryan Kerney

Steven Kerr
Ellen N. Kersh
Jennifer Kertes
Margaret Khaitsa
Ali Khan
Aisha Khatib
Yury Khudyakov
Ananta Khurana
Sarah Kidd
Paul E. Kilgore
Perry Killam
Marie Killerby
Peter Kilmarx
A. Marm Kilpatrick
Eun-Jin Kim
Hee-Jin Kim
Yae-Jean Kim
Laura King
Amy E. Kirby
Marie Kirby
Martyn D. Kirk
Hannah L. Kirking
Peter D. Kirkland
Stephen Kissler
Noriko Kitamura
Moses Chapa Kiti
P.J. Klasse
Stephan Klatt
Terry A. Klein
Boris Klempa
Jackie Kleynhans
Jonas Klingstrom
Michael Klompas
Barbara Knust
Miwako Kobayashi
Marleen Kock
Anson V. Koehler
Patricia Koenig
Claudia Kohl
Haruki Koike
Qingzhong Kong
Mark Kortepeter
Linda Kothera
Barbara Kowalcyk
Alicia N.M. Kraay
Florian Krammer
Wolfgan Kratzer
Barry N. Kreiswirth
Erna G. Kroon
Andi Krumbholz
Steven V. Kubiski
Matthew J. Kuehnert
Sharon Kuhlmann-Berenzon
Thijs Kuiken
Sanjai Kumar
Amber Kunkel
Goro Kuno
Johanna Kurscheid
Vishwanath Kurup
Howard I. Kushner
Preeta K. Kutty
Kin On Kwok
Christos Kyratsous
Marcelo B. Labruna
Jean-Christophe Lagier
Katherine Laiton-Donato
Amy J. Lambert
Patrick J. Lammie
Ruiting Lan
Claudio F. Lanata
Emily W. Lankau
Tatiana Lanzieri
Maureen M. Laroche
Marilynn A. Larson
R. Ryan Lash
Erin Lashnits
E.H.Y. Lau
Rachel Lau
Susanna Kar Pui Lau
Adam Lauring
Michael Lauzardo
Becki Lawson
Kirsty Le Doare
Soizick Le Guyader
Tan Le Van
Sixto M. Leal
David Lee
Dong-Hun Lee
Rogan Lee
Youn-Jeong Lee
Surbhi Leekha
Fabian H. Leendertz
Sophie Lefevre
Giuseppe Legname
Natasha Lelijveld
Adrien Lemaignen
Audrey Lenhart
Robert J. Lentz
David A. Leon
Sebastian Lequime
Eyal Leshem
Michael Letko
Vivian Leung
Michael L. Levin
Min Z. Levine
Eric Lewitus
Joseph Lewnard
Lifang Li
Wen-Ta Li
You Li
Amy Liebman
Efrem Lim
Poh Lian Lim
Travis Lim
Direk Limmathurotsakul
Chung-Ying Lin
Jessica Lin
Yen Ting Lin
Monika Lindemann
Robbin Lindsay
William G. Lindsley
W. Ian Lipkin
Anastasia P. Litvintseva
Carol Y. Liu
Martin LLewellyn
Spencer Lloyd
Shawn R. Lockhart
Christopher H. Logue
Eduardo L. Lopez
Velma Lopez
Olivier Lortholary
Christopher F. Lowe
Xiaoyan Lu
Stephen Luby
Sebastian Lucas
Jay Lucidarme
Martin Ludlow
Oliver Lung
Yaniv Lustig
Joseph D. Lutgring
Laurence D.W. Luu
Joseph Lykins
Maureen Lynch
Michael Lynch
Alexandre Macedo de Oliveira
John Mackenzie
Emily MacLean
Ryan A. Maddox
Jean-Yves Madec
Zachary J. Madewell
Susan Madison-Antenucci
James H. Maguire
Monika Mahajan
Le Quynh Mai
Mark Maire
Anna Majury
Yadira Malavez
Richard Malik
Ryan Malosh
Arie Manangan
Floréale Mangin
Sylvie Manguin
Barbara Mann
Seeralan Manoharan
Tony Marfin
Kieren A. Marr
Linsey Marr
Theodore K. Marras
Tom Marrie
Roosecelis B. Martines
Jaime Martinez-Urtaza
Constanza Martinez-Valdebenito
Talkmore Maruta
Grace Marx
Paul S. Masters
Amy J. Mathers
Yasufumi Matsumura
Keita Matsuno
Salim Mattar
Giada Mattiuzzo
Anthony Maurelli
Max Maurin
Paolo A. Mazzarello
Conor McAloon
C. Patrick McClure
J. Trenton McClure
Andrea McCollum
Patrick McDermott
Anita K. McElroy
Suzanne McEvoy
Lesley McGee
Peter B. McIntyre
Debbie McKenzie
Sarah McKune
Sandra McLellan
Lucy McNamara
Jennifer H. McQuiston
Oleg Mediannikov
Jennifer K. Meece
Jean-Louis Mège
Megha L. Mehrotra
Jacques F. Meis
Cody Meissner
Elissa Meites
Cléa Melenotte
Georgios Meletis
Michael Melgar

Martin I. Meltzer
Leonel Mendoza
Dick Menzies
Nicolas Menzies
Rachel A. Mercaldo
Jeffrey W. Mercante
João Mesquita
Kevin Messacar
Mark Messonnier
Raphaëlle Métras
Lorraine Michelet
Claire M. Midgley
Susan K. Mikota
Gabrielle Miller
Maureen Miller
Imran Mirza
Nischay Mishra
Saroj Mishra
Oriol Mitja
Adriana S. Miu
Kenji Mizumoto
David Modrý
Fawzi Mohamed
Meng Ling Moi
Chris K.P. Mok
Igor Mokrousov
Noelle-Angelique M. Molinari
Michel Monod
Steve Monroe
Susan P. Montgomery
Ana Montoya
Patrick K. Moonan
John P Moore
Andrew Moorehead
Jacob Moran-Gilad
Serge Morand
Gonzalo Moratorio
Guillaume Morel
Pilar Moreno
David Morens
Leah F. Moriarty
Florent Morio
C. Paul Morris
Amy C. Morrison
Eric Mossel
Joel Mossong
Farzad Mostashari
Mina Motaghi
Sara Moutailler
Stephen Muhi
Barbara Mühlemann
Grace Mulcahy
Mick N. Mulders
Shantel Muldrew
Marcel A. Müller
Thomas Müller
Mark Mulligan
Vincent Munster
Peninah Munyua
David R. Murdoch
Manoj Murhekar
Frederick A. Murphy
Matthew Murphy
Kristy O. Murray
Yoshikazu Mutoh
Cameron Myhrvold
Peter J. Myler
Scott A. Nabity
Helen Nabwera
Robyn Nadolny
Céline Nadon
Harish Nair
Satosi Nakano
Allyn K. Nakashima
Fatemeh Namazi
Masa Narita
Farooq Nasar
Josilene Nascimento Seixas
Dean Natalie
Pavithra Natarajan
Sheila Nathan
Muktha Natrajan
Maria Negron
Christina Nelson
Martha Nelson
Nicole Nemeth
Elitieri Neto
Gilles Nevez
Kevin Ng
Terry Fei Fan Ng
Kimberly Nguyen
William L Nicholson
Eva Møller Nielsen
Vladyslav Nikolayevskyy
Carmen Niño-Taravilla
Eduardo Nobile-Orazio
Diego B. Nobrega
Susan M. Noh
Romolo Nonno
Michael Norris
Niels Norskov-Lauritsen
Janin Nouhin
Shannon Novosad
Norbert Nowotny
Ulrich Nubel
David O'Callaghan
Miguel O'Ryan
Kanecia Obie
John E. Oeltmann
Sylvia Ofori
Nick H. Ogden
Myoung-don Oh
Makoto Ohnishi
Tomohiro Oishi
Nisreen M.A. Okba
Peter Olbrich
Jane Oliver
Margaret A. Olsen
Sonja J. Olsen
Donald R. Olson
Victoria A. Olson
Tanja Opreissnig
Kathy A. Orloski
Nancy Ortiz
Matt Oster
Stephen Ostroff
Luis Ostrosky-Zeichner
José A. Oteo
Domenico Otranto
Bas B. Oude Munnink
Christopher D. Paddock
Clinton R. Paden
John Paget
Mark A. Pallansch
Gitika Panicker
Igor A.D. Paploski
John R. Papp
Sang Woo Park
Wan Beom Park
Daniel M. Parker
John James Parker
Julian Parkhill
William Parks
Jonathan B. Parr
Colin Parrish
Christopher M. Parry
Jeffrey Parsonnet
W. Clyde Partin
Frank Pasmans
Dipti Patel
Alessandro Patriarchi
Alex Pauvolid-Correa
David L. Pearl
Carl Pearson
Malik J.S. Peiris
Claudia Perandones
Mariana Perez Duque
Lara Perinet
Kiran M. Perkins
Stanley Perlman
Stephanie Perniciaro
Christian Perronne
Patricia Pesavento
Brett Petersen
Christine Petersen
Maria Skaalum Petersen
A. Townsend Peterson
Jennifer K. Peterson
Josh Petrie
Mary Petrone
Michael Pfaller
Melissa Phuong
Martine Piarroux
Renaud Piarroux
Brad Pickering
Genay Pilarowski
Allan Pillay
Pablo E. Piñeyro
Benjamin A. Pinsky
Johann D.D. Pitout
Brandon Plattner
Mateusz Plucinski
Ian Plumb
Jasmine Plummer
Gerd Pluschke
Thomas Poder
Laurent Poirel
Zvonimir Poljak
Mary Pomeroy
Leo L.M. Poon
Sven Poppert
David Powell
Krista Powell
Edoardo Pozio
Kiesha Prem
Andrew Preston
Bobbi Pritt
Jose L. Proenca-Modena
Christine Prue
Melissa Prusinski
Arto T. Pulliainen
Rachael Pung
Michael A. Purdy
Lawrence J. Purpura
Krista Queen
Laura Quilter
Holger Rabenau
Elisabeth Rabold
Benjamin Rader

Jayna Raghwani
Motiur Rahman
Gabriel Rainisch
M. Ramirez
K.P. Ranjan
Danielle A. Rankin
Stéphane Ranque
Didier Raoult
Mohammed Rasheed
Magnus Rasmussen
Mario Raviglione
Sergio Recuenco
Andrew Reeves
Michael Reid
Arthur Reingold
Michael H. Reiskind
Fredrik Resman
Susan Resnick
Mary G. Reynolds
Ali Rezaei-Matehkolaei
Ketra Rice
Wendy Rice
Stephen M. Rich
William Ristenpart
Scott A. Ritchie
Florence Robert-Gangneux
Gemma Robertson
Emmanuel Robesyn
Ashley Robinson
Anna Roca
Barry Rockx
Jesús Rodríguez-Baño
Pablo Rojo
Morgane Rolland
Pierre E. Rollin
Volle Romain
Claudia Romeo
Hannah E. Romo
Kimberlyn Roosa
Anne-Marie Roque-Afonso
Erica Rose
John Rossow
Christina Rostad
Paul Rota
Virginie Rougeron
Janell A. Routh
Pavitra Roychoudhury
Jose M. Rubio
Fiona Russell
Thomas A. Russo
Daniel Ruzek
Sadie Ryan
Jamal Saad
Rosalie Sacheli
Nasia Safdar
David Safronetz
Masayuki Saijo
Mohammad M. Sajadi
Yoshihiro Sakoda
Stephanie J. Salyer
Steven L. Salzberg
Johanna S. Salzer
Mark Salzman
Samira Sami
Sofia Samper
A Sanchez-Paa
Anna-Lena Sander
Gilberto A. Santiago
Mauricio Santillana
Sarah G.H. Sapp
Sharon Saydah
Sameera Sayeed
Elaine Scallan Walter
Maria Scaturro
William Schaffner
Joni M. Scheftel
Elizabeth Schlaudecker
Jonas Schmidt-Chanasit
Randal J. Schoepp
Tony Schountz
Betsy Schroeder
Claudia Schulz
Amy Schwartz
David Schwartz
Ilan S. Schwartz
Tatjana Schwarz
Jessica S. Schwind
H. Morgan Scott
Zuzana Sekeyova
Tara Kirk Sell
Piseth Seng
Jeffrey Seow
Andrea Servián
Nandini Sethuraman
Daniel J. Sexton
Komal Shah
Melisa Shah
Sharaf Shah
Andi L. Shane
Anupama Shankar
Carrie Shapiro-Mendoza
Adrienne E. Shapiro
Jyoti Sharma
Paul M. Sharp
Tyler Sharp
Frederic E. Shaw
Scott Sherrill-Mix
Kayoko Shioda
Kirsty Short
Adrienne Showler
Susan A. Shriner
Madhumita Shrotri
Emily E. Sickbert-Bennett
Katherine J. Siddle
Alex Sigal
Patricia J. Simner
Eric Simões
Etienne Simon-Loriere
R.J. Simonds
Colin R. Simpson
Les Sims
Andreas Sing
Charlene da Siza
Jan Slapeta
Jonathan Smith
Jessica Smith
Robert P. Smith
Tara C. Smith
Teemu Smura
Olusegun O. Soge
Ranjani Somayaji
Gail L. Sondermeyer Cooksey
Jeongmin Song
Jamie Sookhoo
Frank J. Sorvillo
Thiago Moreno L. Souza
Erica Spatz
Andrej Spec
Barbara Spellerberg
John Spencer
Francesca Sperotto
Kevin Spicer
Andrew Spieker
Gianfranco Spiteri
Armand Sprecher
Siddharth Sridhar
Kirby Stafford
David Stallknecht
J. Erin Staples
Angela Starks
Mieke Steensels
Robert Steffen
Arjan Stegeman
Eike Steinmann
Christen Rune Stensvold
Dennis L. Stevens
Ellen Stevenson
O. Colin Stine
Mars Stone
Neil Stone
J. Russell Stothard
Anne Straily
Susan Stramer
Marc A. Strassburg
Franc Strle
Klemen Strle
Kanta Subbarao
Kaiyuan Sun
Rebecca Sunenshine
Colin Sutherland
Melissa Sutton
John Swartzberg
David E. Swayne
David L. Swerdlow
Susan Swindells
Anna Szczerba-Turek
Thuy-Huong Ta-Tang
Marisa Tait
Sarah Talarico
Leisel Talley
Amish Talwar
Azaibi Tamin
Kathrine R. Tan
Arthur Tang
Julian Wei-Tze Tang
Robert Tanz
Dennis Tappe
Arnaud Tarantola
Cheryl L. Tarr
Phillip I. Tarr
Heather Tate
Robert Tauxe
Bradford Taylor
Asmaa Tazi
Sam Telford
Stefano Tempia
Mark Tenforde
Phil-Robin Tepasse
Karen Terio
Anders Ternhag
Harsh Thaker
Roger Thomas
George Thompson
Peter N. Thompson
Emma Thomson
Natalie Thornburg
Simon Tiberi
Tejpratap Tiwari

Kelvin Kai-Wang To
Mitsuru Toda
Isabelle Toga
Eugenia Tognotti
Rafal Tokarz
Hale Toklu
Keizo Tomonaga
Diana Tordoff
Paul Torgerson
Sergio Torres-Rueda
Pritish K. Tosh
Antonella Totsi
Mathieu Tourdjman
Cuc H. Tran
Rita Traxler
Shaun Truelove
Benedict Truman
Raymond Tsang
Tim K. Tsang
Apichal Tuanyok
Damien Tully
Claire E. Turner
Gregory Tyrrell
Yih-Ling Tzeng
Rainer Ulrich
Agnė Ulytė
Grace Vahey
Ronald O. Valdiserri
Sophie A. Valkenburg
Snigdha Vallabhaneni
Wim van der Hoek
Mark van der Linden
Wim H.M. van der Poel
H. Rogier van Doorn
Neeltje van Doremalen
Welmoed van Loon
Kristien Van Reeth
Debby van Riel
Willem van Schaik
Francois Vandenesch
Stephen Vaughan
Maria Vehreschild
Marietjie Venter
Júlia Vergara-Alert
Andrew Vernon
Guilherme Verocai
Paul E. Verweij
Nicolas Vignier
Julie Villanueva
Jan Vinjé
Benoit Visseaux
Susanna Visser
Chantal Vogels
Karin Jasmijn von Eije
Christian Johannes von Wintersdorff
Neil M. Vora
Duc J. Vugia
Jesse J. Waggoner
Henry Walke
Mark Walker
Megan Wallace
Julia Walochnik
Henry (Xiufeng) Wan
Jianwei Wang
Lin Wang
Lin-Fa Wang
Xin Wang
Honorine Ward
Mary Warrell
David Warren
Michael L. Washington
Stephen Waterman
John Watson
Matthew R. Watts
Scott C. Weaver
J. Todd Weber
J. Scott Weese
Michael R. Weigand
Zachary Weiner
Robert A. Weinstein
Louis M. Weiss
Will Weldon
Rory Welsh
Bruce G. Weniger
Juergen Wenzel
Guido Werner
Kerstin Wernike
Jean Whichard
David M. Whiley
Laura F. White
Lewis White
Peter Andrew White
Richard G. White
Hilary Whitham
Cyndy Whitney
Andreas Widmer
Nathan Wiederhold
Andrew Wiese
Margaret M. Williams
Erica Wilson
Dean L. Winslow
Laila Woc-Colburn
Cameron R. Wolfe
Nicole Wolter
Frank Wong
Kum Thong Wong
Roy Wong
Sirichit Wongkamchai
Jean Woo
Patrick C.Y. Woo
Spencer Woody
Gary Wormser
Jonathan Wortham
Anne L. Wyllie
Jingyi Xiao
Hayley Yaglom
Dafna Yahav
Bingyi Yang
Wan Yang
Yang Yang
Maosheng Yao
Hui-Ling Yen
Eugene Yeung
Xin Yin
Lili Yu
Xue-jie Yu
Kwok-Yung Yuen
Chee Fu Yung
Martin Zacharias
Sherif Zaki
Souheil Zayet
Bianca Zecchin
Adrian Zelazny
Shi Zhao
Stephan Zientara
Jakob Zinsstag
Julio C. Zuniga-Moya

EMERGING INFECTIOUS DISEASES®

Upcoming Issue

- Severe Acute Respiratory Syndrome Coronavirus 2 and Respiratory Virus Sentinel Surveillance, California, USA, May 10, 2020–June 12, 2021
- Outbreak of Mucormycosis in Coronavirus Disease Patients, Pune, India
- Using the Acute Flaccid Paralysis Surveillance System to Identify Cases of Acute Flaccid Myelitis, Australia, 2000–2018
- Potential Association of Legionnaires' Disease with Hot Spring Water, Hot Springs National Park and Hot Springs, Arkansas, USA, 2018–2019
- Extensively Drug-Resistant, Carbapenemase-Producing *Pseudomonas aeruginosa* and Medical Tourism from United States to Mexico, 2018–2019
- SARS-CoV-2 Infections, Including Coronavirus Disease Vaccine Breakthrough Infections, Associated with Large Public Gatherings, Massachusetts, USA
- Global Genome Diversity and Recombination in Mycoplasma pneumoniae
- Transmission Dynamics of Large Coronavirus Disease Outbreak in Homeless Shelter, Chicago, Illinois, USA, 2020
- Mask Effectiveness for Preventing Secondary Cases of COVID-19, Johnson County, Iowa, USA
- Effect of Hepatitis E Virus RNA Universal Blood Donor Screening, Catalonia, Spain, 2017–2020
- Coronavirus Disease Case Definitions, Diagnostic Testing Criteria, and Surveillance in 25 Countries with Highest Reported Case Counts
- Systematic Genomic and Clinical Analysis of Severe Acute Respiratory Syndrome Coronavirus 2 Reinfections and Recurrences Involving the Same Strain, Madrid, Spain
- Emergence of SARS-CoV-2 Delta Variant, Benin, West Africa, May–July 2021
- SARS-CoV-2 Shedding in Semen and Oligozoospermia of Patient with Severe Coronavirus Disease 11 Weeks after Infection
- Use of Private Sector Workforce Respiratory Disease Short-Term Disability Claims to Assess SARS-CoV-2, Mexico, 2020
- Melioidosis Manifesting as Chronic Femoral Osteomyelitis in Patient, Ghana
- Coronavirus Disease Spread during Summer Vacation, Israel, 2020
- Low Seroprevalence among Undetected COVID-19 Cases, Faroe Islands, November 2020
- Use of Incoming Travelers Arriving at Hong Kong for Genomic Surveillance of SARS-CoV-2
- Effectiveness of International Travel Controls for Delaying Local Outbreaks of COVID-19
- Postmortem Antigen-Detecting Rapid Diagnostic Tests to Predict Infectivity of SARS-CoV-2–Associated Deaths
- Atezolizumab Treatment for Progressive Multifocal Leukoencephalopathy
- Unexpectedly High Prevalence of Hepatitis C Virus Infection, Southern Lao People's Democratic Republic

See list of articles in the January issue at https://wwwnc.cdc.gov/eid/#issue-284

Earning CME Credit

To obtain credit, you should first read the journal article. After reading the article, you should be able to answer the following, related, multiple-choice questions. To complete the questions (with a minimum 75% passing score) and earn continuing medical education (CME) credit, please go to http://www.medscape.org/journal/eid. Credit cannot be obtained for tests completed on paper, although you may use the worksheet below to keep a record of your answers.

You must be a registered user on http://www.medscape.org. If you are not registered on http://www.medscape.org, please click on the "Register" link on the right hand side of the website.

Only one answer is correct for each question. Once you successfully answer all post-test questions, you will be able to view and/or print your certificate. For questions regarding this activity, contact the accredited provider, CME@medscape.net. For technical assistance, contact CME@medscape.net. American Medical Association's Physician's Recognition Award (AMA PRA) credits are accepted in the US as evidence of participation in CME activities. For further information on this award, please go to https://www.ama-assn.org. The AMA has determined that physicians not licensed in the US who participate in this CME activity are eligible for AMA PRA Category 1 Credits™. Through agreements that the AMA has made with agencies in some countries, AMA PRA credit may be acceptable as evidence of participation in CME activities. If you are not licensed in the US, please complete the questions online, print the AMA PRA CME credit certificate, and present it to your national medical association for review.

Article Title

Clinical Characteristics of *Corynebacterium* Bacteremia Caused by Different Species, Japan, 2014–2020

CME Questions

1. Your patient is a 67-year-old man with acute myeloid leukemia and positive blood culture for *Corynebacterium*. On the basis of the retrospective medical record review by Yamamuro and colleagues, which one of the following statements about proportion of true bacteremia and differences in clinical characteristics of patients with bacteremia from *C. striatum*, *C. jeikeium*, and other *Corynebacterium* species is correct?

A. Proportions of true bacteremia cases caused by *C. striatum* and *C. jeikeium* were significantly higher than for other *Corynebacterium* species
B. Of the 115 cases evaluated, more than three quarters represented true bacteremia
C. The most common underlying disease was diabetes mellitus
D. Among cases with true bacteremia, central venous port infection was the most common infective focus

2. According to the retrospective medical record review by Yamamuro and colleagues, which one of the following statements about differences in mortality and antimicrobial susceptibility in patients with bacteremia from *C. striatum*, *C. jeikeium*, and other *Corynebacterium* species is correct?

A. Survival in patients with *C. jeikeium* bacteremia was significantly worse than in patients with bacteremia from other *Corynebacterium* species
B. 90-day mortality rate was 34% for *C. striatum* bacteremia
C. Most tested strains were resistant to minocycline
D. *C. striatum* and *C. jeikeium* were more susceptible than other species to meropenem

3. On the basis of the retrospective medical record review by Yamamuro and colleagues, which one of the following statements about clinical implications of differences in clinical characteristics of patients with bacteremia from *C. striatum*, *C. jeikeium*, and other *Corynebacterium* species is correct?

A. *C. striatum* and *C. jeikeium* detected in blood cultures are generally contaminants and need not be evaluated further
B. *C. striatum* and *C. jeikeium* are less likely than other species to form biofilms
C. Antibiotic sensitivity in this study differed substantially from that found in previous studies
D. The authors emphasize the need to actively identifying coryneform in specimens, even if unsterile (e.g., sputum or urine), especially in suspected cases of *Corynebacterium* bacteremia

Earning CME Credit

To obtain credit, you should first read the journal article. After reading the article, you should be able to answer the following, related, multiple-choice questions. To complete the questions (with a minimum 75% passing score) and earn continuing medical education (CME) credit, please go to http://www.medscape.org/journal/eid. Credit cannot be obtained for tests completed on paper, although you may use the worksheet below to keep a record of your answers.

You must be a registered user on http://www.medscape.org. If you are not registered on http://www.medscape.org, please click on the "Register" link on the right hand side of the website.

Only one answer is correct for each question. Once you successfully answer all post-test questions, you will be able to view and/or print your certificate. For questions regarding this activity, contact the accredited provider, CME@medscape.net. For technical assistance, contact CME@medscape.net. American Medical Association's Physician's Recognition Award (AMA PRA) credits are accepted in the US as evidence of participation in CME activities. For further information on this award, please go to https://www.ama-assn.org. The AMA has determined that physicians not licensed in the US who participate in this CME activity are eligible for AMA PRA Category 1 Credits™. Through agreements that the AMA has made with agencies in some countries, AMA PRA credit may be acceptable as evidence of participation in CME activities. If you are not licensed in the US, please complete the questions online, print the AMA PRA CME credit certificate, and present it to your national medical association for review.

Article Title

Trends in Incidence and Clinical Outcomes of *Clostridioides difficile* Infection, Hong Kong

CME Questions

1. You are advising a large hospital regarding anticipated trends in *Clostridioides difficile* infection (CDI). According to the updated territory-wide survey study in Hong Kong by Guo and colleagues, which of the following statements about disease burden, incidence, and clinical outcomes of CDI among hospitalized patients in Hong Kong is correct?

A. Three-quarters of CDI cases were healthcare-associated (HA-CDI), and one-quarter was community-associated (CA-CDI)
B. CDI incidence increased significantly from 2006 to 2017 but plateaued in 2018 and 2019
C. 30-day mortality rates remained stable from 2015 to 2019 whereas 60-day recurrence rates decreased
D. Patients with HA-CDI were significantly younger than patients with CA-CDI and had similar mortality

2. According to the updated territory-wide survey study in Hong Kong by Guo and colleagues, which of the following statements about antibiotic usage and other CDI-associated risk factors and clinical outcomes among hospitalized patients in Hong Kong is correct?

A. CDI incidence trend was significantly correlated with overall antibiotic use ($r = 0.865$; $p<0.0001$), with decreasing incidence since an antibiotic stewardship program began in 2017
B. On multivariate logistic regression analysis, the main predictors for death in 30 days were use of H2 antagonists and comorbid stroke
C. 42% of patients had taken high-risk antibiotics within 8 weeks before CDI diagnosis
D. Tetracycline use within 8 weeks before CDI diagnosis decreased from 2015 to 2019

3. According to the updated territorywide survey study in Hong Kong by Guo and colleagues, which of the following statements about clinical and public health implications of the epidemiologic pattern of CDI, CDI-associated risk factors, and clinical outcomes among hospitalized patients in Hong Kong is correct?

A. The best explanation for changes in *C. difficile* epidemiology was changes in patient comorbidities
B. Sulphonamides and carbapenems are high-risk for CDI
C. The decrease in 30-day mortality rates was attributed solely to improved effectiveness of CDI treatment and management
D. Ribotypes 002 and 017, both virulent strains with high antibiotic resistance, may have been positively selected in the past because of excessive antibiotic use

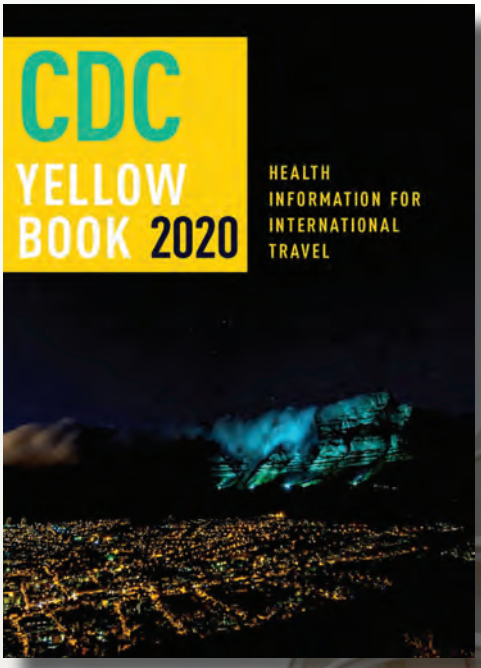

Available Now
Yellow Book 2020

The fully revised and updated CDC Yellow Book 2020: Health Information for International Travel codifies the US government's most current health guidelines and information for clinicians advising international travelers, including pretravel vaccine recommendations, destination-specific health advice, and easy-to-reference maps, tables, and charts.

ISBN: 978-0-19-006597-3 | $115.00 | May 2019 | Hardback | 720 pages

ISBN: 978-0-19-092893-3 | $55.00 | May 2019 | Paperback | 687 pages

Yellow Book 2020 includes important travel medicine updates

- **The latest information on emerging infectious disease threats, such as Zika, Ebola, and henipaviruses**
- **Considerations for treating infectious diseases in the face of increasing antimicrobial resistance**
- **Legal issues facing clinicians who provide travel health care**
- **Special considerations for unique types of travel, such as wilderness expeditions, work-related travel, and study abroad**

OXFORD
UNIVERSITY PRESS

Order your copy at:
www.oup.com/academic